

AGARD-LS-104

AGARD-LS-104

# AGARD

ADVISORY GROUP FOR AEROSPACE RESEARCH & DEVELOPMENT

7 RUE ANCELLE 92200 NEUILLY SUR SEINE FRANCE

ADA 081 645

## LEVELY

AGARD LECTURE SERIES No. 104

### Parameter Identification

DTIC  
ELECTE  
MAR 1 1985

This document has been approved  
for public release and sale; its  
distribution is unlimited.

DDC FILE COPY

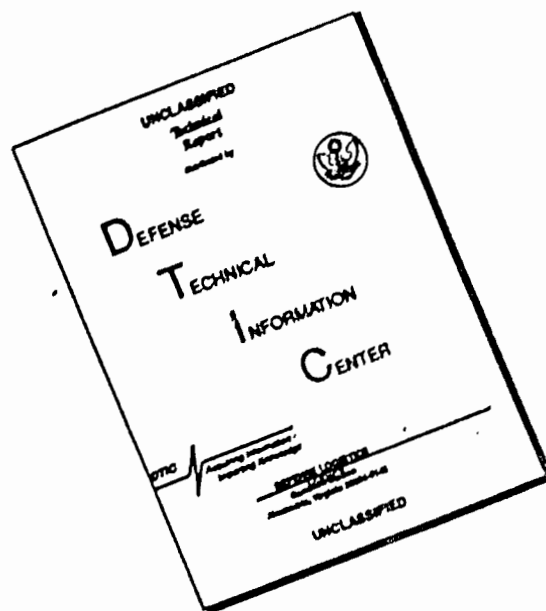
NORTH ATLANTIC TREATY ORGANIZATION



DISTRIBUTION AND AVAILABILITY  
ON BACK COVER

80 3 6 024

# DISCLAIMER NOTICE



THIS DOCUMENT IS BEST QUALITY AVAILABLE. THE COPY FURNISHED TO DTIC CONTAINED A SIGNIFICANT NUMBER OF PAGES WHICH DO NOT REPRODUCE LEGIBLY.

NORTH ATLANTIC TREATY ORGANIZATION  
ADVISORY GROUP FOR AEROSPACE RESEARCH AND DEVELOPMENT  
(ORGANISATION DU TRAITE DE L'ATLANTIQUE NORD)

E R R A T U M

to AGARD Lecture Series No.104 on Parameter Identification.

- Page 1-5: Paragraph 5 should read:  
"It is appropriate to use as a measuring unit a strap-down inertial . . ."
- Page 1-7: Paragraph 8 should read:  
"The introduction of parameter identification techniques into dynamic model testing, employing dynamically . . ."
- Page 1-19/20: Exchange captions of Figure 5 and Figure 6.
- Page 2-8: Equation (56) should read:  
" $\nu(i) = y(i) - \hat{y}(i, \hat{\theta})$ "
- Page 2-8: Line 31 from above should read:  
" $E\{x(0)\} = x_0$  and  $E\{[x(0) - x_0]^2\} = P_0$ "
- Page 2-11: Equation (95) should read:  
" $E\{(\hat{\theta} - \theta)(\hat{\theta} - \theta)^T\} \geq -E\left\{\frac{\partial^2 J(\theta)}{\partial \theta \partial \theta^T}\right\}$ "
- Page 3-1: Summary should read:  
"The discussed input signals, which were used in a flight test program, are compared with respect . . ."
- Page 3-6: Formula should read:  
" $J_{ij} = u_N^T \underline{A_i^T} W^{-1} A_j u_N$ "
- Page 3-10: Paragraph 6 should read:  
"The flight testing was carried out . . ."
- Page 10-2: Equation (2) should read:

$$\begin{bmatrix} \dot{u} \\ \dot{w} \\ \dot{q} \\ \dot{\theta} \end{bmatrix} + \begin{bmatrix} -X_u & -X_w & -X_q & q \\ -Z_u & -Z_w & -(V + Z_q) & 0 \\ -M_u & -M_w & -M_q & 0 \\ 0 & 0 & -1 & 0 \end{bmatrix} \begin{bmatrix} u \\ w \\ q \\ \theta \end{bmatrix} = \begin{bmatrix} X_\delta \\ Z_\delta \\ M_\delta \\ 0 \end{bmatrix} \delta_e$$

P.Hamel  
November 1979

AGARD-LS-104

NORTH ATLANTIC TREATY ORGANIZATION  
ADVISORY GROUP FOR AEROSPACE RESEARCH AND DEVELOPMENT  
(ORGANISATION DU TRAITE DE L'ATLANTIQUE NORD)

DTIC  
ELECTE  
MAR 11 1980

AGARD Lecture Series No. 104

PARAMETER IDENTIFICATION •

① 704 77/  
② 12 317/

This document has been approved  
for public release and sale; its  
distribution is unlimited.

The material in this publication was assembled to support a Lecture Series under the  
sponsorship of the Flight Mechanics Panel and the Consultant and Exchange Programme of  
AGARD presented on 29-30 October 1979 at Delft in The Netherlands and  
1-2 November 1979 in London, UK.

400 043

AB



## THE MISSION OF AGARD

The mission of AGARD is to bring together the leading personalities of the NATO nations in the fields of science and technology relating to aerospace for the following purposes:

- Exchanging of scientific and technical information;
- Continuously stimulating advances in the aerospace sciences relevant to strengthening the common defence posture;
- Improving the co-operation among member nations in aerospace research and development;
- Providing scientific and technical advice and assistance to the North Atlantic Military Committee in the field of aerospace research and development;
- Rendering scientific and technical assistance, as requested, to other NATO bodies and to member nations in connection with research and development problems in the aerospace field;
- Providing assistance to member nations for the purpose of increasing their scientific and technical potential;
- Recommending effective ways for the member nations to use their research and development capabilities for the common benefit of the NATO community.

The highest authority within AGARD is the National Delegates Board consisting of officially appointed senior representatives from each member nation. The mission of AGARD is carried out through the Panels which are composed of experts appointed by the National Delegates, the Consultant and Exchange Programme and the Aerospace Applications Studies Programme. The results of AGARD work are reported to the member nations and the NATO Authorities through the AGARD series of publications of which this is one.

Participation in AGARD activities is by invitation only and is normally limited to citizens of the NATO nations.

The content of this publication has been reproduced directly from material supplied by AGARD or the authors.

Published November 1979

Copyright © AGARD 1979  
All Rights Reserved

ISBN 92-835-1340-1



*Printed by Technical Editing and Reproduction Ltd  
Harford House, 7-9 Charlotte St, London, W1P 1HD*

## PREFACE

✓  
This Lecture Series No.104 on the subject of Parameter Identification is sponsored by the Flight Mechanics Panel of AGARD and implemented by the Consultant and Exchange Programme.

The aim of this Lecture Series is to review the present state of the art of Aircraft Parameter Identification Techniques and to provide a critical appraisal of current methods developed and applied to the problems of Analysis of Flight Test Data in a number of NATO countries. Particular emphasis is placed on the practical aspects of Aircraft Parameter Estimation to generate information useful for the Flight Test Engineer.

P.HAMEL  
Lecture Series  
Director

Accession For	
NTIS GNA&I	<input checked="" type="checkbox"/>
DEC TAB	
Unannounced Justification	
By	
Distribution/	
Availability/	
Dist	Available for special
A	

## LIST OF SPEAKERS

Lecture Series Director: Dr P.Hamel  
Institut für Flugmechanik – DFVLR  
Postfach 3267  
D-3300 Braunschweig  
Germany

Ir. J.H.Breeman  
National Aerospace Laboratory, NLR  
Anthony Fokkerweg 2  
Amsterdam 1017  
The Netherlands

Dipl.-Ing. J.Kaletka  
Institut für Flugmechanik – DFVLR  
Postfach 3267  
D-3300 Braunschweig  
Germany

Dr V.Klein  
Joint Institute for Advance of Flight Science  
George Washington University  
NASA Langley Research Center  
Mail Stop 169  
Hampton, Virginia 23665  
USA

Dipl.-Ing. R.Koehler  
Institut für Flugmechanik – DFVLR  
Postfach 3267  
D-3300 Braunschweig  
Germany

Dr K.W.Iliff  
NASA  
Hugh L.Dryden Flight Research Center  
P.O.Box 273  
Edwards, California 93523  
USA

Ir. J.A.Mulder  
Delft University of Technology  
Department of Aerospace Engineering  
Kluyverweg 1, P.O.Box 126  
Delft  
The Netherlands

Dr E.Plaetschke  
Institut für Flugmechanik – DFVLR  
Postfach 3267  
D-3300 Braunschweig  
Germany

Dr A.J.Ross  
Royal Aircraft Establishment  
Flight Systems Department  
Farnborough  
Hampshire GU14 6TD  
UK

Mr R.A.Verbrugge  
Institut de Mechanique des Fluides  
5 Boulevard Paul Painleve  
5900 Lille  
France

## CONTENTS

	Page
PREFACE	iii
LIST OF SPEAKERS	iv
	Reference
AIRCRAFT PARAMETER IDENTIFICATION METHODS AND THEIR APPLICATIONS – SURVEY AND FUTURE ASPECTS by P.G.Hamel	1
IDENTIFICATION EVALUATION METHODS by V.Klein	2
PRACTICAL INPUT SIGNAL DESIGN by E.Plaetschke and G.Schulz	3
ASPECTS OF FLIGHT TEST INSTRUMENTATION by J.H.Breeman, K.van Woerkom, H.L.Jonkers and J.A.Mulder	4
ANALYSIS OF AIRCRAFT PERFORMANCE, STABILITY AND CONTROL MEASUREMENTS by J.A.Mulder, H.L.Jonkers, J.J.Horsten, J.H.Breeman and J.L.Simons	5
AIRCRAFT IDENTIFICATION EXPERIENCE by K.W.Iliff	6
ROTORCRAFT IDENTIFICATION EXPERIENCE by J.Kaletka	7
IDENTIFICATION EXPERIENCE IN EXTREME FLIGHT REGIMES by A.J.Ross	8
WINDTUNNEL AND FREE-FLIGHT MODEL IDENTIFICATION EXPERIENCE by R.A.Verbrugge, W.Charon and M.Marchand	9
CLOSED LOOP ASPECTS OF AIRCRAFT IDENTIFICATION by R.Koehler and K.Wilhelm	10
BIBLIOGRAPHY	B

# AIRCRAFT PARAMETER IDENTIFICATION METHODS AND THEIR APPLICATIONS - SURVEY AND FUTURE ASPECTS

by

P. G. Hamel

Institut für Flugmechanik

Deutsche Forschungs- und Versuchsanstalt  
für Luft- und Raumfahrt e.V. (DFVLR)  
D 3300 Braunschweig-Flughafen, West Germany

## SUMMARY

This paper is intended to give an overall view of the methods for the determination of aircraft flight mechanic parameters from flight tests and the problems associated with them. Improved technologies in the field of instrumentation, data handling and data processing as well as improved methodologies for optimum control input design have contributed to broaden the application spectrum for parameter identification. For example, these methods are becoming standard procedures for aircraft handling qualities investigations and acceptance testing.

Future relevant research topics will deal with the identification of high order system aircraft dynamics including high angle of attack flight conditions incorporating nonlinear and unsteady flow separation dynamics. In addition, system identification demands for active control technology flight vehicles implementing aeroservoelastic coupling effects and control surface interactions within an extended frequency bandwidth will become subject of increased attention. Further, still existing limitations with regard to the in-flight determination of parameters of highly coupled rotorcraft systems have to be eliminated. New activities in the fields of in-flight determined parameters of missile system flight mechanics and external store separation dynamics may evolve.

## 1. INTRODUCTION

During the past years there has been a constant effort in determining dynamic aircraft parameters, such as stability and control derivatives, from flight test measurements. Several factors are involved in the increased application spectrum of flight test methods for aircraft state and parameter identification. One of which is the fact that the evolution of flight test instrumentation, analytical capability and computational facilities nowadays make aircraft parameter identification methods to routine procedures, which, in turn, have generated sufficient practical experience to gain confidence in utilizing these techniques.

Seen from the aspect of cost-effectiveness another factor involved is the demand to reduce the amount of costly and time consuming aircraft flight testing with respect to specification requirements. It seems possible to further reduce a considerable portion of the flight test programme by application of aircraft parameter identification methods [1].

An additional important factor is emerging from the area of implementation of active-control-technology (ACT) or control-configured-vehicle (CCV) concepts offering the promise of significantly increased aircraft performance and operational capability. It is well-known, that this approach extends the traditional tradeoffs between aerodynamics, structures and propulsion to include the capabilities of a full-time, full-authority fly-by-wire control system [2]. It is imperative that the aerodynamic stability and control parameters of such active control aircraft inflight have to turn out as predicted, since the inherent stability margins will be lower and the flight control system must correct these deficiencies to provide required handling qualities.

The aim of this lecture series of the AGARD Flight Mechanics Panel is to review the present state of the art of aircraft parameter identification techniques and to provide a critical appraisal of current methods developed and applied to the problems of analysis of flight test data in a number of NATO countries. Particular emphasis is placed on practical aspects of aircraft parameter estimation in order to generate information useful to the flight test engineer in industry, applied research facilities and universities. Special reference is also made to comparing different approaches to the aircraft parameter identification flight test and evaluation methodology under equal experimental conditions in order to provide guidelines for the user's selection and application.

## 2. REVIEW OF AGARD ACTIVITIES

Before going into more technical details it is worthwhile mentioning the substantial role of the AGARD Flight Mechanics Panel to identify the importance of extracting aircraft stability and control parameters from flight tests and to provide a multitude of documentation within the various AGARD publication series (Table 1). Included in this review are some informations about dynamic windtunnel test techniques because they play an essential part in predicting aircraft dynamic stability parameters within the preliminary design stage. In addition, these dynamic data obtained from ground testing are valuable as *a priori* parameter estimates for modern computerized aircraft identification methods.

From Table 1 it can be seen that AGARD treated this problem area as early as 1955. Special reference should be made to the AGARD Conference Proceedings CP 172 (1975) on Methods for Aircraft State and Parameter Identification which contain all papers presented at a Specialist's Meeting of the Flight Mechanics Panel of AGARD held at NASA Langley Research Center in November 1974 [3]. The present AGARD Lecture Series 104 is a direct outcome from the above Specialist's Meeting.

In further consequence, the AGARD Flight Mechanics Panel has asked Dr. Kenneth W. Iliff, a most experienced NASA expert in the field of aircraft parameter identification, to prepare an AGARDograph entitled *Parameter Identification* as a follow-up action to the present Lecture Series 104. This AGARDograph is under preparation of the well-known AGARD Flight Test Manual Series and will address the general flight test methodology of aircraft parameter identification in a more unified way including some of the main conclusions of the Panel Discussion of the Lecture Series 104.

Finally, the AGARD Scientific Publication and Technical Information Panel has arranged for this Lecture Series a Bibliography entitled *Parameter Identification*. The Bibliography with abstracts was prepared by the Scientific and Technical Information Branch of the U.S. NASA, Washington, and is enclosed at the end of this Lecture Series Edition.

For quick information references [4, 5, 6] are available from the above list of AGARD publications. They review the main aspects pertinent to the field of methods for aircraft state and parameter identification.

## 3. DEFINITIONS FOR PARAMETER IDENTIFICATION

### QUADRANGLE OF FORCES

Figure 1 represents an aircraft "Ersatz" model from a flight mechanics standpoint. The aircraft dynamic response behaviour (output) due to disturbance (gusts) and control (pilot) inputs is described by the interaction of inertial and aerodynamic forces as well as elastomechanic and control forces.

It is evident that aircraft stability, controllability and sensitivity is in principle influenced by all four kinds of forces. The relative effects of these forces on the aircraft's dynamic response is varying between different aircraft configurations and operations.

Whereas static and dynamic structural and control force influence parameters can be properly modeled without airloads by ground test techniques, the identification of aerodynamic forces and loads require windtunnel and flight testing. Static and dynamic windtunnel testing methods play an important role in the preliminary aircraft design although aerodynamic scale effects and windtunnel model deficiencies may lead to severe limitations in the applicability of windtunnel data.

Therefore, flight tests are important and necessary to isolate limits and uncertainties from the prediction techniques of aircraft aerodynamics and flight mechanics. Perhaps more than any other technique parameter identification provides the basis for flight/ground testing correlation by extracting as much information as possible from subscale and full-scale windtunnel and free flight tests.

Precisely defined, parameter identification is the determination, on the basis of input and output of a system within a specified class of systems to which the system under test is equivalent. This means realistic expressed with respect to the present problem area that aircraft parameter identification is related to the flight test verification of qualitative (model) and quantitative (coefficients) aerodynamics from a flight mechanics standpoint (Figure 1). Hence, aircraft parameter identification may be subdivided into two distinct areas:

- System identification, primarily concerned with the mathematical structure of aircraft models and
- Parameter estimation, the quantifying of parameters or coefficients for a selected aircraft model.

## IDENTIFICATION FRAMEWORK

A fairly general synoptic description of the procedure applied for determining the flight vehicle states and parameters from flight tests is given in Figure 2. The parameter identification framework can be divided into three parts:

The first is *instrumentation and filters* which covers the entire data acquisition process and takes into account the effects of measurement noise.

The second called *flight test techniques* is related to input design. The input signals have to be optimized in their spectral composition in order to achieve accurate identification.

The third describes *analysis of flight test data* which includes the mathematical model of the aircraft and an estimation criterion which devises some iterative computational algorithm to adjust some a-priori estimate of the parameters until a set of best parameter estimates is obtained which minimizes the response error.

Corresponding to the above three strongly interdependent topics on parameter identification the first half of the technical programme of the present Lecture Series will be devoted to these key aspects. The main emphasis in the second part is placed on practical applications of the parameter identification framework to various aircraft and rotorcraft problem areas including extreme flight regimes and closed loop aspects.

## 4. REQUIREMENTS FOR PARAMETER IDENTIFICATION

Although the essential flight vehicle aerodynamic characteristics can be predicted with rather satisfactory accuracy by means of theoretical calculations and windtunnel measurements, the requirements for more precise, experimentally determined aircraft flight mechanics parameters have increased.

### ACCEPTANCE FLIGHT TESTING

For example, the acceptance flight testing of the flying qualities of modern weapon systems with respect to the requirements of military specifications is costly and time consuming. A considerable portion of the flight test programme can be eliminated by implementing aircraft parameter identification techniques. This method would be employed to extract the aircraft stability and control derivatives from data obtained through a preselected limited number of flight test points. The specification of flight test points is a matter to insure that flight envelope parameters like Mach number, angle of attack and normal load factor are adequately covered. In turn, the derivatives would be used to verify the handling qualities of the aircraft with the military specification requirements [1, 78].

### TRACKING FLIGHT TESTING

Also, requirements for increased maneuverability of modern combat aircraft make the task of assessing the overall handling qualities or precision controllability more difficult. The analysis of precision tracking tasks depends heavily on the integration of the pilot, flight control systems and the aircraft dynamics. From a flight mechanics standpoint, the adoption of tracking flight tests offer a closed-loop task that has the advantage of permitting a quantitative evaluation in addition to the qualitative pilot assessment [9, 10]. Such pilot-in-the-loop precision tracking flight test provide actual flight vehicle data not only for the extraction of stability and control derivatives of the aircraft within a matrix of angle of attack and normal load factor but also for the identification of pilot dynamics.

### PIO FLIGHT TESTING

In addition, the identification of closed loop pilot-aircraft dynamics is especially important when pilot induced oscillations (PIO) are encountered. It is probably safe to say that PIO should be expected to occur with each new aircraft because the problem cannot be predicted authentically without accurate knowledge of the aircraft/flight control system dynamics. For advanced aerodynamic configurations and modern digital flight control systems it is therefore essential to require baseline tracking tests during initial stages of flight testing to enable a rapid detection and elimination of hidden PIO problems [11]. Here again, parameter identification techniques can contribute to more effective quantitative flight testing.

### ACT FLIGHT TESTING

Finally, future highly maneuverable aircraft will incorporate active flight control technology (ACT) with blended aerodynamic control surfaces which are very closely coupled aerodynamically. Adverse aerodynamic interactions between the force and moment producers of an ACT aircraft as well as nonlinear aerodynamics at the extremes of the flight envelope can be prime factors of an increased requirement for a better and

accurate definition and estimation of aerodynamic characteristics [12, 13, 14, 15]. The application of ACT using high performance, full authority fly-by-wire control systems will require thorough higher order aerodynamic, structural, electrical and hydraulic mathematical models of the aircraft and its control system. The existing flying qualities requirements of MIL-F 8785 B need updating in order to better handle such complex aircraft dynamics, also called higher order systems (HOS) [16]. The impact of Active Control Technology on aircraft complexity is indicated in Figure 3 where specific items of conventional or low order system (LOS) aircraft dynamics are compared with active control or higher order system (HOS) aircraft dynamics.

By introducing increased flight test data accuracy and improved and reliable parameter estimation techniques the flight test methodology of aircraft parameter identification can be used not only to reduce the amount of ever increasing flight time on specification testing of HOS aircraft but also to contribute toward safer and more effective flight testing.

#### ROTORCRAFT FLIGHT TESTING

In contrary to fixed wing aircraft, rotorcraft identification is a still more complicated task due to strong coupling of all rigid-body modes plus additional flexible modes introduced by the rotor blade system. HOS rotorcraft of the future implementing fly-by-wire control and higher-harmonic active control systems will require unique and sophisticated flight test methods for the accurate identification of not only stability and control derivatives but also aeroelastic (rotor) parameters. High vibration levels and inefficient instrumentation in extreme flight regimes are further aggravating factors.

Due to the fact that rotorcraft have to meet stringent flying qualities requirements arising from various well defined operational needs like NOE or TF flight missions under all weather and severe combat conditions, again it can be stated that the existing military flying qualities requirements for rotorcraft are inadequate for proper application. Also, there is a lack of mutuality with regard to military handling and ride quality requirements within a country among the military services civil service and between countries within NATO [17].

Therefore, joint research in the field of mission oriented flying qualities for advanced rotorcraft systems is required. Practical and reliable parameter identification flight testing can provide a powerful and cost-effective tool to improve and unify rotorcraft handling and ride qualities acceptance testing in the future.

### 5. APPLICATION SPECTRUM FOR PARAMETER IDENTIFICATION

#### BASIC APPLICATIONS

Including the foregoing stated broad requirements for aircraft parameter identification in the field of handling qualities verification the basic application spectrum for exact and reliable stability and control parameters is the following:

- Acceptance testing of aircraft handling qualities including effects of mission and configuration changes as well as external store interference.
- Data correlation for increasing confidence in flight mechanic prediction techniques.
- Data utilization of industry for isolation and identification of nonanticipated aerodynamic effects and further aircraft development.
- Optimization of aircraft stability augmentation and active control systems by accurate description of airframe parameters.
- Data generation for basic computer simulations, fixed and moving base ground simulators and airborne simulators.
- Improvement of flight test and data evaluation methodologies in general.
- On-line identification of aircraft parameters for adaptive control.

#### SPECIFIC APPLICATIONS

Specific problem areas have accentuated the need for parameter identification. Some of these problem areas are concerned with the in-flight determination of:

- High angle of attack flight mechanics generating nonlinear (amplitude dependent) and unsteady (frequency dependent) aerodynamic characteristics [15].
- High angle of attack flight mechanics providing kinematic and aerodynamic cross-coupling between lateral and longitudinal degrees of freedom [12, 15, 18].



- Closed loop stability and control augmentation effects on handling qualities evaluations [1, 19].
- Critical aerodynamic characteristics of full-authority active control surfaces due to flow separation, interference and coupling effects [20, 21].
- Important structural mode parameters for optimizing aeroservoelastic coupling effects by means of active control technology [2].
- Engine-airframe coupling parameters due to inlet control deficiencies or extreme flight conditions [22].
- Critical airload parameters of fixed-wing and rotorcraft in extreme dynamic flight conditions for certification purposes [23].
- Rotor-airframe control and coupling parameters for improved rotorcraft stability and control augmentation [24, 25].
- Aircraft proneness to pilot induced oscillations by gaining adequate information on airframe-flight control system parameters [11, 26].

## 6. INSTRUMENTATION AND FILTERS

### ERROR SOURCES

A principal source of inaccuracy in identifying aircraft parameters is the error in the flight test instrumentation. Therefore, parameter estimation accuracy is highly dependent on the quality of the flight measured data [27, 28].

In order to determine the suitability of the utilized instrumentation, the effects of static (scale factors, misalignments, location uncertainty and vane corrections) and dynamic error sources (airframe vibrations, sensor dynamics, electrical noise and inappropriate signal filters) have to be taken into account.

### RELEVANT DOCUMENTATION

Classic information on flight test instrumentation for parameter identification is given in Ref. [29]. To satisfy the need for specialized documentation in the field of sophisticated flight test instrumentation, and to promote a better understanding between the flight test engineer and the instrumentation and data processing specialists, the AGARD Flight Mechanics Panel started a renewed effort to establish a series of separately published monographs on selected subjects of flight test instrumentation. Within this AGARD Flight Test Instrumentation Series several new Volumes have been produced which provide valuable information on instrumentation system design for parameter identification purposes [30, 31, 32]. Well designed instrumentation and filtering systems have increased the parameter identification accuracy dramatically [33]. More information on aspects of optimum flight test instrumentation design will be given in this Lecture Series by *Breeman*.

### DATA CHANNEL COMPATIBILITY

In order to avoid wasting of valuable flight test, research and computer time due to signal incompatibility between various signals, flight test data analysis should determine as early as possible whether the data channels are compatible. Adjustments can be made by application of special computing techniques for estimating aircraft states (positions, velocities and attitudes) from measurements recorded in-flight [34, 35, 36]. It is appropriate to use as a measuring unit a strapped-down inertial system providing angular rate and acceleration information. If, in addition, an airflow vane is available for measuring the airflow angle of attack and the inertial angle of attack (computed from the inertial velocities) it provides a measure of turbulence acting on the airframe [37].

Finally, nowadays there are software techniques for redundancy management of digital flight control systems at hand which implement observer techniques to the reconstruction of failed sensor outputs. These techniques may offer the advantage to provide additional redundancy, compatibility and confidence between measured signals for parameter identification applications.

## 7. FLIGHT TEST TECHNIQUES

### INPUT DESIGN

The importance of adequate design of flight test maneuvers for parameter identification purposes is well recognized [38, 39]. The reliability of aircraft parameter extraction from flight test maneuvers depends heavily on the amount of information available in the response. Therefore, the shapes of the control inputs should be chosen such that they excite each pertinent mode of the aircraft dynamics as much as possible. Generally, as there is neither an ideally located single control surface nor a single control input shape possible which could excite all modes of the aircraft response equally well, it is mandatory to design and apply specific optimum inputs for all available control surfaces of the aircraft under investigation within the flight envelope of interest.

The design of optimum input signal can be performed in the frequency or time domain considering system criteria and estimation error criteria. Evaluations, practical applications and performance comparisons of optimum inputs will be discussed in a subsequent paper given by *Plaetschke* within this Lecture Series.

### PILOT INPUT IMPLEMENTATION

The optimized inputs can be generated manually by the pilot or if available by some automatic input device like a fly-by-wire control system. With an automatic device any kind of optimum continuous input signals can be performed. In the other case of manual inputs, multistep type sequences like combination of some fundamental types (doublets, pulses and steps) can be implemented by the pilot in practice.

Figure 4 shows two examples of the pilot's ability to realize prescribed control inputs. On the left side of Figure 4 the optimum DFVLR 3211 input signal was flown by a pilot in a small transport aircraft CASA 212 within a Spain-West Germany cooperative flight test programme [40]. The input signal was connected electrically to the left needle of a dual vertical scale instrument. The right needle was driven by the control surface deflection signal (elevator). With this simple visual cue the pilot needed only to try to cause by control column deflection the right needle to follow the left needle commands. The elevator has then to perform the programmed deflections. This system enabled the pilot, after spending a minimum amount of training, to fly the wanted signals quite well.

On the right side of Figure 4 a special designed Calspan rudder input signal was nicely implemented by the pilot in practice on a F-106 A during a flight experiment conducted by the USAF. Alternating with the rudder, additional aileron input signals were applied by the pilot to perform a pseudo-sideslip maneuver [41].

### MULTI INPUT MANEUVER

As was discussed in this section earlier, there are problems to accurately identifying flight vehicle parameters when only one control input is used to excite all modes of the vehicle. The inability to estimate some terms accurately is because the influence of these terms on the flight vehicle dynamics is small. An equivalent situation is given if there exists a strong dependency between two motion variables or between a motion variable and a control input. A classical example in flight mechanics is the difficulty to separate the translational acceleration derivative  $\dot{C}_{M\dot{\alpha}}$  independent of the angular rate derivative  $\dot{C}_{M\dot{\omega}}$  due to the fact that translational acceleration and angular rate are nearly dependent. Selecting and combining physical meaningful different inputs (maneuvers), it was shown, that it is possible to separately estimate both aircraft parameters [42]. In general, it can be concluded that identification problems due to high correlation of measured signals can be overcome by multiple input maneuvers. Also, the interaction of turbulence with the airframe may, if properly modeled, aid in the identification of aircraft parameters. This is because turbulence acts as another input signal in addition to the usual control input [37].

### MULTIPLE MANEUVERS

Further, the evaluation of aircraft parameters can also be improved by using selected multiple maneuvers with single or multiple inputs. The use of a large amount of information from multiple data runs is especially meaningful for identification of rotorcraft parameters in unstable flight regimes as well as for augmented aircraft with various highly correlated measured signals. These aspects will be discussed in more detail in subsequent papers of this Lecture Series presented by *Kaletka* and *Koehler*.

Finally, multiple input design is also attractive for identification of the effectiveness of active control surfaces. In selecting the optimum input for control parameter identification, it is mandatory to excite also the eigenmotion of the airplane since the

technique of identifying active control parameters involves also the identification of stability parameters. A poor identification of the latter parameters would affect the quality of the active control parameters.

#### ACTIVE CONTROL PARAMETER IDENTIFICATION

Figure 5 indicates, as an example, the sequence of control inputs for the identification of active flap and spoiler control parameters of the airborne simulator DFVLR-Hansa Jet. First, the short period and phugoid motions are excited by a DFVLR 3211 elevator signal. Then an equivalent 3211 input signal of either the spoiler and flap separately, or a combined spoiler-flap setting is applied [44]. As illustrated on the left side of Figure 5 the time responses of the flight test data and the model identified using flap and spoiler derivatives from separate identification runs show a relatively good agreement. Some errors in pitch rate and accelerations are due to flap-spoiler interference. This is confirmed by the right hand side of Figure 5, where a better match has been achieved using control parameters identified by a combined flap/spoiler input signal.

Figure 6 indicates the flight test determined flap and spoiler control parameters for different reference (index "0") deflections. It is apparent, that the flap effectiveness derivatives  $c_{M\delta_f}$  and  $c_{L\delta_f}$  are only slightly influenced by superposed spoiler dynamics whereas the spoiler moment effectiveness  $c_{M\delta_{sp}}$  reveals a strong amplitude sensitivity with respect to flap dynamic interference.

Further specific aerodynamic interference effects of active control surfaces have been observed during flight testing of two other airborne simulators. For example, the original midwing located active side-force control surfaces of the airborne simulator Calspan TIFS generated substantial and unexpected flow separation on the wing which caused a large decrease in the aircraft lift and a large increase in induced drag. In addition, there were changes in the side force effectiveness experienced due to interactions with the active lift flap deflections [45]. A modified maximum likelihood estimation technique was used to determine the aerodynamic derivatives of the airborne simulator NASA-Jet Star. The aircraft was equipped with direct lift and side force control surfaces. The two side force control surfaces were mounted side by side beneath the center wing. Figure 7 indicates a significant interference effect of the side force generator on the lateral stiffness ( $c_{l\beta}$ ) and damping ( $c_{l\dot{\beta}}$ ) parameter at low angles of attack, whereas the side force control effectiveness remains merely unchanged. Similar trends of strong interference could be discovered also for other stability and control parameters [46].

Finally, recent flight test experience involving the CCV/YF-16 testbed vehicle demonstrated impressively that active control surfaces used to decouple aircraft motions and implement ACT concepts can be expected to exhibit aerodynamic nonlinearities and interference. These aerodynamic interactions can produce adverse effects and limits beyond which aircraft flight control system fixes of aerodynamic characteristics are no longer feasible [20].

Therefore, it can be concluded that active control parameters have to be estimated from initial flight test data to identify and solve potential adverse aerodynamic interactions problems as early as possible.

#### DYNAMIC MODEL IDENTIFICATION

To improve the identification quality of sensitive, low-influence or highly correlated parameters by careful selected flight test maneuvers it is important to gain sufficient physical insight into the phenomenon to be analyzed. This can be achieved in a more fundamental way by properly defined flight test maneuvers in dynamic windtunnel or free flight model testing facilities.

The introduction of parameter identification techniques into dynamic model testing, employing dynamically scaled and controllable light-weight aircraft models, is attractive because more controlled experiments than flight tests are feasible. If, in addition, realistic and reproducible gust generating devices for discrete gust or continuous turbulence simulation are available the advantage of this type of dynamic windtunnel testing is the good observability of all state, control and disturbance variables acting on the aircraft model. All standard or optimized control or disturbance (turbulence) input signals for parameter identification, such as single and multistep or continuous excitations, can be repeatedly performed [47, 48]. More information and practical experience can be found in a subsequent paper presented by Verbrugge in this Lecture Series.

### 3. ANALYSIS OF FLIGHT TEST DATA

#### TIME DOMAIN ESTIMATION

In recent years three groups of time-domain estimation techniques for the identification of aircraft parameters from flight tests have evolved. They include the equation error and

output error method and two advanced statistical methods. The last two advanced methods, the generalized maximum likelihood and extended Kalman filter method, can solve the general estimation problem including the extraction of aircraft performance, stability and control parameters for a nonlinear model from flight data containing process (turbulence) and measurement noise (sensor errors). At present, the maximum likelihood method is widely accepted as one of the best methods for parameter estimation. Multiple practical experience has been gained during the last decade. For example, the U.S. "Mekka" of aircraft flight testing, the NASA Dryden Flight Research Center has estimated stability and control parameters from over 3000 maneuvers performed by 30 different aircraft [6]. More information about this impressive practical experience in the field of aircraft parameter identification will be presented by *Iliff* in this Lecture Series.

#### FREQUENCY DOMAIN ESTIMATION

It can be shown that the aforementioned three groups of parameter evaluation methods are equally well formulated in the frequency domain for linear models of the system under test. The measured data for these methods can be either the frequency response curves or the transformed input and output time histories. Frequency domain methods for aircraft parameter estimation may be advantageous for the identification of aeroelastic and unsteady aerodynamics effects [49]. In addition, these methods are attractive for estimating so-called equivalent time delay effects of high order system (HOS) dynamics of future active control technology aircraft, as will be seen later. A more detailed overview of the present state of the art of identification evaluation methods and its merits associated with them will be given by *Klein* in his paper on this subject within this Lecture Series.

#### MATHEMATICAL MODELS

It can be stated that linear stability and control derivatives can be determined from flight test data in a routine manner. Nevertheless, the application of parameter identification techniques to each flight test programme must be considered individually, depending on the objectives of that testing. Further problems can develop when modeling errors of the aircraft under test are apparent because the best form of the mathematical model is not always obvious. For example, this can be true for flight dynamics with flow separation at high angles of attack, unsteady aerodynamics due to highly responsive active control surfaces and unsteady interfering aerodynamics of several closely coupled active control surfaces. For V/STOL flight mechanics, effects of powered lift, vectored thrust, or rotor-aeromechanics as well as ground proximity interference have to be taken into account. In all these cases there is a need to get into details of aerodynamic phenomena for adequate modeling of aircraft dynamics.

The consequent way to establish a valid mathematical model is to start with a linear model which is adequate for small-perturbation analysis for conventional aircraft. Nonlinear models become necessary for extreme flight regimes where consideration of non-attached critical flow or controlled vortex flow is essential. In this case, the model form is established using series expansions or high order terms to represent nondimensional forces and moments for selected ranges of angle of attack. Strict care has to be taken when generating such curve-fitting polynomial models for aerodynamic coefficients, that these additional high order terms have physical interpretation from a flight mechanics standpoint. It is also important to notify that the estimated high order coefficient will generally tend to be only close to the actual coefficient in the angle of attack regime for the record from which they were estimated. Outside this range the validity of the estimates are doubtful [41]. More detailed information on aircraft parameter identification experience in extreme flight regimes will be presented in a paper by *Ross* in this Lecture Series.

#### MODE COUPLING IDENTIFICATION PROBLEMS

Investigations of aerodynamic coupling are of current interest because aircraft flying at high angles of attack exhibit kinematic and aerodynamic coupling due to effects of separated flow [15]. Asymmetric flight conditions and corresponding aerodynamic coupling [50, 51] can also arise from asymmetric aircraft components like the oblique wing [52], asymmetric stores and engine out/off conditions as well as from uncoordinated turns and active control disharmony [20].

In principle, the application of the maximum likelihood estimation method is straightforward to the identification of flight vehicles with kinematic, aerodynamic and aeroelastic coupling between the longitudinal and lateral-directional modes. However, a multitude of practical computational and numerical problems may arise from this approach due to a high number of states, observations and control inputs.

This is especially true for rotorcraft parameter estimations where complex mathematical models, mainly due to the periodic rotor aeromechanics, have not only to include the strongly coupled rigid body modes but also elastic modes due to the rotor blades, shaft and fuselage flexibility including tail rotor dynamics. Therefore, a large number of unknown rotorcraft parameters have to be identified. More detailed information about

rotorcraft related identification problems and experience can be found in the paper of *Kaletka* prepared for this Lecture Series.

#### MODE SEPARATION TECHNIQUE

Many problems resulting from the handling of a large number of unknown parameters can be alleviated if the longitudinal and lateral-directional motions are analyzed separately. The longitudinal and lateral models are generally complete in that all cross-coupling terms are included.

Therefore, these models are together capable of describing all degrees of freedom and large amplitude aircraft responses. This is done in the longitudinal analysis by using the measured lateral-directional responses as inputs to the longitudinal equations and, vice versa, the lateral-directional analyses uses the measured longitudinal responses [41, 52]. The assumption necessary for this approach can be seen in analogy to the prerequisite of the classical equation error method, that is, the measurements are relatively accurate and without noise contamination. Also, the cross-coupling terms must be small compared with the standard terms.

#### ASYMMETRIC FLIGHT MODE IDENTIFICATION

An unexpected example of hidden aerodynamic coupling due to aircraft yaw asymmetry was discovered during routine data analysis within a parameter identification flight test programme of the airborne simulator DFVLR-Hansa Jet [53].

From Figure 8 it can be seen that an elevator input signal (DFVLR 3211) generated a normal longitudinal response (run 1). On the other hand, a considerable longitudinal response is also evident with respect to a rudder input command (not shown in Figure 8). At the same time, a negligible elevator input (run 2) can be observed.

The two maneuvers were combined to provide a sufficient amount of information about the aerodynamic coupled system under test. Application of the aforementioned mode separation technique in analyzing the longitudinal modes by including kinematic and aerodynamic coupling terms and using the measured lateral-directional responses yielded reasonable agreement of the measured and computed time responses of the model identified (Figure 8).

From a corresponding evaluation of the estimation errors it was concluded that the main coupling effect was approximately modeled by a first and second order term of the sideslip pitching moment (i.e.  $C_{M\beta}$  and  $C_{M\beta^2}$ ).

Figure 9 describes the modeling schematic and the sequence of events for this case of one-sided coupling due to aircraft yaw asymmetry.

#### HIGH ORDER SYSTEM (HOS) MODELING

To overcome the problems with which analysts are often faced, i.e. problems of selecting the mathematical model which is suited best for determining the desired parameters, several efforts have been undertaken to discuss unified approaches and propose criteria which are useful in deciding how complex a model should be [54, 55, 56]. On the other hand, the possibility to start the parameter estimation sequence with physical meaningful models seem still to be the most attractive alternative. Some general aspects in this context will be discussed with relevance to the modeling of future active control aircraft in the following.

Figure 10 indicates the evolution of aircraft dynamic modeling within the last thirty to forty years. The three steps of rigid, augmented and active control aircraft dynamic modeling including an accumulation of interacting aerodynamic, inertial, control and elastic forces is apparent. The third and last step of aircraft evolution implements the integration of active control technology. This was mainly caused by the constant demand for reduction in direct operating costs of commercial aircraft and improvement of the operational capabilities and mission effectiveness of military flight vehicles. An aircraft utilizing active controls can, in general, be identified as one in which independent from the pilot significant inputs are transmitted to the aerodynamic control surfaces for the purpose of augmenting the vehicle performance, the flying and ride qualities as well as the structural dynamics from a load and fatigue relief standpoint. One important aspect is the necessary high frequency bandwidth of active control systems for controlling from low frequency flight path modes up to high frequency flutter modes. Consequently, high order system (HOS) dynamics have to be modeled in all kinds of aircraft subsystems as indicated in Figure 11. Figure 11 gives an overall impression on what kinds of HOS effects have to be accounted for in order to generate physical convincing aircraft models for accurate parameter identification. Included are modeling aspects for pilot and atmosphere dynamics which, in principle, can also be identified by parameter estimation techniques.

## ACTUATOR MODELING

A relevant example of the importance of correct modeling of aircraft and flight control dynamics is the well-known T-38 A PIO incident some fifteen years ago. Although several analytical studies were performed to test various theories for what causes pilot induced oscillations it was not until recently that an already well-accepted analytical model developed to represent the aircraft [11] had to be questioned. It was finally discovered that the major cause of the PIO problem was a low dynamic performance of a servo valve at higher airloads which, in turn, reduced the control surface deflection rates with increasing hinge moments [57]. As a consequence, the mathematical model of the actuator dynamics had to be corrected for large hinge moments from a second order into a third-order system. Adding another dramatic example of actuator limiting due to high hinge moments causing an uncommanded load factor response [21], it can be concluded that careful actuator dynamic modeling with respect to air loads is of high importance for closed loop active control aircraft parameter identification and pilot-in-the-loop investigations.

## EQUIVALENT LOW ORDER SYSTEM (ELOS) MODELING

Returning to the requirements of aircraft flying qualities using system identification methods, Figure 12 denotes the classical rigid aircraft short period equations of motion (time domain) and the corresponding transfer function (frequency domain) of pitch rate ( $q$ ) to elevator control deflection ( $\delta_e$ ). This low order system (LOS) model is appropriate for conventional aircraft dynamics with negligible flight control system dynamics. Hence, the pilot will not view any additional control system dynamics in the pitch rate response ( $q$ ) to stick-force inputs ( $F$ ). Logically, parameter estimation techniques for handling qualities investigations have to deal only with the identification of the fundamental (LOS) parameters, denoted in Figure 12 by a prime. Standard Flying Qualities Specifications like the MIL-F 8785 B are then readily applicable.

In contrast, the flight control and stability augmentation system (CSAS) dynamics of current modern aircraft may have significant influences on the flight characteristics. Thus the motions of such aircraft have to be modeled by more complex equations or transfer functions. Therefore, aircraft with complex augmentation systems must be represented by high order system (HOS) dynamics, which may greatly alter the aforementioned LOS short period mode response [16, 58]. Since the current Flying Qualities Specifications do consider only the natural low-order short period modes of the rigid aircraft, and no additional HOS modes of the control and stability augmentation system (CSAS), parameters of an equivalent low order system (ELOS) must be found, if the classical specifications should be applicable with any confidence.

The introduction of an equivalent low order system (ELOS) as a substitute of a high order system (HOS) aircraft is shown for the longitudinal short period dynamics in Figure 13. In addition to the equivalent fundamental (LOS) parameters, denoted in Figure 13 by a star, an equivalent time delay parameter  $\tau^*$  is needed to approximate the phase lag. This lag is introduced by the high order flight control dynamics such as actuator and sensor dynamics as well as filter dynamics and digital delays. Accumulated simulation and flight test results indicate that, in general, the implementation of ELOS aircraft modeling is convenient for representing the overall flying qualities of the aircraft [16, 58]. Also, the ELOS parameters, to be identified in the future, should yield an important data base for temporary and new Flying Qualities Specifications of aircraft with modern flight control systems. Frequency domain identification methods may become here attractive especially for the estimation of equivalent time delays.

## EQUIVALENT HIGH ORDER SYSTEM (EHOS) MODELING

The preceding section discussed possibilities to define equivalent low order system parameters in order to determine flying qualities of HOS aircraft along the lines of existing Flying Qualities Specifications. Nevertheless, although the evaluation of flight test data of HOS aircraft by parameter identification techniques may yield satisfactory curve fits, closed loop flying qualities investigations may be unsatisfactory. This is due mainly to an inadequate model structure of the HOS aircraft. In particular, the flight test engineer must be aware of possible shortcomings using equivalent low order system (ELOS) parameters for HOS aircraft flying qualities investigations.

Satisfactory fits and adequate flying qualities results can be obtained by an improved mathematical description of the HOS aircraft dynamics, utilizing

- Basic low order system (LOS) airframe model,
- Equivalent (feedforward) flight control system (EFCS) model,
- Equivalent (feedback) stability augmentation system (ESAS) model.

The integration of feedforward and feedback control system dynamics into two EFCS and ESAS transfer function models leads in combination with the basic (uncontrolled) LOS model of the aircraft to an equivalent high order system EHOS aircraft model (Figure 14). The EFCS and ESAS model structure can be approximated using information supplied by the

manufacturer. The principle of this approach was successfully applied to the flight test data analysis of a combat type aircraft. That flight test programme included open/closed loop identifications yielding relevant stability and control characteristics [11].

More information on closed loop aspects of aircraft parameter identification within this Lecture Series will be given by Kochler.

## 9. FUTURE POTENTIAL

In addition and referring to the wide application spectrum for parameter identification, discussed and described in section 5 of this paper, the following future research topics can be highlighted:

- Identification of nonlinear and unsteady aircraft dynamics including the modeling of high angle of attack and normal load factor aerodynamics,
- Identification of aerodynamic control characteristics for active control applications including aerodynamic interactions for various flight modes,
- Identification of high order system aircraft dynamics including the modeling of structures, electronics and hydraulics of future active control systems,
- Identification of the effects of control system lags and time delays on the pilot-in-the-loop flying qualities,
- Identification improvements for highly coupled rotorcraft systems by elimination of severe modeling limitations,
- Identification of missile captive and launch parameters including the effects of limited instrumentation (Figure 15 gives an impression of the inadequate state of the art of matching model estimates with flight test data [59]),
- Identification of external store interference and separation parameters using non-optical instrumentation (current state of the art in the field of store separation analysis from flight tests is limited to photographic instrumentation [60]).

## 10. CONCLUSION AND RECOMMENDATIONS

It was the purpose of this paper to highlight some of the requirements, applications, advantages and problems as well as present and future potentials of aircraft parameter identification techniques.

Improved technologies in the field of instrumentation, data handling and data processing as well as improved methodologies for optimum control input design have contributed to broaden the application spectrum for parameter identification. For example, these methods are becoming standard procedures for aircraft handling qualities investigations and acceptance testing.

Future relevant research topics will deal with the identification of high order system aircraft dynamics including high angle of attack flight conditions incorporating nonlinear and unsteady flow separation dynamics. In addition, system identification demands for active control technology flight vehicles implementing aeroservoelastic coupling effects and control surface interactions within an extended frequency bandwidth will become subject of increased attention. Further, still existing limitations with regard to the in-flight determination of parameters of highly coupled rotorcraft systems have to be eliminated. New activities in the fields of in-flight determined parameters of missile system flight mechanics and external store separation dynamics may evolve.

For further discussion, the following items are recommended:

- Application of mode separation techniques for rotorcraft parameter identification,
- Application of parameter identification techniques for dynamic wind tunnel testing including optimum gust and control input design,
- Application of reproducible dynamic wind tunnel testing for the estimation of "difficult" aircraft parameters,
- Application of equivalent low order system modeling for parameter identification of aircraft with complex active control systems,
- Application of parameter identification techniques for the evaluation of acceleration/deceleration control responses of combat aircraft,
- Application of system identification techniques for dynamic airload estimations during critical takeoff, landing and heavy turbulence maneuvers,

- Application of common parameter identification methods including unified inputs, instrumentation and data analysis for future standardized acceptance flight testing within the NATO communities. Some steps in this direction have been initiated by a common flight test programme between The Netherlands and West-Germany [61].

It is hoped that the outcome of this Lecture Series will uncover those aspects of parameter identification which have not been treated sufficiently in the past. Also, new or alternative thinking along these lines would be welcomed.



## 11. REFERENCES

1. Koehler, R., Marchand, M. "Open/Closed Loop Identification of Stability and Control Characteristics of Combat Aircraft", AGARD-CP-260, Paper 16, May 1979.
2. Kurzahls, P.R., ed., "Active Controls in Aircraft Design", AGARD-AG-234, November 1978.
3. Anon., "Methods for Aircraft State and Parameter Identification", AGARD Conference Proceedings, AGARD-CP-172, May 1975.
4. Iliff, K.W., Maine, R.E., "Practical Aspects of Using a Maximum Likelihood Estimator", AGARD-CP-172, Paper 16, May 1975.
5. Hamel, P.G., "Status of Methods for Aircraft State and Parameter Identification", AGARD-CP-187, Paper 8, 1976.
6. Iliff, K.W., "Estimation of Aerodynamic Characteristics from Dynamic Flight Test Data", AGARD-CP-235, Paper 15, November 1978.
7. Burton, R.A., "Advancement in Parameter Identification and Aircraft Flight Testing", AGARD-CP-172, Paper 15, May 1975.
8. Jeglum, P.M., "Air Force Flight Test Center Experience in the Identification of Stability and Control Parameters from Dynamic Flight Test Maneuvers", AGARD-CP-235, Paper 14, November 1978.
9. Twisdale, T.R., Jones, G.L., Ashurst, T.A., "A Mission Oriented Flight Test Technique for Identifying Aircraft and Flight Control System Transfer Functions", AGARD-CP-223, Paper 13, April 1977.
10. Sisk, T.R., "A Technique for the Assessment of Fighter Aircraft Precision Controllability", AIAA Paper 78-1364, 1978.
11. Smith, R.H., "A Theory for Longitudinal Short-Period Pilot Induced Oscillations", AFFDL-TR-77-57, June 1977.
12. Ericsson, L.E., "Technical Evaluation Report on the Fluid Dynamics Panel Symposium on Dynamic Stability Parameters", AGARD-AR-137, April 1979.
13. Chalk, C.R., "Technical Evaluation Report on the Flight Mechanics Panel Symposium on Stability and Control", AGARD-AR-134, January 1979.
14. Anon., "Aerodynamic Characteristics of Controls", AGARD Conference Preprint, AGARD-CP-262, April 1979.
15. Anon., "High Angle of Attack Aerodynamics", AGARD Conference Proceedings, AGARD-CP-247, January 1979.
16. A'Harrah, R.C., Lamanna, W.J., Hodgkinson, J., "Are Today's Specifications Appropriate for Tomorrow's Airplanes?", AGARD-CP-260, Paper 23, May 1979.
17. Velkoff, H.R., "Technical Evaluation Report on the Flight Mechanics Panel Symposium on Rotorcraft Design", AGARD-AR-114, January 1978.
18. Anon., "Stall/Spin Problems of Military Aircraft", AGARD Conference Proceedings, AGARD-CP-199, June 1976.
19. Gibson, J.C., "Flying Qualities and the Fly-By-Wire Aeroplane", AGARD-CP-260, Paper 22, May 1979.
20. Whitmoyer, R.A., "Aerodynamic Interactions on the Fighter CCV Test Aircraft", AGARD-CP-235, Paper 16, November 1978.
21. Ross, A.J., Thomas, H.H.B.M., "A Survey of Experimental Data on the Aerodynamics of Controls, in the Light of Future Needs", AGARD-CP-262, Paper 2, April 1979.
22. Gilyard, G.B., "Determination of Propulsion-System-Induced Forces and Moments of a Mach 3 Cruise Aircraft", in NASA TND-7647, April 1974, pp. 369-374.
23. Park, G.D., "Parameter Identification Technology Used in Determining In-Flight Airload Parameters", J. Aircraft, Vol. 14, No. 3, March 1977.
24. Rix, O., Huber, H., Kaletka, J., "Parameter Identification of a Hingeless Rotor Helicopter", Preprint No. 77.33-42, 33rd Annual National Forum of the American Helicopter Society, Washington, D.C., May 1977.

25. Hall, W.E., Gupta, N.K., Hansen, R.S., "Rotorcraft System Identification Techniques for Handling Qualities and Stability and Control Evaluation", Preprint No. 78-30, 34th Annual Forum of the American Helicopter Society, Washington, D.C., May 1978.
26. Anon., "The Effects of Buffeting and other Transonic Phenomena on Maneuvering Combat Aircraft", AGARD Advisory Report, AGARD-AR-82, July 1975.
27. Bryant, W.H., Hodge, W.F., "A Monte Carlo Analysis of the Effects of Instrumentation Errors on Aircraft Parameter Identification", AGARD-CP-172, Paper 5, May 1975.
28. Hosman, R.J.A.W., "Advanced Flight Test Instrumentation: Design and Calibration", AGARD-CP-172, Paper 6, May 1975.
29. Wolowicz, C.H., "Considerations in the Determination of Stability and Control Derivatives and Dynamic Characteristics from Flight Data", AGARD Rep. 549-Part 1, 1966.
30. Bennett, G.E., "Magnetic Recording of Flight Test Data", AGARD Flight Test Instrumentation Series, AGARD-AG-160-Vol. 5, February 1974.
31. McLaren, I., "Open and Closed Loop Accelerometers", AGARD Flight Test Instrumentation Series, AGARD-AG-160-Vol. 6, July 1974.
32. Van Nunen, J.W.G., Piazzoli, G., "Aeroelastic Flight Test Techniques and Instrumentation", AGARD Flight Test Instrumentation Series, AGARD-AG-160-Vol. 9, February 1979.
33. Hosman, R.J.A.W., "Advanced Flight Test Instrumentation: Design and Calibration", AGARD-CP-172, Paper 6, May 1975.
34. Mulder, J.A., "Estimation of the Aircraft State in Non-Steady Flight", Delft University of Technology, Memorandum M-221, October 1974.
35. Wingrove, R.C., "Quasi Linearization Technique for Estimating Aircraft States from Flight Data", J. Aircraft, Vol. 10, No. 5, May 1973.
36. Klein, V., Schiess, J.R., "Compatibility Check of Measured Aircraft Responses Using Kinematic Equations and Extended Kalman Filter", NASA TN D-8514, August 1977.
37. Wingrove, R.C., "Parameter Estimation of Powered-Lift STOL Aircraft Characteristics Including Turbulence and Ground Effects", AGARD-CP-172, Paper 28, May 1975.
38. Mehra, R.K., Gupta, N.K., "Status of Input Design for Aircraft Parameter Identification", AGARD-CP-172, Paper 12, May 1975.
39. Chen, R.T.N., "Input Design for Aircraft Parameter Identification: Using Time-Optimal Control Formulation", AGARD-CP-172, Paper 13, May 1975.
40. McCracken, J.R., Kaletka, J., Meyer, H., Rix, O., Gartung, B., "Spain-Federal Republic of Germany Cooperative Research Program CASA C-212 Flight Test and Parameter Identification", DFVLR IB 154-76/16, 1976.
41. Eulrich, B.J., Govindaraj, K.S., Harrington, W.W., "Estimation of the Aerodynamic Stability and Control Parameters for the F-106 A Aircraft from Flight Data: Maneuver Design and Flight Data Analysis", AIAA Paper 78-1326, 1978.
42. Maine, R.E., Iliff, K.W., "Maximum Likelihood Estimation of Translational Acceleration Derivatives from Flight Data", AIAA Paper 78-1342, 1978.
44. Rix, O., Hanke, D., "In-Flight Measured Characteristics of Combined Flap-Spoiler Direct Lift Controls", AGARD-CP-262, Paper 16, April 1979.
45. Anon., "Total In-Flight Simulator (TIFS)-Preliminary Design Report", Technical Report AFFDL-TR-71-119, August 1971, pp. 25-26.
46. Smith, H.J., "Flight-Determined Stability and Control Derivatives for an Executive Jet Transport", NASA TMX-56034, July 1975.
47. Hamel, P.G., Krag, B., "Dynamic Windtunnel Simulation of Active Control Systems", AGARD-CP-260, Paper 16A, May 1979.
48. Bennett, R.M., Farmer, M.G., Mohr, R.L., Hall Jr., W.E., "Wind-Tunnel Technique for Determining Stability Derivatives from Cable-Mounted Models", J. Aircraft, Vol. 15, No. 5, May 1978.

49. Klein, V., "Aircraft Parameter Estimation in Frequency Domain", AIAA Paper 78-1344, 1978.
50. Hamel, P.G., "A Systems Analysis View of Aerodynamic Coupling", J. Aircraft, Vol. 7, No. 6, Nov.-Dec. 1970.
51. Johnston, D.E., "Identification of Key Maneuver-Limiting Factors in High-Angle-of-Attack Flight", AGARD-CP-235, Paper 36, November 1978.
52. Maine, R.E., "Aerodynamic Derivatives for an Oblique Wing Aircraft Estimated from Flight Data by Using a Maximum Likelihood Technique", NASA Technical Paper 1336, October 1978.
53. Koehler, R., "Identifizierung von Kopplungseffekten zwischen Längs- und Seitenbewegung bei der HFB-320", DFVLR, Institut für Flugmechanik, ARNO 154-618-1, 1979, - unpublished note - .
54. Taylor, Jr., L.W., "A New Criterion for Modeling Systems", in NASA TND-7647, April 1974, pp. 291-313.
55. Gupta, N.K., Hall Jr., W.E., Trankle, T.L., "Advanced Methods of Model Structure Determination from Test Data", J. Guidance and Control, Vol. 1, No. 3, May-June 1978.
56. Klein, V., "On the Adequate Model for Aircraft Parameter Estimation", CIT, Cranfield Report Aero No. 28, March 1975.
57. Chalk, C.R., "Another Study of the T-38A PIO Incident", Calspan Advanced Technology Center, FRM No. 534, August 1978, - unpublished note - .
58. Hodgkinson, J., La Manna, W.J., Heyde, J.L., "Handling Qualities of Aircraft with Stability and Control Augmentation Systems - a Fundamental Approach", Aeronautical Journal, Vol. 80, No. 782, February 1976.
59. Driscoll, T.R., Eckenroth, H.F., "Flight Test Validation of the Patriot Missile Six-Degree-of-Freedom Aerodynamic Simulation Model", Martin Marietta Corporation, Orlando, Florida.
60. Schindel, L.H., "Store Separation", AGARD-AG-202, June 1975.
61. Garretson, H.C., "Beaver Aircraft Parameter Identification - Technical Preparations and Preliminary Results", DFVLR-Mitt. 78-01, August 1978.

#### ACKNOWLEDGEMENTS

The author wishes to thank Mr. P.F. Eckert of NASA Scientific and Technical Information Facility, Baltimore/Washington, for providing the bibliography for this AGARD Lecture Series.

He, furthermore, would like to acknowledge the help in the preparation of this paper:

- Mrs. M. Nagel for drawing the Figures
- Mrs. H.M. Lehmann for assistance in translation
- Dr. D. Schafranek who has done a great deal of technical proof reading and
- Mrs. H. Wedekind for the typewriting work.

Table 1: Review of AGARD Publication in the field of Aircraft Parameter Identification

YEAR	TITLE	AGARD REFERENCE *)
1955	Dynamic Measurements in Windtunnels	AG 11
1956	Some Correlations of Flight-Measured and Wind-Tunnel Measured Stability and Control Characteristics of High-Speed Airplanes	RP 62
1958	An Example of the Determination of Principal Aerodynamic Coefficients from Flight Tests	RP 189
1958	On the Extraction of Stability Derivatives from Full-Scale Flight Data	RP 190
1958	Application of Dynamic Testing Procedures to Stability and Control Flight Test Programs	RP 191
1958	Stability-Derivative Determination from Flight Data	RP 224
1959 (1963)	Stability-Derivative Determination from Flight Data	MN 1/2/10/2
1961	Current Progress in the Estimation of Stability Derivatives	RP 341
1961	Windtunnel and Flight Measurements of Aerodynamic Derivatives	RP 346
1966	Considerations in the Determination of Stability and Control Derivatives and Dynamic Characteristics from Flight Data	RP 549/1
1966	Un Nouveau Type de Fonctions Modulatrices pour la Méthode de Shinbrot	RP 549/2/1
1966	Experience with Shinbrot's Method of Transient Response	RP 549/2/2
1966	Stability and Control	CP 17/1/20,21
1969	Aeroelastic Effects from a Flight Mechanics Standpoint	CP 46/18
1972	Flight Test Techniques	CP 85/10,14,16
1972	Stability and Control	CP 119/13,14,23
1975	Methods for Aircraft State and Parameter Identification	CP 172/1 to 29
1976	Flight/Ground Testing Facilities Correlation	CP 187/6,8,13
1977	Flight Test Techniques	CP 223/5,11,12,13
1978	Rotorcraft Design	CP 233/20
1978	Dynamic Stability Parameters	CP 235/14,15,17,18
1978	Excitation and Analysis Technique for Flight Flutter Tests	RP 672
1979	Aeroelastic Flight Test Techniques and Instrumentation	AG 160/9
1979	High Angle of Attack Aerodynamics	CP 247/1,14
1979	Stability and Control	CP 260/16
1979	Aerodynamic Characteristics of Controls	CP 262/2,3,16
1979	Parameter Identification	LS 104
(1981)	Parameter Identification	AG to be announced

\*) see also AGARD Index of Publications 52/70 PtI, 71/73 and 74/76

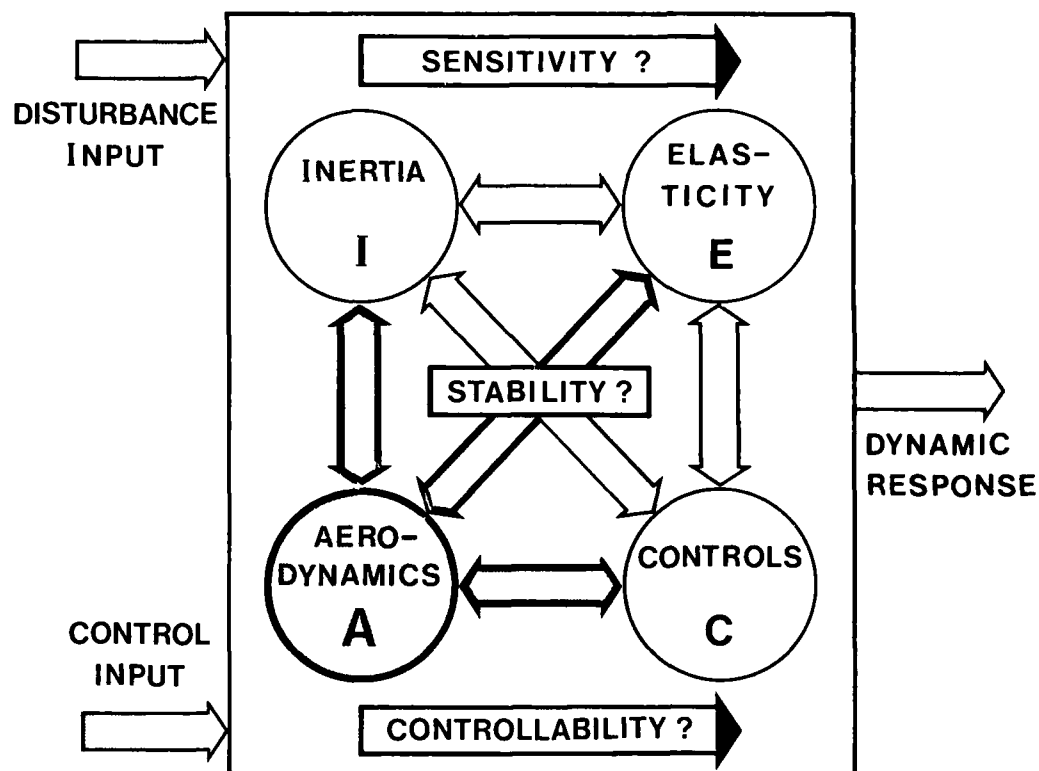
AG = AGARDograph

MN = AGARD Flight Test Manual

RP = AGARD Report

CP = AGARD Conference Proceedings

LS = AGARD Lecture Series



### AIRCRAFT PARAMETER IDENTIFICATION

⇒ FLIGHT TEST VERIFICATION OF  
QUALITATIVE AND QUANTITATIVE  
AERODYNAMICS FROM A FLIGHT  
MECHANICS STANDPOINT

Fig. 1 Aircraft "Ersatz" Model-Quadrangle of Forces

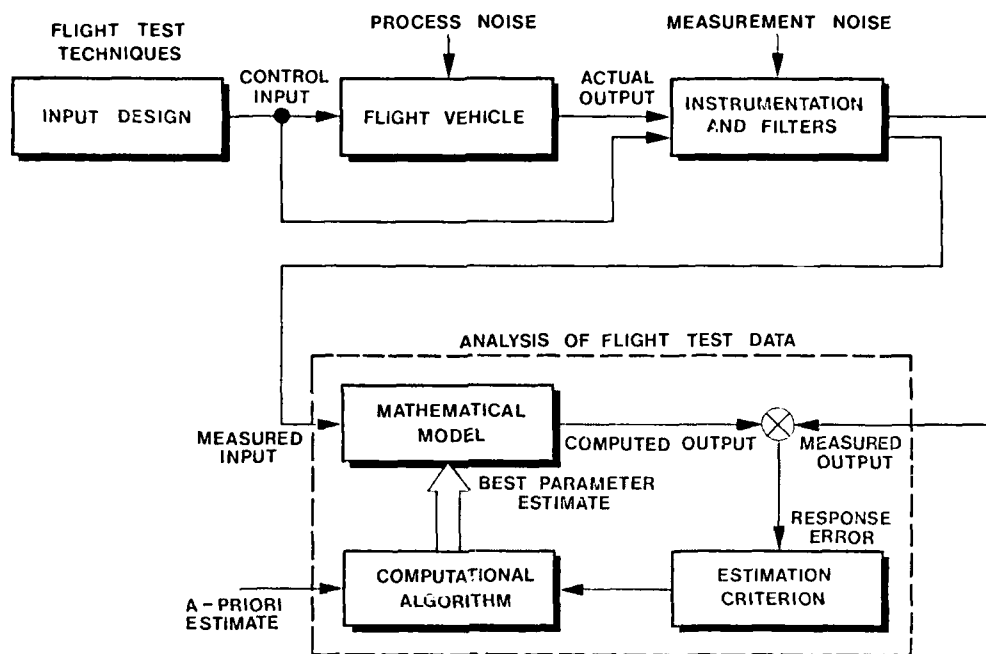


Fig. 2 Basic Parameter Identification Procedure

### • CONVENTIONAL AIRCRAFT

- RIGID BODY MODES
- ADEQUATE AERODYNAMIC (INHERENT) STABILITY
- SINGLE SURFACE CONTROL
- MECHANICAL FCS
- SAS WITH LIMITED CONTROL AUTHORITY
- LOW CONTROL LOOP BANDWIDTH

### • ACTIVE CONTROL AIRCRAFT

- RIGID BODY AND STRUCTURAL MODES
- REDUCED AERODYNAMIC STABILITY
- MULTI SURFACE CONTROL
- COMPLEX DIGITAL FCS
- SCAS WITH HIGH CONTROL AUTHORITY
- HIGH CONTROL LOOP BANDWIDTH

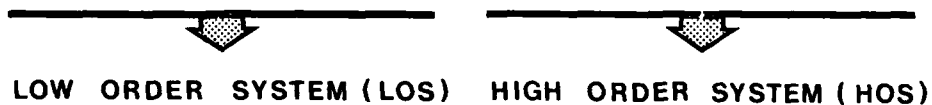


Fig. 3 Impact of Active Control Technology (ACT) on Aircraft Complexity

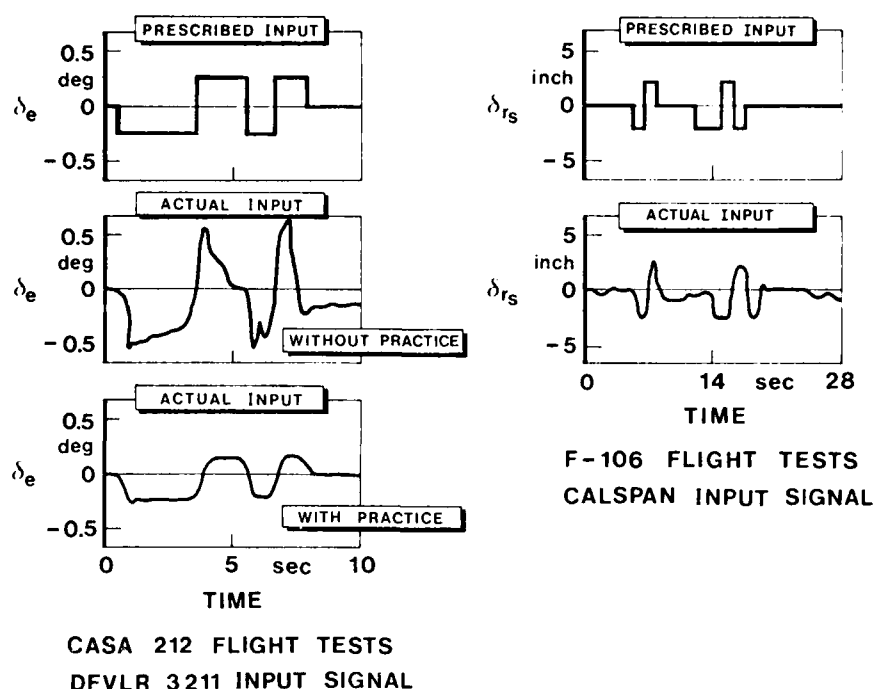
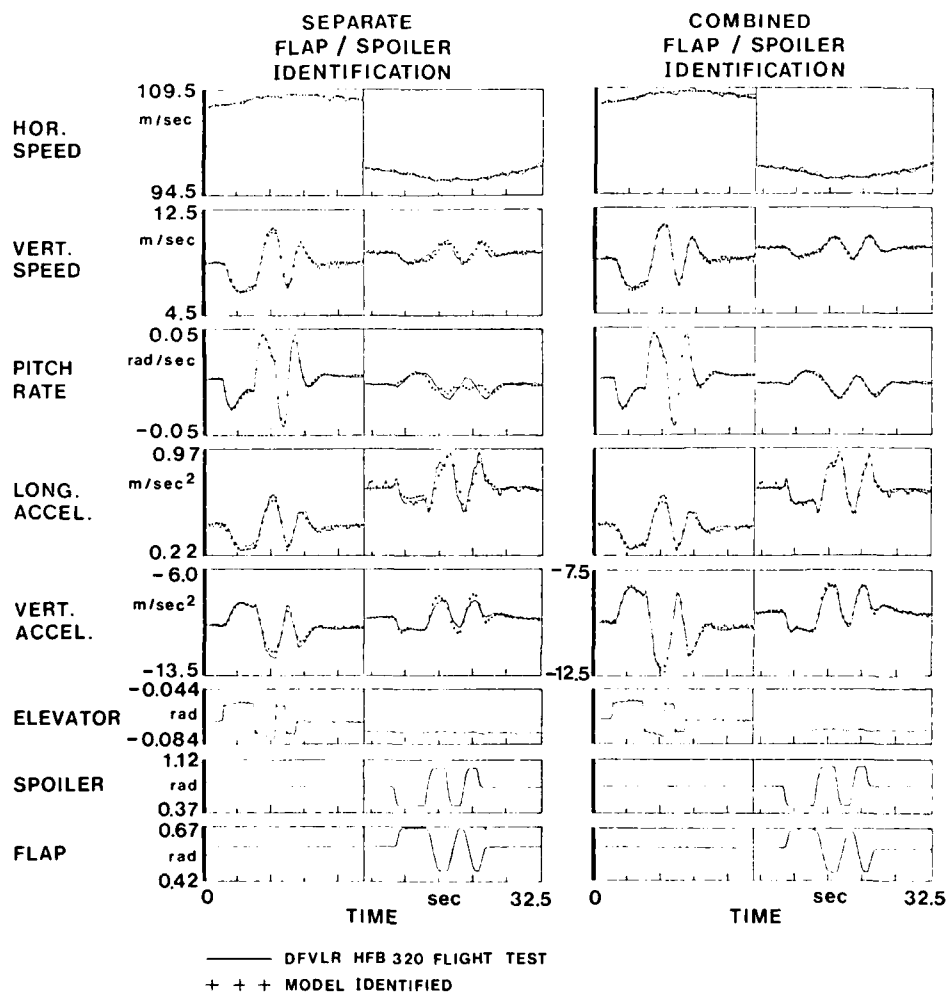


Fig. 4 Manual Optimum Input Realization

Fig. 5 Direct Lift Control Effectiveness and Interference (DFVLR Airborne Simulator *Ranga Jet*)

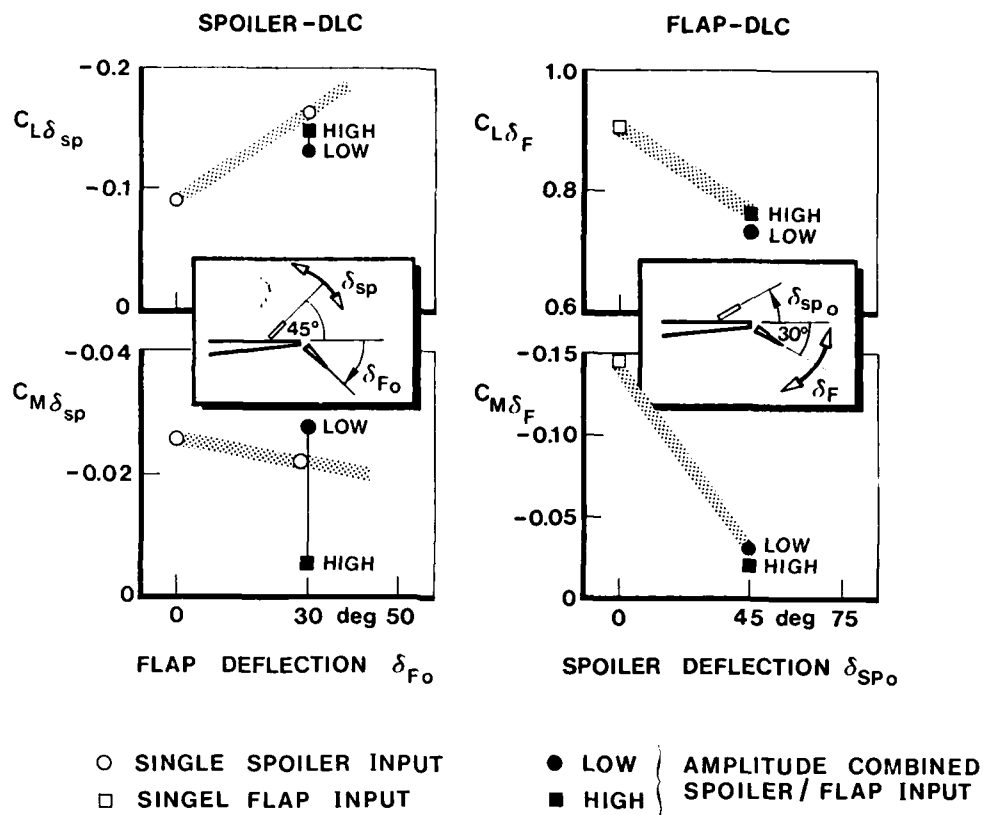


Fig. 6 Identification of Direct Lift Control Effectiveness (DFVLR Airborne Simulator *Hansa Jet*)

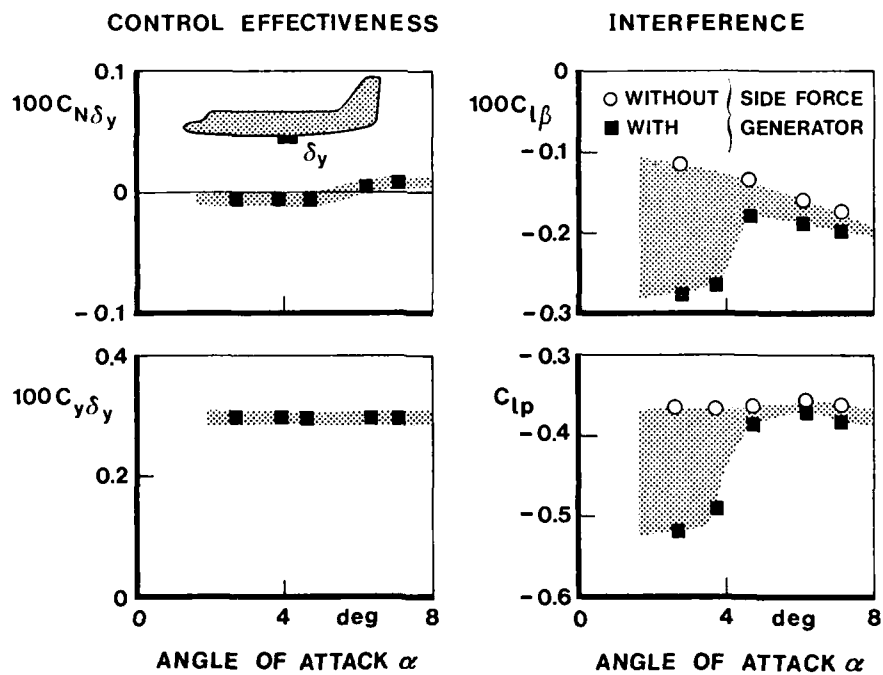


Fig. 7 Direct Side Force Control Effectiveness and Interference (NASA Airborne Simulator *Jet Star*)



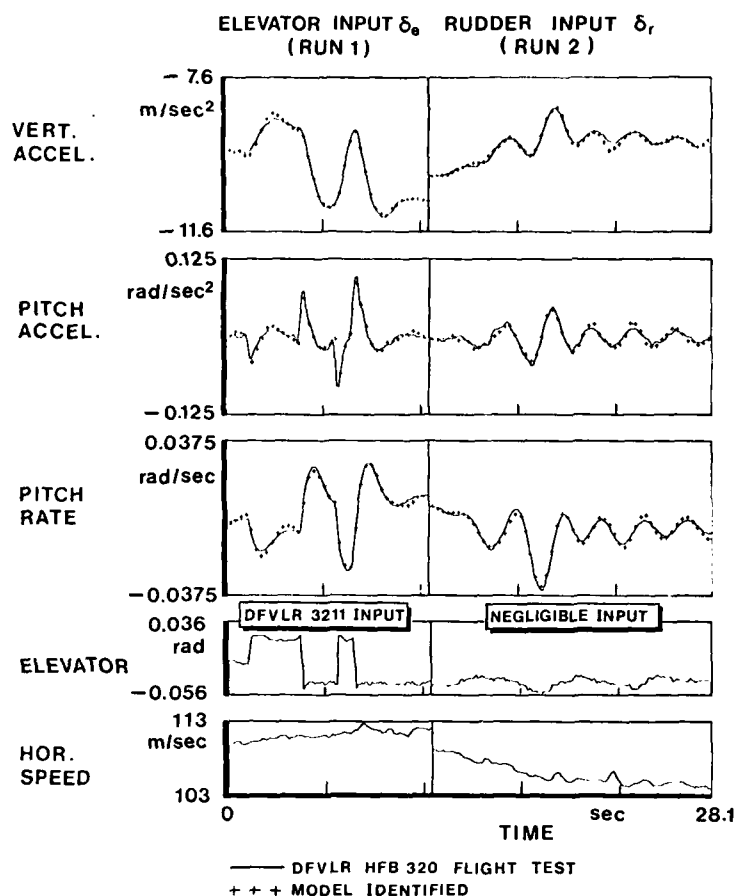
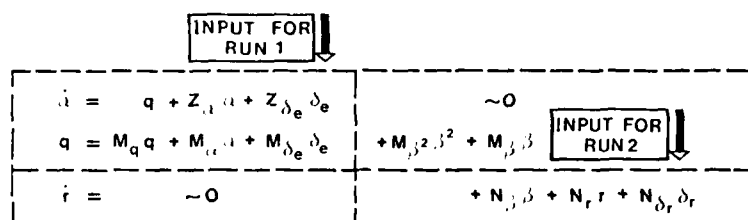
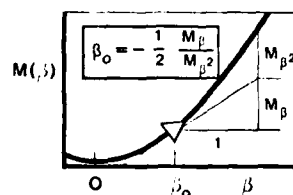


Fig. 8 Identification of One-Sided Aerodynamic Coupling due to Yaw-Asymmetry (DFVLR-Airborne Simulator *Hansa Jet*)



- RUDDER BIAS  $\delta_{r0}$  FOR A/C YAW ASYMMETRY COMPENSATION PRODUCES EQUIVALENT SIDESLIP

$$\beta_0 = -\frac{N_{\delta_r}}{N_{\beta}} \delta_{r0}$$



- EQUIVALENT SIDESLIP INDUCES PITCHING MOMENT  $M(\beta = \beta_0)$
- RUDDER INPUT  $\delta_r$  (RUN 2) PROVIDES EXCITATION OF LONGITUDINAL DYNAMICS THRU  $\beta_0$  - COUPLING
- SUCCESSFUL IDENTIFICATION OF QUASILINEARIZED COUPLING TERMS  $M_{\beta}$  and  $M_{\beta^2}$  WITH MODE SEPARATION TECHNIQUE (FIG. 8)

Fig. 9 Modeling of One-Sided Aerodynamic Coupling (see Fig. 8)

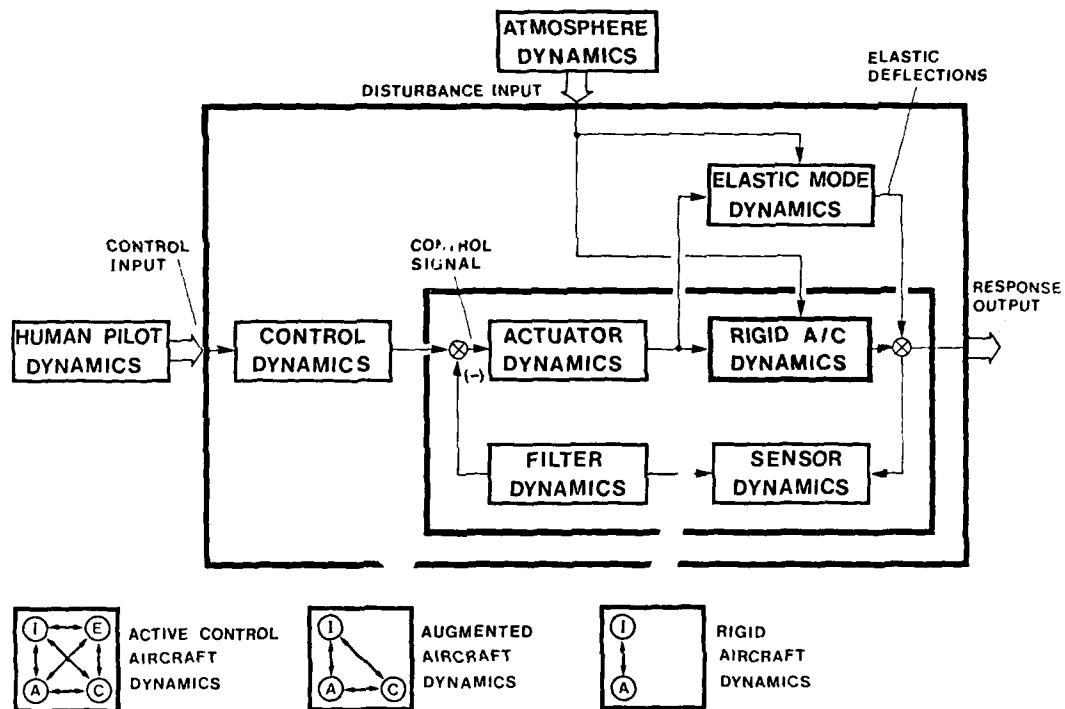


Fig. 10 Modeling Schematic of High Order System (HOS) Aircraft Dynamics

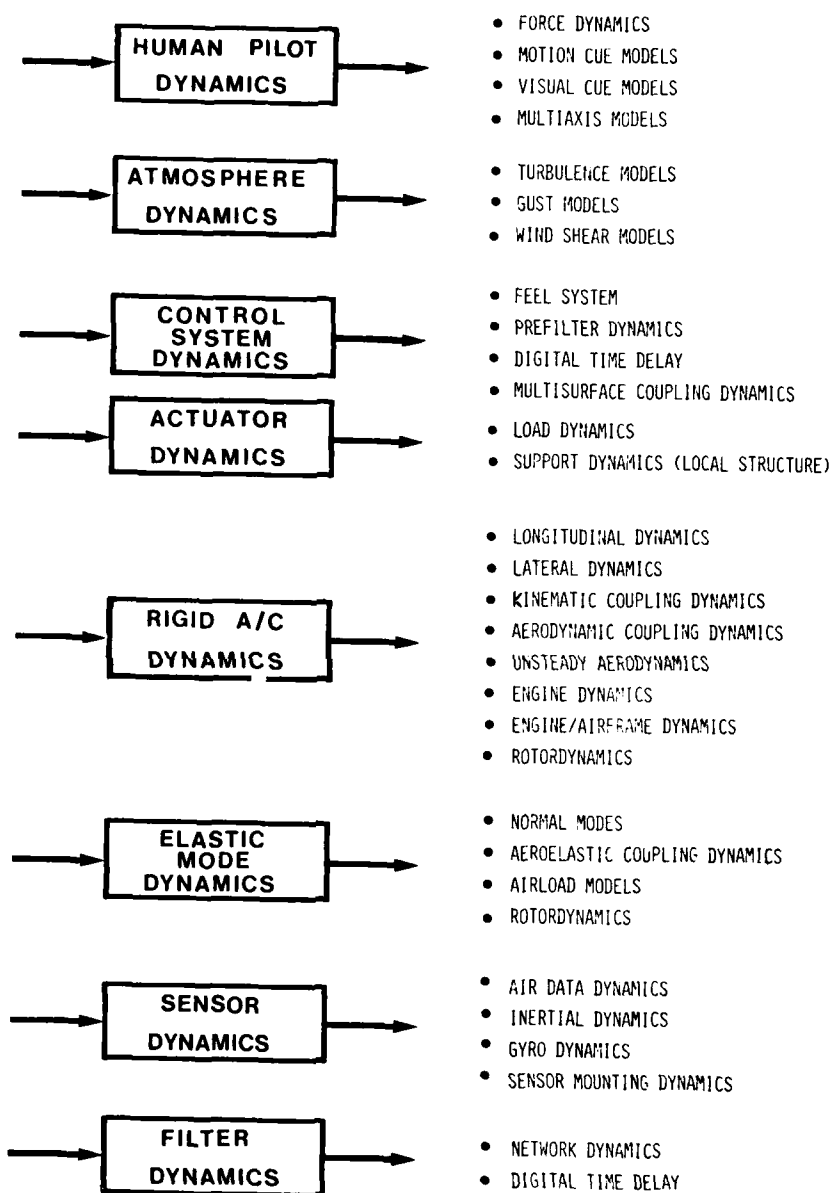
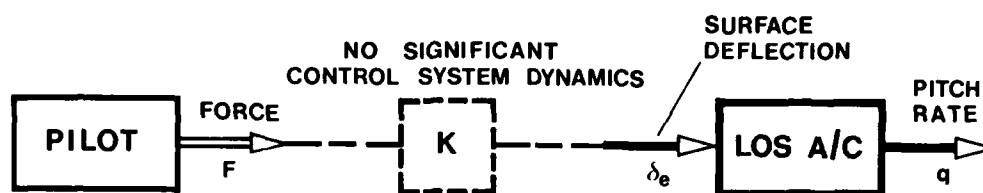


Fig. 11 Subsystem Modeling of High Order System (HOS) Aircraft Dynamics



### LOS A/C MODEL ( BASIC A/C )

#### • TIME DOMAIN

$$\dot{\alpha} = q + Z'_{\alpha}\alpha + Z'_{\delta_e}\delta_e$$

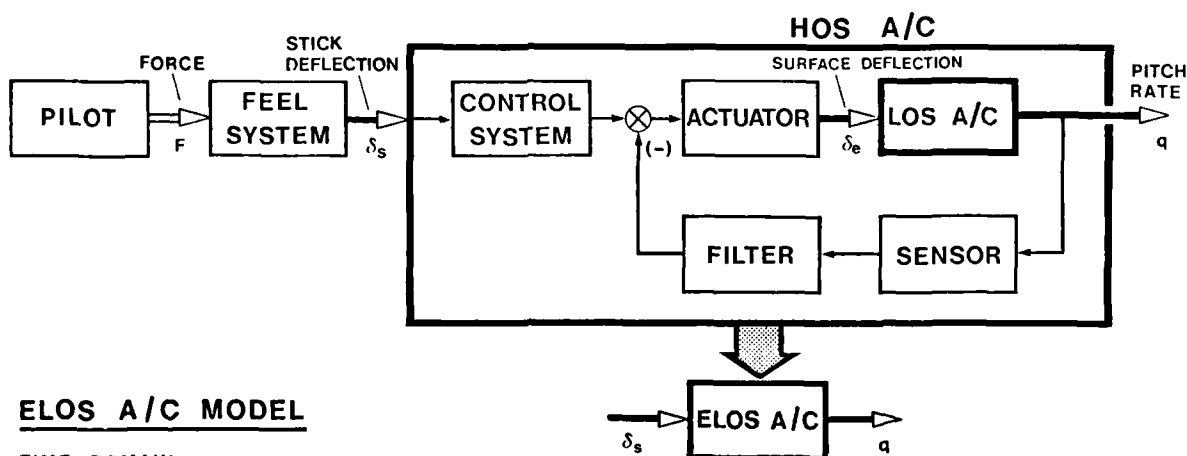
$$\dot{q} = M'_q q + M'_{\alpha}\alpha + M'_{\delta_e}\delta_e$$

#### • FREQUENCY DOMAIN

$$\frac{q}{\delta_e} = \frac{K'_q (s + 1/\tau'_{\theta 2})}{s^2 + 2\zeta'_{sp} \omega'_{sp} s + \omega'^2_{sp}}$$

PRIME (') DENOTES LOS PARAMETER TO BE IDENTIFIED

Fig. 12 Low Order System (LOS)  
Model for Aircraft Parameter Identification



### ELOS A/C MODEL

#### • TIME DOMAIN

$$\dot{\alpha} = q + Z^*_{\alpha}\alpha + Z^*_{\delta_s}\delta_s (t - \tau^*)$$

$$\dot{q} = M^*_q q + M^*_{\alpha}\alpha + M^*_{\delta_s}\delta_s (t - \tau^*)$$

#### • FREQUENCY DOMAIN

$$\frac{q}{\delta_s} = \frac{K^*_q (s + 1/\tau^*_{\theta 2})}{s^2 + 2\zeta^*_{sp} \omega^*_{sp} s + \omega^{*2}_{sp}} \exp(-s\tau^*)$$

STAR (\*) DENOTES ELOS PARAMETER TO BE IDENTIFIED

EQUIVALENT TIME DELAY  $\tau^*$   
REPRESENTS PHASE LAG OF

- ACTUATOR DYNAMICS
- STRUCTURAL FILTERS
- PREFILTER
- SENSOR DYNAMICS
- DIGITAL DELAYS

Fig. 13 Equivalent Low Order System (ELOS)  
Model for Aircraft Parameter Identification

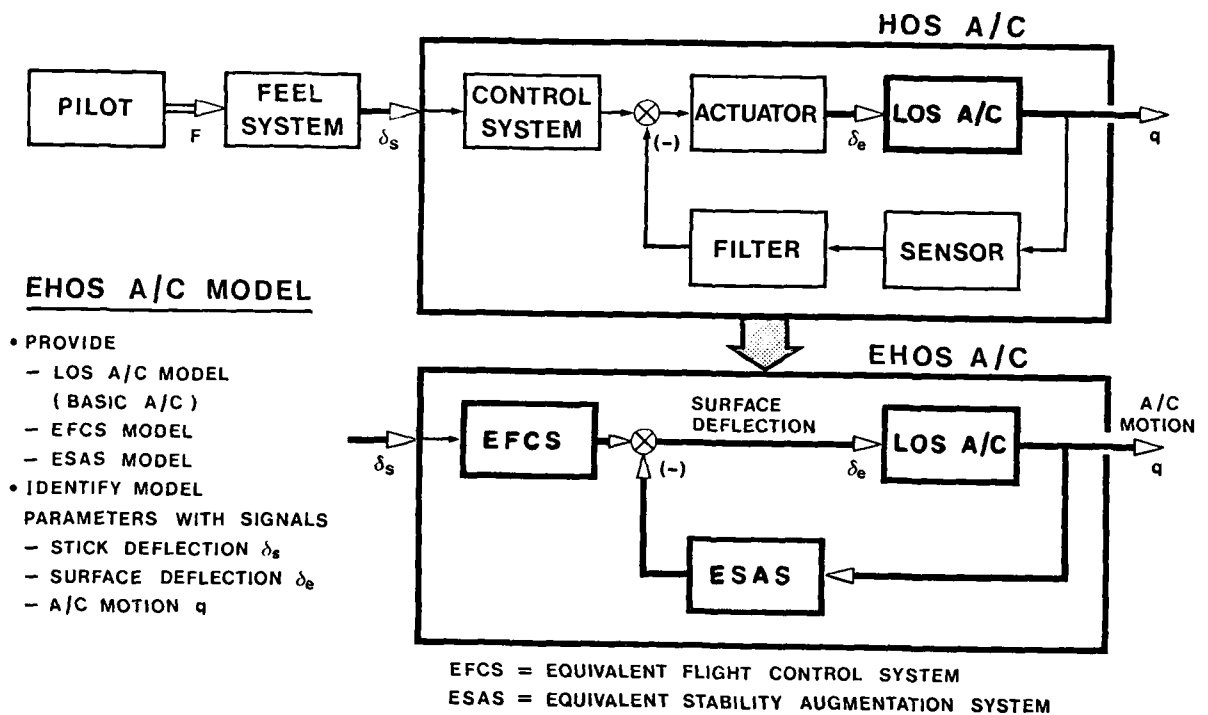


Fig. 14 Equivalent High Order System (EHOS)  
Model for Aircraft Parameter Identification

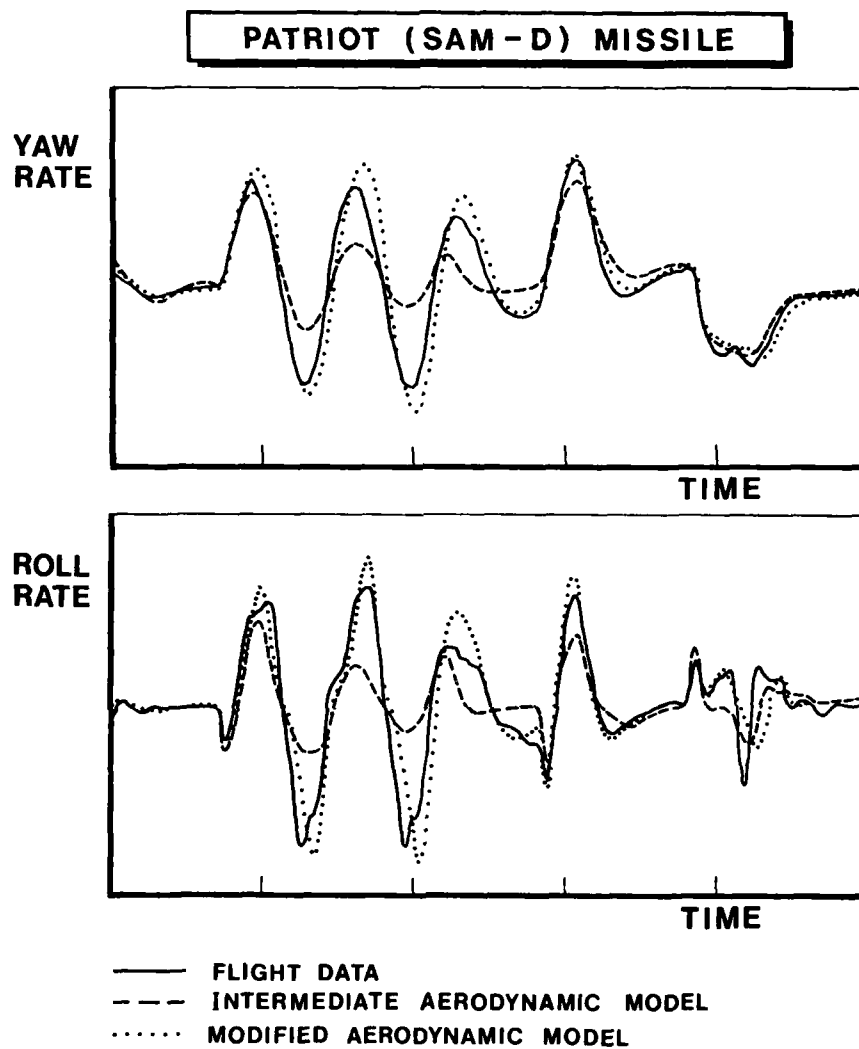


Fig. 15 State of the Art of Missile  
System Identification

## IDENTIFICATION EVALUATION METHODS

by

Vladislav Klein  
The George Washington University  
JIAFS/NASA Langley Research Center  
Hampton, Virginia 23665

## SUMMARY

Three groups of well established methods for airplane parameter estimation, the equation error method, output error method and two advanced methods are presented and their basic properties described. The advanced methods include the maximum likelihood and extended Kalman filter method. For a better understanding of the estimation techniques a first-order scalar differential equation is used as a model of the system under test. Then, the application of the methods to a general multivariable linear system is briefly outlined. A note on the parameter estimation in the frequency domain is also presented. The paper is completed by three numerical examples with the comparison of results from various methods.

## 1. INTRODUCTION

System identification and parameter estimation have been developed over the last 20 years as a strategy and technique for establishing the properties of any system by the measurement of its input and output time histories. During this development several different approaches and methods have been proposed and tested. The process of system identification has also been applied to the determination of airplane parameters (mostly in the form of stability and control derivatives) from flight data.

Previous approaches to the evaluation of stability and control derivatives from flight data were based mainly on time consuming steady-state measurements and on the measurement of free oscillations. The analysis of transient maneuvers based on the least squares procedure was proposed in references 1 and 2. This procedure was, however, applied to very simple maneuvers and resulted in only limited amount of information about system parameters and their accuracies. For the practical analysis of more complicated maneuvers the analog-matching technique has been used. This technique minimizes the errors of the various responses iteratively through the human operator. Finally the increased availability of modern digital computers has made the application of more sophisticated techniques for the estimation of airplane parameters feasible.

The identification of an airplane using modern control theory, theory of statistical inference and new numerical techniques has brought qualitatively new methods of airplane testing and data analysis. This new approach makes it possible to evaluate from one test run all the stability and control derivatives together with their accuracies and confidence intervals. At the same time the accuracy of measured data is also estimated so that this data can be used in the analysis with a corresponding level of confidence. If necessary, there is a possibility of separating the measurement noise in the output variables from the external disturbances to the system caused by gust effects or modeling errors (process noise). Finally the identification methods provide tools for a design of an experiment (optimal input form) to obtain the most accurate results and for testing a hypothesis about an adequate form of the mathematical model describing the analyzed motion of an airplane.

There are several methods for the estimation of airplane parameters. Their basic differences are due to assumptions regarding an optimal criterion, which reflects the existence of external disturbances and the presence of measurement noise in the data. Three groups of well established methods for airplane parameter estimation, the equation error method, output error method and two advanced (statistical) methods will be presented and their basic properties described. The advanced methods are the maximum likelihood method and the extended Kalman filter method.

The paper starts with a short note on the mathematical model of an airplane which must be postulated prior to parameter estimation. For a better understanding of estimation techniques mentioned, a first-order scalar differential equation will be used as a model of the system under test. Then, the application of the methods to a general multivariable linear system representing an airplane will be briefly outlined. Some numerical examples with the comparison of results from various methods will be given. A brief note on the parameter estimation in the frequency domain will also be presented.

## 2. MATHEMATICAL MODEL OF AIRPLANE

For the determination of unknown parameters from flight data the mathematical model of an airplane under test must be postulated. To represent any realistic flying vehicle completely would be a task of immense difficulty. The problem of modeling an airplane raises, therefore, the fundamental question of how complex the model should be. Although a more complex model can be justified for correct description of airplane motion, it is not clear in the case of parameter estimation what should be the best relationship between model complexity and measurement information. If too many unknown parameters are sought for a limited amount of data, then a reduced accuracy of determined parameters can be expected or attempts to estimate all parameters might fail.

In many practical applications the linear model of an aircraft is completely sufficient. The linear equations describing its longitudinal and lateral motion are well developed and can be expressed in the form

$$\dot{x}(t) = F x(t) + G u(t), \quad x(0) = x_0 \quad (1)$$

where  $x$  is the  $(n \times 1)$  state vector,  $u$  is the  $(m \times 1)$  output vector,  $x_0$  is the  $(n \times 1)$  vector of initial conditions,  $F$  and  $G$  are the matrices which include the unknown stability and control derivatives.

In some cases external disturbances to the airplane must be also included. Then model Equation (1) is extended by adding the vector of the so-called process noise which represents a random input due to atmospheric gust and/or certain modeling errors. Equation (1) is changed to

$$\dot{x}(t) = F x(t) + G u(t) + \Gamma w(t) \quad (2)$$

where  $w$  is the  $(r \times 1)$  process noise vector and  $\Gamma$  is the matrix defining the distribution of the process noise into the static equations. Resulting model (2) is a stochastic one with  $x$  being a random variable.

For the measured values it is usually assumed that they are taken at times  $t_1, t_2, \dots, t_N$ , where  $N$  is the number of data points. The measurement equation is formulated as

$$y(i) = H x(i) + D u(i) + v(i) \quad (3)$$

$$i = 1, 2, \dots, N$$

where  $y$  is the measured output vector,  $v$  is the measurement noise vector, and  $H$  and  $D$  are the transformation matrices. The vector  $y$  combines measured state variables and those which can be expressed as a linear combination of states, e.g., linear accelerations, wind vane readings, and so forth.

### 3. EQUATION ERROR METHOD

The equation error (EE) method is based on the principle of least squares which was perhaps the first approach to the concept of optimality. The least squares technique is mainly known in its application to the curve-fitting or regression analysis. In these problems it is desired to represent the measured data by simple functional relationship or by a smooth curve. The solution minimizes the sum of squares of deviations between data points and corresponding points obtained from the solution.

The extension of the least squares techniques to the estimation of parameters of the dynamical system from measured time histories of the input and output is first illustrated on a simple example. It is assumed that the system under test is governed by the scalar differential equation

$$\dot{x}(t) = \theta_1 x(t) + u(t) \quad (4)$$

where  $x$  and  $u$  are the state and input variables, respectively, and  $\theta_1$  is the unknown parameter. It is further assumed that

- (a)  $\dot{x}$ ,  $x$ , and  $u$  are known from measurements,
- (b)  $x$  and  $u$  are measured without errors, whereas the measured values of  $\dot{x}$  are corrupted by measurement errors in such a way that

$$y(i) = \dot{x}(i) + e(i), \quad i = 1, 2, \dots, N \quad (5)$$

where  $y$  is the measured value of  $\dot{x}$  and  $e$  is a random measurement error.

Using the measured data and Equations (4) and (5), then for each time  $t_i$  the following relation holds

$$y(i) - \theta_1 x(i) - u(i) = e(i) \quad (6)$$

The least squares criterion, in this case also termed as the cost function, is

$$J(\theta) = \sum_{i=1}^N e^2(i) = \sum_{i=1}^N [y(i) - \theta_1 x(i) - u(i)]^2 \quad (7)$$

It is now desired to determine the value of  $\theta_1$  for which the cost function has the minimum value. To determine the minimum, Equation (7) is differentiated with respect to  $\theta_1$  obtaining

$$\frac{\partial J(\theta)}{\partial \theta_1} = -2 \sum_{i=1}^N [y(i) - \theta_1 x(i) - u(i)] x(i) \quad (8)$$

For  $J(\theta)$  to be minimum, the right side of Equation (8) is set equal to zero. Then

$$\hat{\theta}_1 \sum_{i=1}^N x^2(i) + \sum_{i=1}^N u(i) x(i) = \sum_{i=1}^N y(i) x(i) \quad (9)$$

Solving Equation (9) the least squares estimate of  $\theta_1$  is obtained.

#### 3.1 ESTIMATION OF AIRPLANE PARAMETERS

The resultant aerodynamic forces and moments acting on the airplane are expressed by means of the aerodynamic model equations which may be written as

$$y(t) = \theta_0 + \theta_1 x_1(t) + \dots + \theta_n x_n(t) + \theta_{n+1} u_1(t) + \dots + \theta_{q-1} u_m(t) \quad (10)$$

In this equation  $y(t)$  represents the resultant coefficient of the aerodynamic force or moment,  $\theta_0$  through  $\theta_{q-1}$  are the stability and control derivatives,  $\theta_0$  is the value of any particular coefficient corresponding to the initial steady-state flight conditions,  $x_1$  to  $x_n$  are the airplane states, and  $u_1$  to  $u_m$  are the control variables.

By substituting the measured values of  $y$ ,  $x$ , and  $u$  into Equation (10), then for each time interval



$$y(i) = \theta_0 + \theta_1 x_1(i) + \dots + \theta_{q-1} u_m(i) = e(i) \quad (11)$$

$$i = 1, 2, \dots, N$$

Because Equation (10) is only an approximation of the actual aerodynamic relations, the right-hand side of Equation (11) is often referred to as the equation error. It can account for the measurement noise and/or modeling errors. Specifying the vectors

$$X_i = [1, x_1(i), \dots, x_n(i), u_1(i), \dots, u_m(i)]$$

$$\theta = [\theta_0, \theta_1, \dots, \theta_{q-1}]^T$$

where the exponent  $T$  denotes the transpose vector or matrix, then the equation error can be expressed as

$$e(i) = y(i) - X_i^T \theta \quad (12)$$

The minimalization of the cost function

$$J(\theta) = \sum_{i=1}^N [y(i) - X_i^T \theta]^2 \quad (13)$$

is obtained by setting

$$\frac{\partial J(\theta)}{\partial \theta} = 0$$

Because of

$$\left. \frac{\partial J(\theta)}{\partial \theta} \right|_{\theta = \hat{\theta}} = -2 \sum_{i=1}^N X_i^T [y(i) - X_i^T \hat{\theta}] = 0$$

then  $\hat{\theta}$  can be solved as

$$\hat{\theta} = \left[ \sum_{i=1}^N X_i^T X_i \right]^{-1} \sum_{i=1}^N X_i^T y(i) \quad (14)$$

This result is called the least squares estimator of  $\theta$ . The block-scheme of the equation error method is shown in Figure 1.

### 3.2 PROPERTIES OF LEAST SQUARES ESTIMATOR

For the examining of the least squares estimator properties the model given by Equation (11) will be changed to

$$y = X\theta + e \quad (15)$$

where

$$y = [y(1), y(2), \dots, y(N)]^T$$

$$e = [e(1), e(2), \dots, e(N)]^T$$

$X$  is the  $(N \times q)$  matrix defined as

$$\begin{bmatrix} 1 & x_1(1) & \dots & u_m(1) \\ 1 & x_1(2) & & u_m(2) \\ \vdots & \vdots & & \vdots \\ 1 & x_1(N) & \dots & u_m(N) \end{bmatrix}$$

and  $q$  indicates the number of unknown parameters. The least squares estimator is obtained from the expression

$$\hat{\theta} = (X^T X)^{-1} X^T y \quad (16)$$

which is identical to Equation (14). It will be further assumed that

- (a)  $e$  is a stationary random vector with zero mean value, i.e.,  $E\{e\} = 0$ ,
- (b)  $e$  is uncorrelated with  $X$ , i.e.,  $E\{X^T e\} = E\{X^T\}E\{e\}$ .

In general,  $\hat{\theta}$  are random variables. The accuracy of  $\hat{\theta}$  can be measured by a number of statistical properties such as bias, error covariance, efficiency and consistency. Substituting of Equation (15) into (16) results in

$$\hat{\theta} = (X^T X)^{-1} X^T X \theta + (X^T X)^{-1} X^T e = \theta + (X^T X)^{-1} X^T e \quad (17)$$

Then expressing the expected value of  $\hat{\theta}$  it is obtained

$$E\{\hat{\theta}\} = \theta + E\{(X^T X)^{-1} X^T\} E\{e\} = 0 \quad (18)$$

Equation (18) indicates that  $\hat{\theta}$  is unbiased.

The covariance matrix corresponding to the estimate error  $\hat{\theta} - \theta$  is

$$\begin{aligned} \text{Cov}\{\hat{\theta} - \theta\} &= E\{(\hat{\theta} - \theta)(\hat{\theta} - \theta)^T\} \\ &= E\{[(X^T X)^{-1} X^T e][(X^T X)^{-1} X^T e]^T\} \\ &= (X^T X)^{-1} X^T E\{e e^T\} X (X^T X)^{-1} \end{aligned} \quad (19)$$

When the measurement noise  $e(i)$  are identically distributed and independent (white noise) with zero mean and variance  $\sigma^2$ , then the measurement noise covariance matrix becomes

$$E\{e e^T\} = \sigma^2 I \quad (20)$$

where  $I$  is the identity matrix. Equation (19) is simplified as

$$\text{Cov}\{\hat{\theta} - \theta\} = \sigma^2 (X^T X)^{-1} \quad (21)$$

Because the variance  $\sigma^2$  is usually not known its estimate  $s^2$  can be used in Equation (21) instead. The variance estimate is found from the residuals  $v(i)$  as

$$s^2 = \frac{1}{N-q} \sum_{i=1}^N v^2(i) \quad (22)$$

where

$$v(i) = y(i) - X_i^T \hat{\theta} \quad (23)$$

In the error covariance matrix (also called the parameter covariance matrix) the main diagonal terms are the variances of the estimated parameters  $\sigma^2(\theta_k)$ . The off-diagonal elements are the covariances  $\rho_{kl} \sigma(\theta_k) \sigma(\theta_l)$ , where  $\rho_{kl}$  is the correlation coefficients for errors in the parameters  $\theta_k$  and  $\theta_l$ .

If the measurement noise has the properties given by Equation (20), it is possible to show that the corresponding estimator is a minimum-variance (efficient) estimator (see e.g., ref. 3). Rewriting the covariance matrix as

$$\text{Cov}\{\hat{\theta} - \theta\} = \frac{\sigma^2}{N} \left( \frac{1}{N} X^T X \right)^{-1}$$

and assuming that

$$\lim_{N \rightarrow \infty} \left[ \frac{1}{N} X^T X \right]^{-1}$$

does exist, then

$$\lim_{N \rightarrow \infty} \text{Cov}\{\hat{\theta} - \theta\} = \lim_{N \rightarrow \infty} \frac{\sigma^2}{N} \left[ \frac{1}{N} X^T X \right]^{-1} = 0 \quad (24)$$

zero parameter covariance matrix means that  $\hat{\theta} = \theta$  at  $N \rightarrow \infty$ . This convergence property indicates that  $\hat{\theta}$  is a consistent estimator.

In any real situation the measured state and input variables are corrupted by errors and the airplane can be exposed to the effect of process noise. The model has, therefore, the form

$$y_T = X_T \theta + w \quad (25)$$

where the index  $T$  indicates true values and  $w$  is the process noise. From the measurements

$$y = y_T + v \quad (26)$$

$$X = X_T + \delta X$$

where  $v$  and  $\delta X$  is the measurement noise in  $y$ , and in  $x$  and  $u$ , respectively. Premultiplying Equation (25) by  $(X^T X)^{-1} X^T$  gives

$$(X^T X)^{-1} X^T y_T = (X^T X)^{-1} X^T X_T \theta + (X^T X)^{-1} X^T w \quad (27)$$

Using Equations (26), Equation (27) is changed as

$$(X^T X)^{-1} X^T (y - v) = (X^T X)^{-1} X^T (X - \delta X) \theta + (X^T X)^{-1} X^T w$$

from which

$$\hat{\theta} = \theta + (X^T X)^{-1} X^T (w + v - \delta X \theta) \quad (28)$$

Then the expected value and covariance matrix of the estimate error have the form

$$E\{\hat{\theta} - \theta\} = -E\{(X^T X)^{-1} X^T \delta X\} \theta \quad (29)$$

and

$$\text{Cov}\{\hat{\theta} - \theta\} = E\{(X^T X)^{-1} X^T e e^T X (X^T X)^{-1}\} + E\{(X^T X)^{-1} X^T \delta X \theta \theta^T \delta X^T X (X^T X)^{-1}\} \quad (30)$$

where  $\epsilon = w + v$ .

From Equations (29) and (30) the following conclusions can be drawn:

1. The estimate  $\hat{A}$  is biased, even if the noise vector  $v$  and  $w$  have zero mean and are independent of  $\delta X$ ,
2. the bias of the estimate is affected solely by the error in the state and input variables as long as the errors  $v$  and  $w$  are zero mean,
3. the bias in the estimates is zero if  $X$  is measured without error or if the equation error is zero mean and white,
4. the variance of the estimates is affected by the noise level of all the measurements and by the process noise.

Despite all these degradations in the accuracy of the estimates resulting from real flight data, the equation error method is often used, sometimes with very consistent results in comparison with more sophisticated techniques. The main appeal of the method is in its simplicity and easy application to any linear or nonlinear model. Results from the EE method can be found in several references, for example, references 4 to 6.

### 3.3 INSTRUMENTAL VARIABLE METHOD

It has been shown in the preceding chapter that the nice properties of the least squares estimates depend critically on the assumption that the equation errors are white. There are several methods which can remove the correlation in  $\epsilon(i)$  and thus obtain unbiased estimates. Unfortunately, these methods are rather complicated for airplane parameter estimation. They require a model for the equation errors as a filter driven by white noise.

To avoid the difficulties with correlated equation errors, the so-called instrumental variable method was proposed (see ref. 7). For airplane aerodynamic model Equation (15) the instrumental variable method requires the formulation of a  $Z$  matrix, which is called the instrumental variable matrix. The elements of the  $Z$  matrix are functions of the data and have the following properties

$$E\{Z^T X\} \text{ is a positive definite matrix}$$

$$E\{Z^T \epsilon\} = 0$$

Premultiplying Equation (15) by  $Z^T$  and solving for  $\theta$  gives

$$\theta = (Z^T X)^{-1} Z^T y - (Z^T X)^{-1} Z^T \epsilon \quad (31)$$

In this equation

$$\hat{\theta}_{IV} = (Z^T X)^{-1} Z^T y \quad (32)$$

is taken as the instrumental variable estimates of  $\theta$ . It is proved in reference 7 that this estimator is consistent, e.g.

$$\lim_{N \rightarrow \infty} \hat{\theta}_{IV} = \theta$$

It can be seen that Equation (32) has the same form as the least squares solution, thus it is simple to compute. The only important question remaining is how to determine the instrumental variables needed to construct  $Z$ . The required properties of this matrix mean that the instrumental variables are uncorrelated with  $\epsilon$  but strongly correlated with the input and state variables in  $X$ .

There are several proposals in references 7 and 8 for the design of an instrumental variables. For the airplane parameter estimation the model using a Kalman filter (given later in Chapter 5) with known input variables and approximate values for the stability and control derivatives might be used. These equations provide the estimates of the state variables,  $\hat{x}$ , which are then used, together with the input variables, in the  $Z$  matrix. For the model represented by Equation (10) the vector  $Z_i$  will have the form

$$Z_i = [1, \hat{x}_1(i), \dots, \hat{x}_n(i), u_1(i), \dots, u_m(i)]$$

The block-scheme of the instrumental variable method comprising a Kalman filter is presented in Figure 2.

### 4. OUTPUT ERROR METHOD

The output error (OE) method minimizes the errors between the actual output and the model output by using the same input. It is assumed that only measured outputs are corrupted by noise and that there are no gust or other disturbances to the airplane. The optimization problem involved is a nonlinear one and requires the use of an iterative solution. The modified Newton-Raphson technique is usually applied because of its good convergence rate even for large number of unknown parameters. Because of the nonlinear estimation involved, the OE method is very often introduced under the names of nonlinear regression, modified Newton-Raphson method, method of quasilinearization, and so forth. The OE method is also called the maximum likelihood method if this estimation technique is used for the parameter estimation in the output error cost function.

When the OE method is applied to the system described by Equation (4), the state and measurement equations have the form

$$\dot{\hat{x}}(t) = a_1 \hat{x}(t) + u(t), \quad \hat{x}(0) = 0 \quad (4)$$

$$y(i) = x(i) + v(i), \quad i = 1, 2, \dots, N \quad (33)$$

where, for the measurement noise, it is assumed that

$$E\{v(i)\} = 0 \quad \text{and} \quad E\{v^2(i)\} = \sigma^2$$

The zero initial condition is introduced for simplicity reason. The cost function is now formed as

$$J(\theta) = \frac{1}{2} \sum_{i=1}^N [y(i) - \hat{x}(i)]^2 \quad (34)$$

where  $\hat{x}$  is the computed output which can be expressed as

$$\hat{x}(t) = \int_0^t e^{\theta_1(t-\tau)} u(\tau) d\tau \quad (35)$$

Equation (35) is the nonlinear expression for the parameter  $\theta_1$ , which means that the estimation of  $\theta_1$  is a nonlinear problem. One of the possible ways for finding the estimate of  $\theta_1$  is based on Taylor's series expansion of  $\hat{x}$  around the initial estimate of the unknown parameter,  $\theta_{1N}$ . The expansion is formulated as

$$\hat{x}(\theta_1) = \hat{x}(\theta_{1N}) + \frac{\partial \hat{x}}{\partial \theta_1} \Delta \theta_1 + \text{higher order terms} \quad (36)$$

Using Equation (34) and the linear terms in Equation (36), the cost function is rewritten as

$$J(\theta) = \frac{1}{2} \sum_{i=1}^N [y(i) - \hat{x}(i, \theta_{1N}) - \frac{\partial \hat{x}(i)}{\partial \theta_1} \Delta \theta_1]^2 \quad (37)$$

where the unknown parameter is now the increment  $\Delta \theta_1$ . The term  $\partial \hat{x} / \partial \theta_1$  is called the sensitivity function. It is obtained from the sensitivity equation

$$\frac{d}{dt} \frac{\partial \hat{x}}{\partial \theta_1} = \theta_1 \frac{\partial \hat{x}}{\partial \theta_1} + \hat{x}, \quad \frac{\partial \hat{x}}{\partial \theta_1}(0) = 0 \quad (38)$$

which results from Equation (4) by differentiation with respect to  $\theta_1$ . The minimalization of the cost function with respect to  $\Delta \theta_1$  is the same as with respect to  $\theta_1$ . It gives the equation

$$\frac{\partial J(\theta)}{\partial \theta_1} = - \sum_{i=1}^N [y(i) - \hat{x}(i, \theta_{1N}) - \frac{\partial \hat{x}}{\partial \theta_1} \Delta \theta_1] \frac{\partial \hat{x}}{\partial \theta_1} = 0 \quad (39)$$

which can be solved for  $\Delta \hat{\theta}_1$ . Then the estimates of  $\theta_1$  is found as

$$\hat{\theta}_1 = \theta_{1N} + \Delta \hat{\theta}_1 \quad (40)$$

Because of the approximation of the cost function, the computing is repeated with  $\hat{\theta}_1$  as the new initial estimate. The iteration is completed when the minimum of the cost function is reached.

#### 4.1 MULTIVARIABLE SYSTEM

When the OE method is used for airplane parameter estimation, the model given by Equations (1) and (3) may be used, that is

$$\dot{\hat{x}}(t) = F \hat{x}(t) + G u(t), \quad \hat{x}(0) = x_0 \quad (1)$$

$$y(i) = H \hat{x}(i) + D u(i) + v(i) \quad (3)$$

$$i = 1, 2, \dots, N$$

For the development of the estimation algorithm it is assumed that

$$E\{v(i)\} = 0 \quad \text{and} \quad E\{v(i)v^T(j)\} = \sigma^2 C \quad \text{for } i = j \\ = 0 \quad \text{for } i \neq j$$

where  $C$  is a known diagonal matrix.

In the multivariable case the cost function can be formulated as

$$J(\theta) = \frac{1}{2} \{ w_1 \sum_{i=1}^N [y_1(i) - \hat{y}_1(i)]^2 + w_2 \sum_{i=1}^N [y_2(i) - \hat{y}_2(i)]^2 \\ + \dots + w_p \sum_{i=1}^N [y_p(i) - \hat{y}_p(i)]^2 \} \quad (41)$$

which can be expressed in the matrix form as

$$J(\theta) = \frac{1}{2} \sum_{i=1}^N [y(i) - \hat{y}(i)]^T W [y(i) - \hat{y}(i)] \quad (42)$$

In this cost function  $\hat{y}$  is the computed output vector and  $W$  is the diagonal weighting matrix with the elements  $w_j$ ,  $j = 1, 2, \dots, p$ . The weights  $w_j$  are the homogeneity factors but they can also reflect a confidence in the measured output variables.

The vector of unknown parameters include, in general, the elements of all matrices in the model equations and the initial conditions. As indicated in reference 9, the minimalization of the cost function with respect to the unknown parameters can be solved by several gradient-based nonlinear programming methods. The iteration in these methods is given as

$$\theta_{r+1} = \theta_r - c_r M_r^{-1} g_r \quad (43)$$

where the index  $r$  denotes the  $r$ th iteration,  $c$  is a scalar step size parameter chosen to improve the convergence,  $M$  and  $g$  are the second- and first-order gradients of the cost function. For the modified Newton-Raphson method the matrix  $M$  is approximated as

$$M_r = \sum_{i=1}^N A_i^T(\theta_r) W A_i(\theta_r) \quad (44)$$

where  $A(\theta)$  is the sensitivity matrix including all sensitivities of  $y$  with respect to  $\theta$ . Therefore, the element of  $A$  is

$$A_{kl} = \frac{\partial \hat{y}_k}{\partial \theta_l}, \quad k = 1, 2, \dots, p \\ l = 1, 2, \dots, q$$

The gradient of the cost function has the form

$$g_r = \left. \frac{\partial J(\theta)}{\partial \theta} \right|_{\theta = \theta_r} = \sum_{i=1}^N A_i^T(\theta_r) W [y(i) - \hat{y}(i, \theta_r)] \quad (45)$$

Then the vector equation for the estimate of the increments  $\Delta\theta$  is given (assuming  $c = 1$ ) as

$$\Delta\hat{\theta} = [\sum_{i=1}^N A_i^T W A_i]^{-1} \sum_{i=1}^N A_i^T W [y(i) - \hat{y}(i)] \quad (46)$$

The sensitivities are computed from two sets of equations

$$\frac{d}{dt} \frac{\partial \hat{x}}{\partial \theta_k} = \frac{\partial F}{\partial \theta_k} \hat{x} + F \frac{\partial \hat{x}}{\partial \theta_k} + \frac{\partial G}{\partial \theta_k} u \quad (47)$$

$$\frac{\partial \hat{y}}{\partial \theta_k} = H \frac{\partial \hat{x}}{\partial \theta_k} + \frac{\partial H}{\partial \theta_k} \hat{x} + \frac{\partial D}{\partial \theta_k} u \quad (48)$$

$$k = 1, 2, \dots, q$$

The computing block-scheme for the OE method is given in Figure 3.

To study the properties of the OE estimates, it will be assumed that after the final iteration

$$\hat{y}(i) = \hat{y}_N(i) + A_1 \Delta\theta \quad (49)$$

where  $\hat{y}_N$  represents the computed vector based on the parameter estimates from the previous iteration. These combinations of Equations (49) and (3) yields

$$y(i) - \hat{y}_N(i) = v(i) - A_1 \Delta\theta \quad (50)$$

By substituting Equation (50) into (46) the following expression is obtained

$$\Delta\hat{\theta} = M^{-1} \sum_{i=1}^N A_i^T W v(i) + M^{-1} \sum_{i=1}^N A_i^T W A_1 \Delta\theta = M^{-1} \sum_{i=1}^N A_i^T W v(i) + \Delta\theta \quad (51)$$

from which the error in the estimates has the form

$$\Delta\hat{\theta} - \Delta\theta = M^{-1} \sum_{i=1}^N A_i^T W v(i) \quad (52)$$

The expected value of this error is zero which indicates, considering the approximation in Equation (49), that the estimates  $\Delta\hat{\theta}$  are unbiased to the first order.

With Equation (52) the parameter covariance matrix has the form

$$\text{Cov}\{\Delta\hat{\theta} - \Delta\theta\} = E\{M^{-1} \sum_{i=1}^N A_i^T W v(i) [\sum_{i=1}^N A_i^T W v(i)]^T M^{-1}\} \quad (53)$$

For the white measurement noise with the covariance matrix  $\sigma^2 W$  the parameter covariance matrix is simplified as

$$\text{Cov}\{\Delta\hat{\theta} - \Delta\theta\} = \sigma^2 M^{-1} \quad (54)$$

The estimate of  $\sigma^2$  can be found from the residuals as

$$s^2 = \frac{1}{pN - q} \sum_{i=1}^N v(i)^T W v(i) \quad (55)$$

where

$$v(i) = [y(i) - \hat{y}(i, \hat{\theta})]^T W [y(i) - \hat{y}(i, \hat{\theta})] \quad (56)$$

Some of the properties of the OE estimator will also be apparent from the presentation of the maximum likelihood method in the following chapter.

The OE method with the modified Newton-Raphson algorithm was introduced in references 10 to 13 and it has been used extensively for the past several years. It usually takes the results from the equation error method as the initial values for the parameter estimates. As long as the method is applied to linear flight regimes or where the form of equations is known, it works very well. The principle disadvantage of the OE method is in the degradation of the results where process noise exists. This may result in the computer program not converging or in poor estimates with large variances and/or high correlation coefficients.

## 5. MAXIMUM LIKELIHOOD METHOD

The most general identification problem involves the extraction of airplane parameters for a nonlinear model from flight data containing both measurement and process noise. One of the advanced techniques that has demonstrated this capability is based on the maximum likelihood (ML) criterion. The principle of ML for use in parameter estimation was introduced by R. A. Fisher in 1912 and further expanded by him in a series of papers (see, e.g., ref. 14). The idea behind this technique is relatively simple. It is assumed that the outcome  $Y$  of an experiment depends on unknown parameters  $\theta$ . The ML estimates of the unknown parameters are those values for which the observed value  $y$  would be "most likely" to occur. "Most likely" is defined to mean maximization of the so-called likelihood function. The likelihood function is the conditional probability density function of the observation  $Y$  given  $\theta$ . The problem of ML estimation can be, therefore, stated as

$$\hat{\theta} = \max_{\theta} p[Y|\theta] \quad (57)$$

where  $\hat{\theta}$  is the maximum likelihood estimator of  $\theta$  and  $p[Y|\theta]$  is the conditional probability of  $Y$  given  $\theta$ .

For the illustration of the ML estimation the scalar first-order system with process noise is considered. The model is formed as

$$\dot{x}(t) = \theta_1 x(t) + u(t) + w(t) \quad (58)$$

$$y(i) = x(i) + v(i) \quad (59)$$

where

$$i = 1, 2, \dots, N$$

$$E\{x(0)\} = x_0 \quad \text{and} \quad E\{[x(0) - x_0]^2\} = p_0$$

In Equations (58) and (59)  $w(t)$  and  $v(i)$  are uncorrelated Gaussian white noise sources with zero mean, that is

$$E\{w(t)\} = 0, \quad E\{w(t)w(\tau)\} = q \delta(t - \tau)$$

$$E\{v(i)\} = 0, \quad E\{v(i)v(j)\} = r \delta_{ij}$$

where  $\delta(t - \tau)$  is the Dirac delta function,  $\delta_{ij}$  is the Kronecker delta notation.

The vector of unknown parameters contains the coefficient  $\theta_1$ , and the variances  $q$  and  $r$ , whereas  $x_0$  and  $p_0$  are assumed to be known. It means that

$$\theta = [\theta_1, q, r]^T$$

The likelihood function is now

$$L(\theta) = p[y(1), y(2), \dots, y(N) | \theta] \quad (60)$$

To obtain this function, the vector  $Y_N$  consisting of all measured outputs is introduced

$$Y_N = [y(1), y(2), \dots, y(N)]^T \quad (61)$$

If the probability distribution of  $Y_N$  has a density  $p[Y_N|\theta]$ , it then follows from the definition of conditional probabilities that

$$p[Y_N|\theta] = p[y(N) | Y_{N-1}, \theta] p[Y_{N-1} | \theta] \quad (62)$$

Repeated use of this formula gives the following expression for the likelihood function

$$L(\theta) = p[Y_N|\theta] = p[y(N) | Y_{N-1}, \theta] p[y(N-1) | Y_{N-2}, \theta] \dots p[y(2) | y(1), \theta] p[y(1)]$$

$$= \prod_{i=1}^N p[y(i) | Y_{i-1}, \theta] \quad (63)$$

To find the probability distribution of  $y(i)$  given  $Y_{i-1}$  and  $\theta$ , the mean value and variance are determined first. By definition

$$E[y(i) | Y_{i-1}, \theta] \triangleq \hat{y}(i | i-1)$$

which means that the expected value is the best possible estimate of measurements at a point given the measurements up to and including the previous point. From the definition of the variance it follows that

$$E\{[y(i) - \hat{y}(i|i-1)]^2\} = E\{v^2(i)\} \triangleq b(i)$$

where  $v$  are the innovations

$$v(i) = y(i) - \hat{y}(i|i-1) \quad (64)$$

It has been shown that for the high sampling rate the innovations  $v(i)$  tend toward having a Gaussian density. The distribution of  $v(i)$  is, therefore, Gaussian, also  $y(i)$  given  $Y_{i-1}$  and  $\theta$  is Gaussian, i.e.

$$p[y(i)|Y_{i-1}, \theta] = \frac{1}{\sqrt{2\pi b(i)}} \exp\left\{-\frac{1}{2} \frac{v^2(i)}{b(i)}\right\} \quad (65)$$

In the parameter estimation problem it is usually more convenient to work with the negative of the logarithm of the likelihood function. It is possible to do so because the logarithm is a monotonic function. From Equation (65) the logarithm of the probability distribution is

$$\log p[y(i)|Y_{i-1}, \theta] = -\frac{1}{2} \frac{v^2(i)}{b(i)} - \frac{1}{2} \log b(i) + \text{const} \quad (66)$$

Then, using Equations (63) and (66), the negative log-likelihood function can be written as

$$J(\theta) = \frac{1}{2} \sum_{i=1}^N \left\{ \frac{v^2(i)}{b(i)} + \log b(i) \right\} \quad (67)$$

The log-likelihood function depends on the innovations and their covariance. To optimize this function, a way must be found for determining these quantities. Both innovations and their covariance are output of a Kalman filter. This filter is an algorithm which can be divided into two parts. In the first part, called the prediction equations, the state equations and state estimate covariance equations are propagated in time from one measurement point to the next. In the second part, called the measurement update equations, the measurements and associated measurement noise covariances are used to improve state covariance estimates.

The Kalman filter equations are developed, for example, in reference 15. For the system described by Equations (58) and (59) they are as follows:

The prediction equations:

$$\frac{d}{dt} \hat{x}(t|t_{i-1}) = a_1 \hat{x}(t|t_{i-1}) + u(t), \quad \hat{x}(t_0|t_0) = x_0 \quad (68)$$

$$\frac{d}{dt} p(t|t_{i-1}) = 2a_1 p(t|t_{i-1}) + q, \quad p(t_0|t_0) = p_0 \quad (69)$$

$$t_{i-1} \leq t \leq t_i$$

the measurement update equations:

$$\hat{x}(i|i) = \hat{x}(i|i-1) + k(i)v(i) \quad (70)$$

$$p(i|i) = [1 - k(i)]p(i|i-1) \quad (71)$$

where

$$v(i) = y(i) - \hat{x}(i|i-1) \quad (72)$$

$$k(i) = p(i|i-1)b^{-1}(i) \quad (73)$$

$$b(i) = p(i|i-1) + r \quad (74)$$

The computing scheme of a Kalman filter for one stage is presented in Figure 4.

The minimalization of  $J(\theta)$  with respect to  $\theta$  subjected to the Kalman filter constraint leads again to the nonlinear parameter estimation. The parameter vector after the  $r$ th iteration is given by Equation (43), that is

$$\theta_{r+1} = \theta_r - M_r^{-1} g_r \quad (43)$$

The gradient vector of the negative log-likelihood function is

$$\frac{\partial J(\theta)}{\partial \theta_k} = \sum_{i=1}^N \left\{ \frac{v}{b} \frac{\partial v}{\partial \theta_k} - \frac{1}{2} \frac{v^2}{b} \frac{\partial b}{\partial \theta_k} + \frac{1}{2b} \frac{\partial b}{\partial \theta_k} \right\} \quad (75)$$

where  $\theta_k$  is the  $k$ th component of the  $\theta$  vector. The matrix  $M$  is now the so-called Fisher information matrix defined as

$$M = -E\left\{\frac{\partial^2 J(\theta)}{\partial \theta \partial \theta^T}\right\} \quad (76)$$

Using the modified Newton-Raphson technique, the elements of the  $M$  matrix can be estimated from the expression

$$M_{kj} = \sum_{i=1}^N \left\{ \frac{1}{b} \frac{\partial v}{\partial \theta_j} \frac{\partial v}{\partial \theta_k} - \frac{v}{b} \left[ \frac{\partial b}{\partial \theta_j} \frac{\partial v}{\partial \theta_k} + \frac{\partial v}{\partial \theta_j} \frac{\partial b}{\partial \theta_k} \right] + \left( \frac{v^2}{b^3} - \frac{1}{2b^2} \right) \frac{\partial b}{\partial \theta_j} \frac{\partial b}{\partial \theta_k} \right\} \quad (77)$$

Because of Equations (72) and (74), the sensitivities in  $v$  and  $b$  can be written as

$$\frac{\partial v}{\partial \theta_k} = - \frac{\partial \hat{x}(t|t-1)}{\partial \theta_k} \quad (78)$$

$$\frac{\partial b}{\partial \theta_k} = \frac{\partial p(t|t-1)}{\partial \theta_k} + \frac{\partial r}{\partial \theta_k} \quad (79)$$

The sensitivity equations follow from Kalman filter Equations (68) to (71) as

$$\frac{d}{dt} \frac{\partial \hat{x}(t|t-1)}{\partial \theta_k} = \theta_1 \frac{\partial \hat{x}(t|t-1)}{\partial \theta_k} + \frac{\partial \theta_1}{\partial \theta_k} \hat{x}(t|t-1), \frac{\partial \hat{x}(t_0|t_0)}{\partial \theta_k} = 0 \quad (80)$$

$$\frac{d}{dt} \frac{\partial p(t|t-1)}{\partial \theta_k} = 2\theta_1 \frac{\partial p(t|t-1)}{\partial \theta_k} + 2 \frac{\partial \theta_1}{\partial \theta_k} p(t|t-1) + \frac{\partial a}{\partial \theta_k}, \frac{\partial p(t_0|t_0)}{\partial \theta_k} = 0 \quad (81)$$

$$\frac{\partial \hat{x}(t|t)}{\partial \theta_k} = \frac{\partial \hat{x}(t|t-1)}{\partial \theta_k} + \frac{\partial k(t)}{\partial \theta_k} v(t) + k(t) \frac{\partial v(t)}{\partial \theta_k} \quad (82)$$

$$\frac{\partial p(t|t)}{\partial \theta_k} = [1 - k(t)] \frac{\partial p(t|t-1)}{\partial \theta_k} - \frac{\partial k(t)}{\partial \theta_k} p(t|t-1) \quad (83)$$

where

$$\frac{\partial k(t)}{\partial \theta_k} = \frac{\partial p(t|t-1)}{\partial \theta_k} b^{-1}(t) - \frac{1}{b^2(t)} \frac{\partial b(t)}{\partial \theta_k} p(t|t-1) \quad (84)$$

The ML estimation method in the form presented can be rather time consuming even for a simple scalar system. Therefore, for a practical use several simplified versions of this method have been suggested. In many applications the Kalman filter is in steady state for the duration of an experiment. Then the Kalman gain  $k$ , the innovation variance  $b$  and the state variance  $p$  approach constant values. Under these conditions it has been suggested in reference 16 to consider  $k$  and  $b$  as unknown parameters rather than  $q$  and  $r$ . Optimizing  $J(\theta)$  with respect to  $b$  gives

$$\hat{b} = \frac{1}{N} \sum_{i=1}^N v^2(i) \quad (85)$$

Then the gradient of the negative log-likelihood function with respect to other unknown parameters  $\theta = [\theta_1, k]^T$  is

$$\frac{\partial J(\theta)}{\partial \theta_k} = \sum_{i=1}^N \frac{v}{\hat{b}} \frac{\partial v}{\partial \theta_k} \quad (86)$$

and the estimate of elements in the Fisher information matrix are

$$M_{kl} = - \sum_{i=1}^N \frac{1}{\hat{b}} \frac{\partial v}{\partial \theta_l} \frac{\partial v}{\partial \theta_k} \quad (87)$$

The sensitivity equations are simplified as

$$\frac{d}{dt} \frac{\partial \hat{x}(t|t-1)}{\partial \theta_k} = \theta_1 \frac{\partial \hat{x}(t|t-1)}{\partial \theta_k} + \frac{\partial \theta_1}{\partial \theta_k} \hat{x}(t|t-1) \quad (88)$$

$$\frac{\partial \hat{x}(t|t)}{\partial \theta_k} = (1 - k) \frac{\partial \hat{x}(t|t-1)}{\partial \theta_k} + \frac{\partial k}{\partial \theta_k} v(t) + k \frac{\partial v(t)}{\partial \theta_k} \quad (89)$$

The maximum likelihood method can be also simplified when either process noise or measurement noise are absent. If the process noise is zero and the initial state is known, the covariance of the error in the predicted state is also zero. It follows from (73) that the Kalman gain is zero and the innovations are the output errors

$$v(i) = y(i) - \hat{x}(i)$$

The innovation variance is  $b(i) = r$  and the negative log-likelihood function is simplified as

$$J(\theta) = \frac{1}{2r} \sum_{i=1}^N v^2(i) + \frac{N}{2} \log r \quad (90)$$

When (90) is optimized for unknown parameter  $r$  it gives

$$\hat{r} = \frac{1}{N} \sum_{i=1}^N v^2(i) \quad (91)$$

Then the log-likelihood function is

$$J(\theta) = \frac{1}{2\hat{r}} \sum_{i=1}^N v^2(i) + \text{const} \quad (92)$$

which is the same as the cost function for the output error method except that the measurement noise variance is used as a weight.



For the case when no measurement noise in the state variable exists, the log-likelihood function is formulated as

$$J(\theta) = \frac{1}{2\sigma^2} \sum_{i=1}^N [\dot{y}(i) - a_1 x(i) - u(i)]^2 \quad (93)$$

which is the sum of squares of the equation error at sampling times. Thus, the ML estimates are identical to the EE estimates where

$$\sigma^2 = E\{[\dot{y}(i) - \dot{x}(i)]^2\}$$

is assumed to be known.

### 5.1 MULTIVARIABLE SYSTEM WITH PROCESS NOISE

For airplane parameter estimation using the ML method linear model Equations (2) and (3) may be used, that is

$$\dot{x}(t) = F x(t) + G u(t) + \Gamma w(t) \quad (2)$$

$$y(i) = H x(i) + D u(i) + v(i) \quad (3)$$

where

$$E\{x(0)\} = 0 \quad \text{and} \quad E\{[x(0) - x_0][x(0) - x_0]^T\} = P_0$$

The process and measurement noise are assumed uncorrelated and Gaussian with

$$E\{w(t)\} = 0, \quad E\{w(t)w^T(\tau)\} = Q\delta(t - \tau)$$

$$E\{v(i)\} = 0, \quad E\{v(i)v^T(j)\} = R\delta_{ij}$$

If the external disturbances should represent the random gust effects then the modeling of gust spectra would have to be included in Equation (2). This is achieved with the help of a filter that is excited by white noise. The airplane state variables are, therefore, augmented by the filter states as indicated in references 17 and 18.

The negative log-likelihood function is formulated as

$$J(\theta) = \frac{1}{2} \sum_{i=1}^N v^T(i, \theta) B^{-1}(i, \theta) v(i, \theta) + \frac{N}{2} \log |B(i, \theta)| \quad (94)$$

where

$$B(i, \theta) \triangleq E\{v(i, \theta)v^T(i, \theta)\}$$

The unknown parameters can occur in matrices  $F, G, \Gamma, H, D, Q, R, P_0$ , and  $x_0$ . However, all these parameters are not, in general, identifiable. To ensure their identifiability, certain conditions mentioned in reference 19 must be met.

The estimation algorithm for a multivariable case can be developed in a similar way to that in the preceding chapter. The resulting expressions and possible simplifications are presented in references 17 and 18, and references 20 and 21. The block-scheme of the ML method is given in Figure 5. It is similar to that for the output error method with the deterministic model replaced by the Kalman filter system representation. In Table I the cost functions for the three methods described so far are summarized.

### 5.2 PROPERTIES OF MAXIMUM LIKELIHOOD ESTIMATOR

The ML estimates of unknown parameters have the following main properties as reviewed and discussed in references 22 and 23:

1. they are consistent, i.e.

$$\lim_{t \rightarrow \infty} P\{|\hat{\theta}(t) - \theta| < \epsilon\} = 1$$

with  $\epsilon$  arbitrary small

where  $P\{\}$  indicates the probability and  $\theta$  the true value of parameters,

2. they are asymptotically unbiased, i.e.

$$\lim_{t \rightarrow \infty} E\{\hat{\theta}(t)\} = \theta$$

3. they are asymptotically efficient with

$$E\{(\hat{\theta} - \theta)(\hat{\theta} - \theta)^T\} < -E\left\{\frac{\partial^2 J(\theta)}{\partial \theta \partial \theta^T}\right\} \quad (95)$$

Because of Equations (76) and (95), the inverse of the information matrix provides the lower bounds on the variance and the covariance of the errors in the estimated parameters. This lower bound is known as the Cramer-Rao lower bound and is to be viewed as the maximum achievable accuracy in the parameter estimates.

4. They are asymptotically normal, that is, they approximate the Gaussian distribution with the mean  $\theta$  and covariance  $M^{-1}$ .

The properties 1 and 2 apply also to the output error method if  $W$  is a diagonal matrix.

## 6. EXTENDED KALMAN FILTER METHOD

The extended Kalman filter (EKF) is an approximate filter for nonlinear systems, based on first-order linearization. The EKF approach to the estimation of parameters in dynamic systems has a rather long history and many applications of this method has been suggested and discussed. When the EKF method is to be used for parameter estimation, it is necessary first to include the unknown parameters in the state vector. Once this is done, a standard Kalman filter program can be applied for the estimation. The resulting algorithm is consequently not very complicated.

When the model of a system is considered given by Equation (53), the augmented system has the form

$$\dot{\mathbf{x}}(t) = \theta_1(t)\mathbf{x}(t) + \mathbf{u}(t) + \mathbf{w}(t) \quad (96)$$

$$\dot{\theta}_1(t) = 0 \quad (97)$$

With the augmented state vector

$$\mathbf{x}_a = [\mathbf{x}, \theta_1]^T$$

Equations (96) and (97) can be expressed as

$$\dot{\mathbf{x}}_a(t) = \mathbf{f}[\mathbf{x}_a(t), \mathbf{u}(t), t] + \mathbf{w}_a(t) \quad (98)$$

where

$$\mathbf{f}[\mathbf{x}_a(t), \mathbf{u}(t), t] = \begin{bmatrix} \theta_1(t)\mathbf{x}(t) + \mathbf{u}(t) \\ 0 \end{bmatrix}$$

$$\mathbf{w}_a(t) = \begin{bmatrix} \mathbf{w}(t) \\ 0 \end{bmatrix}$$

$$E\{\mathbf{x}_a(0)\} = \mathbf{x}_{a0}, E\{[\mathbf{x}_a(0) - \mathbf{x}_{a0}][\mathbf{x}_a(0) - \mathbf{x}_{a0}]^T\} = \mathbf{P}_0$$

$$E\{\mathbf{w}_a(0)\} = 0, E\{\mathbf{w}_a(t)\mathbf{w}_a(\tau)\} = \mathbf{Q}\delta(t - \tau)$$

The measurement equation is given as

$$y(i) = H\mathbf{x}_a(i) + v(i) \quad (99)$$

where

$$H = [1, 0]$$

$$E\{v(i)\} = 0, E\{v(i)v(j)\} = r\delta_{ij}$$

The Kalman filter equations for the system (98) and (99) are as follows:

The prediction equations:

$$\frac{d}{dt} \hat{\mathbf{x}}_a(t|t_{i-1}) = \mathbf{f}[\hat{\mathbf{x}}_a(t|t_{i-1}), \mathbf{u}(t), t] \quad (100)$$

$$\frac{d}{dt} \mathbf{P}(t|t_{i-1}) = \mathbf{F}(t)\mathbf{P}(t|t_{i-1}) + \mathbf{P}(t|t_{i-1})\mathbf{F}^T(t) + \mathbf{Q} \quad (101)$$

$$t_{i-1} \leq t \leq t_i$$

where  $\mathbf{F}(t)$  is a  $(n \times n)$  matrix obtained by linearizing  $\mathbf{f}[\hat{\mathbf{x}}_a(t|t_{i-1}), \mathbf{u}(t), t]$  about the best current estimate

$$\mathbf{F}(t) = \frac{\partial \mathbf{f}[\hat{\mathbf{x}}_a(t|t_{i-1}), \mathbf{u}(t), t]}{\partial \hat{\mathbf{x}}_a(t|t_{i-1})} \quad (102)$$

For the given system the  $\mathbf{F}(t)$  has the form

$$\mathbf{F}(t) = \begin{bmatrix} \theta_1(t) & \mathbf{x}(t) \\ 0 & 0 \end{bmatrix}$$

the measurement update equations:

$$\hat{\mathbf{x}}_a(i|i) = \hat{\mathbf{x}}_a(i|i-1) + \mathbf{K}(i)v(i) \quad (103)$$

$$\mathbf{P}(i|i) = [\mathbf{I} - \mathbf{K}(i)\mathbf{H}]\mathbf{P}(i|i-1) \quad (104)$$

where

$$v(i) = y(i) - H\hat{\mathbf{x}}_a(i|i-1) \quad (105)$$

$$\mathbf{K}(i) = \mathbf{P}(i|i-1)\mathbf{H}^T\mathbf{b}^{-1}(i) \quad (106)$$

$$\mathbf{b}(i) = \mathbf{H}\mathbf{P}(i|i-1)\mathbf{H}^T + r \quad (107)$$

The extension of the algorithm to a multivariable system and, therefore, to the aircraft state and parameter estimation, is straightforward. One of the first applications of the EKF to the estimation of

airplane stability and control derivatives was introduced in references 24 and 25. Because the EKF estimates are essentially the maximum likelihood estimates, the properties of the EKF estimator are identical to these mentioned in the preceding chapter. The disadvantage of the EKF method is that it requires knowledge of the a priori covariances which are unknown for the parameters. This can be one of the reasons why the EKF methods gives unreliable confidence limits on the parameter estimates. If the a priori values for the parameters are poor, the EKF method exhibits poor convergence or the failure to converge at all.

## 7. PARAMETER ESTIMATION IN FREQUENCY DOMAIN

Many of the early approaches to the extraction of aircraft parameters from flight data were based on measurement results presented in the frequency rather than time domain. Usually the measured frequency response curves were used because they provided good insight into the physics of the system and reduced data analysis to the use of simple algebra. With the availability of modern digital computers, the frequency domain for aircraft parameter estimation was almost forgotten and the measured data have been mostly analyzed in the time domain.

However, the recent attempts to identify an aeroelastic airplane with nonsteady aerodynamics, airplane flying in turbulence, and also the search for greater computing efficiency of estimation algorithms brought back the attention to the frequency domain. Reference 26 shows that it is possible to formulate the existing methods for airplane parameter estimation equally well in the frequency domain. For this formulation it is necessary to transform the model and the data and then formulate the cost function. The transformation is based on the Fourier integral. The Fourier transform pair associated with the variable has the form

$$\tilde{x}(j\omega) = \int_0^{\infty} x(t) \exp(-j\omega t) dt \quad (108)$$

$$x(t) = \frac{1}{2\pi} \int_{-\infty}^{\infty} \tilde{x}(j\omega) \exp(j\omega t) d\omega \quad (109)$$

where  $j = \sqrt{-1}$  and  $\omega$  is the angular frequency.

The least squares criterion for a scalar case can be written as the integral square error

$$J = \int_0^{\infty} [y(t) - x(t)]^2 dt \quad (110)$$

According to Parseval's theorem, there is a relationship between the squared magnitude of the Fourier transform pair

$$\int_0^{\infty} [x(t)]^2 dt = \frac{1}{2\pi} \int_{-\infty}^{\infty} |\tilde{x}(j\omega)|^2 d\omega \quad (111)$$

Applying this result to Equation (110), the frequency domain expression for  $J$  has the form

$$J = \frac{1}{2\pi} \int_{-\infty}^{\infty} [\tilde{y}(j\omega) - \tilde{x}(j\omega)]^2 d\omega \quad (112)$$

By separation of Equation (112) into real and imaginary parts the least square criterion is changed to

$$J = \frac{1}{2\pi} \{ [\text{Re } \tilde{y}(j\omega) - \text{Re } \tilde{x}(j\omega)]^2 + [\text{Im } \tilde{y}(j\omega) - \text{Im } \tilde{x}(j\omega)]^2 \} d\omega \quad (113)$$

where  $\text{Re}$  and  $\text{Im}$  denote the real and imaginary parts, respectively. Comparison of Equations (110) and (112) shows that  $J$  depends on the squared scalar deviation in the time domain, and on the squared vectorial deviation in the frequency domain.

Using again the first-order scalar system (4), its transformed form is

$$j\omega \tilde{x}(j\omega) = \theta_1 \tilde{x}(j\omega) + \tilde{u}(j\omega) \quad (114)$$

The cost function for the equation error is then formulated as

$$J(\theta) = \frac{1}{2} \sum_{n=1}^N | (j\omega_n - \theta_1) \tilde{x}(j\omega_n) - \tilde{u}(j\omega_n) |^2 \quad (115)$$

The least squares estimate of  $\theta_1$  is found from the equation

$$\hat{\theta}_1 \text{Re} \sum_{n=1}^N \tilde{x}(n) \tilde{x}^*(n) = \text{Re} \sum_{n=1}^N [j\omega_n \tilde{x}(n) \tilde{x}^*(n) - \tilde{u}(n) \tilde{x}^*(n)] \quad (116)$$

where  $\tilde{x}^*$  is complex conjugate to  $\tilde{x}$  and the notation  $\tilde{x}(n)$  and  $\tilde{u}(n)$  is used to indicate that these variables are functions of  $\omega_n$ .

For the output error method the cost function is

$$J(\theta) = \frac{1}{2} \sum_{n=1}^N [\tilde{y}(n) - \tilde{x}(n, \theta_1)] [\tilde{y}(n) - \tilde{x}(n, \theta_1)]^* \quad (117)$$

where

$$\tilde{y}(n) = \tilde{x}(n) + \tilde{v}(n)$$

The estimates are obtained by an iterative process as

$$\hat{\theta}_1 = \theta_{1N} + \Delta \hat{\theta}_1$$

where  $\Delta \hat{\theta}$  is computed from the equation

$$\sum_{n=1}^N [\tilde{y}(n) - \tilde{x}(n, \theta_1) - \frac{\partial \tilde{x}}{\partial \theta_1} \Delta \theta_1] \frac{\partial \tilde{x}^*}{\partial \theta_1} = 0$$

as

$$\Delta \hat{\theta}_1 = \left[ \text{Re} \sum_{n=1}^N \frac{\partial \tilde{x}}{\partial \theta_1} \frac{\partial \tilde{x}^*}{\partial \theta_1} \right]^{-1} \text{Re} \sum_{n=1}^N \frac{\partial \tilde{x}^*}{\partial \theta_1} [\tilde{y}(n) - \tilde{x}(n, \theta_1)] \quad (118)$$

The sensitivity equation is reduced to an algebraic expression of the form

$$j\omega \frac{\partial \tilde{x}}{\partial \theta_1} = \theta_1 \frac{\partial \tilde{x}}{\partial \theta_1} + \tilde{x} \quad (119)$$

The detailed development of various equation error method is presented in reference 27. The maximum likelihood method is formulated in reference 28 and applied to three problems of airplane parameter estimation. In this reference the advantages and disadvantages of the frequency domain parameter estimation are also discussed.

## 8. EXAMPLES

Three examples with comparisons of airplane parameter estimates from various methods are presented in a very concise form. Further details can be obtained from the pertinent references.

Example 1 (ref. 6):

The lateral responses of a general aviation airplane from eight runs were analyzed using the equation error, instrumental variable and maximum likelihood method. The measured data from one of the runs are plotted in Figure 6 together with the computed responses based on the ML estimates. The results are summarized in Table II which includes the ensemble averages and standard errors of the stability and control derivatives, and the average standard errors of the estimates from each method used. The comparison of the results indicates that there is no significant difference between the EE and ML estimates, perhaps with the exception of the less significant derivative  $C_{\delta_r}$ . This agreement in the average values of the

extracted derivatives could be due to high signal-to-noise ratio in the measured states (can improve the EE estimates) and some uncorrected modeling errors (may degrade the ML estimates). The IV estimates are close to those from the EE method. In some cases, however, the ensemble standard errors from the IV method are higher than those from the remaining two methods. This is in agreement with the observations that the IV estimates are consistent but less efficient than the EE estimates. The comparison of the ensemble standard errors and the average standard errors of the estimates reveals great differences, probably as the result of the small sample size (eight runs only) and modeling errors.

Example 2 (ref. 18):

In this example the effect of turbulence on the ML estimates of the longitudinal stability and control derivatives is shown. From the measurement in turbulent air the parameters were estimated with and without considering the process noise effect. The estimated parameter values are given in the two last columns of Table III. They are also compared in Table III with the results from the measurements in smooth air and from the wind tunnel data. The exclusion of turbulence effect from the model degrades the accuracy of the estimated parameters and also of the computed airplane responses. The last is apparent from the plots of measured and computed data in Figure 7.

Example 3 (ref. 25):

From measurements at high angles of attack the airplane parameters were estimated using the equation error and extended Kalman filter methods. The model was composed from the nonlinear equations of motion and nonlinear aerodynamic model equations, where some of the derivatives were represented by a polynomial approximation. Some of the results from different runs are plotted in Figure 8 and compared with the wind tunnel data. In Figure 8  $C_x$ ,  $C_z$ , and  $C_m$  are the static aerodynamic coefficients. The more complete set of results in reference 25 shows that the agreement between the estimates from both methods was satisfactory and that the estimates were close to the wind tunnel data.

## 9. CONCLUDING REMARKS

For the estimation of airplane parameters from transient flight data three groups of estimation techniques have been developed. They include the equation error method, output error method and two advanced statistical methods, that is, the maximum likelihood and extended Kalman filter method. The last two methods can solve the most general estimation problem which involves the extraction of airplane parameters for a nonlinear model from flight data containing the process and measurement noise. The extended Kalman filter method estimates simultaneously the airplane state variables and unknown parameters. A standard Kalman filter program can be applied for the estimation. The disadvantage of this method is that it requires good a priori values for the parameters and knowledge of the a priori covariances which are unknown for the parameters.

At present the maximum likelihood method is firmly established as the optimal method for parameter estimation. It consists of a combination of a Kalman filter (for linear equations of motion) or an extended Kalman filter (for nonlinear equations) for estimating the state, and a modified Newton-Raphson

iterative procedure for estimating the parameters. In general, the unknown parameters can include airplane stability and control derivatives, bias terms in the state and output equations, initial conditions for state variables, and measurement noise and process noise covariances. Provided that there are no modeling errors, the parameter estimates are consistent, and asymptotically unbiased, efficient and normal. The methods also provide the lower bound on the parameter covariances which can be viewed as the maximum achievable accuracy in the parameter estimates. The maximum likelihood method is simplified where the process noise is absent. Then the method is reduced to the output error method which minimizes the errors between the actual output and the model output by using the same input. The state estimates are obtained by the integration of the equations of motion only.

The simplest technique for airplane parameter estimation is the equation error method. It represents the application of linear regression to each equation of motion separately. Because of the measurement noise in the state and input variables, it gives biased estimates. To obtain consistent estimates, the instrumental variable method, which retains the simplicity of the least squares algorithm, might be used. This technique, however, reduces the efficiency of the estimated parameters. Its application in airplane identification may be, therefore, substantiated only in cases where extensive measurement noise in state variables is present.

It is possible to formulate the existing method for airplane parameter estimation equally well in the frequency domain. The measured data can be used in the form of transformed input and output time histories or frequency response curves. The frequency domain approach may be advantageous for the identification of an aeroelastic airplane or an airplane with nonsteady aerodynamics. It can also provide an algorithm with greater computing efficiency by replacing differential equations by simple algebraic expressions.

#### 10. REFERENCES

1. Greenberg, H.: A Survey of Methods for Determining Stability Parameters of an Airplane From Dynamic Flight Measurement. NACA TN 2340, 1951.
2. Shinbrot, M.: A Least-Squares Curve Fitting Method With Application to the Calculation of Stability Coefficients From Transient Response Data. NACA TN 2341, 1951.
3. Deutsch, R.: Estimation Theory. Prentice Hall, Englewoods Cliffs, N.J., 1965.
4. Gerlach, O. H.: Determination of Performance, Stability and Control Characteristics From Measurements in Non-Steady Maneuvers. Stability and Control--Part 1, AGARD CP No. 17, September 1966, pp. 499-523.
5. Howard, J.: The Determination of Lateral Stability and Control Derivatives From Flight Data. Can. Aeronaut. & Space J., Vol. 13, No. 3, March 1967, pp. 126-134.
6. Klein, V.: Determination of Stability and Control Parameters of a Light Airplane From Flight Data Using Two Estimation Methods. NASA TP-1306, 1979.
7. Wong, K. Y.; and Polak, E.: Identification of Linear Discrete Time Systems Using the Instrumental Variable Method. IEEE Trans. on Aut. Control, Vol. AC-12, No. 6, December 1967, pp. 707-718.
8. Van den Boom, A. J. W.: On the Relation Between Weighted Least-Squares Estimators and Instrumental Variable Estimators. IFAC 4th Symp. on Ident. and System Param. Est., U.S.S.R., September 1976, pp. 457-466.
9. Gupta, N. K.; and Mehra, R. K.: Computational Aspects of Maximum Likelihood Estimation and Reduction in Sensitivity Function Calculations. IEEE Trans. on Aut. Control, Vol. AC-19, No. 6, December 1974, pp. 774-783.
10. Waterfall, A. P.: A Technique for the Automatic Digital Analysis of Flight Dynamic Response Data. ARC R&M 3699 (RAE Techn. Report 70228), 1970.
11. Iliff, K. W.; and Taylor, L. W., Jr.: Determination of Stability Derivatives From Flight Data Using a Newton-Raphson Minimization Technique. NASA TN D-8514, 1972.
12. Grove, R. D.; Bowles, R. L.; and Mayhew, S. C.: A Procedure for Estimating Stability and Control Parameters From Flight Test Data by Using Maximum Likelihood Methods Employing a Real-Time Digital System. NASA TN D-6735, 1972.
13. Klein, V.: Parameter Identification Applied to Aircraft, Cranfield Report Aero No. 26, 1974.
14. Fisher, R. A.: Contributions to Mathematical Statistics. John Wiley & Sons, 1950.
15. Bryson, R. E., Jr.; and Ho, Y. Ch.: Applied Optimal Control. Ginn and Company, 1969.
16. Mehra, R. K.: Identification of Stochastic Linear Dynamic Systems Using Kalman Filter Representation. AIAA Journal, Vol. 9, No. 1, January 1971.
17. Schulz, G.: Maximum Likelihood Identification Using Kalman Filtering Least-Squares Estimation. A Comparison for the Estimation of Stability Derivatives Considering Gust Disturbances. DLR-FB 75-94, 1975 (English translation: European Space Agency TT 258).
18. Iliff, K. W.: Identification of Aircraft Stability and Control Derivatives in the Presence of Turbulence. In: NASA TN D-7647, 1974, pp. 77-113.
19. Mehra, R. K.: Identification in Control and Econometrics; Similarities and Differences. Division of Engineering and Applied Physics, Harvard University, Cambridge, Massachusetts, Techn. Rept. No. 647, 1973.

20. Stephner, D. E.; and Mehra, R. K.: Maximum Likelihood Identification and Optimal Input Design for Identifying Aircraft Stability and Control Derivatives. NASA CR-2200, 1973.
21. Hall, W. E., Jr.; and Gupta, N. K.; and Smith, R. G.: Identification of Aircraft Stability and Control Coefficients for the High Angle of Attack Regime. System Control, Inc., Palo Alto, California, Techn. Rept. No. 2, 1974.
22. Kashyap, R. L.: Maximum Likelihood Identification of Stochastic Linear Systems. IEEE Trans. on Aut. Control, Vol. AC-15, No. 1, February 1970.
23. Eykhoff, P.: System Identification. Parameter and State Estimation. John Wiley & Sons, 1974.
24. Chen, R. T. N.; Eulrich, B. J.; and Lebacqz, J. V.: Development of Advanced Techniques for the Identification of V/STOL Aircraft Stability and Control Parameters. Cornell Aeronautical Lab., Inc., Rept. No. BM-2820-F-1, 1971.
25. Eulrich, B. J.; and Rynaski, E. G.: Identification of Nonlinear Aerodynamic Stability and Control Parameters at High Angle of Attack. In: AGARD-CP-172, 1975, pp. 2-1 - 2-15.
26. Klein, V.: Aircraft Parameter Estimation in Frequency Domain. 1978 AIAA Atmospheric Flight Mechanics Conference, August 7-9, 1978, Palo Alto, California.
27. Gupta, N. K.: New Frequency Domain Methods for System Identification. 1977 Joint Automatic Control Conference, pp. 804-808.
28. Klein, V.; and Keskar, A. D.: Frequency Domain Identification of a Linear System Using Maximum Likelihood Estimation. IFAC 5th Symp. on Ident. and System Param. Est., Darmstadt, FRG, September 1979.

TABLE I. - COST FUNCTIONS, INNOVATIONS AND COVARIANCE MATRICES OF INNOVATIONS FOR VARIOUS ESTIMATION METHODS

Method	Cost Function, $J(\theta)$	Innovations, $v(i)$	Covariance matrix of innovations
Maximum likelihood	$\frac{1}{2} \sum_{i=1}^N v^T(i, \theta) B(i, \theta) v(i, \theta) + \frac{N}{2} \log  B(i, \theta) $	$y(i) - H\hat{x}(i/i-1) - Du(i)$	$B(i)$
Maximum likelihood with steady state Kalman filter	$\frac{1}{2} \sum_{i=1}^N v^T(i, \theta) B v(i, \theta) + \frac{N}{2} \log  B $		$B$
Maximum likelihood with no process noise or output error	$\frac{1}{2} \sum_{i=1}^N v^T(i, \theta) R v(i, \theta) + \frac{N}{2} \log  R $	$y(i) - H\hat{x}(i) - Du(i)$	$R$
Equation error	$\frac{1}{2} \sum_{i=1}^N v_j^2(i)$ $j=1, 2, \dots, n$	$y_j(i) - \hat{x}_j(i)$ $j=1, 2, \dots, n$	$\sigma_j^2$

TABLE II. - PARAMETERS AND THEIR STANDARD ERRORS ESTIMATED FROM EIGHT REPEATED MEASUREMENTS USING THREE ESTIMATION METHODS

Parameter	Equation error method			Instrumental variable method			Maximum likelihood method		
	Mean Value $\bar{u}$	Standard errors		Mean Value $\bar{u}$	Standard errors		Mean Value $\bar{u}$	Standard errors	
		s (u)	c (u)		s (u)	s (v)		s (u)	s (v) lower bound (v)
	(a)	(b)	(c)	(a)	(b)	(c)	(a)	(b)	(c)
$C_{Y_R}$	-0.647	0.012	0.0061	-0.708	0.035	.0063	-0.649	0.0097	0.0064
$C_{Y_P}$	-.04	.093	.016	-.05	.17	.046	-.09	.12	.016
$C_{Y_{\delta r}}$	.097	.011	.0065	.174	.019	.0085	.094	.014	.0068
$C_{l_{\beta}}$	-.0810	.0025	.0025	-.0815	.0038	.0019	-.0816	.0042	.00079
$C_{l_P}$	-.532	.018	.018	-.549	.028	.014	-.559	.053	.0055
$C_{l_r}$	.16	.040	.016	.14	.038	.012	.13	.027	.0053
$C_{l_{\delta a}}$	-.227	.010	.0065	-.233	.013	.0050	-.241	.022	.0018
$C_{l_{\delta r}}$	.015	.0051	.0036	.011	.0057	.0025	.007	.0068	.0012
$C_{n_R}$	.0745	.0043	.00090	.0724	.0081	.00087	.0772	.0055	.00031
$C_{n_P}$	-.042	.029	.0064	-.086	.018	.0062	-.024	.031	.0028
$C_{n_r}$	-.130	.017	.0059	-.129	.014	.0057	-.145	.030	.0022
$C_{n_{\delta a}}$	.019	.0087	.0022	.002	.0064	.0024	.024	.0096	.0016
$C_{n_{\delta r}}$	-.072	.0031	.0013	-.075	.0090	.0012	-.074	.0073	.00060

<sup>a</sup>Ensemble mean value.

<sup>b</sup>Ensemble standard error.

<sup>c</sup>Average standard error of estimates.

TABLE III. - STABILITY AND CONTROL PARAMETERS ESTIMATED BY MAXIMUM LIKELIHOOD METHOD UNDER DIFFERENT CONDITIONS

Parameter	Wind tunnel	Smooth Air	Turbulent air	
		ML estimate	ML estimate	
			no process noise	with process noise
$Z_{\alpha}$	-1.60	-1.94	-1.08	-1.55
$M_{\alpha}$	-7.79	-11.31	-4.79	-8.02
$M_{\beta}$	-1.31	-1.75	-.77	-2.30
$Z_{\delta e}$	-.123	-.093	-.037	-.079
$M_{\delta e}$	-9.75	-9.87	-5.79	-8.46

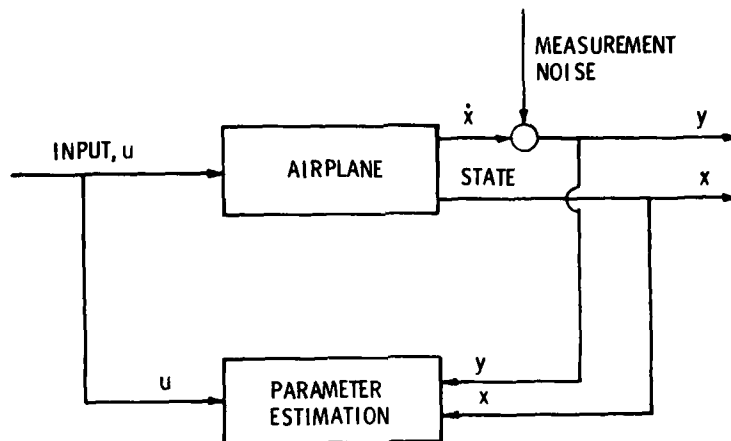


Figure 1. - Computing scheme for parameter estimation using equation error method.

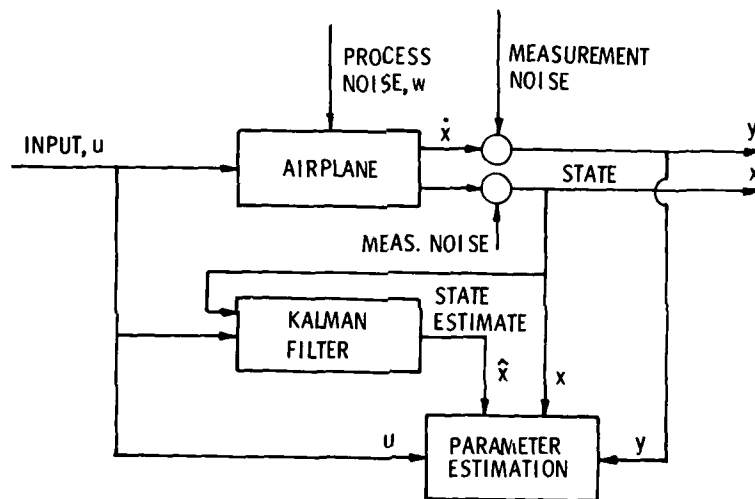


Figure 2. - Computing scheme for parameter estimation using instrumental variable method.

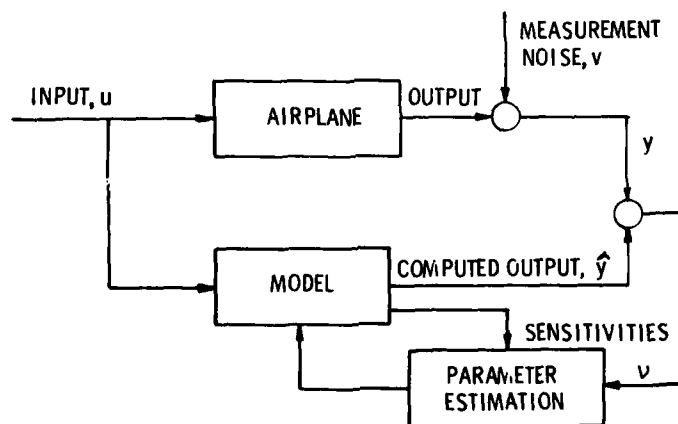


Figure 3. - Computing scheme for parameter estimation using output error method.



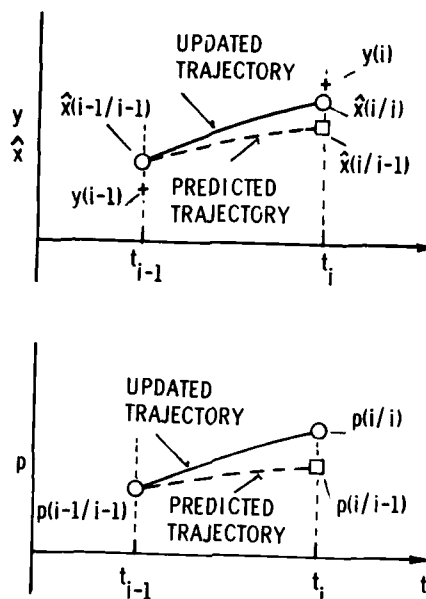


Figure 4. - Computing scheme for Kalman filter.

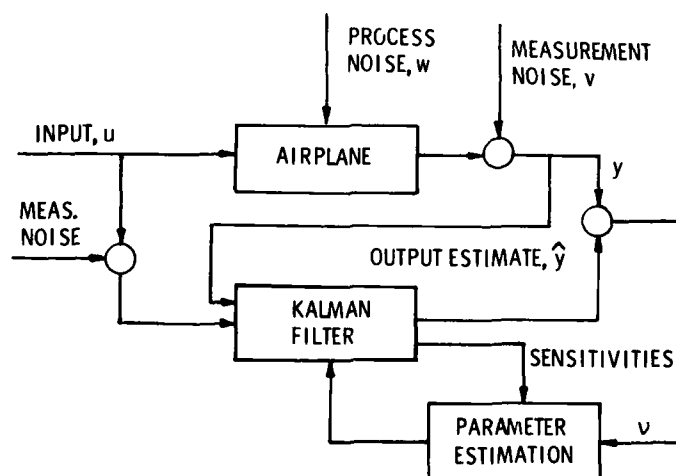


Figure 5. - Computing scheme for parameter estimation using maximum likelihood method.

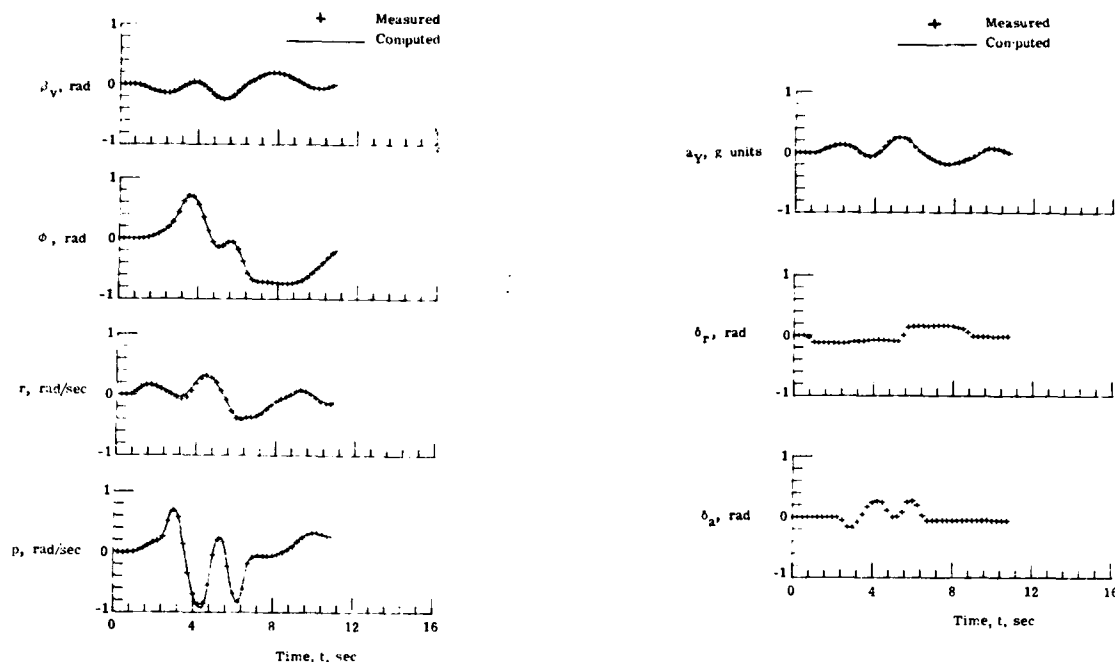


Figure 6. - Measured lateral flight data time histories and those computed by using parameters obtained by maximum likelihood method. (Reference 6.)

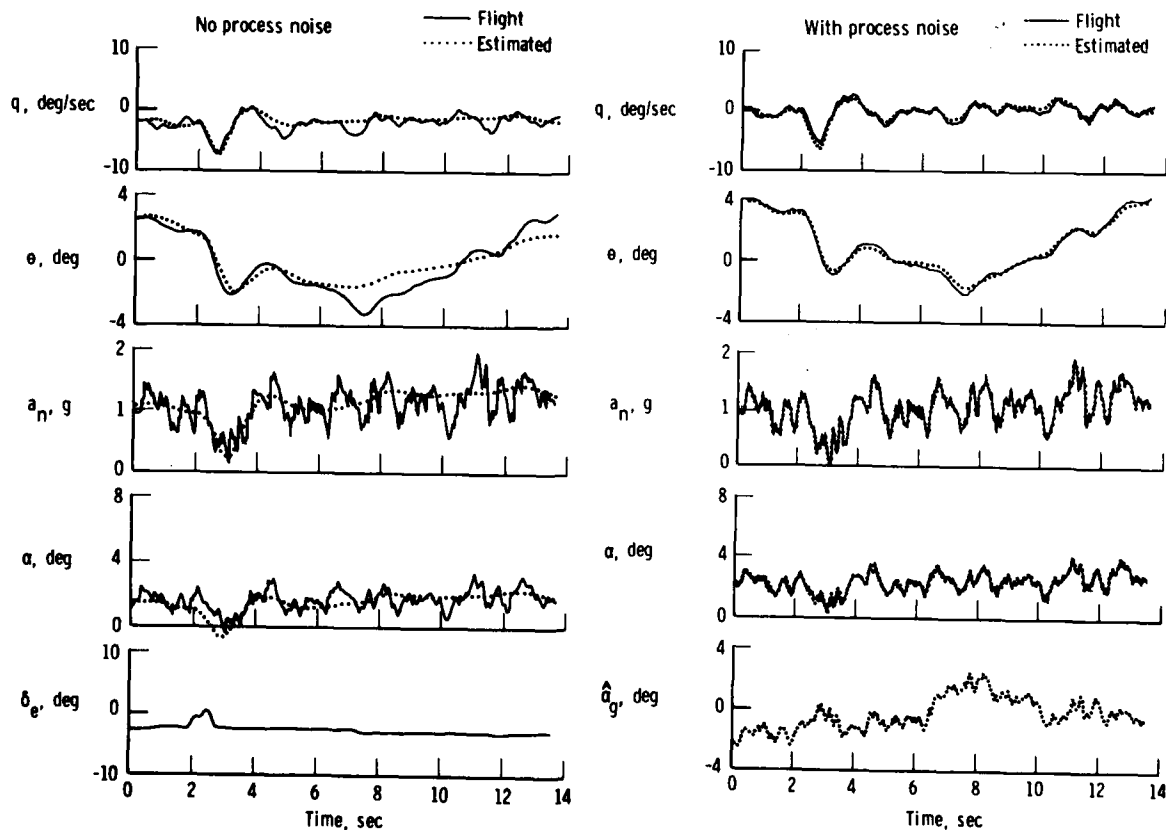


Figure 7. - Measured longitudinal flight data, and those computed by using parameters obtained by maximum likelihood method. (Reference 18.)

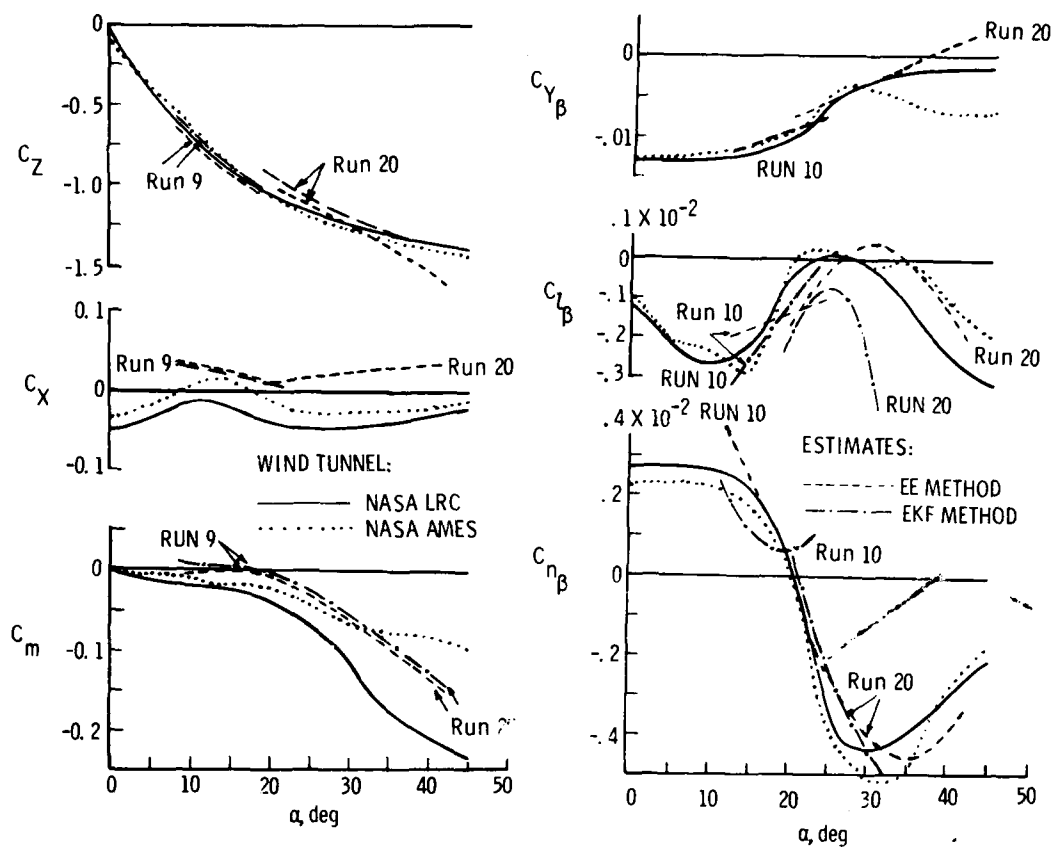


Figure 8. - Comparison of wind tunnel results with parameters estimated from flight data using equation error and maximum likelihood method. (Reference 25.)

## PRACTICAL INPUT SIGNAL DESIGN

by

E. Plaetschke

DFVLR-Institut für Flugmechanik

D-3300 Braunschweig-Flughafen, GERMANY

and

G. Schulz

DFVLR-Institut für Dynamik der Flugsysteme

D-8031 Oberpfaffenhofen, GERMANY

## SUMMARY

This paper considers the design of optimal inputs for identifying stability and control derivatives of the longitudinal and lateral motion of an aircraft. First the purpose of input optimization, the constraints and an overview of the literature is presented. Then two different procedures of input design are treated in more detail. Starting with investigations in the frequency domain the first method yields a multistep input signal, which fulfills specific spectral requirements. Compared with the power spectral densities of the commonly used doublet and single step input, this multistep input has a larger bandwidth. The second way of input design is based on the optimization of different measures of the Fisher information matrix, such as determinant or trace. Depending on the measure used, the designed signals differ with respect to their spectral composition. The discussed input signals, which were used in a flight test program, are compared respect to the achieved accuracy of the identified stability and control derivatives.

## 1. INTRODUCTION

The determination of aircraft stability and control derivatives is of growing importance in the design, testing and certification of modern aircrafts. The greater need for these derivatives has the following reasons:

- (1) They are used to provide model parameters for ground and in-flight aircraft simulators.
- (2) They serve as a basis for the design of flight control systems.
- (3) They define a given aircraft and can be used as quality criteria such as response mode criteria in Flying Qualities Military Specification MIL-F-8785.

Within the procedure of aircraft parameter identification the phase of input design is the first step. Thereby the limitations of the following steps - as there are: selection of the instrumentation system, flight testing under constraints and disturbances, choice of an appropriate identification algorithm - have to be taken into account. During the design phase of test signals the following aspects are of importance:

- (1) The inputs have to excite the modes and parameters of the aircraft appropriately, such that parameter variations cause variations of the measured time response (Sensitivity).
- (2) The amplitude, bandwidth and slope of the input signals have to be bounded, such that first, the signals are realizable by the specific actuators (Realizability), and second, the motion of the aircraft remains within the flight region to be identified (Linearity).
- (3) The noise characteristics and bandwidth of the measuring instruments as well as of the disturbance processes (gusts) have to be considered (Noise characteristics).
- (4) For optimal test signal design good a priori models of the aircraft motion have to be available as to minimize the estimation error variance of the derivatives (A priori model).

The theory of optimal input signal design started with the investigations of Levin [1], Litmann and Huggins [2], and Levadi [3]. The optimization of the Cramér-Rao lower bound, respectively the Fisher information matrix and the estimation error variance was investigated by Aoki and Staley [4], Nahi and Wallis [5], and Nahi and Napjus [6]. The application of optimal input design to the determination of aircraft stability and control derivatives started with the work of Gerlach [7,8] and was strongly influenced in the seventies by the work of Mehra et al. [9,10,11,12]. For detailed lists of references see [11,12].

The design of test signals can be performed in the frequency domain and in the time domain considering system criteria and estimation error criteria. This paper is organized to cover these aspects. After the introductory remarks the "Design of Multistep Input Signals by Frequency Analysis" is presented in section 2. The "Design of Continuous Input Signals by Estimation Error Analysis" is then shown in section 3. A "Comparison of Input Signals in Flight Test", based on an extensive flight test program for aircraft parameter identification, is presented in section 4. This flight test program is being performed in cooperation

between the Delft University of Technology (DUT), the Nationaal Lucht- en Ruimtevaartlaboratorium (NLR, Dutch National Aerospace Laboratory) and the Deutsche Forschungs- und Versuchsanstalt für Luft- und Raumfahrt (DFVLR, German Aerospace Research Establishment), Institut für Flugmechanik. The research aircraft is a de Havilland DHC-2 Beaver.

## 2. DESIGN OF MULTISTEP INPUT SIGNALS BY FREQUENCY ANALYSIS

In this section a practical method for designing optimal inputs is presented which is based on the spectral behaviour of the system. Making use of the Bode diagram one can investigate how the identifiability of the derivatives depends on the frequency of the input signal and which frequencies the input should include for the determination of definite derivatives. Then a multistep input is designed which will excite the aircraft in the required frequency domain.

### 2.1 IDENTIFIABILITY INVESTIGATIONS

The investigation method which will be described here was developed by M. Marchand [13]. We restrict ourselves to the analysis of the longitudinal motion which is represented by the following linearized equations of motion

$$\dot{u} + g\theta - X_u u - X_\alpha \alpha = 0 \quad (2.1)$$

$$\dot{\alpha} - q - Z_u u - Z_\alpha \alpha - Z_{\delta_e} \delta_e = 0 \quad (2.2)$$

$$\dot{q} - M_u u - M_\alpha \alpha - M_q q - M_{\delta_e} \delta_e = 0 \quad (2.3)$$

The identifiability of the derivatives can be investigated using Bode plots in which the frequency response magnitudes of the various terms of the Eqs. (2.1) - (2.3) are plotted as functions of the input signal frequency. As an example, the Figures 1-3 show the frequency response magnitude curves for the Beaver aircraft in horizontal symmetric flight at 45 m/s. The meaning of these plots will be explained for the moment equation (2.3). Figure 3 contains the frequency response magnitudes of the resulting pitch acceleration  $\dot{q}$  (inertial term, dashed line) and of the individual terms  $M_u u$ ,  $M_\alpha \alpha$ ,  $M_q q$  and  $M_{\delta_e} \delta_e$  (control term, solid line) with respect to an elevator input  $\delta_e$ . This means that the curves represent the expressions

$$|\dot{q}(\omega)/\delta_e(\omega)|, |M_u \tilde{u}(\omega)/\delta_e(\omega)|, \dots, |M_{\delta_e}|$$

where  $\sim$  denotes the Fourier transform.

From such a plot the identifiability of the derivatives can be estimated. If at a given frequency the magnitude of a term is large compared with the other terms, it has a great influence within the equation of motion. Its derivative is well identifiable at this frequency. If a term has a small influence, its derivative can not be identified. As a rule of thumb, a derivative is considered to be identifiable when its term has a magnitude of at least 10 % of the largest terms's magnitude.

If the inertial term is small only ratios of the derivatives can be determined. As can be seen from Figure 3, the inertial term  $\dot{q}$  as well as the term  $M_q q$  are negligible in the lower frequency domain. Eq. (2.3) then can be written as

$$-M_u u - M_\alpha \alpha - M_{\delta_e} \delta_e = 0.$$

From this equation only two ratios, e.g.  $M_u/M_{\delta_e}$  and  $M_\alpha/M_{\delta_e}$  can be determined.

The same considerations as for the moment equation can be done for the X- and Z-force equation. In Figure 4 the frequency regions are plotted in which the different derivatives are identifiable. Solid lines represent those regions where the derivatives are directly identifiable. When only ratios are obtainable the lines are dashed.

As can be seen, most of the derivatives are identifiable in the surroundings of the natural frequencies. The lower part of Figure 4 shows these two regions and the derivatives which can be identified there. Those derivatives, which are obtainable only as ratios, are put in parentheses.

## 2.2 DESIGN OF OPTIMAL MULTISTEP INPUTS

After the identifiability regions have been determined the problem is to find input signals which will excite the aircraft in the required frequency domains. Moreover, the signal should have a shape as simple as possible, such that it can be realized in flight by the pilot. A procedure that optimizes a sequence of step functions was developed by R. Koehler [14]. The aim of the optimization is to find a signal the power of which should be distributed uniformly over a wide frequency range (bandpass character with large bandwidth).

In Figure 5 such an optimized multistep input and its power spectral density is presented. Because of its characteristic shape it is called "3211"-signal (3 time units positive, 2 negative, 1 positive, and 1 negative). As can be seen from the power spectral density curve it is a relatively wide-band signal and can effectively excite the aircraft over a decade of frequency. By the choice of the time unit  $\Delta t$  the spectrum can be shifted to match the identifiability regions.

For comparison Figure 5 shows two further inputs, step and doublet. As the step contains energy only at lower frequencies it can not excite the higher frequency natural modes. On the other hand, the aircraft rapidly departs from the linear flight regime when excited by the step. For these reasons the step is unfit for parameter identification. The doublet excites a particular band at a higher frequency. By the choice of  $\Delta t$  the peak of the power spectral density can be shifted to the range of the higher frequency natural oscillations. However, the natural frequencies are not known exactly since they are calculated from the a-priori-values of the derivatives. On the other hand they may vary due to a change of the flight conditions. As the doublet is a relatively narrow-band signal it may happen that the natural modes are not excited effectively.

These difficulties do not occur when the aircraft is excited by a wide-band signal like the "3211"-input. This input has been used for years at the DFVLR Institut für Flugmechanik for aircraft and rotorcraft parameter identification. In some cases it was generated by the pilot and in other cases it was directly transmitted from a tape into the control system. Figure 6 shows that a pilot needs some training to realize the signal.

## 3. DESIGN OF CONTINUOUS INPUT SIGNALS BY ESTIMATION ERROR ANALYSIS

In contrast to the investigations in section 2, the problem of input design is now solved directly by minimizing the estimation error variance of the parameters by means of an appropriate choice of the input signal characteristics. To show the correlation between the estimation error variance and the aircraft response due to a control input, the Cramér-Rao lower bound is first derived.

Theorem: Let  $p(Y|a)$  be the conditional probability density function of the measurement sequence  $Y$  given the single parameter  $a$ ,  $E\{\dots\}$  the expectation value, and  $\text{var}[\dots]$  the variance. If  $\hat{a}(Y)$  is any unbiased estimate of  $a$ , then

$$\text{var}[\hat{a}(Y) - a] \geq E \left\{ \left[ \frac{\partial \ln p(Y|a)}{\partial a} \right]^2 \right\}^{-1} \quad (3.1)$$

or equivalently

$$\text{var}[\hat{a}(Y) - a] \geq - E \left\{ \frac{\partial^2 \ln p(Y|a)}{\partial a^2} \right\}^{-1} \quad (3.2)$$

where the following derivatives

$$\frac{\partial p(Y|a)}{\partial a} \quad \text{and} \quad \frac{\partial^2 p(Y|a)}{\partial a^2} \quad (3.3)$$

exist and are absolutely integrable.

The proof is an application of the Schwarz inequality. Because  $\hat{a}(Y)$  is unbiased

$$E\{\hat{a}(Y) - a\} = \int_{-\infty}^{\infty} [\hat{a}(Y) - a] p(Y|a) dY = 0.$$

Differentiating with respect to the parameter  $a$ , considering condition (3.3) yields

$$-\int_{-\infty}^{\infty} p(Y|a) dY + \int_{-\infty}^{\infty} [\hat{a}(Y) - a] \frac{\partial p(Y|a)}{\partial a} dY = 0.$$

By definition the first integral has a value of 1. Using

$$\frac{\partial p(Y|a)}{\partial a} = \frac{\partial \ln p(Y|a)}{\partial a} \cdot p(Y|a)$$

one gets

$$\int_{-\infty}^{\infty} [\hat{a}(Y) - a] \frac{\partial \ln p(Y|a)}{\partial a} p(Y|a) dY = 1$$

Rewriting the integral

$$\int_{-\infty}^{\infty} [\hat{a}(Y) - a] \sqrt{p(Y|a)} \cdot \frac{\partial \ln p(Y|a)}{\partial a} \sqrt{p(Y|a)} dY = 1$$

and using the Schwarz inequality we have

$$\int_{-\infty}^{\infty} [\hat{a}(Y) - a]^2 p(Y|a) dY \cdot \int_{-\infty}^{\infty} \left[ \frac{\partial \ln p(Y|a)}{\partial a} \right]^2 p(Y|a) dY \geq 1, \quad (3.4)$$

where the equality sign holds for:

$$\frac{\partial \ln p(Y|a)}{\partial a} = [\hat{a}(Y) - a] \cdot k(a). \quad (3.5)$$

The left hand integral of (3.4) is the above-stated estimation error variance:

$$E \{ [\hat{a}(Y) - a]^2 \} \geq E \left\{ \left[ \frac{\partial \ln p(Y|a)}{\partial a} \right]^2 \right\}^{-1}.$$

The second inequality in the theorem is obtained by differentiating

$$\int_{-\infty}^{\infty} p(Y|a) dY = 1$$

twice with respect to  $a$ , which together with condition (3.3) yields

$$E \left\{ \frac{\partial^2 \ln p(Y|a)}{\partial a^2} \right\} = - E \left\{ \left[ \frac{\partial \ln p(Y|a)}{\partial a} \right]^2 \right\}.$$

Comments on the theorem:

1. Any unbiased estimate has a variance greater than or equal to a certain number.
2. If the equality sign of Eq. (3.1) respectively (3.2) is fulfilled, the estimate is called an efficient estimate (minimum variance estimate). The maximum likelihood estimate can be shown to be an efficient estimate. It is defined by the likelihood equation

$$\left. \frac{\partial \ln p(Y|a)}{\partial a} \right|_{a = \hat{a}_{ML}(Y)} = 0.$$

If  $\hat{a}(Y) = \hat{a}_{ML}(Y)$ , then

$$\left. [\hat{a}(Y) - a] \cdot k(a) \right|_{a = \hat{a}_{ML}(Y)} = 0,$$

such that Eq. (3.5) is fulfilled for maximum likelihood estimates.

3. If an efficient estimate does not exist, we do not know how close the variance of the estimate will approach the given bound.

In the multi-parameter case the estimation error variance is given by

$$\text{var} [\hat{a}_i(Y) - a_i] \geq (J^{-1})_{ii}, \quad (3.6)$$

where  $J$  is the Fisher information matrix, the elements of which are derived as

$$\begin{aligned} J_{ij} &= E \left\{ \frac{\partial \ln p(Y|a)}{\partial a_i} \cdot \frac{\partial \ln p(Y|a)}{\partial a_j} \right\} \\ &= - E \left\{ \frac{\partial^2 \ln p(Y|a)}{\partial a_i \partial a_j} \right\}. \end{aligned} \quad (3.7)$$

If an efficient estimate exists, the inverse of the Fisher information matrix  $J$  is equal to the estimation error covariance matrix  $P$ .

As shown by Nahi and Napjus [6], different measures of the Fisher information matrix can be chosen as criteria for the design of optimal input signals  $u(t)$ . Since the volume of the estimation error ellipsoid  $V \sqrt{\det(P)}$  is a convenient measure of the concentration of the probability density about its mean, the minimization of the determinant of the estimation error covariance matrix gives a relevant optimization criterion:

$$\text{I:} \quad \min_{u(t)} \{\det(P)\} \Rightarrow u_{\text{opt}}(t).$$

This minimization is equivalent to the maximization of the determinant of the Fisher information matrix

$$\text{II:} \quad \max_{u(t)} \{\det(J)\} \Rightarrow u_{\text{opt}}(t)$$

as  $\det(J) = 1/\det(P)$ . Other performance measures are the sum or the product of the diagonal elements of the above matrices:

$$\text{III:} \quad \max_{u(t)} \{\text{tr}(J)\} \Rightarrow u_{\text{opt}}(t)$$

$$\text{IV:} \quad \min_{u(t)} \{\text{tr}(P)\} \Rightarrow u_{\text{opt}}(t)$$

$$\text{V:} \quad \min_{u(t)} \left\{ \prod_i P_{ii} \right\} \Rightarrow u_{\text{opt}}(t)$$

In this paper the criteria II, III and IV are used for input design.

The computational burden of the application of these estimation error criteria lies in the problem of expressing the elements of the Fisher information matrix as functions of the input signal  $u(t)$  and the optimization with respect to the characteristic values of the input signal under given constraints.

Let the motion of the aircraft be described by the following system:

$$\dot{x}(t) = F(a) x(t) + G(a) u(t) \quad ; \quad x(0) = 0$$

$$y(t) = H(a) x(t) + v(t) \quad ; \quad 0 \leq t \leq T$$

where  $x$  represents the state vector,  $u$  the input vector (elevator, rudder, aileron, thrust throttle...),  $y$  the measurement vector and  $v$  the measurement noise vector.  $v(t)$  is assumed to be uncorrelated Gaussian white noise with zero mean and covariance matrix  $R_c$  (respectively

$R$  in the discrete time case). The stability and control derivatives to be identified are in a linear or nonlinear manner elements of the matrices  $F$ ,  $G$  and  $H$ . Nahi and Wallis [5] have shown that using the sensitivity equations

$$\frac{\partial \dot{x}(t)}{\partial a_i} = F(a) \frac{\partial x(t)}{\partial a_i} + \frac{\partial F(a)}{\partial a_i} x(t) + \frac{\partial G(a)}{\partial a_i} u(t)$$

$$\frac{\partial y(t)}{\partial a_i} = H(a) \frac{\partial x(t)}{\partial a_i} + \frac{\partial H(a)}{\partial a_i} x(t)$$



the  $(i,j)$ -th element of the Fisher information matrix can be expressed as

$$J_{ij} = \int_0^T \left[ \frac{\partial y(t)}{\partial a_i} \right]^T R_c^{-1} \frac{\partial y(t)}{\partial a_j} dt.$$

In the discrete time case we have

$$J_{ij} = \sum_{k=0}^N \left[ \frac{\partial Y(k)}{\partial a_i} \right]^T R^{-1} \frac{\partial Y(k)}{\partial a_j}.$$

The different methods of optimizing certain performance measures of the Fisher information matrix under practical constraints are now investigated in more detail.

### 3.1 MAXIMIZATION OF THE TRACE OF THE INFORMATION MATRIX

For the determination of the time histories of the input signal for a discrete time model, the following optimization was performed:

$$\max_{u \in U} \{ \text{tr}(J) \} \Rightarrow u_N \text{ opt}$$

with  $u_N^T = [u(0), u(1), \dots, u(N-1)]$  under the energy constraint

$$\sum_{k=0}^{N-1} u^2(k) \leq E.$$

Consider a single input linear discrete-time system

$$x(k+1) = \Phi(a) x(k) + \Gamma(a) u(k) \quad ; \quad x(0) = 0 \quad (3.8)$$

$$y(k) = H(a) x(k) + v(k) \quad ; \quad k = 0, 1, \dots, N-1 \quad (3.9)$$

where  $x$  is a  $n \times 1$  state vector,  $u$  is the single input,  $y$  is a  $m \times 1$  output vector and  $v$  is a  $m \times 1$  measurement noise vector.  $\Phi$ ,  $\Gamma$  and  $H$  are matrices of appropriate dimensions and contain  $q$  unknown parameters  $a$ . It is assumed that  $v(k)$  is an uncorrelated Gaussian white noise sequence with zero mean and covariance matrix  $R$ . For the above system the  $(i,j)$ -th element of the information matrix is determined as

$$J_{ij} = u_N^T A_i W^{-1} A_j u_N$$

where

$$A_i = \begin{bmatrix} H_1^* \Gamma_1^* & & & 0 \\ & \ddots & & \\ & & H_1^* \Phi_1^{*N-1} \Gamma_1^* & \\ & & & H_1^* \Gamma_1^* \end{bmatrix}, \quad W = \begin{bmatrix} R & & \\ & R & \\ & & \ddots \\ & & & R \end{bmatrix},$$

$$H_1^* = \left[ \frac{\partial H}{\partial a_i}, H \right], \quad \Gamma_1^* = \begin{bmatrix} \Gamma \\ \frac{\partial \Gamma}{\partial a_i} \end{bmatrix}, \quad \Phi_1^* = \begin{bmatrix} \Phi & 0 \\ \frac{\partial \Phi}{\partial a_i} & \Phi \end{bmatrix}.$$

The overall optimization criterion then reads as (ref. Schulz [15])

$$\text{tr}(J) = u_N^T \left[ \sum_{i=1}^q A_i^T W^{-1} A_i \right] u_N$$

under the constraint

$$u_N^T u_N \leq E.$$

Following Brockett [16], the maximal value of the above quadratic form with the given constraint is obtained as the normalized eigenvector  $\xi$  that belongs to the maximum eigenvalue of the expression inside the brackets:

$$u_N = \sqrt{E} \xi \left\{ \lambda_{\max} \left[ \sum_{i=1}^q A_i^T W^{-1} A_i \right] \right\}.$$

Using this design criterion, input signals were determined for different flight conditions of the Beaver aircraft. As an example Figure 7 shows an elevator-input which was optimized for the identification of the derivatives in the short-period mode ( $C_{X\alpha}$ ,  $C_{Z\alpha}$ ,  $C_{Zq}$ ,  $C_{Z\delta e}$ ,  $C_{m\alpha}$ ,  $C_{mq}$ ,  $C_{m\delta e}$ ) at an airspeed of 45 m/s. This input will lateron be referred to as Schulz-signal.

### 3.2 MINIMIZATION OF THE TRACE OF THE ESTIMATION ERROR COVARIANCE MATRIX

At the Department of Aerospace Engineering of the Delft University of Technology (DUT) an optimal single input was designed as a sum of sine-functions (cf. Mulder [17]):

$$u(t) = \sum_{i=1}^m k_i \sin \omega_i t.$$

At the beginning and at the end of the test period the input should be zero. This requirement is fulfilled when the frequencies are chosen to be

$$\omega_i = i \cdot 2\pi/T \quad (i = 1, \dots, m)$$

where  $T$  is the length of the test period. Moreover, the total energy of the input should be restricted:

$$\int_0^T u^2 dt = \frac{1}{2} T \cdot \sum_{i=1}^m k_i^2 = E. \quad (3.10)$$

The input can now be optimized by the choice of the  $m$  amplitudes  $k_i$  with regard to the energy constraint.

The energy constraint (3.10) can be considered as the equation of an  $m$ -dimensional sphere with central point at the origin and with radius  $R = \sqrt{2E/T}$ . Thus each combination of the  $m$  amplitudes  $k_i$  can be represented as a point on the sphere. Introducing spherical coordinates each point is defined by  $m-1$  coordinates. By this the number of variables is reduced from  $m$  to  $m-1$ .

The optimization of the input signal was carried out to minimize the trace of the estimation error covariance matrix

$$CF = \text{tr} (P) \quad (3.11)$$

For the minimization of this criterion function the gradient method of Powell was used.

As an example consider an optimal elevator input for the identification of the derivatives in the short-period mode of the Beaver aircraft at 45 m/s. The input was designed for a test duration of  $T = 10$  s. Its total energy was constrained to  $E = 0.01 \text{ rad}^2 \text{ s}$ . As the criterion function (3.11) depends on the number  $m$  of sine-functions of the input it was minimized for different  $m$ . It was found that the minimum values of  $CF$  decrease with increasing  $m$  but remain practically constant for  $m > 8$ . Therefore an input signal with  $m = 8$  sine-functions was selected for further investigations.

When this optimized input was used for simulation it turned out that at the end of the test period some of the state variables had excessively large deviations from the nominal flight conditions. To avoid this a penalty function was added to the criterion function (3.11) resulting in a new criterion function:

$$\overline{CF} = \text{tr} (P) + (0.001 u^2 + 0.1 \alpha^2 + 0.1 \gamma^2)_{t=T}. \quad (3.12)$$

An optimized input which minimizes (3.12) is shown in Figure 8. In the upper part the powers  $k_i^2$  are plotted over the 8 discrete frequencies. As can be seen only two frequencies are really significant. The lower part of Figure 8 shows the time history of the input signal.

### 3.3 MAXIMIZATION OF THE DETERMINANT OF THE INFORMATION MATRIX

Consider the linear discrete-time system (3.8), (3.9) where  $u$  now is a  $p \times 1$  input vector. If the system is stable and time-invariant, the number of data points  $N$  is large and the noise process is stationary, a procedure for computing optimal inputs can be applied, which was developed by Mehra [12, 18]. Making use of the Fourier transformation the problem is transformed into the frequency-domain. Here, the Fisher information matrix ( $q \times q$ ) for parameter set  $a$  of the system (3.8), (3.9) has the elements

$$J_{ij} = \operatorname{Re} \frac{1}{2\pi} \int_{-\infty}^{\infty} \operatorname{tr} (B_{ij}(\omega) dF_{uu}(\omega))$$

where  $\operatorname{Re}$  denotes real part,  $F_{uu}(\omega)$  is the spectral distribution function of  $u(t)$ , and

$$B_{ij}(\omega) = \frac{\partial T^*(\omega)}{\partial a_i} S_{vv}^{-1} \frac{\partial T(\omega)}{\partial a_j}$$

(\* denotes complex conjugate and transpose)

$$T(\omega) = H (e^{-i\omega T} I - \Phi)^{-1} \Gamma.$$

$S_{vv}(\omega)$  is the spectral density of the measurement noise  $v(t)$ .

The information matrix  $J$  has the following properties:

- 1)  $J$  is a real, symmetric, positive-semidefinite matrix.
- 2)  $|J| = 0$  if the spectrum of  $u(t)$  contains less than  $[q/2m]$  points where  $[x]$  denotes the integer part of  $x$ .
- 3) The set of information matrices  $J$  corresponding to all normalized designs (i.e.

$$\frac{1}{2\pi} \int_{-\infty}^{\infty} \operatorname{tr} dF_{uu}(\omega) = 1$$

is convex and closed.

- 4) For any normalized input design  $F_1$  with mixed (continuous and point) spectrum, another normalized design  $F_2$  with a purely point spectrum of less than  $(q(q+1)/2 + 1)$  points can be found such that  $J(F_1) = J(F_2)$ .

The determinant of the information matrix  $|J|$  is now maximized with respect to  $\{F_{uu}(\omega), \omega \in (-\infty, \infty)\}$  subject to the constraint that  $F_{uu}$  is normalized. The optimal normalized input spectrum  $\hat{F}_{uu}$  is shown to fulfill the following equivalent statements:

- 1)  $\hat{F}_{uu}$  maximizes  $|J|$ .
- 2)  $\hat{F}_{uu}$  minimizes  $\max_{\omega} \lambda_{\max} \left[ \operatorname{Re} \sum_{i,j=1}^q p_{ij}(F_{uu}) B_{ij}(\omega) \right]$   
where  $p_{ij}$  is the  $(i, j)$ -th element of  $J^{-1}$  and  $\lambda_{\max}$  is the maximum eigenvalue of the  $p \times p$  matrix inside the parentheses.
- 3)  $\max_{\omega} \lambda_{\max} \left[ \operatorname{Re} \sum_{i,j=1}^q p_{ij}(\hat{F}_{uu}) B_{ij}(\omega) \right] = q$ .

The information matrices of all normalized designs satisfying conditions 1) - 3) are identical, and any linear combination of these designs satisfy 1) - 3).

Based on the above properties an algorithm for computing  $\hat{F}_{uu}$  is proposed.

#### Algorithm:

- 1) Start with any design  $F_0$  such that  $J(F_0)$  is nonsingular. Let  $k=0$ .
- 2) Compute

$$D_k = \operatorname{Re} \sum_{i,j=1}^q p_{ij}(F_k) B_{ij}(\omega)$$

and find its maximum eigenvalue  $\lambda_{\max}^k(\omega)$ . Find  $\omega_k \in (-\infty, \infty)$  by a one-dimensional search so that

$$\lambda_{\max}^k(\omega_k) > \lambda_{\max}^k(\omega).$$

Also compute the eigenvector  $\psi_{\max}^k$ .

3) If  $\lambda_{\max}^k(\omega_k) = q$  stop. Otherwise, proceed to 4).

4) Update the design as follows:

$$F_{k+1} = (1-\alpha_k) F_k + \alpha_k F(\omega_k)$$

where  $F(\omega_k)$  is a design with a single point at  $\omega = \omega_k$  of size  $\psi_{\max}^k (\psi_{\max}^k)^T$ . Choose  $0 < \alpha_k \leq 1$  either by a one-dimensional search or any sequence such that

$$|J^{k+1}| \geq |J^k|, \quad \sum_{k=0}^{\infty} \alpha_k = \infty, \quad \lim_{k \rightarrow \infty} \alpha_k = 0.$$

5) Set  $k=k+1$ . Go back to 2).

For a single input ( $p=1$ ) the spectral distribution of  $u(t)$  is a scalar function

$$df_{uu}(\omega) = 2\pi \sum_{\lambda=1}^1 A_{\lambda} \delta(\omega - \omega_{\lambda}) d\omega$$

where  $A_{\lambda}$  denotes the power corresponding to the frequency  $\omega_{\lambda}$ . The normalization condition then reads

$$\sum_{\lambda=1}^1 A_{\lambda} = 1.$$

The information matrix  $J$  has the elements

$$J_{ij} = \sum_{\lambda=1}^1 A_{\lambda} \cdot \operatorname{Re} b_{ij}(\omega_{\lambda})$$

and

$$\lambda_{\max}^k(\omega) = \sum_{i,j=1}^q p_{ij}(f_k) \cdot \operatorname{Re} b_{ij}(\omega).$$

For practical input design it is convenient to determine the optimal frequencies as integer multiples of a basic frequency, where the basic frequency is defined to have a period corresponding to the observation time. By that we can avoid generating inputs containing frequencies which

1. are so low that they are not significant within the limited observation time,
2. lie so close together that they can not be distinguished within that time.

As an example Figure 9 shows an optimal elevator input. It was optimized to identify the derivatives in the short period mode of the Beaver aircraft at 45 m/s from a maneuver with a duration of 10 seconds. In the upper part of Figure 9 the spectral distribution is given. It contains two frequencies of different powers, one on each side of the short period natural frequency. The hatched line represents the basic frequency.

The optimization procedure yields only optimal frequencies and powers (amplitudes). The phases are still undefined. In order to minimize the starting impuls the phases are chosen such that at the beginning of the observation interval the input is zero and its inclination is a minimum. Since the input is periodic with the observation time, these conditions are also valid at the end of the interval. The lower part of Figure 9 shows the resulting input time history.

#### 4. COMPARISON OF INPUT SIGNALS IN FLIGHT TEST

The input signals described in the previous sections - the doublet, "3211"-signal, Schulz-signal, DUT-signal and Mehra-signal - were applied in the joint Dutch/German Beaver Aircraft Parameter Identification Flight Test Program (cf. [19,20]). This program is being conducted to investigate the various factors affecting aircraft parameter identification. One of the goals of the program is to study the effect of various input signals on the identification process.

The Beaver aircraft has been equipped with a high precision flight test instrumentation by DUT. Moreover, an automatic system for applying the various input signals has been installed. Such a system allows optimized input signals to be applied very precisely without pilot contamination. Additionally, a given signal can be repeated exactly any number of times, allowing statistical analysis of the resulting data.

For the Beaver aircraft this was accomplished by installing three electro-hydraulic actuators (elevator, rudder and aileron). The three actuators were installed in parallel with the normal aircraft control system using pilot controllable electro-mechanical couplers. Shear pins were included in the couplings between each electro-hydraulic actuator and the normal aircraft control system. In case of a malfunction, the pilot could break the shear pins by taking positive control of the aircraft using the normal control system.

Also included in the system was a Lockheed 417 four channel analog FM tape recorder and associated electronics. The optimized test input signals were recorded on the ground and then played back in flight. The outputs from the tape recorder were applied to the electro-hydraulic actuators providing automatic application of test input signals.

The various input signals were optimized to identify the derivatives in the short-period mode and the lateral derivatives. The longitudinal and lateral directional motions were to be identified separately with input signal/maneuver duration of 10 and 16 seconds respectively. Three separate flight conditions were specified: 35, 45 and 55 m/s straight and level cruise flight at 6000 ft.

To allow a valid comparison of results obtained from the different input signal types, all input signals were adjusted to have the same energy content. Additionally, all input signals were filtered via a fourth order low pass filter with boundary frequency  $\omega = 19$  rad/s before being recorded on the input signal tape. This was necessary because of the shear pins between each of the three electro-hydraulic actuators and the normal aircraft control system. Too abrupt or too large input signals would shear the pins.

The flight testing was carried out by DUT. It took place under nonturbulent conditions. For statistical analysis each input signal was flown 10 times at 45 m/s and 3 times at 35 and 55 m/s respectively.

Identification results for the various input signal types are given in Figures 10-14. The figures show the time histories of the variables corresponding to the short-period motion at 45 m/s. The solid lines represent measured flight responses which were processed by the above-mentioned filter, and the crosses represent responses calculated from the identified model. The fit between measured and calculated responses is good. Particularly noteworthy is the high quality of the flight test data provided by DUT.

Some comments should be given on the "3211"-multistep input signal (cf. Figure 11). Because of the energy constraint the relatively short duration "3211"-input would require maximum amplitudes greater than allowable. Therefore, to increase the energy content of this signal and simultaneously reduce its maximum amplitude, the signal was applied twice during the 10 seconds test period. The same was done for the doublet input signal. In addition to this the doublet and the "3211"-input signal were substantially altered by the filtering. This point should be considered when comparing the relative merits of the various input signal types.

To demonstrate the effect of the different input signals on the accuracy of the identification results the relative standard deviations of the derivatives are plotted in Figure 15. The standard deviations were obtained from the Cramér-Rao lower bound and related to the identified values of the derivatives. As can be seen the "3211"-signal, the Mehra-signal and the DUT-signal yield throughout good results while the doublet and the Schulz-signal show large relative standard deviations for the  $q$ - and  $\delta_e$ -derivatives. The reason for this is that higher frequencies are missing in the Schulz-signal. The same is valid for the doublet-signal due to the filtering.

Figure 16 shows the derivatives identified from maneuvers with different inputs. The greatest deviations occur for  $C_{zq}$ . The values identified from maneuvers with doublet and Schulz-input differ considerably from the other identified values and the a-priori-value. This is in accordance with the large standard deviations shown in the previous figure.

As a result of this investigation it can be stated that the "3211"-signal, the Mehra-signal and the DUT-signal are of about the same efficiency. Among these three inputs the "3211"-signal has the following two advantages: (1) It is built up so simply that it is also can be implemented by the pilot, (2) it can be easily adapted to changed flight conditions, requiring only variation of the time unit  $\Delta t$ .

However, it should be pointed out that the results presented here are provisional, because for each input signal only one maneuver was evaluated. Only when all maneuvers are identified can a final valuation of the individual input signals be given.

## 5. CONCLUSIONS

The identifiability investigations have shown that an accurate identification of the stability and control derivatives is guaranteed only if the aircraft is excited by input signals which fulfill certain frequency requirements. For instance, in the short-period mode case the input signal should contain frequencies below and above the natural frequency.

In a flight test program 5 different input signals were tested. It turned out that those inputs which fulfill the above-mentioned frequency requirements provide accurate identifi-

cation results. Among these the "3211"-multistep input signal is advantageous because of its simple design and realizability.

## 6. REFERENCES

- 1 Levin, M.J., "Optimal Estimation of Impulse Response in the Presence of Noise", IRE Trans. Circuit Theory, Vol. CT-7, 1960, pp. 50-56.
- 2 Litmann, S. and Huggins, W.H., "Growing Exponentials as a Probing Signal for System Identification". Proc. IEEE, Vol 51, 1963, pp. 917-923.
- 3 Levadi, V.S., "Design of Input Signals for Parameter Estimation". IEEE Trans. Automatic Control, Vol. 11, No. 2, 1966, pp. 205-211.
- 4 Aoki, M. and Staley, R.M., "On Input Signal Synthesis in Parameter Identification." Preprints 4th IFAC Congress, Warsaw, Poland, 1969, Paper 26.2.
- 5 Nahi, N.E. and Wallis, D.E., "Optimal Inputs for Parameter Estimation in Dynamic Systems with White Observation Noise." Preprints JACC Conf., Boulder, Colorado, 1969.
- 6 Nahi, N. E. and Napjus, G.A., "Design of Optimal Probing Signals for Vector Parameter Estimation." Preprints IEEE Decision and Control Conf., Miami, Florida, 1971.
- 7 Gerlach, O.H., "Analysis of a Possible Method for the Measurement of Performance and Stability and Control Characteristics of an Aircraft in Non-Steady Symmetric Flights." In Dutch with Summary in English, Report VTH-117, Dep. of Aeronautical Engineering, Delft University of Technology, Delft, The Netherlands, 1964.
- 8 Gerlach, O.H., "The Determination of Stability Derivatives and Performance Characteristics from Dynamic Manoeuvres." Report VTH-163, Dep. of Aeronautical Engineering, Delft University of Technology, Delft, The Netherlands, 1971.
- 9 Mehra, R.K., "Optimal Inputs for Linear System Identification." Preprints JACC, Stanford, California, 1972.
- 10 Stepner, D.E. and Mehra, R.K., "Maximum Likelihood Identification and Optimal Input Design for Identifying Aircraft Stability and Control Derivatives." NASA CR-2200, 1973.
- 11 Mehra, R.K., "Optimal Input Signals for Parameter Estimation in Dynamic Systems - Survey and New Results." IEEE Trans. Automatic Control, Vol. 19, No. 6, 1974, pp. 753-768.
- 12 Mehra, R.K. and Gupta, N.K., "Status of Input Design for Aircraft Parameter Identification." Methods for Aircraft State and Parameter Identification, AGARD-CP-172, May 1975, pp. 12-1 - 12-21.
- 13 Marchand, M., "Untersuchung der Bestimmbarkeit der flugmechanischen Derivative des CCV-Versuchsträgers F-104 G." IB 154-77/12, DFVLR Institut für Flugmechanik, Braunschweig, Federal Republic of Germany, March 1977.
- 14 Koehler, R. and Wilhelm, K., "Auslegung von Eingangssignalen für die Kennwertermittlung." IB 154-77/40, DFVLR Institut für Flugmechanik, Braunschweig, Federal Republic of Germany, Dec. 1977.
- 15 Schulz, G., "Entwurf optimaler Eingangssignale für die Systemidentifizierung unter Berücksichtigung von Meß- und Systemrauschen." Regelungstechnik, Heft 10, 1977, pp. 324-330.
- 16 Brockett, R.W., "Finite Dimensional Linear Systems." New York, John Wiley & Sons, Inc., 1970.
- 17 Mulder, J.A., "A Practical Method for the Calculation of Optimum Test Signals." Delft University of Technology, Delft, the Netherlands, to be published.
- 18 Mehra, R.K., "Frequency-Domain Synthesis of Optimal Inputs for Linear System Parameter Estimation." TR 645, Division of Engineering and Applied Physics, Harvard University, Cambridge, Mass., July 1973.
- 19 Garretson, H.C., "Beaver Aircraft Parameter Identification - Technical Preparations and Preliminary Results." DFVLR-Mitt. 78-01, DFVLR Institut für Flugmechanik, Braunschweig, Federal Republic of Germany, July 1978.
- 20 N.N., "Beaver Aircraft Parameter Identification - Final Report", Department of Aerospace Engineering, Delft University of Technology, Delft, the Netherlands; DFVLR Institut für Flugmechanik, Braunschweig, Federal Republic of Germany, to be published.

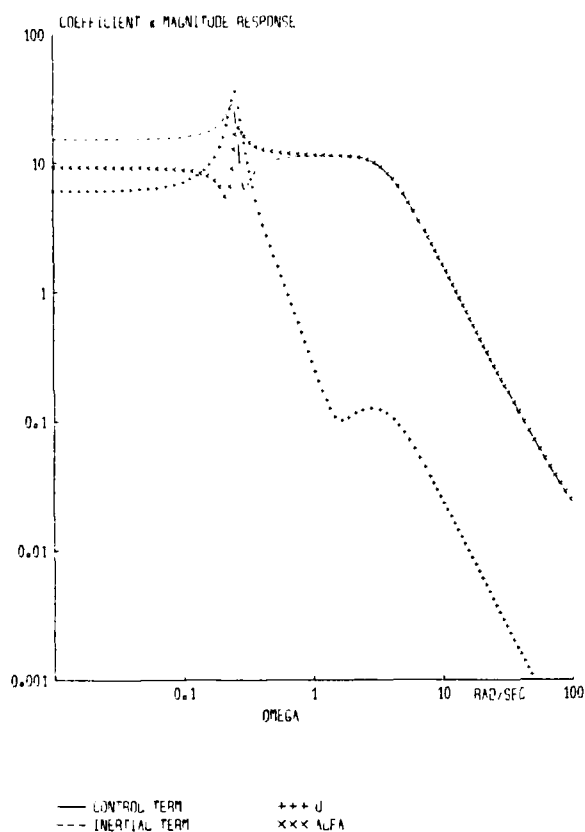
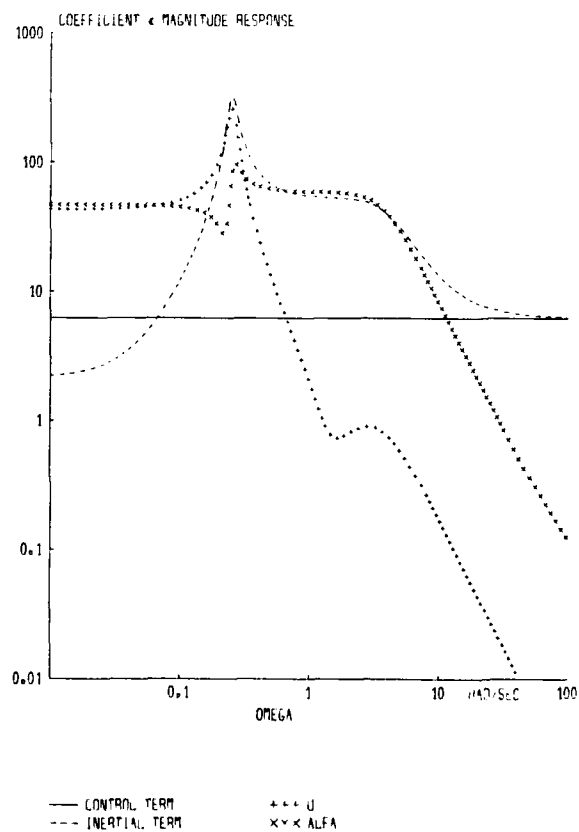
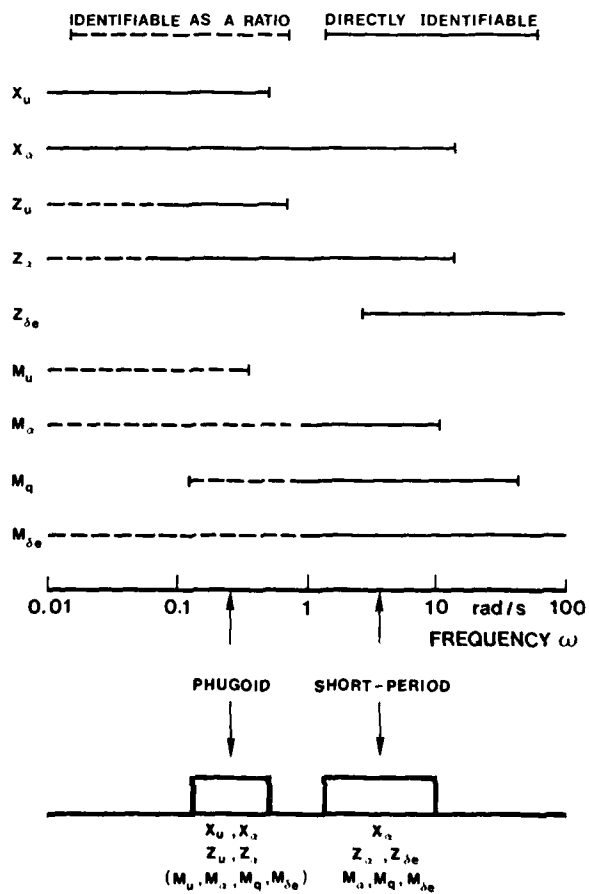
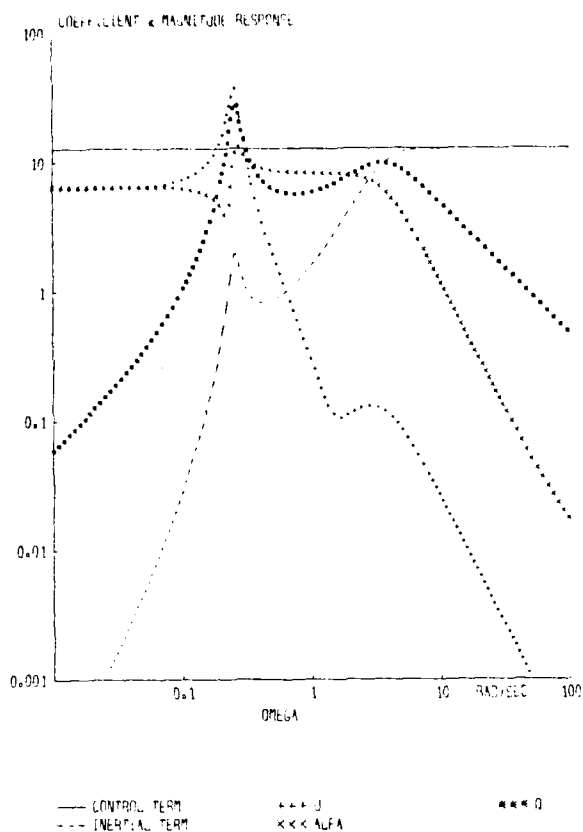


Fig. 2 Bode Plot of the Z-Equation Terms







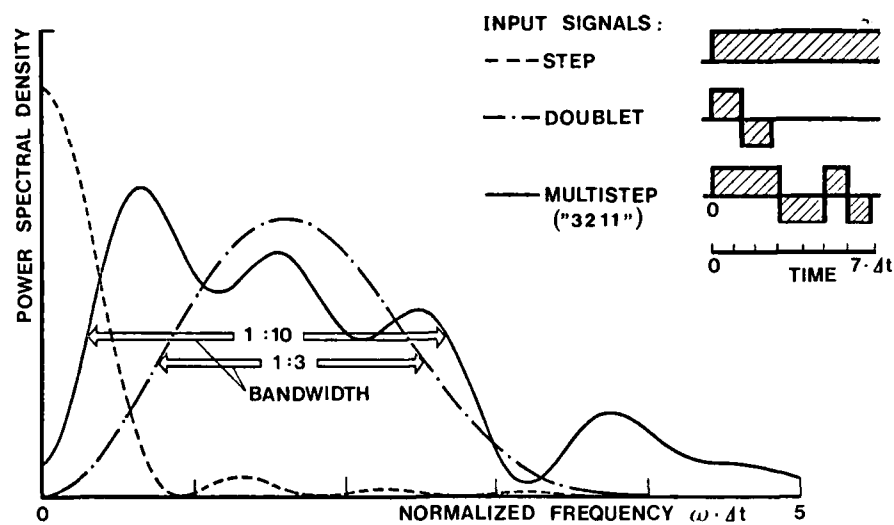


Fig. 5 Frequency Domain Comparison of Various Input Signals

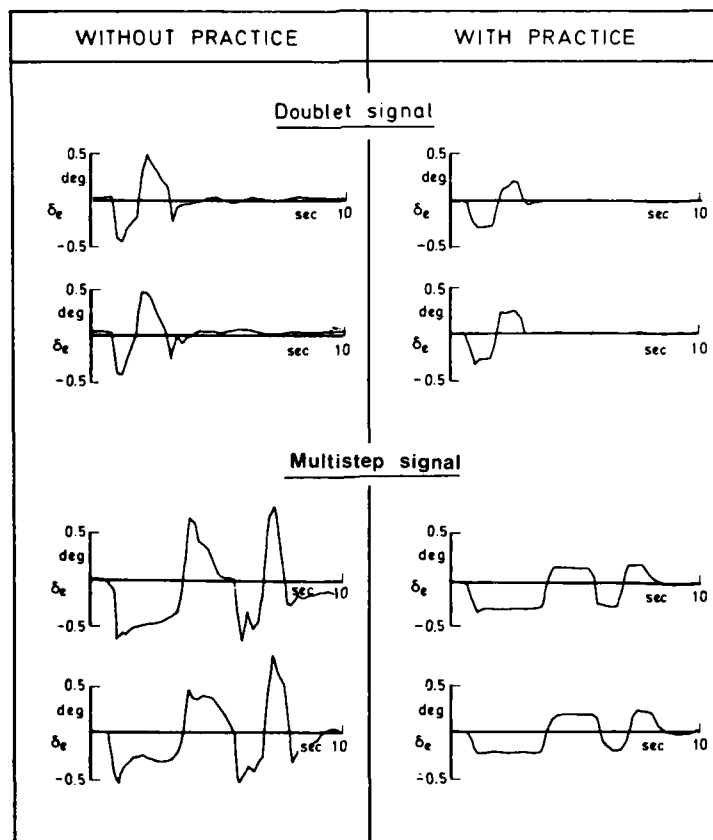


Fig. 6 Pilot Flown Input Signals

Fig. 7 Schulz Elevator-Input

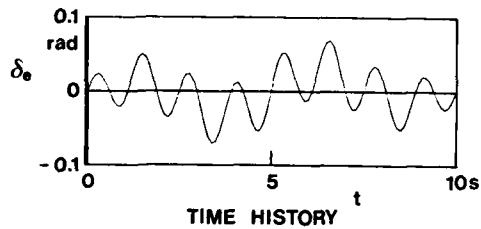
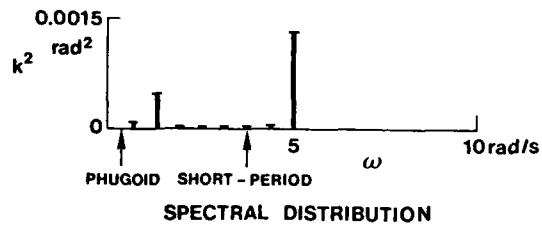
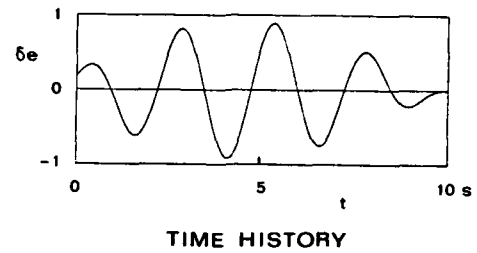
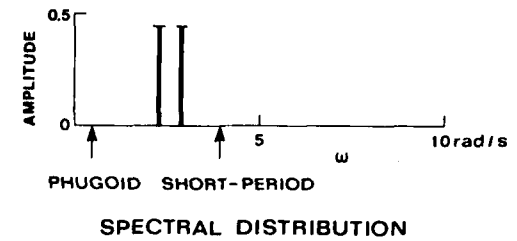


Fig. 8 DUT Elevator-Input

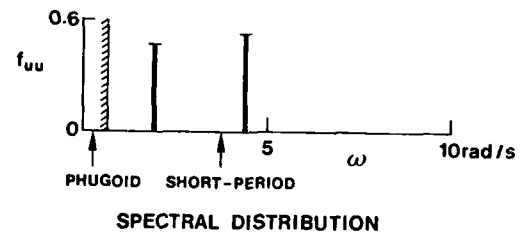
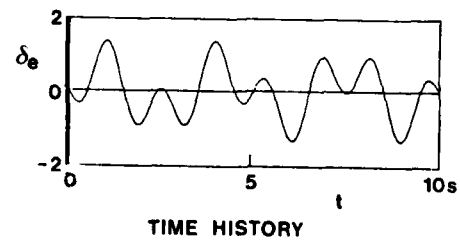


Fig. 9 Mehra Elevator-Input



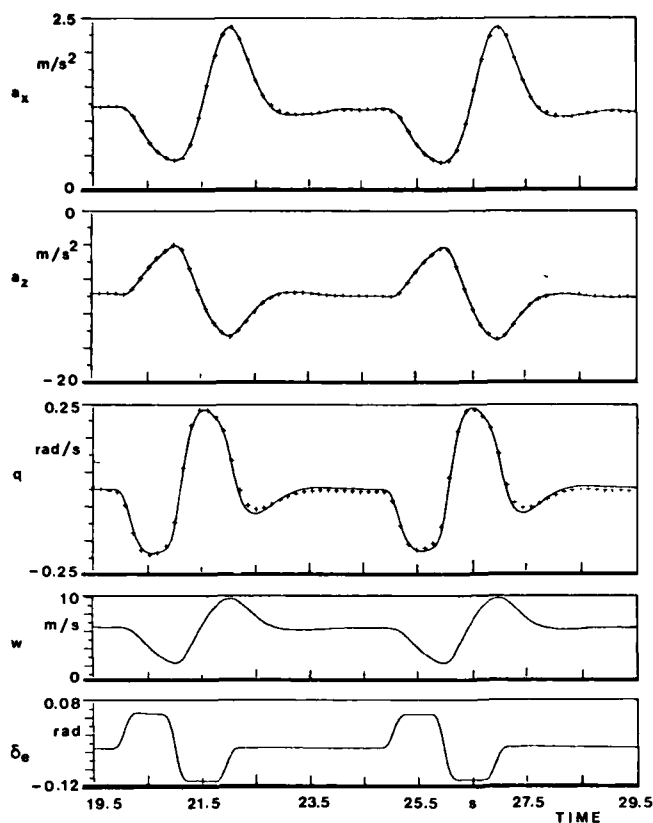


Fig. 10

Time Histories of Flight Test Data (—) and Identified Model Output (+++), Doublet-Input

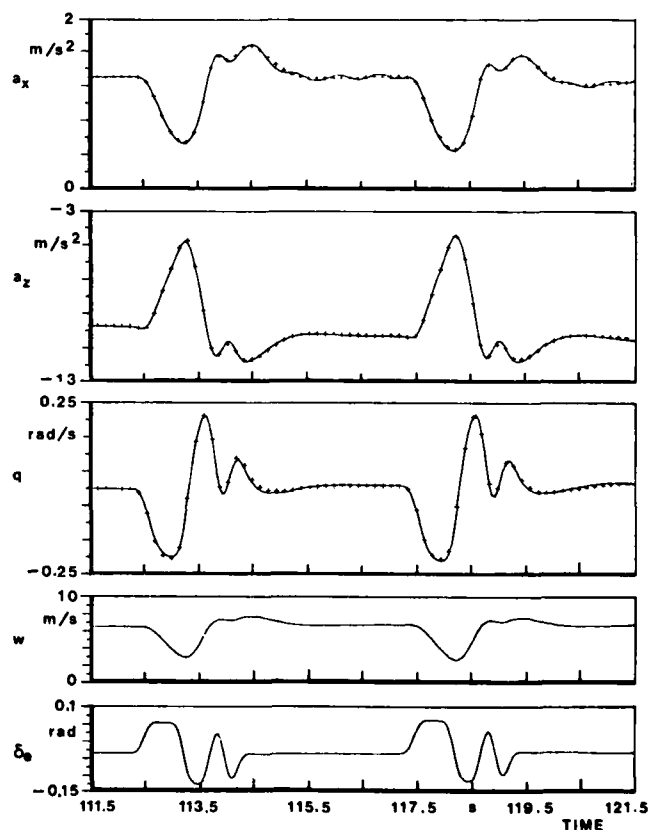


Fig. 11

Time Histories of Flight Test Data (—) and Identified Model Output (+++), "3211"-Input

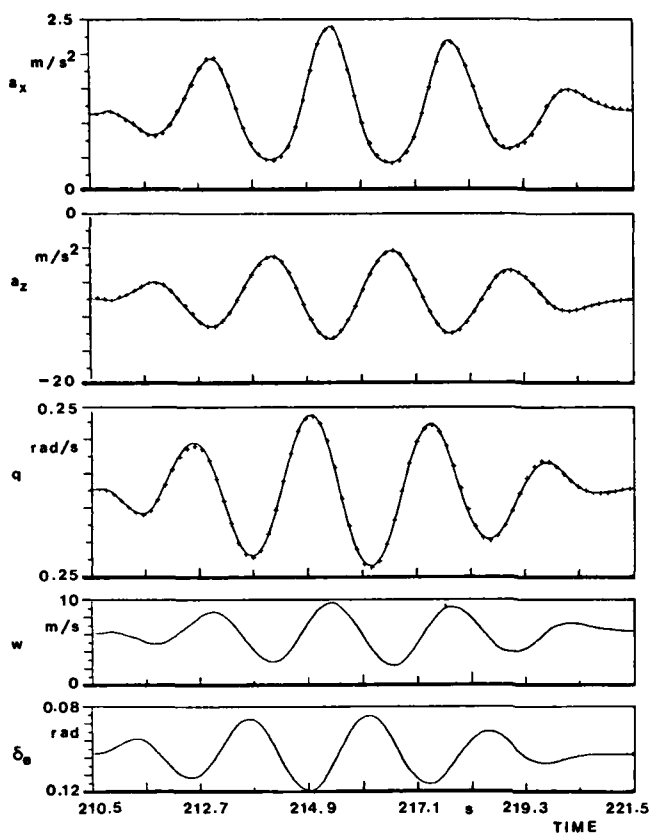


Fig. 12

Time Histories of Flight Test Data (—) and Identified Model Output (+++), Schulz-Input

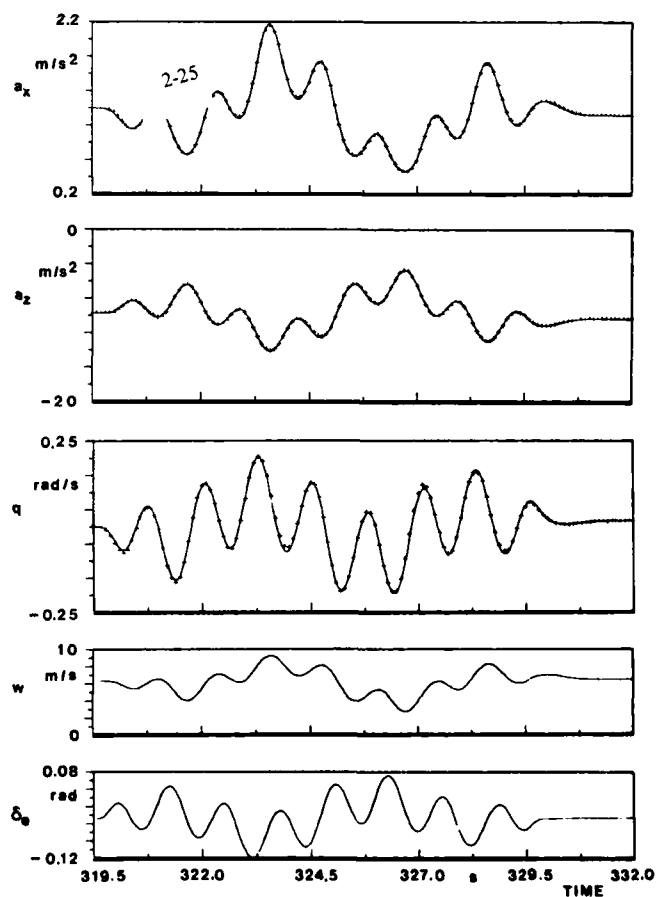


Fig. 13

Time Histories of Flight Test Data (—) and Identified Model Output (+++), DUT-Input

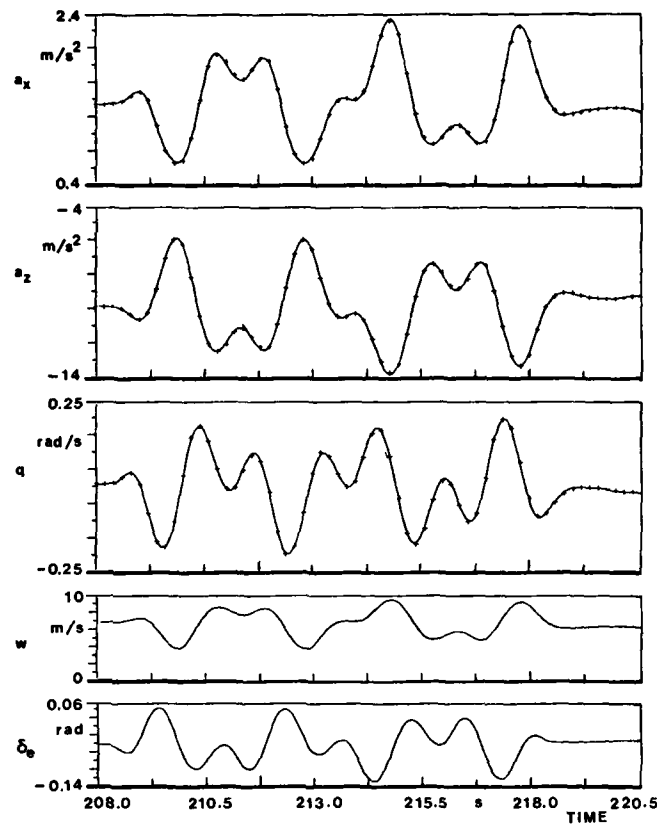


Fig. 14 Time Histories of Flight Test Data (—) and Identified Model Output (+++), Mehra-Input

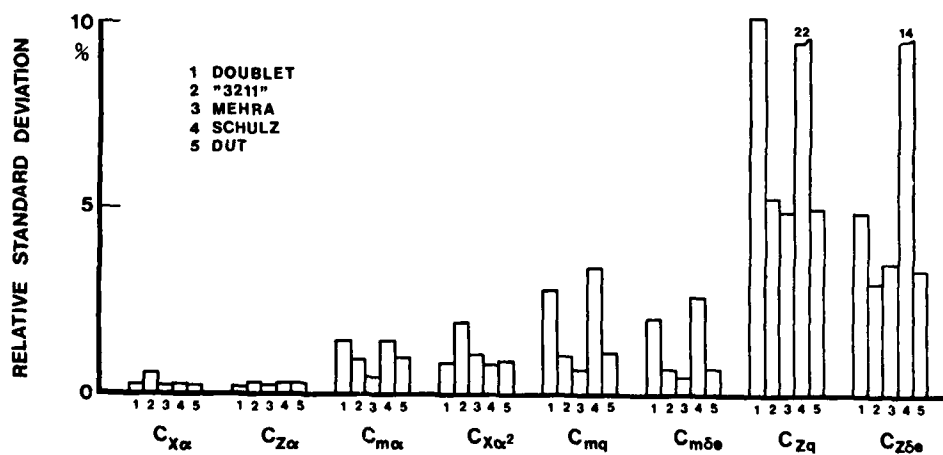


Fig. 15 Effect of Different Input Signals on the Accuracy of the Derivatives

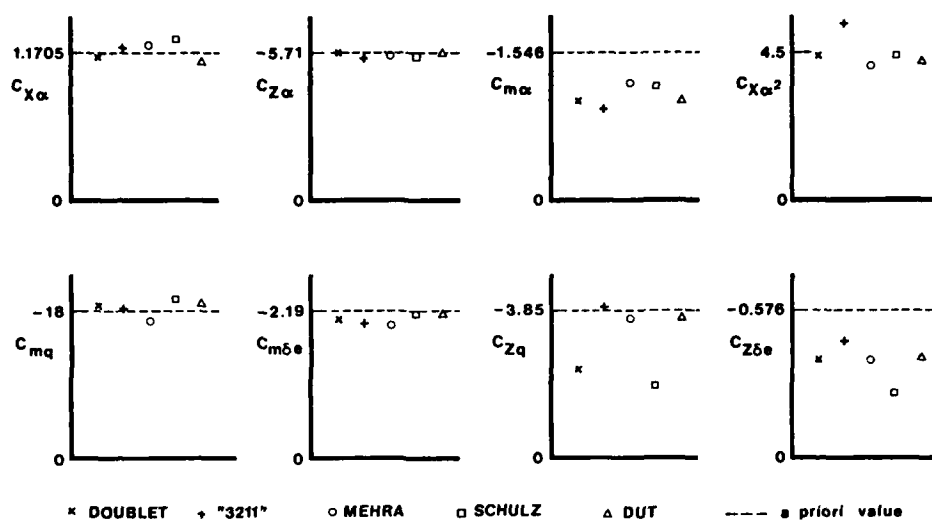


Fig. 16 Identification Results for Different Input Signals

## ASPECTS OF FLIGHT TEST INSTRUMENTATION

by

J.H. Breeman  
National Aerospace Laboratory  
Anthony Fokkerweg 2  
1059 CM AMSTERDAM  
THE NETHERLANDS

K. van Woerkom, H.L. Jonkers, J.A. Mulder  
Delft University of Technology  
Department of Aerospace Engineering  
Kluyverweg 1  
2629 HS DELFT  
THE NETHERLANDS

SUMMARY

The accuracy of aircraft parameters determined from flight test data is dependent on the input signal, the instrumentation system and the data analysis technique. Therefore, the design of a parameter estimation project should be based on an integrated approach. In the last decade there has been considerable progress in the methods for estimating the accuracy as a function of these three components.

This lecture will attempt to give some insight into the design of the instrumentation system for parameter estimation tests. But it must be emphasized that this is just one of the three components necessary for these tests.

As practical examples parts of the high accuracy instrumentation systems developed by the Delft University of Technology and the National Aerospace Laboratory for the determination of performance and stability and control characteristics for dynamic maneuvers will be described.

The most important task is the selection of the sensors. This is complicated by the wide choice of available sensors. In addition, the integrity of the sensor calibrations is a necessary prerequisite for every flight test. The signal conditioning encompasses sensor excitation, output signal demodulation, feedback circuits and temperature control systems. Subsequently the signals have to be filtered in order to remove unwanted signal components before digitalization.

The design of these filters is complicated by the dynamic nature of parameter estimation tests. Traditionally these filters are implemented with analog circuits, but the digital circuits available at present offer the alternative of real time digital filters which offer advantages in terms of stability, flexibility and cost. Large amounts of data can be generated during parameter estimation tests due to the wide bandwidth of dynamic signals, especially when combined with long measurement intervals. This places special demands on the data recording and transmission system.

1. INTRODUCTION

Methods to derive aircraft performance as well as stability and control characteristics from flight test data have been under development in the Netherlands since 1964 (Ref. 1). Attention has been devoted mainly to the derivation of all characteristics of interest from measurements in nonsteady and quasi-steady flight (NSM).

Traditional methods of performance testing are based on measurements in steady-straight flight conditions in which aircraft experience neither translational nor angular accelerations.

Stability and control characteristics were derived mainly from response measurements.

A limited number of efforts, to derive aircraft performance from measurements in nonsteady-flight have been reported in the literature, see Refs. 2, 3, 4.

An important reduction in flight time, required to determine a certain set of aircraft characteristics, may be achieved when deriving all characteristics of interest from measurements in nonsteady manoeuvring flight. The corresponding flight test technique developed at Delft University of Technology, in close cooperation with the National Aerospace Laboratory in Amsterdam, has been described in Refs. 5, 6, 7.

In 1967 and 1968 a flight test program was carried out to evaluate the quality and performance of the flight test methods, the instrumentation system and the data reduction procedures developed for the derivation of aircraft performance stability and control characteristics from measurements in nominally symmetric nonsteady manoeuvring flight. Symmetric flight trials flown with the DHC-2 Beaver aircraft, owned and operated by the Delft University of Technology yielded most encouraging results. In the early seventies a flight test program was carried out with the Hawker Hunter MK VII owned and operated by the National Aerospace Laboratory (NLR). In order to evaluate the applicability of the method to a modern jet transport aircraft a short test program was carried out with the A1 prototype of the Fokker F-28 Fellowship. Preliminary results are reported in Ref. 8. Finally in 1978 a flight test program aimed at the identification of a model for the aircraft symmetric and asymmetric aerodynamics from measurements in symmetric and asymmetric nonsteady manoeuvring flight has been carried out to extend the nonsteady flight test technique to asymmetric flight conditions.

1.1 Flight test technique

In general, successful application of the nonsteady flight test technique depends on a thoughtful combination of:

- the aircraft to be tested
- the flight test instrumentation system
- the signals applied to excite the aircraft
- the models selected for identification
- the procedures devised to analyse test data.

The nonsteady flight test technique developed in the past decade, in particular hinges an accurate measurement of:

- inertial variables; specific aerodynamic forces and angular rates,
- barometric variables; airspeed and static pressure variations,
- control surface deflections.

The flight test method includes:

- utilization of a high accuracy flight test instrumentation system,
- careful calibration of transducers to be used in the instrumentation system,
- analytic or computer aided development of optimal manoeuvre shapes,
- excitation of the aircraft manually or under servo control, during flight test flown under steady atmospheric conditions,
- off-line analysis of the measurements recorded in flight using advanced state and parameter estimation techniques.

### 1.2 Methodology

All aircraft characteristics of interest may in principle be obtained from one single nonsteady or quasi-steady manoeuvring test flight. Obviously for reasons of statistical reliability, measurements recorded during more than one test flight are to be analyzed. During the flight test manoeuvre, the aircraft is made to traverse the entire flight envelope of interest. In an earlier publication (Ref. 1) it has been argued that the procedure applied to derive characteristics of interest from measurements of nonsteady flight demands highly accurate measurements of such variables as the specific aerodynamic forces  $A_x$  and  $A_z$ , the altitude variations  $\Delta h$ , the airspeed  $V$ , the rate of pitch  $q$  and the elevator angle  $\delta_e$ .

The angle of attack  $\alpha$  is of prime importance in the calculation of lift and drag of the aircraft. In order to avoid direct measurement of the angle of attack with a vane with all its inherent problems of calibration and correction for nonsteady effects, the angle of attack is estimated using the so called flight path reconstruction procedure (Ref. 7).

In essence this procedure is as follows.

The angle of attack  $\alpha$  is derived from the pitch angle  $\theta$  and the flight path angle  $\gamma$ . Assuming the air mass traversed by the aircraft is in rest relative to the earth, the following relation between these quantities holds:

$$\alpha = \theta - \gamma$$

In steady rectilinear flight the angle of pitch follows from:

$$\theta = -\arctg \frac{A_x}{A_z}$$

And the flight path angle follows from:

$$\gamma = \arcsin \frac{c}{V}, \text{ where}$$

$$c = \frac{\Delta h}{\Delta t}$$

Obviously  $\Delta h$  represents the altitude variation measured relative to the altitude at manoeuvre initiation. This quantity can be measured with high accuracy with a differential pressure transducer, which measures the difference of the static pressure and the static pressure at manoeuvre initiation, captured in a reference vessel.

Once having computed  $\alpha$ , data points of the polar-drag curve may be computed. For a jet-propelled aircraft

$$C_D = - \frac{mA_x}{\frac{1}{2}\rho V^2 S} \cos \alpha - \frac{mA_z}{\frac{1}{2}\rho V^2 S} \sin \alpha + T_{gT} \cos (\alpha + i_p) - QV$$

$$C_L = + \frac{mA_x}{\frac{1}{2}\rho V^2 S} \sin \alpha - \frac{mA_z}{\frac{1}{2}\rho V^2 S} \cos \alpha - T_{gT} \sin (\alpha + i_p)$$

Here the air density  $\rho$  is derived from measurements of static pressure and air temperature and the gross thrust  $T_{gT}$  and the engine mass flow  $Q$  is derived from measurements of engine variables and from engine calibration data.

Evidently the accuracy of the measurements of the specific forces  $A_x$ ,  $A_z$  directly affect the accuracy of the polar drag curve data points. Also the accurate determination of the engine thrust is of vital importance. In other publications (Ref. 1, 7, 9, 10) the derivation of polar drag curve data points from measurements in quasisteady or nonsteady flight has been shown to require correction of these flight conditions to steady straight flight conditions. This implies correction for the effects of e.g. the rate of pitch and elevator deflection in the nonsteady flight conditions on the aerodynamic forces  $X$  and  $Z$  acting on the aircraft. Hence the rate of pitch and the elevator deflection angle are to be measured accurately.

This discussion exhibits the relation between measurement accuracy and accuracy of the polar drag curve data points derived from these measurements. To grasp the actual arguments for highly accurate instrumentation, as required for the derivation of aircraft characteristics from measurements in nonsteady flight, it should be realized that one polar drag curve data point is derived from a single set of measurements recorded at a single instant of time. In the traditional steady state flight test techniques many sets of measurements may be averaged to obtain one single polar drag curve data point. Modern statistical filtering and smoothing algorithms can be applied to obtain comparable statistical error reduction.

These methods, however, demand exact specification of error models or at least identifiability of error



model parameters in the context of given error model structures. Low quality instrumentation systems tend to exhibit more complicated and less reproducible measurements error structures. Utilization of low quality instrumentation systems will therefore make the application of modern statistical error reduction algorithms far less successful and render them less attractive.

This paper emphasizes aspects of flight test instrumentation with regard to measurements in nonsteady flight.

### 1.3 Organisation of the paper

After defining some terms in section 2, specifications of instrumentation for nonsteady flight testing are discussed in section 3. Section 4 is devoted to general aspects and selection criteria of various transducer types. In addition some practical examples are given. Problems of signal conditioning are discussed in section 5.

## 2. DEFINITIONS

<u>Accuracy</u>	: The ratio of error to full scale output expressed in % of full scale output or in terms of units of measurand.
<u>Resolution</u>	: The magnitude of output step changes as the input is continuously varied over the input range of the device, expressed in % of full scale output.
<u>Hysteresis</u>	: The maximum difference in output at any measurand value within the transducer's range when the value is approached first with increasing and then with decreasing measurand.
<u>Bias or Zero offset</u>	: The output signal at zero-measurand input.
<u>Threshold</u>	: The smallest change in the measurand that results in a measurable change in transducer output.
<u>Repeatability</u>	: The ability of a transducer to reproduce output readings when the same measurand is repeatedly applied to it, under the same conditions and approached in the same direction (in order to eliminate hysteresis).
<u>Stability</u>	: The ability of a transducer to retain its repeatability over a relatively long period of time.
<u>Reliability</u>	: A measure of the probability that a transducer or system will continue to perform within specified error limits for a specified length of time under specified conditions.
<u>Sensitivity shift</u>	: A change of slope of the calibration curve due to a change in sensitivity.
<u>Zero shift</u>	: A change in zero offset over a specified period of time under specified conditions.

## 3. INSTRUMENTATION SPECIFICATIONS

### 3.0 Introduction

The application of the nonsteady flight test technique places special demands on the instrumentation system. As discussed in section 1.2, the determination of performance data requires very accurate measurements of a number of variables, while the determination of stability and control characteristics implies large measuring ranges for variables such as specific forces and angular rates. In this chapter some typical requirements for the accuracy and resolution of a number of variables are presented and reliability and maintainability requirements are discussed. Finally, the influence of rapidly varying measurands on the accuracy of the measurements is considered.

### 3.1 Accuracy requirements

Accuracies better than 0,1% are commonly required for the measurement of accelerations, angular rates, elevator deflection and some differential pressures. Other quantities, such as absolute pressures, engine quantities and temperature have to be measured with accuracies from 0,3 - 1%. These figures are related to entire measuring channels. A measuring channel is considered to comprise a transducer with signal conditioning and one channel of the data collection system. Complete lists of measured variables with range and accuracy for the Hawker Hunter, the Fokker F-28 and the DHC-2 Beaver flight test programs are presented in tables 1, 2 and 3 (see Refs. 11, 12).

### 3.2 Resolution requirements

Digital data collection systems in use today are sometimes very sophisticated. They can be computer controlled and have high sample rate capabilities and a large number of signal inputs of all kinds e.g. analog, synchro/resolver, digital, etc. The number of data bits recorded for each channel defines the theoretical resolution of the particular measuring channel. Accuracy however is not necessarily equal to the resolution of a measuring channel. All kinds of errors of ADC's, multiplexers, sample and holds etc. contribute to the total error of an measuring channel. Also zero-shift and gain shift as function of time and environmental conditions of signal conditioners (filters) play an important role in the measurement accuracy of a channel. In order to realize a measurement accuracy better than 0,1% the resolution of the measuring system has to be at least 14 bits binary or 4 decades BCD, this equals a resolution of resp. 0,006% or 0,01%. The number of bits available is referred to as the available resolution. The actual resolution is less than the available resolution due to internal noise and component drift of the ADC. The resolution of transducers depends on the type of transducer. Output of some transducers will change in small steps when the measurand is varied continuously. This occurs in particular when wire wound potentiometers are used.

meters are used as output device of these transducers. Also transducers with a pulse rate output have a finite resolution when pulses are counted in a finite period of time. The resolution of such pulse rate output sensors increases with increasing measurement time. Usually, the resolution of transducers is more or less constant over the entire range, depending on the linearity of the transducer. Sometimes a number is specified for resolution while threshold is meant. The effect of the presence of a threshold is also shown in the output of a transducer since the output will change with discrete steps with continuously varying input. Output steps, however, are not constant over the entire range. This phenomenon is related to static friction and hysteresis of the transducer. The term threshold should be well understood to be related to the smallest change in the measurand which results in an observable change in the output, while the notion of resolution is related to the smallest step in the output caused by continuous variation of the measurand.

### 3.3 Reliability requirements

The reliability of a flight-test instrumentation system is an important factor, with regard to flight safety as well as to maintain the required accuracy throughout a flight-test program. Flight safety is involved when attaching transducers to the flight controls and to the control surfaces of the aircraft, if the instrumentation system is powered by the aircraft electric/hydraulic power system and if the data collection system is connected to the aircraft's avionics system. Safety measures have to be taken into account in design and development of instrumentation systems, in such a way that under no circumstances, i.e. under proper operation as well as in case of failure of the flight-test instrumentation system, the safety of normal aircraft operation should be affected. Reliability of flight-test instrumentation systems is achieved by utilization of quality components and subsystems, which have already proven their reliability under actual flight-test conditions. Using new parts or newly developed transducers straightaway introduces a large probability for the occurrence of errors or even of failures. Significant benefits may be obtained from using new equipment in preliminary flight-test programs, such even in parallel with already accepted systems or system components. Evaluations of operation and results of new components, leading to changes or modifications may thus be made possible. It is not sensible to prove the validity of complete new instrumentation systems during a new flight-test program, unless this is a special program directed towards instrumentation evaluation. Instrumentation engineers should realise, that flight-test engineers want reliable data presented in the format as agreed upon and are reluctant to accept failures or "lost flights" as a consequence of using new instrumentation "highlights".

### 3.4 Maintenance requirements

Development and integration of instrumentation subsystems must include possibilities for maintenance in the course of the flight-test programs. It is an absolute requirement to have access to all components and transducers for repair or replacement without too much mechanical work. Mountings of some transducers (accelerometers and rate gyros) should be designed in such a way that removal and reinstallation introduce no displacements or rotations and that the alignment is maintained throughout the flight-test program. Measuring relative position and attitude to the aircraft reference axes, especially rotations around the Z-axis is a time consuming job. For routine maintenance, e.g. pre- and post flight checks, it is convenient to have direct access to test points of electronic equipment. Properly locating junction boxes can be most important in this respect.

### 3.5 Dynamic performance

As NSM introduces aircraft motions with frequencies up to about 1 cps it is obvious that not only static performance of the measurement system should be considered, but that also dynamic characteristics should be taken into account. Due to the limited sample rate of data collection systems, aliasing errors are likely to occur. The frequencies in the signals from transducers above 1 cps caused by structure vibration, transducer noise or electromagnetic interference from other systems with frequencies up to 400 cps are to be attenuated. The use of pre-sampling filters is one solution for aliasing problems. Accurate low-pass filtering of transducer outputs is then required without introducing non-recoverable errors into the filtered signals in the frequency range of interest.

## 4. TRANSDUCERS

### 4.0 Introduction

As discussed in section 1.2, a large number of variables have to be measured during nonsteady flight-tests. The discussion in this chapter will be limited to those transducers which have significantly more stringent specifications as compared to the specifications for classical flight-tests. This involves the inertial transducers, the air pressure transducers and the position and angular deflection transducers. For the remaining variables, such as air temperature and engine parameters, we refer to the excellent AGARD Flight Test Instrumentation Series (Ref. 13,15,16,22). A general reference book on transducers is Ref. 17.

### 4.1 Inertial transducers

#### 4.1.1 Accelerometers

Although accelerometers are intended to measure acceleration (linear or angular) they all respond to a force acting upon some inertial mass (the proof mass) which is restrained by a spring. The motion of the proof mass is damped by a second order mass-spring-damper system (Ref. 13). The available accelerometers can be divided into the open-loop transducers and the closed-loop transducers. The open-loop transducers include the direct reading accelerometers calibrated in g-units, potentiometric-reluctive, capacitive, strain gauge and the piezoresistive accelerometers. Measurement of displacement (or rotation) of a proof mass restrained by a spring is the basic principle of these transducers. The accuracy is limited to about 1%. The bandwidth depends on measuring range and damping factor, and varies from 0 - 10 cps for a potentiometric transducer of  $\pm 1g$  up to 0 - 500 cps for a strain-gauge transducer with a measuring range of  $\pm 10g$ .

To the group of closed-loop accelerometers belong the force-feedback and the torque-feedback transducer. The basic principle of force feedback accelerometers is the measurement of the force necessary to restrain the proof mass from moving along the sensitive axis. This is accomplished by sensing the deflection of the proof mass and feeding this signal back to a force coil (see Fig. 1). The current through this coil is a direct measure of the applied acceleration.

In force feedback accelerometers, the proof mass is restrained from motion in any but the sensitive axis of the transducer, by a specially designed suspension, while in the torque-feedback transducer the proof mass is part of a pendulous system.

As result of the high gain of the feedback amplifier displacement of the proof mass is very small, for the pendulous type deflection in the order of 5 min of arc or less. For the torque feedback accelerometers small deflections have the advantage of reduced cross-axis sensitivity, low hysteresis and friction effects and high frequency response. Linearity and accuracy are at least 10 times better than with open-loop transducers, mainly determined by the performance of the torquer in the transducer. In comparison with for example strain-gauge accelerometers the outputs of closed-loop accelerometers are usually rather high (+ 0,05V as compared to 5V).

#### 4.1.2 Rate gyros

Two different types of rate-gyros are commonly used to measure the rate of rotation of an aircraft under flight-test conditions, the open-loop rate gyro and the closed-loop or force-balance rate gyro. In the open-loop rate gyro gimbal deflection is restrained by a spring or torsionbar. The deflection angle is measured by a suitable sensor (e.g. potentiometer or micro-syn). The full scale angular deflection is limited to only a few degrees in order to minimize cross-axis sensitivity. A damping device generates the necessary damping, usually damping coefficients vary between 0,5 and 1 in order to attain acceptable frequency response characteristics of the transducer. Accuracy is limited to about 1% due to changes of spring rate and hysteresis of the restraining spring or torsionbar. Cross-axis sensitivity is 5% with a gimbal deflection of  $3^\circ$  at full scale. The bandwidth depends on measuring range and full scale gimbal deflection, typical figures are 10 cps with  $\pm 6^\circ/\text{sec}$  full scale and 50 cps with  $\pm 100^\circ/\text{sec}$  full scale. Linearity and zero output stability are related to the quality of the gimbal deflection sensor and the restraining spring. The basic principle of the closed-loop rate gyro is the measurement of the torque necessary to restrain the gimbal element of a rate-integrating gyro from rotating around the output axis. This is accomplished by sensing the deflection angle of the gimbal, amplifying this signal and feeding it back to a torque motor which acts on the gimbal (see Fig. 2). The torque generated by the torque motor is proportional to the current through the torquing coil. This current is sensed across a measuring resistor.

Similar to the force balance accelerometer the gimbal deflection is kept very small with a high gain amplifier. Gimbal deflection at full scale input rate is usually smaller than 1 mrad resulting in a cross-axis sensitivity of less than 0,1%. An important advantage of this type of rate gyros is that linearity and stability are not related to the gimbal deflection angle sensor (pick-off) but only to the torquer performance and the open-loop drift rates of the gyro.

#### 4.1.3 Transducer selection

Selection criteria for accelerometers and rate gyros for the use in nonsteady flight testing are as follows:

##### Measuring range

The measuring range of inertial transducers, which are fixed to the aircraft's body axes, has been chosen as small as allowable, in order to maximize the output signal levels and henceforth the resolution of the measuring channel. Usually, the allowable ranges are dictated by the expected inputs resulting from aircraft motions and the vibration level expected at the location of the transducers. Both linear and angular vibration levels have to be considered (Ref. 18). One must avoid saturation of the transducers, because closed-loop transducers produce heavily distorted output signals when the measuring range is exceeded. No matter what kind of filtering is used, the original signal can never be recovered.

##### Frequency response

The upper frequency limit of the signals of interest is about 1 cps. The bandwidth of the transducers, therefore, is an important factor to be considered. Inertial transducers of the force-balance type usually have bandwidths in the order of 80 to 100 cps. A damping ratio of 0,7 results in a flat response throughout the bandwidth of the transducer. The usable frequency range is approximately one tenth of the undamped natural frequency for an attenuation of 0,01% of the output signal. The time shift of the output signal of the transducers is an important factor to consider. With a damping ratio of 0,7, the phase characteristic of a second order system is practically linear up to one tenth of the natural frequency. The time shift of a transducer with a 100 cps natural frequency is about 2,2 msec. up to 10 cps. The maximum error due to time shift in the output at a frequency of 1 cps is 1,4%. This means that this time shift error has to be corrected during the data processing.

##### Accuracy

The accuracy requirements of inertial transducers for the use in nonsteady flight testing are to be considered as severe. As already mentioned in the introduction, the overall accuracy has to be maintained at a level of better than 0,1%. This figure, however, not only concerns the transducer accuracy, but includes the accuracy of the signal conditioning and of the data collection system. It is obvious that the transducer accuracies have to be in the order of 0,02% in order to maintain the required overall accuracy. An important source of error in acceleration measurements is the uncertainty of the output with zero input. A known bias output with zero input is of course not important, but the stability and repeatability are very important. Also zero shift as function of temperature and time and the so called turn-on stiction have to be taken into account. Scale factor (sensitivity) and hysteresis specifications have to be within the accuracy requirements. Scale factor stability depends on the stability of the measuring resistor as well as on the stability of the torquer's permanent magnet. Hysteresis effects are likely to be reduced under operating conditions due to mechanical vibrations. Nonlinearity of output (which depends on torquer linearity) is not too important if careful calibration of the transducer nonlinearity is carried out.

#### Cross-axis sensitivity

This phenomenon is present in pendulous accelerometers as well as in rate gyros. Small cross-axis sensitivity is achieved by stiff servo loops in the force-balance transducers. Figures for cross-axis sensitivity are  $< 0,001$  g/g of applied acceleration for accelerometers and  $< 0,001$  rad  $s^{-1}$ /rad  $s^{-1}$  of applied input rate, or 0,1%. For steady state conditions it is not too important, since careful calibration enables compensation for the effects of cross-axis sensitivity.

Cross-axis sensitivity, however, can be the source of so called rectification errors. This error is the result of the simultaneous presence of sinusoidal accelerations along the cross-axis and along the sensitive axis. It results in a bias when the output of the transducer is filtered to remove unwanted noise and vibrations measured by the transducer (Ref. 13).

Rectilinear accelerometers of the force-balance type do not have the disadvantage of cross-axis sensitivity, but have more problems with the stability of the mechanical suspension. It may be worthwhile to mention, that recent development of force-balance accelerometers for strapped-down applications has resulted in transducers with a very small cross-axis sensitivity of approximately  $5 \cdot 10^{-6}$  g/g of applied acceleration (e.g. Donner 4841).

#### 4.1.4 Practical example

For the NSM with the Hawker Hunter MK VII of the National Aerospace Laboratory a strapped-down inertial package was developed consisting of 3 accelerometers and 2 rate gyro's. The measurements in flight were performed during symmetric nonsteady manoeuvres. Therefore, one precision rate gyro and one gyro of the moderate accuracy were used (Ref. 11). Table 4 shows the type of the transducers used.

The three accelerometers were mounted orthogonally on a stainless steel frame. The mounting flanges of the frame were machined to an accuracy of 0,1 min of arc. Repeatability of the alignment of the transducers after replacement was assured by endplates. The frame was mounted in a cubic stainless steel box on 4 thermo isolators (see Fig. 3). The outer surface of the box was also machined to an accuracy of 0,1 min of arc. Temperature sensitivity of the scale factor of the transducers equaled about 0,02% per  $^{\circ}C$ , the temperature sensitivity of the output with zero input equaled about 0,002% F.R. per  $^{\circ}C$ . With an expected temperature range from  $-30^{\circ}C$  to  $+30^{\circ}C$  the scale factor will change as much as 0,6%, the output related to zero-input will change about 0,06% F.R. Laboratory tests showed that scale factor changes due to temperature were mainly caused by the change of the value of the measuring resistor inside the accelerometer. Replacing this resistor by a high stability low tempco resistor (20 ppm) improved the scale factor stability. Improvement of zero stability was achieved by temperature stabilization of the box containing the accelerometers at  $45^{\circ}C \pm 1^{\circ}C$  with a temperature sensor controlled heater circuit. A small blower circulated the air in the box assuring homogeneous temperature distribution inside the box. The accelerometers were placed in such a way that the transverse-axes of X- and Z-accelerometer were aligned along the Y-axis whereas transverse axis of the Y-accelerometer was along the X-axis of the box. The Y-accelerometer was only used for the purpose of applying relatively small corrections.

The full scale output level of each accelerometer was scaled to the required level of the data collection system. Floating power supplies were used and signal returns were connected to the high quality ground of the instrumentation system, in order to avoid possible ground loops.

The pitch-rate gyro was a wide angle miniature integrating gyro, the dynamic range equaled  $10^5$ . The gyro was procured without electronics and the required electronic circuits were developed to perform rate measurement applying the torque balance principle.

The necessary electronic circuits including power supplies were contained in a box of  $30 \times 12 \times 10$  cm<sup>3</sup>. The gyro was mounted in a frame which was attached to the rear side of the accelerometer box. Adjustment screws permitted exact alignment of the spin reference-axis with the X-axis and of the output-axis with the Z-axis of the accelerometer box. The input-axis of the gyro, henceforth, was aligned with the Y-axis (q). The alignment procedure was carried out using a precision turntable while the gyro was operating in open-loop configuration. The alignment thus achieved was in the order of  $\pm 0,1$  mrad.

The gyro was provided with an internal heater and a temperature sensor. With an electronic circuit the operating temperature was set equal to  $80^{\circ}C$ . To prevent heat transfer from the gyro to the accelerometer box thermal isolation was used in the gyro mounting frame.

The yaw-rate gyro, which was only used for corrections during data processing, was an open loop potentiometer type gyro of moderate performance.

The accelerometer box with the pitch-rate gyro the yaw-rate gyro and the amplifier box were mounted on a noral plate of 18 mm thickness. This plate, which was strainfree, was strapped on a rigid frame. Alignment with the aircraft reference axes was achieved with the aid of three adjustment screws. The alignment procedure was carried out with a precision inclinometer and a theodolite. The natural frequency of the accelerometer was about 100 cps and of the pitch rate gyro 80 cps. Although these frequencies were high as compared to the frequency of aircraft motion during the measurements the timeshift error (group delay) was a factor which had to be taken into account.

This will be shown in the following example.

Suppose a transducer with a natural frequency  $f_n = 80$  cps and a damping ratio 0,7 is excited with a frequency of 0,5 cps. The time shift error of a second order system assuming linear phase characteristics equals:

$$\Delta t = \frac{\lambda}{\pi f_n} \rightarrow \Delta t \approx 2,8 \text{ ms}$$

With an arbitrary sinusoidal input signal  $a = \hat{a} \sin 2\pi f t$ , the maximum slope of the input signal is (see Fig. 4)

$$\frac{\Delta a}{\Delta t} = 2\pi f_n \hat{a}$$

therefore, the maximum relative error  $e_{\text{max}}$  equals:

$$e_{\text{max}} = \frac{\Delta a}{\hat{a}} = 2\lambda \frac{f}{f_n}$$

in this example:

$$e_{\max} = 0,9\%$$

Therefore, the maximum relative error which occurs around the zero crossings of the input signal equals about 1% of the amplitude of the input signal.

Two methods for the correction of these errors will now be discussed briefly. The first method can be formulated as follows:

1. Make sure that the damping coefficients of all inertial transducers are kept close to 0,7.
2. Determine the natural frequency of each transducer.
3. Calculate the time shift for each transducer.
4. Correct during data processing the measurement data for the time shifts of the corresponding transducers by interpolation.

The second method consists of the following steps:

1. Equalize all inertial transducers with respect to their transfer functions, if necessary by adding special equalization filters in each measurement channel (see Ref. 14).
2. Determine the time shift of the inertial transducers.
3. Correct during data processing the measurement data for the time shifts of all other transducers with respect to the time shift of the inertial transducers.

## 4.2. Air data transducers

### 4.2.1. Some definitions

Pressure is a force acting on a surface, pressure is measured as force per unit area.

Absolute pressure is measured relative to vacuum.

Differential pressure is measured relative to a reference pressure.

Static pressure is the pressure exerted normal to the surface along the flow.

Impact pressure is the pressure in a moving fluid exerted parallel to direction of flow, due to flow velocity.

Stagnation pressure (total pressure) is the sum of static and impact pressure.

### 4.2.2. Classification of pressure transducers

In this chapter some of the principles of measuring pressure to provide air data will be discussed. Pressure transducers sense pressure by measuring the deflection of mechanical sensing elements. These elements are usually relatively thin walled elastic members (plates or tubes) which offer the pressure a surface to act upon. The deflection, which is converted into a secondary motion in some transducers, is used to produce a change in the output of the transducer. To produce electrical outputs a wide variety of transduction elements is applied in pressure transducers. For example: potentiometers, strain gauge, inductive and capacitive displacement sensors. A separate group of pressure transducers includes those fitted with vibrating elements, such as for example: vibrating cylinder, vibrating wire, and vibrating quartz beam. They usually produce digital outputs. The servo type pressure transducers are available in two basic versions, the null balance and the force balance transducer.

Pressure transducers with output potentiometers are seldom applied to flight testing for generation of air data. The accuracy is limited (1-3%) due to wiper friction especially in low range transducers. Wear of resistance elements might cause nonlinearity. Wirewound elements have limited resolution. To achieve acceleration insensitivity the moving parts have to be carefully balanced. Advantages are however low cost and the possibility to obtain high output levels directly.

Strain gauge pressure transducers are widely used for flight testing. They are available in many different types. For example: bonded- and unbonded wire gauges, bonded semiconductor- and diffused semiconductor gauges. Measuring ranges are available from ~ 10 kPa up to ~70 MPa thus covering a wide range of applications. Outputs of strain gauge transducers are in the mV ranges, ~ 40 mV for bonded- and unbonded strain gauges, up to ~ 500 mV for semiconductor strain gauges. Signal conditioners have to be applied, to obtain the signal levels commonly required by data collection systems. Those conditioners also provide bridge power supply, either a.c. or d.c., for the transducers. They are available as separate units which operate on aircraft d.c. power supply. Several types of strain gauge transducers at present are integrated with the corresponding electronics, thus eliminating low level signal wires from the transducer to the signal conditioning unit.

In inductive pressure transducers, several methods are applied to generate output signals. One of the methods is based on the principle of a moving core in a triple coil assembly connected as a differential transformer. Displacement of the core, connected to the sensing element of the transducer, increases the magnetic coupling between one secondary coil and the primary coil and at the same time decreases the magnetic coupling of the other secondary coil and the primary coil. The sum of the outputs of the secondary coils is constant, the difference of the outputs, however, is proportional to the displacement of the core. A second method is based on the deflections of a magnetically permeable diaphragm. This diaphragm is supported between two coils which are connected in series as a two-arm inductance bridge. Applied pressure deflects the diaphragm, decreasing the gap between the diaphragm and one coil and at the same time increasing the gap on the other side. When the half-bridge is connected to an a.c. supply, the output voltage is proportional to the ratio between the inductances of the two coils. Pressure transducers with a moving core are available with measuring ranges down to levels as low as 200 Pa. To reduce acceleration sensitivity, sometimes two pressure sensitive elements are combined into one transducer. Electrical connections of the coils are made in such a way that diaphragm deflections due to acceleration have practically no effect on the output of the transducer. Outputs are up to 10% of the

applied power supply, which is usually about 20 V at 1000 cps.

The essential element of capacitive pressure transducers is a metal membrane stretched flat under radial tension. Pressure differentials cause a deflection of the diaphragm thus introducing a change in the capacitance with respect to one or two adjacent electrodes. Diaphragm displacement is a function of the exerted force per unit area and henceforth represents a true pressure. The tensioned membrane has a low mass and very low hysteresis (0,02% typical). The low mass and high radial tension usually results in a very low acceleration sensitivity normal to the diaphragm, in the order of 0,1%-0,01% F.S. per g. For low range pressure transducers (~ 15 kPa) usually the dual stator sensing element is employed in order to increase the sensitivity.

Different electronic circuits (separate from or integrated in the transducer housing) are used to generate either analog or digital outputs.

A typical example of a capacitive pressure transducer may be described as follows. The fixed electrodes are at an a.c. voltage with a stable amplitude and frequency. If pressure deflects the diaphragm, the change in capacitance between the diaphragm and each fixed electrode results in a voltage change across the two capacitors. The two capacitors act like an a.c. powered voltage divider. The voltage change is amplified and phase sensitive demodulated to achieve bidirectional operation for differential pressure transducers. Filters are applied to suppress the carrier frequency. Sometimes sensor linearity is increased by a feedback circuit which changes the excitation voltage as a function of the output signal. A typical value obtained for non linearity by application of this technique is about 0,05%. To reduce sensitivity for temperature variations of the sensor, feedback controlled heaters are applied with the additional advantage of eliminating the effects of condensing humidity.

Capacitive pressure transducers are available for a wide range of applications, absolute, gauge and true differential measurements in the range of 1 kPa to 15 MPa.

Also available are height-linear and airspeed-linear capacitive pressure transducers which are employed in air data systems.

In force balance pressure transducers the sensing element is restrained from motion by a force generator and displacement of the sensing element is thus kept very small. The deflection of the sensing element is detected by a pick-off. The output is fed to a servo amplifier which drives an electric motor. This motor is connected through a suitable gear box to an output device (potentiometer, synchro/resolver), while generating a force which acts upon the pressure sensitive element. Usually this is done by a very well machined screw spindle and a helical spring. The output of the transducers is proportional to the force required to keep the sensing element in the null-position. Linearity achieved with this principle is very good, depending practically only on the spring characteristics. Due to the relatively high masses of the moving parts, it is very difficult to achieve insensitivity for accelerations such as those resulting from rotational vibrations. Usually heaters are required to reduce temperature sensitivity of null and of scale factor. Stability is mainly determined by the force generator (spring). The frequency response depends on the pressure amplitude, due to the limited slew rate of the mechanical servo system. The application of this type of pressure transducer is mainly restricted to air data systems and sometimes pressure ratio measurements.

#### 4.2.2. Pressure transducer selection

Selection of pressure transducers for nonsteady flight testing depends on the required measuring range, accuracy, output, frequency response and environmental conditions during the flight tests.

##### Measuring range

From the configuration of the pressure measurement system and the expected pressure changes in flight the measurement ranges of the transducers are to be determined. A priori information concerning maximum airspeed and altitude variations in manoeuvring flight may aid in deriving correct range estimates. Over-ranges have to be kept small as possible in order to maximize relative accuracy. Usually the overrange is determined by the transducers selected, since transducers rarely have precisely the required measuring range.

When selecting differential pressure transducers one has to distinguish between two different types: the (true differential) bidirectional transducers and the unidirectional differential transducer. The first one is designed to accept pressure reversals and should not suffer from "frog effects" on zero differential pressure input and should exhibit no scale factor difference between positive and negative output.

The second one only accepts pressure difference excursions from zero to full scale.

In types with dual sensing elements minor differences between both systems (mechanical and/or electrical) may result to different outputs corresponding with the same differential pressure applied at a higher or lower absolute pressure level (common mode pressure).

##### Accuracy

Accuracy achieved with pressure measurements not only depends on the transducer but is also affected by the required electronic circuits. Transducers with separate electronics are usually specified without the required signal conditioning circuits. Although specifications of separate electronics exceed those of the transducers, attention has to be paid to the effects of temperature on zero-offset and scale factor (gain) and to the effects of power supply variations.

The accuracy of static pressure measurements required for non steady flight testing equals 0,05% equivalent with an altitude deviation of 4 m at sea level. This high degree of accuracy has to be maintained throughout the calibration and flight test period, thus stability and repeatability are of great significance.

It is not recommended to use altitude-linear absolute pressure transducer systems, since the outputs are less accurate, as a result of the electronic linearization applied. The linearity of the transducers is not too important since careful calibration enables adequate correction of the nonlinearity during data processing, provided that there are no significant step changes in the slope of the calibration curve. This may occur in some differential pressure transducers at zero input pressure.

##### Output signal requirements

Outputs of transducers have to be made acceptable for the data collection system. Only potentiometric

transducers usually offer high level outputs, depending on the reference supply voltage. Practically all other types of pressure transducers need some electronic circuit to demodulate and/or amplify the output signal to the appropriate level. Strain gauge transducers with integrated electronics have outputs of up to  $\pm 5$  V d.c. with the advantage of short connections of the strain gauges to the amplifier, and low output impedance. Capacitive transducers sometimes are provided with partially integrated electronics, usually the first stage a.c. amplifier. Demodulation amplification and filtering is realized with the aid of separate electronic circuits. Digital outputs are obtained from vibrating element transducers or from transducers with internal analog to digital converters. Outputs can be generated in serial or parallel format usually under control of the digital data collection system. Some pressure transducer systems offer the advantage of separate power supply and signal return connections in order to avoid possible ground loops in instrumentation systems. For differential pressure transducers it is advisable to have a so-called "live zero" to avoid any misinterpretation of zero pressure difference during pre- and postflight checks.

#### Environmental conditions

Two effects of temperature changes on pressure transducers are to be considered; i.e. the effect of temperature on the output with zero-input pressure, and the effect on the sensitivity (scale factor).

Strain gauge pressure transducers are usually fitted with temperature compensating resistors. Temperature coefficients achieved over rather large temperature ranges ( $-50^{\circ}\text{C}/+120^{\circ}\text{C}$ ) are in the order of  $0,02\%/^{\circ}\text{C}$  for zero shift and sensitivity. The same figures apply for reluctance transducers, although in the lower ranges ( $\sim 100$  Pa) somewhat larger figures have to be expected.

Force-balance and capacitive transducers are often provided with controlled heaters to maintain a fairly constant temperature of the sensing element. In capacitive transducers heaters have the additional advantage that they reduce the influence of relative humidity on the sensing element. Disadvantages are: the warm-up times required and the additional electronic circuits.

Single sensing element transducers, especially those with unbonded strain gauges, have rather high g-sensitivity in the direction normal to the diaphragm, sometimes up to  $1\%$  F.S. at  $1g$ . This figure also applies to moving core reluctance transducers. This property is caused by the weight added to the diaphragm. Capacitive and semiconductor strain gauge transducers normally have very low g-sensitivity. About  $0,005\%/g$  F.S. for a  $10\text{ kPa}$  range semiconductor strain gauge transducer and about  $0,01\%/g$  F.S. for a  $100\text{ kPa}$  capacitive transducer. If possible, pressure transducers should be installed with their g-sensitive axis parallel to the Y-axis of the aircraft, especially when symmetrical manoeuvres are to be performed. A priori information on the vibration levels at the transducer locations aids in the design of the transducer mountings. Sometimes shock mounts are required. Some transducers are provided with internal shock mounts for the sensing elements.

Close attention should be paid to Electro Magnetic Interference (EMI), since sensitive electronic circuits tend to pick up noise from electromagnetic fields, which may be generated by operating VHF transmitters or by switching transients in the AC power lines. These effects may be observed as noise or DC offsets in the outputs of the electronic circuits affected.

Integration of amplifiers within transducers and careful shielding of circuits and wiring are recommended. In addition, circuits and instrument housing should be properly grounded.

It is not recommended that pressure transducers and their associated electronics directly use the aircraft's DC power bus as a supply, in view of the voltage variations and transients on this bus.

#### Frequency response

The bandwidth of pressure transducers is large compared to the frequency of aircraft motions, even during nonsteady manoeuvres. Motor driven force-balance transducers have very limited bandwidths, depending on pressure amplitude, due to the slew rate restriction. The frequency response of any transducer depends on the type and the measuring range. Reluctance transducers with moving core have smaller bandwidth compared to those with permeable diaphragms. Capacitive and semiconductor strain gauge transducers have usually high frequency responses. These high bandwidths, however, are usually limited in the signal conditioning equipment. Cut-off frequency of low-pass filters then determines the overall frequency characteristic. Vibrating element transducers also have a rather low frequency response ( $10\text{--}30$  cps), due not to the properties of the sensing element but to the long counting intervals required.

The frequency response of air data measurement systems during flight tests is limited in practice by the length and the diameter of the tubing which connects the transducers with the measuring probes. A useful approximation formula for this time delay is:

$$\tau = \frac{128\mu l}{\pi d^4 P_s} \left[ v_d + \frac{v_t}{2} \right] + \frac{l}{a}$$

where:  $\mu$  = coefficient of viscosity of air  
 $l$  = length of tubing  
 $d$  = internal diameter of tubing  
 $P_s$  = static pressure  
 $v_d$  = volume of transducer  
 $v_t$  = volume of tubing  
 $a$  = velocity of sound

This formula may be up to  $20\%$  in error. Therefore, it is strongly recommended that the frequency transfer function of the pitot-static system is measured on the ground over the frequency range of interest and at different static pressures. In the Hawker Hunter pitot-static system the time delay was in the order of  $250\text{ ms}$  at sealevel, while in the case of the F-28 trailing cone installation the time delay was  $2$  seconds at a pressure altitude of  $10000\text{ m}$  and the cut-off frequency equalled  $0,5\text{ cps}$ . The results for the F-28 were obtained by sinusoidal excitation of the static system while measuring the input and output pressure signals with the pressure measurement system itself (see 4.2.3.).

#### 4.2.3 Practical example

The air data measurement system used for flight tests with the Fokker F-28 was designed to measure the impact pressure PI, the static pressure PS and the static deviation pressure dPS. The transducers used in this measurement system are shown in Table 5. The high resolution required for the altitude measurement (0,1 m) at sea level was achieved by measuring the static pressure deviation (dPS) related to the value of the static pressure (PS) at manoeuvre-initiation.

##### Pneumatics

In the pneumatic part of the system the pressure storage vessel is an important item (see Fig. 5). This vessel is disconnected from the PS input at manoeuvre initiation and the captured pressure is used as reference pressure for the dPS measurement. In order to achieve the high accuracy of 1 Pa for dPS the reference must be stable within 0,3 Pa. Therefore, it is necessary to keep the vessel temperature within 0,002°C at 48°C nominal. This is achieved with a three step temperature control: the reference vessel is contained in a pot which is controlled at a temperature  $0,5 \pm 0,05^\circ\text{C}$  lower than the vessel temperature and this pot is contained in a box together with the rest of the pressure measurement system, which is maintained at a temperature of  $45 \pm 0,7^\circ\text{C}$ . The capacity of the heaters assures a warm up period of less than one hour. The dPS and PS transducers are mounted in the second temperature region for two reasons: short pneumatic connections and high temperature stability. The PI transducer is placed inside the temperature controlled box. Static pressure was sensed with a trailing cone connected to the tip of the vertical fin of the aircraft by a 14 m tube, while impact pressure was sensed with a NLR designed pitot tube which is insensitive to the direction of the airflow. A problem was the fact that the transfer function of the tubes is dependent on the frequency and on the static pressure. Therefore, the static pressure tube and the impact pressure tube were matched in length and diameter in order to achieve equal transfer functions.

##### Transducers

The pressure transducers used in this system were:

- dPS Druck type PDCR 22 with a range of  $\pm 5$  kPa,
- PI Druck type PDCR 22 with a range of  $\pm 17,5$  kPa and
- PS Rosemount absolute transducer 1201F with a range of 0 to 105 kPa.

These transducers are connected with static pressure, pitot pressure, the reference vessel and the calibration nipples via a pneumatic valve. The first position of the valve ("Zero") is used between the measurements and during transport: the reference vessel and the PS transducer are connected to the static cone pressure, the dPS and PI transducers are short circuited and also connected to static cone pressure. The second position ("Measure") disconnects and closes the reference vessel, connects one side of the dPS transducer and the PS transducer to the static cone pressure, and the PI transducer is connected between static pressure and pitot pressure. The third position ("Calibrate") connects all transducer pressure inputs to the calibration nipples. During flight all calibration nipples were connected to static pressure to avoid connection to cabin air which can create temperature problems in the vessel. The valve rotates only in the cycle zero, measure, calibrate.

##### Electronics

The electronic part of the system consists of the temperature control circuits, voltage references, amplifiers and filters for the transducer signals, analog multiplexer and A/D converter, and a microprocessor with interfaces. The microprocessor arranges the digital data in a ARINC 429 serial data stream and controls upon command the pneumatic valve and the internal timing which can be slaved to an external signal. High precision NTC resistors are used in the temperature control circuits. An alarm is raised when temperatures are too high or too low. Installed heater power is 6W for the reference vessel, 80 W for the pot with the reference vessel and 110 W for the box containing pot and electronics. The differential transducers for dPS and PI are of the semiconductor strain gauge type and have a output of about 10 mV. Effects of acceleration are minimized by mounting the sensors in the most favourable direction in the aircraft, effects of bridge supply are minimized by relating this voltage to the A/D converters reference voltage. Also the output of the PS transducer (a single sided capacitive type) is related to the reference voltage of A/D converter. Transducer signals are amplified and fed to the anti-aliasing filters. These filters are 5th order linear phase (Bessel) filters with a cut-off frequency of 4 cps. The filtered signals are connected to a 16 bit A/D converter by means of an analog multiplexer. The digitized measurements are input to the microprocessor system which arranges the data in a 8 bit label +24 bits data ARINC 419 format, establishes the timing relation to the input clock/synchronization signal and controls the pneumatic valve upon external command. The system is housed in a 1/1 ATR box ( $45,5 \times 49,5 \times 20,5 \text{ cm}^3$ ), power regulators and filters are separate in a 1/2 ATR short box ( $12,5 \times 19,5 \times 31,5 \text{ cm}^3$ ). The system is powered by the aircraft's 28V DC and 115 V 400 Hz which are converted into filtered 28V for the heaters,  $\pm 15\text{V}$  for the analog circuits and  $\pm 5\text{V}$  for the logic circuits.

##### Position/deflection transducers

###### General aspects

For steady flight testing very accurate measurements of control surface deflections are required. In the case of the elevator deflection measurement equals about 0,1% or 0,05 to 0,1 mm. Usually it is required to measure the elevator deflection, the aileron deflection, the rudder deflection and the elevator trim deflection. For asymmetrical manoeuvres rudder trim deflection measurement is required as well. If measurements are to be made during take-off and landing, flap deflection measurement is required.

###### Position/deflection measurements

Position transducers are widely used for position measurements. The principle is very simple: a



sliding contact or wiper moves over a resistive element, which is connected to a reference voltage source. The voltage taken from the wiper with reference to one of the end points is a direct measure of the position of the wiper. The motion of the wiper can be either angular or linear.

Resistive elements of both angular and linear potentiometers are made of resistance wire or film deposited on a substrate.

The slide wire potentiometer, a device in which the wiper moves along a single wire, is seldom used for position measurement. However, it is used in force-balance air data transducers as a multiturn (100 or more revolutions) output device. Resistance is low (1k), the resolution is infinite and the linearity is very good, depending only on constancy of the cross section of the wire. The wire wound potentiometer is provided with a resistive element which consists of resistance wire uniformly wound around an insulated core. Linearity depends on spacing of the wire and on eccentricity of the wiper shaft in angular potentiometers. The resolution depends on the number of wires used. If high resolution is required very thin wire has to be used. The smallest wire diameter applicable with regard to reliability is about 0,02 mm. A resolution of 0,05% can be achieved with an angular wire wound potentiometer with an outside diameter of 7/8" or size 8. The total resistance value however will be in the order of 100k, which can be a disadvantage, since high input impedance of the measuring equipment is required. Otherwise nonlinearities due to loading effects have to be dealt with in the calibration procedure. Linearity achieved in wire wound angular potentiometers (depending on case diameter) is from 0,5% for a size 8 up to 0,01% for case diameters over 3".

Film potentiometers have resistance elements of metal, cermet, conductive plastic or carbon.

The advantages of film potentiometers are the infinite resolution, the high power rating and the high reliability combined with a wide range of resistance values. Some metal film potentiometers have limited life expectancy, due to very thin film elements.

Cermet potentiometers may have positive or negative temperature coefficients depending on total resistance, for example 0 to +500 ppm per °C for a 100% total resistance or 0 to -250 ppm per °C for a 200k total resistance potentiometer. Life expectancy for cermet is up to  $15 \cdot 10^6$  and for conductive plastic film up to  $40 \cdot 10^6$  revolutions.

Attention must be paid to the so called "end resistance" of film potentiometers, since linearity is specified from 1% to 99% of the mechanical travel.

Practically all types of film elements are available in angular as well as in linear potentiometers.

#### Synchros

The synchro consists basically of a three phase stator and a single phase rotor. The stator windings are spaced at 120 degrees. The rotor is energized with an a.c voltage, usually 26V at 400 cps. The output voltages of the stator windings contain in their amplitude and phase (with reference to the rotor voltage) unique information about the angular position of the rotor.

The type of synchro used for angular position measurements is usually the so-called synchro-control-transmitter. This is a device primarily designed to operate with control-transformers and high input impedance electronic circuits. The resolution of synchros is infinite, the linearity achieved with some types is in the order of 7-10 minutes of arc. The accuracy of synchros, depending on mechanical construction and electrical error, is approximately 0,02 to 0,03% or approximately 0,1 degree.

The stability of synchros is very good, temperature changes have little effect on the output characteristics.

In flight test instrumentation systems the output voltages of synchros have to be converted either into an analog d.c. voltage or directly into a digital signal. Several types of applicable converters are readily available.

#### 4.3.3 Design considerations

In order to perform reliable, high accuracy control surface deflection measurements, the deflection transducers should be connected to the control surfaces as close to the hinges as possible (Ref. 16). Under no circumstances, during normal operation or in case of failure of the transducer, should the operation of the aircraft's control surfaces be affected.

Deflection sensors, either linear or angular, either synchro or potentiometer type, have to be isolated from high loads on shafts and bearings. Such loads may result from forces and moments exerted by additional masses of levers, pushrods, etc., or from vibration of aircraft structures in flight.

For angular sensors isolation is achieved by coupling the sensor shaft with precision (split) gears to a strong and rigid intermediate shaft which in turn runs in rigidly mounted ball-bearing. To the intermediate shaft relatively strong levers can be clamped which in turn are connected by means of a pushrod to the lever of the control surface. Precision ball-joints are usually applied at the ends of pushrods to reduce bending moments due to minor misalignment of the transducer input axis and the control surface rotation axis.

Usually only limited space is available in an aircraft for housing of deflection transducer gear.

Lever-arms, however, should be made as long as possible in order to reduce the effect of minor play in pushrod connections. If so required, material of pushrods and leverarms should be matched to the aircraft's structural material to reduce temperature effect on the zero position and the sensitivity of the position transducer. To achieve maximum linearity, the lever arm of the transducer must be fitted parallel to the lever arm of the control surface, and if possible these lever arms should have the same effective length (see Fig. 6 which was taken from Ref.16). The gear ratio in the transducer can be chosen so as to obtain full range output for any given control surface deflection range.

Sometimes linear displacement transducers are applied for control surface deflection measurements. Such transducers are available in ruggedized design, provided with balljoints at the housing and at the end of the shaft.

Two problems have to be considered when applying this type of transducer.

- What happens in case of a transducer failure e.g. jammed shafts, breakdown of wiper assembly etc.
- Is the transducer capable to withstand relatively high loads normal to the transducer axis, in fully extended position.

A possible application of linear potentiometers is described in 4.3.4.

#### 4.3.4 Practical examples

Two position transducers were designed for nonsteady flight testing of the Hawker Hunter MK VII of the National Aerospace Laboratory. One transducer was used for measurement of the deflection of the horizontal stabilizer relative to the aircraft's X-axis and the other was used for measurement of the elevator angle relative to the horizontal stabilizer (see Fig. 7).

The ranges of the stabilizer and elevator deflection angles were respectively 6 degrees and 33 degrees. In order to minimize production cost, both transducers were designed to be basically similar. The transducers are provided with angular cermet potentiometers type 6603 of Beckman Instruments Inc. This type of potentiometer has a servo mount (size 20) and is provided with ball bearings. A resistance value of 100 k was specified to achieve a temperature coefficient of only 50 ppm per degree C. The linearity tolerance of this potentiometer equals 0,1%. In the transducers the potentiometers are driven by precision split gears (DIN 867). The ratio of the gears equals 1:6. This ratio results in a rotation of 290 degrees for the stabilizer potentiometer and of 330 degrees for the elevator potentiometer. The split gears in the transducers are preloaded with a small spring in order to keep play as small as possible even during the expected temperature changes. Intermediate shafts are provided with ball bearings, while the pushrods connecting the levers are provided with steel-bronze-teflon ball joints, in order to minimize effects of forces due to small misalignments. The levers of the stabilizer transducer have unequal lengths, in order to provide reasonable potentiometer rotation for relatively small deflection angles.

The price to be paid for this amplification of the measurand is a minor nonlinearity.

The static accuracy of the elevator and stabilizer deflection transducer respectively equaled 0,04 degree, and 0,01 degree.

As a result of play in the elevator control horn bearing the accuracy of the elevator deflection measurements was reduced to 0,08 degree of arc.

For the 1978 nonsteady flight test program carried through with the DHC-2 Beaver, linear film potentiometers CIC type 116 were used to perform the control surface deflection measurements. The stroke of the potentiometers equals 100 mm, the resistance value is 5k. The transducers used for measurement of left and right aileron deflection, elevator and rudder deflection and left and right flap deflection are basically of similar construction, in order to keep production costs low.

To isolate the potentiometer shafts from loads normal to the measuring direction, the free ends of the potentiometer shafts are both rigidly fixed on two sustaining shafts, thus forming a three shaft assembly. These two sustaining shafts are beared in two precision bearing blocks fixed on the mounting plate of the potentiometer. The mounting plate as well as the free end of the shaft are provided with steel-bronze-teflon bearings. The ball joint of the shaft end is connected to the shaft assembly by a shear pin (maximum allowable force about 50 N) for safety reasons. Special care is taken to prevent any play and to provide for easy and reproducible replacement of the shearpin. Aileron, rudder and elevator transducers are located respectively inside the wing and the tailcone and are linked directly to the control horns of the control surfaces. The wing flap transducers are located outside the wing directly connected to the flap joints. The flap transducers are provided with an additional dust cover, to prevent the entrance of dust and water into the sensing element.

In addition to these transducers also two trimtab deflection transducers were provided. These are very small transducers also fitted with linear potentiometers ("Bourns linipot") and mounted outside the aircraft directly on the rudder and elevator control surfaces. The free shaft ends are connected to the trimtabs through miniature ball joints. The static accuracy achieved with the deflection transducers ranges from 0,02 to 0,1 degree for the control surfaces, up to 0,3 degree for the trimtabs.

The accuracy of the deflection measurements is degraded by the play in the control surface hinges and the lever joints. This statement holds in particular for the trim tab deflection measurements.

### 5. Signal conditioning

#### 5.0 Introduction

Signal conditioning embraces all modifying operations applied to signals (electrical or physical) to satisfy input conditions of the subsequent stages of the instrumentation system. Several reasons exist for signal conditioning in a flight test instrumentation system (Ref. 22). The emphasis is on the accuracy required for performing measurements in nonsteady flight.

Signal conditioning includes among others:

- a. Adaptation of transducer outputs to the input requirements of a data collection system.
- b. Extraction of signals, relevant to flight testing, from the standard aircraft instrumentation.
- c. Satisfying impedance matching requirements between components of a measuring channel.
- d. Filtering of signals prior to feeding a subsequent signal processing stage.
- e. Multiplexing.
- f. Analog to digital conversion.

#### 5.1 Modification of transducer outputs

##### 5.1.1 Elementary adaptation

Flight test instrumentation systems usually incorporate transducers with many different types of output signals, as some transducers, relevant to flight testing, are already available in the aircraft and others are selected with regard to accuracy, resolution, stability, etc. rather than with regard to output signal specifications. Transducers in general may have analog low or high level d.c. outputs e.g. strain gauges, potentiometers, accelerometers or analog low or high level a.c. outputs, e.g. reductive transducers, synchros. Transducer output signals are passed through signal conditioning units, for instance for amplification, rectification or demodulation and sometimes for level shifting. Level shifting is required if the desired output signal range of the transducer must be matched to the input range of the A/D converter.

### 5.1.2 Interaction with cockpit instruments

If standard aircraft transducers are to be utilized for flight test purposes, care has to be taken not to introduce possible misreading of cockpit instruments. For example:

- Synchro outputs of attitude reference systems should be coupled into recording equipment using high input impedance converters to produce either an analog or a digital output signal.
- Total temperature measurement performed with resistive elements can be adapted to data collection systems, using high input impedance differential amplifiers.
- Engine RPM measurements are usually performed with the aid of the a.c. generator coupled to the aircraft's engine. In this case signal conditioning should satisfy two requirements: i.e. isolation from the generator-cockpit indicator combination and conversion from the frequency of the a.c. voltage into either an analog d.c. voltage or directly into a digital signal.

In general it is sensible to have the possibility to disconnect the data collection system from aircraft instruments or systems. This operation is easily performed with the "normal open" contacts of a multipole relay, which is energized simultaneously with the data collection system.

### 5.1.3 Impedance adaptation

Sometimes relatively high output impedance transducers have to be used, such as potentiometers with a high resistance value, some types of accelerometers and capacitive transducers. Connection of high output impedance transducers directly to the measuring equipment usually results in a change in linearity and/or the scale factor of the transducer. To reduce these effects impedance conversion is required in the signal conditioning unit, with high input impedance (buffer) amplifiers. Also noise and d.c. susceptibility are reduced when this kind of signal conditioning is performed close to the sensing element. A disadvantage, however, is the requirement for additional power supply leads to the signal conditioner at a remote location in the aircraft.

### 5.1.4 Analog filtering

Filters are used in measuring systems to attenuate the amplitude of the high frequency contents of the signals. For nonsteady flight test work, signals with frequencies of up to approximately 1 cps have to be recorded. There are several reasons for filtering signals in measuring channels. Transducers with high bandwidths are able to pick up unwanted inputs due to vibration. This holds in particular for accelerometers and rate gyros. To prevent saturation of these transducers it may be necessary to install some form of mechanical filter between the aircraft structure and the transducer, such as shock mounts or anti-vibration mountings.

Extreme care must be taken when such filters are applied since they should never affect transducer alignment in the signal frequency range of interest. The damping of mechanical filters is usually low, resulting in nonlinear phase characteristics, which in turn introduces signal distortion. A priori information about the environmental conditions at the location of the transducer package is required, to establish mechanical filter characteristics (See Ref. 18). Apart from preventing transducer saturation, it is required to reduce high frequency signal amplitude due to vibration or electrical noise. Attenuation of high frequency signal components is required to reduce aliasing error caused by the finite sampling rate of the data collection system. The specification of anti-aliasing filters depends on sampling rate and the desired measurement accuracy, in relation to the signal frequency contents. Two conflicting requirements arise in designing anti-aliasing filters.

Firstly: The filter cut-off frequency must be high compared to the frequency range of the signal of interest. Such in order to obtain a flat frequency response and a constant group delay over the specified frequency range.

Secondly: The filter cut-off frequency must be low compared to the sample frequency of the data collection system. Such in order to keep amplitudes of fold-over frequencies within the specified accuracy limits.

A valuable reference book on the design of analog filters is Ref. 19.

### 5.2 Multiplexing

In digital data collection systems signals of a large number of measuring channels have to be recorded. This is achieved by multiplexing the analog or digital transducer signals in a predetermined sequence. Analog multiplexers are provided either with high quality relays or with electronic switches. The quality of multiplexers directly affects the accuracy of the instrumentation system.

Some key specifications of switches used for signal commutation are:

- the "on-resistance",
- the "off resistance"
- the leakage current in open state
- the "settling time"
- the "cross talk" between adjacent switches.

Electronic switches for signal commutation are available as complete multichannel devices, with control inputs which are compatible with digital circuits. For multiplexing digital signals several standard integrated circuits are available. For nonsteady flight testing analog multiplexers are required with an accuracy of 1 mV on a 10V signal amplitude.

### 5.3 Sample and hold unit

A sample and hold circuit preceding the analog to digital converter is required if signal variation during the analog to digital conversion period exceeds the A/D converter resolution. Such a sample and hold circuit tracks the input signal during a sample command signal and holds the input signal within the specified accuracy limits upon a hold command signal.

The signal frequency and amplitude determine the rate of change, i.e. the slewrate, of the input signal. The maximum error developed by the A/D converter measuring a sinusoidal signal can be calculated as:

$$e_m = \frac{2\pi\Delta t}{T} \cdot 100 \%$$

where  $\Delta t$  is the A/D conversion time and  $T$  is the signal period time.

The maximum error,  $e_m$ , represents a worst case error which occurs only if a so called successive approximation A/D converter is used and for measurements performed at the zero crossings of the input signal. In case of random measurements the probable error is much smaller;

$$e_p \approx \frac{0.3\pi\Delta t}{T} \cdot 100 \% \approx \frac{\Delta t}{T} \cdot 100 \%$$

If for example an A/D converter is used with a conversion time of 1 ms to measure a full scale sine input signal with a frequency of 1 cps, the probable error is 0,1 % and the maximum error is about 0,6 %.

Key specifications of sample and hold circuits are:

<u>Acquisition time</u>	: the time interval between sample command and the moment the output tracks the input signal within the accuracy limits.
<u>Aperture uncertainty</u>	: the difference between the maximum and minimum time required to change from sample to hold (turn off time).
<u>Settling time</u>	: the time required for the output to track the input signal for a full scale step input change within the specified accuracy limits.
<u>Decay rate</u>	: the maximum rate of change of the output in the hold mode.
<u>Gain accuracy</u>	: a measure of gain stability under specified environmental conditions.
<u>Output offset</u>	: the maximum value of output when zero input is sampled.

#### 5.4.1 General aspects.

Analog to digital conversion in a measuring system is considered as signal conditioning; the pre-conditioned analog signals are converted into a digital word. In a rather simple instrumentation system only one analog to digital converter (ADC) may be used under the condition that all signals to be digitized have the same range. This requirement has to be satisfied in the preceding signal conditioning units.

#### 5.4.2 Design consideration

A wide variety of A/D converters in modular form is commercially available. Consideration of the following converter characteristics may guide the system designer in the selection of a suitable A/D converter (Ref. 20,21)

##### Conversion speed

The maximum time available for one complete conversion may be derived from the instrumentation system requirements. The number of channels which have to be digitized and the sampling rate of each individual signal determine the processing time available for the multiplexer, the sample and hold (if applicable) and the A/D converter. The available time for one complete measurement leads to the decision whether a rather slow dual slope integrating or a fast successive approximation converter is required. When a very fast A/D converter is applied (e.g. 20  $\mu$ s conversion time) a sample and hold circuit, which affects system cost and complexity, might not be required.

##### System consideration

The converter characteristics affected by the system configuration (design) include: the digital code, e.g. (offset) binary, two's complement, binary coded decimal (BCD); the input voltage range (unipolar or bipolar); the input impedance; power supplies etc. For high accuracy measurements a special grounding technique or a differential buffer amplifier may be required. Some converters have separate analog and digital grounds, in these converters digital currents do not interfere with analog signals. Optical coupling of digital outputs provide for complete electric isolation of the A/D converter from the data recording system. It is convenient to have access to the reference voltage of the A/D converter in order to control the instrumentation system's reference power supply, since this will allow ratiometric measurements (fig.8). However, extreme care must be taken not to affect any of the converter's specifications, when connections are made to the reference voltage.

##### Resolution and accuracy

The practical resolution of A/D converters is usually less than the number of bits presented at the output. This phenomenon is caused by noise generated in the analog circuits of the converter. Sometimes noise level referred to the analog input of the converter is specified as RMS noise, the momentary error, however, may be up to 6 times the specified RMS value. The noise is generated in the reference voltage source, the input buffer or scaling amplifier, the comparator and in the precision resistor network. The absolute accuracy of an A/D converter is the ability of the converter to produce an output code which defines the input voltage with reference to the "Standard Volt". The relative accuracy is related to the linearity of the converter and is defined in terms of deviations from the best fitted straight calibration line. To maintain accuracy during the measurement period it is important that the converter is provided with means for offset and range adjustment. When external adjustment components have to be installed, careful selection of these components is required, as the stability and the overall temperature coefficient may be affected.

##### Environmental conditions

When high resolution, high accuracy A/D converters are used in flight test instrumentation systems, the sensitivity of the converter to temperature changes, humidity, electromagnetic and electrostatic fields has to be considered. Also susceptibility to power supply ripple and noise may affect the performance of the converter. High resolution converters usually have very low temperature coefficients in the order of a few

ppm per degree C for gain and offset, such in order to match the accuracy to the resolution of 14 or 16 bits.

Some shielding from EMI is provided by the metal housing of the converter module, but additional shielding may be required depending on the location of the converter. Sources of EMI may be Distance Measuring Equipment, transmitters, transponders, a.c and d.c. power conductors and natural lightning. Power supply noise has to be suppressed as much as possible. This is usually achieved by application of bypass capacitors and RF chokes in the converter module.

### 5.5 Practical Example

In the instrumentation system for the measurements in nonsteady flight with the Hawker Hunter MK VII as well as in the system for the DHC-2 Beaver (Fig. 9), high quality anti-aliasing filters are applied. Each analog measuring channel is provided with fourth-order low pass filters, which are nominally equal with respect to gain, damping ratio and cut-off frequency. The cut-off frequency of the filters was established at  $19 \text{ rad s}^{-1}$ . With a sampling rate of 20 measurements per sec, the aliasing error of combined images is kept below 0.1% up to about  $10 \text{ rad s}^{-1}$ . The calculation of the damping ratio was carried out as follows. Each fourth-order filter is considered to consist of two equal second-order filters connected in series (actually the fourth order filters are constructed in this way). The normalized frequency characteristic of a second-order low pass filter only depends on the static gain and the damping coefficient. With given gain limits the damping coefficient which allows for the highest possible frequency is calculated. With the gain limits set equal to unity  $\pm 0.001$  the calculated damping coefficient is 0.691. This value is slightly smaller than the critical value which equals 0.707. This results in a frequency characteristic with an increasing gain to 1.001 from zero frequency to  $4 \text{ rad s}^{-1}$  and a decreasing gain to 0.999 from  $4 \text{ rad s}^{-1}$  to  $6.3 \text{ rad s}^{-1}$ . The gain equals 1.000 at  $5.6 \text{ rad s}^{-1}$ . So the maximum bandwidth of the filter between the gain limits is  $6.3 \text{ rad s}^{-1}$  or 1 cps which equals approximately one third of the cut-off frequency (Fig. 10, 11).

The phase shift of the low-pass filters has to be considered next. The time shift of a second order system at zero frequency always equals two times the damping factor divided by the cut-off frequency:  $2\lambda/\omega_0$ . At the cut-off frequency the time shift equals:  $\pi/2\omega_0$ . Hence, in the low pass filters mentioned above with a cut-off frequency of  $19 \text{ rad s}^{-1}$  and a damping factor equal to 0.691 the time shift will vary from 73 ms at zero frequency to 83 ms at the cut-off frequency. However, up to the usable bandwidth of  $6.3 \text{ rad s}^{-1}$  the time shift varies from 73 to 75 ms resulting in a maximum time shift error of  $\pm 1 \text{ ms}$  for signals with a frequency of up to 1 cps, being the frequency range relevant to flight testing (Fig. 12).

The practical realization of the second order filters is performed with chopper-stabilized operational amplifiers and high stability resistor/capacitor networks (Fig. 13). Four filters are mounted together in one unit measuring approximately  $3 \times 10 \times 30 \text{ cm}^3$ . The front panel is provided with one switch and one screw driver potentiometer for zero-adjustment of each amplifier. Each filter has provisions for the adjustment of static gain, damping factor and cut-off frequency (Fig. 14). A kind of model matching technique was applied, using a high precision analog computer, to perform the final adjustment of the filters (Fig. 15).

### 6. FINAL REMARKS

The development of the nonsteady flight test technique has resulted in a steady improvement in the accuracy of the flight test instrumentation systems used. It should be realized, however, that the accuracy of the results derived from nonsteady flight tests is at present primarily limited by factors other than the transducer accuracies. These factors are among others: wind velocity variations and turbulence, engine thrust uncertainties and errors in the aerodynamic models used. Other factors are more closely connected to the instrumentation system, such as position error correction uncertainties and pitot-static delay uncertainties. Also, the deformation of each control surface under aerodynamic loading introduces discrepancies between the actual effectiveness of the control and the deflection measured by the instrumentation system. This raises the question whether the cost and effort of developing high accuracy instrumentation systems is really justified. A few remarks will be made on this point:

As already mentioned in section 1.2, less accurate transducers tend to have a more complicated error behaviour. For example, the bias error of the inertial transducers is very important for the quality of the results of the flight path estimation procedure (Ref. 7). This is the reason that these bias errors are estimated using an extended Kalman filter procedure. In this procedure it is assumed that the bias errors are constant during the measurement, but this is not necessarily true for low quality transducers. Since the uncertainty of the bias error estimates heavily depends on the shape of the nonsteady manoeuvre and on the set of variables selected for measurement (Ref. 23), it is obvious that it will not be possible to estimate time-varying bias errors.

A second example is the variation in the magnitudes of the horizontal components of the wind vector, which may result in large errors in the estimated angle of attack. In the F-28 flight test program, it turned out that the wind velocity variation could be adequately modelled as being proportional to altitude. The wind gradient, however, could not be estimated simultaneously with the bias errors of the inertial transducers. Fortunately, these bias errors, estimated from measurements that did not suffer from wind velocity changes, proved to be negligibly small, which confirmed the high quality of the inertial transducers used. This justifies the deletion of the bias errors from the flight path estimation procedure and the incorporation of the wind gradients into this procedure.

Another viewpoint is the need for reproducibility of the flight test results. For example, the determination of engine thrust is a difficult subject and there is never complete certainty that the estimated aircraft drag coefficient is not corrupted by systematic errors in the determination of the engine thrust. If, however, the determination of the drag coefficient is aimed at the calculation of the actual performance of the aircraft, such as rate of climb, with the same engine under approximately the same circumstances, the reproducibility of the calculated engine thrust is more important than the absolute accuracy. Therefore, the accuracy of the measurements of the engine variables should not degrade the reproducibility of the calculated engine thrust. A similar argument can be put forward with respect to the uncertainty in the control surface deflection measurements. It is clear, that the actual deflection is not as important as whether the angle measured by the transducer gives reproducible results in the aerodynamic model identification.

Obviously only high quality instrumentation offers the accuracy and the stability required for an acceptable reproducibility of the flight test results.

The final motivation for the high accuracy instrumentation system is the ability to detect, to estimate and to correct for all perturbations, other than from instrumentation errors, that affect the accuracy of the flight test results. The determination of some of these effects, such as the influence of aeroelasticity, require even more extensive instrumentation than the systems referred to in this paper.

#### REFERENCES

1. O.H. Gerlach: "Analyse van een mogelijke methode voor het meten van prestaties en stabiliteits- en besturingseigenschappen van een vliegtuig in niet-stationaire, symmetrische vluchten" (In Dutch with summary in English), Delft University of Technology, Department of Aerospace Engineering, Delft, Report VTH-117, 1964.
2. Hussenot: "Methodes nouvelles d'essais en vol", Technique et Science Aeronautique, Vol. 6, pp 38-49, 1950.
3. J.P.K. Vlegghert: "Measuring climb performance of a propellor engined transport aeroplane using the acceleration technique", AGARD Report 127, 1957.
4. H.B. Klopfenstein: "Obtaining airplane-drag from nonsteady flight", AIAA Paper no. 65-211, 1965.
5. O.H. Gerlach: "Determination of performance and stability parameters from nonsteady flight test maneuvers", Society of Automotive Engineers, Inc. National Business Aircraft Meeting, Wichita, Kansas, SAE Paper no. 700236, 1970.
6. O.H. Gerlach: "The determination of stability derivatives and performance characteristics from dynamic manoeuvres", AGARD Conference Proceedings, no. 85, 1971 (VTH-163).
7. H.L. Jonkers: "Application of the Kalman filter to flight path reconstruction from flight test data including estimation of instrumental bias error corrections", Delft University of Technology, Department of Aerospace Engineering, Delft, Report VTH-162, 1976.
8. J.H. Breeman, J.L. Simons: "Evaluation of a method to extract performance data from dynamic maneuvers for a jet transport aircraft", 11th Congress of the International Council of the Aeronautical Sciences, Lisbon, September 1978.
9. H.L. Jonkers, J.A. Mulder: "Accuracy limits in nonsteady flight testing", the Tenth Congress of the International Council of the Aeronautical Sciences, ICAS Paper no. 76-46, Ottawa, Oct. 1976.
10. H.L. Jonkers, J.A. Mulder: "New Developments and accuracy limits in aircraft flight testing", AIAA Aircraft Systems and Technology Meeting, Dallas, Texas, AIAA Paper no. 76-897, Sept. 1976.
11. R.J.A.W. Hosman: "Advanced flight test instrumentation: Design and calibration", Delft University of Technology, Department of Aerospace Engineering, Memorandum M-222, 1974.
12. H. Pouwels: "Instrumentation for the determination of aircraft performance from dynamic maneuvers", 25th International Instrumentation Symposium, Anaheim, May 1979.
13. J. McLaren: "Open and closed loop accelerometers", AGARD Flight Test Instrumentation Series, AGARDograph no. 160, vol. 6, 1974.
14. L.J.M. Joosten: "Determination of performance and stability characteristics from dynamic longitudinal maneuvers with the Fokker F-28 transport aircraft; Description of inertial strapdown system", National Aerospace Laboratory, NLR TR 78058L, 1978.
15. F. Trenkle, M. Reinhardt: "In flight temperature measurements", AGARD Flight Test Instrumentation Series, AGARDograph no. 160, Vol.2, 1973.
16. J.C. van der Linden, H.A. Mensink: "Linear and angular position measurement of aircraft components", AGARD Flight Test Instrumentation Series, AGARDograph no. 160, Vol.8, 1977.

17. H.N. Norton: "Handbook of transducers for electronic measuring systems", Prentice Hall, 1969.
18. J.H. Breeman: "Vibration measurements in the Beaver of the Department of Aerospace Engineering of the Delft University of Technology", (In Dutch), National Aerospace Laboratory, NLR VV74-040.
19. A.I. Zverev: "Handbook of filter synthesis", Wiley, 1967.
20. H. Schmid: "Electronic analog/digital conversions", Van Nostrand-Reinhold, 1970.
21. B.M. Gordon: "The Analogic data conversion systems digest", Analogic Corporation, 1977.
22. A. Pool, D. Bosman: "Basic principles of flight test instrumentation engineering", AGARD Flight Test Instrumentation Series, AGARDograph no. 160, Vol. 1, 1974.
23. A. Mulder, H.L. Jonkers, J.J. Horsten, J.H. Breeman, J.L. Simons: "Analysis of aircraft performance, stability and control measurements, Part I: Theoretical aspects", AGARD LS-104, 1979.

Table 1: LIST OF MEASURED VARIABLES HUNTER Mk VII

	Variable	Unit	Range	Calibrated range	Static accuracy (10)
A <sub>x</sub>	specific force X-axis	ms <sup>-2</sup>	+ 10	+ 10	0.002
A <sub>y</sub>	specific force Y-axis	ms <sup>-2</sup>	+ 5	+ 5	0.001
A <sub>z</sub>	specific force Z-axis	ms <sup>-2</sup>	+ 100	-15/+45	0.004
q	rate of pitch	deg s <sup>-1</sup>	+ 23	+ 20	0.002
r	rate of yaw	deg s <sup>-1</sup>	+ 7	+ 7	0.02
ψ	change in yaw	deg	360	+ 90	0.06
φ	angle of roll	deg	+ 90	+ 16	0.03
δ <sub>e</sub>	elevator angle	deg	-9/+21	-9/+21	0.04
ih	elevator trim angle	deg	+ 2.5	+ 2.5	0.01
α	angle of attack (vane)	deg	+ 30	+ 30	0.03
P <sub>ref</sub>	reference pressure	kPa	110	110	0.03
q <sub>c</sub>	P <sub>t</sub> -P <sub>ref</sub>	kPa	70	0/50	0.01
ΔP <sub>1</sub>	P <sub>1</sub> -P <sub>ref</sub>	kPa	+ 7	+ 5	0.004
ΔP <sub>4</sub>	P <sub>c</sub> -P <sub>ref</sub>	kPa	+ 2	+ 1.7	0.006
ΔP <sub>5</sub>	P <sub>s</sub> -P <sub>ref</sub>	kPa	+ 2	+ 1.7	0.004
ΔP <sub>6</sub>	P <sub>c</sub> -P <sub>ref</sub>	kPa	+ 2	+ 1.7	0.005
ΔP <sub>sj</sub>	P <sub>sj</sub> -P <sub>ref</sub>	kPa	+ 70	-30/+70	0.03
ΔP <sub>tj</sub>	P <sub>tj</sub> -P <sub>ref</sub>	kPa	+ 175	0/170	0.1
n	engine speed	rpm	8200	8200	1.2
EGT	exhaust gas temperature	K	273/1473	273/1050	1.1
T <sub>t</sub>	total air temperature	K	173/473	223/323	0.02

TABLE 2: LIST OF MEASURED VARIABLES FOKKER F-28

	Variable	Unit	Range	Calibrated range	Static accuracy*
A <sub>x</sub>	specific force X-axis	ms <sup>-2</sup>	+ 100	+ 25	0.001
A <sub>y</sub>	specific force Y-axis	ms <sup>-2</sup>	+ 100	+ 25	0.001
A <sub>z</sub>	specific force Z-axis	ms <sup>-2</sup>	+ 100	+ 25	0.001
p	rate of roll	deg s <sup>-1</sup>	+ 23	+ 10	0.001
q	rate of pitch	deg s <sup>-1</sup>	+ 23	+ 10	0.001
r	rate of yaw	deg s <sup>-1</sup>	+ 23	+ 10	0.001
ψ	yaw angle	deg	360	360	0.2
θ	pitch angle	deg	+ 90	+ 25	0.1
φ	roll angle	deg	+ 90	+ 25	0.1
δ <sub>el</sub>	elevator deflection left	deg	-26/+14	-26/+14	0.1
δ <sub>er</sub>	elevator deflection right	deg	-26/+14	-26/+14	0.1
δ <sub>al</sub>	aileron deflection left	deg	-22/+22	-22/+22	0.3
δ <sub>ar</sub>	aileron deflection right	deg	-22/+22	-22/+22	0.3
δ <sub>r</sub>	rudder deflection	deg	-33/+33	-33/+33	0.2
δ <sub>s</sub>	stabilizer deflection	deg	-10/+ 4	-10/+ 4	0.05
α	angle of attack (vane)	deg	+ 90	- 5/+25	0.03
β	angle of sideslip (vane)	deg	+ 90	+ 15	0.03
q <sub>c</sub>	impact pressure	kPa	+ 25	0/17.5	0.010
ΔP <sub>s</sub>	deviation in P <sub>s</sub>	kPa	+ 5	+ 5	0.001
P <sub>s</sub>	static pressure	kPa	0/130	15/105	0.050
P <sub>2l</sub>	deliv.press.lp.comp.left	kPa	0/175	0/175	2
P <sub>2r</sub>	deliv.press.lp.comp.right	kPa	0/175	0/175	2
P <sub>3l</sub>	deliv.press.hp.comp.left	kPa	0/1600	0/1600	20
P <sub>3r</sub>	deliv.press.hp.comp.right	kPa	0/1600	0/1600	20
P <sub>7l</sub>	thrust pressure left	kPa	0/240	0/240	0.2
P <sub>7r</sub>	thrust pressure right	kPa	0/240	0/240	0.2
n <sub>1pl</sub>	left eng.speed lp. shaft	rpm	1600/8900	1600/8900	9
n <sub>1pr</sub>	right eng.speed lp.shaft	rpm	1600/8900	1600/8900	9
n <sub>hpl</sub>	left eng.speed hp.shaft	rpm	2300/13000	2300/13000	13
n <sub>hpr</sub>	right eng.speed hp.shaft	rpm	2300/13000	2300/13000	13
T <sub>7l</sub>	turbine gas temp. left	K	573/1023	573/1023	5
T <sub>7r</sub>	turbine gas temp. right	K	573/1023	573/1023	5
T <sub>t</sub>	total air temperature	K	190/330	190/330	0.3
h <sub>p</sub>	pressure altitude	m	0/24000	0/24000	5
V <sub>ias</sub>	indicated airspeed	ms <sup>-1</sup>	0/230	0/230	0.5
V <sub>NS</sub>	N-S velocity	ms <sup>-1</sup>	+ 1600	+ 1600	1
V <sub>EW</sub>	E-W velocity	ms <sup>-1</sup>	+ 1600	+ 1600	1
λ	present position latitude	deg	+ 90	+ 90	0.02
μ	present position longitude	deg	+ 180	+ 180	0.02

\* These accuracy figures are the largest deviations between the results of six independent calibrations performed before, during, and after the flight test program.



TABLE 3: LIST OF MEASURED VARIABLES DHC-2 BEAVER

	Variable	Unit	Range	Calibrated range	Static accuracy (1σ)
A <sub>x</sub>	specific force X-axis	ms <sup>-2</sup>	+ 10	+ 10	0.001
A <sub>y</sub>	specific force Y-axis	ms <sup>-2</sup>	+ 5	+ 5	0.0005
A <sub>z</sub>	specific force Z-axis	ms <sup>-2</sup>	+ 20	0/-20	0.001
p	rate of roll	deg s <sup>-1</sup>	+ 23	+ 20	0.002
q	rate of pitch	deg s <sup>-1</sup>	+ 23	+ 20	0.002
r	rate of yaw	deg s <sup>-1</sup>	+ 23	+ 20	0.002
ψ	yaw angle	deg	360	0/360	0.2
δ <sub>e</sub>	elevator angle	deg	51	-28/23	0.02
δ <sub>a<sub>l</sub></sub>	aileron angle left	deg	50	-17/33	0.06
δ <sub>a<sub>r</sub></sub>	aileron angle right	deg	50	-33/+17	0.06
δ <sub>r</sub>	rudder angle	deg	50	-25/+25	0.04
δ <sub>f<sub>l</sub></sub>	flap angle left	deg	58	0/+58	0.05
δ <sub>f<sub>r</sub></sub>	flap angle right	deg	58	0/+58	0.05
δ <sub>e<sub>t</sub></sub>	elevator trim angle	deg	44	-18/+26	0.3
δ <sub>r<sub>t</sub></sub>	rudder trim angle	deg	36	-18/+18	0.3
α	angle of attack (vane)	deg	90	-10/+30	0.1
β	angle of sideslip (vane)	deg	90	-30/+30	0.1
q <sub>c</sub>	impact pressure	kPa	+ 4	0/+3	0.0005
ΔP <sub>l</sub>	change in static pressure	kPa	+ 4	-3/+3	0.0005
P <sub>s</sub>	static pressure	kPa	130	+50/+105	0.01
ΔP <sub>t</sub>	slipstream pressure	kPa	+ 4	0/+3	0.0005
P <sub>z</sub>	manifold pressure	kPa	130	+50/+130	0.01
n	engine speed	rpm	3000	500/2400	0.2
T <sub>e</sub>	carburetor temp.	K	243/303	243/303	0.1
T <sub>t</sub>	total air temp.	K	173/473	243/303	0.03
DME	distance meas.equ	n.m.	200	0/90	0.004
U <sub>ref</sub>	d.c. reference voltage	mV	9985	-	-

TABLE 4: INERTIAL TRANSDUCERS

Variable	Hawker Hunter	Fokker F-28	Beaver
A <sub>x</sub>	Donner 4810	Sagem 10625A	Donner 4810
A <sub>y</sub>	Donner 4310	Sagem 10625A	Donner 4310
A <sub>z</sub>	Donner 4810	Sagem 10625A	Sundstrand QA1100
p	-	Honeywell GG87B7	Honeywell GG87B7
q	Honeywell GG87B7	Honeywell GG87B7	Honeywell GG87B7
r	SFIM I14	Honeywell GG87B7	Honeywell GG87B7

TABLE 5: PRESSURE TRANSDUCERS

Variable	Hawker Hunter	Fokker F-28	Beaver
P <sub>s</sub>	Kelvin Hughes KTG1902	Rosemount 1201F	Baraton 145A
ΔP <sub>s</sub>	Statham PM6TC	Druck PDCR22	Baraton 145D
q <sub>c</sub>	Statham PM6TC	Druck PDCR22	Baraton 145D

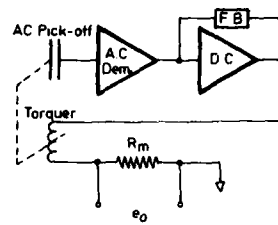


Fig. 1 Schematic diagram of a force balance accelerometer

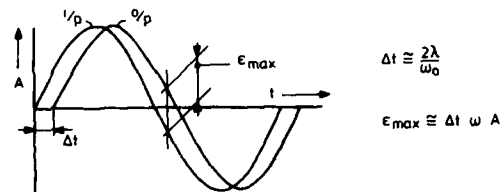


Fig. 4 Maximum relative error due to phase shift.

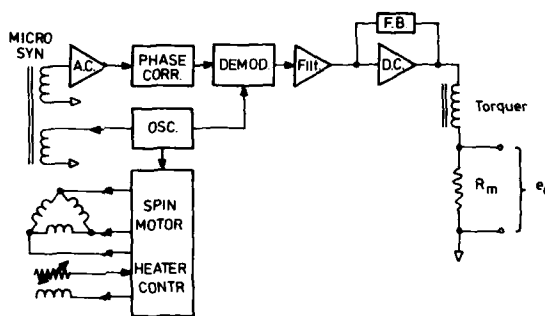


Fig. 2 Schematic diagram of rate gyro electronics.

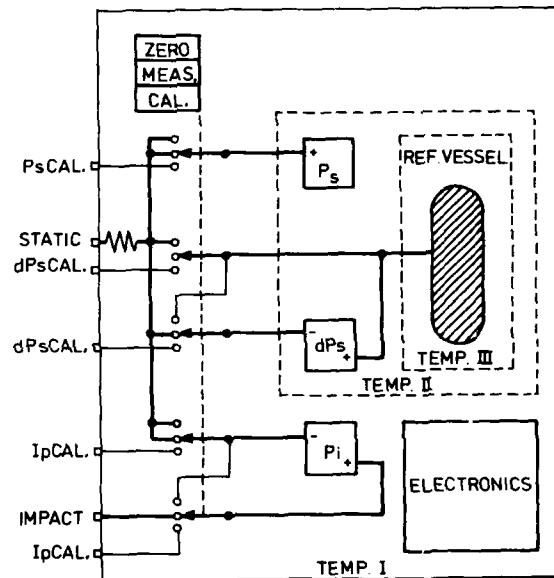
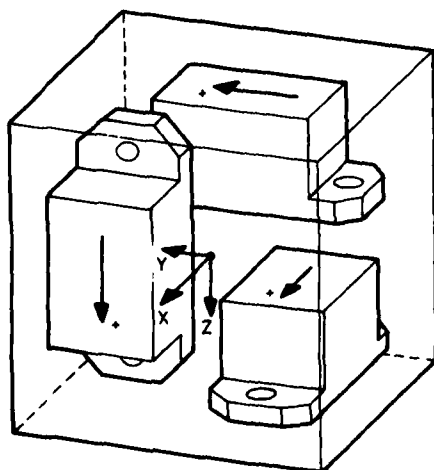


Fig. 5 Pneumatic diagram airdata measurement system

Fig. 3 Arrangement of three accelerometers in cubic box of  $14 \times 14 \times 14 \text{ cm}^3$

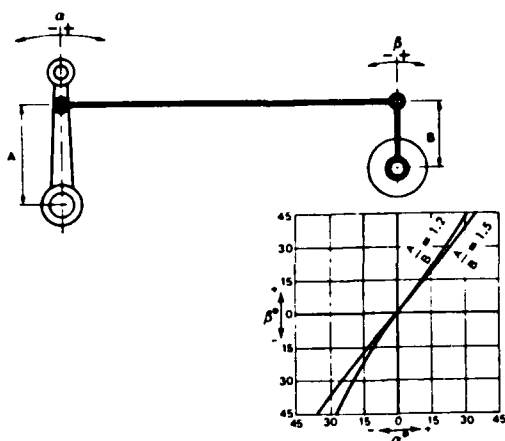


Fig. 6a Linearity errors due to difference in lever length

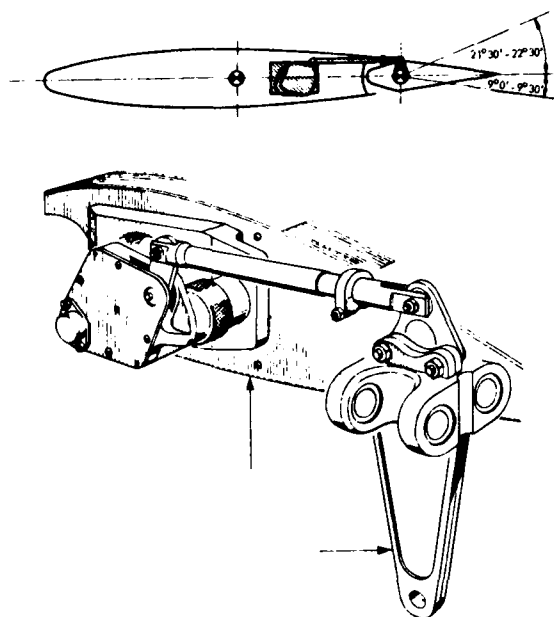


Fig. 7 Elevator deflection transducer

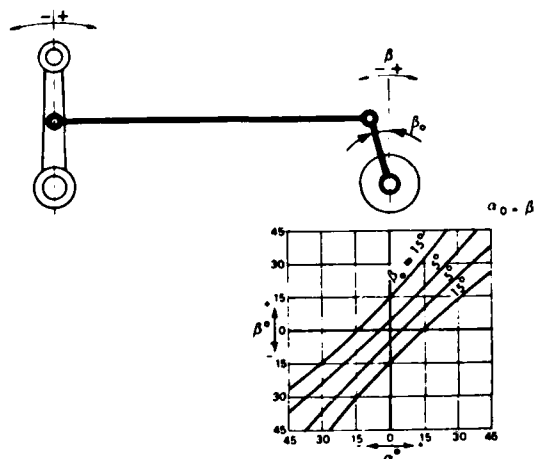


Fig. 6b Linearity errors due to non-parallel levers

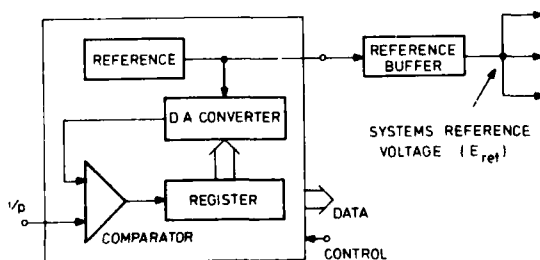


Fig. 8 Principle of using a/d converters reference for systems reference voltage.

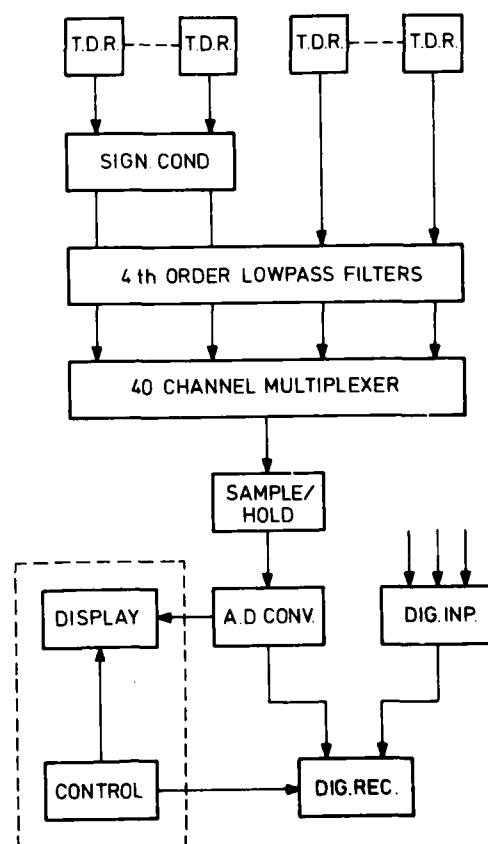


Fig. 9 General arrangement of "Hunter" and "Beaver" instrumentation system.

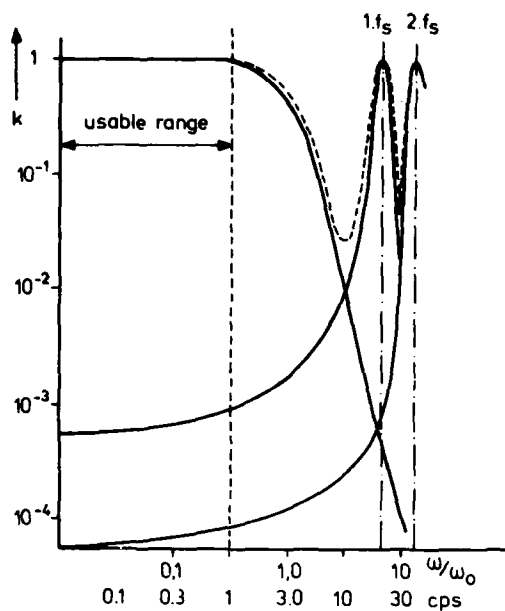


Fig. 10 Fourth order lowpass frequency characteristic.  
 $f_0 = 3.0$  cps  $\lambda = 0.691$   $f_s = 20$  samples. sec<sup>-1</sup>

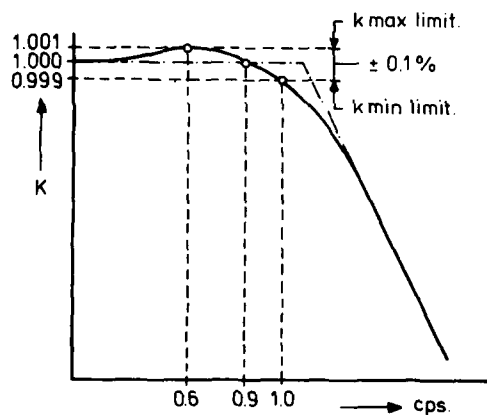


Fig. 11 Second order lowpass frequency characteristic  
 with gain limits (drawn not to scale)

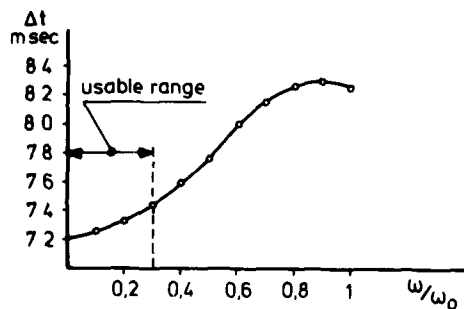


Fig. 12 Time shift of second order filter with:  
 $f_0 = 3.0$  cps  $\lambda = 0.691$

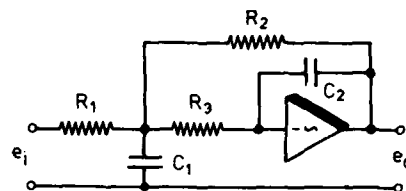


Fig. 13 General components arrangement for a  
 second order lowpass filter.

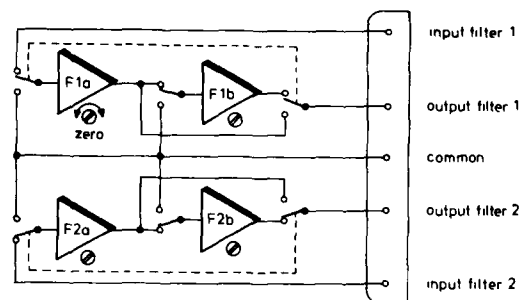


Fig. 14 Switch arrangement to provide zero adjustment of  
 four 2nd order filters of one filter unit.

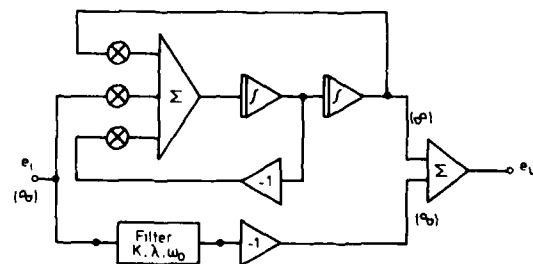


Fig. 15 Schematic adjustment procedure of  
 second-order lowpass filters.

# ANALYSIS OF AIRCRAFT PERFORMANCE, STABILITY AND CONTROL MEASUREMENTS

Ir. J.A. Mulder, Dr. H.L. Jonkers, Ir. J.J. Horsten  
Delft University of Technology  
Department of Aerospace Engineering  
Delft, THE NETHERLANDS

Ir. J.H. Breeman, Dr. J.L. Simons  
National Aerospace Laboratory, NLR  
Amsterdam, THE NETHERLANDS

## PREFACE

In this paper an overview is presented of the nonsteady flight test technique as developed by both Delft University of Technology and the National Aerospace Laboratory during the past two decades. Principal elements of this technique which is directed towards time efficient and accurate determination of performance characteristics as well as stability and control characteristics from measurements in nonsteady or quasi-steady flight, are:

- application of high quality flight test instrumentation systems
- accurate reconstruction of the aircraft's motions
- identification of nonlinear aerodynamic models
- calculation of performance, stability and control characteristics by correction of nonsteady or quasi-steady flight conditions towards prespecified nominal conditions.

Main emphasis of this paper is on a tutorial exposition of the first three of these elements. The fourth of these principal elements is delineated in a future publication. In addition to the tutorial presentation some experimental results of various flight test programs are present.

## C. CONTENTS

	<u>page</u>
1. Introduction	2
1.1. Historical background	2
1.2. Flight test technique	3
1.3. The flight test data analysis	3
1.3.0. Outline	3
1.3.1. Methodology	3
1.3.2. Statistical analysis	4
1.4. Organization of this paper	4
2. Symbol definitions and reference frames	4
2.1. Alphabetic symbols	4
2.2. Index notations	6
2.3. Reference frames	6
Part I: Theoretical aspects	7
3. The flight path reconstruction problem	7
3.0. Introduction	7
3.1. System models for the flight path reconstruction problem	7
3.1.0. Introduction	7
3.1.1. Equations of motion	7
3.1.2. System state and observation equations	9
3.1.3. Error models	10
3.1.4. The augmented system model, linearization and discretization	11
3.2. Principles of flight path reconstruction	14
3.2.0. Introduction	14
3.2.1. Basic system definition	14
3.2.2. Example 1: Estimation of the initial state	15
3.2.3. Example 2: Estimation of the initial state from measurements corrupted with random errors	16
3.2.4. Example 3: Estimation of initial state and correction for bias errors	20
3.2.5. Example 4: State estimation	22
3.3. Flight path reconstruction algorithms	24
3.3.0. Introduction	24
3.3.1. Weighted least squares and least squares estimation	25
3.3.2. The Kalman filter algorithm	26
3.3.3. The Maximum Likelihood algorithm	28
4. Aerodynamic model identification	31
4.0. Introduction	31
4.1. Regression analysis	32
4.1.0. Introduction	32
4.1.1. Basic principles	33
4.1.2. Model simplifications and identifiability	35
4.1.3. Residual analysis	36
4.2. Advanced numerical methods for the solution of the normal equations	37
4.2.0. Introduction	37
4.2.1. Orthogonal transformation	38

4.2.2. Householder transformations	38
4.2.3. Givens rotations	39
4.2.4. Use of a priori/a fortiori information on the aerodynamic model	40
4.2.5. Batch versus sequential processing	40
Part II: Technical aspects and results	40
5. Technical aspects and results of flight path reconstruction	40
5.0. Introduction	40
5.1. Flight test instrumentation and data analysis	40
5.1.0. Introduction	40
5.1.1. The flight test instrumentation system	41
5.1.2. Data analysis	42
5.2. Initial condition computation	43
5.2.0. Introduction	43
5.2.1. Simple algorithm for the calculation of the nominal initial state vector	43
5.2.2. Advanced algorithm for the calculation of the nominal initial state vector	46
5.3. Flight path reconstruction results	48
5.3.0. Introduction	48
5.3.1. Flight path reconstruction from simulated flight test data	48
5.3.1.0. Simulation of the flight test data	48
5.3.1.1. The augmented state vector and a priori statistics	49
5.3.1.2. Results of the simulation experiment	49
5.3.2. Flight path reconstruction from actual flight test data	51
5.4. Conclusions	51
6. Aerodynamic model identification with an interactive computer program	52
6.0. Introduction	52
6.1. Flight test method	52
6.2. Statement of the problem	52
6.3. Aerodynamic model identification	52
6.4. Structure of PIAS	53
6.5. Description of a typical run	53
6.6. Conclusions	54
7. Concluding remarks	54
8. References	55
Appendix A: The aircraft's equations of motion in the aircraft's body frame of reference $F_B$	58
A.0. Introduction	58
A.1. Acceleration in an arbitrarily moving frame $F_M$	58
A.2. Acceleration in the earth fixed reference frame $F_E$	58
A.3. The aircraft's acceleration in the aircraft's body frame of reference $F_B$	59
A.4. The aircraft's Euler angle rates	62
A.5. The aircraft's position	63
A.6. Summary of the equations of motion relative to $F_B$	63
Appendix B: Derivation of the batch regression algorithm	64
Tables	65
Figures	73

## 1. INTRODUCTION

### 1.1. Historical background

Since the early sixties the Department of Aerospace Engineering of the Delft University of Technology has been engaged in the development of methods to derive aircraft performance as well as stability and control characteristics from flight test data. Attention has been devoted mainly to the derivation of all characteristics of interest from measurements in nonsteady and quasi-steady flight. Traditional methods of performance testing are based on measurements in steady straight flight conditions in which the aircraft experiences neither translational nor angular accelerations. Stability and control characteristics were derived mainly from dynamic response measurements. A limited number of efforts to derive aircraft performance from measurements in nonsteady flight have been reported in the literature, see Refs. 8, 9, 15, 32.

An important reduction in flight time, required to determine a certain set of aircraft characteristics, may be achieved when deriving all characteristics of interest from measurements in nonsteady manoeuvring flight. The corresponding flight test technique has been described in Refs. 2-4, 10-12, 17-19, 20, 21.

In 1967 and 1968 a flight test program was carried through to evaluate the quality and performance of the flight test methods, the instrumentation system and the data reduction procedures developed for the derivation of aircraft performance, stability and control characteristics from measurements in nominally symmetric nonsteady manoeuvring flight. Symmetric flight trials flown with the DHC-2 Beaver aircraft, owned and operated by the Delft University of Technology, yielded most encouraging results. It was decided to extend these

investigations to high speed jet flight. In the early seventies a flight test program was carried through with the Hawker Hunter Mk 7 owned and operated by the National Aerospace Laboratory (NLR). Preliminary results of these flight tests have been presented in Ref. 19. In 1978 a flight test program aimed at the identification of a model for the aircraft's symmetric and asymmetric aerodynamics from measurements in symmetric and asymmetric nonsteady manoeuvring flight has been carried through, Ref. 29.

Based upon experience gained in these flight test programs a flight test program was carried through by the National Aerospace Laboratory to investigate the applicability for the case of a twin engined transport type aircraft, the Fokker F-28 "Fellowship". Initial results of this flight test program have been presented in Ref. 31.

### 1.2. Flight test technique

In general, succesful application of the nonsteady flight test technique depends on a thoughtful combination of the aircraft to be tested, the flight test instrumentation system, the signals applied to excite the aircraft, the models selected for identification and the procedures devised to analyse test data.

The nonsteady flight test technique, developed at the Delft University of Technology in the past decade, in particular hinges on accurate measurement of several inertial variables, e.g. specific aerodynamic forces and angular rates, and barometric variables, e.g. airspeed and static airpressure variations.

This flight test method includes:

1. the utilization of a high accuracy flight test instrumentation system, comprising high quality inertial and barometric sensors, see Refs. 23, 27, 28;
2. careful calibration of all transducers to be used in the flight test instrumentation system, Ref. 7;
3. analytic or computer aided development of optimal manoeuvre shapes, i.e. optimal time histories for the control surface deflections required to excite the aircraft, so as for example to maximize the amount of information in the measurements, concerning the characteristic parameters of interest, Refs. 3, 30;
4. excitation of the aircraft manually or under servo control (according to the optimal test signals developed) during test flights flown in fine weather;
5. off-line analysis of the measurements recorded in flight, using advanced state and parameter estimation techniques.

### 1.3. The flight test data analysis

#### 1.3.0. Outline

To provide an outline of the procedure used for the analysis of nonsteady manoeuvring flight test data, the following procedure steps are distinguished:

1. the first step includes transformation of transducer output voltages, accurately measured, periodically sampled, digitized and recorded in flight into physical magnitudes, using the results of laboratory calibrations of the flight test instrumentation system and applying various corrections;
2. the second procedure step results in accurate reconstruction of the aircraft's motions in symmetric or asymmetric nonsteady manoeuvring flight from the flight test measurements recorded;
3. the third procedure step is directed towards the identification of the aircraft's aerodynamic model, using the flight path reconstruction results. This includes specification of the relations between the aircraft's state and control variables and the resulting aerodynamic forces and moments, as well as estimation of the aerodynamic derivatives, governing these relations;
4. the final step comprises the derivation of aircraft performance as well as stability and control characteristics, either from the aerodynamic model obtained or from the reconstructed state variable time histories of the nonsteady manoeuvring test aircraft, Refs. 11, 18, 19.

#### 1.3.1. Methodology

As already stated in subsection 1.1. and as may be seen from the outline of the flight test data analysis procedure, presented above, the final goal of the nonsteady flight test technique developed is the determination of the performance characteristics of the aircraft in combination with stability and control characteristics. Static performance and control characteristics such as trim curves, polar drag curves, lift curves, rate of climb as a function of airspeed in steady straight flight and power curves, are derived from measurements in nearly- or quasi-steady conditions. Measurements recorded under highly non-steady conditions are analyzed to determine aerodynamic or stability derivatives.

All characteristics of interest may in principle be obtained from one single nonsteady manoeuvring test flight. Obviously for reasons of statistical reliability measurements recorded during more than one test flight are to be analyzed.

During the test flight manoeuvre, the aircraft is made to traverse the entire flight envelope of interest. The quasi-steady flight test conditions are selected so that the total aerodynamic forces and moments, acting upon the aircraft during the manoeuvre, will result in small translational and angular accelerations. To derive data points of the aircraft characteristics the aerodynamic forces and moments, as recorded under the quasi-steady conditions, have to be corrected towards steady conditions. The correction of quasi-steady to steady conditions boils down in fact to extrapolation of the aircraft's dynamics. Extrapolation from one condition of a dynamic process to another in general requires:

- determination of the first condition,
- knowledge concerning the laws governing the dynamic process,
- specifications concerning the second condition.

The laws governing the dynamic process may be represented by mathematic models of the relations between all quantities characterizing the dynamics of the process.

In atmospheric flight dynamics the characteristic quantities are for example: the aircraft's airspeed, the angle of attack, the angle of sideslip, the angles of pitch, roll and yaw, angular rotation rates, control surface deflections and the engine thrust. These quantities may be related to the aerodynamic forces

and moments, or to the corresponding dimensionless aerodynamic coefficients, using polynomial relations, i.e. the aerodynamic model. Deriving equilibrium conditions from measurements in quasi-steady flight, may thus be concluded to demand for knowledge of the time histories of the variables mentioned, as well as knowledge concerning the aerodynamic model relations. Moreover, it is remarked that the parameters in these relations are to be computed, equating time histories of the respective aerodynamic forces and moments to combinations of the time histories of the variables mentioned. To limit the detrimental effects of possible modelling errors on the accuracy of the equilibrium conditions, steady state data points should be derived from the nearest possible quasi-steady state data points recorded in flight.

From this discussion it may be clear that derivation of performance and control characteristics requires accurate knowledge of the aircraft's motions. Considerable effort has consequently been devoted to the development of techniques for the reconstruction of these motions from on-board inertial and barometric measurements. The reconstruction of these motions, the so-called flight path reconstruction, is discussed in considerable detail in the present lecture.

It should be noticed here that accurate flight path reconstruction is not only of prime interest for the analysis of measurements in nonsteady flight. Traditional flight testing and automatic aircraft navigation, control and flight management may also demand accurate off-line or on-line reconstruction of the aircraft's motions relative to a certain frame of reference.

### 1.3.2. Statistical analysis

Most aircraft variables relevant in this context may be measured directly with more or less accuracy, pain and costs.

Variables such as for example the aerodynamic forces<sup>1)</sup>, the rates of pitch, yaw and roll and the airspeed can be directly measured with acceptable accuracy; this does not hold however for variables as the angle of attack and the angle of sideslip. In particular on a single engine propeller driven aircraft such as the DHC-2 Beaver, it is not possible to directly measure these quantities with adequate accuracy, using the conventional boom-mounted vanes or pitot-spheres. Methods are therefore devised to estimate these quantities from all available measurements, including wind vane measurements. These methods, including simultaneous calibration of the wind vanes, are based on the application of statistical estimation procedures such as Kalman filtering, Kalman smoothing or Maximum Likelihood analysis, to minimize the effects of measurement errors on the reconstructed flight path data.

Once having achieved flight path reconstruction, the time histories of the aircraft's state variables, as obtained are used for aerodynamic model identification applying regression analysis. The characteristics of interest may subsequently be derived either from the aerodynamic model or correcting nonsteady aircraft states to steady states, using the reconstructed flight path data and the aerodynamic model identified. As the aerodynamic model is identified using the flight path reconstruction results, the accuracy of all characteristics derived from flight test data may thus be seen to depend either indirectly or directly on the accuracy of these results.

### 1.4. Organization of this paper

Section 3 of this report is devoted to the description of the dynamic system models used for flight path reconstruction. Basic principles and concepts underlying the data reduction procedures are introduced and discussed. In addition a survey of the procedures applicable to flight path reconstruction is given in this section. Results obtained processing simulated and actual flight test measurements are presented in Section 5.

The subject of Section 4 is the identification of the aerodynamic model from the flight path reconstruction results. An application of the theory as developed in Section 4 is presented in Section 6.

## 2. SYMBOL DEFINITIONS AND REFERENCE FRAMES

### 2.1. Alphabetic symbols

$a$	net thrust moment arm
$\underline{a}$	acceleration, parameter vector
$a_i$	regression coefficient
$A(t)$	system matrix
$A_{XB}, A_{YB}, A_{ZB}$	specific forces along the $X_B$ -, $Y_B$ - and $Z_B$ -axes
$b$	span
$B(t)$	input distribution matrix
$\bar{c}$	mean aerodynamic chord
$C(t)$	observation matrix
$C_L$	lift coefficient
$C_{LB}, C_{MB}, C_{NB}$	dimensionless aerodynamic moments respectively about the $X_B$ -, $Y_B$ - and $Z_B$ -axes
$C_{XB}, C_{YB}, C_{ZB}$	dimensionless aerodynamic forces respectively along the $X_B$ -, $Y_B$ - and $Z_B$ -axes
$C_{si}$	sidewash correction factor
$C_\beta$	zero shift of the $\beta_v$ wind vane
$D(t)$	matrix in Eq. (3.126)
$e(n)$	state estimation error in Section 3, residual in Section 4
$E$	expected value
$\underline{f}_B$	force vector
$\underline{f}_{cor}$	coriolis acceleration

1) aerodynamic forces per unit mass are measured with accelerometers strapped on the aircraft's body frame.



$f_{cen}$	centripetal acceleration
$\vec{F}$	aerodynamic force vector
$F$	Fisher information matrix
$F_B$	aircraft's body frame of reference
$F_E$	earth-fixed reference frame
$F_I$	inertial reference frame
$F_V$	vehicle carried vertical frame
$F_W$	vehicle carried air trajectory reference frame
$g_h$	gravitational acceleration
$g_o$	gravitational acceleration at sea level
$G$	Givens rotation
$\Delta h$	altitude variation defined relative to the initial altitude
$i_p$	engine gross or net thrust inclination angle
$I$	identity matrix
$I_x, I_y, I_z$	moments of inertia respectively about the $X_B$ -, $Y_B$ - and $Z_B$ -axes
$I_{xz}$	product of inertia
$J$	optimization criterion
$k$	discrete-time indication (abbreviated notation of $t_k$ )
$K^O$	optimal gain
$K(k)$	Kalman filter gain matrix
$K_S(k)$	Kalman smoother gain matrix
$L_B$	aerodynamic moment about $X_B$ -axis
$L$	weighting matrix
$L$	likelihood function
$L_{BV}$	transformation matrix for rotation from $F_V$ into $F_B$
$L_{BE}$	transformation matrix for rotation from $F_E$ into $F_B$
$L_{IM}$	transformation matrix for rotation from $F_M$ into $F_I$
$L_{EI}$	transformation matrix for rotation from $F_I$ into $F_E$
$m$	aircraft mass
$\vec{m}(t)$	vector-valued correction for the observation perturbation vector
$M_B$	aerodynamic moment about $Y_B$ -axis
$\vec{M}(t)$	system output signal
$M$	matrix in Eq. (A-40)
$M$	Mach number
$N_B$	aerodynamic moment about $Z_B$ -axis
$p$	probability density function
$p_B$	angular rate of roll
$p_B^E, q_B^E, r_B^E$	components of $\vec{\omega}_B$ in $F_E$
$\vec{p}$	vector in Eq. (B-2)
$\bar{p}$	component of $\vec{\omega}_B$ along $X_B$
$p_i$	orthogonal transformation matrix
$P(k k)$	estimation error covariance matrix
$P_M(k n)$	error covariance matrix of $\underline{M}$
$q$	dynamic pressure
$q_B$	angular rate of pitch
$q_c$	impact pressure
$\vec{q}(t)$	vector-valued correction for the random errors in the system output signal measurements $\underline{M}_m(t)$
$Q$	component of $\vec{\omega}_B$ along $Y_B$ , engine mass flow
$Q, Q^i$	Householder transformation matrix
$Q(t)$	covariance matrix of $\vec{q}(t)$
$r$	radius
$r_B$	angular rate of yaw
$\vec{r}_{rot}$	rotation of the aircraft resulting from the earth rotation
$\vec{r}_{spher}$	rotation of the aircraft travelling over a spherical earth
$\vec{r}(k)$	vector in Eq. (3.64)
$R(k)$	matrix in Eq. (3.138)
$R$	component of $\vec{\omega}_B$ along $Z_B$
$R_t$	total correlation coefficient
$R^E$	local radius of the earth corresponding with the latitude of the flight test area
$S$	wind area
$S(t)$	matrix in Eq. (3.172)
$TG_T$	engine gross thrust
$T_N$	engine net thrust
$t$	time
$\Delta t$	sampling time interval
$T$	sampling time interval
$\vec{u}(t)$	input perturbation corrections
$\underline{U}(t)$	vector-valued input signal
$\bar{V}$	covariance matrix of estimation errors
$\vec{V}$	velocity of the aircraft's c.g.
$\vec{V}_{XB}, \vec{V}_{YB}, \vec{V}_{ZB}$	components of $\vec{V}$ in $F_B$
$\vec{w}(t)$	vector-valued correction for the random errors in the input signal measurements $\underline{U}_m(t)$
$\bar{W}$	aircraft weight
$W(t)$	covariance matrix of $\vec{w}(t)$
$x_i$	independent variable in regression theory
$\vec{x}$	vector-valued state perturbation
$x_E, y_E, z_E$	aircraft's position relative to $F_E$
$x_{\beta B}, y_{\beta B}$	position coordinates of the $\beta_v$ wind vane in the $X_B$ - $Y_B$ -plane
$X$	matrix of independent variables in regression theory
$X^i$	matrix of independent variables in regression theory, first $i$ columns in upper triangular form

$x_B, y_B, z_B$	aerodynamic force along $X_B$ axis
$\underline{x}(t)$	system state vector
$y$	dependent variable in regression theory
$\underline{y}(t)$	discrete-time state perturbation correction vector
$\underline{Y}(t)$	augmented state vector
$y_B$	aerodynamic force along $Y_B$ axis
$z_B$	aerodynamic force along $Z_B$ axis
$\alpha$	angle of attack
$\alpha_v$	wind vane angle of attack
$\beta$	angle of sideslip
$\beta_v$	wind vane angle of sideslip
$\Gamma(k, k-1)$	disturbance distribution matrix
$\delta_d$	Dirac delta
$\delta_{k,j}$	Kronecker delta
$\delta_e$	elevator angle
$\delta_a$	aileron angle
$\delta_r$	rudder angle
$\delta_h$	horizontal stabilisor trim angle
$\epsilon$	random error in Section 3, model error in regression theory
$\theta$	angle of pitch
$\lambda$	latitude
$\bar{\lambda}$	constant input signal bias error corrections
$\kappa$	matrix rank
$\mu$	longitude
$\sigma$	standard deviation
$\tau$	time
$\phi$	angle of roll
$\Phi(k k-1)$	transition matrix
$\psi$	angle of yaw
$\rho_{ij}$	simple correlation coefficient
$\omega_E$	rotation rate of the earth $\omega_E$ in $F_B$
$\omega_B$	matrix equivalent of $\omega_E$
$\frac{\partial}{\partial x}$	row vector of partial derivatives

## 2.2. Index notations

### Subscript

B	in the aircraft's body frame of reference $F_B$
E	in the earth fixed reference frame $F_E$
I	in the inertial reference frame $F_I$
m	measured magnitude
nom	nominal
T	in the vehicle carried vertical reference frame $F_T$
V	in the vehicle carried vertical reference frame $F_V$
W	in the vehicle carried air-trajectory reference frame $F_W$

## 2.3. Reference frames

All reference frames are right-handed and orthogonal.

### 1. The aircraft's body-fixed reference frame $F_B$ (see fig. 1)

The origin  $O_B$  of  $F_B$  lies in the aircraft's c.g. The  $X_BO_BZ_B$ -plane coincides with the aircraft's plane of symmetry. The positive  $X_B$ -axis points forward. The positive  $Y_B$ -axis points to the right. The positive  $Z_B$ -axis points downwards.

### 2. The earth-fixed reference frame $F_E$ (see fig. 1)

The positive  $X_E$  axis points to the north. The positive  $Y_E$ -axis points to the east. The positive  $Z_E$ -axis points downwards.

### 3. The vehicle carried vertical frame $F_V$ (see fig. A-2, 1)

The origin  $O_V$  of  $F_V$  lies in the aircraft's c.g. The positive  $X_V$ -axis points to the north. The positive  $Y_V$ -axis points to the east. The positive  $Z_V$ -axis points vertically downwards.

### 4. The vehicle carried vertical reference frame $F_T$ (see fig. 1)

The origin  $O_T$  of  $F_T$  lies in the aircraft's c.g. The positive  $X_T$ -axis coincides with the aircraft's plane of symmetry and points forward. The positive  $Z_T$ -axis points vertically downwards.

### 5. The vehicle carried air-trajectory reference frame $F_W$

The origin lies in the aircraft's c.g. The  $X_W$ -axis is directed along the velocity vector  $V$ , the  $Z_W$ -axis points downwards and is in the aircraft's plane of symmetry.

## PART I

## 3. THE FLIGHT PATH RECONSTRUCTION PROBLEM

## 3.0. Introduction

The accuracy of performance measurements in nonsteady flight conditions depends to a large extent on the accuracy of the measurement of the specific forces  $A_{x_B}$  and  $A_{z_B}$  and on the accuracy of the measurements of the angle of attack  $\alpha$  and airspeed  $V$ .

Airspeed is usually deduced from total and static pressure measurements. The requirement for maximum accuracy dictates the application of sophisticated instrumentation techniques as for instance described in Refs. 26, 27 and 28. Essential are also the correction of barometric measurements for instrumental bias- and static pressure position errors. The fundamental problem here is that the achievable accuracy decreases in nonsteady flight conditions. The dynamic response of air pressure tubes being difficult or even impossible to correct for exactly and the sensitivity of barometric transducers to accelerations are probably the most significant additional error sources in nonsteady flight conditions.

The angle of attack  $\alpha$  and slip angle  $\beta$  are usually measured with vanes on wing or nose mounted booms in order to minimize aircraft induced air velocities. Still, an in flight calibration is usually necessary even when windtunnel data on the aircraft induced flow angle is available. This requires a series of measurements in steady straight conditions in which the effect of several variables as angle of attack, Mach number, engine thrust and aircraft configuration must be evaluated. Then, it still remains questionable to what extent the resulting calibrations may be exploited in nonsteady flight conditions.

The philosophy of the present paper is that in order to on the one hand circumvent the practical difficulties mentioned above and on the other, improve the achievable accuracy, the angle of attack should be calculated instead of directly measured. In several earlier references the technique for calculating these variables has been named "flight path reconstruction". However, the technique for the calculation of the angle of attack and airspeed encompasses much more than the mere reconstruction of the flight path. Several other variables as pitch angle and accelerometer zero shifts are reconstructed or estimated simultaneously.

Besides for performance measurements in nonsteady flight and as a basis for aerodynamic model identification, flight path estimation has by now been adopted for other applications e.g. the measurement of wake turbulence, Ref. 36, and for proving the integrity of flight test instrumentation systems, Ref. 14.

The organization of this chapter is as follows. In 3.1. a description is given of the mathematical or system model, employed for flight path reconstruction, which comprises a set of first order differential equations representing the kinematical relations of the motion of the body fixed reference frame  $F_B$  with respect to a spherical and rotating earth, an observation and an error model. Subsequently the model is linearized and discretized. The principles and basic philosophy of flight path reconstruction is the subject of Section 3.2. On the basis of four examples of increasing complexity several notions as nominal trajectory, state estimation, input bias estimation, the effect of measurement and of system noise are introduced and clarified. Section 3.3. deals with the details of the statistical estimation algorithms which have in the course of the present work been actually applied to the flight path reconstruction problem i.e. least squares estimation, extended Kalman Filtering and Smoothing, the square root information filter and Maximum Likelihood estimation. A summary is presented in Section 3.4.

## 3.1. System models for the flight path reconstruction problem

## 3.1.0. Introduction

Flight path reconstruction can be formulated as the problem of generating knowledge on the aircraft's motion from on board measurements. The solution of this problem starts with the development of a mathematical model representing the kinematics of the motion of the body fixed reference frame  $F_B$  with respect to a spherical rotating earth. Because the mathematical model can be interpreted as to represent a dynamical system, the model will in the sequence be indicated as the system model.

Section 3.1.1. starts with the development of a simplified model describing the motion with respect to a flat and non-rotating earth. It is argued that, because attention is restricted to the kinematics of the body fixed reference frame  $F_B$ , the resulting kinematical relations hold for flexible as well as rigid aircraft. In Appendix A it is shown that these relations can readily be extended to the case of a spherical rotating earth.

In Section 3.1.2. the kinematical relations are reformulated using system theoretical concepts. A system is defined with corresponding state vector, input vector and observation model.

In Section 3.1.3. error models are postulated for the measurements of the input vector and observation vector so as to pave the way for the application of statistical estimation algorithms for the solution of the flight path reconstruction problem.

Finally in Section 3.1.4., the system model is reformulated in terms of an augmented system model and a corresponding augmented state vector is introduced. It is shown also that the nonlinear time continuous model can be discretized and linearized about a nominal trajectory.

## 3.1.1. Equations of motion

The translational dynamics of the aircraft are described by the following equations relating all relevant forces such as the aerodynamic forces  $X_B$ ,  $Y_B$  and  $Z_B$ , the centrifugal forces and the gravitational forces:

$$X_B = m(\dot{V}_{x_B} + q_B V_{z_B} - r_B V_{y_B}) + W \sin \theta \quad (3.1)$$

$$\dot{y}_B = m(\dot{v}_{yB} + r_B v_{xB} - p_B v_{zB}) - W \cos \theta \sin \varphi \quad (3.2)$$

$$\dot{z}_B = m(\dot{v}_{zB} + p_B v_{yB} - q_B v_{xB}) - W \cos \theta \cos \varphi \quad (3.3)$$

The rotational dynamics of the aircraft are represented by the following equations:

$$L_B = I_x \dot{p}_B + (I_z - I_y) q_B r_B - I_{xz} (\dot{r}_B + p_B q_B) \quad (3.4)$$

$$M_B = I_y \dot{q}_B + (I_x - I_z) r_B p_B + I_{xz} (p_B^2 - r_B^2) \quad (3.5)$$

$$N_B = I_z \dot{r}_B + (I_y - I_x) p_B q_B - I_{xz} (\dot{p}_B - r_B q_B) \quad (3.6)$$

In these relations the possible effects of rotating propellers or turbines have been neglected. Furthermore  $I_{xy}$  and  $I_{yz}$  have been taken equal to zero because the  $X_B$  and  $Z_B$  are in the aircraft's plane of symmetry.

Equations (3.1) through (3.6) hold for the case of a rigid aircraft and a flat and non-rotating earth.

The orientation of  $F_B$  with respect to the vehicle carried vertical reference frame  $F_V$ , expressed by the rotation rates  $p_B$ ,  $q_B$  and  $r_B$  and the time derivatives of these angles, reads:

$$\dot{\psi} = q_B \frac{\sin \varphi}{\cos \theta} + r_B \frac{\cos \varphi}{\cos \theta} \quad (3.7)$$

$$\dot{\theta} = q_B \cos \varphi - r_B \sin \varphi \quad (3.8)$$

$$\dot{\varphi} = p_B + q_B \sin \varphi \tan \theta + r_B \cos \varphi \tan \theta \quad (3.9)$$

It is interesting to notice that equations (3.1) through (3.9) can be solved by means of numerical integration, if the aerodynamic forces  $X_B$ ,  $Y_B$  and  $Z_B$ , the aerodynamic moments  $L_B$ ,  $M_B$  and  $N_B$ , the aircraft's weight ( $W = mg$ ), the moments and products of inertia and the initial condition  $v_{xB}(0)$ ,  $v_{yB}(0)$ ,  $v_{zB}(0)$ ,  $p_B(0)$ ,  $q_B(0)$ ,  $r_B(0)$ ,  $\psi(0)$ ,  $\theta(0)$  and  $\varphi(0)$  were known. Solution of these equations yields time histories of the variables  $v_{xB}(t)$ ,  $v_{yB}(t)$ ,  $v_{zB}(t)$ ,  $p_B(t)$ ,  $q_B(t)$ ,  $r_B(t)$ ,  $\psi(t)$ ,  $\theta(t)$  and  $\varphi(t)$ .

It is even more important to remark that the dynamic equations (3.1) through (3.3) and the kinematic equations (3.7) through (3.9) could numerically be integrated independently of the rotational dynamic equations (3.4) through (3.6) if the angular velocities  $p_B$ ,  $q_B$  and  $r_B$  were measured. In that case the determination of the aerodynamic moments  $L_B$ ,  $M_B$  and  $N_B$  and the integration of the corresponding equations is no longer necessary.

The aerodynamic forces  $X_B$ ,  $Y_B$  and  $Z_B$  can be written in terms of specific aerodynamic forces  $A_{xB}$ ,  $A_{yB}$  and  $A_{zB}$ :

$$X_B = m A_{xB} \quad (3.10)$$

$$Y_B = m A_{yB} \quad (3.11)$$

$$Z_B = m A_{zB} \quad (3.12)$$

In the hypothetical case of a rigid aircraft,  $A_{xB}$ ,  $A_{yB}$  and  $A_{zB}$  are the quantities sensed by accelerometers in the aircraft's centre of gravity and aligned along the axes of the body fixed reference frame  $F_B$ . Substitution of (3.10) through (3.12) into (3.1) through (3.3) results in the following set of kinematic equations:

$$\dot{v}_{xB} = A_{xB} - g_h \sin \theta - q_B v_{zB} + r_B v_{yB} \quad (3.13)$$

$$\dot{v}_{yB} = A_{yB} + g_h \cos \theta \sin \varphi - r_B v_{xB} + p_B v_{zB} \quad (3.14)$$

$$\dot{v}_{zB} = A_{zB} + g_h \cos \theta \cos \varphi - p_B v_{yB} + q_B v_{xB} \quad (3.15)$$

Now, if in addition to the angular velocities  $p_B$ ,  $q_B$  and  $r_B$ , the specific aerodynamic forces  $A_{xB}$ ,  $A_{yB}$  and  $A_{zB}$  were measured, equations (3.13) through (3.15) and (3.7) through (3.9) could be numerically integrated if only the following initial values  $v_{xB}(0)$ ,  $v_{yB}(0)$ ,  $v_{zB}(0)$ ,  $\psi(0)$ ,  $\theta(0)$  and  $\varphi(0)$  were known.

The foregoing discussion can be summarized as follows. Numerical integration of the equation of motion (3.1.) through (3.6.) and the kinematic equations (3.7) through (3.9) would, in addition to initial conditions, aircraft weight and moments and products of inertia also require knowledge of the aerodynamic forces and moments. When however, measurements are made of specific forces and angular velocities the kinematic equations (3.13) through (3.15) and (3.7) through (3.9) can be integrated instead. This integration requires nothing more than a set of initial values.

While for the integration of the original equations of motion (3.1) through (3.6) an aerodynamic model must be specified, the aerodynamic forces are eliminated all together in the kinematic equations (3.13) through (3.15). The accuracy of these equations has therefore become independent of the accuracy of any aerodynamic model.

If the inertial quantities  $A_{x_B}$ ,  $A_{y_B}$ ,  $A_{z_B}$ ,  $p_B$ ,  $q_B$  and  $r_B$  could be measured with absolute precision as a function of time and if the relevant initial condition was exactly specified, the flight path reconstruction problem would reduce to integration of a set of first order nonlinear differential equations.

Evidently the measurements recorded in flight are never completely free of errors. Moreover the initial condition cannot be exactly specified from the measurements recorded. Application of statistical estimation procedures is therefore required to attenuate the effects of these errors on the time histories of the state variables as derived from flight test data.

If the position of the aircraft's c.g. relative to  $E$  should be computed as a function of time, the following set of equations has to be solved in addition to (3.13) through (3.15) and (3.7) through (3.9):

$$\begin{aligned}\dot{x}_E &= V_{x_B} \cos \theta \cos \psi + V_{y_B} (\sin \varphi \sin \theta \cos \psi - \cos \varphi \sin \psi) + \\ &+ V_{z_B} (\cos \varphi \sin \theta \cos \psi + \sin \varphi \sin \psi)\end{aligned}\quad (3.16)$$

$$\begin{aligned}\dot{y}_E &= V_{x_B} \cos \theta \sin \psi + V_{y_B} (\sin \varphi \sin \theta \sin \psi + \cos \varphi \cos \psi) + \\ &+ V_{z_B} (\cos \varphi \sin \theta \sin \psi - \sin \varphi \cos \psi)\end{aligned}\quad (3.17)$$

$$\dot{z}_E = -V_{x_B} \sin \theta + V_{y_B} \sin \varphi \cos \theta + V_{z_B} \cos \varphi \cos \theta \quad (3.18)$$

Equations (3.13) - (3.15), (3.7) - (3.9) and (3.16) - (3.18) hold for the case of motion with respect to a flat and non-rotating earth. The effects of the curvature and rotation of the earth are treated in Appendix A.

In the case of flexible aircraft, the specific aerodynamic forces and the quantities sensed by accelerometers can in principle no longer be assumed identical. Even then however, the kinematical equations (3.13) - (3.15) for the motion of the aircraft's c.g. remain valid. To see this, (3.1) - (3.3) might be interpreted as the equations of motion of a hypothetical inertial unit containing the accelerometers and fixed in the c.g.  $x_B$ ,  $y_B$  and  $z_B$  would then represent suspension forces and  $m$  the mass of the inertial unit. In (3.13) - (3.15)  $A_{x_B}$ ,  $A_{y_B}$  and  $A_{z_B}$  would then represent specific suspension forces, identical to the quantities sensed by the accelerometers.

### 3.1.2. System state and observation equations

The representation of the aircraft's dynamics in terms of a state vector equation is established to set the stage for the application of the statistical estimation procedures for the solution of the flight path reconstruction problem.

The following vector-valued quantities are introduced:

$$\underline{X} \triangleq \text{col} [V_{x_B}, V_{y_B}, V_{z_B}, \psi, \theta, \varphi, x_E, y_E, z_E] \quad (3.19)$$

$$\underline{U} \triangleq \text{col} [A_{x_B}, A_{y_B}, A_{z_B}, p_B, q_B, r_B] \quad (3.20)$$

Equations (3.13) - (3.15), (3.7) - (3.9) and (3.16) - (3.18) may be represented together by the following symbolic vector differential equation:

$$\dot{\underline{X}}(t) = \underline{f}(\underline{X}(t), \underline{U}(t)) \quad (3.21)$$

$$\underline{X}(t_0) = \underline{X}(0) \quad (3.22)$$

The quantity  $\underline{X}(t)$  is referred to as the state vector of the dynamic system under consideration. The quantity  $\underline{U}(t)$  is called the system input signal. The function  $\underline{f}$  is a vector-valued quantity of the same dimension as  $\underline{X}(t)$ .

In the previous subsection, numerical solution of Eqs. (3.13) - (3.15), (3.7) - (3.9) and (3.16) - (3.18) has already been shown to demand for measurement of the specific forces and angular velocities, i.e. the components of  $\underline{U}(t)$ .

In addition, an estimate is required of the initial state  $\underline{X}(0)$ . Errors in  $\underline{U}_m(t)$ , being the measured magnitude of  $\underline{U}(t)$  as well as errors in the estimate  $\hat{\underline{X}}(0)$  of the initial state, will lead to deviations between the calculated time history of the system state vector and the actual time history.

From the calculated magnitudes of various state vector components, the magnitudes of several related quantities, such as the airspeed  $V$ , the altitude variation  $\Delta h$  and the wind vane angle of sideslip  $\beta_v$  may be computed, according to:

$$V = \sqrt{v_{x_B}^2 + v_{y_B}^2 + v_{z_B}^2} \quad (3.23)$$

$$\Delta h = -z_E \quad (3.24)$$

$$\beta_v = \arctg \left( \frac{v_{y_B} + x_{\beta_B} r_B - z_{\beta_B} p_B}{v_{x_B}} \right) + C_{si} \arctg \frac{v_{y_B}}{v_{x_B}} - C_{\beta} \quad (3.25)$$

Here  $x_{\beta_B}$  and  $z_{\beta_B}$  are the coordinates of the wind vane relative to  $F_B$ ,  $C_{si}$  is the sidewash coefficient and  $C_{\beta}$  is the zero shift of the wind vane. The quantities  $C_{si}$  and  $C_{\beta}$  should either be given or be estimated from flight test data.

The quantities  $V$ ,  $\Delta h$  and  $\beta_v$  are referred to as the components of the vector-valued system output signal  $\underline{M}$ :

$$\underline{M} \triangleq \text{col} [V, \Delta h, \beta_v] \quad (3.26)$$

These quantities are important for flightpath reconstruction purposes, since they may also be directly measured with barometric sensors or boom-mounted windvanes. The latter measurements will again contain measurement errors. It is emphasized here that the composition of  $\underline{M}$  given in Eq. (3.26) should be considered merely as a possible example of the output signal observation configuration. Other variables, algebraically (i.e. memoryless) related to the system state vector components, such as for example the angle of yaw  $\psi$ , the angle of roll  $\phi$ , the wind vane angle of attack  $\alpha_v$ , DME based aircraft position fixes or inertial platform measured velocity components, may also be considered as system output signals. Equations (3.23) - (3.25) may be considered as the constituent components of the following time dependent equation:

$$\underline{M}(t) = \underline{h}(\underline{X}(t), \underline{U}(t)) \quad (3.27)$$

The calculated output variables can be compared to the measured output variables, taking account of the relative accuracies.

From the deviations between the calculated and the measured outputs, information can be extracted concerning the deviations of the estimated state  $\hat{\underline{X}}(t)$  from the actual state  $\underline{X}(t)$ .

The estimation procedures to be discussed center around optimal use of this information.

The equations (3.21) and (3.27) are respectively called the system state equation and the system observation equation.

### 3.1.3. Error models

The outputs of the sensors used for measurement of the system input and output signal components are assumed to be corrupted with time dependent errors.

More precisely the accelerometer and rate gyroscope measurements are supposed to be contaminated with constant bias errors as well as with random measurement errors. The barometric measurements are assumed to be corrupted only with random measurement errors, since short-circuiting of the pneumatic sensor systems, prior and posterior to each test flight manoeuvre, allows for accurate post flight compensation of possible bias errors.

Henceforth the following expressions may be used to relate variable magnitudes measured with the corresponding actual or better exact magnitudes:

$$\underline{U}_m(t) \triangleq \underline{U}(t) - \underline{\lambda} - \underline{w}(t) \quad (3.28)$$

$$\underline{M}_m(t) \triangleq \underline{M}(t) - \underline{q}(t) \quad (3.29)$$

The vector-valued quantities  $\underline{\lambda}$ ,  $\underline{w}(t)$  and  $\underline{q}(t)$  are defined respectively as:

$$\underline{\lambda} \triangleq \text{col} [\lambda_x, \lambda_y, \lambda_z, \lambda_p, \lambda_q, \lambda_r] \quad (3.30)$$

$$\underline{w} \triangleq \text{col} [w_x, w_y, w_z, w_p, w_q, w_r] \quad (3.31)$$

$$\underline{q} \triangleq \text{col} [q_v, q_{\Delta h}, q_{\beta_v}] \quad (3.32)$$

The bias errors are assumed constant, hence:

$$\dot{\underline{\lambda}} = 0 \quad (3.33)$$

The time dependent random errors  $\underline{w}(t)$  and  $\underline{q}(t)$  are considered as Gaussian white noise processes with the following statistical properties:

1. The mean values are assumed equal to zero:

$$\left. \begin{aligned} E[\underline{w}(t)] &= 0 \\ E[\underline{q}(t)] &= 0 \end{aligned} \right\} \text{ for all } t \quad (3.34)$$

$$(3.35)$$

2. The random error variances satisfy:

$$E[\underline{w}(t) \underline{w}^T(\tau)] = \underline{W}(t) \delta_d(t - \tau) \quad (3.36)$$

$$E[\underline{q}(t) \underline{q}^T(\tau)] = \underline{Q}(t) \delta_d(t - \tau) \quad (3.37)$$

As discussed in the previous subsections the flight path reconstruction problem would be reduced to the numerical solution (integration) of the system equation (3.21) when the initial state vector  $\underline{x}(0)$  were exactly known and the input signal  $\underline{u}(t)$  could be measured absolutely precise. In practice, the estimated initial state vector  $\hat{\underline{x}}(0)$  differs from the actual state vector according to:

$$\underline{x}(0) \triangleq \underline{x}(0) - \hat{\underline{x}}(0) \quad (3.38)$$

The components of the input vector are measured very accurately, meaning that the random measurement errors are very small. However in any case the effect of the bias errors on the result of an integration of the system equation (3.21) cannot be neglected.

The comparison of calculated system output variables and measured output variables provides "information" to correct for these effects. This is the subject of the following Sections where different statistical estimation procedures are applied to the flight path reconstruction problem.

#### 3.1.4. The augmented system model, linearization and discretization

As will be delineated in the following Sections the simultaneous estimation of the initial state  $\underline{x}(0)$  or the system state  $\underline{x}(t)$  and the corrections  $\underline{\lambda}$  for the bias errors in the input signal measurements requires the introduction of an augmented system model. The augmented system state is defined as:

$$\begin{aligned} \underline{y} &\triangleq \text{col} [\underline{x}(t), \underline{\lambda}] = \\ &= \text{col} [v_{x_B}, v_{y_B}, v_{z_B}, \psi, \theta, \phi, x_E, y_E, z_E, \lambda_x, \lambda_y, \lambda_z, \lambda_p, \lambda_q, \lambda_r] \end{aligned} \quad (3.39)$$

From Eqs. (3.21) and (3.27) through (3.32) it follows that the system and observation models can be written as:

$$\dot{\underline{x}}(t) = \underline{f}(\underline{x}(t), \underline{u}_m(t), \underline{\lambda}, \underline{w}(t)) \quad (3.40)$$

$$\underline{m}_m(t) = \underline{h}(\underline{x}(t), \underline{u}_m(t), \underline{\lambda}, \underline{w}(t)) - \underline{q}(t) \quad (3.41)$$

With the concept of the augmented state vector (3.40) can be written as:

$$\begin{aligned} \dot{\underline{y}}(t) &= \underline{f}'(\underline{y}(t), \underline{u}_m(t), \underline{w}(t)) = \\ &= \underline{f}'(\underline{y}(t), \underline{u}'(t)) \end{aligned} \quad (3.42)$$

where:

$$\underline{u}'(t) \triangleq \underline{u}_m(t) + \underline{w}(t) \quad (3.43)$$

The input vector (3.43) can be interpreted as the deterministic component of the measured input vector  $\underline{u}_m(t)$ . The observation equation corresponding to the augmented system now reads:

$$\underline{m}(t) = \underline{h}'(\underline{y}(t), \underline{u}'(t)) \quad (3.44)$$

Many estimation procedures require linearization of the nonlinear state and observation equations presented above with respect to a nominal trajectory  $\underline{y}_{nom}(t)$ , computed from the recorded input signal measurements  $\underline{u}_m(t)$  by integration of the nominal state equation:

$$\begin{aligned} \dot{\underline{y}}_{nom}(t) &= \underline{f}'(\underline{y}_{nom}(t), \underline{u}'_{nom}(t)) \\ &= \underline{f}'(\underline{y}_{nom}(t), \underline{u}_m(t)) \end{aligned} \quad (3.45)$$

for given

$$\underline{y}_{nom}(0) = \text{col} [\underline{x}_{nom}(0), \underline{\lambda}_{nom}] = \text{col} [\underline{x}_{nom}(0), 0] \quad (3.46)$$

Linearization of the augmented system state equation (3.42) and the corresponding observation equation (3.44), is based on the introduction of the corrections for the state perturbations:

$$\underline{y}(t) \triangleq \underline{y}(t) - \underline{y}_{nom}(t) \quad (3.47)$$

and the input signal perturbation corrections to the nominal input signals:

$$\begin{aligned} \underline{u}(t) &\triangleq \underline{u}'(t) - \underline{u}'_{nom}(t) = \\ &= \underline{u}'(t) - \underline{u}_m(t) = \underline{w}(t) \end{aligned} \quad (3.48)$$

Linearization of the augmented system model around the nominal trajectory  $\underline{y}_{nom}(t)$  and the corresponding nominal input signal  $\underline{u}_{nom}(t)$  results in:

$$\begin{aligned} \dot{\underline{y}}(t) &= \underline{f}'(\underline{y}(t), \underline{u}'(t)) - \underline{f}'(\underline{y}_{nom}(t), \underline{u}'_{nom}(t)) \\ &\approx \left[ \frac{\partial \underline{f}'}{\partial \underline{y}} \right]_{\underline{y}_{nom}, \underline{u}'_{nom}} \underline{y}(t) + \left[ \frac{\partial \underline{f}'}{\partial \underline{u}'} \right]_{\underline{y}_{nom}, \underline{u}'_{nom}} \underline{w}(t) \end{aligned} \quad (3.49)$$

Linearization of the observation equation yields:

$$\begin{aligned} \underline{m}(t) &\triangleq \underline{m}(t) - \underline{m}_{nom}(t) \\ &= \underline{m}(t) - \underline{q}(t) - \underline{m}_{nom}(t) \\ &= \underline{h}'(\underline{y}(t), \underline{u}'(t)) - \underline{h}'(\underline{y}_{nom}(t), \underline{u}'_{nom}(t)) - \underline{q}(t) \\ &= \left[ \frac{\partial \underline{h}'}{\partial \underline{y}} \right]_{\underline{y}_{nom}, \underline{u}'_{nom}} \underline{y}(t) + \left[ \frac{\partial \underline{h}'}{\partial \underline{u}'} \right]_{\underline{y}_{nom}, \underline{u}'_{nom}} \underline{w}(t) - \underline{q}(t) \end{aligned} \quad (3.50)$$

The initial condition of the linearized state equation is in many cases not known and therefore set equal to zero

$$\underline{y}(0) = 0 \quad (3.51)$$

The linearized state and observation equations, presented above, may be symbolically represented by:

$$\dot{\underline{y}}(t) = \underline{A}(t) \underline{y}(t) + \underline{B}(t) \underline{w}(t) \quad (3.52)$$

and



$$\underline{m}(t) = C(t) \underline{y}(t) + D(t) \underline{w}(t) - \underline{q}(t) \quad (3.53)$$

Under the conditions characterizing the problem of flight path reconstruction from flight test data, the contribution of the term  $D(t) \underline{w}(t)$  in  $\underline{m}(t)$  is negligibly small. This contribution results in the present case from the correction of the side slip vane measurements  $\beta_v$  for the effects of the angular velocities  $p_B$  and  $r_B$  according to Eq. (3.25). This correction is small and furthermore the measurements of  $p_B$  and  $r_B$  are highly accurate. The linearized observation equation therefore reduces to:

$$\underline{m}(t) = C(t) \underline{y}(t) - \underline{q}(t) \quad (3.54)$$

Applying present day instrumentation and data logging systems to aircraft flight testing, the input signals  $\underline{U}(t)$  and the output signals  $\underline{M}(t)$  are periodically sampled in time. Moreover, digital computers are used to perform all computations required for flight path reconstruction and further reduction of flight test data. Therefore the discrete time versions of the linearized state and observation equations are required. These discrete time versions relate the state perturbation correction  $\underline{y}(k)$  and the observation perturbation correction  $\underline{m}(k)$  to the quantities  $\underline{y}(k-1)$  and  $\underline{w}(k-1)$ . Assume that the continuous time stochastic process  $\underline{w}(t)$  can adequately be approximated by letting  $\underline{w}(t_{k-1}) = \underline{w}(k-1)$  be constant in the time interval  $[t_{k-1}, t_k]$ . Linear system theory then teaches that:

$$\underline{y}(k) = \Phi(k, k-1) \underline{y}(k-1) + \Gamma(k, k-1) \underline{w}(k-1) \quad (3.55)$$

and:

$$\underline{m}(k) = C(k) \underline{y}(k) - \underline{q}(k) \quad (3.56)$$

The transition matrix  $\Phi(k, k-1)$  is derived from the linear system matrix  $A(t)$ , approximating  $A(t)$  for  $t$  in  $[t_{k-1}, t_k]$  by  $A(t_{k-1})$ , according to:

$$\begin{aligned} \Phi(k, k-1) &= e^{A(t_{k-1}) [t_k - t_{k-1}]} \\ &\approx I + A(t_{k-1}) [t_k - t_{k-1}] + \frac{A^2(t_{k-1}) [t_k - t_{k-1}]^2}{2!} + \dots \end{aligned} \quad (3.57)$$

The control distribution matrix  $\Gamma(k, k-1)$  is derived from  $B(t_{k-1})$  according to:

$$\begin{aligned} \Gamma(k, k-1) &= \int_{t_{k-1}}^{t_k} \Phi(t_k, \tau) B(\tau) d\tau \\ &\approx \int_{t_{k-1}}^{t_k} \Phi(t_k, \tau) B(t_{k-1}) d\tau \\ &= B(t_{k-1}) (t_k - t_{k-1}) + \frac{A(t_{k-1}) B(t_{k-1}) (t_k - t_{k-1})^2}{2!} + \\ &\quad + \frac{A^2(t_{k-1}) B(t_{k-1}) (t_k - t_{k-1})^3}{3!} + \dots \end{aligned} \quad (3.58)$$

From linear system theory the following properties of the transition matrix are recalled:

$$\Phi(k, k-1) \Phi(k-1, k-2) = \Phi(k, k-2) \quad (3.59)$$

$$\Phi(k, k-1) \Phi(k-1, k) = I$$

$$\Phi(k, k) = I \quad (3.60)$$

Combining the discrete-time linear state equation with the linear observation equation, the following relations may be derived for the linearized observations  $\underline{m}(k)$ :

$$\underline{m}(k) = C(k) \Phi(k, k-1) \underline{y}(k-1) + C(k) \Gamma(k, k-1) \underline{w}(k-1) - \underline{q}(k) \quad (3.61)$$

or:

$$\underline{m}(k) = C(k) \Phi(k, 0) \underline{y}(0) + C(k) \sum_{i=1}^k \Phi(k, i) \Gamma(i, i-1) \underline{w}(i-1) - \underline{g}(k) \quad (3.62)$$

It should be noticed that the latter expression drastically simplifies if the contributions to  $\underline{m}(k)$  governed by the perturbations  $\underline{w}(i-1)$ , for  $i = 1, 2, \dots, k$ , may be neglected for all  $k$ . Neglecting  $\underline{w}(i-1)$ , for  $i = 1, 2, \dots, k$ , implies that the stochastic linear system, represented by Eqs. (3.55) and (3.56), is approximated by a deterministic system with stochastic output signal observations. This simplification yields the following relation:

$$\underline{m}(k) = C(k) \Phi(k, 0) \underline{y}(0) - \underline{g}(k) \quad (3.63)$$

## 3.2. Principles of flight path reconstruction

### 3.2.0. Introduction

In this Section four simple examples of increasing complexity serve for the introduction and clarification of several notions as nominal trajectory, state estimation, input bias estimation and the effects of measurement and of system noise. The reader more familiar with basic concepts of estimation theory is referred directly to Section 3.3. for which this Section serves as an introduction.

### 3.2.1. Basic system definition

In this subsection a description will be given of a simple scalar linear dynamic system. This system description is presented to set the stage for the problems to be discussed in the following subsections.

Let the scalar variable  $X(t)$  denote the state of a one-dimensional linear system with input  $U(t)$  and output  $M(t)$ . The evolution of the linear system state  $X(t)$  as a result of the system input  $U(t)$  and the corresponding output  $M(t)$ , are described by the following equations:

$$\dot{X}(t) = A X(t) + B U(t) \quad (3.64)$$

$$M(t) = C X(t) \quad (3.65)$$

Here  $A$ ,  $B$ ,  $C$  are scalar system parameters.

Solution of Eq. (3.64) obviously requires specification of the initial state:

$$X(t_0) \triangleq X(0) \quad (3.66)$$

In addition, the input  $U(t)$  should be given for  $t \geq 0$ . See fig. 2.

According to linear system theory, the solution of Eq. (3.64), i.e. the system's state as a function of time, may then be computed as follows:

$$X(t) = e^{A(t-t_0)} X(0) + \int_0^t e^{A(t-\tau)} B U(\tau) d\tau \quad (3.67)$$

$$X(t) = \Phi(t, t_0) X(0) + \int_0^t \Gamma(t, \tau) U(\tau) d\tau \quad (3.68)$$

where:

$$\Gamma(t, \tau) = e^{A(t-\tau)} B = \Phi(t, \tau) B \quad (3.69)$$

The output signal is given by (3.65).

Definitions for the state transition parameter  $\Phi(t, t_0)$  and the impulse response parameter  $\Gamma(t, \tau)$  occurring in Eq. (3.68) are apparent from that equation.

Now suppose that the system input  $U$  and the system output  $M$  are measured and that these measurements are corrupted with errors as follows:

$$U_m(t) = U(t) - \lambda - w(t) \quad (3.70)$$

$$M_m(t) = M(t) - q(t) \quad (3.71)$$

The subscript  $m$  is used to indicate measured magnitudes. The parameter  $\lambda$  represents a constant bias error, hence:

$$\dot{\lambda} = 0 \quad (3.72)$$

The variables  $w(t)$  and  $q(t)$  represent measurement noise. Both of these noise signals are assumed to be Gaussian, white and zero-mean. Hence:

$$E[w(t)] = E[q(t)] = 0 \quad \text{for all } t \quad (4.73)$$

The second order moments of the noise statistics are specified as follows:

$$E[w(t) w(\tau)] = W \delta_d(t - \tau) \quad (3.74)$$

$$E[q(t) q(\tau)] = Q \delta_d(t - \tau) \quad (3.75)$$

In accordance with present-day flight test instrumentation technology, the system input and output signals are assumed to be sampled periodically in time. Consequently, Eqs. (3.70) and (3.71) are to be reformulated, writing:

$$U_m(t_k) = U(t_k) - \lambda - w(t_k) \quad (3.76)$$

$$M_m(t_k) = M(t_k) - q(t_k) \quad (3.77)$$

To simplify the notation only the sequence number  $k$  will be used instead of the notation  $t_k$  to indicate the sample of interest.

It should be noticed that the Gaussian noise processes  $w(t)$  and  $q(t)$  are replaced by the Gaussian random sequences  $w(k)$  and  $q(k)$ . Equations (3.68) and (3.69) may now be replaced by the following expressions:

$$X(k) = \Phi(k, k-1) X(k-1) + \Gamma(k, k-1) U(k-1) \quad (3.78)$$

$$M(k) = C X(k) \quad (3.79)$$

Here:

$$U(\tau) = U(k-1) \quad \text{for } \tau \in [t_{k-1}, t_k)$$

In principle now the task is set to reconstruct the system state  $X(k)$  from the measurements  $U_m(i)$  and  $M_m(i)$ , where  $i < k$ ,  $i = k$  or  $i > k$ . In the following subsections further simplifications of the system delineated above will be introduced to facilitate the explanation of elementary problems and solution principles relevant to flight path reconstruction.

### 3.2.2. Example 1: Estimation of the initial state

In this example flight path reconstruction, or more precisely, estimation of the trajectory of the system state in its state space, is reduced to calculation of the initial condition  $X(0)$  followed by direct integration of the system state equation, see Eqs. (3.68) and (3.78).

For clarity sake the linear system model discussed in subsection 3.3.1. is simplified as much as possible. The system parameter  $A$  is assumed equal to 0, whereas the parameters  $B$  and  $C$  are supposed to be equal to 1, see fig. 3.

Hence:

$$A \triangleq 0 \quad (3.80)$$

$$B = C \triangleq 1 \quad (3.81)$$

It follows that the system parameters  $\Phi$  and  $\Gamma$  satisfy:

$$\Phi(k, k-1) = 1 \quad (3.82)$$

$$\Gamma(k, k-1) = t_k - t_{k-1} = T \quad (3.83)$$

To further simplify the system introduced in subsection 3.1.1., the system input  $U$  is assumed constant in time. The measurements  $U_m(k)$  and  $M_m(k)$  are supposed to be free of any errors.

$$U_m(k) = U \quad (3.84)$$

$$M_m(k) = M(k) \quad (3.85)$$

Compare with Eqs. (3.70) and (3.71).

To solve this almost trivial problem, the concept of nominal quantities is introduced. Nominal quantities are those computed directly from the input signal measurements recorded. First of all the nominal system state  $X_{nom}(k)$  is computed. It is assumed that:

$$X_{nom}(0) = 0 \quad (3.86)$$

The nominal system state is then computed as:

$$X_{nom}(k) = X_{nom}(0) + \sum_{j=1}^k U_m(j) T \quad (3.87)$$

Since  $X_{nom}(0) = 0$  and  $U_m(k) = U$  for all  $k$ , it follows that:

$$X_{nom}(k) = U k T \quad (3.88)$$

The nominal output signal observations are:

$$M_{nom}(k) = X_{nom}(k) = U k T \quad (3.89)$$

The measured output signal observations are:

$$M_m(k) = X(k) = X(0) + U k T \quad (3.90)$$

Comparison of  $M_m(k)$  with  $M_{nom}(k)$  reveals the required information concerning the initial condition  $X(0)$  as (see fig. 4):

$$\begin{aligned} m(k) &\triangleq M_m(k) - M_{nom}(k) = X(k) - X_{nom}(k) \\ &= X(0) + U k T - U k T = X(0) \end{aligned} \quad (3.91)$$

In this very simple deterministic example, a single measurement of the system input  $U$  and the system output  $M(k)$  should be noticed to suffice for determination of the initial condition  $X(0)$ , once  $k$  is specified. Evidently the system state  $X(k)$  can now be computed for all  $k$ , according to:

$$X(k) = X(0) + U k T \quad (3.92)$$

or in more general terms, by integration of the system input signal.

Summarizing in this example the flight path reconstruction problem has been reduced to straightforward calculation of the initial state followed by integration of the system input signal. Essential to flight path reconstruction from on-board measurements is the notion of nominal quantities and the fact that comparison of nominal output signal observations with actual measurements of the output signal reveals most relevant information concerning the parameters to be estimated.

### 3.2.3. Example 2: Estimation of the initial state from measurements corrupted with random errors

The problem discussed in the previous subsection is now complicated by the assumption that the output signal measurements  $M_m(k)$  for  $k = 1, 2, \dots, n$ , are corrupted with random errors  $q(k)$  (see fig. 5). Now it is no longer possible to determine  $X(0)$  from a single pair of measurements  $U_m(k)$  and  $M_m(k)$ . To obtain the information required for estimation of  $X(0)$ , the application of statistical methods is unavoidable. Referring to Eqs. (3.80) through (3.85) it is assumed again that:

$$A = 0$$

$$B = 1$$

$$\begin{aligned}
C &= 1 \\
U &= \text{constant} \\
X(t_0) &= X(0) \\
U_m(k) &= U \\
M_m(k) &= M(k) - q(k)
\end{aligned} \tag{3.93}$$

The output signal observations are supposed to be corrupted with random errors  $-q(k)$ , which are considered as an uncorrelated Gaussian sequence with:

$$E[q(k)] = 0 \tag{3.94}$$

$$E[q(k) q(j)] = Q \delta_{k,j} \tag{3.95}$$

For state trajectory reconstruction now again the task is set first of all to estimate  $X(0)$  from the available measurements  $U_m(k)$  and  $M_m(k)$  for  $k = 0, 1, 2, \dots, n$ , using the input signal measurements. Again nominal observations  $M_{nom}(k)$  can be computed (see fig. 6):

$$M_{nom}(k) = X_{nom}(k) = X_{nom}(0) + \sum_{j=1}^k U_m(j) T = U k T \tag{3.96}$$

The output signal observations  $M_m(k)$  are related to the initial state  $X(0)$  according to:

$$M_m(k) = X(k) - q(k) = X(0) + U k T - q(k) \tag{3.97}$$

Subtraction of the nominal output signal observations  $M_{nom}(k)$ , derived from the input signal measurements  $U_m(k)$ , from the actual output signal measurements  $M_m(k)$ , yields:

$$m(k) = M_m(k) - M_{nom}(k) = X(0) - q(k) \tag{3.98}$$

See Eqs. (3.96) and (3.97).

As the random errors  $-q(k)$  are supposed to be zero-mean, see Eq. (3.94), and to have a Gaussian, hence symmetric distribution it seems reasonable to estimate the initial state  $X(0)$  by averaging the deviations  $m(k)$ .

Hence:

$$\hat{X}(0|n) = \frac{1}{n} \sum_{k=1}^n m(k) \tag{3.99}$$

This estimation algorithm is the most simple "linear" estimation algorithm, since  $\hat{X}(0|n)$  is calculated linearly combining the available measurements.

With reference to the fact that  $\hat{X}(0|n)$  is, according to the preceding algorithm, derived at once from a batch of  $n$  observations  $m(k)$ , for  $k = 1, 2, \dots, n$ , this algorithm may be referred to as a batch algorithm. Alternatively, a recursive algorithm may be derived from the same averaging principle underlying the preceding batch algorithm.

It is now assumed that an estimate of  $X(0)$  is to be derived from  $n+1$  measurements. From the batch algorithm given above, it follows that:

$$(n+1) \hat{X}(0|n+1) - n \hat{X}(0|n) = m(n+1) \tag{3.100}$$

Hence:

$$\begin{aligned}
\hat{X}(0|n+1) &= \frac{n}{n+1} \hat{X}(0|n) + \frac{1}{n+1} m(n+1) \\
&= \left(1 - \frac{1}{n+1}\right) \hat{X}(0|n) + \frac{1}{n+1} m(n+1)
\end{aligned} \tag{3.101}$$

Defining the confidence factor:

$$K(n+1) \triangleq \frac{1}{n+1} \tag{3.102}$$

Combination of Eqs. (3.101) and (3.102) yields:

$$\hat{X}(0|n+1) = (1 - K(n+1)) \hat{X}(0|n) + K(n+1) m(n+1) \quad (3.103)$$

or:

$$\hat{X}(0|n+1) = \hat{X}(0|n) + K(n+1) [m(n+1) - \hat{X}(0|n)] \quad (3.104)$$

As the last two equations will return frequently in the subsequent text, it is highly relevant to discuss these equations in more detail.

The factors  $(1 - K(n+1))$  and  $K(n+1)$  occurring in Eq. (3.103) may be considered as confidence factors or weighting factors. This expression may therefore be understood to describe a weighted combination of the preceding estimate  $\hat{X}(0|n)$  and the following observation perturbation correction  $m(n+1)$ . If  $n$  is very small, the estimate  $\hat{X}(0|n+1)$  may be seen to rely more on the new measurement  $m(n+1)$  than on the preceding estimate  $\hat{X}(0|n)$ . For large  $n$  however,  $\hat{X}(0|n+1)$  is almost entirely determined by  $\hat{X}(0|n)$ . In the limit for  $n \rightarrow \infty$  the contribution to  $\hat{X}(0|n+1)$ , governed by  $m(n+1)$ , may be seen to vanish.

Equation (3.104) shows that the recursive algorithm may be considered as a kind of prediction-correction scheme. When  $m(n+1)$  is recorded, the best available estimate of  $X(0)$  is  $\hat{X}(0|n)$ .

Hence  $\hat{X}(0|n)$  can be considered as the best prediction of  $m(n+1)$  at  $t_{n+1}$ , obtained by processing all measurements up to and including  $m(n)$ , recorded at  $t_n$ . The deviation between  $m(n+1)$  and  $\hat{X}(0|n)$  is then used to correct  $\hat{X}(0|n)$ . Obviously the relevant information contained in  $m(n+1)$  is corrupted with the measurement error  $-q(n+1)$ .

From Eqs. (3.103) and (3.104) recursive expressions may be derived for the propagation in time of the error in the estimate of the initial state.

Let:

$$e(0|n+1) \triangleq X(0) - \hat{X}(0|n+1) \quad (3.105)$$

Equation (3.105) may then be rewritten as:

$$X(0) - \hat{X}(0|n+1) = X(0) - (1 - K(n+1)) \hat{X}(0|n) - K(n+1) m(n+1) \quad (3.106)$$

$$= (1 - K(n+1)) X(0) - (1 - K(n+1)) \hat{X}(0|n) + K(n+1) q(n+1) \quad (3.107)$$

Hence:

$$e(n+1) = (1 - K(n+1)) e(n) + K(n+1) q(n+1) \quad (3.108)$$

A measure for the dispersion or scatter in the estimates  $\hat{X}(0|n+1)$ , for all  $n$ , is given by the variance  $E[e^2(n+1)]$ . As the estimation error  $e(n)$  and the observation error  $-q(n+1)$  may be assumed uncorrelated, the following equation may be derived from Eq. (3.108), when defining:

$$P(0|n+1) \triangleq E[e^2(0|n+1)] = (1 - K(n+1))^2 P(0|n) + K^2(n+1) Q \quad (3.109)$$

Studying the weighted combination of  $\hat{X}(0|n)$  and  $m(n+1)$ , see Eq. (3.103), computed to obtain the estimate  $\hat{X}(0|n+1)$ , the question arises what relation should exist between the best or optimal  $K(n+1)$  at one hand and  $P(0|n)$  and  $Q$  at the other, to minimize  $P(0|n+1)$ . This relation may easily be derived satisfying the following condition:

$$\frac{\partial P(0|n+1)}{\partial K(n+1)} = -2 (1 - K(n+1)) P(0|n) + 2K(n+1) Q = 0 \quad (3.110)$$

From this condition it follows that  $P(0|n+1)$  is minimal, for given  $P(0|n)$  and  $Q$  if:

$$K^0(n+1) = \frac{P(0|n)}{P(0|n) + Q} \quad (3.111)$$

Substitution of this expression for the confidence factor  $K(n+1)$  in the expression for  $P(0|n+1)$ , see Eq. (3.109), yields the following recursive relation for the variance in the estimation error:

$$P(0|n+1) = \frac{P(0|n) Q}{P(0|n) + Q} = (1 - K^0(n+1)) P(0|n) \quad (3.112)$$

A recursive algorithm for  $K^0(n+1)$ , for the optimal confidence factor given  $K^0(0)$ , can also be derived according to:

$$\begin{aligned}
 K^0(n+1) &= \frac{P(0|n)}{P(0|n) + Q} = \frac{1}{1 + Q/P(0|n)} = \\
 &= \frac{1}{1 + \frac{P(0|n-1) + Q}{P(0|n-1)}} = \frac{1}{1 + 1/K^0(n)} = \\
 &= \frac{K^0(n)}{K^0(n) + 1}
 \end{aligned} \tag{3.113}$$

In contrast to the batch algorithm discussed, the application of recursive algorithms demands for a priori specification of the initial estimate  $\hat{x}(0|0)$ , the variance  $P(0|0)$  of the errors in the initial estimate as well as the variance  $Q$  of the measurement errors  $-q(k)$ .

The question may now arise, as to what extent more accurate results can be achieved, estimating the initial condition  $x(0)$  by means of the optimal recursive estimation scheme as compared to the results obtained, when applying the batch algorithm.

After processing  $n+1$  observations  $m(k)$ ;  $k = 1, 2, \dots, n+1$ , the error in the estimate  $\hat{x}(0|n+1)$  may be derived as follows:

$$\hat{x}(0|n+1) - x(0) = \frac{1}{n+1} \sum_{k=1}^{n+1} m(k) - x(0) = \frac{1}{n+1} \sum_{k=1}^{n+1} q(k) \tag{3.114}$$

see Eq. (3.109).

The variance of the error in the estimate  $\hat{x}(0|n+1)$  may thus be derived as (see fig. 7):

$$P(0|n+1) = E \left[ \left\{ \frac{1}{n+1} \sum_{k=1}^{n+1} q(k) \right\}^2 \right] = \frac{1}{n+1} Q \tag{3.115}$$

When applying the batch estimation scheme no a priori information concerning  $x(0)$  is required. This situation is reflected, when specifying:

$$P(0|0) = \infty \tag{3.116}$$

The following results are obtained in this case:

$$\lim_{P(0|0) \rightarrow \infty} K^0(1) = \lim_{P(0|0) \rightarrow \infty} \frac{P(0|0)}{P(0|0) + Q} = 1 \tag{3.117}$$

and:

$$\lim_{P(0|0) \rightarrow \infty} P(0|1) = \lim_{P(0|0) \rightarrow \infty} \frac{P(0|0) Q}{P(0|0) + Q} = Q \tag{3.118}$$

Recursively applying the relation between  $P(0|k)$  and  $P(0|k-1)$ , for  $k = 2, 3, \dots, n+1$ , it can easily be verified that in this case:

$$P(0|n+1) = \frac{1}{n+1} Q \tag{3.119}$$

Hence, when setting  $P(0|0) = \infty$ , the optimal recursive estimation scheme should be observed to yield exactly the same estimation results as obtained when applying the batch estimation algorithm, such for any magnitude of the observation error variance  $Q$ . Although different magnitudes of  $P(0|0)$  may affect the error variance  $P(0|n)$  it follows from recursive application of Eqs. (3.112) and (3.113) that these effects vanish for  $n \rightarrow \infty$ .

As the task was set to estimate the system state  $x(k)$  after processing a sufficiently large number of measurements, to obtain an estimate of the initial state  $x(0)$  with adequate accuracy, the estimate  $\hat{x}(k)$  remains to be computed according to:

$$\hat{x}(k|n+1) = \hat{x}(0|n+1) + \sum_{i=2}^k U_m(k) T = \hat{x}(0|n+1) + U_k T \tag{3.120}$$

The accuracy of  $\hat{x}(k)$  may thus be seen to depend in this case only on the accuracy of the initial state estimate  $\hat{x}(0|n+1)$ :

$$P(k|n) = E[(x(k) - \hat{x}(k|n))^2]$$

$$= E[(X(0) - \hat{X}(0|n))^2]$$

$$= P(0|n)$$

Summarizing it should be noticed that the preceding example has been used to introduce statistical estimation concepts applying simple averaging of observation differences  $m(k)$ , for  $k = 1, 2, \dots, n$ , between the actual output signal observations  $M_m(k)$  and the calculated observations  $M_{nom}(k)$ . In addition the concepts of recursive and batch estimation have been exhibited.

### 3.2.4. Example 3: Estimation of initial state and correction for bias errors

The third example problem differs from the second only in that a constant bias error is supposed to offset the measurements  $U_m$  of the output signal  $U$ , such in order to facilitate the introduction of the concept of an augmented vector (see fig. 8). It should be noticed however, that the bias error can be introduced conserving model linearity.

Hence:

$$U_m \triangleq U - \lambda \quad (3.121)$$

Reconstruction of the time history of the system state  $X(k)$  now requires estimation of the initial state  $X(0)$  as well as estimation of a correction for the bias error  $-\lambda$ .

Again, the required information is obtained, comparing nominal observations  $M_{nom}(k)$ , calculated from the measured input signals  $U_m(k)$  with the actual output signal observations  $M_m(k)$ .

As in the previous example problems (see fig. 9):

$$M_{nom}(k) = X_{nom}(k) = X_{nom}(0) + U_m k T = (U - \lambda) k T \quad (3.122)$$

whereas:

$$M_m(k) = X(k) - q(k) = X(0) + U k T - q(k) \quad (3.123)$$

From Eqs. (3.122) and (3.123) it follows that:

$$m(k) = M_m(k) - M_{nom}(k) = X(0) + \lambda k T - q(k) \quad (3.124)$$

As components of an augmented parameter vector  $\underline{Y}(0)$  the parameters  $X(0)$  and  $\lambda$  can now be estimated, processing a batch of say  $n$  observation differences  $m(k)$ ,  $k = 1, 2, \dots, n$ , with the aid of a statistical estimation algorithm, often referred to as regression analysis.

Let:

$$\underline{Y}(0) \triangleq \text{col } [X(0), \lambda] \quad (3.125)$$

and:

$$\underline{r}(k) = \text{row } [1, k T] \quad (3.126)$$

Equation (3.124) may then be reformulated writing:

$$m(k) = \underline{r}(k) \underline{Y}(0) - q(k) \quad (3.127)$$

According to regression analysis, the optimal estimate  $\hat{\underline{Y}}(0|n)$  minimizing the quadratic cost function:

$$J_n = \sum_{k=1}^n (m(k) - \underline{r}(k) \hat{\underline{Y}}(0))^2 Q^{-1} \quad (3.128)$$

is then obtained according to (see appendix B):

$$\hat{\underline{Y}}(0|n) = \left( \sum_{k=1}^n \underline{r}^T(k) Q^{-1} \underline{r}(k) \right)^{-1} \sum_{k=1}^n \underline{r}^T(k) Q^{-1} m(k) \quad (3.129)$$

The covariance matrix  $P(0|n)$  of the error in the batch estimate  $\hat{\underline{Y}}(0|n)$  can be derived from Eq. (3.129), using:



$$\begin{aligned}
\underline{e}(0|n) &= \underline{y}(0) - \hat{\underline{y}}(0|n) \\
&= \underline{y}(0) - \left( \sum_{k=1}^n \underline{r}^T(k) \underline{Q}^{-1} \underline{r}(k) \right)^{-1} \sum_{k=1}^n \underline{r}^T(k) \underline{Q}^{-1} m(k) \\
&= \underline{y}(0) - \left( \sum_{k=1}^n \underline{r}^T(k) \underline{Q}^{-1} \underline{r}(k) \right)^{-1} \sum_{k=1}^n \underline{r}^T(k) \underline{Q}^{-1} \left( \underline{r}(k) \underline{y}(0) - q(k) \right) \\
&= \sum_{k=1}^n \left( \underline{r}^T(k) \underline{Q}^{-1} \underline{r}(k) \right)^{-1} \sum_{k=1}^n \underline{r}^T(k) \underline{Q}^{-1} q(k)
\end{aligned} \tag{3.130}$$

Now:

$$\begin{aligned}
P(0|n) &= E \left[ \underline{e}(0|n) \underline{e}^T(0|n) \right] \\
&= E \left[ \left( \sum_{k=1}^n \underline{r}^T(k) \underline{Q}^{-1} \underline{r}(k) \right)^{-1} \sum_{k=1}^n \underline{r}^T(k) \underline{Q}^{-1} q(k) \sum_{j=1}^n q(j) \underline{Q}^{-1} \underline{r}(j) \left( \sum_{k=1}^n \underline{r}^T(k) \underline{Q}^{-1} \underline{r}(k) \right)^{-1} \right]
\end{aligned} \tag{3.131}$$

Recalling the fact that  $q(k)$  is sequentially uncorrelated, now:

$$P(0|n) = \left( \sum_{k=1}^n \underline{r}^T(k) \underline{Q}^{-1} \underline{r}(k) \right)^{-1} \tag{3.132}$$

Substituting in Eq. (3.129) yields:

$$\hat{\underline{y}}(0|n) = P(0|n) \sum_{k=1}^n \underline{r}^T(k) \underline{Q}^{-1} m(k) \tag{3.133}$$

The recursive regression algorithm, corresponding with the batch algorithm discussed in this example, now follows from Eq. (3.129) and comparison of  $\hat{\underline{y}}(0|n)$  with  $\hat{\underline{y}}(0|n+1)$  see also Eq. (3.100):

$$\begin{aligned}
\left( \sum_{k=1}^{n+1} \underline{r}^T(k) \underline{Q}^{-1} \underline{r}(k) \right) \hat{\underline{y}}(0|n+1) - \left( \sum_{k=1}^n \underline{r}^T(k) \underline{Q}^{-1} \underline{r}(k) \right) \hat{\underline{y}}(0|n) &= \\
= \underline{r}^T(n+1) \underline{Q}^{-1} m(n+1)
\end{aligned} \tag{3.134}$$

This expression may be rearranged using Eq. (3.132):

$$\begin{aligned}
P(0|n+1)^{-1} \hat{\underline{y}}(0|n+1) - (P(0|n+1)^{-1} - \underline{r}^T(n+1) \underline{Q}^{-1} \underline{r}(n+1)) \hat{\underline{y}}(0|n) &= \\
= \underline{r}^T(n+1) \underline{Q}^{-1} m(n+1)
\end{aligned} \tag{3.135}$$

Now rewriting this equation:

$$\begin{aligned}
\hat{\underline{y}}(0|n+1) &= \hat{\underline{y}}(0|n) + P(0|n+1) \underline{r}^T(n+1) \underline{Q}^{-1} [m(n+1) - \underline{r}(n+1) \hat{\underline{y}}(0|n)] \\
&\triangleq \hat{\underline{y}}(0|n) + K(n+1) [m(n+1) - \underline{r}(n+1) \hat{\underline{y}}(0|n)]
\end{aligned} \tag{3.136}$$

or:

$$\hat{\underline{y}}(0|n+1) = (1 - K(n+1) \underline{r}^T(n+1)) \hat{\underline{y}}(0|n) + K(n+1) m(n+1) \tag{3.137}$$

where:

$$K(n+1) \triangleq P(0|n+1) \underline{r}^T(n+1) \underline{Q}^{-1} \tag{3.138}$$

Using the expressions for  $P(0|n)$  and  $K(n+1)$  a recursive propagation equation can be derived for the covariance matrix  $P(0|n+1)$  of the errors  $\underline{e}(0|n+1)$  in the estimate  $\hat{\underline{y}}(0|n+1)$ :

$$P(0|n+1) - P(0|n) = -P(0|n+1) \left\{ P(0|n+1)^{-1} - P(0|n)^{-1} \right\} P(0|n)$$

$$\begin{aligned}
&= -P(0|n+1) \left\{ \sum_{k=1}^{n+1} \underline{r}^T(k) Q^{-1} \underline{r}(k) - \sum_{k=1}^n \underline{r}^T(k) Q^{-1} \underline{r}(k) \right\} P(0|n) \\
&= -P(0|n+1) \underline{r}^T(n+1) Q^{-1} \underline{r}(n+1) P(0|n) \\
&= -K(n+1) \underline{r}(n+1) P(0|n)
\end{aligned} \tag{3.139}$$

So,

$$P(0|n+1) = (1 - K(n+1) \underline{r}^T(n+1)) P(0|n) \tag{3.140}$$

After estimation of  $X(0)$  and  $\lambda$ , the time history of the system state may then be computed according to:

$$\hat{X}(k|n) = \hat{X}(0|n) + (U_m + \hat{\lambda}(0|n)) k T \tag{3.141}$$

Summarizing it should be noticed that this example has been presented to illustrate the introduction of a so-called augmented parameter vector used to facilitate simultaneous estimation of all parameters of interest. In addition it has been shown how to estimate corrections for constant bias errors in the measurements to be processed and how to apply these corrections. The augmented parameter vector approach is permitted since model linearity was conserved, when introducing the bias error  $-\lambda$ .

### 3.2.5. Example 4: State estimation

This example is presented to introduce the notion of recursive estimation of the system state  $X(k)$  as a function of time, such in contrast to estimation of only the initial state  $X(0)$ , see Refs. 34, 35. To set the stage the measurements  $U_m(k)$  are assumed to be corrupted with random errors  $w(k)$  (see fig. 10):

$$U_m(k) \triangleq U - w(k) \tag{3.142}$$

The random errors  $-w(k)$  for  $k = 0, 1, 2, \dots$ , are considered as a zero-mean, sequentially uncorrelated, Gaussian random sequence:

$$E\{w(k)\} = 0 \quad \text{for all } k \tag{3.143}$$

with variance:

$$E\{w(k) w(j)\} = W \delta_{k,j} \tag{3.144}$$

Calculation of system state estimates  $\hat{X}(k)$  by estimation of the initial state  $X(0)$ , followed by integration of the measured input signal  $U_m(k)$  does not yield the most accurate results, since integration of  $U_m(k)$  for  $k = 0, 1, \dots$ , obviously implies integration of the measurement errors  $w(k)$ . In fact a method should be devised to attenuate the effects of the errors  $-w(k)$  and  $-q(k)$  on the estimates  $\hat{X}(k)$ . To this end Kalman and Bucy developed in the early 1960's recursive algorithms which can be used to derive an estimate  $\hat{X}(k|k)$  from all measurements up to and including those recorded at time  $t_k$ . Application of these recursive algorithms to the estimation problem in this example results in attenuation of the errors  $-q(k)$  in the output signal measurements  $M_m(k)$  and in estimation of the effects of the errors  $-w(k)$  in the measurements  $U_m(k)$  on the estimates of the system state  $X(k)$ . Estimation of the latter effects enables adequate correction. Again most relevant information is squeezed out of the deviations  $m(k)$  between the output signal measurements  $M_m(k)$  and the nominal or computed output signal measurements  $M_{nom}(k)$ . The nominal output signal measurements are computed according to:

$$M_{nom}(k) = X_{nom}(k) = X_{nom}(k-1) + U_m(k) T \tag{3.145}$$

The actual system state evolves according to:

$$X(k) = X(k-1) + U T \tag{3.146}$$

The actual output signal measurements are again given by:

$$M_m(k) = X(k) - q(k) \tag{3.147}$$

From these equations it follows that:

$$\begin{aligned}
 m(k) &= M_m(k) - M_{nom}(k) \\
 &= X(k) - X_{nom}(k) - q(k) \\
 &= X(k-1) - X_{nom}(k-1) + w(k-1)T - q(k)
 \end{aligned} \tag{3.148}$$

Recursive substitution of the relations:

$$X(i) = X(i-1) + U T \tag{3.149}$$

and:

$$X_{nom}(i) = X_{nom}(i-1) + U_m(i-1) T \tag{3.150}$$

In the expression derived for  $m(k)$ , see Eq. (3.148), yields:

$$m(k) = X(0) - X_{nom}(0) + \sum_{i=1}^k w(i-1)T - q(k) \tag{3.151}$$

$$= X(0) + \sum_{i=1}^k w(i-1)T - q(k) \tag{3.152}$$

From the assumptions that  $-w(k)$  and  $-q(k)$  are zero-mean, sequentially uncorrelated, Gaussian, random error sequences it follows that the sum of these random errors, occurring in the preceding expression, may also be considered as a zero-mean random error process  $\varepsilon(k)$ .

As  $X_{nom}(0)$  is assumed equal to zero, the preceding expression may be rewritten as:

$$m(k) = X(0) + \varepsilon(k) \tag{3.153}$$

The variance of  $\varepsilon(k)$  however increases with increasing  $k$ , since:

$$\begin{aligned}
 \sigma_{\varepsilon}^2(k) &= E[\varepsilon^2(k)] = \sum_{i=1}^k E[w^2(i-1)T^2] + E[q^2(k)] \\
 &= k W T^2 + Q
 \end{aligned} \tag{3.154}$$

Application of regression analysis algorithms to the problem of estimating  $X(0)$  from a batch of measurement differences  $m(1), m(2), \dots, m(n)$ , under this condition, requires introduction of a weighting factor  $\sigma_{\varepsilon}^2(k)$  in the cost-function given in subsection 3.2.4., Eq. (3.128), such that:

$$J_n = \sum_{k=1}^n \frac{(m(k) - \underline{r}(k) \hat{X}(0))^2}{\sigma_{\varepsilon}^2(k)} \tag{3.155}$$

Instead of further developing the batch estimation algorithms minimizing the cost-function  $J_n$ , with the subsequent disadvantages inherent to merely estimating  $X(0)$  discussed before in this example, now the discrete time version of the Kalman-Bucy filter will be introduced.

It will be shown that an optimal estimate of  $X(k)$  can be obtained applying a recursive estimation algorithm which is designed to take account of both the input signal and output signal noise statistics.

To initiate the recursive estimation process it is assumed that an estimate  $X(k-1|k-1)$  of the system state  $X(k-1)$  is derived from all measurements up to and including those recorded at  $t_{k-1}$ .

The task is set to derive the optimal estimate  $\hat{X}(k|k)$  from the measurements  $U_m(k)$  and  $M_m(k)$ . First of all the most accurate prediction of  $X(k)$ , i.e.  $\hat{X}(k|k-1)$  is computed according to:

$$\hat{X}(k|k-1) = \hat{X}(k-1|k-1) + U_m(k) T \tag{3.156}$$

The error  $e(k|k-1)$  in the prediction  $\hat{X}(k|k-1)$  satisfies:

$$\begin{aligned}
 e(k|k-1) &= X(k) - \hat{X}(k|k-1) \\
 &= X(k-1) + U T - \hat{X}(k-1|k-1) - U T + w(k-1) T
 \end{aligned} \tag{3.157}$$

$$= e(k-1|k-1) + w(k-1) T$$

The variance of the error in the prediction  $\hat{x}(k|k-1)$  hence equals:

$$\begin{aligned} P(k|k-1) &= E [e^2(k|k-1)] \\ &= P(k-1|k-1) + T^2 w \end{aligned} \quad (3.158)$$

For estimation of  $x(k)$  the discrete time Kalman filter algorithm, showing great similarity with the recursive algorithm delineated in subsection 3.2.3. (example 2), will be applied:

$$\hat{x}(k|k) = \hat{x}(k|k-1) + K(k) [m(k) - \hat{x}(k|k-1)] \quad (3.159)$$

Or equivalently:

$$\hat{x}(k|k) = (1 - K(k)) \hat{x}(k|k-1) + K(k) m(k) \quad (3.160)$$

These expressions may be considered as the discrete time version of a linear signal filter. The confidence factor  $K(k)$ , also referred to as the filter gain, is still to be derived. The optimal filter gain should be derived so as to minimize the variance of the error in the estimate  $\hat{x}(k|k)$ . Applying Eq. (3.159) it may easily be derived that the error in the optimal estimate  $\hat{x}(k|k)$  satisfies:

$$e(k|k) = x(k) - \hat{x}(k|k) = (1 - K(k)) e(k|k-1) + K(k) q(k) \quad (3.161)$$

Hence:

$$P(k|k) = (1 - K(k))^2 P(k|k-1) + K^2(k) Q \quad (3.162)$$

If  $K^0(k)$  is the optimal gain, then  $P(k|k)$  should be minimal if:

$$\left( \frac{\partial P(k|k)}{\partial K(k)} \right)_{K^0(k)} = 0 \quad (3.163)$$

which yields:

$$K^0(k) = \frac{P(k|k-1)}{P(k|k-1) + Q} \quad (3.164)$$

A remarkable similarity between this expression for  $K^0(k)$  and the corresponding expression for the confidence factor in example 2 should be observed. Therefore it should not surprise that the similarity also holds for the error propagation equation obtained when substituting the expression for the optimal filter gain  $K^0(k)$  in Eq. (3.162), which yields:

$$P^0(k|k) = \frac{P(k|k-1) Q}{P(k|k-1) + Q} \quad (3.165)$$

Summarizing, example 4 has been presented to show that flight path reconstruction from on board measurements in the presence of input signal errors  $-w(t)$  and random errors in the output signal observations  $-q(t)$  cannot be achieved simply by estimation of the initial state with recursive or batch regression analysis procedures followed by integration of  $U_m(t)$ . Instead the Kalman filter algorithm was introduced to directly obtain and estimate  $\hat{x}(k|k)$  from all measurements  $U_m(i-1)$  and  $M_m(i)$  for  $i = 1, 2, \dots, k$ .

### 3.3. Flight path reconstruction algorithms

#### 3.3.0. Introduction

A survey of the algorithms used for estimation of flight path variables and corrections for instrumental bias errors from measurements of system input and output signals will be presented in this section. Depending on the characteristics of the flight path reconstruction problem facing the flight test engineer, he may choose from these algorithms the one that suits him best. The selection may be affected not only by the characteristics of the underlying dynamic system model, the flight test instrumentation system to be used, or the type of manoeuvres to be reconstructed. Moreover, economic factors such as the computing time required, the computer capacity available, available standard software, available skill and experience may have to be taken into account, when selecting the algorithm to be applied.

Presenting the reconstruction algorithms in the subsequent subsections, no simplifications will be introduced. The algorithms will be based on the model formulations developed in Section 3.1.

### 3.3.1. Weighted least squares and least squares estimation

If the accelerometers used to measure the specific aerodynamic forces  $A_{x_B}$ ,  $A_{y_B}$  and  $A_{z_B}$  and the rate gyroscopes used to measure the angular rates  $p_B$ ,  $q_B$  and  $r_B$  of the aircraft are of sufficiently high accuracy it may be acceptable to neglect the measurement errors  $-w(k)$  in the measurements  $\underline{u}_m(k)$  of the vector valued input signal  $\underline{u}(k)$ . The observations  $\underline{m}(k)$ , see Eq. (3.50), are in that case linearly related to the initial state perturbation corrections  $\underline{y}(0)$  according to Eq. (3.63):

$$\underline{m}(k) = C(k) \Phi(k, 0) \underline{y}(0) - \underline{q}(k) \quad (3.166)$$

Definition of:

$$R(k) \triangleq C(k) \Phi(k, 0) \quad (3.167)$$

and substitution in Eq. (3.167) yields:

$$\underline{m}(k) = R(k) \underline{y}(0) - \underline{q}(k) \quad (3.168)$$

This linear relation closely resembles Eq. (3.127) presented in Subsection (3.24).

If:

$$E [\underline{q}(k) \underline{q}^T(j)] = Q(k) \delta_{k,j} \quad (3.169)$$

then the estimate minimizing the quadratic cost function:

$$J_k = \sum_{i=1}^k (\underline{m}(i) - R(i) \underline{y}(0))^T Q^{-1}(i) (\underline{m}(i) - R(i) \underline{y}(0)) \quad (3.170)$$

follows from the weighted linear regression algorithm:

$$\hat{\underline{y}}(0|k) = \left( \sum_{i=1}^k R^T(i) Q^{-1}(i) R(i) \right)^{-1} \sum_{i=1}^k R^T(i) Q^{-1} \underline{m}(i) \quad (3.171)$$

If:

$$Q(i) = Q \quad \text{for all } i \quad (3.172)$$

i.e. if:

$$Q = \text{constant} \quad (3.173)$$

then the weighted linear regression algorithm, see Eq. (3.171), reduces to the simpler linear regression algorithm:

$$\hat{\underline{y}}(0|k) = \left( \sum_{i=1}^k R^T(i) Q^{-1} R(i) \right)^{-1} \sum_{i=1}^k R^T(i) Q^{-1} \underline{m}(i) \quad (3.174)$$

If:

$$Q(i) = Q = \sigma_q^2 I \quad (3.175)$$

the preceding expression may again be simplified to yield:

$$\hat{\underline{y}}(0|k) = \left( \sum_{i=1}^k R^T(i) R(i) \right)^{-1} \sum_{i=1}^k R^T(i) \underline{m}(i) \quad (3.176)$$

The reconstructed time histories of the flight path quantities of interest then follow from:

$$\hat{\underline{y}}(k|k) = \underline{y}_{nom}(k) + \phi(k, 0) \hat{\underline{y}}(0|k) \quad (3.177)$$

or from recalculation of the nominal state vector trajectory  $\underline{y}_{nom}(k)$  posterior to correction of the nominal initial state according to:

$$\hat{\underline{y}}(0|k) = \underline{y}_{nom}(0) + \hat{\underline{y}}(0|k) \quad (3.178)$$

This process may be repeated until no significant deviations between two consecutive estimates of the initial state are observed. The covariance matrix  $P(0|k)$  of the errors in the estimate  $\hat{\underline{y}}(0|k)$  and henceforth in the estimate  $\hat{\underline{y}}(0|k)$  may be computed according to:

$$P(0|k) = \left( \sum_{i=1}^k R^T(i) Q^{-1} R(i) \right)^{-1} \quad (3.179)$$

Alternatively  $\hat{\underline{y}}(0|k)$  may also be obtained applying a recursive estimation scheme, as follows:

$$\hat{\underline{y}}(0|k) = \hat{\underline{y}}(0|k-1) + K(k) [\underline{m}(k) - R(k) \hat{\underline{y}}(0|k-1)] \quad (3.180)$$

The confidence or gain matrix is given by:

$$K(k) = P(0|k) R^T(k) Q^{-1} \quad (3.181)$$

The optimal error covariance matrix follows from:

$$P(0|k) = (I - K(k) R(k)) P(0|k-1) \quad (3.182)$$

### 3.3.2. The Kalman Filter Algorithm

If the input signal  $w(k-1)$  is not to be neglected, computation of a correction  $\hat{\underline{y}}(k|k)$  for the corresponding state perturbation  $-\underline{y}(k)$ , by estimation of a correction  $\hat{\underline{y}}(0|k)$  for the initial state perturbation  $-\underline{y}(0)$ , followed by integration of the linearized state equation, see Eq. (3.55), derived in Section 3.1., is not possible, since the random input signal  $w(k-1)$  is unknown as a function of time.

Only the statistical distribution function of the random sequence  $w(k-1)$  is given in terms of the first and second order moment of a Gaussian distribution, see Section 3.1. and 3.2. A similar remark holds for the observation noise  $q(k)$ . In addition both random error sequences are considered sequentially uncorrelated. If estimation of the correction for the initial state perturbation  $-\underline{y}(0)$ , followed by integration of the linearized state equation Eq. (3.55), cannot be accomplished, the question arises how to arrive at accurate estimates  $\hat{\underline{y}}(k|k)$  of the state perturbation corrections required for correction of the corresponding nominal state vector quantities  $\underline{y}_{nom}(k)$ . In other words and more technically speaking, the flight test engineer faces the problem to find a method which enables him to correct the nominal state vector quantities  $\underline{y}_{nom}(k)$ , computed by straight forward integration of the equations of motion (using the measured inputs  $\underline{u}_m(k) = \underline{u}_{nom}(k)$ ) for the effects of the random errors  $-w(k)$  in these measurements. Therefore a method should be devised to estimate corrections for the contribution  $-\underline{y}(k)$  to  $\underline{y}_{nom}(k)$ , resulting from integration of the random measurement errors  $-w(k)$ . Again information concerning the deviations of  $\underline{y}_{nom}(k)$  from the actual system state  $\underline{y}(k)$  is revealed by the observation perturbations  $\underline{m}(k)$  obtained when comparing the actual system outputs measured  $\underline{M}_m(k)$  with the computed or nominal system outputs  $\underline{M}_{nom}(k)$ . As shown in Section 3.1., see Eq. (3.56), these observation perturbation corrections are linearly related to the linearized system state perturbation  $\underline{y}(k)$ , which in turn results from the initial state perturbation vector  $\underline{y}(0)$  and the linear system response on the random input  $w(i)$ , for  $i = 1, 2, \dots, k-1$ . To state the problem more precisely an algorithm should be found enabling estimation of the linear state perturbation correction vector  $\underline{y}(k)$  from measurements  $\underline{m}(1), \underline{m}(2), \dots, \underline{m}(n)$ .

If  $n < k$  the estimation process is referred to as "statistical prediction".

If  $n = k$  the process is referred to as "filtering" and if  $n > k$  it is called "smoothing".

First of all the filtering process will be delineated.

Let the linearized system dynamics related to the propagation of the corrections for the state perturbations be given by the following equations:

$$\underline{y}(k) = \phi(k, k-1) \underline{y}(k-1) + \Gamma(k, k-1) w(k-1) \quad (3.183)$$

$$\underline{m}(k) = C(k) \underline{y}(k) - q(k) \quad (3.184)$$

The Kalman filter algorithm is then represented by the following set of recursive equations (time update):

$$\hat{\underline{y}}(k|k-1) = \phi(k, k-1) \hat{\underline{y}}(k-1|k-1) \quad (3.185)$$

$$P(k|k-1) = \Phi(k, k-1) P(k-1|k-1) \Phi^T(k, k-1) + \Gamma(k, k-1) W \Gamma^T(k, k-1) \quad (3.186)$$

The gain matrix is given by (measurement update):

$$K(k) = P(k|k-1) C^T(k) [C(k) P(k|k-1) C^T(k) + Q]^{-1} \quad (3.187)$$

It should be remarked here that the covariance matrices of the random errors  $-w(k-1)$  and  $-q(k)$  may be time dependent. In that case  $W$  and  $Q$  in the previous expressions are replaced respectively by the time dependent covariance matrices  $W(k-1)$  and  $Q(k)$ .

The optimal estimate of the correction  $\underline{y}(k)$  for the state perturbation is then obtained from:

$$\hat{\underline{y}}(k|k) = \hat{\underline{y}}(k|k-1) + K(k) [\underline{m}(k) - C(k) \hat{\underline{y}}(k|k-1)] \quad (3.188)$$

The corresponding covariance matrix of the errors in  $\hat{\underline{y}}(k|k)$  is computed according to:

$$P(k|k) = (I - K(k) C(k)) P(k|k-1) \quad (3.189)$$

Finally actual estimates of the system state  $\underline{y}(k)$  are obtained from:

$$\hat{\underline{y}}(k|k) = \underline{y}_{nom}(k) + \hat{\underline{y}}(k|k) \quad (3.190)$$

For actual application of the Kalman filter to flight path reconstruction from on board measurements a so called extended form of the Kalman filter is applied. The extended Kalman filter differs from the original filter in that the nominal state vector trajectory  $\underline{y}_{nom}(k)$ , is not computed entirely before mechanizing the Kalman filter algorithm.

Instead, for  $k = 1, 2, \dots$ , the nominal state vector quantity  $\underline{y}_{nom}(k)$  is computed by integration of the nonlinear state equation, see Eq. (3.40), using the previous optimal estimate  $\hat{\underline{y}}(k-1|k-1)$  as initial condition.

Hence:

$$\begin{aligned} \hat{\underline{y}}_{nom}(k) &= \hat{\underline{y}}(k|k-1) \\ &= \hat{\underline{y}}(k-1|k-1) + \int_{t_{k-1}}^{t_k} \underline{f}(\underline{y}(\tau), \underline{u}_m(k-1)) d\tau \end{aligned} \quad (3.191)$$

The observation perturbation correction is in this case computed according to:

$$\underline{m}(k) = \underline{M}_m(k) - h(\hat{\underline{y}}(k|k-1)) \quad (3.192)$$

The optimal estimate now follows from:

$$\hat{\underline{y}}(k|k) = \hat{\underline{y}}(k|k-1) + K(k) \underline{m}(k) \quad (3.193)$$

since  $\hat{\underline{y}}(k|k-1) = 0$ .

If:

$$1 > k \quad (3.194)$$

then the estimate  $\hat{\underline{y}}(1|1)$  relies on more observations than  $\hat{\underline{y}}(k|k)$ .

To compensate for this effect the so called fixed interval smoothing algorithms may be applied. Although in this text attention will be devoted only to fixed interval smoothing it should be remarked here that there exist three types of smoothing algorithms. There is fixed-point smoothing, yielding an estimate  $\hat{\underline{y}}(k|j)$ , for:

$$k \approx \text{constant} \quad (3.195)$$

and

$$j \geq k \quad (3.196)$$

The estimate  $\hat{Y}(k|k+n)$  for fixed  $n$  results from fixed lag smoothing. The term "fixed-interval smoothing" refers to the algorithm yielding  $\hat{Y}(k|n)$  where  $n$  is a fixed integer and  $k = 0, 1, 2, \dots, n$ . The initial condition of the extended fixed interval smoothing algorithm is  $\hat{Y}(n|n)$  generated by the Kalman filter. Working backward in time, this procedure corrects the estimate  $\hat{Y}(k|k)$  obtained from the Kalman filter algorithm according to:

$$\hat{Y}(k|n) = \hat{Y}(k|k) + K_S(k) [\hat{Y}(k+1|n) - \hat{Y}(k+1|k)] \quad (3.197)$$

$k = n-1, n-2, \dots, 0$ .

The gain matrix of the smoothing algorithm is given by:

$$K_S(k) = P(k|k) \Phi^T(k+1|k) P^{-1}(k+1|k) \quad (3.198)$$

The covariance matrix of the errors in  $\hat{Y}(k|n)$  is given by:

$$P(k|n) = P(k|k) + K_S(k) [P(k+1|n) - P(k+1|k)] K_S^T(k) \quad (3.199)$$

Instead of the conventional Kalman approach to discrete filtering, an square-root information filter may be applied. Although algebraically equivalent to the conventional approach, the square-root filters have improved numerical characteristics. The resulting algorithms have been compiled and elucidated in Ref. 31 and 32.

### 3.3.3. The Maximum Likelihood algorithm

Another method applicable to the flight path reconstruction problem is the so called Maximum Likelihood algorithm. If the system and observation models are linear, the Maximum Likelihood estimation theory results in an algorithm identical to the weighted least square algorithm discussed in subsection 3.3.1. The Maximum Likelihood method however differs from the estimation procedures discussed so far in that the models of the dynamic system and the output signal observations may be nonlinear. Furthermore the Maximum Likelihood algorithm when applied to a nonlinear estimation problem is to be implemented as an iterative batch processing algorithm. This implies that an estimate of the parameters of interest, obtained after processing a certain batch of measurements, may be improved by repeated application of the same algorithm to the same batch of measurements, using the previous estimate as a reference condition.

The following assumptions underly the application of the Maximum Likelihood theory:

- The system and observation models are assumed highly accurate.
- The input signal noise, i.e.  $-w(k)$  in the measurements  $U_m(k)$  is assumed negligibly small.
- The observation noise  $-q(k)$  is represented by the models for the output signal observations; the noise is assumed zero mean and Gaussian, but the variance  $Q(k)$  is assumed unknown, though it is usually assumed to be constant thus  $Q(k) = Q$ .

Application of the Maximum Likelihood algorithm to flight path reconstruction from on board measurements is directed again towards extraction of an estimate  $\hat{Y}(0|n)$  from the corrections  $\underline{m}(k)$  for the observation perturbations:

$$\underline{m}(k) = \underline{M}_m(k) - \underline{M}_{nom}(k) \quad k = 1, 2, \dots, n \quad (3.200)$$

In addition to estimation of the initial state for flight path reconstruction followed by integration of the equations of motions the Maximum Likelihood algorithm can be used to estimate the variance  $Q$  of the observation noise  $-q(k)$ .

Each iteration cycle of the Maximum Likelihood procedure comprises the following steps:

1. An estimate of the initial state  $\underline{Y}(0)$  is extracted manually or by any other means from the flight test data or else obtained as a result of the previous procedure iteration cycle.
2. An estimate of the covariance matrix  $Q$  is either extracted from instrument calibration data or else obtained as a result of the previous procedure iteration cycle. In practice the initial estimate  $Q$  is set equal to the identity matrix  $I$ .
3. Using the available estimate of the initial state  $\underline{Y}(0)$  as an initial condition the dynamic system state equations:

$$\dot{\underline{Y}}_{nom} = f(\underline{Y}_{nom}(t), \underline{U}_m(t)) \quad (3.201)$$

are numerically integrated to obtain a nominal state vector trajectory  $\underline{Y}_{nom}(k)$ ,  $k = 1, 2, \dots, n$ . Nominal observations  $\underline{M}_{nom}(k)$  are then derived from  $\underline{Y}_{nom}(k)$ :

$$\underline{M}_{nom}(k) = h(\underline{Y}_{nom}(k), \underline{U}_m(k)) \quad (3.202)$$



4. The nominal output signals  $\underline{m}_{nom}(k)$  are then compared with the measured output signals  $\underline{m}(k)$  to obtain the corrections  $\underline{m}(k)$ , see Eq. (3.200).
5. To obtain the required estimates of  $\underline{y}(0)$  and the covariance matrix  $Q$ , an attempt is made to find the values  $\hat{\underline{y}}(0|k)$  and  $\hat{Q}$  maximizing the magnitude of the conditional probability density function:

$$p(\underline{m}(1), \underline{m}(2), \dots, \underline{m}(n) | \underline{y}(0), Q) \quad (3.203)$$

To obtain a maximum of the conditional probability density function given, it is required to formulate the sensitivity of  $\underline{m}(k)$ ,  $k = 1, 2, \dots, n$ , to variations in  $\underline{y}(0|k)$ . Since  $\underline{m}_{nom}(k)$  is the only contribution to  $\underline{m}(k)$  depending on  $\underline{y}_{nom}(0)$ , it is required to formulate the sensitivity of  $\underline{m}_{nom}(k)$  for the variations in  $\underline{y}_{nom}(0)$ .

Using Eq. (3.202) the following sensitivity relations are found:

$$\begin{aligned} \underline{m}_{nom}(\underline{y}_{nom}(0) + \underline{y}(0), \underline{u}_m, t) &= \underline{m}_{nom}(\underline{y}_{nom}(0), \underline{u}_m, t) + \left( \frac{\partial \underline{m}(\underline{y}(0), t)}{\partial \underline{y}(0)} \right)_{\underline{y}_{nom}, \underline{u}'_{nom}} \underline{y}(0) \\ \underline{m}_{nom}(\underline{y}_{nom}(0) + \underline{y}(0), \underline{u}_m, t) - \underline{m}_{nom}(\underline{y}_{nom}(0), \underline{u}_m, t) &= \\ &= \left( \frac{\partial \underline{h}}{\partial \underline{y}} \right)_{\underline{y}_{nom}, \underline{u}'_{nom}} \left( \frac{\partial \underline{y}}{\partial \underline{y}(0)} \right)_{\underline{y}_{nom}, \underline{u}'_{nom}} \underline{y}(0) \\ &= C(t) \left( \frac{\partial \underline{y}}{\partial \underline{y}(0)} \right)_{\underline{y}_{nom}, \underline{u}'_{nom}} \underline{y}(0) \\ &\triangleq C(t) S(t) \underline{y}(0) \end{aligned} \quad (3.204)$$

The elements of the matrix product  $C(t) S(t)$  are referred to as the sensitivity coefficients. The elements of the matrix  $S(t)$  can be found formulating and solving a differential propagation equation for  $S(t)$  with respect to time. This differential equation may be derived as follows:

$$\begin{aligned} \frac{d}{dt} (S(t)) &= \frac{d}{dt} \left( \frac{\partial \underline{y}}{\partial \underline{y}(0)} \right)_{\underline{y}_{nom}, \underline{u}'_{nom}} = \left( \frac{\partial}{\partial \underline{y}(0)} \frac{d\underline{y}}{dt} \right)_{\underline{y}_{nom}, \underline{u}'_{nom}} \\ &= \left( \frac{\partial}{\partial \underline{y}(0)} f(\underline{y}, \underline{u}, t) \right)_{\underline{y}_{nom}, \underline{u}'_{nom}} \\ &= \left( \frac{\partial f(\underline{y}, \underline{u}, t)}{\partial \underline{y}} \frac{\partial \underline{y}}{\partial \underline{y}(0)} \right)_{\underline{y}_{nom}, \underline{u}'_{nom}} \\ &= \left( \frac{\partial f(\underline{y}, \underline{u}, t)}{\partial \underline{y}} \right)_{\underline{y}_{nom}, \underline{u}'_{nom}} S(t) \end{aligned} \quad (3.205)$$

This may be written as:

$$\dot{S}(t) = A(t) S(t) \quad (3.206)$$

in which  $A(t)$  is identical to the matrix of derivatives as defined in (3.49) and (3.52).

The required solution  $S(t)$  and henceforth the sensitivity coefficients, elements of  $C(t) S(t)$  can be computed solving this propagation equation. It should be realized that the initial condition:

$$S(0) = \left( \frac{\partial \underline{y}}{\partial \underline{y}(0)} \right)_{\underline{y}_{nom}(0), \underline{u}'_{nom}(0)} = I \quad (3.207)$$

The estimation procedure is now initialized, specifying an initial estimate  $\underline{y}_{nom}(0)$  and  $Q$ . The likelihood function of the measurements is defined as:

$$L(\underline{y}_{nom}(0), Q) \triangleq p(\underline{m}(1), \underline{m}(2), \dots, \underline{m}(n) | \underline{y}_{nom}(0), Q) \quad (3.208)$$

From (3.200) and (3.204) it follows that  $\underline{m}(k)$  depends only on  $\underline{y}_{nom}(0)$  and on  $\underline{q}(k)$ . Because  $\underline{q}(k)$  is an independent process, (3.208) may be written as a product of conditional densities according to:

$$\begin{aligned}
 L(\underline{y}_{\text{nom}}(0), Q) &= \prod_{k=1}^n p(\underline{m}(k) | \underline{y}_{\text{nom}}(0), Q) = \\
 &= \frac{1}{(2\pi |Q|)^{n/2}} \exp \left[ -\frac{1}{2} \sum_{k=1}^n (\underline{m}^T(k) Q^{-1} \underline{m}(k)) \right]
 \end{aligned} \quad (3.209)$$

because  $\underline{q}(k)$  is gaussian.

To obtain the required Maximum Likelihood estimates of  $\underline{y}(0)$  and  $Q$ ,  $L(\underline{y}_{\text{nom}}(0), Q)$  should be maximized. Maximizing  $L(\underline{y}_{\text{nom}}(0), Q)$  is equivalent to maximizing  $\ln(L(\underline{y}_{\text{nom}}(0), Q))$ :

$$\ln(L(\underline{y}_{\text{nom}}(0), Q)) = -\frac{1}{2} \sum_{k=1}^n \underline{m}^T(k) Q^{-1} \underline{m}(k) - \frac{n}{2} \ln |Q| + C \quad (3.210)$$

According to ref. 5, maximization of  $L(\underline{y}_{\text{nom}}(0), Q)$  with respect to  $\underline{y}_{\text{nom}}(0)$  and  $Q$  is replaced by maximization of  $L(\underline{y}_{\text{nom}}(0) + \underline{y}(0), Q)$  with respect to  $\underline{y}(0)$  and  $Q$ . With  $\underline{y}(0)$ , an improved estimate of  $\underline{m}(k)$ , denoted by  $\underline{m}_1(k)$  follows directly from (3.200) and (3.205):

$$\underline{m}_1(k) \triangleq \underline{m}(k) - \underline{m}_{\text{nom}}(\underline{y}_{\text{nom}}(0) + \underline{y}(0), k) \quad (3.211)$$

$$\underline{m}_1(k) = \underline{m}(k) - C(k) S(k) \underline{y}(0)$$

Substitution of  $\underline{m}_1(k)$  in Eq. (3.210) yields:

$$\begin{aligned}
 \ln L(\underline{y}_{\text{nom}}(0) + \underline{y}(0), Q) &= -\frac{1}{2} \sum_{k=1}^n [\underline{m}(k) - C(k) S(k) \underline{y}(0)]^T Q^{-1} \\
 &\quad [\underline{m}(k) - C(k) S(k) \underline{y}(0)] - \frac{n}{2} \ln |Q| + C
 \end{aligned} \quad (3.212)$$

To obtain the estimates  $\hat{\underline{y}}(0|n)$  and  $\hat{Q}$  the following equations are set equal to zero:

$$\left( \frac{\partial \ln L(\underline{y}_{\text{nom}}(0) + \underline{y}(0), Q)}{\partial \underline{y}(0)} \right)_{\hat{\underline{y}}(0), \hat{Q}} = 0 \quad (3.213)$$

and:

$$\left( \frac{\partial \ln L(\underline{y}_{\text{nom}}(0) + \underline{y}(0), Q)}{\partial Q} \right)_{\hat{\underline{y}}(0), \hat{Q}} = 0 \quad (3.214)$$

Using Eq. (3.212) the following results are obtained:

$$\hat{\underline{y}}(0|n) = \left\{ \sum_{k=1}^n \left[ S^T(k) C^T(k) Q^{-1} C(k) S(k) \right] \right\}^{-1} \left\{ \sum_{k=1}^n \left[ C(k) S(k) Q^{-1} \underline{m}(k) \right] \right\} \quad (3.215)$$

$$\hat{Q} = \frac{1}{n} \sum_{k=1}^n \left[ \underline{m}(k) - C(k) S(k) \underline{y}(0) \right] \left[ \underline{m}(k) - C(k) S(k) \underline{y}(0) \right]^T \quad (3.216)$$

The estimated correction  $\hat{\underline{y}}(0|n)$  is used to obtain the Maximum Likelihood estimate:

$$\underline{\hat{y}}(0|n) = \underline{y}_{\text{nom}}(0) + \hat{\underline{y}}(0|n) \quad (3.217)$$

Now the performance index  $J_n$  is computed:

$$J_n = |\hat{Q}|$$

If the difference between two consecutive magnitudes of  $J_n$  is greater than a prespecified magnitude  $\epsilon$ , the estimate  $\underline{\hat{y}}(0|n)$  is used to initiate the next iteration cycle.

The covariance matrix  $P(0|n)$  of the errors in the estimate  $\underline{\hat{y}}(0|n)$  is defined as:

$$P(0|n) \triangleq E \left\{ \left[ \underline{\hat{y}}(0|n) - E(\underline{\hat{y}}(0|n)) \right] \left[ \underline{\hat{y}}(0|n) - E(\underline{\hat{y}}(0|n)) \right]^T \right\} \quad (3.218)$$

The following remarks can be made concerning various properties of the Maximum Likelihood estimation results:

1. Under certain general conditions, Maximum Likelihood estimates are consistent and asymptotically efficient. This implies that the accuracy of  $\hat{Y}(0|n)$  will approach the maximally accuracy achievable if the number of measurements increases:

$$P(0|n) = F^{-1} \quad (3.219)$$

$n \rightarrow \infty$

The matrix  $F^{-1}$  is a lower bound of the covariance matrix  $P(0|n)$  and is called the Cramér-Rao lower bound. The matrix  $F$  denotes the so-called Fisher information matrix defined as:

$$F \triangleq E \left\{ \left[ \frac{\partial \ln L(\underline{Y}_{nom}(0) + \underline{Y}(0), \underline{Q})}{\partial \underline{Y}(0)} \right]_{\underline{\hat{Y}}(0), \underline{\hat{Q}}} \left[ \frac{\partial \ln L(\underline{Y}_{nom}(0) + \underline{Y}(0), \underline{Q})}{\partial \underline{Y}(0)} \right]^T_{\underline{\hat{Y}}(0), \underline{\hat{Q}}} \right\} \quad (3.220)$$

An approximation to this information matrix can be calculated according to:

$$F = \sum_{k=1}^n S^T(k) C^T(k) \bar{Q}^{-1} C(k) S(k) \quad (3.221)$$

This matrix also appears in Eq. (3.216). Usually the information matrix is calculated by substituting the best estimates of  $\bar{Q}$  and  $S(k)$ , for all  $k$ , in Eq. (3.221) after the iteration scheme for  $\hat{Y}(0|n)$  has converged.

2. In practice  $P(0|n)$  is usually approximated by setting:

$$P(0|n) = F^{-1} \quad (3.222)$$

even if  $n < \infty$ . With  $P(0|n)$  it is simple to approximate the covariance matrix of  $\hat{Y}(k|n)$ , indicated by  $P(k|n)$  according to:

$$P(k|n) = S(k) P(0|n) S^T(k) \quad (3.223)$$

3. In cases where the information matrix, as defined in Eq. (3.221), is ill-conditioned numerical difficulties may arise in the matrix inversion, required for computation of  $P(0|n)$ . If the information matrix  $F$  is singular, one or more components of  $\underline{Y}(0)$  can not be estimated from the available measurements and subsequent elimination is then demanded. If the matrix  $F$  is ill-conditioned but still invertible, then the iterative estimation scheme may diverge. This difficulty may be circumvented by resorting to alternative optimization algorithms or by modifying the information matrix, eliminating the smallest eigenvalues and corresponding eigenvectors. Numerical details of Maximum Likelihood estimates have been discussed in Ref. 16.
4. The iteration scheme presented above is in the literature also referred to as the quasi-linearization method or modified Newton-Raphson. In the literature on aircraft dynamic response analysis, the algorithm is frequently applied to the problem of estimating the stability derivatives and initial conditions of the linearized equations of motion. From the discussion above it follows that the algorithm may equally well be applied to the flight path reconstruction problem, refs. 17, 21.
5. In case where the process noise can not be neglected it is still possible to derive an expression for the likelihood function and the corresponding Maximum Likelihood estimates. However, the resulting optimization problem becomes very difficult to solve. Analytical and numerical details are discussed in Ref. 33.

Summarizing, various estimation procedures, applicable to the flight path reconstruction problem, have been shown.

Comparing Eqs. (3.171), (3.174) and (3.215), a considerable similarity should be observed between the corresponding expressions used for computation of the required estimates. In fact all expressions given can be considered as weighted least squares estimates with different weighting matrices. Except for the Kalman filter - Kalman smoothing method, all flight path reconstruction procedures presented are based on the assumption that the system input noise, i.e. the random errors in the inertial measurements are negligibly small. This assumption obviously only holds if accelerometers and rate gyroscopes of high quality are used for measurement of the specific aerodynamic forces and angular rotation rates.

#### 4. AERODYNAMIC MODEL IDENTIFICATION

##### 4.0. Introduction

The mathematical model for the aircraft's aerodynamics includes a set of polynomials, relating aerodynamic forces and moments acting upon the aircraft to its state variables and control inputs. Aerodynamic model

identification is the process of searching for the structure of these polynomials and of extracting numerical values for the aerodynamic derivatives, appearing as parameters in these polynomials, from recorded time histories of the control inputs and the resulting aircraft responses.

The identification process is based on the assumption that the dimensionless coefficients  $C_{X_B}$ ,  $C_{Y_B}$ ,  $C_{Z_B}$ ,  $C_{L_B}$ ,  $C_{m_B}$  and  $C_{n_B}$  are relatively simple functions of the time histories of such quantities as the angle of attack  $\alpha$ , the angle of sideslip  $\beta$ , the angular rates  $p_B$ ,  $q_B$  and  $r_B$  and the control surface deflections  $\delta_a$ ,  $\delta_e$  and  $\delta_r$ . Obviously, when formulating the aerodynamic model relations, the aerodynamic forces and moments should be specified relative to any suitable frame of reference such as the body frame  $F_B$  or the air trajectory reference frame  $F_W$ .

Modelling the aircraft's aerodynamics is most significant to prediction of its behaviour in terms of responses to control inputs as well as in terms of aircraft performance, stability and control characteristics. The complexity of an aerodynamic model depends on the class and type of aircraft under consideration, on the section of its flight envelope and response frequency ranges to be covered. In fact the model complexity is somewhat arbitrary, as the model structure depends not only on these aspects but also on the accuracy required and the purpose of the model. In the literature several aerodynamic model equations have been formulated and motivated. A systematic introduction to aerodynamic models is given in Ref. 1. Alternatives for the mathematical description of aerodynamic models are discussed in Ref. 24.

Given the time histories of all the model variables mentioned above model complexity is in practice limited by the identifiability of the model parameters. Here, with identifiability is meant whether or not and to what extent numerical values for the model parameters can be extracted from the available flight test data.

When setting out for aerodynamic model identification it should be realized that first of all pre-specified model structures are to be validated and secondly, the magnitudes of the parameters occurring in the model structure are to be estimated. The estimation results obtained in terms of the parameter estimates and the estimation error covariance matrices, model fit, residual statistics and correlation coefficients may be exploited for evaluation of a given set of prespecified model structures.

Different approaches towards model identification from test data are possible:

1. A rather simple model structure can be specified, followed by parameter estimation from a subset of the available flight test data belonging to a rather limited part of the aircraft's flight envelope. Subsequently, by processing several test data subsets, variations in the resulting parameter estimates guide the flight test engineer in specifying different or more complex model structures representing larger subsets of aircraft response data. Cues for model extensions for improved model fit may be deduced from a careful analysis of the residuals of a particular model and flight test data subset.
2. Alternatively, a fairly general and therefore rather complex model structure may be defined at the outset. When trying to estimate the parameters of such a model from the available test data, the flight test engineer may find several parameter or linear parameter combinations to be unidentifiable. This implies that one or more of the parameters cannot be estimated from the available flight test data. The model has to be simplified by elimination of the parameters involved.

In this Section some aspects of aerodynamic model identification are discussed in more detail. In Section 5.1. it is shown that the aerodynamic model parameter estimation problem can be formulated as a linear parameter estimation problem when use is made of the results of the flight path reconstruction. Some general principles of linear least squares estimation are introduced. The notions of identifiability and bias due to model simplifications are discussed and some aspects of residual analysis are presented. Numerical techniques are discussed in Section 5.2. It is shown that loss of numerical accuracy while calculating the well known  $X^T X$  matrix can be circumvented. The principles of Householder transformations are introduced.

#### 4.1. Regression analysis

##### 4.1.0. Introduction

Regression analysis may be applied to estimate parameters of the class of mathematical models which are linear with respect to the parameters to be estimated. The structure of those models is given by:

$$y = a_0 x_0 + a_1 x_1 + \dots + a_r x_r \quad (4.1)$$

Aerodynamic models usually have an identical structure. As an example may serve the aerodynamic model of the lift coefficient of a high subsonic aircraft as presented in Ref. 19:

$$C_L = C_{L0} + C_{L\alpha} \alpha + C_{L\alpha M} \alpha M + C_{L\alpha M^2} \alpha M^2 \quad (4.2)$$

In (4.1),  $x_0, x_1, \dots, x_r$  are the independent variables. The parameters  $a_0, a_1, \dots, a_r$  are estimated from  $n$  sets of values of the independent variables and the dependent variable  $y$ . Clearly, the estimation of the aerodynamic derivatives  $C_{L0}, C_{L\alpha}, C_{L\alpha M}$  and  $C_{L\alpha M^2}$  in (4.2) constitutes an identical problem. In general, aerodynamic model identification is preceded by the reconstruction of the aircraft's flight path as described in the previous Section. As a result of flight path reconstruction, accurate time histories of the angle of attack  $\alpha$  and airspeed  $V$  are calculated. Obviously, also time histories of  $\alpha M$  and  $\alpha M^2$  may then be obtained while the lift coefficient  $C_L$  would follow from:

$$C_L = \frac{m}{4\rho V^2 S} (A_{x_B} \sin \alpha - A_{z_B} \cos \alpha) - \frac{T_{G_T}}{4\rho V^2 S} \sin(\alpha + i_p) \quad (4.3)$$

where the last term in (4.3) accounts for the effect of engine gross thrust. Thus at  $n$  discrete instants of time,  $n$  sets of values of the dependent and independent variables in (4.2) may be deduced from the accelerometer measurements  $A_{x_B}$  and  $A_{z_B}$  and the results of the flight path reconstruction. In (4.3),  $A_{x_B}$  and  $A_{z_B}$  will have been corrected for the estimated zero shifts  $\lambda_x$  and  $\lambda_z$ , Eq. (3. ).

Mathematical models structurally identical to the model of Eq. (4.1) may be developed for  $C_{x_B}$ ,  $C_{z_B}$ ,  $C_{y_B}$ ,  $C_{l_B}$ ,  $C_{m_B}$  and  $C_{n_B}$ . One other example is presented in Section 6. The remaining part of this Section is devoted to basic principles, practical aspects and numerical techniques of regression analysis.

#### 4.1.1. Basic principles

In regression analysis the following problem is posed. Estimate the parameters  $a_0, a_1, \dots, a_r$  of the linear model:

$$y(i) = a_0 x_0(i) + a_1 x_1(i) + \dots + a_r x_r(i) + \varepsilon(i) \quad (4.4)$$

when  $N$  sets of values are given of the independent variables  $x_0(i), x_1(i), \dots, x_r(i)$  and the dependent variables  $y(i)$ , while  $\varepsilon(i)$  is unknown.

In Eq. (4.4)  $\varepsilon(i)$  results from model or measurement errors.  $\varepsilon(i)$  is usually assumed to be adequately represented by an independent random sequence with:

$$\begin{aligned} E\{\varepsilon(i)\} &= 0 \\ E\{\varepsilon(i) \varepsilon(j)\} &= \sigma^2 \delta_{ij} \\ i &= 1, \dots, n \end{aligned}$$

Eq. (4.4) can be written more compactly by defining the row vector  $\underline{x}(i) = [x_0(i), x_1(i), \dots, x_r(i)]$  and the column vector  $[a_0, a_1, \dots, a_r]$ :

$$\begin{aligned} y(i) &= \underline{x}(i) \underline{a} + \varepsilon(i) \\ i &= 1, \dots, n \end{aligned} \quad (4.5)$$

In regression analysis it will be convenient to manipulate with all  $n$  equations (4.5) simultaneously. To achieve this the  $n$  dimensional column vectors  $\underline{y}$  and  $\underline{\varepsilon}$  are defined as  $\underline{y} = \text{col}[y(1), y(2), \dots, y(n)]$  and  $\underline{\varepsilon} = \text{col}[\varepsilon(1), \varepsilon(2), \dots, \varepsilon(n)]$ . Furthermore the  $n \times r$  matrix  $X$  is defined as:

$$X = \begin{bmatrix} \underline{x}(1) \\ \underline{x}(2) \\ \vdots \\ \underline{x}(n) \end{bmatrix}$$

after which Eq. (4.5) can be written as:

$$\underline{y} = X \underline{a} + \underline{\varepsilon} \quad (4.6)$$

When  $\hat{\underline{a}}$  is an estimate of the parameter vector  $\underline{a}$  the residual  $e(i)$  is defined as  $e(i) = y(i) - \underline{x}(i) \hat{\underline{a}}$ . Defining the  $n$  dimensional column vector  $\underline{e}$  in the usual way by  $\underline{e} = \text{col}[e(1), e(2), \dots, e(n)]$  the sum of the squares of the residuals can be written as:

$$\underline{e}^T \underline{e} = (\underline{y} - X \hat{\underline{a}})^T (\underline{y} - X \hat{\underline{a}}) \quad (4.7)$$

The least squares estimate of  $\underline{a}$  is obtained by minimizing Eq. (4.7) with respect to  $\hat{\underline{a}}$ . A necessary condition for  $\hat{\underline{a}}$  to minimize Eq. (4.7) is:

$$\frac{\partial \underline{e}^T \underline{e}}{\partial \hat{\underline{a}}} = 0 \quad (4.8)$$

Substitution of Eq. (4.7) in Eq. (4.8) leads directly to the so-called normal equations:

$$[X^T X] \hat{a} = X^T Y \quad (4.9)$$

When the matrix  $[X^T X]$  is positive definite (i.e. its inverse exists) the least squares estimate of  $\underline{a}$  follows from:

$$\hat{a} = [X^T X]^{-1} X^T Y \quad (4.10)$$

Besides the numerical value an important characteristic of the least squares estimate constitutes the accuracy of  $\hat{a}$  which is expressed by:

$$\Delta \underline{a} = \hat{a} - E(\hat{a}) \quad (4.11)$$

$E(\hat{a})$  can be calculated by substituting Eq. (4.6) into Eq. (4.10) which then yields:

$$E(\hat{a}) = E \left\{ [X^T X]^{-1} X^T X \underline{a} + [X^T X]^{-1} X^T \underline{\epsilon} \right\} = \underline{a} \quad (4.12)$$

because  $E(\underline{\epsilon}) = 0$  and  $X$  is deterministic. This means that  $\hat{a}$  is a so-called unbiased estimate of  $\underline{a}$ .

The covariance matrix of the estimate errors  $\Delta \underline{a}$  may now be written as:

$$\begin{aligned} V(\hat{a}) &= E \left\{ \Delta \underline{a} \Delta \underline{a}^T \right\} = E \left\{ [\hat{a} - E(\hat{a})] [\hat{a} - E(\hat{a})]^T \right\} = \\ &= E \left\{ [\hat{a} - \underline{a}] [\hat{a} - \underline{a}]^T \right\} \end{aligned} \quad (4.13)$$

Substitution of Eq. (4.10) then results in:

$$V(\hat{a}) = \sigma^2 [X^T X]^{-1} \quad (4.14)$$

From Eq. (4.14) the matrix of simple estimation error correlation coefficients may be obtained from:

$$[\rho_{ij}] = \frac{v_{ij}}{\sqrt{v_{ii} v_{jj}}}$$

In many applications  $\sigma^2$  is not precisely known. This will be the case in particular when  $\epsilon(i)$  must be attributed to model errors rather than measurement errors of  $y(i)$ .

Then  $\sigma^2$  may be estimated by:

$$\hat{\sigma}^2 = \frac{1}{n - r - 1} \underline{e}^T \underline{e} \quad (4.15)$$

which can be calculated posterior to the calculation of  $\hat{a}$ .

The goodness of fit of the mathematical model to the measurements is expressed by the so-called total correlation coefficient  $R_t$  defined as:

$$R_t = \left\{ 1 - \frac{\underline{e}^T \underline{e}}{\underline{Y}^T \underline{Y}} \right\}^{1/2} \quad 0 \leq R_t \leq 1$$

In case of perfect fit  $\underline{e}^T \underline{e} = 0$  and thus  $R_t = 1$ . When the model Eq. (4.6) is completely invalid the parameter estimate will be identical zero:

$$\hat{a} = 0$$

because of:

$$X^T Y = 0$$

Then it follows that  $\underline{e} = Y$  and  $R_t$  reaches its minimum value of zero.

Eqs. (4.10), (4.14) and (4.15) are well known results in regression analysis.

#### 4.1.2. Model simplifications and identifiability

In flight testing problems, when accurate instrumentation systems are exploited measurement errors can be relatively small. It is therefore important to further evaluate the effect of modelling errors on the accuracy and the numerical value of the least square estimate  $\hat{\underline{a}}$ .

Assume the actual model to be:

$$\underline{y} = \underline{x}_1 \underline{a}_1 + \underline{x}_2 \underline{a}_2 + \underline{\epsilon} \quad (4.16)$$

in which  $\underline{a}_1$  and  $\underline{a}_2$  are  $r$  and  $s$  dimensional vectors of parameters.

A least squares estimate of  $\underline{a}_1$  is made by using a simplified model:

$$\underline{y} = \underline{x}_1 \underline{a}_1 \quad (4.17)$$

Minimization of  $\underline{\epsilon}_1^T \underline{\epsilon}_1$  with  $\underline{\epsilon}_1 = \underline{y} - \underline{x}_1 \hat{\underline{a}}_1$  leads via the necessary conditions to the set of normal equations:

$$[\underline{x}_1^T \underline{x}_1] \hat{\underline{a}}_1 = \underline{x}_1^T \underline{y} \quad (4.18)$$

and the estimate of  $\underline{a}_1$ :

$$\hat{\underline{a}}_1 = [\underline{x}_1^T \underline{x}_1]^{-1} \underline{x}_1^T \underline{y} \quad (4.19)$$

when  $[\underline{x}_1^T \underline{x}_1]$  is positive definite.

From:

$$\begin{aligned} E(\hat{\underline{a}}_1) &= [\underline{x}_1^T \underline{x}_1]^{-1} \underline{x}_1^T E(\underline{y}) = [\underline{x}_1^T \underline{x}_1]^{-1} \underline{x}_1^T [\underline{x}_1 \underline{a}_1 + \underline{x}_2 \underline{a}_2] = \\ &= \underline{a}_1 + [\underline{x}_1^T \underline{x}_1]^{-1} [\underline{x}_1^T \underline{x}_2] \underline{a}_2 \end{aligned} \quad (4.20)$$

follows that now  $\hat{\underline{a}}_1$  will in general be a biased estimate of  $\underline{a}_1$ .  
The estimate variance of the residuals may now be obtained from:

$$\hat{\sigma}_1^2 = \frac{1}{n - r - 1} \underline{\epsilon}_1^T \underline{\epsilon}_1 \quad (4.21)$$

In practical applications a major problem is the selection of the "optimum" number of parameters in the mathematical model. In general a trade-off must be made between reduced estimation accuracies after an additional parameter is added and a better fit of the model to the measurements. This may be clarified as follows.

The matrix  $\underline{X}_2$  can always be written as:

$$\underline{X}_2 = \underline{X}_1 \underline{C} + \Delta \underline{X}_2 \quad (4.22)$$

in which  $\underline{C}$  denotes a constant  $r \times s$  matrix. It follows from Eq. (4.22) that each column of the matrix  $\underline{X}_2$  may be composed out of a linear combination of the columns of the matrix  $\underline{X}_1$  and one column of the matrix  $\Delta \underline{X}_2$ . The geometrical interpretation of this composition becomes clear when interpreting every column of  $\underline{X}_2$  as a vector in  $n$ -dimensional Euclidean space. This vector can be decomposed into two components perpendicular to and in the  $r$ -dimensional subspace of the columns of  $\underline{X}_1$ .

1. When  $\Delta \underline{X}_2$  is very small, i.e. the columns of  $\underline{X}_2$  depend linearly on the columns of  $\underline{X}_1$ , the estimate of the parameter  $\underline{a}_1$  using the simplified model will be biased according to:

$$E(\hat{\underline{a}}_1) = \underline{a}_1 + \underline{C} \underline{a}_2 \quad (4.23)$$

When attempting however to eliminate this bias by adding the parameters  $\underline{a}_2$  to the model it can be shown that:

- a)  $\hat{\sigma}_1^2 = \hat{\sigma}^2$ , the variance of the residuals has not been decreased,
  - b) parameter estimation errors tend to infinity due to singularity of the matrix  $\underline{X}^T \underline{X}$ , one or more simple correlation coefficients in the estimation error correlation matrix will approach 1.
2. In case all elements of  $\underline{C}$  are identical zero ( $\underline{X}_2 = \Delta \underline{X}_2$ ), the estimate of the parameter  $\underline{a}_1$  using the simplified model will be unbiased because of:

$$x_1^T \Delta x_2 = 0$$

(4.24)

When adding now the parameters  $a_2$  to the model it follows that:

- a)  $\hat{\sigma}_1^2$  decreases to  $\hat{\sigma}^2$ ,
- b) parameter estimation errors of  $a_1$  will remain unchanged.

It may be deduced that in case 1 extra parameters should not, while in case 2 extra parameters may be added to the model.

The notion of identifiability is now introduced. A parameter vector  $a$  is called identifiable when the rank of the corresponding  $X^T X$  matrix is equal to the dimension of  $a$ . This means that the matrix  $X^T X$  can in principle be inverted and thus all elements of  $a$  be estimated. In many instances the rank of  $X^T X$  is equal to the dimension of  $a$  but the matrix  $X^T X$  is ill-conditioned. In practice, the condition of the matrix  $X^T X$  is degraded even further due to the effect of finite word length in digital computing. In Subsection 4.2. it is shown that a least squares estimate of  $a$  can be calculated without actually calculating the matrix  $X^T X$  of the normal equations.

When the matrix  $X^T X$  is nonsingular and can be inverted, all diagonal elements of the variance matrix of the parameter estimation errors remain finite. In case of an ill conditioned matrix  $X^T X$  (indicating an over-parameterization for the given data set) some or all diagonal elements of the variance matrix will be large and some or all non-diagonal elements of the corresponding matrix of simple correlation coefficients will be very close to + or - unity.

#### 4.1.3. Residual analysis

More often than not an aerodynamic model structure is adapted to the available measurements in the sense that non-identifiable parameters or parameter sets will be eliminated and on the other hand, an effort will be made to increase the fit of the model. Improving the fit of the model implies a reduction of  $\underline{e}^T \underline{e}$ , the sum of the squares of the residuals.

From the previous subsection it follows that when an additional variable is added to the existing model, this variable may be decomposed into two orthogonal components as follows:

$$\underline{x}_2 = X_1 \underline{C} + \Delta \underline{x}_2$$

The matrix  $X_2$  defined in the preceding subsection reduces here to a vector  $\underline{x}_2$  because the effect of adding one single variable is studied in this subsection. The matrix  $C$  reduces correspondingly to a  $r$  dimensional row vector.

In many cases the aerodynamic model is extended to include additional terms because of the fit of the model is unsatisfactory. This means that the variance of the residuals is large compared to what might be expected on the basis of the accuracy of the instrumentation system. Terms which are added to the model are usually based on physical considerations. For example, an extra term  $C_{mq2} \alpha^2$  might be added because windtunnel experiments clearly exhibit a nonlinear  $C_m$  versus  $\alpha$  relation.

As has been argued in the preceding subsection only the orthogonal component  $\Delta \underline{x}_2$  may contribute to a reduction of the residuals. When therefore an additional variable  $\underline{x}_2$  is added to the model it may as well be replaced by its orthogonal component  $\Delta \underline{x}_2$ .

The vector  $\underline{C}$  can be calculated from  $\underline{x}_2$  and  $X_1$  by interpreting  $\underline{x}_2$  as the measurements of the dependent variable and  $X_1$  the matrix of independent variables of a regression model. Then it follows directly that:

$$\underline{C} = [X_1^T X_1]^{-1} X_1^T \underline{x}_2 \quad (4.25)$$

The orthogonal component of  $\underline{x}_2$  then follows directly according to:

$$\Delta \underline{x}_2 = \underline{x}_2 - X_1 \underline{C} = \underline{x}_2 - X_1 [X_1^T X_1]^{-1} X_1^T \underline{x}_2 \quad (4.26)$$

It is easily proved that  $\Delta \underline{x}_2$  is orthogonal to  $X_1$ :

$$X_1^T \Delta \underline{x}_2 = X_1^T \underline{x}_2 - X_1^T X_1 [X_1^T X_1]^{-1} X_1^T \underline{x}_2 = X_1^T \underline{x}_2 - X_1^T \underline{x}_2 = 0$$

The new matrix of independent variables is partitioned according to:

$$X = [X_1 \mid \Delta \underline{x}_2]$$

and the corresponding parameter vector can be written as:



$$\underline{a} = \text{col} [\underline{a}_1^T, \underline{a}^{\#}]$$

The least squares estimate of  $\underline{a}$  is:

$$\begin{aligned} \hat{\underline{a}} &= \begin{bmatrix} \hat{\underline{a}}_1 \\ \hat{\underline{a}}^{\#} \end{bmatrix} = [X^T X]^{-1} X^T \underline{y} = \\ &= \begin{bmatrix} X_1^T X_1 & X_1^T \Delta x_2 \\ \Delta x_2^T X_1 & \Delta x_2^T \Delta x_2 \end{bmatrix}^{-1} \begin{bmatrix} X_1^T \\ \Delta x_2^T \end{bmatrix} \underline{y} \end{aligned} \quad (4.27)$$

Because  $\Delta x_2$  is orthogonal to the column space of  $X_1$  it follows that:

$$\begin{aligned} \begin{bmatrix} \hat{\underline{a}}_1 \\ \hat{\underline{a}}^{\#} \end{bmatrix} &= \begin{bmatrix} X_1^T X_1 & 0 \\ 0 & \Delta x_2^T \Delta x_2 \end{bmatrix}^{-1} \begin{bmatrix} X_1^T \\ \Delta x_2^T \end{bmatrix} \underline{y} = \\ &= \begin{bmatrix} [X_1^T X_1]^{-1} X_1^T \underline{y} \\ (\Delta x_2^T \Delta x_2)^{-1} \Delta x_2^T \underline{y} \end{bmatrix} \end{aligned} \quad (4.28)$$

Thus  $\hat{\underline{a}}^{\#}$  is independent of  $\hat{\underline{a}}_1$ . An attractive property which follows from the orthogonality of  $\Delta x_2$  is that  $\hat{\underline{a}}^{\#}$  can also be calculated from the residuals  $\underline{e}$  corresponding to the original model.

When  $\underline{e}$  is interpreted as the measurements of the dependent variable and  $\Delta x_2$  the vector of independent variables the regression model becomes:

$$\underline{e} = \Delta x_2 \underline{a}^{\#} + \underline{e}_2 \quad (4.29)$$

The least squares estimate can then be written as:

$$\hat{\underline{a}}^{\#} = (\Delta x_2^T \Delta x_2)^{-1} \Delta x_2^T \underline{e}$$

Because of  $\underline{e} = \underline{y} - X_1 \hat{\underline{a}}_1$  and the orthogonality of  $\Delta x_2$  to the column space of  $X_1$  the resulting estimate is identical to the result obtained when  $\hat{\underline{a}}^{\#}$  is determined simultaneously to  $\hat{\underline{a}}_1$ .

This leads to a stepwise regression procedure in which the model fit is sequentially improved by regressing additional orthogonal variables to the residuals of the previous model.

#### 4.2. Advanced numerical methods for the solution of the normal equations

##### 4.2.0. Introduction

In those cases where the matrix  $X^T X$  of the normal equations, Eq. (4.9) is ill-conditioned, its condition will usually even further degrade when actually computing its numerical value due to the finite word length in digital computing.

In the following subsections it is shown that the original problem of finding the least squares (LS) or minimum length solution of:

$$X \underline{a} + \underline{\varepsilon} = \underline{y} \quad (4.30)$$

in which  $X$  denotes a  $n \times r$  matrix and  $\underline{y}$  a  $n$  dimensional column vector, can be transformed into the problem of solving the following set of linear equations:

$$X^T \underline{a} = \underline{y}^T \quad (4.31)$$

in which  $X^T$  denotes a  $n \times r$  matrix and  $\underline{y}^T$  a  $n$  dimensional vector. Because the matrix  $X^T$  is constructed to be upper triangular, the solution of  $\underline{a}$  does not require inversion of the matrix  $X^T$ . The last element of  $\underline{a}$

is calculated from:

$$x_{rr}^r a_r = y_r^r \quad (4.32)$$

in which  $x_{rr}^r$  denotes the  $r, r$  th element of  $X^r$  and  $a_r, y_r^r$  the  $r$  th elements of  $\underline{a}$  and  $\underline{y}^r$ . Subsequently, by substituting  $a_r = y_r^r / x_{rr}^r$  in:

$$x_{r-1, r-1}^r a_{r-1} + x_{r-1, r}^r a_r = y_{r-1}^r \quad (4.33)$$

the element  $a_{r-1}$  can be calculated in the second step.

Continuing in this way, all elements of  $\underline{a}$  can be calculated in  $r$  steps. In the following subsections the subject is the transformation of the matrix  $X$  into the matrix  $X^r$ . In 4.2.1. the invariance of the least squares solution  $\underline{a}$  of Eq. (4.39) under orthogonal transformations is discussed. Householder transformations are defined in 4.2.2. Recursive estimation via Givens rotations is mentioned in 4.2.3. Finally the implementation of a priori knowledge is the subject of 4.2.4. In the following Eq. (4.30) is written as:

$$X \underline{a} \approx \underline{y} \quad (4.34)$$

A detailed discussion on the numerical aspects of the least squares problem can be found in Ref. 25.

#### 4.2.1. Orthogonal transformation

A well known theorem in numerical analysis states that for every  $n \times r$  matrix  $X$ , there exists an  $n \times n$  orthogonal<sup>\*)</sup> matrix  $Q$  such that  $QX = R$  is an upper triangular  $n \times r$  matrix. If  $\text{rank}(X) = \kappa = r \leq n$  then all diagonal elements of  $R$  are non zero. If  $\text{rank}(X) = \kappa < r \leq n$  then some diagonal elements will be zero.

A property of orthogonal matrices is that they preserve Euclidean length i.e.  $\|Q \underline{y}\| = \|\underline{y}\|$  for every  $\underline{y}$ . Thus for every orthogonal matrix  $Q$  and every vector  $\underline{a}$  one has:

$$\|Q(X \underline{a} - \underline{y})\| = \|QX \underline{a} - Q \underline{y}\| = \|X \underline{a} - \underline{y}\| \quad (4.34)$$

Now let  $\hat{\underline{a}}_1$  be the minimum length solution of  $X \underline{a} \approx \underline{y}$  and let  $\hat{\underline{a}}_2$  be the minimum length solution of  $QX \underline{a} \approx Q \underline{y}$ . Both solutions are unique. Now one has:

$$\begin{aligned} \|QX \hat{\underline{a}}_2 - Q \underline{y}\| &= \|X \hat{\underline{a}}_2 - \underline{y}\| \\ \|QX(\hat{\underline{a}}_2 + \delta \hat{\underline{a}}_2) - Q \underline{y}\| &\geq \|QX \hat{\underline{a}}_2 - Q \underline{y}\| \quad \text{for all } \delta \hat{\underline{a}}_2 \\ \|X(\hat{\underline{a}}_2 + \delta \hat{\underline{a}}_2) - \underline{y}\| &\geq \|X \hat{\underline{a}}_2 - \underline{y}\| \quad \text{for all } \delta \hat{\underline{a}}_2 \end{aligned} \quad (4.35)$$

Consequently  $\hat{\underline{a}}_2$  is also a minimum length solution of  $X \underline{a} \approx \underline{y}$  and thus  $\hat{\underline{a}}_1 = \hat{\underline{a}}_2$ . This leads to the following conclusion.

If a least squares (LS) problem  $X \underline{a} \approx \underline{y}$  has to be solved one may multiply this system with an orthogonal matrix. The LS solution for the transformed system is the same as for the original system. In the two following subsections commonly used orthogonal transformations are discussed.

#### 4.2.2. Householder transformations

In this subsection it is shown that the  $n \times r$  matrix  $X$  can be transformed into an upper triangular  $n \times r$  matrix  $X^r$  via  $r$  successive orthogonal transformations according to:

$$\begin{aligned} X^r &= P^r X^{r-1} = P^r P^{r-1} X^{r-2} = \\ &= P^r P^{r-1} \dots P^2 Q^1 X \end{aligned} \quad (4.36)$$

The orthogonal  $n \times n$  matrix  $X$  is constructed as follows.

Consider an  $n \times 1$  vector  $\underline{v}$  (not the zero vector). Define a vector  $\underline{u} = \underline{v} + \sigma \frac{\|\underline{v}\|}{2} \underline{e}_1$ , where  $\underline{e}_1 = \text{col}[1, 0, \dots, 0]$ ,  $\sigma = +1$  if  $v_1 \geq 0$  and  $\sigma = -1$  if  $v_1 < 0$ . For the matrix  $Q = I - \frac{\underline{u} \underline{u}^T}{\underline{u}^T \underline{u}}$  one has:

\*) A square matrix  $Q$  is orthogonal if  $Q^T Q = I$ .

$$\begin{aligned}
 Q^T Q &= \left\{ I - \frac{2}{\underline{u}^T \underline{u}} \underline{u} \underline{u}^T \right\}^T \left\{ I - \frac{2}{\underline{u}^T \underline{u}} \underline{u} \underline{u}^T \right\} \\
 &= I - \frac{4}{\underline{u}^T \underline{u}} \underline{u} \underline{u}^T + \frac{4 \underline{u} \underline{u}^T \underline{u} \underline{u}^T}{\underline{u}^T \underline{u} \underline{u}^T \underline{u}} \\
 &= I
 \end{aligned} \tag{4.37}$$

and:

$$Q \underline{v} = \underline{v} - 2 \frac{\underline{u} \underline{u}^T \underline{v}}{\underline{u}^T \underline{u}} = \underline{v} - \underline{u} = -\sigma \frac{\underline{u}}{\|\underline{u}\|} = \underline{e}_1 \tag{4.38}$$

$Q$  is the well-known Householder transformation matrix, that zeroes all elements of a vector except for the first. If this transformation is applied to a matrix  $[X : \underline{y}]$  from a system  $X \underline{a} \approx \underline{y}$  then only the first element of the first column of the matrix  $Q [X : \underline{y}]$  will not be equal to zero. Because  $Q$  is designed to zero the elements of the first column of  $X$ , a superscript 1 is added, to  $Q = Q^1$ . The Householder matrix  $Q^1$  transforms the matrix  $X$  into  $X^1$ :

$$X^1 = Q^1 X \tag{4.39}$$

In the second step the elements of the second column of the matrix  $X^1$  have to be zeroed except for the first two elements. To accomplish this, a  $(n-1) \times (n-1)$  dimensional Householder matrix  $Q^2$  can be designed for the lower  $n-1$  elements of the second column of  $X^1$ . The matrix  $P^2$  defined as:

$$P^2 = \begin{bmatrix} 1 & 0 \\ 0 & Q^2 \end{bmatrix} \tag{4.40}$$

leaves consequently the first row and column of  $X^1$  unchanged. The first two columns of  $X^2 = P^2 X^1 = P^2 Q^1 X$  have become upper triangular. Proceeding in this way results in an upper triangular matrix  $X^r$  in  $r$  steps. Simultaneously the vector  $\underline{y}$  has been transformed into  $\underline{y}^r$  according to:

$$\underline{y}^r = P^r \underline{y}^{r-1} = P^r P^{r-1} \underline{y}^{r-2} = P^r P^{r-1} \dots P^2 Q^1 \underline{y} \tag{4.41}$$

The result is a set of  $r$  equations for the elements of  $\underline{a}$  which can easily be solved as discussed in 4.2.0. resulting in the LS solution of Eq. (4.30).

#### 4.2.3. Givens rotations

Orthogonal matrices with the following structure:

$$G = \begin{bmatrix} 1 & & & & & \\ & 1 & & & & \\ & & \ddots & & & \\ & & & 1 & & \\ & & & & c_1 & s \\ & & & & s & -c_1 \end{bmatrix} \tag{4.42}$$

are called Givens rotations. These matrices are employed to zero one particular element of a general matrix.

In the preceding section it was shown that a sequence of Householder transformations transforms the matrix  $[X : \underline{y}]$  into upper triangular form according to:

$$[X^r : \underline{y}^r] = \begin{bmatrix} x_{11}^r & \dots & x_{1r}^r & y_1^r \\ & \ddots & \vdots & \vdots \\ 0 & & x_{rr}^r & y_r^r \\ & & & y_{r+1}^r \end{bmatrix} \tag{4.43}$$

When this matrix is adjoined by a new row representing an additional measurement or an a fortiori relation between the parameters, a matrix of the following general structure results:

$$\begin{bmatrix} x^r & y^r \\ \hline b \end{bmatrix} = \begin{bmatrix} x_{11}^r & x_{1r}^r & y_1^r \\ \vdots & \vdots & \vdots \\ x_{rr}^r & y_r^r \\ \hline 0 \dots 0 & b_1 & b_{1+1} \dots b_{r+1} \end{bmatrix} \quad (4.44)$$

One way to bring this matrix again into upper triangular form is via a new sequence of Householder transformations. A more direct and less time consuming way however is via a sequence of  $r+1$  Givens rotations. When premultiplying the matrix of Eq. (4.44) by  $G$ , only the elements  $x_{11}^r, x_{1,1+1}^r, \dots, y_1^r$  and the elements  $b_1, b_{1+1}, \dots, b_{r+1}$  are changed. In particular, the element  $b_1$  becomes  $s x_{11}^r - c b_1$ . By choosing:

$$s = \frac{b_1}{\sqrt{x_{11}^{r2} + b_1^2}}, \quad c = \frac{x_{11}^r}{\sqrt{x_{11}^{r2} + b_1^2}} \quad (4.45)$$

this element vanishes. Repeated application of this concept restores the upper triangular structure of the original matrix of Eq. (4.43). Since Givens rotation are orthogonal matrices, the LS solution of the transformed system is still identical to the LS solution of the original system.

#### 4.2.4. Use of a priori/a fortiori information on the aerodynamic model

Householder transformations may be applied to transform the original  $X a \approx y$  system into upper triangular form. If the upper triangular matrix has non-zero diagonal elements the solution is straightforward and gives the aerodynamic model parameters. However, if some diagonal elements are zero, the system cannot be solved. Theoretically, the minimal length solution in the solution space can be sought via additional after-multiplication with Householder matrices. Details of this technique can be found in Ref. 25. Another, more practical, approach is to accept these zeroes as a result of one or more unidentifiable parameters. A solution from the solution space (not the one with minimum length) can now be chosen by setting the unidentifiable parameter to any value. A realistic approach however is to use a fortiori information on the aerodynamic model. Any relation between parameters can be added as an equation and via Givens rotations be incorporated in the upper triangular matrix. This process should eliminate all zeroes on the diagonal without increasing the sum of squared residuals significantly. In practical diagonal elements may become approximately zero. Now an error  $\delta X$  has to be specified to recognize small values on the diagonal as zero.

#### 4.2.5. Batch versus sequential processing

In a practical application the actual matrix  $X$  may become quite large. Typical values for  $n$  and  $r$  are 4000 and 10 for example. In such cases it may be impossible to have the whole matrix  $X$  or even two columns in core storage at one time and consequently standard Householder transformations cannot be applied.

In Ref. 25 a detailed description is given of a sequential form of the Householder transformation technique. This technique partitions the original matrix  $[X \mid y]$  into blocks of appropriate length and the same width as the original matrix  $[X \mid y]$ . The length is chosen in such a way that two blocks can be kept in core storage simultaneously.

After upper triangularization of the first two blocks a new block is loaded in the place of the second and the process goes on until the last block is processed.

This technique opens the way to two important features:

- (i) It can be performed real time.
- (ii) If intermediate upper triangular systems are solved an insight can be obtained into the identifiability of the aerodynamic model as a function of the number of processed data blocks.

## PART II

### 5. TECHNICAL ASPECTS AND RESULTS OF FLIGHT PATH RECONSTRUCTION

#### 5.0. Introduction

This section emphasizes technical aspects of flight test instrumentation and computational aspects of data analysis with emphasis on flight path reconstruction. Experimental results are shown and discussed.

#### 5.1. Flight test instrumentation and data analysis

##### 5.1.0. Introduction

A brief description of the flight test instrumentation system used and a survey of the entire data analysis procedure will be presented in this subsection.

The reader interested in more detailed descriptions of the instrumentation systems used for various flight

test programs is referred to other publications (see refs. 27, 28). Procedures developed for accurate calibration of the sensors to be used are described in ref. 7.

#### 5.1.1. The flight test instrumentation system

Various flight test programs have been carried through for validation of the nonsteady flight test technique. Aircraft flight tested were the De Havilland DHC-2 Beaver aircraft owned and operated by the Delft University of Technology, a Hunter Mk VII of the National Aerospace Laboratory and the Fokker owned F-28 test aircraft. For these flight test programs including tests in steady as well as in non-steady flight, instrumentation systems were developed by the Department of Aerospace Engineering of the Delft University of Technology as well as by the National Aerospace Laboratory. Fig. 11 shows a general lay-out of these systems.

The instrumentation system used for the 1978 flight test program directed towards measuring performance, stability and control characteristics of the laboratory aircraft of the Delft University in symmetric as well as in asymmetric flight, will be considered as an example system. The system is capable of measuring and recording 38 variables at a sample rate of 10 samples per second each. To be more specific, the variables to be measured are sequentially scanned by means of a 38 channel scanner at a scanning rate of 10 cycles per second. As in the instrumentation system under concern 24 variables are measured, some variables such as for instance the inertial quantities and the control surface deflections, were sampled at a double sample frequency (20 samples/s) by connecting the corresponding outputs to two multiplexer switches.

In the data logging part of the system an information from 20 channels is recorded on magnetic tape. The tape recorder used for data recording is a simple NAGRA audio tape recorder with modified circuitry. As only a two track system is used, information of each channel is to be recorded in serial form. The amount of information per sample to be stored equals 25 bits. Hence the total amount of the information to be recorded per second equals 10.000 bits. The output voltages of the transducers are conditioned to range from 0 to 10.000 mV dc.

The transducer signals are each filtered by an active filter network. The filter outputs are sequentially scanned, then sampled by a sample and hold unit. The hold unit output is digitized by an analog to digital converter. The 16 bits of information presented in parallel by the analog to digital converter are transformed into 16 bits of serial information by a parallel series converter.

Nine bits of information generated in the parallel series converter are added to this information. These 9 bits are used to identify operational modes of the system as well as to separate the information of consecutive channels. One channel is used to record administrative data generated in the parallel series converter. The instrumentation system has been designed to operate in one of three modes. The first mode (balance mode) permits the registration of the mV offsets of the filter amplifiers. The second mode (zero output mode) provides the possibility for recording the zero outputs of the differential pressure transducers in the instrumentation system. In this mode both sides of each differential pressure transducer are interconnected. The third mode (manoeuvre mode) is directed towards taking actual in-flight measurements.

A small and simple control panel provides a mode selection facility as well as a digital read-out for single channel monitoring and checking purposes.

Filtering the transducer output signals before recording in the system is essential for the application of digital measuring techniques to in-flight measurements. The frequency spectrum of the transducer output signals can be separated into two parts. The frequencies related to the pilot induced aircraft motions usually ranging from zero to 6 rad/s and the frequencies higher than those related to the aircraft motions. The latter frequencies are considered as noise, originating from engine induced structural vibration, transducer noise and electromagnetic interference of other on-board systems.

In the instrumentation system under consideration each transducer output voltage is sampled at a finite sampling rate. It follows from Shannon's sampling theorem that the frequency contents of the signal above a certain frequency must be suppressed. In the instrumentation system all signals of the transducers are filtered by identical fourth order filters. Each filter consists of two identical second order filters connected in series.

The second order filters contain a chopper stabilized operational amplifier and a network of high quality capacitor's and resistors. The cut-off frequency of these second order filters equals 19 rad/s. The damping ratio of 0.691 is chosen so as to obtain a constant gain and almost linear phase characteristic in the region of the low frequency part of the signal spectrum. It is assumed that this filter characteristic results in a constant time shift of the filter output relative to the corresponding filter input, equal for all filtered signals. The static error introduced by the filters is smaller than 1 mV which equals 0.01% of the maximum filter output voltage range. Deviations of the actual phase characteristics from the ideal linear characteristics may cause errors in the order of several mV's in the dynamic parts of the manoeuvres. Good zero stability of the electronic filters is highly important to accurate signal processing. Tests made in the laboratory reveal the zero shifts of the filters in a temperature range from -25° up to 25° and over periods of several hours to be less than 1 mV.

The scanner is operated by a crystal controlled clock. The clock is built into the parallel-series converter unit and operates at 40 kHz. The scanner contains 38 analog switches and is considered to introduce no significant errors in the signals.

The analog to digital converter is a modified digital volt meter (EAI series 6000). The ADC inputs range from 0 to 10.000 mV. The resolution equals 1 mV, the static accuracy of the digital volt meter equals 0.01% + 1 digit, 0.02% full scale. The output is specified in 16 bits BCD for the parallel-series converter. A decimal coded output is available for the display panel. The conversion time of the ADC equals 1 ms. The highest frequencies in the transducer output signals related to aircraft motion are in the order of 6 rad/s. Hence signal variations occurring during ADC conversion time may be in the order of 30 mV. This demonstrates the need for a sample and hold unit at the ADC input side.

The sample and hold circuit switches sequentially from the sampling mode to the hold mode. The uncertainty in the switching time instant, the aperture uncertainty, is typically in the order of 100 nano seconds. The decay of the sample and hold circuit is about 1 mV/s. The DC offset in hold equals about 0.2 mV. It follows from these data that the sample and hold unit does not significantly contribute to the error in the signals measured by the instrumentation system. The maximum sample rate achievable with the instrumentation system is limited by the conversion time of the analog to digital converter and the acquisition time of the sample and hold unit.

A comprehensive list of variables measured and transducers employed in the instrumentation system, measurement ranges and accuracies as deduced from calibration data is presented in Table 1.

A discussion of the calibration technique employed is given in Ref. 7. It followed from the calibrations that the random errors in the outputs of the accelerometers and the pitch rate gyroscopes are smaller than 0.01% full scale, i.e. in the order of 1 mV.

The inertial transducer measurement errors, i.e. the measurement errors of the accelerometers and rate gyro's are typically in the order of 0.01% of full scale. These errors are composed out of a random error and a constant bias error. The bias error changes from one calibration to the next. In actual flight test conditions, these bias errors are of course unknown but they may be estimated simultaneously with the flight path reconstruction as described in the previous chapter. The inertial transducers can thus be corrected for bias errors.

The accuracy of the absolute and relative pressure transducers is in the order of 0.01% to 0.05% of full scale. These transducers serve for the measurement of air density, true airspeed and altitude variations with respect to a nominal altitude. To fully exploit the inherent capabilities of carefully selected modern pressure transducers in actual flight test conditions extreme care is taken to eliminate or reduce the effect of accelerations and temperature variations on the transducer outputs. The transducers are placed in a temperature controlled box. Before and after every flight test manoeuvre the zero outputs of the relative pressure transducers are measured in the instrumentation system. Changes in zero outputs can thus be corrected for a posteriori in the data analysis process. At the nominal altitude the static pressure is sampled by means of thermoflask. To reduce the effects of warming up or cooling of due to compression or expansion of the air while the flask is not closed the heat capacity of the inside of the flask is increased to as high a level as possible. Linear film-type potentiometers were used for the measurement of rudder, aileron, elevator and flap angle deflections. The resulting accuracies are in the order of 0.05% to 0.1%. Different types of flow angle transducers are used. The angle of attack vane is based on a film type potentiometer, the side slip angle vane on a synchro transducer. Accuracies are in the order of 0.1%. A detailed description of the instrumentation system is given in refs. 27 and 28.

The transducer outputs are sequentially scanned and measured by the instrumentation system. Hence, all measurements are made at different instances in time. Further analysis, however, requires the values of the measured quantities pertaining to one measuring cycle to be specified at one particular instance of time characterizing that cycle. Hence, a shift in time of  $n-1$  out of the  $n$  voltages recorded is required. The output voltage of the  $A_{x3}$  accelerometer is taken as the time reference variable. The other subsequent transducer voltage recordings are shifted backwards or forwards in time using numerical interpolation procedures. Transducer output voltage measurements are delayed by the electronic filters discussed earlier. Since all filters are constructed so as to have identical time constants these time delays need no further interpolations.

#### 5.1.2. Data analysis

The digital magnetic tape produced in flight by means of the flight test instrumentation system is transcribed in IBM compatible format and stored on nine track tape in order to achieve compatibility with the digital computer system to be used for further data analysis. Simultaneously, quick-look time histories of the sensor output voltages are produced.

The digitized voltages are subsequently converted to the corresponding physical quantities. Information required for this conversion process includes:

- transducer calibration data, specified in terms of nonlinear polynomials,
- the aircraft's c.g. position, to correct for effects of aircraft body angular rates and angular accelerations on the outputs of the accelerometers,
- dynamic response data of the air pressure tubes of the barometric sensor system, to correct for the time required by small pressure fluctuations to travel through these tubes to the transducers,
- the zero shifts of the differential pressure transducers measured shortly prior and posterior to each manoeuvre by short circuiting both sides of these differential pressure transducers,
- amount of fuel carried as a function of time, computed by linear interpolation of fuel contents measurements, taken manually before and after each flight test manoeuvre,
- the aircraft weight, mass and moments of inertia as a function of time.

Finally in this step of the data reduction procedure elementary calculations are carried through resulting in such variables as airspeed, Mach number, total and static outside air temperature, air density and altitude variations.

Table 2 provides a survey of the magnitudes recorded as resulting from the first step of the data reduction procedure. It is remarked that this procedure step also includes calculation of the gravitational acceleration as a function of latitude and altitude, such because of the fact that variations of the gravitational acceleration with geographical position and altitude should not be neglected for accurate flight path reconstruction, which is the goal set for the next, i.e. the second step of the data reduction procedure.

The algorithms applied to reconstruct the aircraft's flight path and all pertaining descriptive variables from the data shown in Table 2 have been discussed in the preceding sections. In the following subsections some technical aspects of flight path reconstruction and some results obtained will be discussed. After flightpath reconstruction, the aerodynamic model is identified. This is the subject of Chapter 6. Several performance characteristics and stability and control characteristics are derived. Examples are: drag polar, excess thrust and rate of climb versus airspeed curves, stick displacement per "g" and stability derivatives, see Refs. 4 and 19.

## 5.2. Initial condition computation

### 5.2.0. Introduction

This subsection is devoted to the presentation of the procedure followed by calculation of:

- 1) the nominal initial state  $\underline{y}_{nom}(0)$  as required for nominal flight path computation, i.e. for integration of Eq. (3.45),
- 2) the initial error covariance matrix  $P(0|0)$  as required for the solution of Eq. (3.186) and (3.189), of the Kalman Filtering and Smoothing algorithms are applied to the solution of the flight path reconstruction problem.

After estimation of  $\underline{y}(0)$ , the nominal flight path  $\underline{y}_{nom}(t)$  can be computed starting from:

$$\underline{y}_{nom}(0) = \hat{\underline{y}}(0) \quad (5.1)$$

The initial perturbation correction, i.e. the correction for the deviation of  $\underline{y}_{nom}(0)$  from  $\underline{y}(0)$ , is defined as:

$$\underline{\chi}(0) \triangleq \underline{y}(0) - \underline{y}_{nom}(0) \quad (5.2)$$

See Eq. (3.47).

Obviously,  $\underline{\chi}(0)$  is unknown. Consequently, the estimated initial state vector of the Kalman Filter, see Eq. (3.185), is taken as:

$$\hat{\underline{\chi}}(0|0) = 0 \quad (5.3)$$

The error made is reflected in statistical terms by the elements of the initial error covariance matrix  $P(0|0)$  defined as:

$$P(0|0) \triangleq E \left\{ [\hat{\underline{\chi}}(0|0) - \underline{\chi}(0)] [\hat{\underline{\chi}}(0|0) - \underline{\chi}(0)]^T \right\} \quad (5.4)$$

It should be noticed that accurate estimation of the nominal initial state is required to minimize linearization errors in the linear system matrices  $A(t)$  and  $B(t)$  occurring in Eq. (3.52).

While performing test flights, each manoeuvre is preceded by an interval of approximately 10 seconds of steady rectilinear flight with wings level and constant angle of yaw.

Several components of the nominal initial state vector  $\underline{y}_{nom}(0)$  can be estimated from measurements recorded during this time interval.

Two algorithms for estimation of these components, one simple and straightforward the other more complex and requiring iterative computations are described in the following subsections.

#### 5.2.1. Simple algorithm for the calculation of the nominal initial state vector

To obtain the flight path reconstruction results to be presented in Subsection 5.3., no effort was made as yet to estimate the horizontal position coordinates  $x_E$  and  $y_E$ . These components are therefore dropped from the augmented system state vector  $\underline{y}$  as defined by Eq. (3.39).

The augmented system state then reduces to:

$$\begin{aligned} \underline{y}(t) &\triangleq \text{col} [\underline{x}(t), \underline{\lambda}] = \\ &= \text{col} [v_{x_B}, v_{y_B}, v_{z_B}, \psi, \theta, \varphi, z_E, \lambda_x, \lambda_y, \lambda_z, \lambda_p, \lambda_q, \lambda_r] \end{aligned} \quad (5.5)$$

Obviously, the nominal initial state vector  $\underline{y}_{nom}(0)$  can be written as:

$$\begin{aligned} \underline{y}_{nom}(0) &\triangleq \text{col} [\underline{x}_{nom}(0), \underline{\lambda}_{nom}(0)] \\ &= \text{col} [v_{x_{B_{nom}}}(0), v_{y_{B_{nom}}}(0), v_{z_{B_{nom}}}(0), \psi_{nom}(0), \theta_{nom}(0), \\ &\quad \varphi_{nom}(0), z_{E_{nom}}(0), \lambda_{x_{nom}}(0), \lambda_{y_{nom}}(0), \lambda_{x_{nom}}(0), \\ &\quad \lambda_{p_{nom}}(0), \lambda_{q_{nom}}(0), \lambda_{r_{nom}}(0)] \end{aligned} \quad (5.6)$$

In (5.5),  $\underline{\lambda}$  does not vary with time since the bias errors are assumed to be constant.

Since no a priori knowledge is available concerning the components of  $\underline{\lambda}_{nom}(0)$  these components are set equal to zero. The remaining elements of  $\underline{y}_{nom}(0)$  are derived from the equations of motion taking account of the condition of steady rectilinear flight.

From the steady flight condition assumed it follows that:

$$\dot{v}_{x_B} = \dot{v}_{y_B} = \dot{v}_{z_B} = p_B = q_B = r_B = 0 \quad (5.7)$$

neglecting the effects of the curvature and rotation of the earth, the pitch angle  $\theta_{nom}(0)$  and roll angle  $\varphi_{nom}(0)$ , may be expressed as a function of  $A_{x_{B_{nom}}}$ ,  $A_{y_{B_{nom}}}$ ,  $A_{z_{B_{nom}}}$ :

$$\theta_{nom}(0) = -\text{arctg} \frac{A_{x_{B_{nom}}}}{A_{z_{B_{nom}}}} \quad (5.8)$$

$$\varphi_{nom}(0) = \text{arctg} \frac{A_{y_{B_{nom}}}}{A_{z_{B_{nom}}}} \quad (5.9)$$

These expressions follow directly from Eqs. (3.13), (3.14) and (3.15). Reasonable estimates are obtained by substitution of measurements for the specific forces according to:

$$\hat{\theta}(0) = -\text{arctg} \frac{A_{x_{B_m}}(0)}{A_{z_{B_m}}(0)} \quad (5.10)$$

$$\hat{\varphi}(0) = \text{arctg} \frac{A_{y_{B_m}}(0)}{A_{z_{B_m}}(0)} \quad (5.11)$$

An estimate of  $\psi_{nom}(0)$  may be derived directly from the corresponding measurement:

$$\hat{\psi}(0) = \hat{\psi}_m(0) \quad (5.12)$$

In steady rectilinear flights with zero angle of roll (wings level),  $A_{y_B}$  is equal to zero as follows directly from Eq. (3.14). For perfectly symmetric aircraft in steady rectilinear flight, this implies that the velocity vector  $\underline{v}$  lies in the aircraft's plane of symmetry. Consequently the lateral velocity component  $V_{y_B} = 0$ . The angle of sideslip  $\beta$  is therefore also equal to zero. If, however, the airflow is not strictly symmetric, relative to the aircraft's plane of symmetry, the condition that  $A_{y_B} = 0$  does not necessarily imply that  $V_{y_B} = 0$ .

This condition holds for example for single-engined, propeller driven aircraft. Asymmetric airflow contributions resulting in these cases from the propeller slipstream, may induce an unknown offset  $-C_\beta$  in the side slip vane angle. From the remarks made, the lateral component  $V_{y_B}(0)$  and henceforth the initial slip angle  $\beta(0)$  may be concluded to be unobservable.

Processing the flight test measurements, recorded during the 1978 flight test program, for flight path reconstruction, the asymmetric airflow effects were neglected. This implies that  $\dot{V}_{y_B}(t)$  and henceforth  $\dot{\beta}(t)$  are set equal to zero for  $t \in [t_0, t_s]$ , the time span of the initial steady rectilinear flight section, preceding each nonsteady manoeuvring test flight. Consequently, for  $t = 0$ :

$$\dot{V}_{y_B}(0) \triangleq 0 \quad (5.13)$$

Hence:

$$\hat{\beta}(0) \triangleq 0$$

An estimate of the wind vane zero shift may then be derived from the initial wind vane measurements according to Eq. (3.25):

$$\hat{C}_\beta = -\beta_{v_m}(0) \quad (5.14)$$

Estimates of the remaining components  $V_{x_B}(0)$  and  $V_{z_B}(0)$  of  $\underline{v}(0)$  are still to be generated. The following relations may be derived from Fig. 12:

$$V_{x_B} = V \cos \alpha \cos \beta \quad (5.15)$$

$$V_{z_B} = V \sin \alpha \cos \beta \quad (5.16)$$

Since it is assumed that  $\beta(t) = 0$ , for  $t \in [t_0, t_s]$  i.e. during the initial steady straight part of the flight test manoeuvre these relations reduce to:

$$V_{x_B} = V \cos \alpha \quad (5.17)$$



$$V_{z_B} = V \sin \alpha \quad (5.18)$$

The angle of attack  $\alpha$  may be derived from the angle of pitch  $\theta$  and the flight path angle  $\gamma$  according to the relation:

$$\alpha = \theta - \gamma \quad (5.19)$$

which holds under conditions of strictly symmetric flight.  
The flight path angle  $\gamma$  follows from:

$$\gamma = \arcsin \left( \frac{-\dot{z}_E}{V} \right) \quad (5.20)$$

An estimate of  $\dot{z}_E(\tau)$ , for  $\tau \in [t_0, t_1]$  may be computed from test flight measurements as follows:

$$\dot{z}_E = - \frac{\Delta h_m(1) - \Delta h_m(0)}{t_1 - t_0} \quad (5.21)$$

The flight path angle  $\gamma$  and the angle of attack  $\alpha$  are subsequently estimated according to:

$$\hat{\gamma}(0) = \arcsin \left( \frac{-\hat{\dot{z}}_E}{V_m(0)} \right) \quad (5.22)$$

$$\hat{\alpha}(0) = \hat{\theta}(0) - \hat{\gamma}(0) \quad (5.23)$$

see Eq. (5.10).

Now:

$$\hat{V}_{x_B}(0) = V_m(0) \cos \hat{\alpha}(0) \quad (5.24)$$

$$\hat{V}_{z_B}(0) = V_m(0) \sin \hat{\alpha}(0) \quad (5.25)$$

The vertical displacement  $z_E(0)$  is by definition set equal to zero. All components of  $\hat{\mathbf{y}}(0)$  have now either been estimated from test flight measurements recorded at time  $t_0$  and  $t_1$ , or a priori specified.

Errors in  $\hat{\mathbf{y}}(0)$  may result from:

1. random measurement errors,
2. constant bias errors in the accelerometer and rate gyroscope measurements,
3. deviations of the actual flight conditions from the nominally steady rectilinear flight conditions.

The effects of random measurement errors on the estimated initial state can be attenuated averaging  $s + 1$  estimates  $\hat{y}_i(k)$ , for  $y_i = V_{x_B}, V_{z_B}, \psi, \theta, \phi$  and  $k = 0, 1, 2, \dots, s$ . It is recalled that the nominally steady, rectilinear flight condition is assumed to be maintained from  $t_0$  until  $t_s$ .

Hence:

$$\hat{y}_i(0) \triangleq \frac{1}{s+1} \sum_{k=0}^s \hat{y}_i(k) \quad (5.26)$$

Some of the diagonal elements of the estimation error covariance matrix  $P(0|0)$  may also be derived from the estimates  $\hat{y}_i(k)$ ,  $k = 0, 1, 2, \dots, s$ .

$$P_{ii}(0|0) = \sigma_{y_i}^2 \approx \frac{1}{s+1} \sum_{k=0}^s \left\{ \hat{y}_i(k) - \frac{1}{s+1} \sum_{k=0}^s \hat{y}_i(k) \right\}^2 \quad (5.27)$$

Estimation of the actual vertical displacement  $z_E(0)$  may be achieved as follows:

$$\hat{z}_E(0) = - \frac{1}{s+1} \sum_{k=0}^s \{ \Delta h_m(k) + \hat{z}_E(0) (t_k - t_0) \} \quad (5.28)$$

where:

$$\hat{z}_E(0) \triangleq - \frac{\Delta h_m(s) - \Delta h_m(0)}{t_s - t_0} \quad (5.29)$$

The variance of the error in the estimate  $\hat{z}_E(0)$  may be derived as follows from the measured altitude deviations:

$$P_{\hat{z}_E}(0|0) = \sigma_{\hat{z}_E}^2 \approx \frac{1}{s+1} \sum_{k=0}^s \left\{ -\Delta h_m(k) - (\hat{z}_E(0) + \hat{z}_E(0)(t_k - t_0)) \right\}^2 \quad (5.30)$$

The remaining diagonal elements of  $P(0|0)$  are to be specified, according to instrument calibration data.

### 5.2.2. Advanced algorithm for the calculation of the nominal initial state vector

Depending on the quality of the steady rectilinear flight flown, the variable components  $\hat{v}_{xB}(k)$ ,  $\hat{v}_{zB}(k)$ ,  $\hat{\psi}(k)$ ,  $\hat{\theta}(k)$  and  $\hat{\varphi}(k)$  of  $\hat{Y}(k)$ , computed from measurements at  $t_{k-1}$  and  $t_k$ , for  $k = 1, 2, \dots, s$ , may vary as a function of time due to deviations of the actual flight condition from steady, rectilinear flight. Correction for the effects of these flight path deviations on the estimated initial state components may be achieved as follows:

$$\hat{Y}_{i_k}(0) = \hat{Y}_i(k) - \int_{t_0}^{t_k} \hat{Y}_i(\tau) d\tau \quad (5.31)$$

for  $Y_i = v_{xB}, v_{zB}, \psi, \theta, \varphi$   
and:

$$\hat{z}_{E_k}(0) = -\Delta h_m(k) - \int_{t_0}^{t_k} \hat{z}_E(\tau) d\tau \quad (5.32)$$

In Eq. (5.31) the quantity  $\hat{Y}_{i_k}(0)$  represents the estimate of  $Y_i(0)$ , as deduced from  $\hat{Y}_i(k)$ , by correction for nonsteady effects, i.e. by elimination of departures of the actual flight conditions from the nominally steady rectilinear flight condition. The estimate of the initial state  $\hat{Y}(0)$  may now be computed, by averaging  $\hat{Y}_{i_k}(0)$ , for  $Y_i = v_{xB}, v_{zB}, \psi, \theta, \varphi, z_E$ :

$$\hat{Y}_i(0) = \frac{1}{s+1} \sum_{k=0}^s \hat{Y}_{i_k}(0) \quad (5.33)$$

Estimates of the diagonal elements of the covariance matrix  $P(0|0)$  are again computed according to Eq. (5.33), replacing  $Y_i(k)$  by  $\hat{Y}_{i_k}(0)$ .

The expressions, Eqs. (5.10) and (5.11), used so far for computation of  $\hat{\theta}(0)$  and  $\hat{\varphi}(0)$  are based on the assumed steady straight flight condition and will therefore in practice yield more or less "rough" approximations.

Taking account of nonsteady effects Eqs. (5.10) and (5.11) can be extended applying Eqs. (3.13) through (3.15) and neglecting the terms in those equations depending on  $v_{yB}(k)$ , since  $v_{yB}(k) \triangleq 0$ :

$$\begin{aligned} \hat{\theta}(k) &= -\arctg \left[ \frac{A_{xB_m}(k) - q_{B_m}(k) \hat{v}_{zB}(k) - \hat{v}_{xB}(k)}{A_{zB_m}(k) + q_{B_m}(k) \hat{v}_{xB}(k) - \hat{v}_{zB}(k)} \cos \hat{\varphi}(k) \right] \\ &\approx -\arctg \left[ \frac{A_{xB_m}(k) - q_{B_m}(k) \hat{v}_{zB}(k) - \hat{v}_{xB}(k)}{A_{zB_m}(k) + q_{B_m}(k) \hat{v}_{xB}(k)} \cos \hat{\varphi}(k) \right] \end{aligned} \quad (5.34)$$

for  $k = 0, 1, 2, \dots, s$ , since  $\hat{v}_{zB}(k) \ll A_{zB_m}(k)$   
and:

$$\begin{aligned} \hat{\varphi}(k) &= \arctg \left[ \frac{A_{yB_m}(k) - r_{B_m}(k) \hat{v}_{xB}(k) + p_{B_m}(k) \hat{v}_{zB}(k) - \hat{v}_{yB}(k)}{A_{zB_m}(k) + q_{B_m}(k) \hat{v}_{xB}(k) - \hat{v}_{zB}(k)} \right] \\ &\approx \arctg \left[ \frac{A_{yB_m}(k) - r_{B_m}(k) \hat{v}_{xB}(k) + p_{B_m}(k) \hat{v}_{zB}(k) - \hat{v}_{yB}(k)}{A_{zB_m}(k) + q_{B_m}(k) \hat{v}_{xB}(k)} \right] \end{aligned} \quad (5.35)$$

for  $k = 0, 1, 2, \dots, s$ .

The corresponding estimates of  $\theta(0)$  and  $\varphi(0)$  may then be computed, according to Eq. (5.31), as:

$$\hat{\theta}_k(0) = \hat{\theta}(k) - \int_{t_0}^{t_k} \hat{\theta}(\tau) d\tau \quad (5.36)$$

$$\hat{\varphi}_k(0) = \hat{\varphi}(k) - \int_{t_0}^{t_k} \hat{\varphi}(\tau) d\tau \quad (5.37)$$

Estimates of  $\hat{z}_E(0)$  may be computed from the altitude deviation measurements  $\Delta h_m(k)$  according to:

$$\begin{aligned}\hat{z}_{E_k}(0) &= \left\{ z_{E_m}(k) - \int_{t_0}^{t_k} a_{z_T}(\tau) d\tau^2 - z_{E_m}(0) \right\} / (t_k - t_0) \\ &= - \left\{ \Delta h_m(k) + \int_{t_0}^{t_k} a_{z_T}(\tau) d\tau^2 - \Delta h_m(0) \right\} / (t_k - t_0)\end{aligned}\quad (5.38)$$

for  $k = 1, 2, \dots, s$ .

where:

$$\begin{aligned}A_{z_T}(t) &= -A_{x_{B_m}}(t) \sin \hat{\theta}(k) + A_{y_{B_m}}(k) \cos \hat{\theta}(t) \sin \hat{\varphi}(k) + \\ &+ A_{z_{B_m}}(k) \cos \hat{\theta}(k) \cos \hat{\varphi}(k) + g_h(k)\end{aligned}\quad (5.39)$$

for  $t \in [t_k, t_{k+1})$

The gravitational acceleration  $g_h(k)$  at the test flight altitude is computed as:

$$g_h(k) = g_0 \left( \frac{R^E}{R^E + h(k)} \right)^2 \quad (5.40)$$

Here  $g_0$  is the gravitational acceleration at sea level computed according to Lambert's formula taking account of the latitude  $\lambda$  of the test site:

$$g_0 = 9,80616 (1 - 0,0026373 \cos 2\lambda + 0,0000059 \cos^2 2\lambda) \quad (5.41)$$

The angle of yaw may be estimated, writing:

$$\hat{\psi}_k(0) = \psi_m(k) - \int_{t_0}^{t_k} \hat{\psi}(\tau) d\tau \quad (5.42)$$

The computations then proceed as follows:

$$\hat{z}_E(0) = \frac{1}{s} \sum_{k=1}^s \hat{z}_{E_k}(0) \quad (5.43)$$

$$\hat{\gamma}(k) = \arcsin \left( - \frac{\hat{z}_E(0) + \int_{t_0}^{t_k} a_{z_T}(\tau) d\tau}{v_m(k)} \right) \quad (5.44)$$

Estimates of the angle of attack  $\alpha$  at time  $t_k$  may now be computed as follows:

$$\hat{\alpha}(k) = \hat{\theta}(k) - \hat{\gamma}(k) \quad (5.45)$$

or, more accurately, as:

$$\hat{\alpha}(k) = \left\{ \hat{\theta}(0) + \int_{t_0}^{t_k} \hat{\theta}(\tau) d\tau - \hat{\gamma}(k) \right\} \quad (5.46)$$

The components of  $\underline{v}$  in the aircraft's plane of symmetry, then follow from:

$$\hat{v}_{x_{B_k}}(0) = v_m(k) \cos \hat{\alpha}(k) - \int_{t_0}^{t_k} \hat{v}_{x_B}(\tau) d\tau \quad (5.47)$$

$$\hat{v}_{z_{B_k}}(0) = v_m(k) \sin \hat{\alpha}(k) - \int_{t_0}^{t_k} \hat{v}_{z_B}(\tau) d\tau \quad (5.48)$$

Estimates of  $z_E(0)$  may be obtained, writing:

$$\hat{z}_{E_k}(0) = -\Delta h_m(k) - \int_{t_0}^k \hat{\dot{z}}_E(\tau) d\tau \quad (5.49)$$

Averaging the  $s + 1$  estimates  $\hat{y}_{1k}(0)$  thus obtained, the required estimates  $\hat{y}_1(0)$  are found. Obviously, application of the equations (5.34) through (5.49) requires the availability of estimates  $\hat{y}_1(k)$  amongst others for computation of estimated time derivatives  $\hat{\dot{y}}_1(\tau)$  as occurring in the preceding equations. The estimates  $\hat{y}_1(k)$  are calculated as:

$$\hat{y}_1(k) = \hat{y}_1(0) + \int_{t_0}^k \hat{\dot{y}}_1(\tau) d\tau \quad (5.50)$$

Computation of the estimated time derivatives  $\hat{\dot{y}}_1(k)$  may be achieved applying Eqs. (3.7) through (3.9) and (3.13) through (3.18).

The expressions Eqs. (5.34) through (5.49) be used for rather accurate estimation of the initial state variables  $y_i$  if incorporated in an iterative algorithm. This algorithm can be initialized using the simplified expressions, presented in Subsection 5.2.1. and 5.2.2.

Flight test experience has shown that the simplified expressions may suffice for calculation of the initial state, if adequately long duration test flight manoeuvres are to be reconstructed and provided that highly accurate flight test instrumentation systems are used. In addition, it should be possible to estimate the state variable components as a function of time with adequate accuracy by application of the linear Kalman estimation procedures. If some state variable cannot be estimated with adequate accuracy after processing the available measurements, accurate initial state estimation by application of the nonlinear expressions, Eqs. (5.36) through (5.49) should be considered more desirable.

### 5.3. Flight path reconstruction results

#### 5.3.0. Introduction

The flight path reconstruction procedures as discussed in the previous sections have been applied to actual flight test data of the flight test programs mentioned in Section 1 as well as to simulated flight test data. In this section some results are presented of the 1978 flight test program carried through with the De Havilland DHC-2 "Beaver" laboratory aircraft.

The aim of the 1978 flight test program was to extend the techniques for flight path reconstruction and aerodynamic model identification for symmetric nonsteady flight test manoeuvres as developed in earlier flight test programs with the DHC-2 "Beaver" and the Hawker Hunter mk VII laboratory aircraft to asymmetric nonsteady flight test manoeuvres. Also the effect of the shape of the control surface input signals on the accuracy of the aerodynamic model identification results was investigated. To this end, a hydraulic control system was installed in the test aircraft with which precalculated test signals for the elevator as well as for the ailerons and rudder could be implemented in flight. The flight test program was carried through in cooperation with the Deutsche Forschungs- und Versuchsanstalt für Luft- und Raumfahrt (DFVLR) in Braunschweig and the National Aerospace Laboratory (NLR) in Amsterdam.

The flight test manoeuvre includes a nominally symmetric and an asymmetric part. Starting from a steady straight flight condition, the elevator control signal was implemented in the hydraulic control system. Then, after returning to the original steady straight flight condition, the asymmetric aileron and rudder control input signals were implemented.

Different types of "optimal" symmetric and asymmetric test signals were designed by DFVLR and Delft University of Technology. The time histories of Fig. 21 represent an example of one of the symmetric/asymmetric test signals which were actually flown in the flight test program.

The experimental results presented in this section only represent some of the flight path reconstruction experiments of the 1978 flight test program. In Subsection 5.3.1. the Kalman filtering and fixed interval smoothing algorithms as described in the previous section are applied to flight path reconstruction from digitally simulated flight test data.

In Subsection 5.3.2. corresponding results from actual flight test data are presented. More results of the 1978 flight test program in particular with respect to aerodynamic model identification and the comparison of different input signals will be covered by future publications, refs. 24, 25, 26.

#### 5.3.1. Flight path reconstruction from simulated flight test data

##### 5.3.1.0. Simulation of the flight test data

Simulation and analysis of simulated flight test data is essential for the development of flight test data analysis algorithms. The algorithms for the reconstruction of the aircraft's flight path in nonsteady asymmetric flight conditions have therefore been evaluated, processing simulated flight test data prior to application to actual flight test data.

The elevator, aileron and rudder control signals simulated are presented in Fig. 13. These signals should be compared to the corresponding signals, actually generated in flight, Fig. 21.

The initial steady straight flight condition  $y_{sim}(0)$  and the measurement error statistics are specified in

Table 4 and Table 5.

### 5.3.1.1. The augmented state vector and a priori statistics

The state vector  $\underline{x}$  of the dynamic system (3.21) under consideration is defined in Section 3 as:

$$\underline{x} \triangleq \text{col} [v_{xB}, v_{yB}, v_{zB}, \psi, \theta, \phi, x_E, y_E, z_E] \quad (3.19)$$

As described in Section 3, when unknown parameters have to be estimated simultaneously with the elements of  $\underline{x}$  an augmented state vector can be defined according to:

$$\underline{y} = \text{col} [v_{xB}, v_{yB}, v_{zB}, \psi, \theta, \phi, x_E, y_E, z_E, \lambda_x, \lambda_y, \lambda_z, \lambda_p, \lambda_q, \lambda_r] \quad (3.49)$$

In practical applications, the number and type of components of  $\underline{y}$  may vary depending on the characteristics of the instrumentation system and on the shape of the nonsteady flight manoeuvre.

As pointed out earlier, flight path reconstruction dictates the demand for very accurate instrumentation system. In one recent application it followed from extensive calibrations that the zero shifts  $\lambda_x, \lambda_y, \lambda_z, \lambda_p, \lambda_q$  and  $\lambda_r$  of the inertial transducers were small as compared to the stochastic measurement errors of these transducers, Ref. 31. Without making too large an error, these zero shifts may then be set equal to zero and may consequently be dropped all together from the augmented system state vector  $\underline{y}$ .

On the other hand, if the zero shifts are not to be neglected a priori, it cannot be warranted in advance that estimates can actually be derived from the available sets of flight test data. One or more of these zero shifts may turn out to be unobservable or "nearly" unobservable. The a priori accuracy, expressed by the relevant diagonal elements of the initial variance matrix  $P(0|0)$  will in those cases not - or hardly improve after processing the available flight test measurements. This implies that such zero shifts may as well be set equal to zero and consequently be dropped from the augmented system state  $\underline{y}(t)$ . From Eqs. (3.49) through (3.55) the observability of the components of  $\underline{y}(t)$  and consequently of  $\underline{x}(t)$  may be seen to depend on the shape of the nonsteady manoeuvre flown.

The observability of the elements of  $\underline{y}$  also depends on the measurement configuration i.e. the number and type of the elements of the observation vector  $\underline{m}$ . In the present experiments on simulated flight test data for example, no measurements of geographical position were included in  $\underline{m}$ . This means that  $x_E$  and  $y_E$  are unobservable and should therefore not be included in the augmented state vector  $\underline{y}$ .

In future publications the relation between observability of the augmented state vector and the measurement configuration and shape of the nonsteady flight test manoeuvre will be covered in more detail.

In practical applications, a sideslip vane calibration is usually not a priori available and thus the sideslip correction factor  $C_{\beta}$  has to be estimated as an extra element of the augmented state vector  $\underline{y}$ .

The input vector of the simulation experiment was as defined in Eq. (3.20):

$$\underline{u}_m = \text{col} [A_{xB_m}, A_{yB_m}, A_{zB_m}, p_{B_m}, q_{B_m}, r_{B_m}] \quad (5.51)$$

and the output signal as defined in Eq. (3.26):

$$\underline{m}_m = \text{col} [v_m, \Delta h_m, \beta_{v_m}] \quad (5.52)$$

The elements of the variance matrices  $W$  and  $Q$ , which are in practical applications to be specified a priori were in the present simulation experiment not set equal to the measurement error statistics of the simulation, as these measurement error statistics are seldom exactly known in practice. In the present case  $W$  and  $Q$  were assumed to be diagonal and the diagonal elements were specified rather conservatively as shown in Table 6.

### 5.3.1.2. Results of the simulation experiment

In the present simulation experiment the "advanced" algorithm for the calculation of the initial condition was used as described in 5.2. By definition the elements of  $\hat{\underline{y}}(0|0)$  are set equal to zero. By processing the measurements generated during the first 3 seconds of simulated steady straight flight, the estimated magnitudes of the elements of  $\underline{y}(0)$  were obtained as listed in Table 4. The initial condition algorithm provides also estimates of the accuracy of those elements of  $\hat{\underline{y}}(0|0)$  corresponding to the components of the state vector  $\underline{x}$  as described in 5.2. The accuracy of the elements of  $\hat{\underline{y}}(0|0)$  representing the zero shifts  $\underline{\lambda}$  were deduced from a set of laboratory instrumentation calibrations. The magnitude of the initial error variance of  $\hat{C}_{\beta}(0|0)$  has been specified conservatively. The resulting r.m.s. magnitudes are listed in Table 4 in the column  $\sigma_{\hat{\underline{y}}(0|0)}$  and the corresponding variances are assigned to the diagonal elements of the variance matrix  $P(0|0)$ . The off-diagonal elements of  $P(0|0)$  are set equal to zero.

From the simulation experiments it followed that not all of the elements of the augmented state vector, as defined in the previous section, could be estimated from the available simulated flight test data. This remark holds for  $\lambda_x, \lambda_y$  and  $\lambda_r$ .

Fig. 14 exhibits the unobservability of  $\lambda_y$ . The apriori variance of  $\hat{\lambda}_y(0|0)$  was set equal to  $(0.01)^2 \text{ m}^2/\text{s}^4$ , see Table 4.

It follows from Fig. 14 that the r.m.s. error magnitude and henceforth the variance of  $\hat{\lambda}_y(k|k)$  does not decrease as a function of time. This implies that  $\lambda_y$  can be dropped from the augmented state vector  $\underline{Y}$ . Similar conclusions could be drawn with respect to the estimation of  $\lambda_x$ . Fig. 15 represents a counter example of an experiment where it was assumed that the yaw angle  $\psi$  could be measured. Therefore  $\psi$  was considered as a component of the output signal  $\underline{M}_m$ :

$$\underline{M}_m = \text{col} [v_m, \Delta h_m, \beta_{v_m}, \psi_m] \quad (5.53)$$

In this experiment the zero shift of the yaw rate gyro  $\lambda_r$  (its simulated magnitude set equal to zero, Table 4) could be estimated accurately as illustrated in Fig. 15. The variance of  $\hat{\lambda}_r(k|k)$  decreases as a function of the number of observations processed.

In the actual 1978 "Beaver" flight test program the yaw angle transducer turned out to be unreliable. Considerable measurement errors occurred during the nonsteady asymmetric sections of the flight test manoeuvre. The recorded yaw angle measurements were therefore disregarded. The output signal observation vector was thus reduced to:

$$\underline{M} = \text{col} [v_m, \Delta h_m, \beta_{v_m}] \quad (5.54)$$

Processing this output signal,  $\lambda_r$  could no longer be estimated and was consequently dropped from  $\underline{Y}$ .

The resulting augmented state vector  $\underline{Y}$  can be written as:

$$\underline{Y} = \text{col} [v_{xB}, v_{yB}, v_{zB}, \psi, \theta, \varphi, z_E, \lambda_z, \lambda_p, \lambda_q, C_{si}] \quad (5.55)$$

As pointed out in the previous subsection, the sidewash correction factor is unknown and is therefore to be estimated.

The result of the Kalman filter algorithm obtained, estimating the zero shifts  $\lambda_z$ ,  $\lambda_q$  and  $\lambda_p$  and the sidewash correction factor  $C_{si}$  are shown in Figs. 16 and 17. Some results of the Kalman smoothing algorithm are added as an illustration in Figs. 18, 19 and 20. In these figures the smoothed estimates of the elements of the output signal  $\underline{M}$  are presented which can be derived from the smoothed estimate of  $\underline{Y}$  via Eq. (3.23), (3.24) and (3.25). The error covariance matrix  $P_M(k|n)$  of  $\underline{M}(k|n)$  can be calculated from the error covariance matrix  $P(k|n)$ , generated by the Kalman fixed interval smoothing procedure, according to:

$$P_M(k|n) = C(k) P(k|n) C^T(k) \quad (5.56)$$

The time histories of the diagonal elements of  $P_M(k|n)$  are also presented in Figs. 18, 19 and 20. Finally the smoother residuals defined as:

$$\hat{m}(k|n) = \underline{M}_m(k) - \hat{\underline{M}}(k|n) \quad (5.57)$$

are presented. Because the error of  $\hat{\underline{M}}(k|n)$  is small compared to the measurement error in  $\underline{M}_m(k)$  these residuals are almost identical to the simulated measurement errors in  $\underline{M}_m(k)$ .

With respect to the simulation experiment and actual flight test measurements it should be remarked that the stationarity of the measurement error statistics, as assumed in the simulation of the flight test manoeuvre, is not guaranteed in actual flight test conditions. In particular, experience has shown that especially the barometric measurements become less reliable in nonsteady flight conditions. From an estimation theoretical point of view even more serious is the fact that the barometric measurement errors in nonsteady flight conditions are highly correlated with the elements of the system state vector  $\underline{X}$ . To circumvent the inherent theoretical and practical problems arising from this correlation, the barometric output measurements (i.e.  $v_m$  and  $\Delta h_m$ ), recorded during the highly nonsteady symmetric and asymmetric sections of the flight test manoeuvre, are neglected. This was concluded, from simulation experiments, to result only in a very slight reduction of Kalman smoother estimation accuracy. When no observations are processed at time  $t_k$ , either the observation matrix  $C(k)$  or the gain matrix  $K(k)$  of Eq. (3.187), should be set equal to zero. Eqs. (3.188) and (3.189) then reduce to:

$$\hat{\underline{Y}}(k|k) = \hat{\underline{Y}}(k|k-1) \quad (5.58)$$

$$P(k|k) = P(k|k-1) \quad (5.59)$$

The zero shifts and sidewash factor are assumed constant, see Eq. (3.33). For these quantities Eq. (3.185) reduces to:

$$\hat{y}_1(k|k-1) = \hat{y}_1(k-1|k-1) \quad (5.60)$$

This implies that  $\hat{y}(k|k)$  and  $\hat{y}(k|k-1)$  remain zero, and thus  $\hat{y}(k|k)$  and  $\hat{y}(k|k-1)$  are equal, when no new observations are processed in the Kalman filter, see Eq. (3.188). The stationarity of  $\hat{y}(k|k)$  in for instance Fig. 16, indicates the time intervals of nonsteady symmetric or asymmetric flight.

In Table 7 the smoother residual statistics, resulting after flight path reconstruction, are presented. These results should be compared to the a priori assumed statistics, Table 6, and the statistics of the simulated measurement errors, Table 5, of the output signal.

### 5.3.2. Flight path reconstruction from actual flight test data

The input signal for the actual flight test manoeuvre and for the nominal flight condition as specified in Table 4, was calculated in advance according to the technique described in Ref. 30 and subsequently stored on magnetic tape for reproduction in flight with the aid of the three-axes hydraulic control system, Ref. 29.

To obtain the experimental results to be discussed here, yaw angle measurements were disregarded for reasons stated in the previous subsection, see Eq. (5.53).

In correspondence with the simulation results the zero shifts  $\lambda_x$ ,  $\lambda_y$  and  $\lambda_r$  were unobservable and could consequently be dropped from the augmented state vector; see Eq. (5.55).

Initial state estimation, processing actual flight test measurements, was performed applying the most advanced estimation method discussed in subsection 5.2.

The diagonal elements of the initial covariance matrix  $P(0|0)$ , corresponding to  $\hat{v}_{yB}(0|0)$ ,  $\hat{\lambda}_z(0|0)$ ,  $\hat{\lambda}_x(0|0)$ ,  $\hat{\lambda}_q(0|0)$ ,  $\hat{c}_{si}(0|0)$ , as well as the covariance matrices of the input and output measurement errors  $W$  and  $Q$  were assigned the same magnitudes as specified for the simulation experiment, Table 3 and 6.

Both for the simulation as well as for the analysis of actual flight test measurements, the aircraft was assumed to fly over a flat non-rotating earth.

In Figs. 22 and 23 the Kalman filter estimates of the zero shifts  $\lambda_z$ ,  $\lambda_q$  and  $\lambda_r$  and the sidewash correction factor  $C_{si}$  are presented. In Fig. 22 the intervals where  $\hat{\lambda}(k|k)$  and  $\sigma_{\hat{\lambda}}(k|k)$  remain constant, correspond to the nonsteady symmetric and asymmetric sections of the flight test manoeuvre, where barometric output measurements are neglected as discussed in 5.3.1.2.

In Figs. 24-26 the smoothed estimates are shown of  $V$ ,  $\Delta h$  and  $\beta$ , with the corresponding Kalman smoother residuals. These figures may be compared to the corresponding results of the simulation experiments, Figs. 18-20. Kalman smoother residual statistics are presented in Table 8 and 9. Zero shift estimation results are presented in Table 10.

As mentioned in 5.1., the results of the flight path reconstruction are stored on tape prior to aerodynamic model identification, Table 3.

A most significant result is the angle of attack which, as has been discussed earlier, may readily be computed from the results of the flight path reconstruction, i.e. the smoothed time histories of the components of  $\underline{y}$ . As pointed out in earlier publications, e.g. Ref. 20, the calculation of an accurate time history of the angle of attack constitutes the basis for the derivation of aircraft performance characteristics from measurements in nonsteady manoeuvring flight.

### 5.4. Conclusions

Accurate reconstruction of the aircraft's motions relative to the surrounding airmass is of paramount importance when models for the aircraft's aerodynamics, in terms of polynomial relations, or aircraft performance, stability and control characteristics are to be deduced from measurements in nonsteady or quasi-steady manoeuvring test flights.

This Section in particular addresses the flight path reconstruction problem.

A bird's eye view on the entire nonsteady flight test technique, as developed at the Department of Aerospace Engineering of the Delft University of Technology, has been presented in section 1.

The mathematical models and algorithms used for estimation of the time histories of aircraft state variables from measurements, corrupted with random and constant errors, are discussed in considerable detail in section 3. The flight test instrumentation system used throughout the most recent flight test programs, as well as the procedures applied, to solve the problem of initial state estimation are discussed in the present section.

Some results obtained, processing digitally simulated and actual flight test measurements with the extended Kalman estimation algorithms, are finally presented.

From these results it may be concluded that the angle of pitch, the angle of roll and the flight path angle and subsequently the angle of attack and the angle of sideslip can be estimated with adequate accuracy from the measurements recorded in quasi-steady or nonsteady flight.

A similar conclusion can be drawn from the experimental results, concerning various other components of the augmented state vector  $\underline{y}(t)$ .

It is of prime importance to notice that the angle of attack can be calculated without being measured directly.

The problem of calibrating the angle of attack vane from measurements in steady rectilinear flight and the subsequent problem of correcting the corresponding measurements in nonsteady flight for the effects of aircraft motions on the airflow has thus been effectively circumvented. Except for  $\lambda_x$  and  $\lambda_y$ , the constant bias errors in the inertial measurements could be estimated with sufficient accuracy.

The zero shift of the angle of sideslip vane could not be estimated, as explained in section 5.2., such in contrast to the sidewash correction factor  $C_{si}$ .

Augmentation of the output signal observation vector  $M$  with geographic position measurements may relieve these problems. Processing geographical position measurements in addition to the measurements already incorporated in the output signal observation vector, it may turn out to be possible to accurately estimate windshear as a function of flight altitude.

If no geographical position - or ground velocity measurements are available, processing  $\beta_v$  measurements has been found to be essential for reconstruction of the roll angle  $\phi$  and the angle of sideslip  $\beta$  as a function of time. Analyzing actual flight test measurements it has been observed, that the barometric measurements, recorded during the highly nonsteady symmetric and asymmetric manoeuvring test flight sections, should not be assigned much weight, in order to prevent nonsteady airflow effects on the barometer sensor readings from degrading flight path reconstruction.

Application of the Maximum Likelihood algorithms as discussed in section 3 and the square root information filters have been found to yield similar results, see Ref. 21 and 38. The accuracy or validity of flight path reconstruction results obtained has been extensively proved by the reproducibility of the aerodynamic models and aircraft performance stability and control characteristics derived using the flight path reconstruction, see Refs. 10, 11 and 12.

Problems of flight path reconstruction from nonsteady flight measurements may arise from the fact that the airmass traversed by the aircraft is not in rest relative to the earth, as well as from insufficient observability of the augmented system state variables. In turn, insufficient observability of the state variables and system parameters to be estimated, may result from either imperfect - or incomplete flight test instrumentation.

## 6. AERODYNAMIC MODEL IDENTIFICATION WITH AN INTERACTIVE COMPUTER PROGRAM

### 6.0. Introduction

With the advance of interactive computer graphics in the last few years, a new way of utilizing the tremendous storage capacity and calculation speed of modern computers has arisen.

In the analysis of flight test data, direct conversational communication between user and computer can be advantageous in those cases where new numerical experiments can be scheduled only after the results of previous experiments are completely known. A typical example is the identification of the aerodynamic model where the effects of model extensions or simplifications on the model fit and parameter estimation accuracy have to be evaluated.

In order to close the gap between man and machine a computer program has been developed by the National Aerospace Laboratory for interactive aerodynamic model identification and computer graphics of residuals, model predictions and time histories. The computer program has been named "Processing of dynamic manoeuvre measurements with an Interactive Adaptive System (PIAS)", see Ref. 39. PIAS is based upon the theory of Householder transformations and Givens rotations as described in Part I, Section 4. In this Section PIAS is applied to a typical nonsteady symmetrical flight test manoeuvre with a twinengined jet transport type aircraft mentioned in Section 1. The application is presented only to demonstrate the interactive aspect and the flexibility of the computer program. Prior to aerodynamic model identification with PIAS, the flight path has been reconstructed according to the theory as developed in Section 3. A modified form of the Kalman Filtering and Smoothing algorithm (the square root information version) has been applied in this case, see Refs. 31 and 38.

### 6.1. Flight test method

The flight test program with the twin engined transport jet aircraft was devoted mainly to evaluate the merits of performance measurements in quasi-steady flight conditions. However, for the purpose of aerodynamic model identification, several nonsteady symmetrical manoeuvres were also executed. Analysis of the measurements of these nonsteady manoeuvres with PIAS is the subject of the following subsections.

The nonsteady symmetrical manoeuvres all started from a condition of steady horizontal flight. Subsequently the aircraft was excited by means of the elevator control. An optimal test signal (see Fig. 27) was implemented manually. The test pilots were able to reproduce these signals rather accurately in flight because of prior training on the moving base flight simulator of the National Aerospace Laboratory.

### 6.2. Statement of the problem

Development of an accurate mathematical model is essential for the evaluation of flying and handling qualities, the design of automatic flight control systems as well as for flight simulation. Two groups of engineers are involved in identification of aerodynamic models from flight test measurements i.e. mathematicians and flight dynamicists. In PIAS it has been attempted to optimize the final result by creating a computer program flexible enough for the flight dynamicist not to be troubled in his analyses by too many mathematical problems and thus to be able to concentrate fully on the physical interpretation of the results.

Obviously, the flight dynamicist still has to have some knowledge of the mathematical background of the program.

### 6.3. Aerodynamic model identification

The variables (time histories) used in the aerodynamic model identification procedure are the result of the flight path reconstruction as described in Sections 3 and 5.

In the present example it is assumed that precise measurements could be made of engine nett thrust  $T_N$ . Prior to model identification the contribution of  $T_N$  to the dimensionless aerodynamic forces  $C_{XB}$  and  $C_{ZB}$  and the dimensionless aerodynamic moment  $C_{MB}$  is subtracted according to:



$$C_{XB}^* = C_{XB} - \frac{T_N}{\frac{1}{2}\rho V^2 S} \cos i_p \quad (6.1)$$

$$C_{ZB}^* = C_{ZB} - \frac{T_N}{\frac{1}{2}\rho V^2 S} \sin i_p \quad (6.2)$$

$$C_{mB}^* = C_{mB} - \frac{T_N}{\frac{1}{2}\rho V^2 S} \frac{a}{\bar{c}} \quad (6.3)$$

For the subcritical flight region the following aerodynamic model is postulated:

$$C_{XB}^* = C_{X0} + C_{X\alpha} \alpha + C_{X\alpha^2} \alpha^2 + C_{X\dot{\alpha}} \frac{\dot{\alpha}\bar{c}}{V} + C_{X\dot{q}} \frac{\dot{q}\bar{c}}{V} + C_{X\delta_h} \delta_h + C_{X\delta_e} \delta_e + \\ + C_{XM} M + C_{X\alpha M} \alpha M + C_{XM^2} M^2 \quad (6.4)$$

$$C_{ZB}^* = C_{Z0} + C_{Z\alpha} \alpha + C_{Z\alpha^2} \alpha^2 + C_{Z\dot{\alpha}} \frac{\dot{\alpha}\bar{c}}{V} + C_{Z\dot{q}} \frac{\dot{q}\bar{c}}{V} + C_{Z\delta_h} \delta_h + C_{Z\delta_e} \delta_e + \\ + C_{ZM} M + C_{Z\alpha M} \alpha M + C_{ZM^2} M^2 \quad (6.5)$$

$$C_{mB}^* = C_{m0} + C_{m\alpha} \alpha + C_{m\alpha^2} \alpha^2 + C_{m\dot{\alpha}} \frac{\dot{\alpha}\bar{c}}{V} + C_{m\dot{q}} \frac{\dot{q}\bar{c}}{V} + C_{m\delta_h} \delta_h + C_{m\delta_e} \delta_e + \\ + C_{mM} M + C_{m\alpha M} \alpha M + C_{mM^2} M^2 \quad (6.6)$$

For the sake of notational simplicity the index B, referring to the body fixed reference frame  $F_B$  in the aerodynamic derivatives, has been dropped. Consequently,  $C_{X\alpha}$  for example should be interpreted as  $C_{XB\alpha}$ . The effect of the compressibility of the air has been modelled via terms containing  $M$ ,  $\alpha M$  and  $M^2$ , Ref. 19.

It is important to notice that although the aerodynamic model is build up out of both linear and nonlinear terms the model is still linear with respect to the aerodynamic derivatives. Regression theory as developed in Section 4 is therefore applicable for the estimation of the aerodynamic derivatives. In for example Eq. (6.5) the parameter vector  $\underline{a}$  is:

$$\underline{a} = \text{col} [C_{Z0}, C_{Z\alpha}, C_{Z\alpha^2}, C_{Z\dot{\alpha}}, C_{Z\dot{q}}, C_{Z\delta_h}, C_{Z\delta_e}, C_{ZM}, C_{Z\alpha M}, C_{ZM^2}] \quad (6.7)$$

while the row vector  $\underline{x}$  of the independent variables can be written as:

$$\underline{x} = [1, \alpha, \alpha^2, \frac{\dot{\alpha}\bar{c}}{V}, \frac{\dot{q}\bar{c}}{V}, \delta_h, \delta_e, M, \alpha M, M^2] \quad (6.8)$$

#### 6.4. Structure of PIAS

PIAS is based upon the theory for the solution of linear least squares problems as described in Section 4, i.e. Householder transformations and Givens rotations. The resulting algorithms turn out to be very computing time efficient.

The program may be employed in two different modes:

- interactive mode
- batch mode

The interactive mode is useful in the initial phase of the aerodynamic model identification where the structure of the model is yet unknown and where the identifiability of the parameters in the a priori postulated model has to be evaluated. In the second phase the repeatability of the model parameters is investigated via batch processing of measurements of several flight test manoeuvres using the model structure as developed in the first phase. Finally, any discrepancies found during batch processing can be studied in the interactive mode with the aid of its extensive graphical capabilities.

The resulting aerodynamic derivative estimates are subsequently judged on the basis of:

- physical significance and correspondence with windtunnel results,
- estimation accuracy as resulting from processing the measurements of one single flight test manoeuvre and repeatability by comparing the results from several flight test manoeuvres.

During the development of PIAS it has been kept in mind that the main purpose of PIAS is the rapid evaluation of several alternative aerodynamic models. As a consequence, great pains have been taken to assure that the user working with the program will neither experience long delays in waiting for results nor be overwhelmed with useless information.

#### 6.5. Description of a typical run

In this subsection the application of PIAS to the measurements of one flight test manoeuvre is discussed

as an illustration of the interactive aspects of PIAS. The program starts after supplying the flight manoeuvre registration number and the required time interval.

At this point the user has the option to combine measurements data from several different flight test manoeuvres. This can be used to improve the identifiability of some parameters in a given model structure. For example the parameters  $C_{Z_M}$ ,  $C_{Z_{\alpha M}}$  and  $C_{Z_{M^2}}$  can be identified when measurements are combined of manoeuvres performed at different nominal values of the flight Mach number. This possibility is the result of the fact that the data analyzed were first processed by a flight path reconstruction procedure.

The selected flight test manoeuvre started from a condition of steady rectilinear horizontal flight. Next the input signal of Fig. 27 is implemented in the elevator.

The results of the identification of the model of  $C_{Z_B}$ , Eq. (6.2) and (6.5) are presented as an example in Table 11.

It is first attempted to estimate all the derivatives in Eq. (6.5). From Table 11 it may be deduced that though the rank of the matrix  $X$  is equal to the number of parameters to be estimated (10), the resulting estimated values are nevertheless unrealistic.

It is realized then that because the Mach number remained approximately constant in this particular flight path manoeuvre, the derivatives with respect to  $M$ ,  $\alpha M$  and  $M^2$  can in principle not be estimated from these measurements.

In the second solution these derivatives are set equal to zero. The resulting estimated values are still not very realistic. This is true in particular for the estimates of  $C_{Z_q}$  and  $C_{Z_{\dot{\alpha}}}$  which corresponds to the well-known fact that the estimates of these derivatives will be highly correlated. This is also indicated by a simple correlation coefficient of approximately -1 in the matrix of simple correlation coefficients.

In the third solution this ambiguity is solved by substitution of an a priori value of -8 for  $C_{Z_q}$ . The next result still shows unrealistic values for the derivatives  $C_{Z_0}$  and  $C_{Z_{\delta_h}}$ . The underlying cause in this case is the fact that the stabilizer deflection angle  $\delta_h$  remained nominally constant during the flight test manoeuvre. From windtunnel measurements the following relation between  $C_{Z_{\delta_e}}$  and  $C_{Z_{\delta_h}}$  could be deduced:

$$\frac{C_{Z_{\delta_h}}}{C_{Z_{\delta_e}}} = 3 \quad (6.9)$$

This relation is brought in the following form:

$$\begin{aligned} 0 \cdot C_{Z_0} + 0 \cdot C_{Z_q} + 0 \cdot C_{Z_{\alpha}} - 3000 C_{Z_{\delta_e}} + 1000 C_{Z_{\delta_h}} + 0 \cdot C_{Z_{\alpha}} + \\ + 0 \cdot C_{Z_{\alpha^2}} + 0 \cdot C_{Z_M} + 0 \cdot C_{Z_{\alpha M}} + 0 \cdot C_{Z_{M^2}} = 0 \end{aligned} \quad (6.10)$$

and subsequently added as an extra equation.

The PIAS program now applies Givens rotations to the extended design matrix to restore the upper triangular form as described in Subsection 4.2.2. By substitution of 3000 and 1000 in Eq. (6.10) instead of 3 and 1 this equation is heavily weighted in the solution of the resulting least squares problem. The resulting 4th solution seems satisfactory and the square roots of the diagonal elements of the parameter covariance matrix and the matrix of simple correlation coefficients confirm this impression.

Finally residual statistics are printed out and a plot is made of the residual time history, Fig. 28.

## 6.6. Conclusions

After the reconstruction of the aircraft's flight path, the aerodynamic model identification problem can be formulated as a linear least squares problem. This permits the application of powerful numerical techniques for the calculation of parameter estimates as described in Section 4.

The resulting algorithms turn out to be very computer time efficient, which paves the way for the development of an interactive identification computer program. Combined with extensive computer graphics facilities, this program allows the analyst to rapidly evaluate alternative model structures on a few selected measurements.

As a result of the flight test data analysis procedure described in this lecture i.e. via flight path reconstruction, the possibility exists to combine measurement data from several different flight test manoeuvres for the purpose of aerodynamic model identification.

The batch mode of the program allows the routine analysis of nonsteady flight test manoeuvres for a given structural form of the aerodynamic model. These results are used to determine the parameter values and associated confidence levels on an ensemble basis.

## 7. CONCLUDING REMARKS

In part I of this lecture theoretical aspects and in part II some experimental results are presented of a flight test method for nonlinear aerodynamic model identification.

Typical aspects of the flight test method are the application of high accuracy instrumentation systems and

flight path reconstruction.

The goal of the flight test technique discussed, is the derivation of aircraft performance, stability and control characteristics from measurements in nonsteady and quasi-steady (accelerated) flight conditions. Aerodynamic model identification from these measurements plays a central role in the derivation of all characteristics of interest from the recorded flight test data.

After aerodynamic model identification, the stability and control derivatives can be derived in a straightforward manner by linearization. As described in Ref. 19, performance characteristics related to steady flight conditions, such as rate of climb versus airspeed, the polar drag curve, and excess thrust versus airspeed may be deduced from measurements in quasi-steady flight, applying so-called correction methods. In these methods the estimated aerodynamic model parameters are essential. By correction of measurements in nonsteady to steady flight conditions several control characteristics such as elevator angle versus normal acceleration and excess thrust versus normal acceleration in horizontal manoeuvring flight can be derived.

As has been discussed in Section 4 and 6 linear least squares theory can be applied to the aerodynamic model identification problem provided that the aircraft's flight path has been reconstructed a priori, according to the techniques discussed in Section 3 and 5. The resulting algorithms are very computer-time efficient and consequently pave the way for interactive aerodynamic model identification as described in Section 6. An important aspect of the aerodynamic model identification procedure is the freedom the experimentalist has in skipping data points of a particular flight test manoeuvre or combining data points from different flight test manoeuvres.

The flight test method has been applied to several flight test programs in both symmetrical and asymmetrical nonsteady flight conditions. Different aircraft have been used for these flight test programs i.e. a low speed single propeller driven aircraft, a high subsonic jet propelled aircraft and a twin jet engined transport aircraft.

The results discussed in this paper and elsewhere, see Ref. 19, confirmed the applicability of the nonsteady flight test technique to a wide variety of flight test problems. It should be noticed however that this technique has not yet been applied to flight testing of large, highly flexible or supersonic aircraft.

Application of the nonsteady flight test technique to these types of aircraft will certainly require additional research programmes, aimed at the development of adequate instrumentation systems and the synthesis of extended transsonic/supersonic aerodynamic models as well as aero elastic models. Benefits gained by application of the nonsteady flight test techniques are amongst others a reduction in flight test time required for performance as well as stability and control testing and more accurate results.

## 8. REFERENCES

1. B. Etkin: "Dynamics of atmospheric flight", John Wiley and Sons, Inc., New York, London, Sydney, Toronto, 1971.
2. O.H. Gerlach: "Determination of performance and stability parameters from nonsteady flight test maneuvers" Society of Automotive Engineering, Inc., National Business Aircraft Meeting, Wichita, Kansas, SAE Paper no. 700236, 1970.
3. O.H. Gerlach: "Analyse van een mogelijke methode voor het meten van prestaties en stabiliteits- en besturingseigenschappen van een vliegtuig in niet-stationaire, symmetrische vluchten" (in Dutch with summary in English), Delft University of Technology, Department of Aerospace Engineering, Delft, Report VTH-117, 1964.
4. O.H. Gerlach: "The determination of stability derivatives and performance characteristics from dynamic maneuvers", AGARD Conference Proceedings, no. 85, 1971 (VTH-163).
5. R.D. Grove, R.L. Bowles, S.C. Mayhew: "A procedure for estimating stability and control parameters from flight test data by using Maximum Likelihood Methods employing a real time digital system", NASA TN D-6735.
6. R.J.A.W. Hosman: "A method to derive angle of pitch, flight-path angle and angle of attack from measurements in nonsteady flight", Delft University of Technology, Department of Aerospace Engineering, Delft, Report VTH-156, 1971.
7. R.J.A.W. Hosman: "Advanced flight test instrumentation: design and calibration", AGARD Conference Proceedings, no. 172, 1974.
8. Hussenot: "Méthodes nouvelles d'essais en vol", Technique et Science Aeronautique, Vol. 6, pp. 38-49, 1950.
9. Anon.: "Methods of testing at constant attitude", ICAO Circular 16-AN/13, 1951.
10. H.L. Jonkers: "Application of the Kalman filter to flight path reconstruction from flight test data including estimation of instrumental bias error corrections", Delft University of Technology, Department of Aerospace Engineering, Delft, Report VTH-162, 1976.
11. H.L. Jonkers, J.A. Mulder: "Accuracy limits in nonsteady flight testing", the Tenth Congress of the International Council of the Aeronautical Sciences, ICAS Paper no. 76-46, Ottawa, Oct. 1976.
12. H.L. Jonkers, J.A. Mulder: "New developments and accuracy limits in aircraft flight testing", AIAA

Aircraft Systems and Technology Meeting, Dallas, Texas, Sept. 1976, AIAA Paper no. 76-897.

13. R.E. Kalman, R.S. Bucy: "New results in linear filtering and prediction theory", transactions ASME, Series D, Journal of basic engineering, Vol. 63, pp. 95-107, 1961.
14. V. Klein, J.R. Schiess: "Compatibility check of measured aircraft responses using kinematic equations and extended Kalman filter", NASA TN D-8514, Langley Research Center, Hampton, 1977.
15. H.B. Klopfenstein: "Obtaining airplane-drag data from nonsteady flight", AIAA Paper no. 65-211, 1965.
16. M.K. Gupta, R.K. Mehra: "Computational aspect of Maximum Likelihood Estimation and reduction in sensitivity function calculations, IEEE Transactions on Automatic Control, Vol. AC19, no. 6, December 1974.
17. J.A. Mulder: "Aircraft performance measurements in nonsteady flights", Proceedings 3rd IFAC Symposium on "Identification and system parameter estimation", Delft-The Hague, 1973.
18. J.A. Mulder: "Estimation of thrust and drag in nonsteady flight", Proceedings 4th IFAC Symposium on "Identification and system parameter estimation", Tbilisi, USSR, September 1976.
19. J.A. Mulder: "Estimation of drag and thrust of jet-propelled aircraft by nonsteady flight test maneuvers", AGARD FMP Symposium on Flight Test Techniques, Porz-Wahn, October 1976.
20. J.A. Mulder, R.J.A.W. Hosman: "The application of high accuracy instrumentation techniques to aircraft flight testing", Shell Aviation News, no. 425, 1974.
21. J.A. Mulder: "Estimation of the aircraft state in nonsteady flight", Methods for aircraft state and parameter identification, AGARD CP-172, May 1975.
22. A.P. Sage, J.L. Melsa: "Estimation theory with application to communications and control", McGraw-Hill, New York, 1971.
23. H.L. Jonkers, J.A. Mulder, K. van Woerkom: "Measurements in nonsteady flight: Instrumentation and analysis", Proceedings of the 7th International Aerospace Instrumentation Symposium, Cranfield, 1972.
24. N.K. Gupta, W.E. Hall: "Advanced methods for model structure determination from test data", Journal of Guidance and Control, May-June 1978.
25. C.L. Lawson, R.J. Hanson: "Solving least squares problems", Prentice-Hall, 1974.
26. J.H. Breeman, K. van Woerkom: "Aspects of flight test instrumentation", AGARD Lecture Series No. 104 on Parameter Identification, October 1979.
27. K. van Woerkom: "Design and evaluation of an instrumentation system for measurements in nonsteady symmetrical flight conditions with the Hawker Hunter Mk VII", Delft University of Technology, Department of Aerospace Engineering, Delft, The Netherlands, to be published.
28. K. van Woerkom: "The instrumentation system for measurements in nonsteady symmetrical and asymmetrical flight conditions with the De Havilland DHC-2 "Beaver"", Delft University of Technology, Department of Aerospace Engineering, Delft, The Netherlands, to be published.
29. H.C. Garretson, III: "Beaver aircraft parameter identification - Technical preparations and preliminary results", DFVLR-Mitt. 78-01, Deutsche Forschungs- und Versuchsanstalt für Luft- und Raumfahrt, Braunschweig, Juli 1978.
30. J.A. Mulder: "A practical method for the calculation of optimal test signals", Delft University of Technology, Department of Aerospace Engineering, Delft, The Netherlands, to be published.
31. J.H. Breeman, J.L. Simons: "Evaluation of a method to extract performance data from dynamic maneuvers for a jet transport aircraft", 11th Congress of the International Council of the Aeronautical Sciences, Lissabon, September 1978.
32. J.J. Bierman: "Factorization methods for discrete sequential estimation", Academic Press, 1977.
33. D.E. Stepner, R.K. Mehra: "Maximum Likelihood identification and optimal input design for identifying aircraft stability and control derivatives", NASA CR-2200, March 1973.
34. S.L. Fagin: "Recursive linear regression theory, optimal filter theory and error analysis of optimal systems", IEEE International Convention Record, Part I, Session 30, 1964.
35. Y.C. Ho: "Introduction to probability, random process and estimation theory with aerospace applications". AIAA Recorded Lecture Series.
36. R.C. Wingrove: "Applications of a technique for estimating aircraft states from recorded flight test data", AIAA paper No. 72-965.
37. J.J. Horsten, H.L. Jonkers, J.A. Mulder: "Flight path reconstruction in the context of nonsteady flight testing", Report LR-280, Delft University of Technology, May 1979.
38. M. van der Wil't: "Flight-path reconstruction of symmetric unsteady flights", NLR TR 76133 U, National Aerospace Laboratory NLR, The Netherlands, 1976.

39. J. Doekes, J.L. Simons: "Description of program PIAS (Processing of dynamic manoeuvre measurements with an Interactive Addaptive System)", NLR Memorandum WN-73-006, National Aerospace Laboratory, NLR, The Netherlands, 1978.

APPENDIX AA. THE AIRCRAFT'S EQUATIONS OF MOTION IN THE AIRCRAFT'S BODY FRAME OF REFERENCE  $F_B$ A.0. Introduction

In this appendix the nonlinear differential equations describing six degree of freedom motions of a rigid aircraft will be derived (see Ref. 1).

The aircraft will be considered flying over a spherical rotating earth. The magnitude describing the aircraft's trajectory will be computed in the aircraft's body frame of reference  $F_B$ .

A.1. Acceleration in an arbitrarily moving frame  $F_M$ 

Consider an arbitrarily moving reference frame  $F_M(O_M X_M Y_M Z_M)$  with an angular velocity  $\tilde{\omega}_I^M$  in the inertial reference frame  $F_I$  (see Fig. A-1).

Where the matrix  $\tilde{\omega}_I^M$  is composed out of absolute angular velocities  $F_M$  (superscript M) along the axis of  $F_I$  (subscript I).

The position of a point P of  $F_M$  relative to  $F_I$  is:

$$\underline{r}_I = \underline{r}_{OI}^M + \underline{r}_I' = \underline{r}_{OI}^M + L_{IM} \underline{r}_M' \quad (A-1)$$

In which the matrix  $L_{IM}$  denotes the transformation matrix from  $F_M$  into  $F_I$ .  
The velocity and acceleration of P relative to  $F_I$  follows from:

$$\dot{\underline{r}}_I = \dot{\underline{r}}_{OI}^M + \dot{L}_{IM} \underline{r}_M' + L_{IM} \dot{\underline{r}}_M' \quad (A-2)$$

$$\ddot{\underline{r}}_I = \ddot{\underline{r}}_{OI}^M + \dot{L}_{IM} \underline{r}_M' + 2\dot{L}_{IM} \dot{\underline{r}}_M' + L_{IM} \ddot{\underline{r}}_M' \quad (A-3)$$

The components of the acceleration of P relative to  $F_I$  in  $F_M$  follow from:

$$\begin{aligned} \underline{a}_M = \ddot{\underline{r}}_M &= L_{MI} \ddot{\underline{r}}_I \\ &= L_{MI} \ddot{\underline{r}}_{OI}^M + L_{MI} \dot{L}_{IM} \underline{r}_M' + 2L_{MI} \dot{L}_{IM} \dot{\underline{r}}_M' + L_{MI} L_{IM} \ddot{\underline{r}}_M' \end{aligned} \quad (A-4)$$

From the rules of transforming derivatives it follows, by substitution of  $\dot{L}_{IM} = \tilde{\omega}_I^M L_{IM}$ , that:

$$\begin{aligned} \underline{a}_M &= \ddot{\underline{r}}_{OI}^M + L_{MI} \frac{d}{dt} \left( \tilde{\omega}_I^M L_{IM} \right) \underline{r}_M' + 2L_{MI} \left( \tilde{\omega}_I^M L_{IM} \right) \dot{\underline{r}}_M' + \ddot{\underline{r}}_M' \\ &= \ddot{\underline{r}}_{OI}^M + L_{MI} \left\{ \tilde{\omega}_I^M L_{IM} + \tilde{\omega}_I^M \left( \tilde{\omega}_I^M L_{IM} \right) \right\} \underline{r}_M' + 2\tilde{\omega}_I^M \dot{\underline{r}}_M' + \ddot{\underline{r}}_M' \\ &= \ddot{\underline{r}}_{OI}^M + \tilde{\omega}_I^M \underline{r}_M' + \tilde{\omega}_I^M \tilde{\omega}_I^M \underline{r}_M' + 2\tilde{\omega}_I^M \dot{\underline{r}}_M' + \ddot{\underline{r}}_M' \end{aligned} \quad (A-5)$$

The total inertial acceleration of P consists of the following parts:

- $\ddot{\underline{r}}_{OI}^M$  : the acceleration of the origin of the moving frame  $F_M$
- $\tilde{\omega}_I^M \underline{r}_M'$  : the "tangential" acceleration owing to rotational acceleration of the frame  $F_M$
- $\tilde{\omega}_I^M \tilde{\omega}_I^M \underline{r}_M'$  : the centripetal acceleration
- $2\tilde{\omega}_I^M \dot{\underline{r}}_M'$  : the Coriolis acceleration
- $\ddot{\underline{r}}_M'$  : the acceleration of P relative to the moving frame

A.2. Acceleration in the earth fixed reference frame  $F_E$ 

Now consider the acceleration in the earth fixed reference frame  $F_E$  relative to  $F_I$ .  
From Equation (A-5) it follows that:

$$\underline{a}_E = \ddot{\underline{r}}_{OE}^E + \tilde{\omega}_E^E \underline{r}_E' + \tilde{\omega}_E^E \tilde{\omega}_E^E \underline{r}_E' + 2\tilde{\omega}_E^E \dot{\underline{r}}_E' + \ddot{\underline{r}}_E' \quad (A-6)$$

The acceleration of the origin of  $F_E$ ,  $\underline{\ddot{a}}_{OE}^E$  can be written as:

$$\begin{aligned}\underline{\ddot{a}}_{OE}^E &= \underline{\dot{r}}_{OE}^E = L_{EI} \underline{\dot{r}}_{OI}^E = L_{EI} \underline{\dot{v}}_{OI}^E = L_{EI} \frac{d}{dt} \left( L_{IE} \underline{v}_{OE}^E \right) \\ &= L_{EI} \left( \dot{L}_{IE} \underline{v}_{OE}^E + L_{IE} \underline{\dot{v}}_{OE}^E \right) \\ &= L_{EI} \tilde{\omega}_I^E L_{IE} \underline{v}_{OE}^E + L_{EI} L_{IE} \underline{\dot{v}}_{OE}^E \\ &= \tilde{\omega}_E^E \underline{v}_{OE}^E + \underline{\dot{v}}_{OE}^E\end{aligned}\quad (A-7)$$

It is assumed that the angular rotation of the earth is constant and that its translation relative to  $F_I$  is rectilinear at constant velocity, so:

$$\tilde{\omega}_E^E = 0 \quad (A-8)$$

and:

$$\underline{\dot{v}}_{OE}^E = 0 \quad (A-9)$$

Substitution of Eq. (A-9) into Eq. (A-7) gives:

$$\underline{\ddot{a}}_{OE}^E = \tilde{\omega}_E^E \underline{v}_{OE}^E = \tilde{\omega}_E^E \left( \underline{\dot{r}}_{OE}^E + \tilde{\omega}_E^E \underline{r}_{OE}^E \right) \quad (A-10)$$

As  $\underline{r}_{OE}^E$  is fixed relative to  $F_E$ , Eq. (A-10) can be rewritten using:

$$\underline{\dot{r}}_{OE}^E = 0 \quad (A-11)$$

Now:

$$\underline{\ddot{a}}_{OE}^E = \tilde{\omega}_E^E \tilde{\omega}_E^E \underline{r}_{OE}^E \quad (A-12)$$

Substitution of Eq. (A-8) and Eq. (A-12) into Eq. (A-6) gives:

$$\underline{\ddot{a}}_E = \underline{\dot{r}}_E^E + 2\tilde{\omega}_E^E \underline{\dot{r}}_E^E + \tilde{\omega}_E^E \tilde{\omega}_E^E \left( \underline{r}_{OE}^E + \underline{r}_E^E \right) \quad (A-13)$$

As  $\underline{\dot{r}}_E^E = \underline{v}_E$  and  $\left( \underline{r}_{OE}^E + \underline{r}_E^E \right) \approx \underline{R}_E^E$  it follows that:

$$\underline{\ddot{a}}_E = \underline{\dot{v}}_E + 2\tilde{\omega}_E^E \underline{v}_E + \tilde{\omega}_E^E \tilde{\omega}_E^E \underline{R}_E^E \quad (A-14)$$

### A.3. The aircraft's acceleration in the aircraft's body frame of reference $F_B$

The acceleration components in  $F_B$  follows from Eq. (A-14):

$$\begin{aligned}\underline{\ddot{a}}_B &= L_{BE} \underline{\ddot{a}}_E = L_{BE} \underline{\dot{v}}_E + 2L_{BE} \tilde{\omega}_E^E \underline{v}_E + L_{BE} \tilde{\omega}_E^E \tilde{\omega}_E^E \underline{R}_E^E \\ &= L_{BE} \underline{\dot{v}}_E + 2 \left( L_{BE} \tilde{\omega}_E^E L_{EB} \right) L_{BE} \underline{v}_E + \left( L_{BE} \tilde{\omega}_E^E L_{EB} \right) \left( L_{BE} \tilde{\omega}_E^E L_{EB} \right) L_{BE} \underline{R}_E^E \\ &= L_{BE} \underline{\dot{v}}_E + 2\tilde{\omega}_B^E \underline{v}_B + \tilde{\omega}_B^E \tilde{\omega}_B^E \underline{R}_B^E\end{aligned}$$

Using the rules of transformation of the derivative of a vector (see ref. 1):

$$\underline{\ddot{a}}_B = \underline{\dot{v}}_B + \tilde{\omega}_B^E \underline{v}_B + 2\tilde{\omega}_B^E \underline{v}_B + \tilde{\omega}_B^E \tilde{\omega}_B^E \underline{R}_B^E \quad (A-15)$$

where:

$$\tilde{\omega}_B = \tilde{\omega}_B^B - \tilde{\omega}_B^E \quad (A-16)$$

Combination of Eqs. (A-15) and (A-16) gives for the aircraft's acceleration  $\dot{V}_B$  relative to  $F_B$ :

$$\dot{V}_B = \underline{a}_B - \tilde{\omega}_B^B V_B - \tilde{\omega}_B^E V_B - \tilde{\omega}_B^E \tilde{\omega}_B^E R_B^E \quad (A-17)$$

The acceleration components  $\underline{a}_B$  in  $F_B$  relative to  $F_I$  can be derived from the force vector  $\underline{f}_B$  which consists of two parts, the aerodynamic reaction (including propulsive force)  $\underline{F}$  and the weight  $m \underline{g}_B$ , i.e.:

$$\underline{f}_B = m \underline{a}_B = \underline{F} + m \underline{g}_B \quad (A-18)$$

where:

$$\underline{F} = \text{col } [x_B, y_B, z_B]$$

and:

$$\underline{g}_B = L_{BV} \underline{g}_V = L_{BV} \begin{bmatrix} 0 \\ 0 \\ g_h \end{bmatrix} \quad (A-20)$$

Using the definition for the specific aerodynamic forces:

$$\underline{A}_B = \frac{\underline{F}}{m} \quad (A-21)$$

and the transformation matrix:

$$L_{BV} = \begin{bmatrix} \cos \theta \cos \psi & \cos \theta \sin \psi & -\sin \theta \\ \sin \varphi \sin \theta \cos \psi - \cos \varphi \sin \psi & \sin \psi \sin \theta \sin \psi + \cos \varphi \cos \psi & \sin \varphi \cos \theta \\ \cos \varphi \sin \theta \cos \psi + \sin \varphi \sin \psi & \cos \varphi \sin \theta \sin \psi - \sin \varphi \cos \psi & \cos \varphi \cos \theta \end{bmatrix} \quad (A-22)$$

The components of  $\underline{a}_B$  can be expressed as:

$$a_{x_B} = A_{x_B} - g_h \sin \theta \quad (A-23)$$

$$a_{y_B} = A_{y_B} + g_h \sin \varphi \cos \theta \quad (A-23)$$

$$a_{z_B} = A_{z_B} + g_h \cos \varphi \cos \theta \quad (A-24)$$

It should be noticed that the components of the specific aerodynamic force  $\underline{A}_B$  can be measured, using accelerometers.

The rotation of the aircraft  $\underline{\omega}_B^B$  relative to  $F_B$  is defined as:

$$\underline{\omega}_B^B \triangleq \text{col } [p_B, q_B, r_B] \quad (A-25)$$

The matrix equivalent of this vector can be expressed as:

$$\underline{\omega}_B^B = \begin{bmatrix} 0 & -r_B & q_B \\ r_B & 0 & -p_B \\ -q_B & p_B & 0 \end{bmatrix} \quad (A-26)$$



So the second term in Eq. (A-17) follows from:

$$\underline{\dot{\omega}}_B^E \underline{v}_B = - \begin{bmatrix} -r_B v_{yB} + q_B v_{zB} \\ r_B v_{xB} - p_B v_{zB} \\ -q_B v_{xB} + p_B v_{yB} \end{bmatrix} \quad (A-27)$$

The rotation  $\underline{\omega}_B^E$  of  $F_E$  in  $F_B$  is defined as:

$$\underline{\omega}_B^E \triangleq \text{col } [p_B^E, q_B^E, r_B^E] \quad (A-28)$$

The components of  $\underline{\omega}_B^E$  can be derived using the rotation  $\underline{\omega}_V^E$  in the vehicle carried vertical frame  $F_V$ . This rotation follows from Fig. A-2.

$$\underline{\omega}_V^E = \begin{bmatrix} \cos \lambda \\ 0 \\ -\sin \lambda \end{bmatrix} \omega_E^E \quad (A-29)$$

The earth rotation in the aircraft's body frame of reference  $F_B$  follows from:

$$\underline{\omega}_B^E = L_{BV} \underline{\omega}_V^E = L_{BV} \begin{bmatrix} \cos \lambda \\ 0 \\ -\sin \lambda \end{bmatrix} \omega_E^E \quad (A-30)$$

Now:

$$\underline{\omega}_B^E = \begin{bmatrix} p_B^E \\ q_B^E \\ r_B^E \end{bmatrix} = \begin{bmatrix} \cos \theta \cos \psi \cos \lambda + \sin \theta \sin \lambda \\ \sin \varphi \sin \theta \cos \psi \cos \lambda - \cos \varphi \sin \psi \cos \lambda - \sin \varphi \cos \theta \sin \lambda \\ \cos \varphi \sin \theta \cos \psi \cos \lambda + \sin \varphi \sin \psi \cos \lambda + \cos \varphi \cos \theta \sin \lambda \end{bmatrix} \omega_E^E \quad (A-31)$$

Using the matrix equivalent  $\tilde{\omega}_B^E$  of  $\underline{\omega}_B^E$ , see Eq. (A-26), the terms  $\tilde{\omega}_B^E \underline{v}_B$  and  $\tilde{\omega}_B^E \tilde{\omega}_B^E \underline{R}_B^E$  of Eq. (A-17) can be computed.

The radius  $\underline{R}_B^E$  in  $F_B$  can be computed from the radius  $\underline{R}_V^E$  in  $F_V$  according to:

$$\underline{R}_B^E = L_{BV} \underline{R}_V^E = L_{BV} \begin{bmatrix} 0 \\ 0 \\ R^E \end{bmatrix} \quad (A-32)$$

Summarized the components of the aircraft's acceleration  $\underline{\dot{v}}_B$  in  $F_B$ , describing an aircraft moving over a spherical rotating earth, can be expressed as:

$$\dot{v}_{xB} = A_{xB} - g_h \sin \theta + r_B v_{yB} - q_B v_{zB} + f_{x_{cor}} + f_{x_{cen}} \quad (A-33)$$

$$\dot{v}_{yB} = A_{yB} + g_h \cos \theta \sin \varphi - r_B v_{xB} + p_B v_{zB} + f_{y_{cor}} + f_{y_{cen}} \quad (A-34)$$

$$\dot{v}_{zB} = A_{zB} + g_h \cos \theta \cos \varphi + q_B v_{zB} - p_B v_{yB} + f_{z_{cor}} + f_{z_{cen}} \quad (A-35)$$

where:

$$\underline{f}_{cor} = \text{col } [f_{x_{cor}}, f_{y_{cor}}, f_{z_{cor}}] = -\tilde{\omega}_B^E \underline{v}_B \quad (A-36)$$

and:

$$\underline{f}_{\text{cen}} = \text{col} [f_{x_{\text{cen}}}, f_{y_{\text{cen}}}, f_{z_{\text{cen}}}] = -\underline{\omega}_B^E \underline{\omega}_B^E \underline{R}_B^E \quad (\text{A-37})$$

#### A.4. The aircraft's Euler angle rates

The aircraft's rotation  $\underline{\omega}_B$  in  $F_B$  relative to  $F_V$  consists of the aircraft's rotation  $\underline{\omega}_B^B$  of  $F_B$  in  $F_B$  and the rotating  $\underline{\omega}_B^V$  of  $F_V$  in  $F_B$  according to:

$$\underline{\omega}_B = \underline{\omega}_B^B + \underline{\omega}_B^V \quad (\text{A-38})$$

The components P, Q and R of  $\underline{\omega}_B$  are equal to the rotation rates  $p_B$ ,  $q_B$  and  $r_B$  for the flat non-rotating earth.

$$\underline{\omega}_B = \begin{bmatrix} P \\ Q \\ R \end{bmatrix} = \underline{\omega}_B^B = \begin{bmatrix} p_B \\ q_B \\ r_B \end{bmatrix} \quad (\text{A-39})$$

In that case the Euler angle rates  $\dot{\phi}$ ,  $\dot{\theta}$  and  $\dot{\psi}$  can directly be derived from the components  $p_B$ ,  $q_B$  and  $r_B$  of  $\underline{\omega}_B^B$  (see Fig. 1), so:

$$\begin{bmatrix} \dot{\phi} \\ \dot{\theta} \\ \dot{\psi} \end{bmatrix} = \begin{bmatrix} 1 & \sin \phi \tan \theta & \cos \phi \tan \theta \\ 0 & \cos \phi & -\sin \phi \\ 0 & \frac{\sin \phi}{\cos \theta} & \frac{\cos \phi}{\cos \theta} \end{bmatrix} \begin{bmatrix} P \\ Q \\ R \end{bmatrix} = M \begin{bmatrix} p_B \\ q_B \\ r_B \end{bmatrix} \quad (\text{A-40})$$

For the spherical rotating earth this equation should be augmented to include terms for the earth rotation as well as for the translation over a spherical earth. In  $F_V$  the translation over a spherical earth can be expressed as:

$$\underline{\omega}_V^V - \underline{\omega}_V^E = \begin{bmatrix} \dot{\mu} \cos \lambda \\ -\dot{\lambda} \\ -\dot{\mu} \sin \lambda \end{bmatrix} \quad (\text{A-41})$$

Using Eq. (A-29), Eq. (A-41) can be written as:

$$\underline{\omega}_V^V = \begin{bmatrix} \omega^E \cos \lambda \\ 0 \\ -\omega^E \sin \lambda \end{bmatrix} + \begin{bmatrix} \dot{\mu} \cos \lambda \\ -\dot{\lambda} \\ -\dot{\mu} \sin \lambda \end{bmatrix} = \begin{bmatrix} (\omega^E + \dot{\mu}) \cos \lambda \\ -\dot{\lambda} \\ -(\omega^E + \dot{\mu}) \sin \lambda \end{bmatrix} \quad (\text{A-42})$$

The vector  $\underline{\omega}_B^V$  can also be decomposed along the axes of  $F_B$  according to:

$$\underline{\omega}_B^V = L_{BV} \underline{\omega}_V^V \quad (\text{A-43})$$

Now combining Eqs. (A-38) through (A-42) the Euler angle rates for a spherical rotating earth are described by the equations:

$$\begin{bmatrix} \dot{\phi} \\ \dot{\theta} \\ \dot{\psi} \end{bmatrix} = M \begin{bmatrix} p_B \\ q_B \\ r_B \end{bmatrix} - M L_{BV} \begin{bmatrix} (\omega^E + \dot{\mu}) \cos \lambda \\ -\dot{\lambda} \\ -(\omega^E + \dot{\mu}) \sin \lambda \end{bmatrix} \quad (\text{A-44})$$

Now writing:

$$\underline{r}_{\text{spher}} + \underline{r}_{\text{rot}} = -M L_{BV} \begin{bmatrix} (\omega^E + \dot{\mu}) \cos \lambda \\ -\dot{\lambda} \\ -(\omega^E + \dot{\mu}) \sin \lambda \end{bmatrix} \quad (\text{A-45})$$

substitution of Eq. (A-45) into Eq. (A-44) finally yields:

$$\dot{\varphi} = p_B + q_B \sin \varphi \tan \theta + r_B \cos \varphi \tan \theta + r_{x\text{spher}} + r_{x\text{rot}} \quad (\text{A-46})$$

$$\dot{\theta} = q_B \cos \varphi - r_B \sin \varphi + r_{y\text{spher}} + r_{y\text{rot}} \quad (\text{A-47})$$

$$\dot{\psi} = q_B \frac{\sin \varphi}{\cos \theta} + r_B \frac{\cos \varphi}{\cos \theta} + r_{z\text{spher}} + r_{y\text{rot}} \quad (\text{A-48})$$

#### A.5. The aircraft's position

The location of the aircraft relative to the earth is presented in the spherical polar coordinates  $\lambda$ ,  $\mu$  and  $R_E$ . Their rates of change are related to the components of the velocity  $V_V$  in  $V_V$  according to (see Fig. A-2):

$$\begin{bmatrix} \dot{\lambda} \\ \dot{\mu} \\ \dot{R}_E \end{bmatrix} = \begin{bmatrix} \frac{1}{R_E} & 0 & 0 \\ 0 & \frac{1}{R_E \cos \lambda} & 0 \\ 0 & 0 & -1 \end{bmatrix} \underline{V}_V \quad (\text{A-49})$$

Using the velocity components in  $F_B$ , this equation can be rewritten:

$$\begin{bmatrix} \dot{\lambda} \\ \dot{\mu} \\ \dot{R}_E \end{bmatrix} = \begin{bmatrix} \frac{1}{R_E} & 0 & 0 \\ 0 & \frac{1}{R_E \cos \lambda} & 0 \\ 0 & 0 & -1 \end{bmatrix} L_{VB} \underline{V}_B \quad (\text{A-50})$$

#### A.6. Summary of the equations of motion

Summarized, the aircraft's motions over a spherical rotating earth in the aircraft's body frame of reference  $F_B$  are described by the following equations:

$$\dot{V}_{x_B} = A_{x_B} - g_h \sin \theta + r_B V_{y_B} - q_B V_{z_B} + f_{x\text{cor}} + f_{x\text{cen}} \quad (\text{A-51})$$

$$\dot{V}_{y_B} = A_{y_B} + g_h \cos \theta \sin \varphi - r_B V_{x_B} + p_B V_{z_B} + f_{y\text{cor}} + f_{y\text{cen}} \quad (\text{A-52})$$

$$\dot{V}_{z_B} = A_{z_B} + g_h \cos \theta \cos \varphi + q_B V_{x_B} - p_B V_{y_B} + f_{z\text{cor}} + f_{z\text{cen}} \quad (\text{A-53})$$

$$\dot{\varphi} = p_B + q_B \sin \varphi \tan \theta + r_B \cos \varphi \tan \theta + r_{x\text{spher}} + r_{x\text{rot}} \quad (\text{A-54})$$

$$\dot{\theta} = q_B \cos \varphi - r_B \sin \varphi + r_{y\text{spher}} + r_{y\text{rot}} \quad (\text{A-55})$$

$$\dot{\psi} = q_B \frac{\sin \varphi}{\cos \theta} + r_B \frac{\cos \varphi}{\cos \theta} + r_{z\text{spher}} + r_{z\text{rot}} \quad (\text{A-56})$$

$$\dot{\lambda} = \frac{1}{R_E} V_{x_V} \quad (\text{A-57})$$

$$\dot{\mu} = \frac{1}{R_E \cos \lambda} V_{y_V} \quad (\text{A-58})$$

$$\dot{R}_E = -V_{z_V} \quad (\text{A-59})$$

## APPENDIX B

## B. DERIVATION OF THE BATCH REGRESSION ALGORITHM

In this appendix the algorithm for the batch regression will be derived, minimizing the cost function:

$$J_n = \sum_{k=1}^n (\underline{m}(k) - R(k) \hat{\underline{y}})^T Q^{-1} (\underline{m}(k) - R(k) \hat{\underline{y}}) \quad (B-1)$$

$$= \sum_{k=1}^n \underline{P}^T(k) Q^{-1} \underline{P}(k) \quad (B-2)$$

The cost function is minimal for:

$$\begin{aligned} \frac{\partial J_n}{\partial \hat{\underline{y}}} &= \frac{\partial J_n}{\partial \underline{P}(k)} \frac{\partial \underline{P}(k)}{\partial \hat{\underline{y}}} \\ &= \frac{\partial \left( \sum_{k=1}^n \underline{P}^T(k) Q^{-1} \underline{P}(k) \right)}{\partial \underline{P}(k)} \frac{\partial \underline{P}(k)}{\partial \hat{\underline{y}}} \\ &= \sum_{k=1}^n \left\{ 2 \underline{P}^T(k) Q^{-1} \frac{\partial \underline{P}(k)}{\partial \underline{P}(k)} \right\} \frac{\partial \underline{P}(k)}{\partial \hat{\underline{y}}} \end{aligned} \quad (B-3)$$

since  $Q^{-1}$  is symmetric.

Now because of  $\frac{\partial \underline{P}(k)}{\partial \underline{P}(k)} = I$  and using the rule  $\frac{\partial A \underline{x}}{\partial \underline{x}} = A$ :

$$\frac{\partial J_n}{\partial \hat{\underline{y}}} = -2 \sum_{k=1}^n \underline{P}^T(k) Q^{-1} R(k) \quad (B-4)$$

Now:

$$\begin{aligned} \frac{\partial J_n}{\partial \hat{\underline{y}}} &= -2 \sum_{k=1}^n R^T(k) Q^{-1} \underline{P}(k) \\ &= -2 \sum_{k=1}^n R^T(k) Q^{-1} (\underline{m}(k) - R(k) \hat{\underline{y}}) = 0 \end{aligned} \quad (B-5)$$

so:

$$\hat{\underline{y}} = \left( \sum_{k=1}^n R^T(k) Q^{-1} R(k) \right)^{-1} \sum_{k=1}^n R^T(k) Q^{-1} \underline{m}(k) \quad (B-6)$$

Sequence number	Variable	Instrument type	Transducer input range	Calibrated input range	Dimension
1	$A_{x_B}$	Donner 4810	-10 → +10	- 10 → +10	m/sec
2	$A_{y_B}$	Donner 4310	- 5 → + 5	- 5 → + 5	m/sec
3	$A_{z_B}$	Donner 4310/ Q-Flex	-20 → +20	0 → +20	m/sec
4	$P_B$	Honeywell GG87B	-23 → +23	- 20 → +20	°/sec
5	$q_B$	Honeywell GG87B	-23 → +23	- 20 → +20	°/sec
6	$r_B$	Honeywell GG87B	-23 → +23	- 20 → +20	°/sec
7	$\psi$	Sperry Tarsyn 333	0 → 360	0 → 360	°
8	$n$	General Electric	500 → 3000	500 → 2400	rpm
9	$T$	Rosemount 102	-40 → +40	- 30 → +30	K
10	$\delta_e$	CIC lin. potm.	51	- 28 → +23	°
11	$\delta_{a_l}$	CIC lin. potm.	50	- 33 → +17	°
12	$\delta_{a_r}$	CIC lin. potm.	50	- 17 → +33	°
13	$\delta_r$	CIC lin. potm.	50	- 25 → +25	°
14	$\delta_{f_l}$	CIC lin. potm.	58	0 → +58	°
15	$\delta_{f_r}$	CIC lin. potm.	58	0 → +58	°
16	$\delta_{t_e}$	Bourns lin. potm.	44	- 18 → +26	°
17	$\delta_{t_r}$	Bourns lin. potm.	36	- 18 → +18	°
18	$\alpha_v$	Delft Univ. of Techn.	90	- 10 → +30	°
19	$\beta_v$	National Aerospace Lab.	90	- 30 → +30	°
20	$\Delta p_t$	MKS 145	- 4 → +4	0 → +3	kPa
21	$\Delta p_i$	MKS 145	- 4 → +4	- 3 → +3	kPa
22	$q_c$	MKS 145	- 4 → +4	0 → +3	kPa
23	$P_z$	MKS 145	0 → 130	+ 50 → +130	kPa
24	$P_{st}$	MKS 145	0 → 130	+ 50 → +105	kPa
25	DME	KING 705A	0 → 200	0 → 90	nm
26	Tcarb	Standard onboard instrument	-30 → +30	- 30 → +30	K

Description

See Table 2

$\Delta p_i$  static pressure variation defined with respect to static pressure at the start of test flight manoeuvre.

Table 1: List of transducers of the flight test instrumentation system.

Sequence number	Variables	Type	Description
1	$\delta_e$	input	elevator angle (rad)
2	$\delta_r$		rudder angle (rad)
3	$\delta_{a_l}$		port aileron angle (rad)
4	$\delta_{a_r}$		starboard aileron angle (rad)
5	$\delta_{f_l}$		port flap angle (rad)
6	$\delta_{f_r}$		starboard flap angle (rad)
7	$\delta_{t_e}$		elevator trim angle (rad)
8	$\delta_{t_r}$		rudder trim angle (rad)
9	$n$	inertial	engine speed (Hz)
10	$P_z$		engine manifold pressure ( $N/m^2$ )
11	$P^*$		engine power (kW)
12	$T_{carb}$		carburettor temperature ( $^{\circ}K$ )
13	$A_{x_B}$		specific forces along the X-, Y- and Z-axis, of the aircraft's body frame of reference ( $m/s^2$ )
14	$A_{y_B}$		
15	$A_{z_B}$		
16	$p_B$		roll rate (rad/s)
17	$q_B$		pitch rate (rad/s)
18	$r_B$		yaw rate (rad/s)
19	$\dot{p}_B^*$		roll acceleration ( $rad/s^2$ )
20	$\dot{q}_B^*$		pitch acceleration ( $rad/s^2$ )
21	$\dot{r}_B^*$		yaw acceleration ( $rad/s^2$ )
22	$\psi$	wind angle	measured heading (rad)
23	DME		distance measured with respect to DME beacon position (m)
24	$\alpha_v$		angle of attack (rad) measured with vane
25	$\beta_v$	pressure	angle of sideslip (rad) measured with vane
26	$P_{st}$		static pressure ( $N/m^2$ )
27	$M^*$		Mach number
28	$T$		free stream air temperature ( $^{\circ}K$ )
29	$\rho^*$	output	air density ( $kg/m^3$ )
30	$\Delta p_t$		increase in total pressure in propeller slipstream ( $N/m^2$ )
31	$\Delta h^*$		altitude variation defined with respect to initial altitude of test flight manoeuvre (m)
32	$v^*$		airspeed from dynamic pressure (m/s)

\* The quantities marked with an asterisk are not directly measured.

Table 2: Flight path quantities after initial data reduction.

Sequence number	Variables	Type	Description
1	$\delta_e$	input	elevator angle (rad)
2	$\delta_r$		rudder angle (rad)
3	$\delta_{a_l}$		port aileron angle (rad)
4	$\delta_{a_r}$		starboard aileron angle (rad)
5	$\delta_{f_l}$		port flap angle (rad)
6	$\delta_{f_r}$		starboard flap angle (rad)
7	$\delta_{t_e}$		elevator trim angle (rad)
8	$\delta_{t_r}$		rudder trim angle (rad)
9	$n$	inertial	engine speed (Hz)
10	$P_z$		engine manifold pressure ( $N/m^2$ )
11	$P/\rho V^3$		"dimensionless" engine power
12	$A_{x_B} + \lambda_x$		specific forces along X-, Y- and
13	$A_{y_B} + \lambda_y$		Z-axis of the aircraft's body
14	$A_{z_B} + \lambda_z$		frame of reference ( $m/s^2$ )
15	$p_B + \lambda_p$		roll rate (rad/s)
16	$q_B + \lambda_q$		pitch rate (rad/s)
17	$r_B + \lambda_r$		yaw rate (rad/s)
18	$\psi$		estimated true heading (rad)
19	$\theta$		estimated angle of pitch (rad)
20	$\phi$		estimated angle of roll (rad)
21	$C_X$		dimensionless aerodynamic coefficients
22	$C_Y$		
23	$C_Z$		
24	$C_l$		
25	$C_m$		
26	$C_n$		
27	$\alpha_v$	wind angles	vane angle of attack (rad)
28	$\alpha$		estimated angle of attack (rad)
29	$\beta_v$		vane angle of sideslip (rad)
30	$\beta$		estimated angle of sideslip (rad)
31	$\dot{\alpha}$		time derivative of $\alpha$ (rad/s)
32	$\dot{\beta}$		time derivative of $\beta$ (rad/s)
33	$M$	pressure	Mach number
34	$T$		free stream air temperature ( $^{\circ}K$ )
35	$\rho$		air density ( $kg/m^3$ )
36	$\Delta P_t / \rho V^2$		dimensionless increase in total pressure in propeller slipstream ( $N/m^2$ )
37	$\Delta h$	output	estimated altitude variation defined with respect to initial altitude of test flight manoeuvres (m)
38	$V$		estimated airspeed (m/s)
39	$C$		rate of climb (m/s)
40	$\gamma$		flight path angle (rad)
41	$q$		dynamic pressure ( $N/m^2$ )

Table 3: Flight path quantities after flight path reconstruction.

Quantity	$\underline{y}_{sim}(0)$	$\underline{y}(0)$	$\sigma_{\hat{\underline{y}}(0 0)}$	unit
$v_{xB}$	44.55	0.044	0.209	m/s
$v_{yB}$	0.0	0.00009	0.500	m/s
$v_{zB}$	6.35	-0.036	0.030	m/s
$\varphi$	0.0	-0.00006	0.031	rad
$\theta$	0.1315	0.0003	0.0003	rad
$\psi$	0.0	-0.0008	0.007	rad
$\Delta h$	0.0	0.012	0.42	m
$\lambda_x$	0.0	0.0	0.04	m/s <sup>2</sup>
$\lambda_y$	0.0	0.0	0.04	m/s <sup>2</sup>
$\lambda_z$	0.02	0.0	0.039	m/s <sup>2</sup>
$\lambda_p$	0.0	0.0	0.001	rad/s
$\lambda_q$	0.0	0.0	0.001	rad/s
$\lambda_r$	0.0	0.0	0.001	rad/s
$C_{si}$	0.1	0.0	0.1	-
Aircraft configuration		Initial flight condition		
$W = 22418 \text{ N}$ $I_x = 5268 \text{ Nm}^2$ $I_y = 6928 \text{ Nm}^2$ $I_z = 11159 \text{ Nm}^2$ $I_{xz} = 178 \text{ Nm}^2$ $x_{cg} = 0.35 \bar{c}$ $y_{cg} = 0$ $z_{cg} = 0.52 \bar{c}$		$V = 45 \text{ m/s}$ $h = 1828.8 \text{ m}$ $n = 33.33 \text{ Hz}$ $p_z = 77966 \text{ N/m}^2$		

Table 4: Survey of the initial condition for the simulation experiment.

Input signal	$\sigma_{w_i}$	unit
$A_{xB}$	$0.278 \times 10^{-2}$	m/s <sup>2</sup>
$A_{yB}$	$0.137 \times 10^{-2}$	m/s <sup>2</sup>
$A_{zB}$	$0.698 \times 10^{-2}$	m/s <sup>2</sup>
$P_B$	$0.678 \times 10^{-4}$	rad/s
$q_B$	$0.697 \times 10^{-4}$	rad/s
$r_B$	$0.679 \times 10^{-4}$	rad/s
Output signal	$\sigma_{q_i}$	unit
$V$	0.206	m/s
$\Delta h$	0.410	m
$\beta$	$0.685 \times 10^{-2}$	rad

Table 5: Standard deviation of the digitally simulated input and output signal errors.



System state vector:

$$\underline{y} = \text{col} [v_{x_B}, v_{y_B}, v_{z_B}, \varphi, \theta, \psi, z_B, \lambda_z, \lambda_p, \lambda_q, c_{s1}]$$

Input signal:

$$\underline{u} = \text{col} [A_{x_B}, A_{y_B}, A_{z_B}, p_B, q_B, r_B]$$

Output signal:

$$\underline{m} = \text{col} [v, \Delta h, \beta]$$

Input signal	$\sigma_{W_{i,i}}$	unit
$A_{x_B}$	$0.32 \times 10^{-2}$	$\text{m}^2/\text{s}^4$
$A_{y_B}$	$0.14 \times 10^{-2}$	$\text{m}^2/\text{s}^4$
$A_{z_B}$	$0.56 \times 10^{-2}$	$\text{m}^2/\text{s}^4$
$p_B$	$0.56 \times 10^{-4}$	$\text{rad}^2/\text{s}^2$
$q_B$	$0.56 \times 10^{-4}$	$\text{rad}^2/\text{s}^2$
$r_B$	$0.56 \times 10^{-4}$	$\text{rad}^2/\text{s}^2$
Output signal	$\sigma_{Q_{i,i}}$	unit
$v$	0.30	$\text{m}^2/\text{s}^2$
$\Delta h$	0.40	$\text{m}^2$
$\beta$	$0.15 \times 10^{-1}$	$\text{rad}^2$

Table 6: System models and measurement error statistics for the Kalman filter, i.e. the diagonal elements of the covariance matrices  $W$  and  $Q$ .

Quantity	Filter		Smoother		
	$\hat{\underline{m}}(k k)$	$\sigma_{\hat{\underline{m}}}(k k)$	$\hat{\underline{m}}(k n)$	$\sigma_{\hat{\underline{m}}}(k n)$	unit
$v$	$-.39 \times 10^{-2}$	0.257	$.37 \times 10^{-2}$	0.206	m/s
$\Delta h$	-.19	0.473	$-.18 \times 10^{-1}$	0.409	m
$\beta$	$-.82 \times 10^{-4}$	0.0067	$-.97 \times 10^{-4}$	0.0068	rad

Table 7: The statistics of the observation residuals for the simulation experiment

Quantity	Filter		Smoother		
	$\bar{m}(k k)$	$\sigma_{\bar{m}(k k)}$	$\bar{m}(k n)$	$\sigma_{\bar{m}(k n)}$	unit
v	-0.088	0.310	0.0096	0.174	m/s
$\Delta h$	-0.084	0.605	0.171	0.463	m
$\beta$	-0.0016	0.0044	-0.0008	0.0036	rad

Table 8: The statistics of the observation residuals of an actual flight manoeuvre.

	$\sigma_{rv_s}$	$\sigma_{r\Delta h_s}$	$\sigma_{r\beta_s}$
	m/s	m	rad
1	0.210	0.450	0.0034
2	0.241	0.592	0.0059
3	0.167	0.467	0.0031
4	0.197	0.517	0.0043
5	0.208	0.485	0.0037
6	0.164	0.402	0.0056
7	0.260	0.566	0.0058
8	0.149	0.379	0.0036
9	0.197	0.464	0.0037
10	0.189	0.434	0.0037

Table 9: Standard deviations of the residuals of ten nonsteady manoeuvring test flights.

	$\lambda_z$	$\sigma_{\lambda_z}$	$\lambda_p$	$\sigma_{\lambda_p}$	$\lambda_q$	$\sigma_{\lambda_q}$	$C_{si}$	$\sigma_{C_{si}}$
	m/s		rad/s		rad/s		-	
1	.043	.24 $\times 10^{-3}$	.48 $\times 10^{-5}$	.69 $\times 10^{-5}$	.13 $\times 10^{-3}$	.48 $\times 10^{-5}$	.031	.13 $\times 10^{-1}$
2	.044	.27 $\times 10^{-3}$	-.13 $\times 10^{-4}$	.14 $\times 10^{-4}$	.14 $\times 10^{-3}$	.69 $\times 10^{-5}$	.013	.91 $\times 10^{-2}$
3	.040	.29 $\times 10^{-3}$	-.12 $\times 10^{-3}$	.20 $\times 10^{-4}$	.10 $\times 10^{-3}$	.96 $\times 10^{-5}$	.027	.23 $\times 10^{-1}$
4	.040	.25 $\times 10^{-3}$	-.43 $\times 10^{-4}$	.11 $\times 10^{-4}$	.11 $\times 10^{-3}$	.57 $\times 10^{-5}$	.024	.13 $\times 10^{-1}$
5	.048	.24 $\times 10^{-3}$	-.65 $\times 10^{-4}$	.69 $\times 10^{-5}$	.43 $\times 10^{-4}$	.51 $\times 10^{-5}$	.024	.13 $\times 10^{-1}$
6	.039	.28 $\times 10^{-3}$	-.85 $\times 10^{-4}$	.15 $\times 10^{-4}$	.14 $\times 10^{-3}$	.80 $\times 10^{-5}$	.028	.11 $\times 10^{-1}$
7	.045	.28 $\times 10^{-3}$	.19 $\times 10^{-5}$	.12 $\times 10^{-4}$	.45 $\times 10^{-4}$	.77 $\times 10^{-5}$	.015	.89 $\times 10^{-2}$
8	.049	.24 $\times 10^{-3}$	-.32 $\times 10^{-4}$	.10 $\times 10^{-4}$	.51 $\times 10^{-4}$	.49 $\times 10^{-5}$	.025	.24 $\times 10^{-1}$
9	.049	.23 $\times 10^{-3}$	-.40 $\times 10^{-4}$	.79 $\times 10^{-5}$	.67 $\times 10^{-4}$	.42 $\times 10^{-5}$	.021	.13 $\times 10^{-1}$
10	.045	.25 $\times 10^{-3}$	-.22 $\times 10^{-4}$	.12 $\times 10^{-4}$	.14 $\times 10^{-3}$	.54 $\times 10^{-5}$	.013	.11 $\times 10^{-1}$

Table 10: Estimated zero shifts and sidewash coefficients including estimation accuracy of ten nonsteady manoeuvring test flights.

CALCULATION OF REGRESSION COEFFICIENTS  
FIRST SOLUTION IS OF UNDISTURBED SYSTEM  
STANDARD ANSWERS ARE Y/N

1. RANK IS 10  
SOLUTION IS

CZ0	CZQ	CZAD	CZDE	CZDH	CZA	CZAA	CZM	CZAM	CZMM
-25.93	-270.3	268.1	-.1515	-2.511	-3.729	.2245E-01	172.4	14.80	-300.9

RMS OF 272 RESIDUES .59552E-03

2. DO YOU WANT TO FIX SOME PARAMETERS? Y

TYPE NUMBER OF FIXES, SEQNUMBERS AND FIX-VALUES  
3,8,0,9,0,10,0

RANK IS 10  
SOLUTION IS

CZ0	CZQ	CZAD	CZDE	CZDH	CZA	CZAA	CZM	CZAM	CZMM
-1.013	-65.27	56.52	-.4411	-10.86	-5.310	3.339	0	0	0

RMS OF 272 RESIDUES .19238E-02

DO YOU WANT TO FIX SOME PARAMETERS? N

DO YOU WANT TO SPECIFY EXTRA EQUATIONS? N

STANDARD ERRORS  
.1405 5.708 5.905 .1358E-01 2.058 .1456 .9527E-01 0 0 0

DO YOU WANT THE SCALED COVARIANCE MATRIX? Y

SCALED COVARIANCE MATRIX

1.00	-.28	.30	.65	.99	.39	-.32	-.00	-.00	-.00
-.28	1.00	-1.00	-.40	-.41	-.97	.32	-.00	-.00	-.00
.30	-1.00	1.00	.45	.43	.97	-.32	.00	.00	.00
.65	-.40	.45	1.00	.67	.46	-.17	.00	.00	.00
.99	-.41	.43	.67	1.00	.51	-.36	.00	.00	.00
.39	-.97	.97	.46	.51	1.00	-.53	.00	-.00	.00
-.32	.32	-.32	-.17	-.36	-.53	1.00	-.00	-.00	-.00
-.00	-.00	.00	.00	.00	.00	-.00	1.00	-.00	-.00
-.00	-.00	.00	.00	.00	-.00	-.00	-.00	1.00	-.00
-.00	-.00	.00	.00	.00	.00	-.00	-.00	-.00	1.00

DO YOU WANT THE RESIDUE STATISTICS? Y

RESIDUE STATISTICS  
MEAN SD MAX MIN  
.4611E-12 .1924E-02 .5457E-02 -.3947E-02

DO YOU WANT A PRINT OF THE RESIDUES? N

3. DO YOU WANT TO FIX SOME PARAMETERS? Y

TYPE NUMBER OF FIXES, SEQNUMBERS AND FIX-VALUES  
1,2,-8

RANK IS 10  
SOLUTION IS

CZ0	CZQ	CZAD	CZDE	CZDH	CZA	CZAA	CZM	CZAM	CZMM
-1.403	-8.000	-2.650	-.4961	-19.35	-6.727	3.644	0	0	0

RMS OF 272 RESIDUES .22634E-02

4. DO YOU WANT TO SPECIFY EXTRA EQUATIONS? Y

TYPE COEFFICIENTS OF EXTRA EQUATION 0,0,0,-3000,1000,0,0,0,0,0

RANK IS 10  
SOLUTION IS

CZ0	CZQ	CZAD	CZDE	CZDH	CZA	CZAA	CZM	CZAM	CZMM
-.1030	-8.000	-1.261	-.4246	-1.274	-6.550	3.407	0	0	0

■ For key see next page.

Table 11: Example of an actual interactive session with PIAS.

```

RMS OF 272 RESIDUES      .25366E-02

DO YOU WANT TO FIX SOME PARAMETERS? N

DO YOU WANT TO SPECIFY EXTRA EQUATIONS? N

STANDARD ERRORS
.4247E-02   0   .3371   .1314E-01   .3941E-01   .4007E-01   .1146   0   0   0

DO YOU WANT THE SCALED COVARIANCE MATRIX? Y

SCALED COVARIANCE MATRIX

1.00   .00   .54   .57   .57   -.81   .87   -.00   -.00   -.00
.00   1.00   -.00   -.00   -.00   -.00   .00   -.00   -.00   -.00
.54   -.00   1.00   .94   .94   .01   .14   .00   .00   .00
.57   -.00   .94   1.00   1.00   .01   .15   .00   .00   .00
.57   -.00   .94   1.00   1.00   .01   .15   .00   .00   .00
-.81   -.00   .01   .01   .01   1.00   -.98   .00   -.00   .00
.87   .00   .14   .15   .15   -.98   1.00   -.00   -.00   -.00
-.00   -.00   .00   .00   .00   .00   -.00   1.00   -.00   -.00
-.00   -.00   .00   .00   .00   -.00   -.00   -.00   1.00   -.00
-.00   -.00   .00   .00   .00   .00   -.00   -.00   -.00   1.00

DO YOU WANT THE RESIDUE STATISTICS? Y

RESIDUE STATISTICS
MEAN      SD      MAX      MIN
.5993E-13 .2537E-02 .5463E-02 -.5181E-02

```

```

KEY: CZO  ≡ CZO      CZA  ≡ CZ
      CZQ  ≡ CZq      CZAA ≡ CZα2
      CZAD ≡ CZα      CZM  ≡ CZM
      CZDE ≡ CZδe     CZAM ≡ CZαM
      CZDH ≡ CZδh     CZMM ≡ CZM2

```

Table 11. Continued.

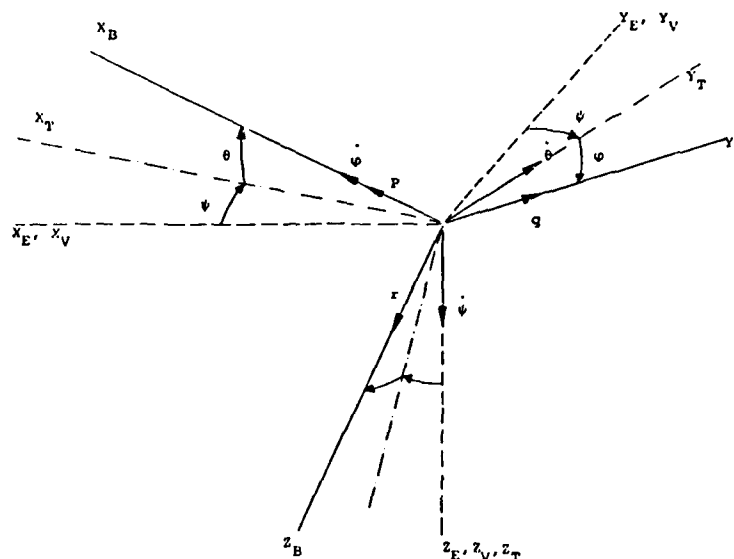


Fig. 1. The aircraft's body frame of reference  $F_B$  relative to the vehicle carried vertical frame  $F_V$  and the vehicle carried vertical frame  $F_T$ .

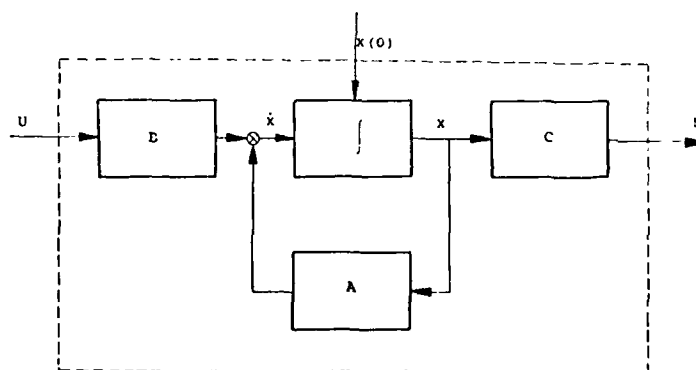


Fig. 2. Block diagram of the linear system:  $\dot{X} = A X + B U$   
 $M = C X$

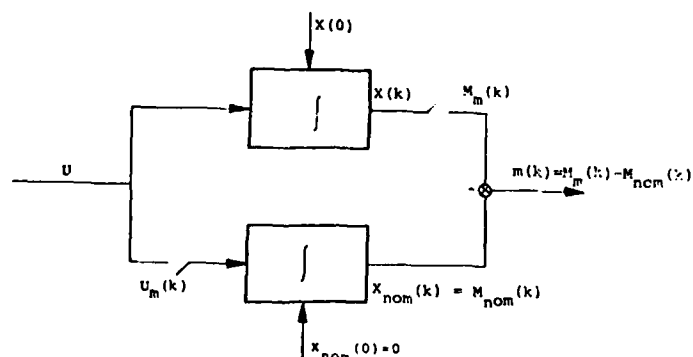


Fig. 3. The simplified system of example 1, subsection 3.2.1.

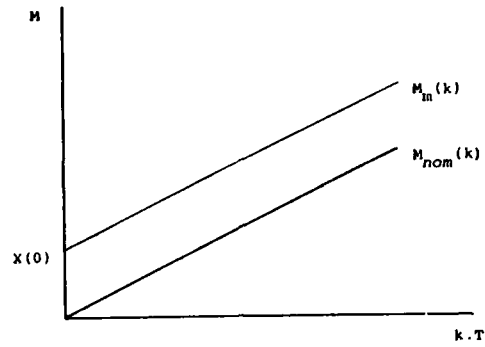


Fig. 4. Nominal and measured output signal of example 1, subsection 3.2.1.

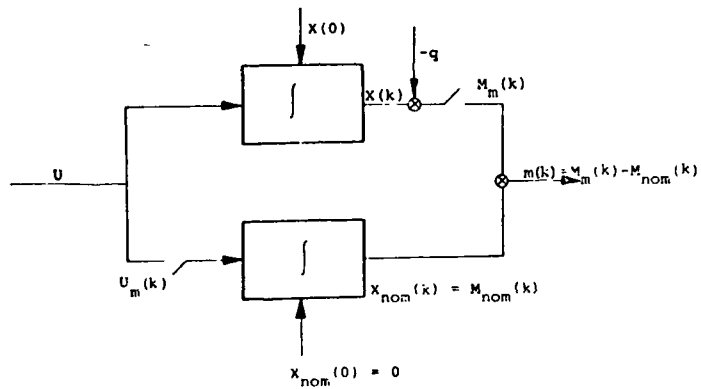


Fig. 5. The system of example 2, subsection 3.2.3., taking account of observation noise.

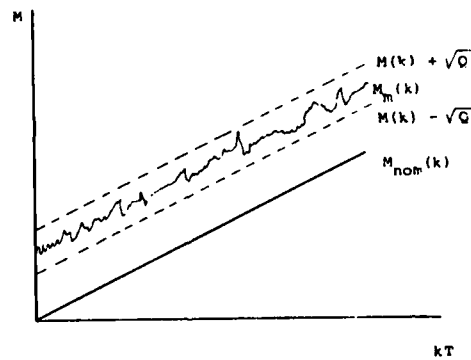


Fig. 6. Nominal and measured output signal of example 2, subsection 3.2.3.

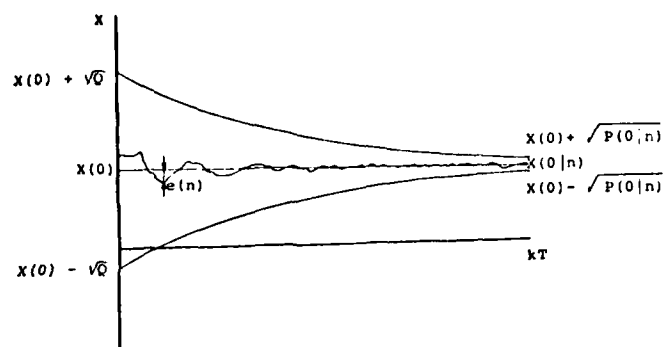


Fig. 7. Estimate of  $X(0)$  and corresponding r.m.s.-error.

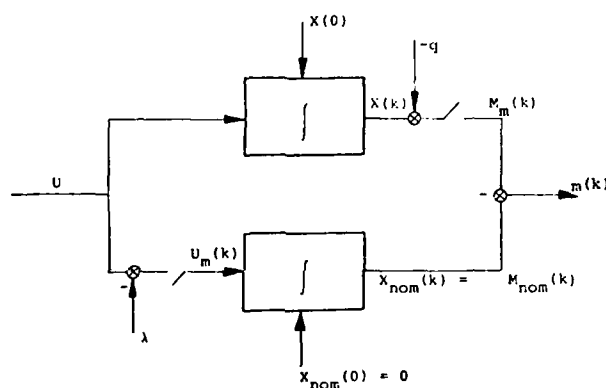


Fig. 8. The system of example 3, subsection 3.2.4., taking account of observation noise and a bias error.

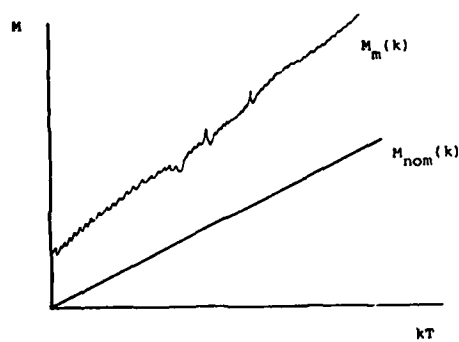


Fig. 9. Nominal and measured output signal of the system of example 3, subsection 3.2.4.

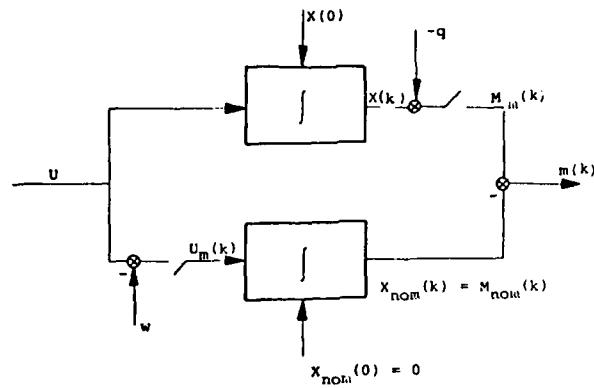


Fig. 10. The system of example 4, subsection 3.2.5., taking account of input- and output signal noise.

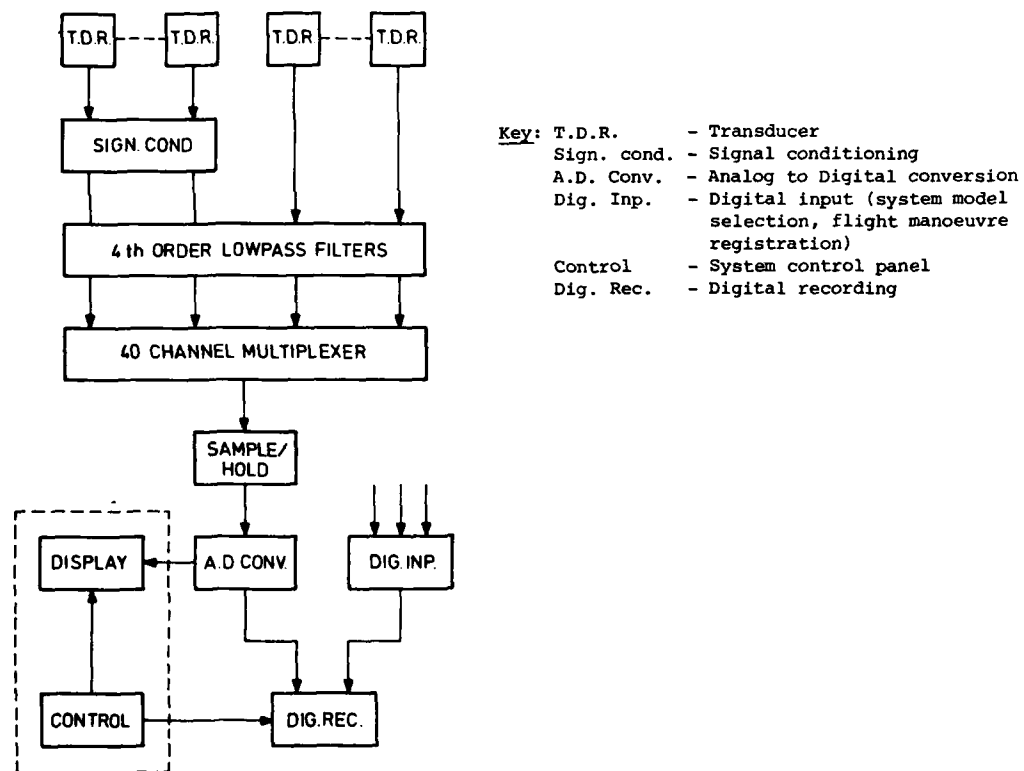


Fig. 11. General arrangement of instrumentation system, ref. 26.



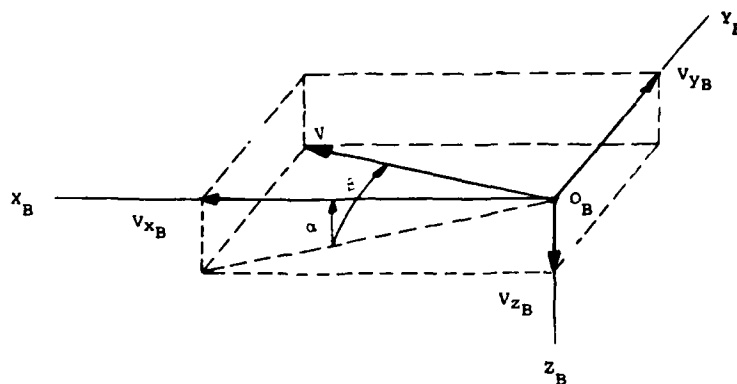


Fig. 12. The angles of attack and sideslip in the aircraft's body frame of reference  $F_B$ .

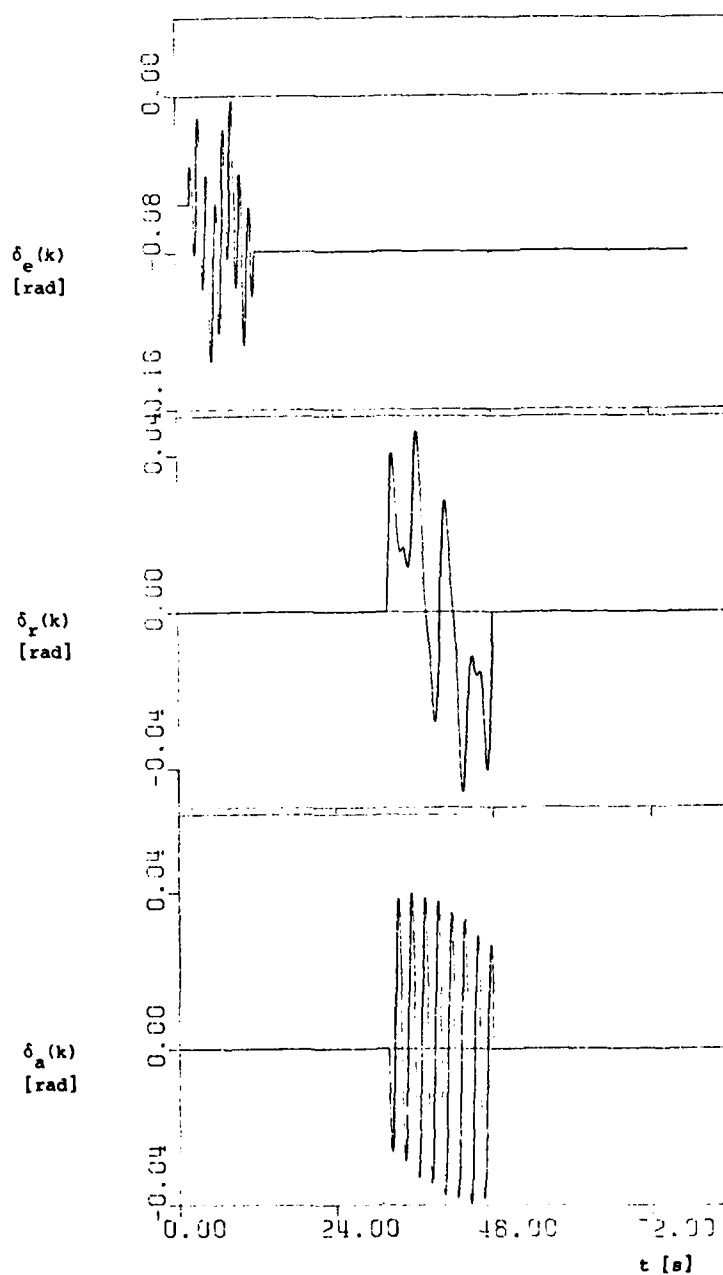
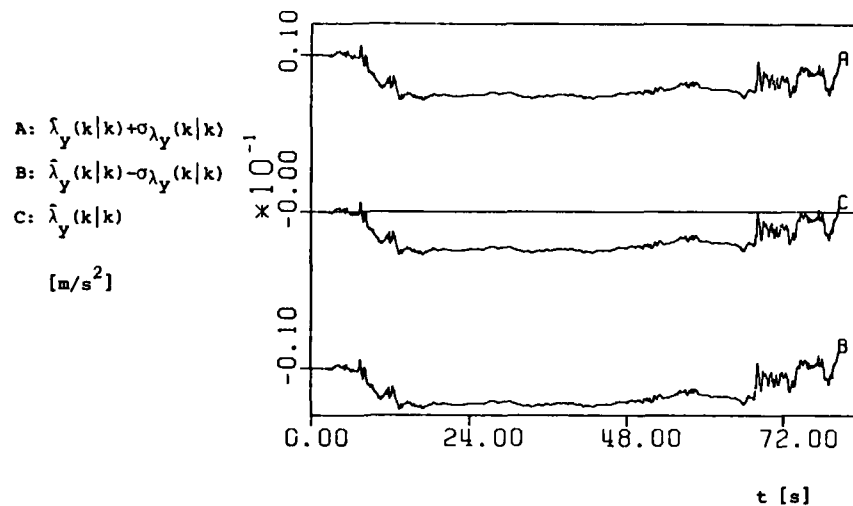
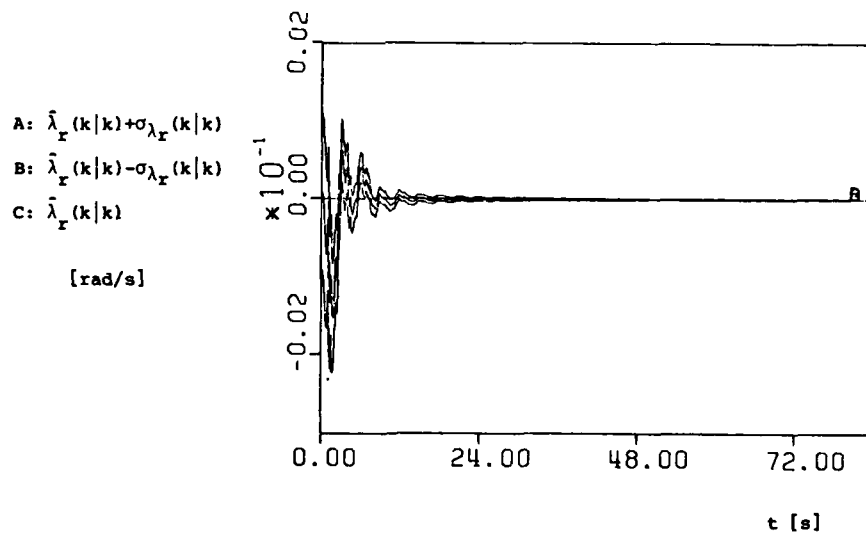


Fig. 13. Elevator, rudder and aileron input signals for the simulated flight test manoeuvre.



**Fig. 14.** Kalman filter estimate of the bias error correction  $\lambda_y$  for the simulated flight test manoeuvre.



**Fig. 15.** Kalman filter estimate of the bias error correction  $\lambda_x$  for the simulated flight test manoeuvre.

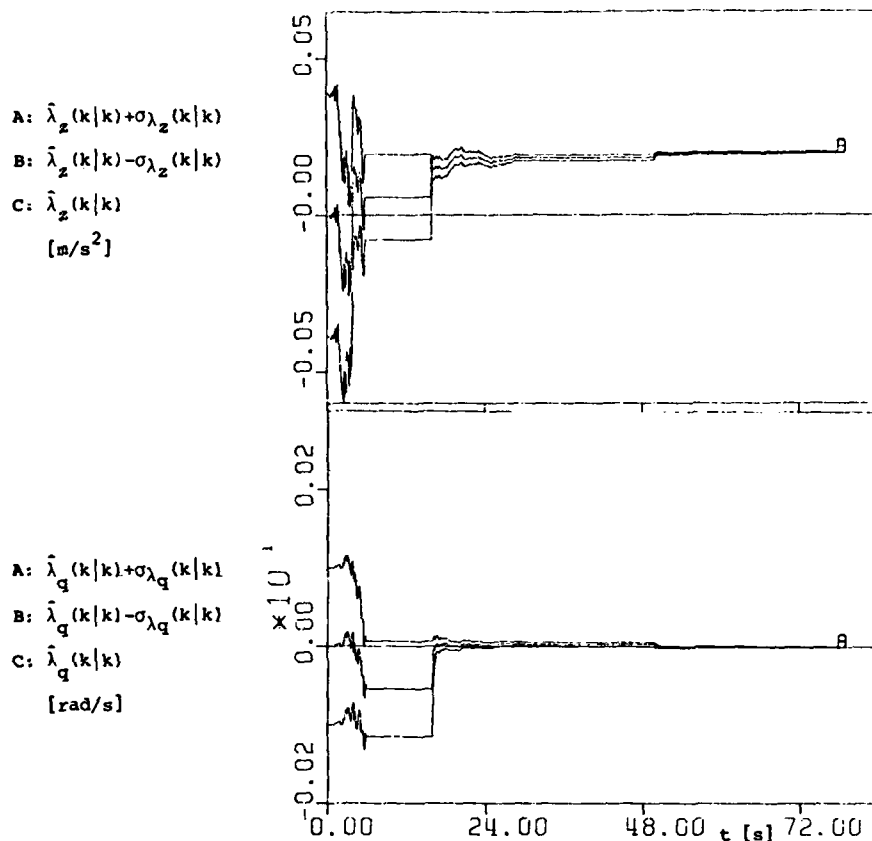


Fig. 16. Kalman filter estimates of the bias error corrections  $\lambda_z$  and  $\lambda_q$  for the simulated flight test manoeuvre.

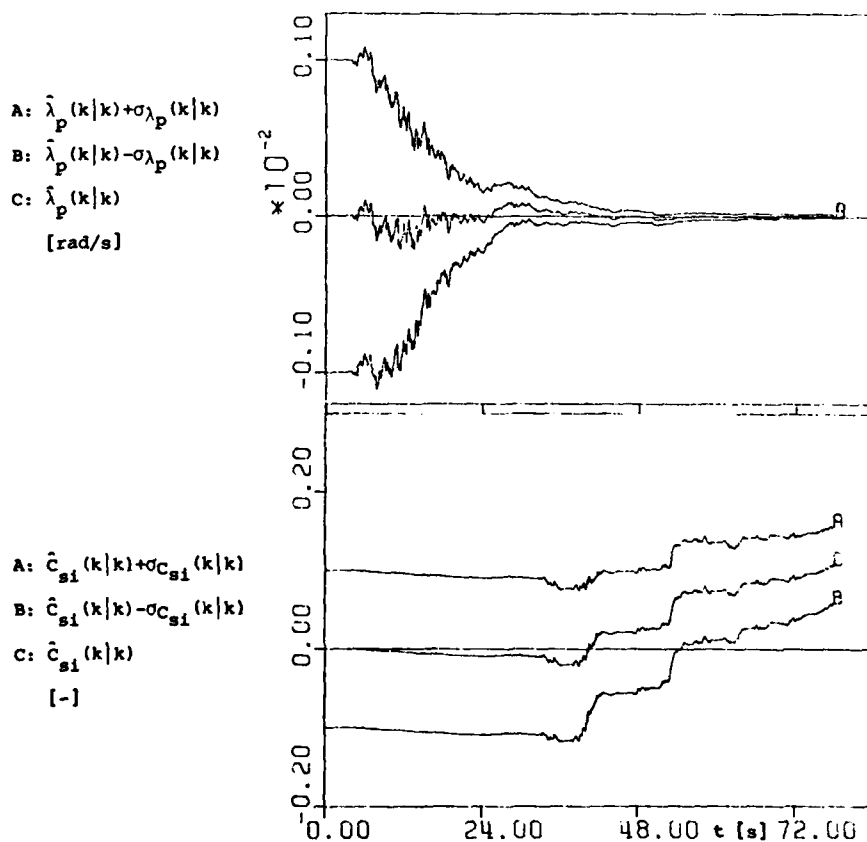


Fig. 17. Kalman filter estimates of the bias error correction  $\lambda_p$  and sidewash coefficient  $C_{si}$  for the simulated flight test manoeuvre.

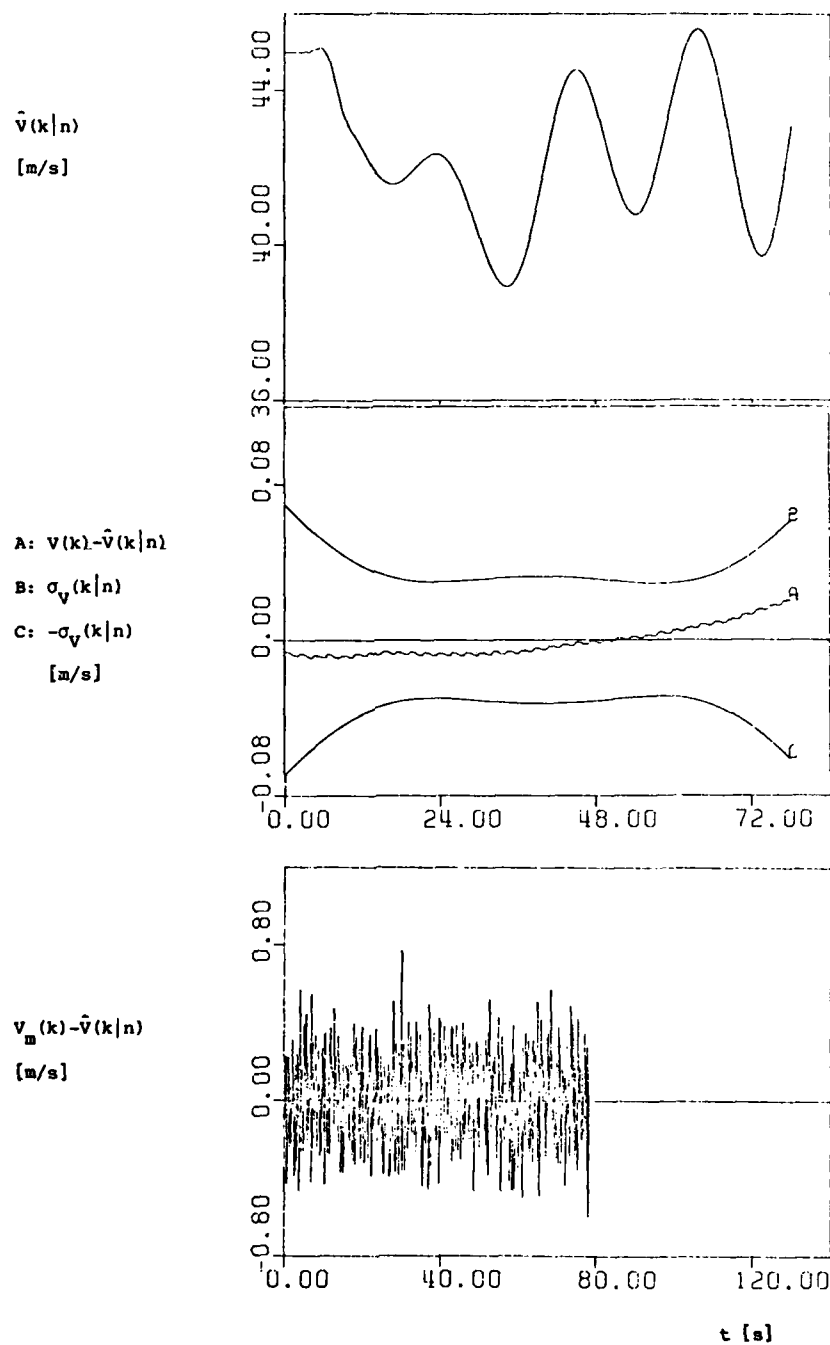


Fig. 18. Kalman smoother estimate, estimation error and residual of the aircraft's velocity for the simulated flight test manoeuvre.

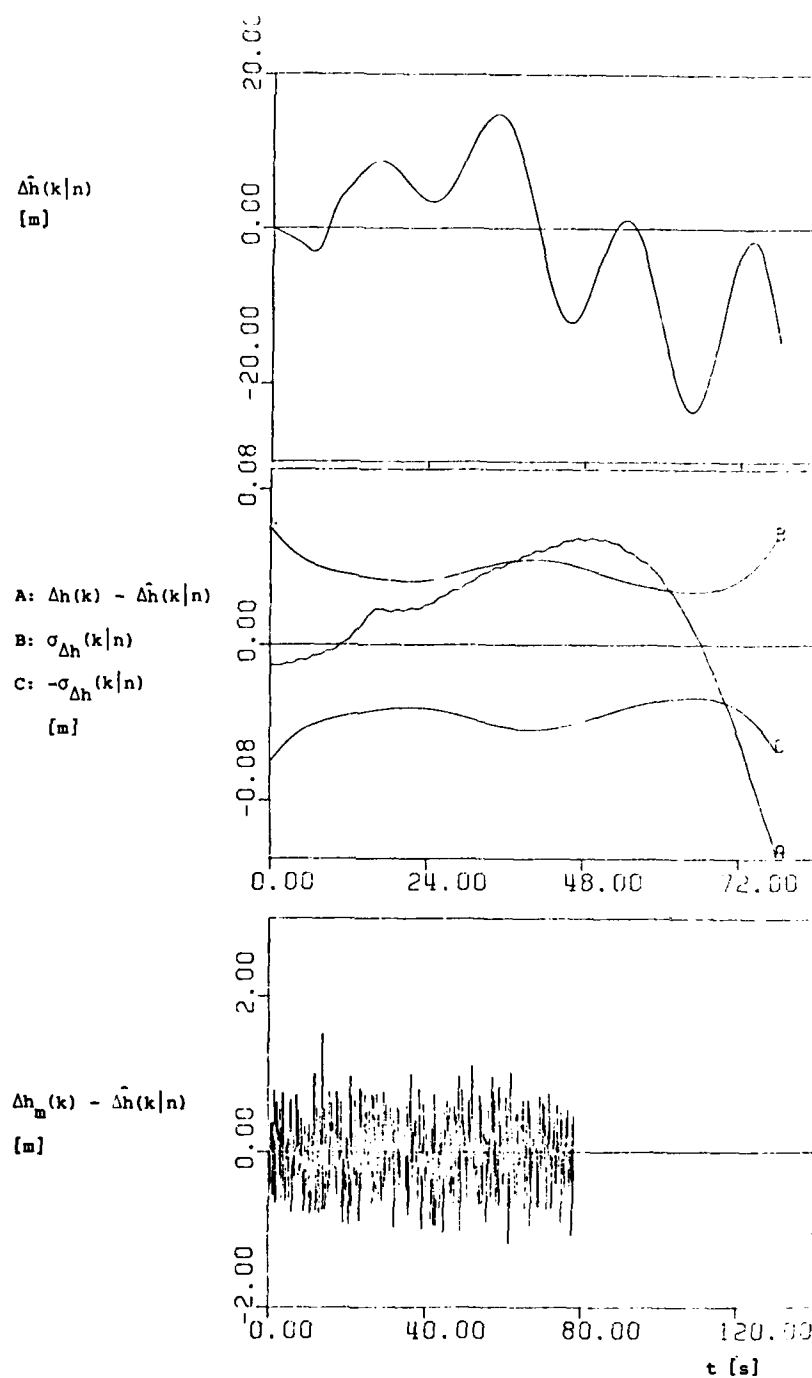


Fig. 19. Kalman smoother estimate, estimation error and residual of the altitude variation for the simulated flight test manoeuvre.

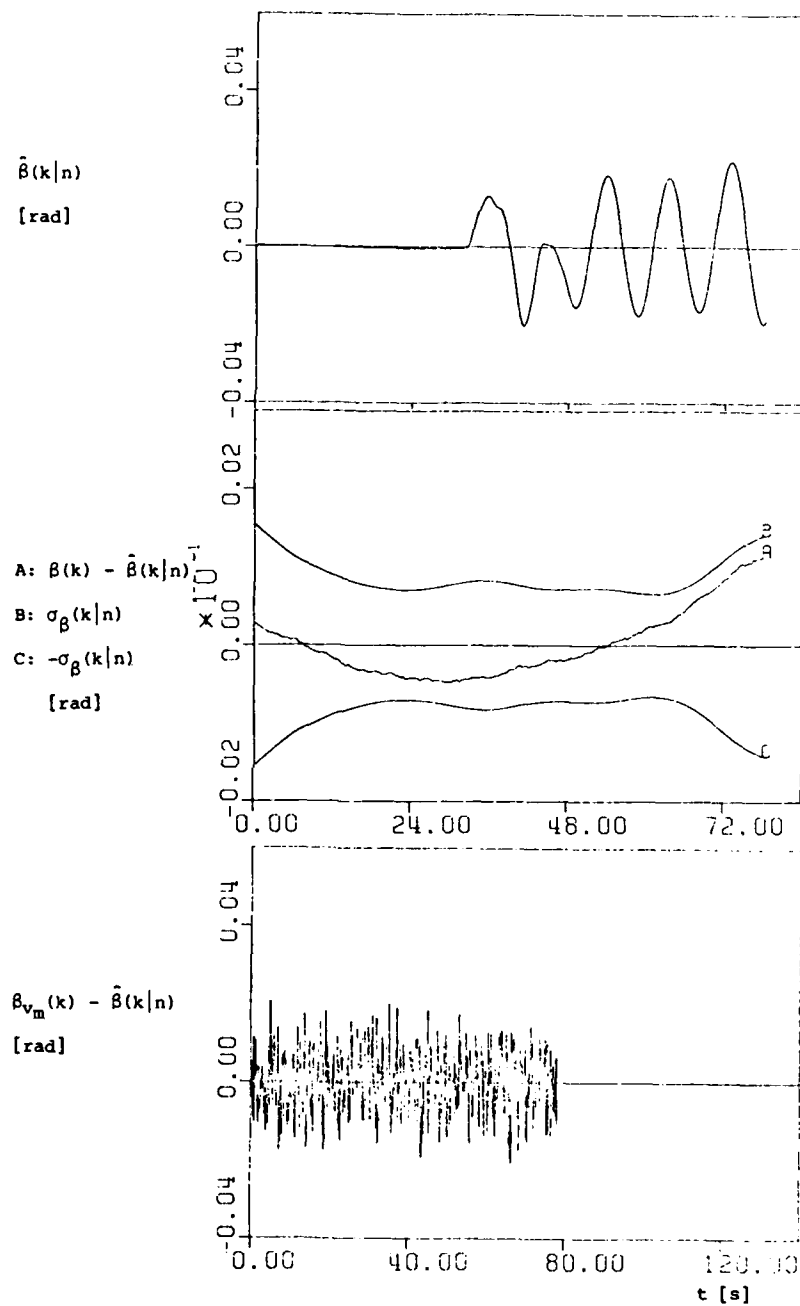
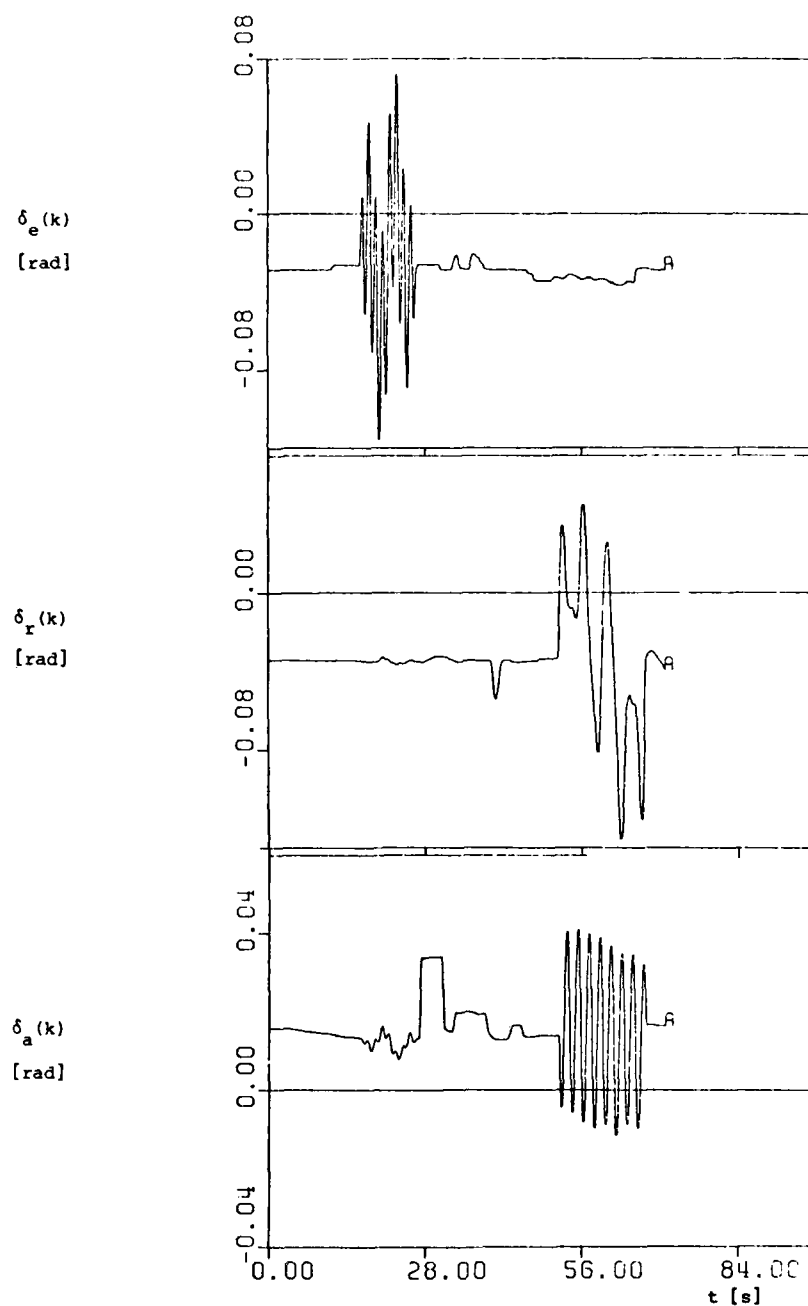


Fig. 20. Kalman smoother estimate, estimation error and residual of the angle of sideslip for the simulated flight test manoeuvre.



**Fig. 21.** Elevator, rudder and aileron input signals for the actual flight test manoeuvre.

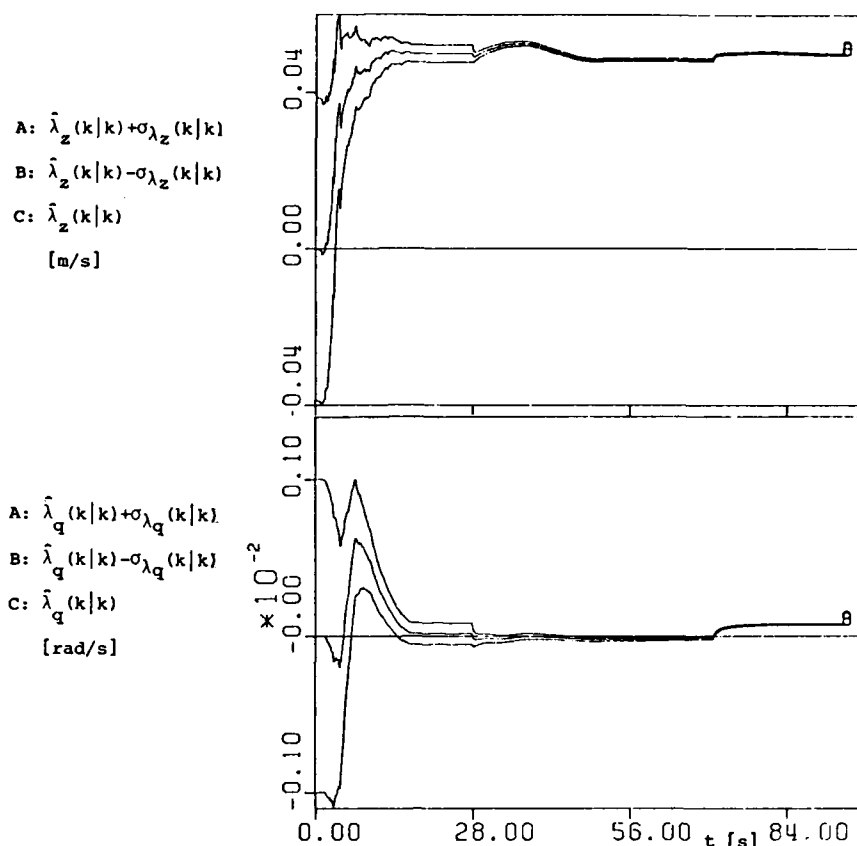


Fig. 22. Kalman filter estimate of the bias error corrections  $\lambda_z$  and  $\lambda_q$  for the actual flight test manoeuvre.

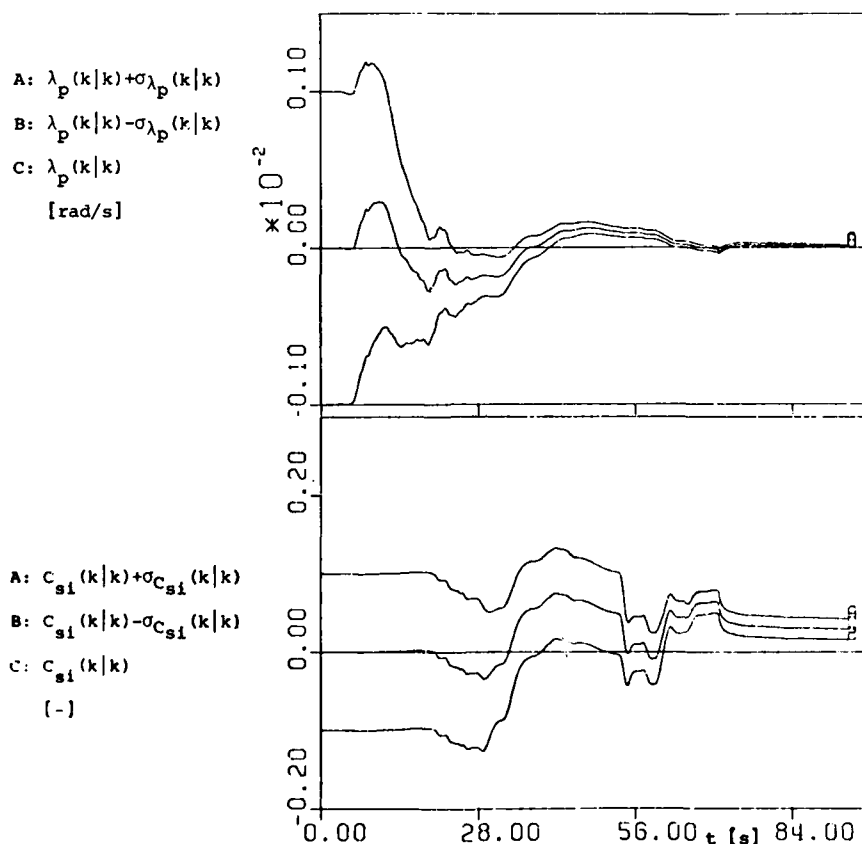


Fig. 23. Kalman filter estimate of the bias error correction  $\lambda_p$  and sidewash  $C_{si}$  for the actual flight test manoeuvre.



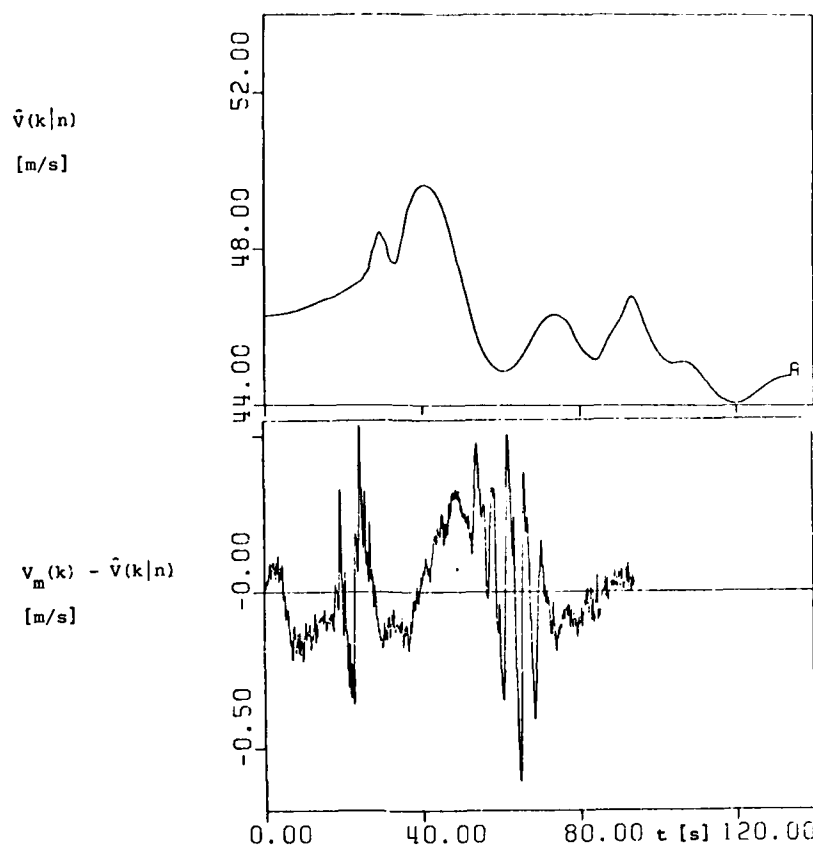


Fig. 24. Kalman smoother estimate and residual of the aircraft's velocity for an actual flight test manoeuvre.

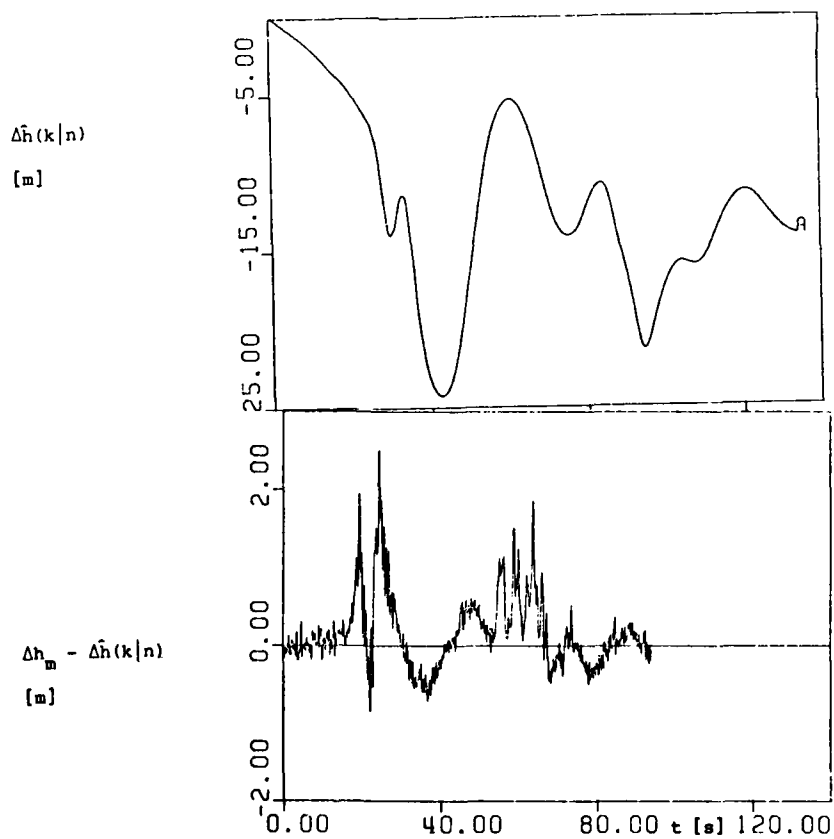


Fig. 25. Kalman smoother estimate and residual of the altitude variation for an actual flight test manoeuvre.

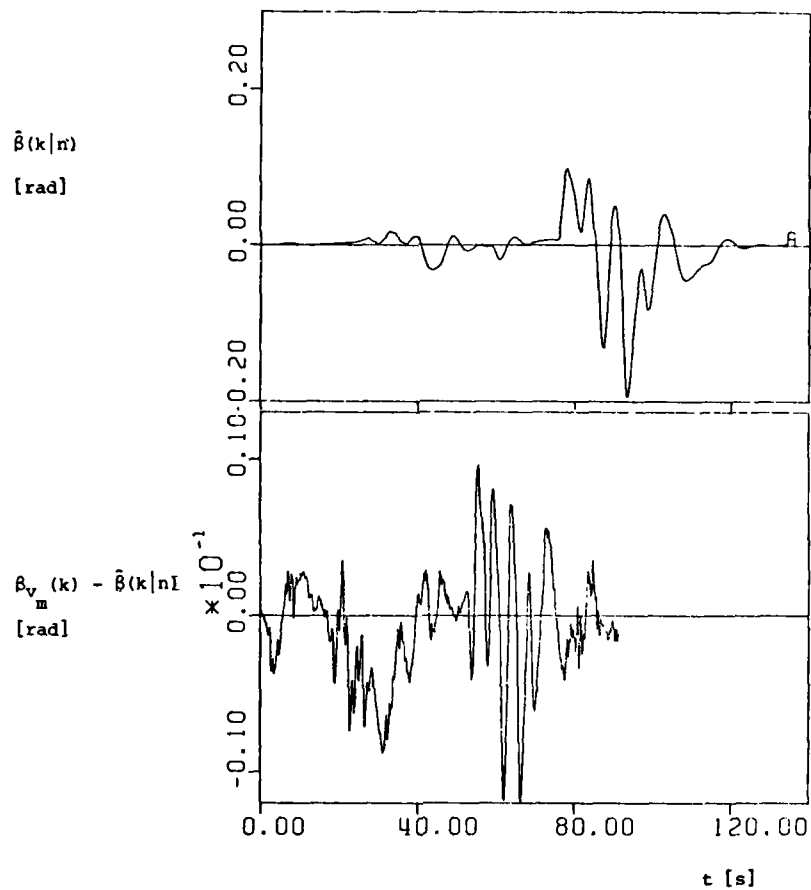


Fig. 26. Kalman smoother estimate and residual of the angle of sideslip for an actual flight test manoeuvre.

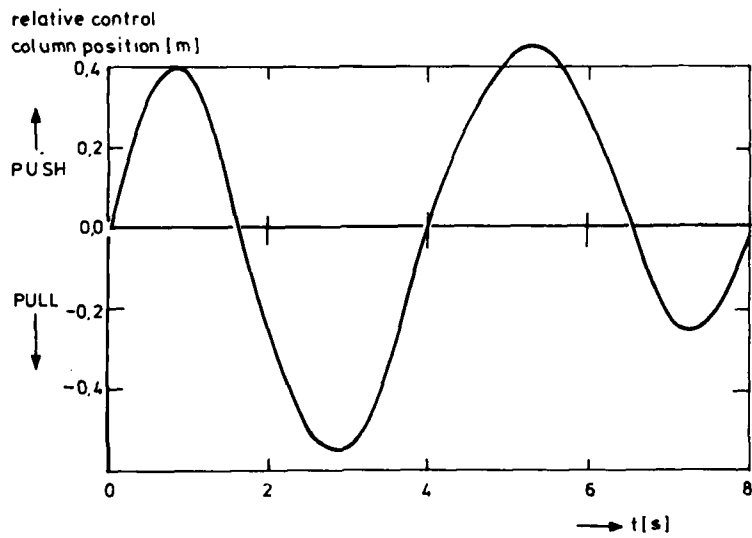


Fig. 27. Example of optimal F-28 elevator input signal, ref. 30.

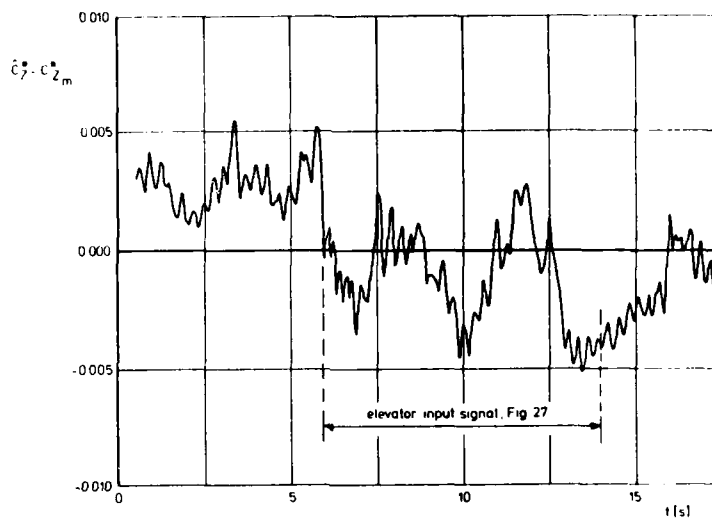


Fig. 28. Residuals of  $C_Z^*$  model.

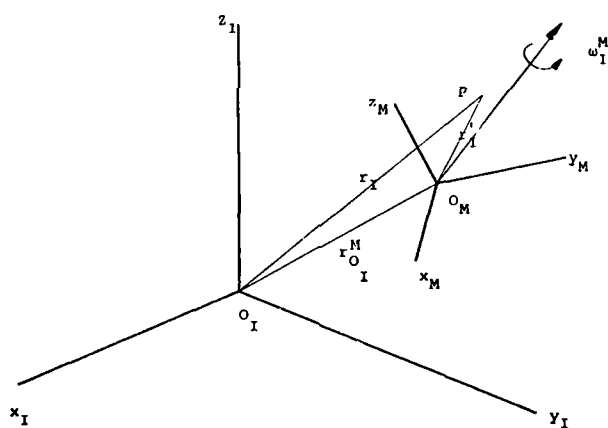


Fig. A-1. Arbitrary moving frame  $F_M$  relative to the inertial reference frame  $F_I$ .

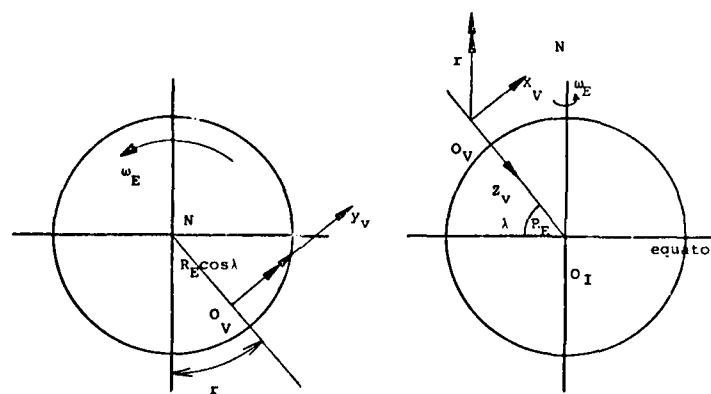


Fig. A-2. The earth rotation relative to  $F_V$ .

## AIRCRAFT IDENTIFICATION EXPERIENCE

Kenneth W. Iliff  
Aerospace Engineer  
NASA Dryden Flight Research Center  
P.O. Box 273  
Edwards, California 93523  
U.S.A.

## SUMMARY

This lecture discusses some of the important aspects of estimating the unknown coefficients of the aircraft equations of motion from dynamic flight data. The primary topic is the experience at the NASA Dryden Flight Research Center in the application of the maximum likelihood estimation technique to such data. The lecture covers basic considerations that must be addressed in the estimation of stability and control derivatives from conventional flight maneuvers, and the assessment of the reliability and quality of the estimates obtained. Some complex areas of estimation (such as estimation in the presence of atmospheric turbulence, estimation of acceleration derivatives, and analysis of maneuvers where both kinematic and aerodynamic coupling are present) are also discussed.

## NOMENCLATURE

$A, B, C, D$	system matrices	$M$	normalized pitching moment, $\text{rad/sec}^2$
$a_n$	normal acceleration, g	$m$	mass, N
$a_x$	longitudinal acceleration, g	$N$	normalized yawing moment, $\text{rad/sec}^2$
$a_y$	lateral acceleration, g	$n$	state noise vector
$b$	reference span, m	PSD	power spectral density
$C_D$	coefficient of drag	$p$	roll rate, $\text{deg/sec}$ or $\text{rad/sec}$
$C_{D_I}$	coefficient of induced drag	$q$	pitch rate, $\text{deg/sec}$ or $\text{rad/sec}$
$C_L$	coefficient of lift	$\bar{q}$	dynamic pressure, $\text{kN/m}^2$
$C_l$	coefficient of rolling moment	$R$	covariance of weighted residual measurement error
$C_m$	coefficient of pitching moment	$r$	yaw rate, $\text{deg/sec}$ or $\text{rad/sec}$
$C_N$	coefficient of normal force	$s$	reference area, $\text{m}^2$
$C_n$	coefficient of yawing moment	$T$	maneuver duration, sec
$C_Y$	coefficient of side force	$t$	time, sec
$c$	reference chord, m	$\Delta t$	sample interval, sec
$E\{ \}$	expected value	$u$	input vector
$f( )$	general function	$V$	velocity, $\text{m/sec}$
$GG^*$	power spectral density of measurement noise	$x$	state vector
$g$	acceleration due to gravity, $\text{m/sec}^2$	$Y$	normalized lateral force, $\text{rad/sec}$
$g( )$	general function	$y$	observation vector
$I_X, I_Y, I_Z,$ $I_{XY}, I_{XZ}$	inertias, $\text{kg-m}^2$	$Z$	normalized normal force, $\text{rad/sec}$
$J$	cost functional	$z$	measured observation vector
$L$	normalized rolling moment, $\text{rad/sec}^2$	$\hat{z}$	Kalman-filtered estimate of the observation vector
		$\alpha$	angle of attack, deg
		$\hat{\alpha}_g$	angle of attack induced by vertical velocity component of turbulence, deg
		$\beta$	angle of sideslip, deg

$\delta_a$	aileron deflection, deg	$\omega_0$	true frequency, rad/sec
$\delta_e$	elevator deflection, deg	Subscripts:	
$\delta_r$	rudder deflection, deg	$p, q, r, \alpha, \dot{\alpha}, \beta, \delta_a, \delta_e, \delta_r$	measured derivative with respect to indicated quantity
$\eta$	measurement noise vector	trim	trimmed value
$\theta$	pitch angle, deg	0	bias
$\xi$	vector of unknowns	Superscript:	
$\varphi$	bank angle, deg	*	matrix transpose
$\omega$	frequency, rad/sec		

## INTRODUCTION

One of the primary goals of an aircraft flight test program is to estimate flight-determined aircraft characteristics, such as the aircraft's performance, structural, and stability and control coefficients. As estimates of these coefficients become available, they can be used to expand the flight test envelope, update the simulators, and improve the aircraft propulsion and control systems. After the analysis of the flight test data, the estimated coefficients can be compared with calculated and wind tunnel predictions, and this comparison can be used to update prediction methods for the improvement of future aircraft design.

Today the primary method of obtaining estimated coefficients from flight data is maximum likelihood estimation (ref. 1), or the output error method. The results reported in this lecture were obtained from the MMLE computer program (ref. 2) and the more general program, MMLE 3, described in reference 3. In addition to the results reported here, extensive worldwide experience with the use of maximum likelihood estimation on actual flight data has been reported, as exemplified by references 4 to 17. References 18 and 19 give a comprehensive sampling of papers reporting the results of aircraft parameter estimation. Reference 20 provides an overview of the papers contained in reference 19.

The preceding lectures in this series provide a detailed treatment of various aspects of aircraft parameter estimation. This lecture presents the results obtained at the NASA Dryden Flight Research Center from the application of a maximum likelihood estimator to dynamic flight data. The estimation process and the maximum likelihood estimator are described, and the instrumentation for and analysis of dynamic flight maneuvers are discussed in detail. Because most of the estimation experience to date has been with stability and control derivatives, the discussion emphasizes the estimation of these derivatives.

## MAXIMUM LIKELIHOOD ESTIMATION

The aircraft parameter estimation problem can be defined quite simply in general terms. The system investigated is assumed to be modeled by a set of dynamic equations containing unknown parameters. To determine the values of the unknown parameters, the system is excited by a suitable input, and the input and actual system response are measured. The values of the unknown parameters are then inferred based on the requirement that the model response to the given input match the actual system response. When formulated in this manner, the problem of identifying the unknown parameters can be easily solved by many methods; however, complicating factors arise when application to a real system is considered.

The first complication results from the impossibility of obtaining perfect measurements of the response of any real system. The inevitable sensor errors are usually included as additive measurement noise in the dynamic model. Once this noise is introduced, the theoretical nature of the problem changes drastically. It is no longer possible to exactly identify the values of the unknown parameters; instead, the values must be estimated by some statistical criterion. For discrete time systems, the theory of estimation in the presence of measurement noise is relatively straightforward, requiring only basic probability. In continuous time, however, the problem of rigorously defining a useful probability measure requires background in functional analysis and advanced probability.

The second complication of real systems is the presence of state noise. State noise is random excitation of the system from unmeasured sources, the standard example for the aircraft stability and control problem being atmospheric turbulence. If state noise is present and measurement noise is neglected, the analysis results in the regression algorithm discussed in a preceding lecture.

When both state and measurement noise are considered, the continuous time theory involves extensive mathematical background for a rigorous treatment. The algorithm that results, however, is actually quite simple. (The results presented in this lecture were obtained with the continuous time results and discretized only at the stage of implementation on a digital computer.)

The final problem for real systems is modeling. It has been assumed throughout the above discussion that for some value (called the "true" value) of the unknown parameter vector, the system is correctly described by the dynamic model. Physical systems are seldom described exactly by simple dynamic models, so the question of modeling error arises. There is no comprehensive theory of modeling error available. The most common approach taken amounts to ignoring it. Any modeling error is simply treated as state noise or measurement noise, or both, in spite of the fact that the modeling error may be deterministic rather than random. The assumed noise statistics can then be adjusted to include the contribution of the modeling error. This procedure is not rigorously justifiable, but combined with a carefully chosen model, it is probably the best approach available.

With the above discussion in mind, it is possible to make a more precise mathematically probabilistic statement of the parameter estimation problem. For each possible estimate of the unknown parameters, a probability that the aircraft response time histories attain values near the observed values can be defined. The estimates, which are referred to as the maximum likelihood estimates, should be chosen such that this probability is maximized. Maximum likelihood estimation has many desirable statistical characteristics; for example, it yields asymptotically unbiased, consistent, and efficient estimates (refs. 21 and 22).

The mathematical model for the dynamic system is

$$\dot{x}(t) = f(x, u, \xi) + n(t) \quad (1)$$

$$y(t) = g(x, u, \xi) \quad (2)$$

$$z(t) = y(t) + \eta(t) \quad (3)$$

The noise is assumed to be zero mean, white, Gaussian, and stationary. The maximum likelihood estimates are obtained by maximizing the likelihood functional or, equivalently, by minimizing the following negative log likelihood functional (ref. 22):

$$J(\xi) = \frac{1}{T} \int_0^T (z - \hat{z}_\xi)^* (GG^*)^{-1} (z - \hat{z}_\xi) dt + \text{Trace } R \quad (4)$$

where  $\hat{z}_\xi$  is the Kalman-filtered estimate of  $y$  and  $R$  is the covariance matrix of the weighted observation estimation error. This algorithm, in contrast to the extended Kalman filter method (ref. 23), uses the Kalman filter only to estimate the states and measurements, not to estimate the unknown coefficients.

When there is no state noise,  $R$  is the null matrix and  $\hat{z}_\xi$  is obtained by simply integrating the system equations; no linearity assumptions are required. If state noise is present, the system equations must be linear in order to rigorously define the likelihood functional as in equation (4). For nonlinear systems with state noise, an estimator can be defined by replacing the Kalman filter for  $\hat{z}_\xi$  with an extended Kalman filter, but such an estimate is no longer maximum likelihood.

Figure 1 illustrates the maximum likelihood estimation concept. The measured response of the aircraft is compared with the estimated response and the difference between these responses is called the response error.

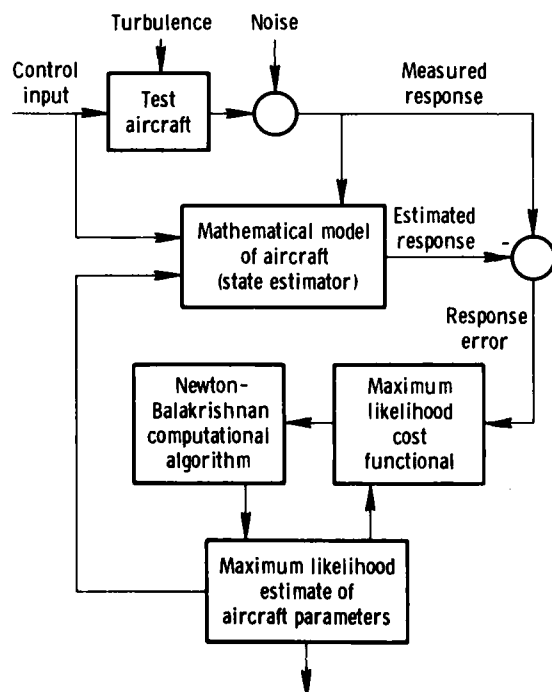


Figure 1. Maximum likelihood estimation concept.

The Newton-Balakrishnan (ref. 22) computational algorithm (formerly referred to as the modified Newton-Raphson algorithm) is used to find the coefficient values that maximize the likelihood functional. Each iteration of this algorithm provides a new estimate of the unknown coefficients on the basis of the response error. These new estimates of the coefficients are then used to update the mathematical model of the aircraft, providing a new estimated response and, therefore, a new response error. The updating of the mathematical model continues iteratively until a convergence criterion is satisfied. The estimates resulting from this procedure are the maximum likelihood estimates.

The maximum likelihood estimator also provides a measure of the reliability of each estimate based on the information obtained from each dynamic maneuver. This measure of the reliability, analogous to the standard deviation, is called the Cramer-Rao bound (ref. 24) or the uncertainty level. The Cramer-Rao bound as computed by current programs should generally be used as a measure of relative accuracy rather than absolute accuracy. Recent insight regarding the computation and interpretation of the absolute magnitude of the bound is discussed in reference 25 and later in this lecture. When carefully used, the Cramer-Rao bound has proven to be a useful tool for assessing the validity of the estimates.

At the Dryden Flight Research Center the algorithm described by equations (1) to (4) is currently implemented with a program called MMLE 3. A general description of this program is given in reference 3. The MMLE 3 program, which is an outgrowth of MMLE (ref. 2), was developed

to satisfy the need for more versatility and is designed to handle a general set of linear or bilinear dynamic equations of arbitrary order. All current analysis at Dryden is done with MMLE 3. Measurement noise and, optionally, state noise (such as turbulence) are included in the equations. The results presented in this lecture were obtained from the application of maximum likelihood estimation through the use of either MMLE or MMLE 3.

## INSTRUMENTATION AND DATA ACQUISITION

This section discusses the data requirements that the Dryden Flight Research Center has found to be important for performing maximum likelihood estimation. Previous lectures have covered instrumentation requirements in greater depth; the intention here is to place these requirements in the perspective of an overall flight test program, with the primary emphasis on the effect that the instrumentation may have on the estimation process.

## Signals Required

The signals required for maximum likelihood estimation fall into two partially overlapping classes. The first class consists of signals for which only an average value is required for each maneuver. The second class consists of signals for which the complete time history must be available. Some signals can fall in either class, depending on the particular maneuver or the coefficients to be estimated. Signals for which only average values are required include those that define the vehicle configuration, flight condition, and mass characteristics. These signals need not be recorded on the data tape; pilot lap notes or similar hand-kept records may be adequate in some cases. However, for large numbers of maneuvers it may prove convenient to record these parameters on the data tape in order to automate the bookkeeping.

For stability and control analysis, the vehicle configuration includes the positions of all flaps, canards, landing gear, wings (sweep angle), engine controls, and other items that affect the aerodynamic characteristics of the vehicle and are held fixed during a maneuver. The flight condition is defined by velocity, altitude, Mach number, dynamic pressure, angle of attack, and other quantities used to nondimensionalize the derivatives or plot the results. Some flight test programs may only require the estimation of dimensional derivatives, in which case some of the nondimensionalizing parameters may not be required. The mass characteristics that should be known are the weight, center of gravity, and inertias. These mass characteristics are usually determined from tables based on vehicle configuration, fuel weights, and cargo loading. An accurate determination of the mass characteristics is essential because errors in the mass characteristics result in proportional errors in the nondimensional derivatives. Weight can be readily determined. With sufficient care, the inertias of the vehicle can be either measured (ref. 26) or calculated; however, the ideal approach is to obtain both measured and calculated values. A frequently overlooked quantity is the vertical center of gravity position, the importance of which is discussed later in this lecture in reference to accelerometer locations.

The signals for which time histories are most necessary are the external inputs that vary during a maneuver and the response variables to be matched. For stability and control analyses where cross coupling is important (see Cross Coupling), the longitudinal response variables are needed to match the lateral responses, and the lateral response variables are needed to match the longitudinal responses. The longitudinal response variables are  $u$ ,  $q$ ,  $\theta$ ,  $a_n$ ,  $a_x$ , and  $\dot{q}$ ; the lateral directional response variables are  $\beta$ ,  $p$ ,  $r$ ,  $\phi$ ,  $a_y$ ,  $\dot{p}$ , and  $\dot{r}$ . The variables  $\dot{p}$ ,  $\dot{q}$ , and  $\dot{r}$  are often not available; however, differentiated values of  $p$ ,  $q$ , and  $r$  should not be substituted as they add no new information. Not all the response variables must be measured for each maneuver, but the more that are available, the more reliable will be the derivative estimates.

Aircraft carry a wide range of instrumentation to sense angle of attack and angle of sideslip, including boom-mounted vanes, "cheek" or "chin" vanes, differential pressure ports (ref. 27), and inertial navigation systems. Care should be exercised in choosing the type of instrumentation for derivative estimation purposes. "Cheek" and "chin" vanes are subject to local flow effects and require extensive calibration; pressure ports are noted for measurement lags; and inertial navigation systems do not account for wind shears or turbulence. The best available instrumentation is probably the boom-mounted vane, as it appears to have the fewest deficiencies. Most of the data analyzed to date at the Dryden Flight Research Center have been obtained from boom-mounted vanes.

In special situations, time histories of some of the normally constant parameters are required. The most common example of this is the necessity for time histories of velocity and dynamic pressure if those signals change enough during a maneuver to have significant effects on the estimates. In general, any signal that changes significantly during a maneuver should be recorded as a function of time.

## Data Quality

Considerations in the quality of data can be separated into two basic problem groups: problems that cannot be accounted for after the data are obtained and problems that can. Examples of the first group are the data resolution and sampling rate, and some effects of basic data filtering. Examples of the second group are found in the specification of known instrument locations and orientations, and the effects of basic data filtering that result in known time shifting of the data. This section contains a brief discussion of some of these problems and in some instances shows the effect on the data or the analysis, or both.

## Resolution, sampling rate, and record length

Two basic factors in data quality are the instrument resolutions and the sampling rates. Experience indicates that in general neither of these factors alone is critical (ref. 24). However, the additive effects of these and other problems can be significant. Fairly low resolution can be tolerated in any noncontrol measurement if measurement noise is small. This is particularly true if many signals are used for time history matches and some of the signals have good resolution. If the data clearly define the aircraft response and no other data problems exist, the estimator can be expected to perform well. Much the same conclusion can be drawn in regard to the sampling rate. For typical aircraft at typical flight conditions, sampling rates of 10 samples per second are often adequate for the analysis (ref. 4); however, problems can arise for aircraft with fast responses or for data resulting from rapid control inputs. Sampling rate requirements are also related to the duration of the maneuvers (ref. 28). As discussed later under *Filtering*, the sampling rate is often dictated by considerations other than the estimation procedure. Sampling rates as high as 200 samples per second are sometimes needed to filter out structural vibrations.

To assess more completely the effect of data resolution, sampling rate, and record length on the maximum likelihood estimates, a study was undertaken using the high quality data obtained from the PA-30 aircraft. The data were obtained at a sampling rate of 200 samples per second on a 9-bit pulse code modulation system and

thinned to 50 samples per second for analysis. The basic resolutions for the signals of interest are shown in the following table. Four lateral-directional maneuvers obtained at the same flight condition and with the same computer-generated control input were chosen for the study. Figure 2 shows the time history of one of these maneuvers and the fit obtained with the maximum likelihood estimation method.

Signal	Resolution
$\beta$ , deg . . . . .	0.1
$q$ , deg/sec . . . . .	0.25
$r$ , deg/sec . . . . .	0.15
$\phi$ , deg . . . . .	0.75
$a_y$ , g . . . . .	0.003
$\delta_a$ , deg . . . . .	0.1

The effect of reduced resolution on these maneuvers was assessed by obtaining estimates from the maneuvers with simulated reduced resolution. The resolution was reduced by factors of 2, 4, 8, 16, 32, and 64 for each of the four maneuvers. The maximum likelihood estimation method was applied to each case to obtain a complete set of lateral-directional stability and control derivatives from the reduced resolution data. Figure 3 shows

the data of figure 2 with the resolution reduced by a factor of 16 and the fit obtained with the maximum likelihood estimation method. The fit is still remarkably representative of the actual data. Note that even at this drastically reduced resolution, the control input in particular is still representative of the measured signal. If the control input had been affected more dramatically by reduced resolution, the fit and estimates would have deteriorated greatly.

The effects of the reduced data resolution on three estimated coefficients,  $C_{l\beta}$ ,  $C_{l\delta_a}$ , and  $C_{n_r}$ , are presented

in figure 4. There is little effect on these estimates until the resolution is reduced by a factor of 16. The reduction of the resolution by a factor of 32 results in a significant degradation in the estimates, as evidenced by the change in the average estimate and the increased scatter of the estimates. These results indicate that for high quality data, fairly low resolution can be tolerated without significantly reducing the quality of the estimates. For poorer data where greater nonlinearity is present, reduced resolution should be expected to have a larger effect on the fit and the estimates.

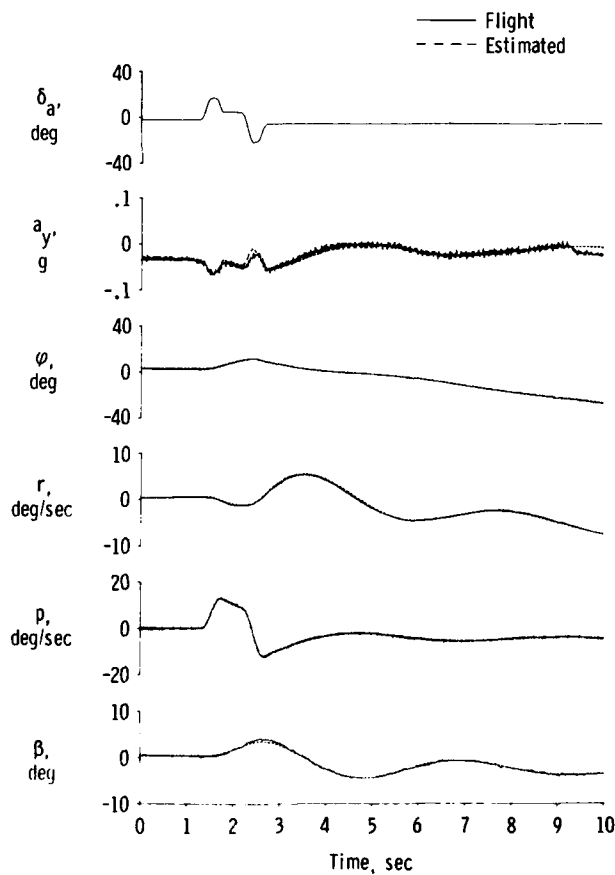


Figure 2. Fit of computed and flight data for lateral-directional maneuver.



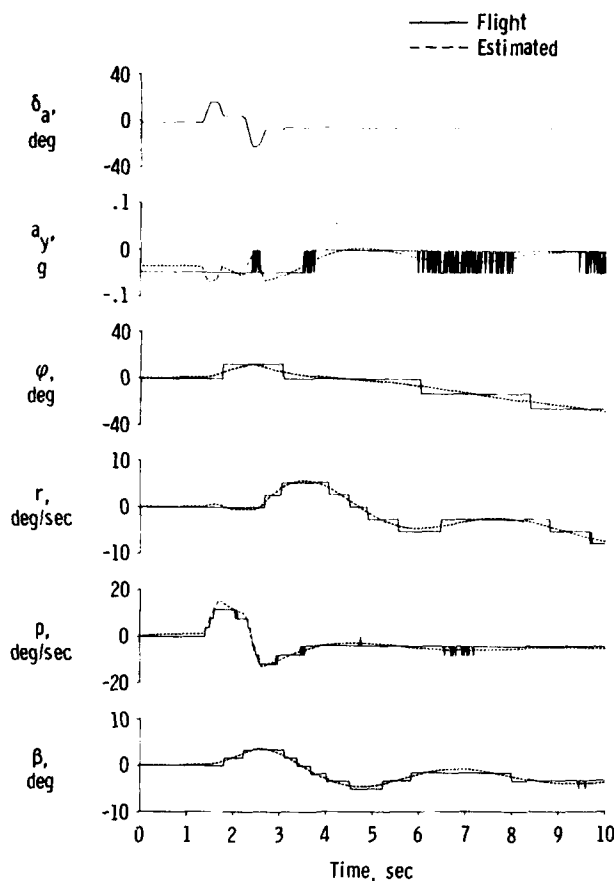


Figure 3. Fit of computed and flight data of figure 2 with resolution reduced by a factor of 16.

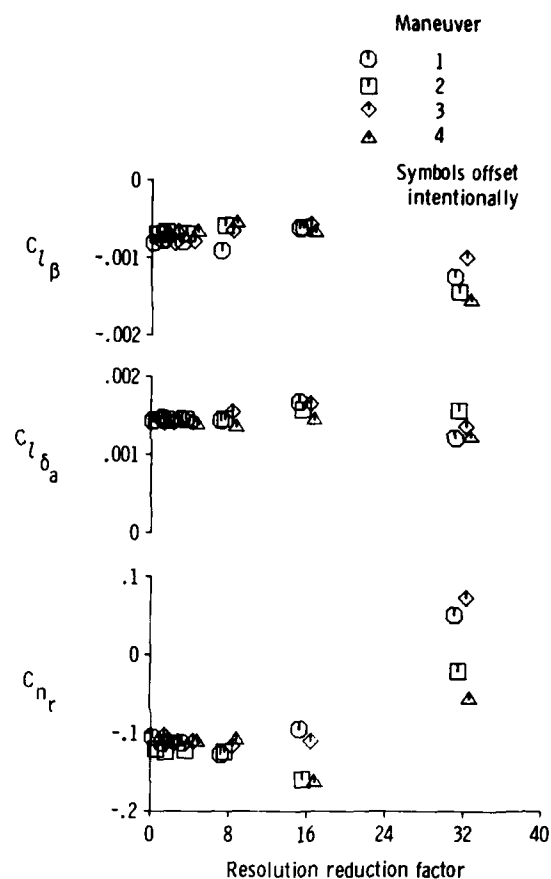


Figure 4. Selected stability and control derivatives as functions of measurement signal resolution.

The computer time required to perform a derivative estimation is directly proportional to the number of data points, which is proportional to the sampling rate and record length. In addition, lowering the sampling rate results in lessening the requirements on the data acquisition system. However, the sampling rate and record length obviously have lower limits where any greater reduction would result in meaningless estimates (ref. 28). To determine these lower limits, the four lateral-directional maneuvers were analyzed for data obtained at a basic sampling rate of 50 samples per second and for data with sampling rates reduced by factors of 2, 3, 4, 5, 10, 15, and 20. This resulted in sampling rates from 2.5 samples per second to 50 samples per second. The estimates of the derivatives were obtained for each maneuver at each sampling rate. Figure 5 presents the estimates of  $C_{l\beta}$ ,  $C_{l\delta_a}$ , and  $C_{n_r}$  as functions of sampling rate. For this aircraft, the estimates show little change until the sampling rate is reduced to less than 5 samples per second. At a sampling rate of 2.5 samples per second, the estimates of  $C_{l\beta}$  and  $C_{l\delta_a}$  become unacceptable.

Since the number of data points used is a function of both the sampling rate and the record length, it is of interest to investigate the combined effect of sampling rate and record length. To evaluate this effect, the same four maneuvers were analyzed using only one-fourth of the total record. The data used include the portion of each maneuver where the control input occurred and correspond to the time segment from 1 second to 3.5 seconds in figure 2. The results of this analysis are presented in figure 6 for  $C_{l\beta}$ ,  $C_{l\delta_a}$ , and  $C_{n_r}$ . The scatter in the estimates for  $C_{l\beta}$  and  $C_{n_r}$  is unacceptable for all sampling rates. The estimates of  $C_{l\delta_a}$  are unaffected by sampling rate; the record length also has no effect on the estimates of  $C_{l\delta_a}$ , as might be expected since the control input portion of the maneuver was retained. (It should be noted that the same number of data points are used for the analysis of the entire record length at 12.5 samples per second (fig. 5) as are used for the quarter record length at 50 samples per second (fig. 6).) For  $C_{l\beta}$  and  $C_{n_r}$ , the scatter is five to ten times as great for the shorter record length. This result indicates that, in the absence of other considerations, reducing the sampling rate is more effective than reducing the record length as a method of reducing the total computer time required without greatly degrading the quality of the estimates.

The preceding results indicate that fairly low resolution or sampling rate can be tolerated on this aircraft for the derivatives shown. If the resolution and sampling rate were reduced simultaneously, the magnitude of the tolerable reductions might be smaller.

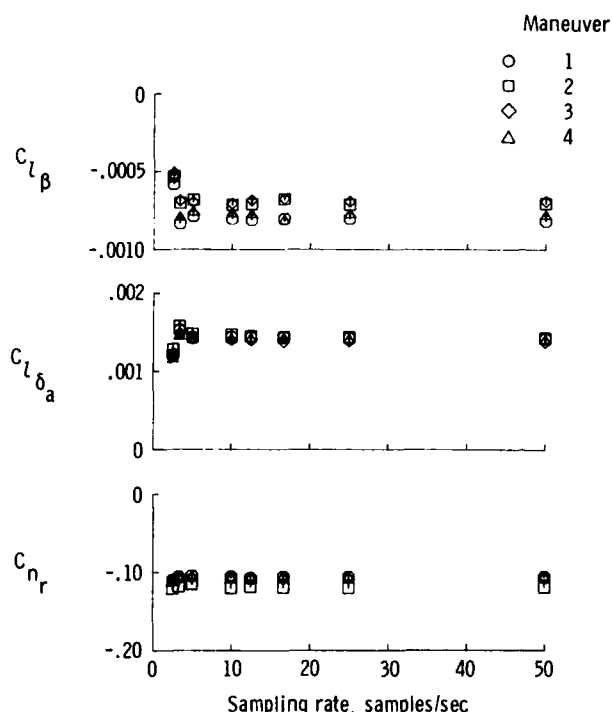


Figure 5. Selected stability and control derivatives as functions of sampling rate for original lateral-directional maneuvers.

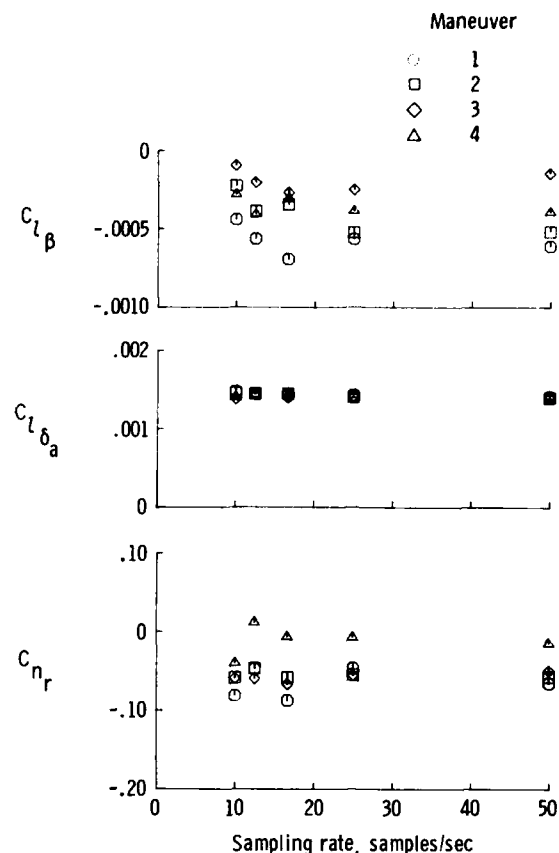


Figure 6. Selected stability and control derivatives as functions of sampling rate for the one-fourth record length lateral-directional maneuvers.

### Filtering

Sometimes data must be filtered prior to analysis to remove unwanted noise from the measurements. In general, however, unnecessary filtering of data should be avoided. One of the primary problems caused by filtering is the introduction of phase or time shifts in the data, the effect of which is discussed in the next section. If filtering is necessary, all filter roll-off frequencies should be kept much higher than the aerodynamic frequencies of interest.

Figure 7 shows a longitudinal time history obtained from the oblique wing aircraft (ref. 17). Due to the construction of the vehicle, it was difficult to mount the instrumentation package in a vibration-free environment. Therefore, to analyze the data, the structural noise (particularly evident on  $q_n$  and  $q$ ) was reduced with a digital filter. The specification of the filter characteristics was based on the results of an analysis of the power spectral densities of the measured data. The power spectral density of the  $q_n$  signal (fig. 8) shows several modes between 40 and 80 hertz, and one broad mode centered at 17.7 hertz. The strong peak at 60 hertz is a result of engine vibration. Based on the power spectral density analysis, it was determined that a notch filter at 17.7 hertz and a third-order Butterworth low-pass filter with a break frequency of 20 hertz (ref. 17) would remove most of the noise from the signals shown in figure 7. The power spectral density of the filtered  $q_n$  signal is shown in figure 9. A significant reduction in the power at 17.7 hertz and above 20 hertz is apparent. All the data in figure 7 were filtered with the same filter, and the filtered data are shown in figure 10. Marked improvement in  $q_n$  and  $q$  is apparent in the filtered data with no noticeable phase shift or attenuation in the aerodynamic responses.

If the unfiltered data are thinned below 200 samples per second, aliasing of the 40-hertz to 80-hertz structural responses becomes a problem. In the thinned data, these responses are folded down to lower frequencies and cannot be separated from the rigid-body response. The folding is illustrated by figure 11, which is the power spectral density of the unfiltered  $q_n$  signal thinned to 25 samples per second. The structural modes from figure 8 have folded down and spread over the spectrum between 0 hertz and 12.5 hertz, with the result that the spectrum is nearly white. It would be almost impossible to recover a good signal from these data; therefore, 200-sample-per-second data were necessary for filtering out the structural response. After filtering, the data were thinned to 25 samples per second for analysis.

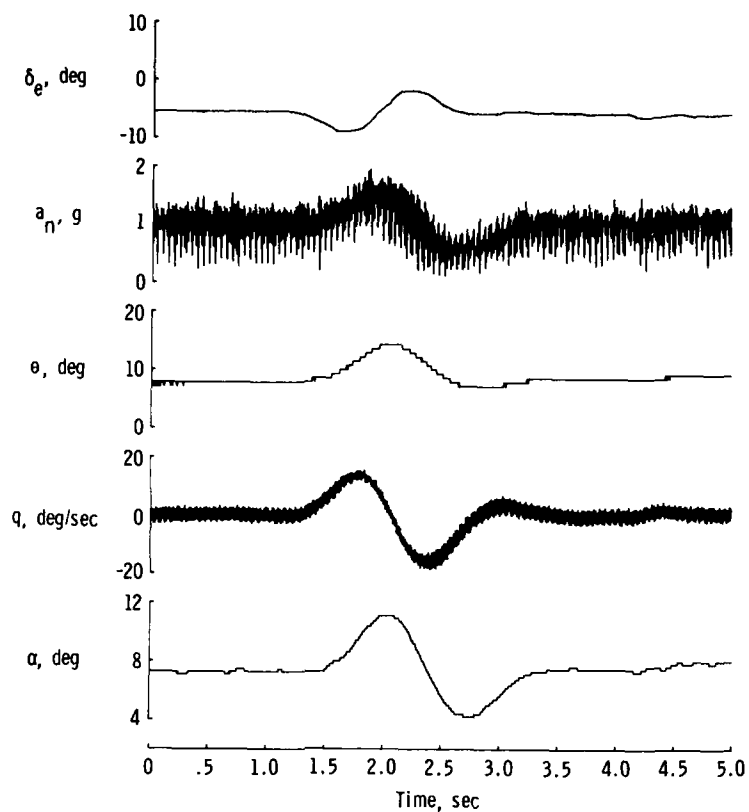


Figure 7. Time history of unfiltered longitudinal data.

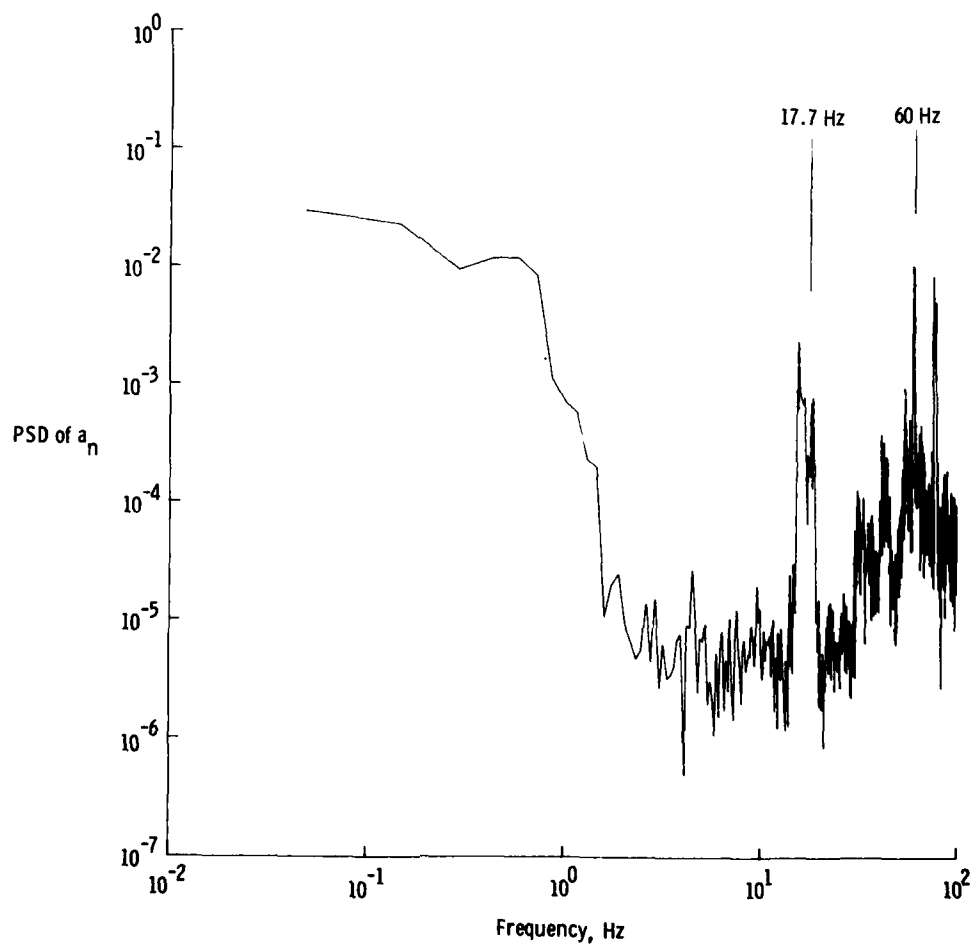


Figure 8. Power spectral density of unfiltered 200-sample-per-second data.

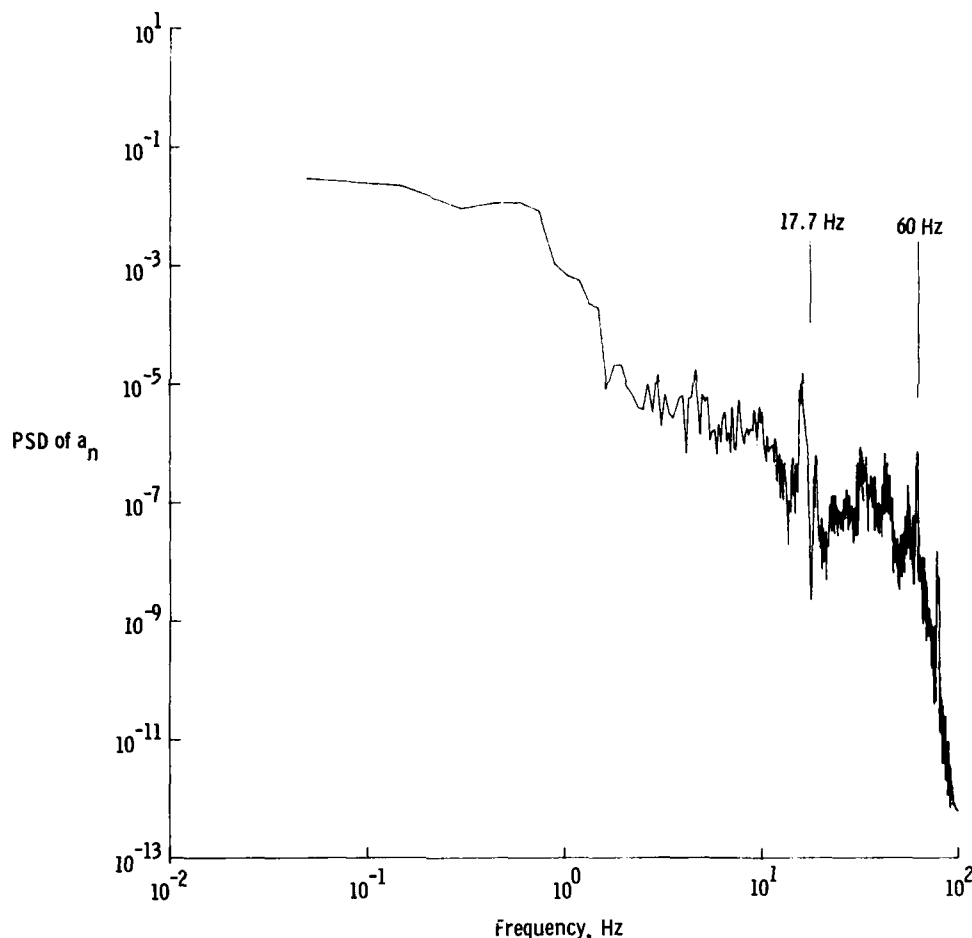


Figure 9. Power spectral density of filtered 200-sample-per-second data.

#### Time Shifts

The maximum likelihood estimator is very sensitive to small time or phase shifts between parameters (ref. 29). One cause of such shifts is the instrumentation filtering discussed in the previous section. If it is not possible to avoid filters, all the measurements should be filtered with the same filter, or phase shift corrections should be applied to the raw data for all the filtered measurements.

Time shifts may also be caused by the effects of data sampling. Most data sampling techniques result in small time skews between parameters. For example, if the data are sampled at 10 samples per second, the sample of one parameter may be separated by up to 0.1 second from the sample of another parameter in the same time frame of data. The maximum likelihood estimation algorithm assumes that all measurements in one time frame are sampled simultaneously, so any time shift causes errors in the estimated coefficients. This type of time shift becomes particularly important when the control input is sampled at a significantly different time than one or more of the response measurements within the sample interval. If the skew due to sampling is large, its effect can be compensated for by time shifting the appropriate signals before the analysis is begun.

There are causes for time or phase shifts other than filtering and sampling, such as the lag in the response of pressure instrumentation when long tubes are involved (ref. 27). Whatever the cause of these shifts, every effort must be made to eliminate or account for them if the estimation process is to yield high quality estimates.

The effects of time and phase shifts in the flight data on the stability and control derivative estimates are documented in reference 29. An example from reference 29 of the effect on  $L_\beta$  of a time shift in  $p$ ,  $\beta$ , or  $\delta_a$  is shown in figure 12. The yaw rate,  $r$ , and lateral acceleration,  $a_y$ , were also used in the analysis, but they were not time shifted. The zero-shift value is assumed to be the correct value, and a positive shift indicates that all the other signals lead the shifted variable. As shown in the figure, shifts in  $p$  or  $\delta_a$  have significant effects on the estimated value of  $L_\beta$ . A positive time shift of 0.1 second for  $\delta_a$  results in a 50-percent error in  $L_\beta$ . A negative time shift of 0.1 second in  $p$  also results in a 50-percent error. Time shifts larger than 0.1 second have been observed in flight data. Reference 29 shows similar results for most of the stability and control derivatives of five aircraft, although the magnitude and direction of the effect of the shift on the derivatives are not necessarily the same as shown in figure 12.

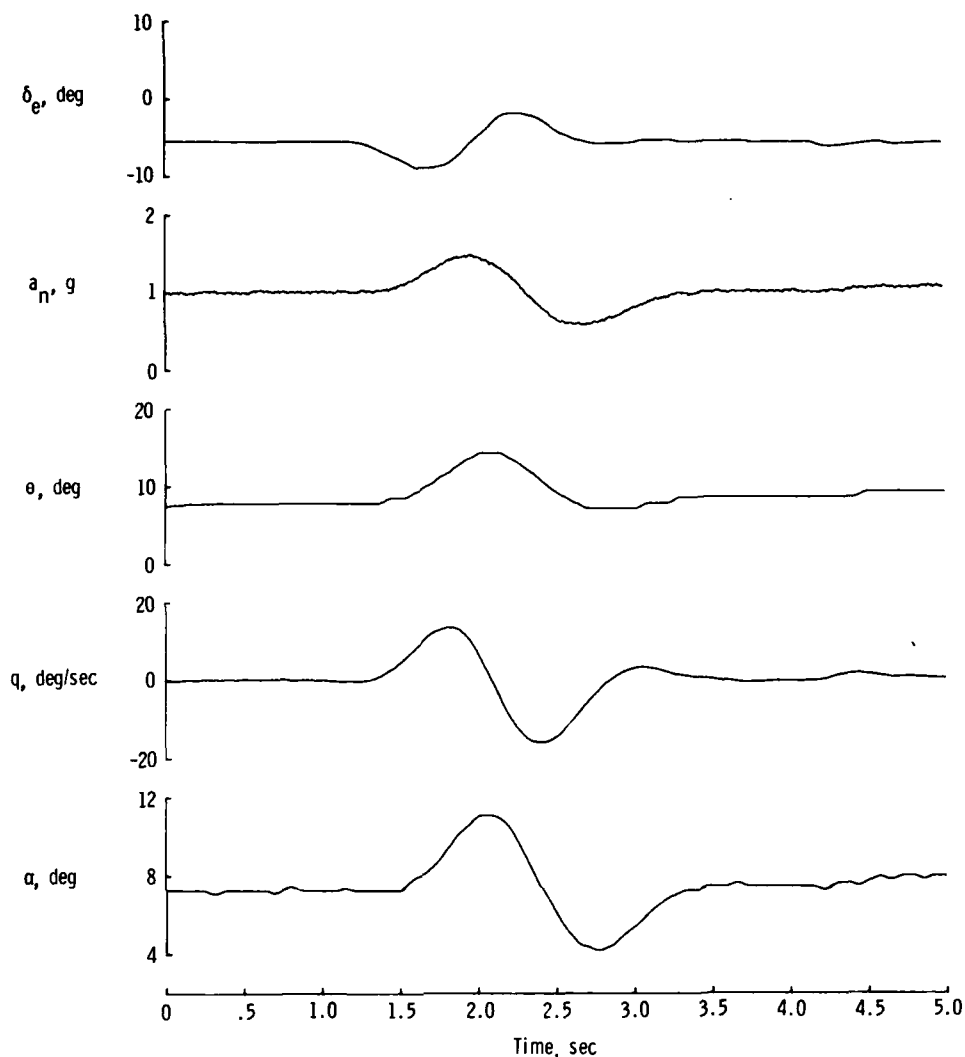


Figure 10. Time history of filtered longitudinal data.

#### Measurement Corrections

Instrument positions and angular orientations in the aircraft are important factors in analyzing flight data. There are usually no particular requirements on where the instruments must be, but it is important to know precisely where they are in order to account for the effects of their displacement from the center of gravity.

Knowing the positions of the accelerometers and the angle-of-attack and angle-of-sideslip vanes is particularly important in estimating stability and control derivatives. If these instruments are offset from the center of gravity, corrections can be made in the analysis. If the data are not corrected for vane location, the fit of the data will be poor, particularly when angular rates are high. If the data are not corrected for accelerometer position, some of the estimated derivatives ( $C_{Y\beta}$  and  $C_{L\alpha}$ , in particular) will be affected.

If the correction for accelerometer location has not been made, it usually becomes evident when the measured and estimated data are compared. In figure 13(a), for example, the fit of the flight and estimated data for the 3/8-scale F-15 remotely piloted research vehicle (RPRV, ref. 30) for roll rate,  $p$ , is excellent, but there are some discrepancies in the fit of the data for  $a_y$ , particularly where  $\dot{p}$  is large. This is the type of mismatch that occurs if the accelerometer location is different from that assumed in the model. If a more precise determination of the location of the lateral accelerometer is made and included in the estimation process, a better fit results. The fit that resulted when the assumed vertical location on the RPRV was changed by 15 centimeters (which corresponds to 40 centimeters on an F-15 aircraft) is shown in figure 13(b). The fit for  $a_y$  is much better and the fit for  $p$  is slightly improved.

It might be thought that such a small inconsistency would have an insignificant effect on the estimates of the derivatives. Figure 14(a) shows the coefficient  $C_{Y\beta}$  estimated from the accelerometer position assumed in figure 13(a); figure 14(b) shows the coefficient estimated when the assumed accelerometer position was changed by 15 centimeters, as in figure 13(b). The values of  $C_{Y\beta}$  in figure 14(b) are approximately 50-percent greater in magnitude than those in figure 14(a). Obviously, the stability and control derivative estimates are sensitive to instrument location.

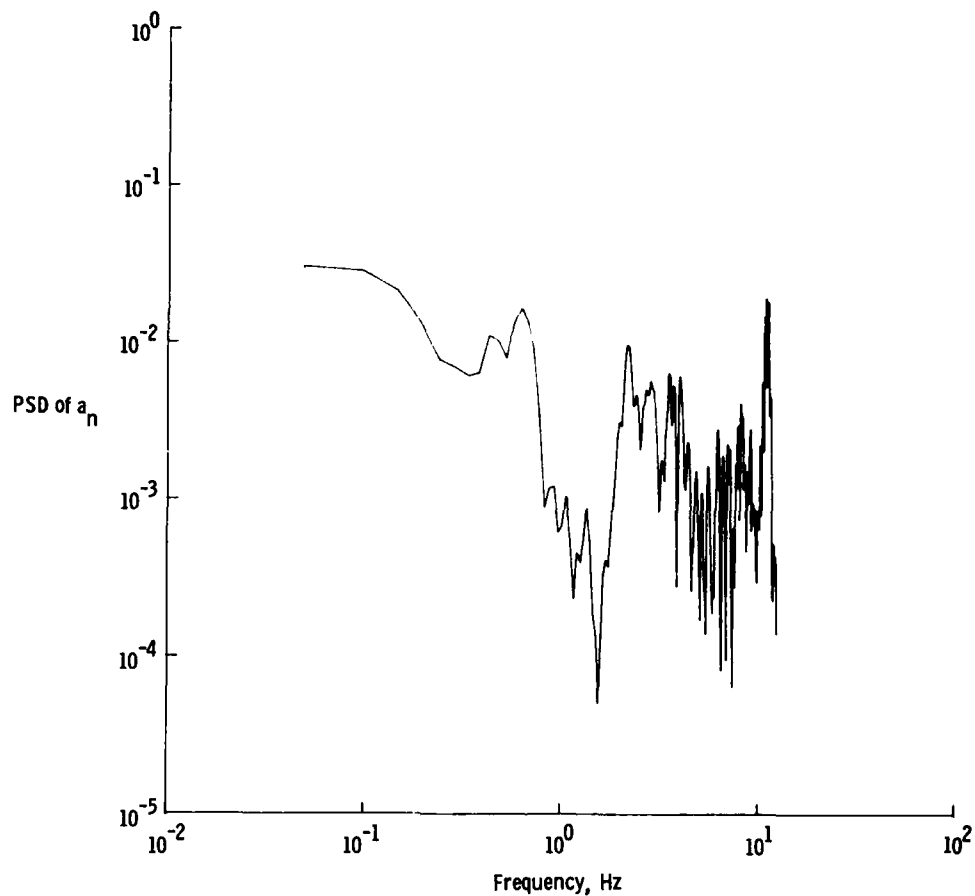


Figure 11. Power spectral density of unfiltered 25-sample-per-second normal acceleration.

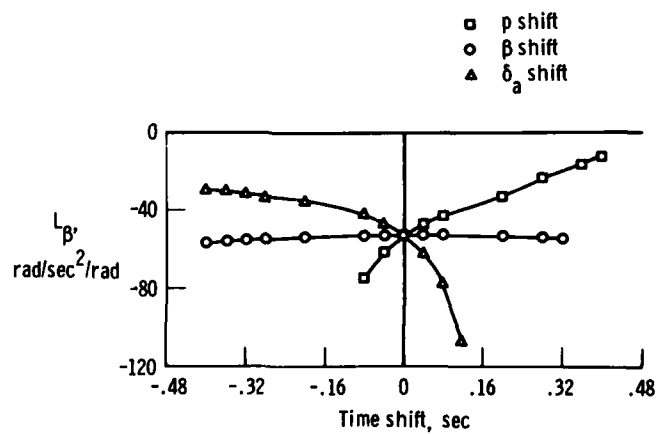
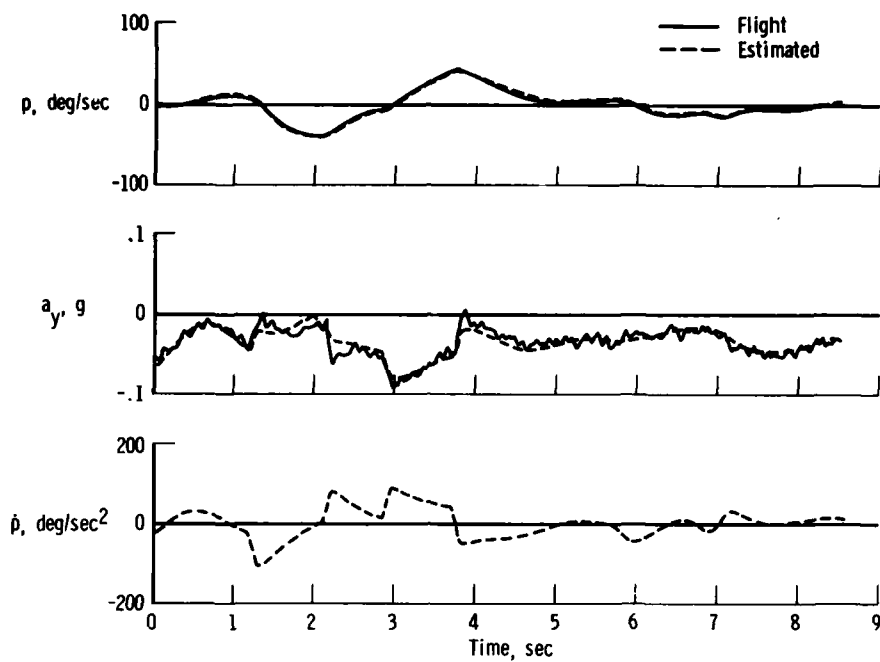
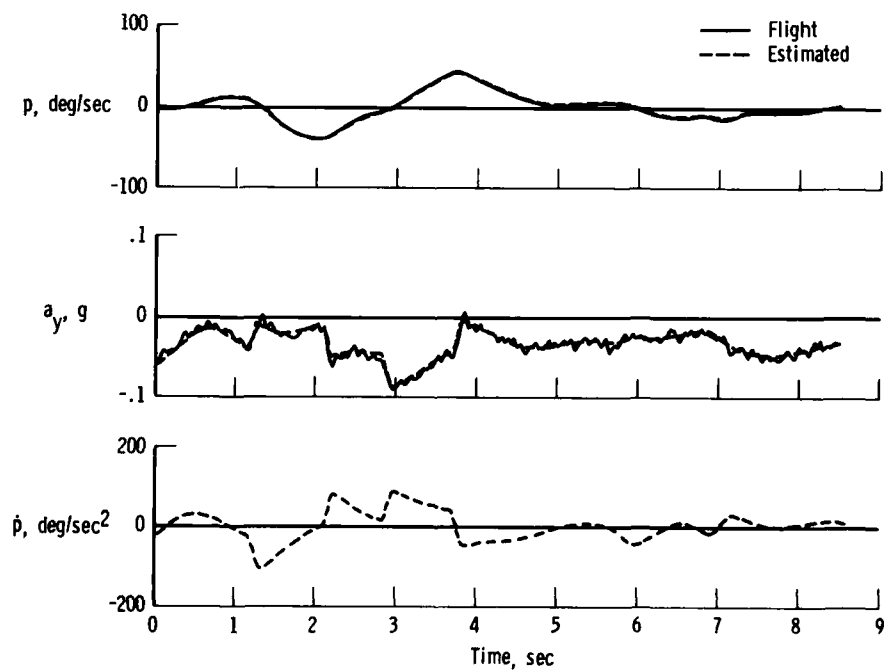


Figure 12. Estimated  $L_\beta$  as a function of time shift.

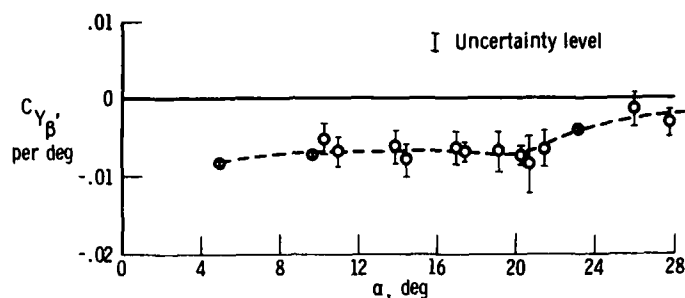


(a) Incorrect accelerometer location.

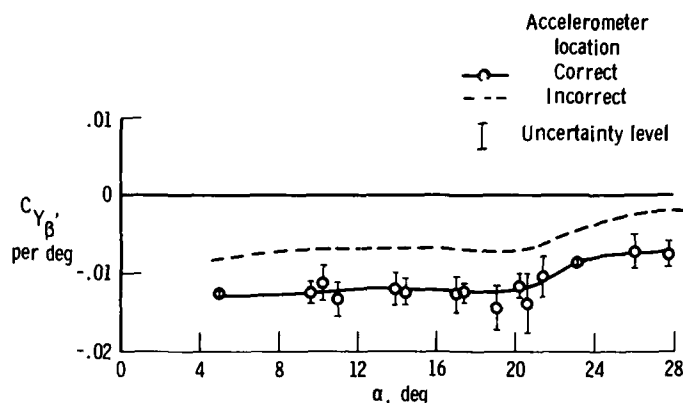


(b) Correct accelerometer location.

Figure 13. Effect of correct identification of lateral accelerometer location on fit of computed and flight data.



(a) Incorrect accelerometer location.



(b) Correct accelerometer location.

Figure 14. Values of  $C_{Y_{\beta}}$  found when location of lateral accelerometer is specified correctly and incorrectly.

While instrumentation and data acquisition can pose unexpected problems for the analyst, these problems can usually be overcome by care and planning. The analyst need only know what the instruments actually measure and to what effects the estimator is sensitive.

#### ESTIMATION EXAMPLES

For 13 years, the NASA Dryden Flight Research Center has used the maximum likelihood technique to estimate stability and control derivatives from flight data. During this time, a considerable amount of experience has been gained in both the theoretical and practical aspects of using this method. Dryden has obtained stability and control derivatives with this method from over 3500 maneuvers from 32 different aircraft including many unusual configurations. Among these aircraft have been a hypersonic rocket-powered research vehicle (the X-15); a series of lifting bodies (the M2-F2, HL-10, M2-F3, X-24A, and X-24B); two large commercial airliners (the CV-990 and B-747); several general aviation aircraft (including the Piper Twin Comanche and the Beech 99); a high-altitude reconnaissance aircraft (the YF-12); two large supersonic bombers (the B-70 and B-1); several remotely piloted aircraft (including an oblique wing aircraft, the Firebee, the Minisniffer, and the spin research vehicle); a large number of fighter aircraft (the F-8, F-111, F-111 transonic aircraft technology (TACT), F-14, F-15, YF-16, and YF-17); and the space shuttle and space shuttle carrier aircraft. The flight conditions have included Mach numbers up to 5, altitudes up to 30 kilometers, angles of attack from  $-20^\circ$  to  $53^\circ$ , and normal accelerations up to 4 g's. Virtually all derivative extraction at the Dryden Flight Research Center is now done with maximum likelihood estimators.

Most of the stability and control analysis at Dryden has been done with a simple linear model, but occasionally a more complete model is needed. In general, the MMLE 3 program is capable of handling both types of analysis. An example of the more complete, five-degree-of-freedom model is given in the appendix. For a linear model, equations (1) and (2) can be written in the following form:

$$\dot{x}(t) = Ax(t) + Bu(t) \quad (5)$$

$$y(t) = Cx(t) + Du(t) \quad (6)$$



The simple linear two-degree-of-freedom model for the longitudinal dynamics of an aircraft is given by the following equations.

$$\dot{\mathbf{x}}(t) = \begin{bmatrix} \dot{\alpha}(t) \\ \dot{q}(t) \\ \dot{\theta}(t) \end{bmatrix} = \begin{bmatrix} Z_\alpha & 1 & (-\sin \theta)(\cos \varphi)g/V \\ M_\alpha & M_q & 0 \\ 0 & \cos \varphi & 0 \end{bmatrix} \begin{bmatrix} \alpha(t) \\ q(t) \\ \theta(t) \end{bmatrix} + \begin{bmatrix} Z_{\delta_e} & Z_0 \\ M_{\delta_e} & M_0 \\ 0 & \dot{\theta}_0 \end{bmatrix} \begin{bmatrix} \delta_e(t) \\ 1 \end{bmatrix} \quad (7)$$

$$\mathbf{y}(t) = \begin{bmatrix} \alpha(t) \\ q(t) \\ \theta(t) \\ a_n(t) \end{bmatrix} = \begin{bmatrix} 1 & 0 & 0 \\ 0 & 1 & 0 \\ 0 & 0 & 1 \\ (-V/g)Z_\alpha & 0 & 0 \end{bmatrix} \begin{bmatrix} \alpha(t) \\ q(t) \\ \theta(t) \end{bmatrix} + \begin{bmatrix} 0 & 0 \\ 0 & 0 \\ 0 & 0 \\ (-V/g)Z_{\delta_e} & a_{n_{bias}} \end{bmatrix} \begin{bmatrix} \delta_e(t) \\ 1 \end{bmatrix} \quad (8)$$

$$\mathbf{z}(t) = \mathbf{y}(t) + \boldsymbol{\eta}(t) \quad (9)$$

$$\boldsymbol{\xi}^* = (Z_\alpha \ M_\alpha \ M_q \ Z_{\delta_e} \ M_{\delta_e} \ Z_0 \ M_0 \ \dot{\theta}_0 \ a_{n_{bias}})$$

$J(\boldsymbol{\xi})$  of equation (4) is then minimized over the time interval  $T$  by adjusting the five stability and control derivatives and the three bias terms in the vector  $\boldsymbol{\xi}$  to minimize the difference between the measured response and the computed response,  $\mathbf{z}(t)$  and  $\hat{\mathbf{z}}_{\boldsymbol{\xi}}(t)$ .

The simple linear lateral-directional model is given by the equations

$$\dot{\mathbf{x}}(t) = \begin{bmatrix} \dot{\beta}(t) \\ \dot{p}(t) \\ \dot{r}(t) \\ \dot{\phi}(t) \end{bmatrix} = \begin{bmatrix} Y_\beta & \sin \alpha & -\cos \alpha & (\cos \varphi)(\cos \theta)g/V \\ L_\beta & L_p & L_r & 0 \\ N_\beta & N_p & N_r & 0 \\ 0 & 1 & (\cos \varphi)(\tan \theta) & 0 \end{bmatrix} \begin{bmatrix} \beta(t) \\ p(t) \\ r(t) \\ \phi(t) \end{bmatrix} + \begin{bmatrix} Y_{\delta_a} & Y_{\delta_r} & Y_0 \\ L_{\delta_a} & L_{\delta_r} & L_0 \\ N_{\delta_a} & N_{\delta_r} & N_0 \\ 0 & 0 & \dot{\phi}_0 \end{bmatrix} \begin{bmatrix} \delta_a(t) \\ \delta_r(t) \\ 1 \end{bmatrix} \quad (10)$$

$$\mathbf{y}(t) = \begin{bmatrix} \beta(t) \\ p(t) \\ r(t) \\ \phi(t) \\ a_y(t) \end{bmatrix} = \begin{bmatrix} 1 & 0 & 0 & 0 \\ 0 & 1 & 0 & 0 \\ 0 & 0 & 1 & 0 \\ 0 & 0 & 0 & 1 \\ (V/g)Y_\beta & 0 & 0 & 0 \end{bmatrix} \begin{bmatrix} \beta(t) \\ p(t) \\ r(t) \\ \phi(t) \end{bmatrix} + \begin{bmatrix} 0 & 0 & 0 \\ 0 & 0 & 0 \\ 0 & 0 & 0 \\ 0 & 0 & 0 \\ (V/g)Y_{\delta_a} & (V/g)Y_{\delta_r} & a_{y_{bias}} \end{bmatrix} \begin{bmatrix} \delta_a(t) \\ \delta_r(t) \\ 1 \end{bmatrix} \quad (11)$$

$$\mathbf{z}(t) = \mathbf{y}(t) + \boldsymbol{\eta}(t) \quad (12)$$

$$\boldsymbol{\xi}^* = [Y_\beta \ (\sin \alpha) \ L_\beta \ L_p \ L_r \ N_\beta \ N_p \ N_r \ Y_{\delta_a} \ Y_{\delta_r} \ Y_0 \ L_{\delta_a} \ L_{\delta_r} \ L_0 \ N_{\delta_a} \ N_{\delta_r} \ N_0 \ \dot{\phi}_0 \ a_{y_{bias}}]$$

These models are representative of most aircraft at many flight conditions, but occasionally unusual aircraft configurations, unusual analysis requirements, or unusual flight conditions create special problems for the analyst. Several of these problems are discussed in the sections that follow.

#### Measures of Estimate Accuracy

With any parameter estimation method, it is important to have a measure of the accuracy of the estimates. In the absence of modeling error or bias, the scatter of the estimates is a reasonable indication of the overall accuracy. Accuracy can also be assessed by observing the consistency of the trend in the estimates as a function of the primary variables defining the flight condition, such as angle of attack or Mach number. However, if only one or two cases are available at a given condition, neither the scatter nor the established trend can be evaluated. In addition, even when many cases are available, it is useful to have an indication of which individual estimates are the most reliable. The Cramer-Rao bound provides the best known analytical measure of the accuracy of each estimate.

### Common accuracy measures

The Cramer-Rao bound for unbiased estimators is

$$\text{Variance } (\xi) \geq \left\{ E \left\{ \left[ \nabla_{\xi} \log p(Z/\xi) \right] \left[ \nabla_{\xi} \log p(Z/\xi) \right]^* \right\} \right\}^{-1} \quad (13)$$

This equation gives only a lower bound for the variance of the estimates. The maximum likelihood estimates, however, are asymptotically efficient; this means that for large time intervals, the variance is approximately equal to the expression in the above inequality, provided that the system and noise are correctly modeled.

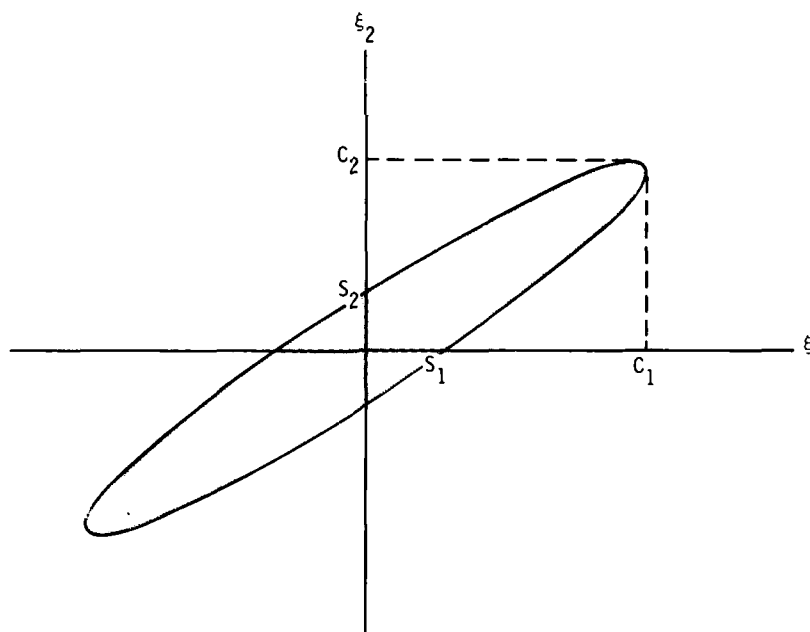
For the no-state-noise case, equation (13) can be evaluated as

$$\text{Variance } (\xi) \approx \left\{ \int_0^T \left[ \nabla_{\xi} \hat{z}_{\xi}(t) \right] (GG^*)^{-1} \left[ \nabla_{\xi} \hat{z}_{\xi}(t) \right]^* dt \right\}^{-1} \quad (14)$$

When state noise is present, it is awkward to compute the exact Cramer-Rao bound, but Balakrishnan has shown (ref. 22) that equation (14) approaches the bound for large time intervals. The expression in equation (14) is easily shown to be the inverse of the portion of the second gradient matrix used in the Newton-Balakrishnan algorithm. Most maximum likelihood estimation computer programs compute this matrix, so the Cramer-Rao bounds are available with negligible extra computational effort.

The matrix used in the Cramer-Rao bound is referred to, before inversion, as the Fisher information matrix. Two other measures of estimate accuracy based on this matrix are in common use—the sensitivities and the correlations. In some instances, these quantities are poor measures. The Cramer-Rao bounds include the desirable properties of both the sensitivities and the correlations.

A diagram is helpful in illustrating the features of the three accuracy measures just mentioned. Consider a system with only two unknown parameters, and assume the cost functional,  $J(\xi)$ , is quadratic in these two parameters. The locus of points at which  $J(\xi)$  is constant is an ellipse centered at the minimum point of  $J(\xi)$ . The sketch below shows such an ellipse where the constant has been chosen such that there is a 63.2-percent ( $1\sigma$ ) probability that the true value lies inside the ellipse (shaded area).



The sensitivities are defined as the square roots of the diagonal elements of the Fisher information matrix. The inverses of the sensitivities are indicated on the diagram by the points  $S_1$  and  $S_2$ . As shown, the sensitivity measures how much an individual coefficient can change when all the other coefficients are fixed, without leaving the shaded area. The sensitivity is known to be a poor measure of accuracy because it neglects all correlation between coefficients. The value of  $\xi_1$  can be increased to about five times  $S_1$  without leaving the shaded area, if  $\xi_2$  is increased correspondingly.

The correlations (normalized off-diagonal elements of the inverse of the information matrix) are related to the eccentricity of the ellipse. As has just been demonstrated, the eccentricity is important in gauging the accuracy of the estimates. The correlations do not tell the full story, however, as they give no information on the size of the ellipse. A small ellipse with high eccentricity obviously provides better estimates than a large circle. Thus, accurate estimates can exist with high correlations, and inaccurate estimates can exist with low correlations, which are undesirable properties for a measure of accuracy. Other problems with the correlations

arise if more than two unknowns exist, because the correlations are essentially two-dimensional tools, in the same sense that the sensitivities are one-dimensional tools.

In regard to the above diagram, the best measure of the accuracy of  $\xi_1$  is the largest value of  $\xi_1$  contained inside the ellipse (hyperellipse, if there are more than two unknowns), regardless of the values of any other unknowns. This value is indicated on the diagram by  $C_1$ , and the corresponding value for  $\xi_2$  is indicated by  $C_2$ . The values of  $C_1$  and  $C_2$  are given by the Cramer-Rao bounds (the square roots of the diagonal elements of the inverse of the information matrix). It is evident that the Cramer-Rao bound takes into account the eccentricity (correlation) and size (sensitivity) of the ellipse in precisely the correct manner. In addition, the Cramer-Rao bound remains valid in any number of dimensions because it accounts for multidimensional correlations of any order.

No discussion of estimate accuracy is complete without a mention of modeling error. It is difficult even to define estimation accuracy unless the system is described exactly by the assumed dynamic model with some "true" values of the parameters. Physical systems are seldom so agreeable as to conform exactly to simple dynamic models. Neither the Cramer-Rao bound nor any other known technique can evaluate all the possible effects of modeling error with complete confidence. All the attempts known to the author have involved modeling the modeling error. Although such efforts can provide improved fidelity and better understanding of the effects of specific errors, they are circular in nature and do not address the basic theoretical problem. Therefore, the Cramer-Rao bound should not be taken as an incontestable value for the accuracy of the estimate, but instead as one of the tools available to assist in the evaluation. The usefulness of this tool has been well established in practice in many investigations; examples are given later in this lecture.

#### Assessment of Cramer-Rao bounds

In spite of the strong theoretical rigor behind the Cramer-Rao bound, it would be wise to evaluate its reasonability in applications to typical aircraft data before placing too much dependence on it. A simple reasonability check can be made by comparing the Cramer-Rao bound with the amount of scatter of the estimates. Figure 15

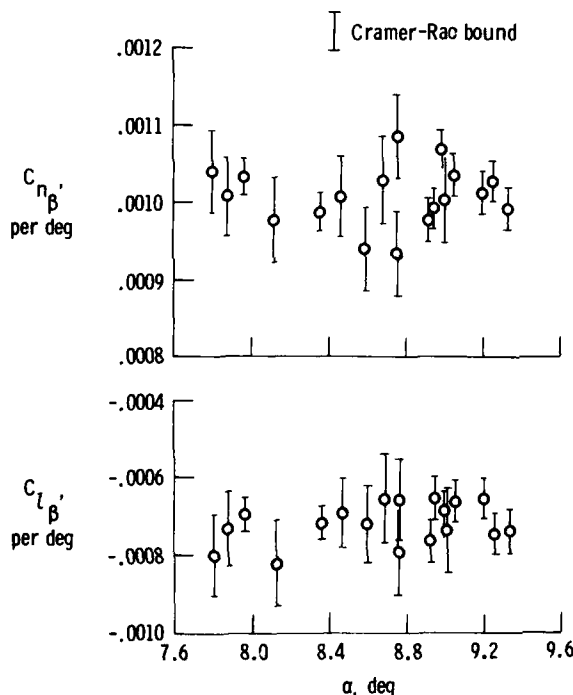


Figure 15. Stability derivative estimates and Cramer-Rao bounds for computed data.

illustrates this comparison for simulated data with artificial Gaussian white measurement noise. The scales of the figure are expanded to show the effect. The symbols indicate the maximum likelihood estimates of  $C_{n\beta}$  and  $C_{l\beta}$  based on the data from 18

simulated maneuvers with measurement noise added. Derivatives and input signals were taken from the PA-30 flight data discussed in the following paragraph and used to create the simulated data. The magnitude of the simulated measurement noise was chosen to make the scatter of  $C_{l\beta}$  and  $C_{n\beta}$  typical of the scatter

observed in flight data. The vertical bars show the magnitudes of the Cramer-Rao bounds. In theory, the magnitudes of the Cramer-Rao bounds should approximately equal the standard deviations of the estimates. This can be visually verified in figure 15.

Although the Cramer-Rao bound checks out excellently on computed data, it has long been known that a large anomaly exists in results from flight data. Figure 16 shows a comparison of the same type as that shown in figure 15, except that the actual flight data from the PA-30 aircraft were used to obtain the derivative estimates and the Cramer-Rao bounds. These data were obtained at the same flight condition as was used for the simulated data. The data scatter in figure 16 is obviously far greater than predicted by the Cramer-Rao bounds. This phenomenon of greater scatter than predicted by the Cramer-Rao bound is common to all flight data. In reference 24 it was proven useful to multiply the Cramer-Rao bound by a factor of 5 to 10 to make the bound representative of the scatter observed in flight data. (The Cramer-Rao bound times this factor is called the uncertainty level.) The factor was purely empirical, and no

rigorous theoretical explanation was available for why the disagreement existed or whether it could be properly accounted for by a constant factor. The necessity for this unexplained factor considerably weakened the confidence that could be placed in the Cramer-Rao bound.

Recent investigations have shown that the disagreement can be explained by carefully accounting for the spectral characteristics of the residual errors of flight data. Previous analysis has assumed that the measurement noise was band-limited white, with the band limit equal to the Nyquist frequency,  $\frac{1}{2\Delta t}$  (typically 10 to 25 hertz). A band limit of approximately 1 hertz is more typical of that observed in actual data, but the Nyquist frequency was chosen as the assumed band limit because the frequency of the band limit did not seem important. In addition, the assumption of the Nyquist frequency greatly simplified the analysis in the discrete time case since the noise samples at each point were then independent. However, if the primary analysis is done in continuous time and discretized for the actual computation only at the last step of analysis, it is equally easy to assume any band limit. In fact, both the maximum likelihood estimation algorithm and the Cramer-Rao bound are unaffected by the band limit in the continuous time analysis.

This result seems to verify the earlier assumption that the bandwidth is unimportant to the analysis. However, the bandwidth is also used explicitly (in the continuous time case) or implicitly (in the discrete time case) to determine the weighting matrix,  $(GG^*)^{-1}$ , from real data. The usual procedure to compute  $GG^*$  is to compute the total power of the residual error and divide by the Nyquist frequency; in the discrete time case, the total power itself is used and the division by the Nyquist frequency is done implicitly in the algorithm.

The source of the problem can be easily seen: If the band limit is lower than the Nyquist frequency, the usual computation of the spectral density will be incorrect; the total power should properly be divided by the actual band limit instead of the Nyquist frequency. Since actual data are not strictly band limited but decrease in power over a finite frequency range, some error is inherent in selecting any single frequency as the band limit. This error, however, would be of an acceptable magnitude, unlike the factor-of-25 error between a realistic 1-hertz band limit and the 25-hertz Nyquist frequency of data obtained at 50 samples per second. Since the Cramer-Rao bound is given by the square root of equation (14), errors in the determination of the spectral density,  $G$ , will directly influence the bound.

The flight data from figure 16 can be used to illustrate these principles. An average band limit of approximately 1 hertz was observed in the power spectral densities of the residual measurement errors. Using this band limit increased the estimate of  $G$  by a factor of 5 over that obtained when the 25-hertz Nyquist frequency was assumed to be the band limit. Figure 17 shows the resulting Cramer-Rao bounds, which are five times larger than those in figure 16. The agreement between the scatter and the Cramer-Rao bounds is much better in figure 17.

Naturally, the same band limit does not have to be used for all the signals. If different band limits are used, the change in the Cramer-Rao bound cannot be expressed as a simple factor, but the bound can still be computed simply by using the correct  $G$  matrix. Other acceptable methods of estimating  $G$  are available, including direct examination of the magnitude of the power spectral density of the residual error.

These results are consistent with the good agreement already observed on simulated data because the additive noise used with the simulated data studies was band limited at the Nyquist frequency. Recent simulated data studies have succeeded in reproducing the disagreement observed in flight data by using simulated noise with lower bandwidths. This lends support to the interpretation of the Cramer-Rao bound presented here.

#### Linear Dependence Problems

Many of the difficulties in estimating stability and control coefficients from flight data fall into the category of linear dependence problems; that is, two or more of the variables to be estimated are linearly dependent and cannot be separately estimated from the data available. A simple example of linear dependence occurs in an

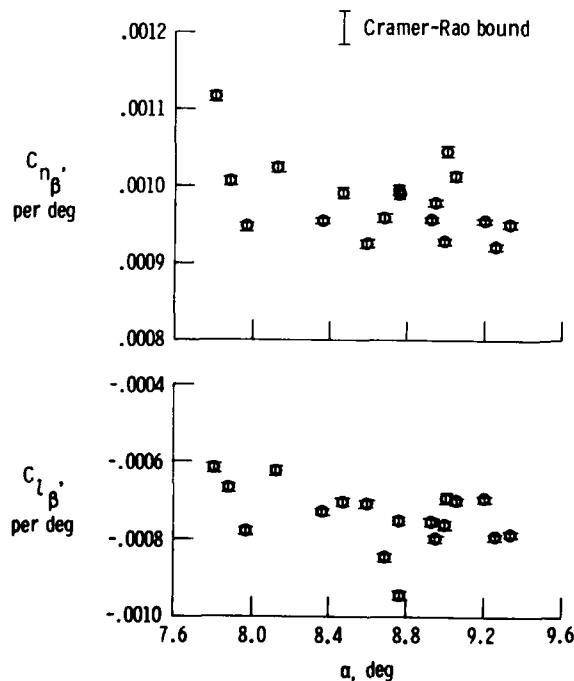


Figure 16. Stability derivative estimates and Cramer-Rao bounds for flight data.

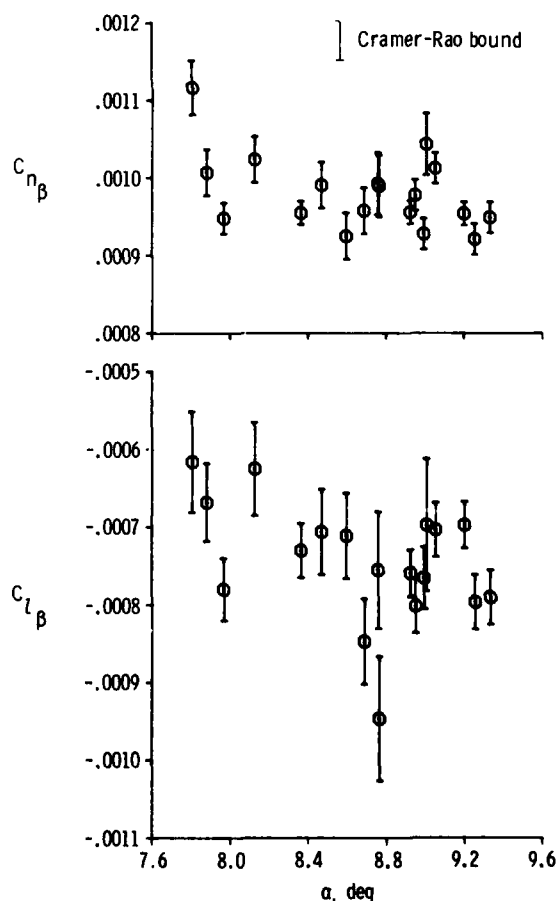


Figure 17. Stability derivative estimates and Cramer-Rao bounds for flight data obtained by modifying assumed spectral densities.

undamped lateral-directional maneuver. In this type of maneuver,  $\beta$ ,  $p$ , and  $r$  are all pure sinusoids; therefore, any one of the signals can be written as a linear combination of the other two.

There are two basic causes of linear dependence problems. One cause is an overly complex model. There is a temptation for the analyst to make the model as detailed and accurate as possible, including every term that might conceivably arise in any situation. The increased computational costs are accepted in exchange for the presumably increased accuracy and greater generality. If the additional terms are completely known, as in the case of kinematic cross-coupling terms (see Cross Coupling section), there are no particular problems with this approach. However, the additional terms often include unknown coefficients, which must be estimated along with the basic stability and control derivatives. If too many coefficients are unknown, there will not be enough information in the data to obtain accurate estimates. Not only will the estimates of the added coefficients be poor, but the estimates of the basic coefficients will also be degraded. Therefore, a complicated model can actually result in poorer estimates rather than increased accuracy. In some cases, the algorithm will not converge and no estimates can be obtained. Because of these difficulties, a program should not be set up to handle all situations, then left in the hands of an inexperienced technician. Rather, the program should be designed for a basic set of equations, with options or modifications to apply to specific circumstances. The analyst must have the experience, or be guided by someone with the experience, to recognize the important factors in each situation and invoke the appropriate options or modifications.

The second cause of linear dependence problems is inadequate control input. If the input used does not adequately excite all the dynamic modes of the model, it may not be possible to estimate all the coefficients. Problems with inadequate control inputs are common when the airplane is flown with the stability augmentation system (SAS) on. Without additional information, it is impossible to adequately distinguish between the basic airframe damping and the damping induced by the control feedback. To obtain derivatives from SAS-on maneuvers, each control surface must have an independent control input in addition to the SAS feedback.

The Cramer-Rao bounds (or, more precisely, the uncertainty levels described in the section on Cramer-Rao bounds) can be used as a tool for evaluating whether linear dependence problems exist. Figure 18 shows estimates of  $C_{n_p}$  for a PA-30 airplane at three flap settings.

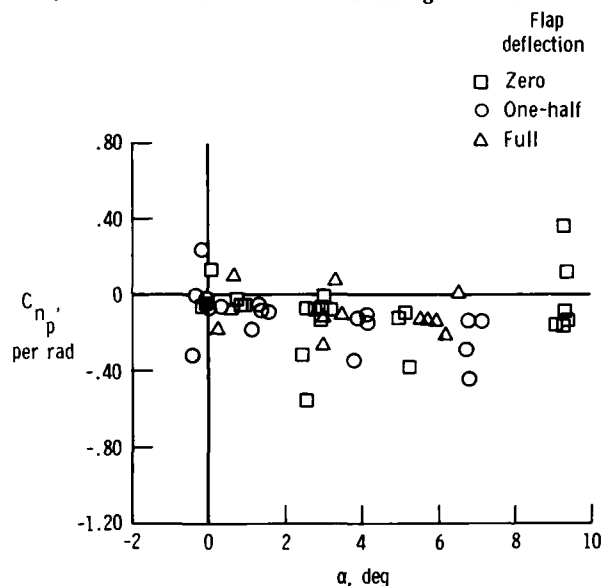


Figure 18. Variations of  $C_{n_p}$  with angle of attack without uncertainty levels.

There is a significant amount of scatter, and little information about  $C_{n_p}$  can be gleaned from this figure.

In figure 19, the same data are shown with uncertainty levels. The points with small Cramer-Rao bounds lead to a well-defined fairing when the points with large Cramer-Rao bounds are ignored.

In an attempt to discover the reason for the poor Cramer-Rao bounds associated with some of the data in figures 18 and 19, the data from rudder and aileron maneuvers were plotted separately (fig. 20). The data from the aileron maneuvers form a well-defined line with little scatter and good Cramer-Rao bounds, but the rudder maneuvers result in a large amount of scatter and poor Cramer-Rao bounds. It is obvious that the rudder pulse does not excite the airplane motion adequately for identification purposes. To best identify all the stability and control derivatives of the PA-30 airplane, maneuvers with both aileron and rudder inputs should be used. As a substitute, an aileron maneuver can be analyzed along with a rudder maneuver to obtain a single set of estimates based on both sets of data. Figure 21 shows the same data as in figure 20, reanalyzed with the multiple maneuver approach. The scatter and poor Cramer-Rao bounds have disappeared, and the fairing from the aileron maneuvers is shown to be a good representation of the response to both aileron and rudder pulses.

These PA-30 data provide a good example of a linear dependence problem and the use of the Cramer-Rao bound to deduce the reasons for the problem and devise a solution.

#### Aircraft Scale Effects

One way to assess the quality of flight estimates is to compare the estimates with predictions from other sources. When making this comparison, great care must be taken to assess any possible sources of error that may contaminate the estimates or predictions. Errors may enter the flight-determined maximum likelihood estimates from many sources, some of which are discussed elsewhere in this lecture. Sometimes, after all apparent sources of error have been investigated, differences between the estimates still exist. Such differences have been observed when comparing wind tunnel estimates with flight-determined estimates. The differences are frequently attributed to either scale effects or the differences in aerodynamic flow between the static wind tunnel tests and the dynamic flight maneuvers. It is therefore of interest to compare flight-determined estimates from the same configuration for two scales.

The F-15 airplane (described in ref. 31) and the 3/8-scale model F-15 RPRV (ref. 30) are of the same configuration. Other than scale, the primary difference between the two vehicles is that the F-15 RPRV is unpowered with blocked inlets and the F-15 airplane is powered.

Stability and control maneuvers were performed on the F-15 airplane and the F-15 RPRV. The maneuvers on the F-15 airplane were performed at three engine mass flow rates to assess the effect of the propulsion system on the stability and control derivatives. A complete set of stability and control derivatives were obtained for both vehicles using the maximum likelihood estimation method. These derivatives were obtained on both vehicles over an angle-of-attack range of approximately  $-15^\circ$  to  $20^\circ$ . The propulsion system appeared to have little effect on the derivatives. In general, very good agreement was found between the estimates from the two vehicles.

Figure 22 shows the maximum likelihood estimates of  $C_{n_\beta}$ ,  $C_{n_r}$ , and  $C_{n_{\delta_r}}$  from the F-15 RPRV. The vertical bars represent the uncertainty levels (see Cramer-Rao bounds section). The fairing of the data was determined by considering the estimates with the smaller uncertainty levels to be more reliable. Figure 23 presents estimates from the F-15 airplane of the same derivatives in the same format. The various symbols represent various mass flow rates. The fairing from figure 22 is repeated in figure 23. The agreement between the two vehicles is good for  $C_{n_\beta}$  and  $C_{n_r}$ . The trend for  $C_{n_{\delta_r}}$  is the same for both vehicles, but the F-15 airplane indicates more rudder control effectiveness. There is no trend in  $C_{n_{\delta_r}}$  for the F-15 airplane

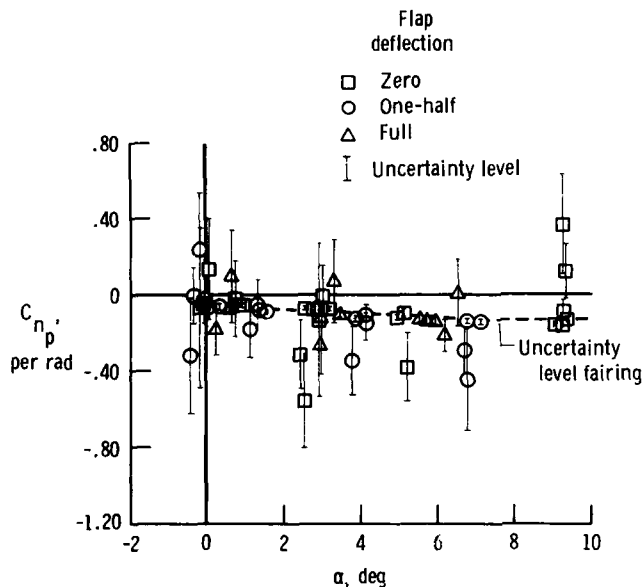


Figure 19. Variations of  $C_{n_p}$  with angle of attack with uncertainty levels.

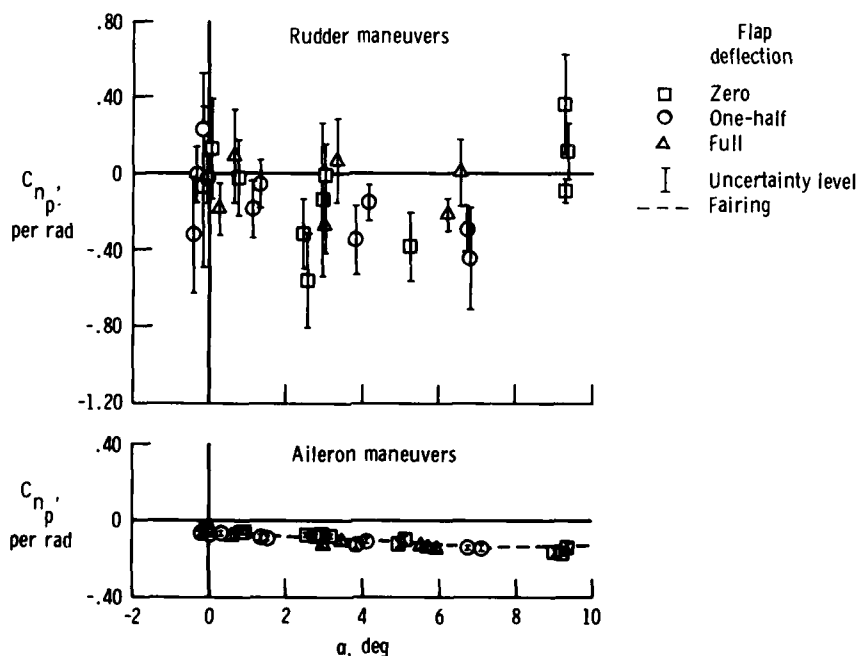


Figure 20. Variation of  $C_{n_p}$  with angle of attack for rudder and aileron maneuvers.

to indicate that an extrapolation of the mass flow rates would account for this difference. Since  $C_{n_\beta}$  and  $C_{n_r}$  for the two vehicles are in good agreement, it is unlikely that an error in dynamic pressure or the moment of inertia in one of the vehicles would account for the difference. Therefore, the difference in  $C_{n_{\delta_r}}$  between these vehicles may be attributable to scale effects.

#### Structural Modes

The identification of structural coefficients from flight data is of great importance to the overall definition of the aircraft characteristics. Research is currently being conducted in this area by many aircraft organizations, and certain successes have already been reported (ref. 11). Structural modes are also of interest when performing a stability and control analysis.

When data measured for stability and control analysis are corrupted by structural vibration, several techniques are available for treating the data to improve the results of the analysis. Three of these techniques—the removal of the structural effects, pseudostatic structural modeling, and dynamic structural modeling—are discussed in this section.

The most common approach to structural vibration problems is to remove the effects of the structural vibration as shown in the *Filtering* section. This approach assumes that the structural vibration is at relatively high frequency and therefore uncoupled from the rigid-body oscillation. The power spectra of the signals are obtained, and digital notch or low-pass filters are designed (ref. 32) to remove the structural effects without degrading the rigid-body data. Care must be exercised to avoid introducing data time skews by filtering. Such time skews could present more problems than the original structural vibration (ref. 29). The advisable approach is to filter all the signals with the same digital filter. The necessity for such digital filters must be considered when the

data system sampling rates are chosen. Sampling rates of 100 to 200 samples per second are often required for input to the filter, even though the filtered data are only used at 10 to 50 samples per second (ref. 17). The increased sampling rate requirement can be eliminated by using active analog filters before the data are sampled; however, this method creates other problems. For example, the unfiltered data measured by the sensor cannot be recovered and the filter characteristics cannot be changed after the flight. Also, the addition of analog filters requires hardware changes in the data system. Passive analog filters should be avoided if possible, because the filter break frequency, and thus the time lag, changes with the impedance loading. Unless the lags are very small, each passive filter in the system must be checked to determine its actual lag.

High-frequency structural vibration in the measurements is often due to mounting the instrument package on a flexible member. Therefore, the effects of such vibrations on the data can often be alleviated by mounting the instrument package at a location less subject to vibration. Obviously, such a solution is not always practical, as shown in an earlier example (*Filtering* section).

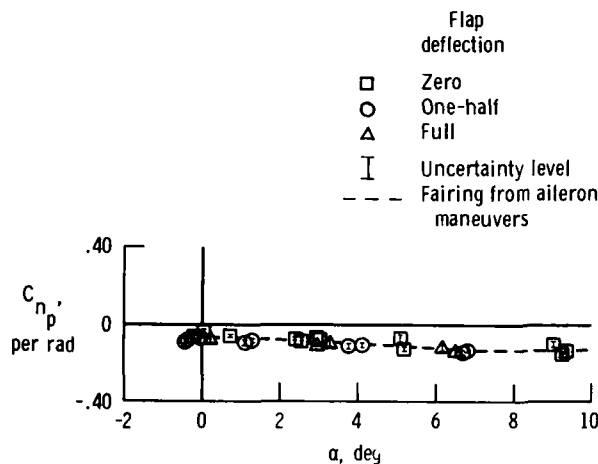


Figure 21. Variation of  $C_{n_p}$  with angle of attack for multiple maneuver analysis.

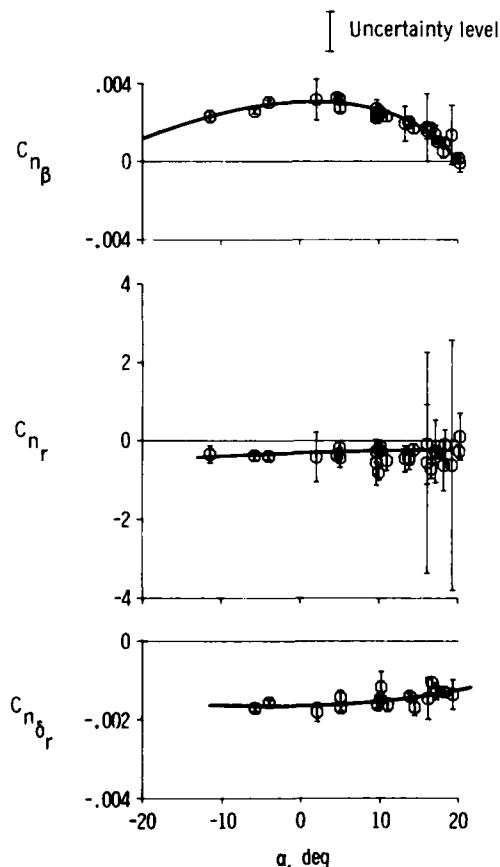


Figure 22. Selected low-speed stability and control derivatives as functions of angle of attack obtained from 3/8-scale F-15 RPRV.

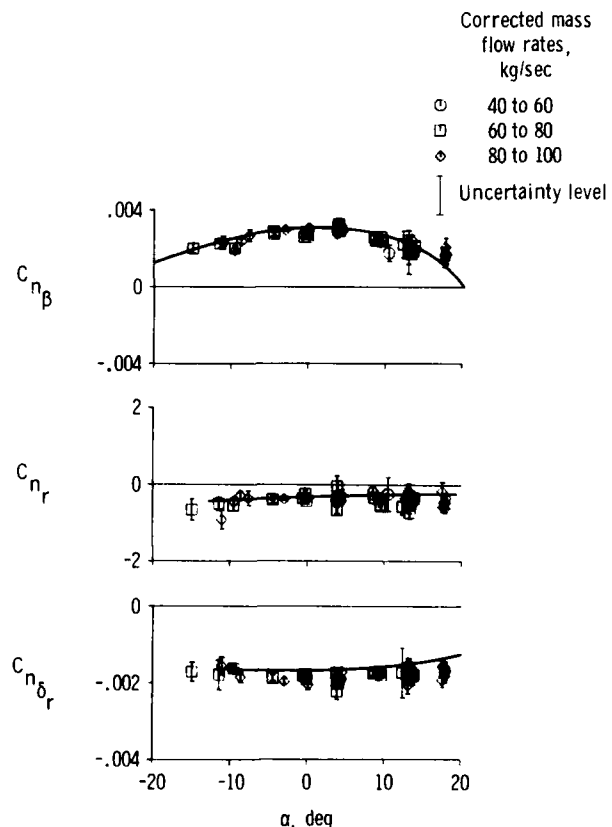


Figure 23. Selected low-speed stability and control derivatives as functions of angle of attack obtained from F-15 airplane at three engine mass flow rates.

The second approach to accounting for structural effects is pseudostatic structural modeling. This approach is appropriate for aircraft that deform under load, causing the vehicle shape to be significantly different for different flight conditions. For such aircraft, the aerodynamic coefficients are functions of load factor, or more precisely, dynamic pressure. This pseudostatic deformation effect requires no modification of the analysis technique. It does, however, require the investigation of a wide range of flight conditions to determine the trends of the coefficients as a function of flight condition.

The stability and control derivatives determined from flight data can be quite insensitive to pseudostatic structural deformations. Figure 24 shows flight-determined estimates of  $C_{N_\alpha}$  and  $C_{m_{\delta_e}}$  for an F-111A airplane

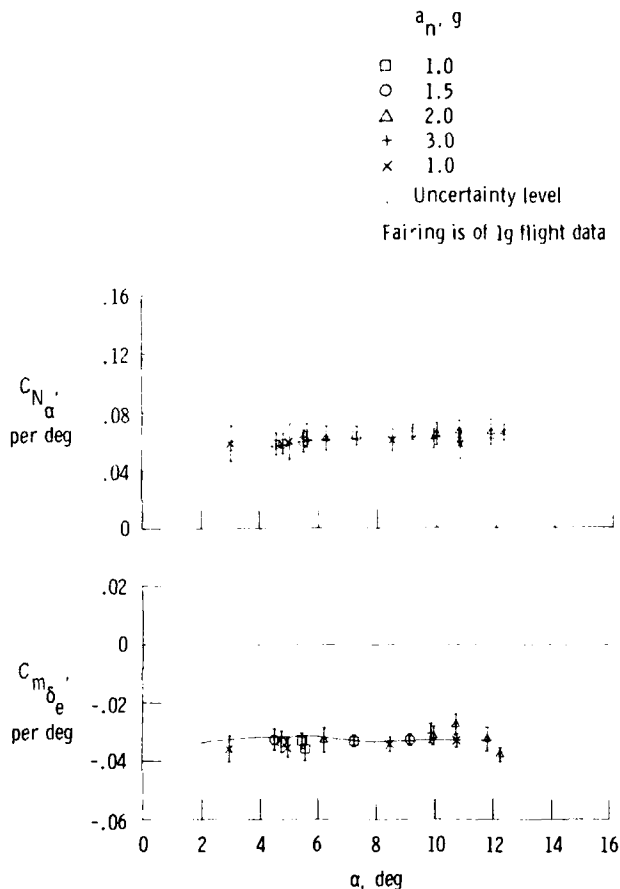


Figure 24.  $C_{N_\alpha}$  and  $C_{m_{\delta_e}}$  for an F-111A airplane with a wing sweep of  $58^\circ$  for elevated g flight.

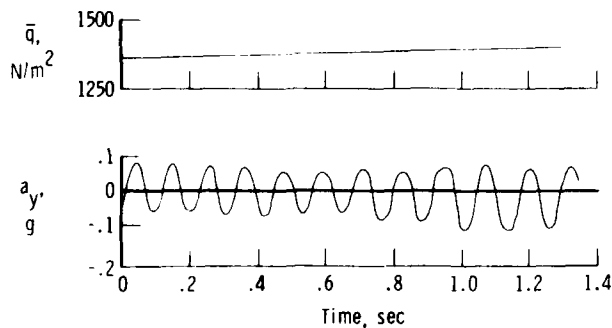


Figure 25. Structural mode oscillation observed on the lateral acceleration.

with a wing sweep of  $58^\circ$  and load factors of 1 to 3 g's (ref. 33). Although the F-111A airplane is fairly large and relatively flexible longitudinally for a fighter airplane, no effects of structural deformation on the estimated stability and control derivatives are apparent in the data shown.

The third method of accounting for structural effects is to dynamically model the structural modes and their interactions with the aerodynamics. For large flexible aircraft, where the structural modes have low frequencies and couple significantly with the rigid-body motion, this may be the only applicable analysis technique. This is a currently active research area, and many investigations are addressing the structural identification problem. Therefore, no definite list is available of the instrumentation, maneuvers, and ground test data required to obtain accurate coefficient estimates in the presence of dynamic aerostuctural interaction.

Even though no completely satisfying practical results are available that account for structural modes and their interactions with the aerodynamics, it is interesting to assess the time domain maximum likelihood analysis of the structural modes independent of any interaction. This can be done where a structural mode is observed and no significant coupling is apparent.

Figure 25 shows a structural mode on the lateral acceleration of an aircraft where little effect was observed for structural/aerodynamic coupling. The frequency of the mode is high enough so that the mode does not interact with the aerodynamic modes. Therefore, the stability and control derivatives were obtained separately and held constant for the succeeding analysis. The analysis consisted of using the maximum likelihood estimation program MMLE 3 (ref. 3) with a sixth-order model that included the lateral-directional aerodynamic modes plus one structural mode. The dynamic pressure and the velocity were allowed to vary in the analysis. The structural mode frequency and damping were estimated as linear functions of dynamic pressure. The initial conditions were also estimated. A structural mode frequency of 7.84 hertz was chosen to start the estimation process. The comparison between the original data and the fit obtained with the maximum likelihood estimation method is shown in figure 26. The two time histories are in good agreement at the beginning of the maneuver and at the end of the maneuver, but they are  $180^\circ$  out of phase at a time of approximately 0.3 second. The fit shown in figure 26 suggests that the maximum likelihood estimator has reached a local minimum but not the global minimum. Multiple minima are not normally a problem when obtaining the stability and control derivatives with the maximum likelihood estimation method. They can be a problem, however, if a technique is used that incorporates the extended Kalman filter. Multiple



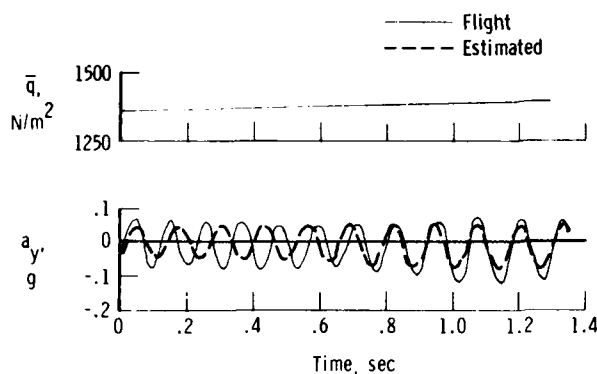


Figure 26. Fit of measured and computed lateral acceleration obtained when maximum likelihood estimator converged to local minimum.

$\hat{z}_g = \sin(\omega t)$ , where  $\omega$  is the only unknown coefficient. Then, by equation (4), the cost functional becomes

$$\begin{aligned}
 J(\omega, T) &= \int_0^T [\sin(\omega_0 t) - \sin(\omega t)]^2 dt \\
 &= T - \frac{1}{4\omega_0} \sin(2\omega_0 T) - \frac{1}{4\omega} \sin(2\omega T) \\
 &\quad - \frac{2\omega}{\omega^2 - \omega_0^2} \left[ \frac{\omega_0}{\omega} \sin(\omega T) \cos(\omega_0 T) - \cos(\omega T) \sin(\omega_0 T) \right]
 \end{aligned}$$

If  $T$  is chosen to represent 10 cycles as shown in figure 26, then for an  $\omega_0$  of 1 radian per second,  $T$  equals  $20\pi$ .

In figure 27, the cost functional  $J(\omega, 20\pi)$  is shown as a function of  $\omega$ . The global minimum is at an  $\omega$  of 1 radian per second, as it should be, but there are many local minima at increments of approximately 0.05 radian per second.

If a value of less than 0.97 or greater than 1.03 were chosen for a starting estimate of  $\omega$ , the algorithm would converge to a local minimum. If a value of between 0.98 and 1.02 were chosen, it would converge to the global minimum. Therefore, for this example where 10 cycles were observed, the starting value of  $\omega$  must be less than 3 percent from the correct answer to converge to the global minimum.

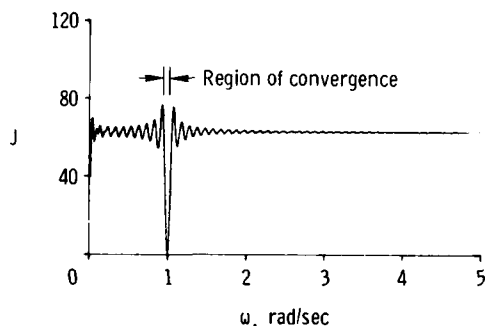


Figure 27. Cost functional for ten cycles of data as function of frequency showing close proximity of local minima to global minimum.

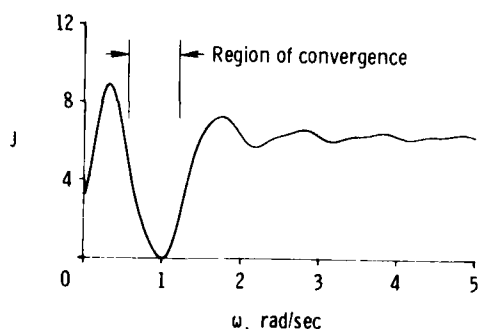


Figure 28. Cost functional for one cycle of data as function of frequency showing wide region of convergence for global minimum.

minima have been observed when the short-period and phugoid modes are analyzed simultaneously with the maximum likelihood estimation technique. This problem is caused by the long record length required to identify the coefficients of the phugoid mode. The long record length dictates that many cycles of the short-period mode occur and, if the short-period coefficients are not started very close to the correct answer, multiple minima occur. Experience has shown that it is best to first determine the short-period characteristics and then hold those constant while the phugoid characteristics are determined (ref. 34). The problem observed in figure 27 is similar to the short-period analysis discussed above in that many cycles of the structural mode are observed.

The reason for the multiple minima is demonstrated by the following simple scalar example. Let the noiseless measured response be  $z(t) = \sin(\omega_0 t)$  and the estimated response be

If  $T$  is chosen to represent only one cycle and  $\omega_0$  remains equal to 1 radian per second, then  $T$  equals  $2\pi$ . The cost functional  $J(\omega, 2\pi)$  is presented as a function of  $\omega$  in figure 28. The global minimum is correctly at an  $\omega$  of 1 radian per second, but now the algorithm converges to the global minimum if  $\omega$  is started within approximately 25 percent of the correct value.

Knowing the sensitivity of the algorithm when a record with many lightly damped cycles is being analyzed, the data of figure 25 can be reanalyzed starting closer to the observed frequency. Starting the maximum likelihood estimation method with an  $\omega$  of 9.0 results in the fit shown in figure 29. This is an acceptable fit of the data.

Based on the preceding results, if data are to be analyzed where many cycles of a structural mode are present, the structural mode frequency,  $\omega$ , must be closely approximated before starting the estimation process.

#### Turbulence

Most flight data analysis to date has been done with algorithms that do not model the effect of turbulence. These algorithms give poor results when significant turbulence is present. As stated in the MAXIMUM LIKELIHOOD ESTIMATION section, the difference between an analysis that accounts for state

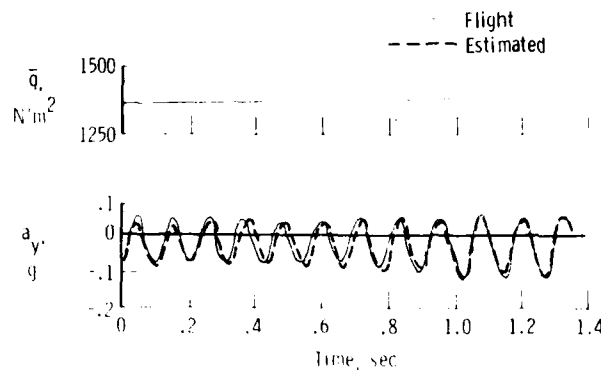


Figure 29. Acceptable fit of measured and computed lateral acceleration.

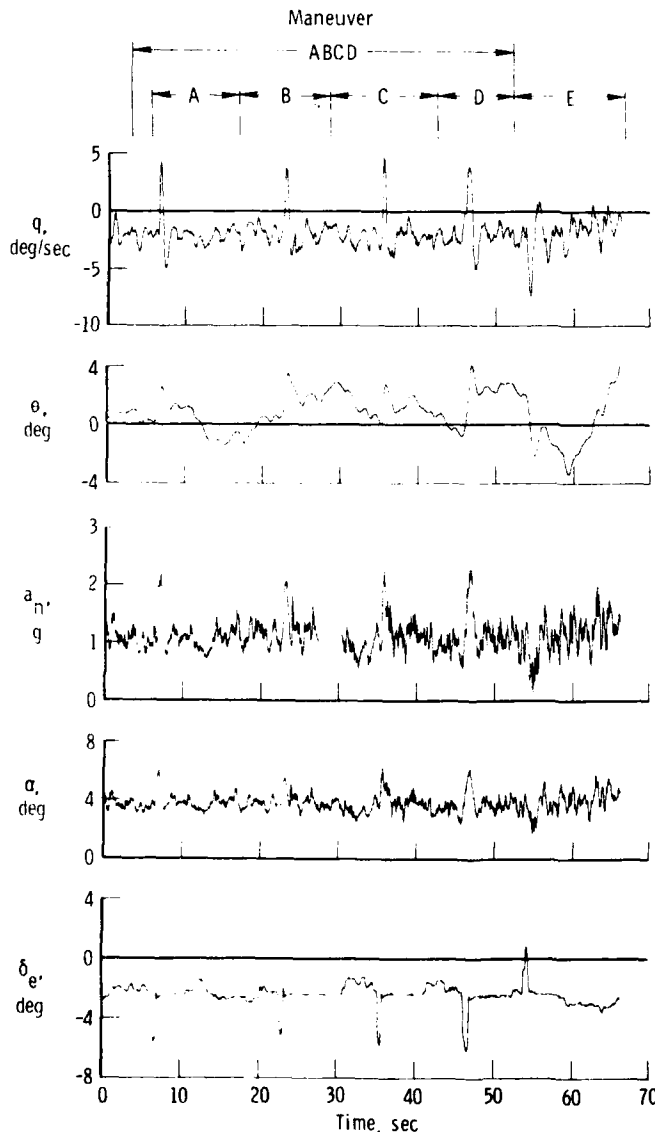


Figure 30. Total aircraft turbulence time history showing time interval for each maneuver.

noise (such as turbulence) and one that does not account for state noise is in the interpretation of equations (1) and (4). It is of interest to test the maximum likelihood algorithm on flight data obtained in turbulence. Two forms of the algorithm are evaluated in this section: one where the turbulence is not accounted for and one where it is. For simplicity, these will be referred to throughout this section as algorithm I and algorithm II, respectively.

Approximately 65 seconds of data (fig. 30) were obtained from a JetStar aircraft (ref. 35) flying in turbulence. The data were acquired during an interval in which turbulence was continuous and the pilot made five prominent inputs. Five longitudinal maneuvers of approximately equal length (13 seconds), referred to here as maneuvers A, B, C, D, and E, resulted from these inputs.

The need to account for turbulence or state noise when the maximum likelihood estimation algorithm is applied becomes obvious when the results obtained with the state noise assumed to be negligible are examined. Figure 31 compares the data measured for an aircraft flying in turbulence (maneuver E) with the computed time history based on the maximum likelihood estimator that does not account for turbulence (algorithm I). The fit shows that the assumed mathematical model is inadequate. Figure 32 shows the same comparison when the maximum likelihood estimation algorithm that accounts for the turbulence (algorithm II) is applied. The agreement is now excellent.

Each of the five maneuvers was analyzed with both algorithms (ref. 36), and only algorithm II provided acceptable matches between the computed and flight data. The mean values and the standard deviations of the estimates of the stability and control derivatives obtained from algorithms I and II from these five maneuvers are shown in figure 33, along with flight-determined estimates for smooth air and wind tunnel estimates. The standard deviations of the estimates obtained from algorithm I are unacceptable.

To complete the evaluation of algorithm II, its estimates of the state noise were compared with those defined by the Dryden expression. Figure 34 compares the power spectral density of the estimated turbulence for maneuver ABCD (fig. 30) with the asymptote for the Dryden expression. The level of the Dryden asymptote is based on the mean square of the estimated turbulence power. The shape of the power spectrum is in excellent agreement with the asymptote.

The preceding results show that the complete algorithm described by equation (4) provides good estimates of the unknown coefficients and the state noise for the longitudinal case. Some results of analysis for the lateral-directional case are given in reference 25.

The capability for obtaining derivative estimates in the presence of turbulence does exist. However, several cautions must be stated. First, there is an added computational cost, generally on the order of 30 percent. Second, it is conceivable that the aerodynamic derivatives are different in turbulence and smooth air. Although such differences have not been documented in

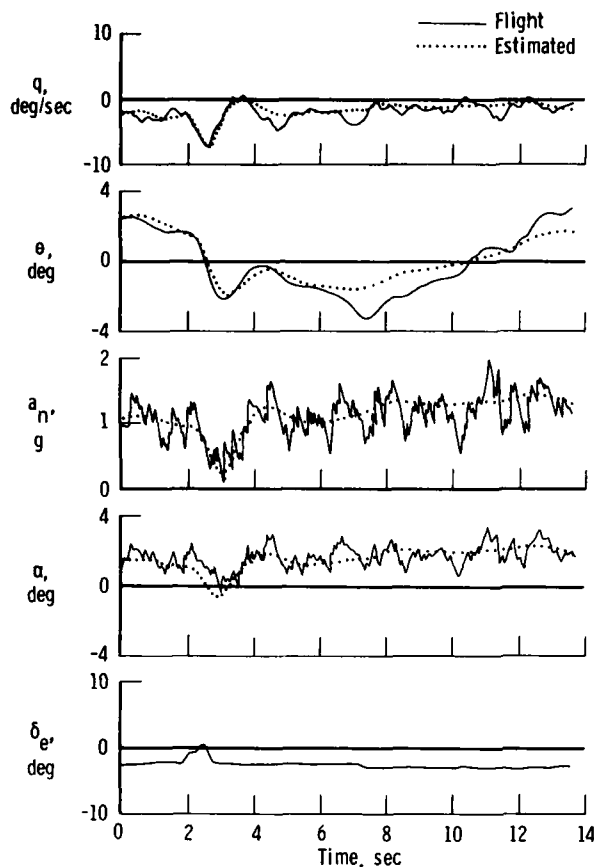


Figure 31. Comparison of flight data for maneuver E with values estimated by using algorithm 1.

sional derivatives in the equations of motion are then written as the nondimensional derivatives multiplied by the dimensionalization ratios. The dimensionalization ratios are computed as known functions of time using the measured velocity and dynamic pressure. By writing the equations in this manner, the known time variation of the system can be accounted for.

The problem of determining time-varying coefficients is then replaced by the problem of determining constant coefficients with known time-varying multipliers. This technique relies on noise-free measurements of velocity, dynamic pressure, and other changing flight conditions. The technique cannot be applied to transonic data where significant changes in Mach number occur because the dimensionless derivatives themselves are functions of Mach number.

In both the case of large variations in altitude and the case of varying flight conditions, the time-varying nature of the system is reduced to known effects. Thus, the analyst is not determining time-varying derivatives in the general sense. The computer costs for the analysis of these "time-varying" systems are high. As implemented, the "time-varying" option available in the MMLE 3 program results in a threefold increase in computer time use. Although expensive, the "time-varying" option permits analysis of the most commonly encountered time-varying systems in aircraft stability and control derivative determination while retaining the basic simplicity of the model used.

#### Nonlinearities

Most airplanes show great nonlinearities in total forces and moments when considered over large ranges of flow angles. These nonlinearities are neglected in the typical derivative estimation process because the derivatives are local linearizations of the total forces and moments. For example, the pitching moment coefficient,  $C_{m_\alpha}$ , as a function of  $\alpha$  is quite nonlinear over a large angle-of-attack range. If the change in angle of attack can be kept small enough for a given maneuver, the locally linearized derivative,  $C_{m_\alpha}$ , can be estimated and plotted as a function of angle of attack. Figure 35 shows  $C_{m_\alpha}$  as a function of  $\alpha$  for an angle-of-attack range of  $-20^\circ$  to  $50^\circ$ .

The estimates are consistent and show a clear trend that is in fair agreement with wind tunnel estimates. By using the linear perturbation model for each maneuver, an excellent comparison can be made with the globally nonlinear wind tunnel data. This simple and widely used technique avoids many of the problems of modeling nonlinear systems and is readily applied to aircraft where maneuvers typically are small perturbations about a point in a much larger envelope.

flight, care must be taken in using derivatives obtained in turbulence for application in smooth air. Of course, if handling qualities in turbulence are being studied, the converse problem exists. Third, questions arise about the accuracy of the turbulence model used and the sensitivity of the algorithm to errors in modeling the turbulence. Because of these three considerations, every attempt should be made to obtain most data in smooth air. However, for data that are difficult or expensive to repeat, or for experiments explicitly related to turbulence, the algorithm that accounts for turbulence is available.

#### Time-Varying Systems

One of the most common simplifications used by the data analyst is the assumption that the system being studied does not vary significantly during the brief time span of a maneuver. This simplification translates into especially simple models. In terms of the two-degree-of-freedom example given earlier (eqs. (7) and (9)), this means that the dimensional derivatives ( $Z_\alpha$ ,  $M_\alpha$ ,  $M_q$ ,  $Z_{\delta_e}$ , and  $M_{\delta_e}$ ), the biases ( $Z_0$ ,  $M_0$ , and  $a_{n_{bias}}$ ), and the terms composed of  $V$ ,  $\sin \theta$ , and  $\cos \phi$  are all assumed constant during the maneuver. However, in a variety of circumstances the system varies significantly during the maneuver. In some of these cases, the analysis technique can be extended to cover the time variation of the system.

If dynamic pressure or velocity changes significantly during a maneuver, the dimensional derivatives will change correspondingly. Fortunately, the dependence of the dimensional derivatives on dynamic pressure and velocity is well known. The nondimensional derivatives do not usually vary significantly with velocity and dynamic pressure. The approach taken, therefore, is to identify the nondimensional derivatives. The dimen-

In some cases the linear model of the aircraft is inadequate to determine the needed information, and the known system nonlinearity may need to be addressed directly by the maximum likelihood technique. An example of this type of problem is the need to estimate the drag polar of an aircraft. A simplified illustration can be shown by assuming the drag polar can be represented by

$$C_D = C_{D_0} + C_{D_I} C_L^2$$

where the second term,  $C_{D_I} C_L^2$ , accounts for the induced drag. This term results in a nonlinearity in the problem; that is, although  $C_L$  can be written as a linear function of the angle of attack and elevator position,  $C_D$  cannot. Therefore, the estimation of  $C_D$  from dynamic data involves equations that cannot be written in the linear form given by equations (5) and (6), and the more general function form of equations (1) and (2) must be used. A complete description of this analysis is given in reference 37, and the following results are taken from this reference.

To obtain estimates of the drag polars, pushover-pullup maneuvers were performed in flight. Figure 36 is a comparison of longitudinal maneuver data and data computed on the basis of estimates from a nonlinear model for the algorithm just discussed. The fit is excellent. The drag polar obtained from this maneuver is compared in figure 37 with wind tunnel estimates of the drag polar. The agreement is reasonably good.

To assess the usefulness of the maximum likelihood estimation technique for obtaining drag information from dynamic maneuvers, the maximum likelihood estimates were compared with wind tunnel estimates as a function of the drag-rise Mach number ratio at four constant lift coefficients. The drag-rise Mach number ratio,  $M_r$ , is calculated by dividing the Mach number by the wind tunnel estimate of the drag-rise Mach number at a lift coefficient of 0.25. The drag rise Mach number is defined

as the Mach number where  $\frac{\partial C_D}{\partial \text{Mach number}} = 0.1$ .

The maximum estimates of the trimmed drag are compared with wind tunnel results in figure 38. The dashed lines are fairings of the maximum likelihood estimates (similar to those shown in fig. 37) obtained at various Mach numbers. In general, the correlation is good and indicates that the drag-rise Mach number determined by the maximum likelihood estimation technique is somewhat lower than that determined by the wind tunnel estimates.

The fundamental problem of nonlinear maximum likelihood estimation is that, in practice, the form of the nonlinear model is unknown. In cases where the form of the model is known, as in the drag polar case, meaningful estimates can be expected if the maneuvers excite the nonlinearity of the system. Very little useful experience is available to guide the analysis of nonlinear systems where a linearized model is inadequate and the form of the nonlinearity is not known. If *ad hoc* techniques are used in modeling unknown nonlinearities, great care must be taken or meaningless results may be obtained.

#### Cross Coupling

The standard aircraft equations of motion are separated into longitudinal and lateral-directional modes, and it is assumed that no cross coupling exists. When significant coupling does exist, there are two approaches that can be used. The most obvious approach is to use the full nonlinear five- or six-degree-of-freedom equations of motion with coupling terms. Although simple in principle, this method is plagued with practical difficulties. The equations given in the appendix are for the nonlinear five-degree-of-freedom equations of motion. The second approach is to use the measured lateral-directional data as inputs to the longitudinal equations and the measured longitudinal data as inputs to the lateral-directional equations. This approach requires that the measurements of all the state variables be available and have low noise levels.

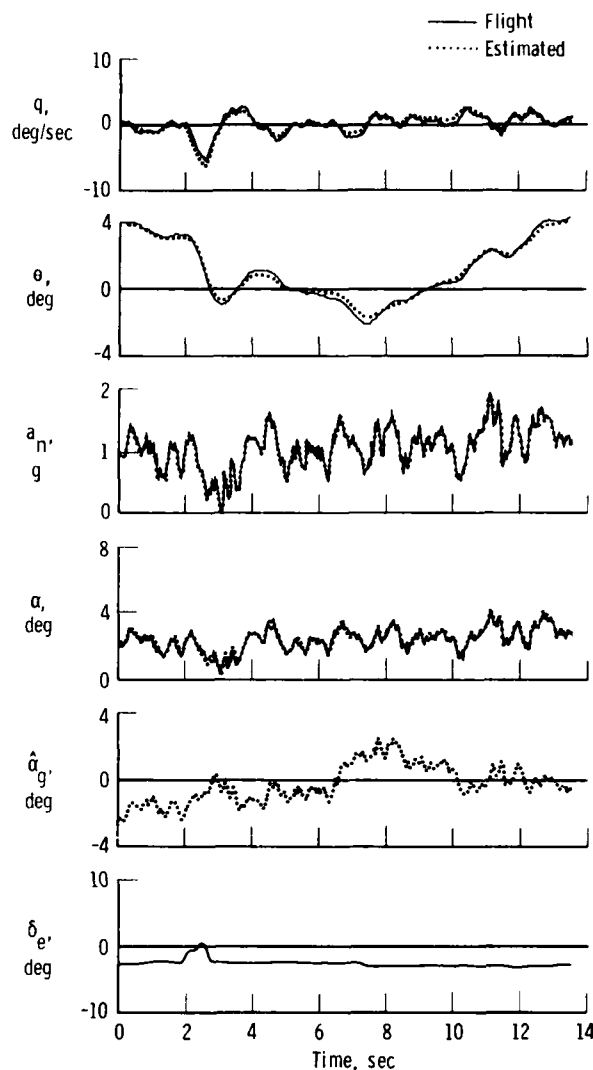


Figure 32. Comparison of flight data for maneuver E with values estimated by using algorithm II.

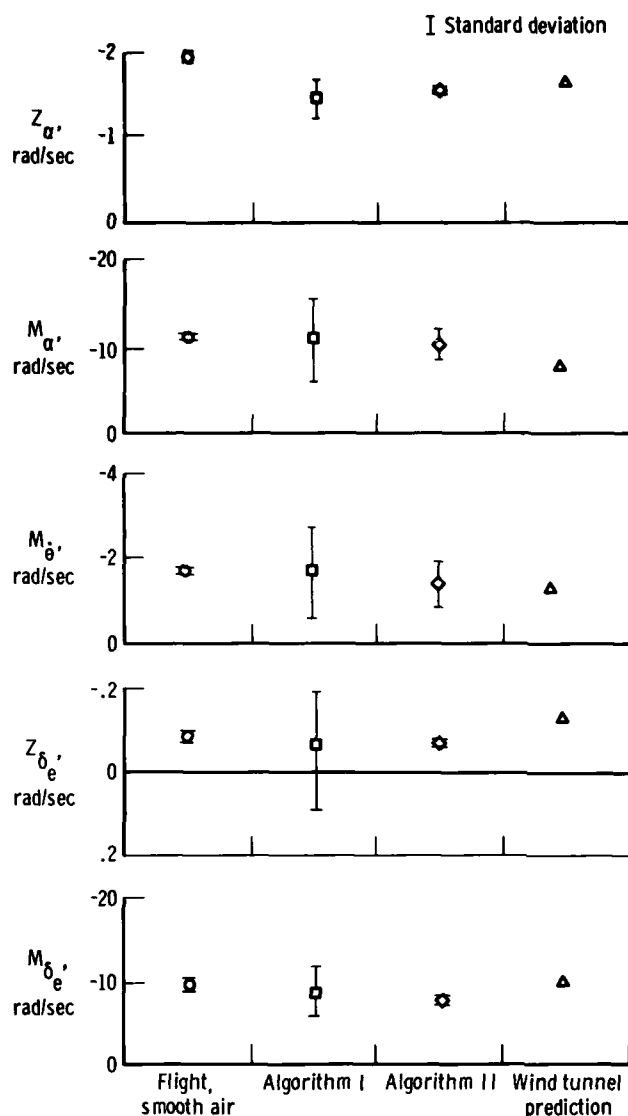


Figure 33. Means and standard deviations for four methods of estimating stability and control derivatives.

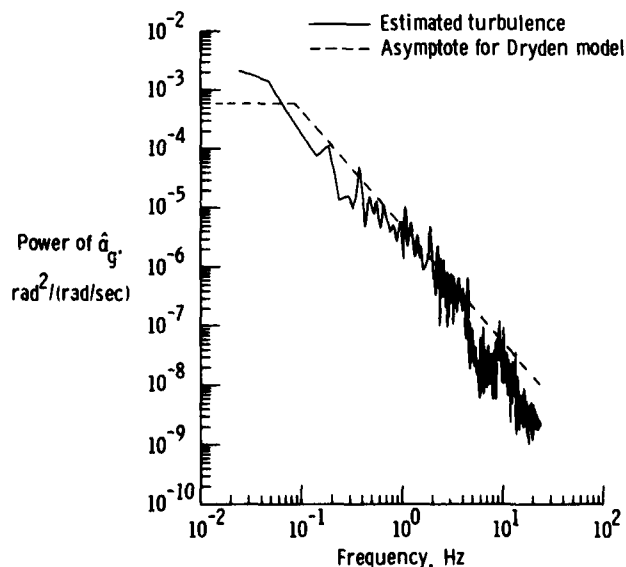


Figure 34. Power spectral density of  $\delta_g$  for maneuver ABCD.

There are two distinct types of cross coupling. The first type is kinematic cross coupling, which is cross coupling arising from the equations of motion. A typical example is gyroscopic forces. Kinematic cross coupling can be a problem even with symmetrical aircraft. One of the most common kinematic cross coupling problems is nose slice during longitudinal pulses obtained in steady turns. To account for nose slice, the kinematic cross coupling term  $r(\sin \phi)$  must be added to the  $\dot{\theta}$  equation.

The second type of cross coupling is aerodynamic cross coupling, which is that appearing in the expansions of the force and moment coefficients. Aerodynamic cross coupling is predicted to be significant at high angles of attack even for symmetric aircraft (ref. 38). For asymmetric aircraft, of course, aerodynamic cross coupling exists at all angles of attack.

Figure 39 is a three-view drawing of an oblique wing RPRV flown at the Dryden Flight Research Center (ref. 17). The wing of this aircraft can be skewed up to  $45^\circ$ . The oblique wing concept is of interest because of its potential for transonic drag reduction. When the wing is skewed, both aerodynamic and kinematic cross coupling must be accounted for. The additional terms needed for this analysis are the underlined terms in equations (22) to (26), which are given in the appendix. Figure 40 shows a fit of lateral-directional data obtained with the wing skewed to  $45^\circ$ . All the cross-coupling terms were ignored for this fit. This unconventional maneuver was an unintentional one caused by interference with the radio control system. The fit is totally unacceptable. Figure 41 shows the fit for the same maneuver when both kinematic and aerodynamic cross-coupling terms are included. The fit is now very good considering the unconventional nature of the maneuver. This example shows that cross-coupling effects can be accurately accounted for. All the lateral-directional maneuvers obtained from the oblique wing aircraft with the wing skewed to  $0^\circ$  and  $45^\circ$  were analyzed, and a complete set of stability and control derivatives including the aerodynamic coupling terms were successfully determined. Figure 42 shows the comparison of the estimated values from flight with the wind tunnel estimates obtained for wing skew angles of  $0^\circ$  and  $45^\circ$  for the aerodynamic coupling terms  $C_{m_{\delta_a}}$  and  $C_{m_p}$ .

These derivatives, which are important when leaving or entering a turn, show reasonably good agreement between the sets of estimates.

#### Estimation of Pitching Moment Due to Vertical Acceleration

The estimation of  $C_{m_{\ddot{a}}}$  from flight data is a problem that exemplifies many of the considerations discussed previously. The derivative  $C_{m_{\ddot{a}}}$

cannot normally be estimated from flight data because  $C_{m_{\ddot{a}}}$  and  $C_{m_q}$  are linearly dependent.

Analysts have had to be content with estimating  $C_{m_{\ddot{a}}} + C_{m_q}$ . At the Dryden Flight Research Center, maneuvers specifically designed to remove the dependence of  $C_{m_{\ddot{a}}}$  and  $C_{m_q}$  (ref. 39)

have recently been developed. Figure 43 shows a comparison of flight and estimated data for one of these maneuvers, an aileron roll with a series of elevator pulses. The fit is excellent,

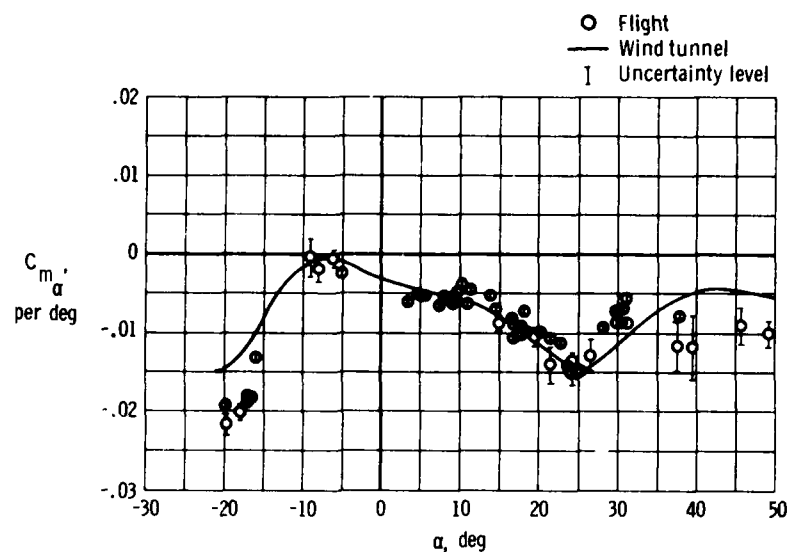


Figure 35. Comparison of flight and wind tunnel estimates of  $C_{m_\alpha}$  over a large angle-of-attack range.

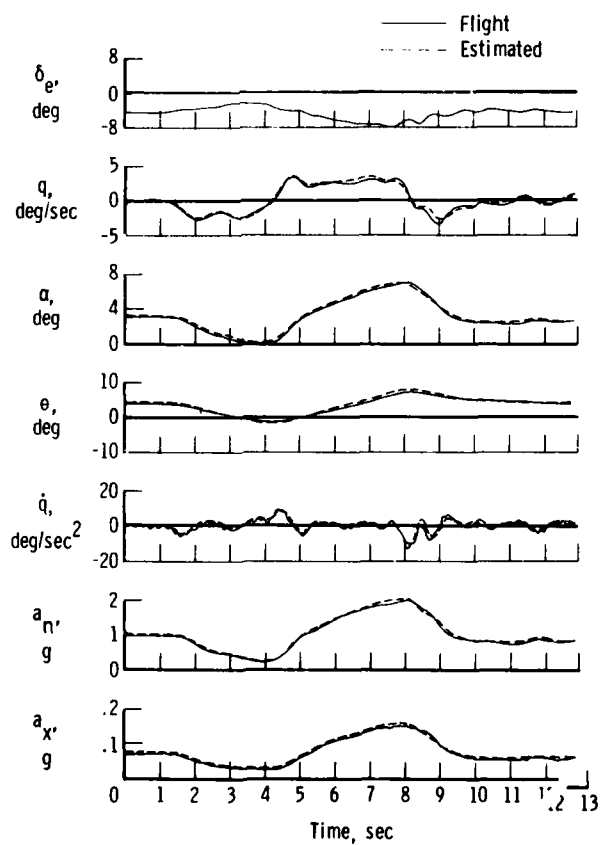


Figure 36. Comparison of flight data and data estimated by using a nonlinear model.

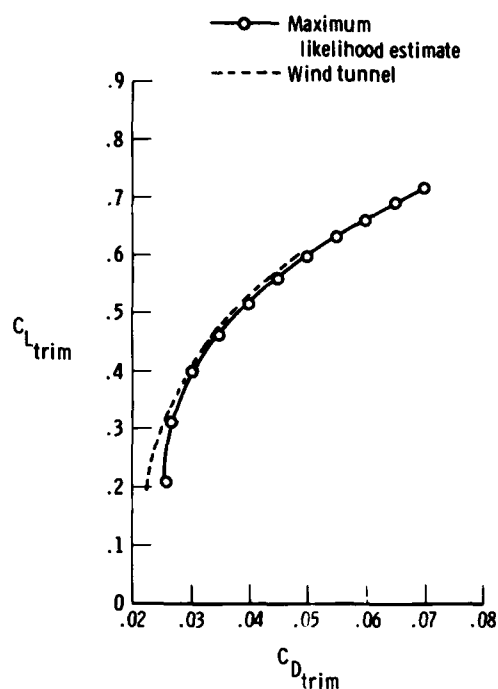


Figure 37. Comparison of drag polars obtained from estimates based on wind tunnel and flight data.

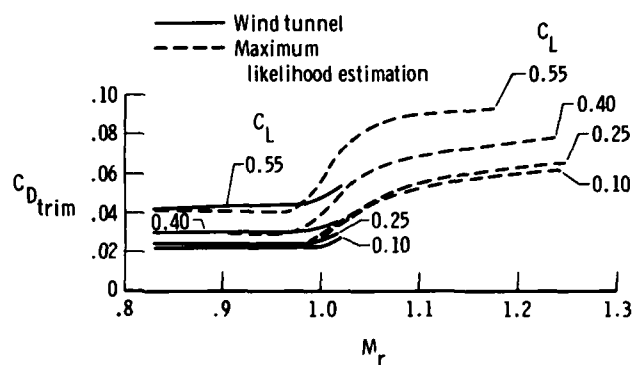


Figure 38. Summary of coefficient of drag as a function of  $M_r$  for estimates from the wind tunnel and the maximum likelihood estimation technique.

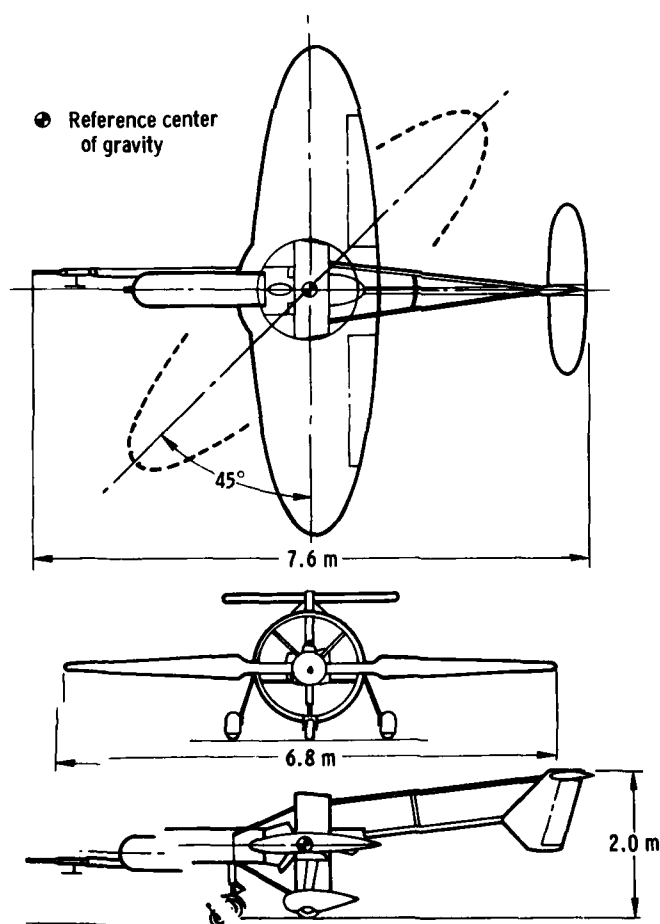


Figure 39. Three-view drawing of remotely piloted oblique wing aircraft.

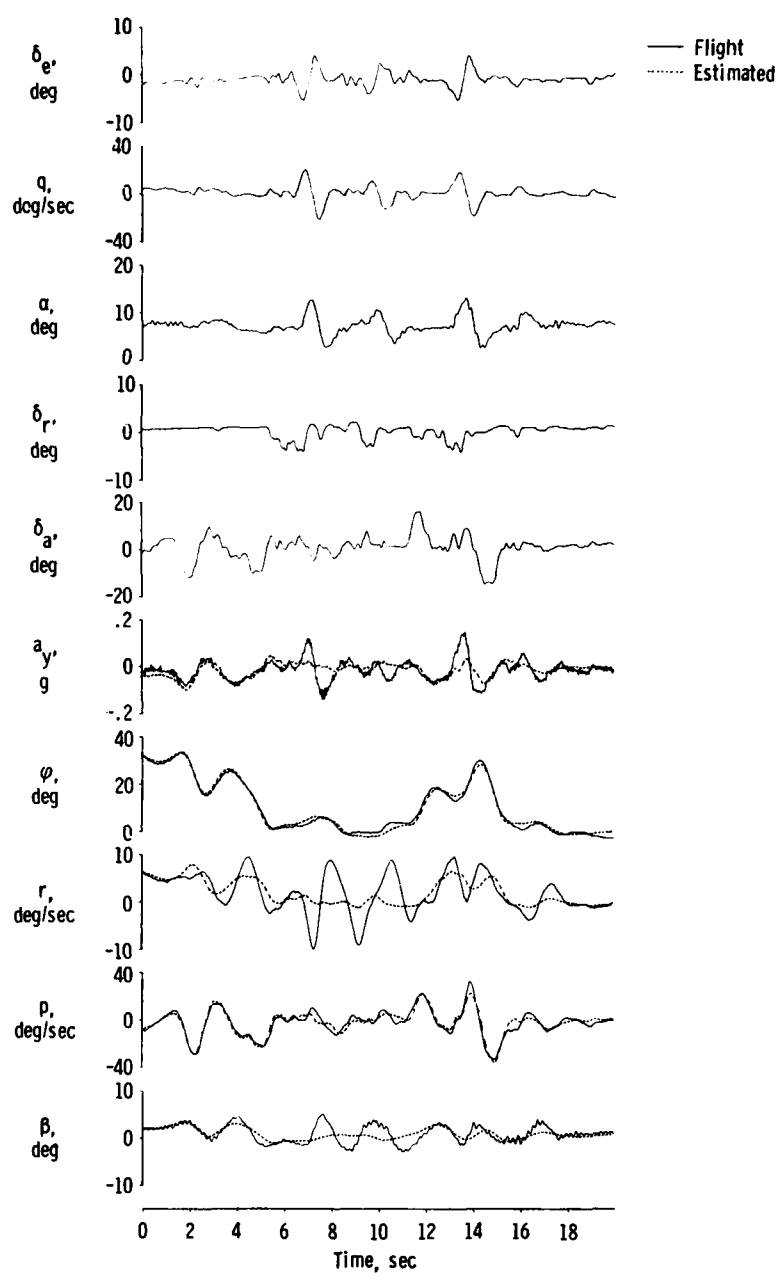


Figure 40. Comparison of measured and computed lateral-directional motions of oblique wing aircraft with 45° of wing skew where cross-coupling terms are omitted.



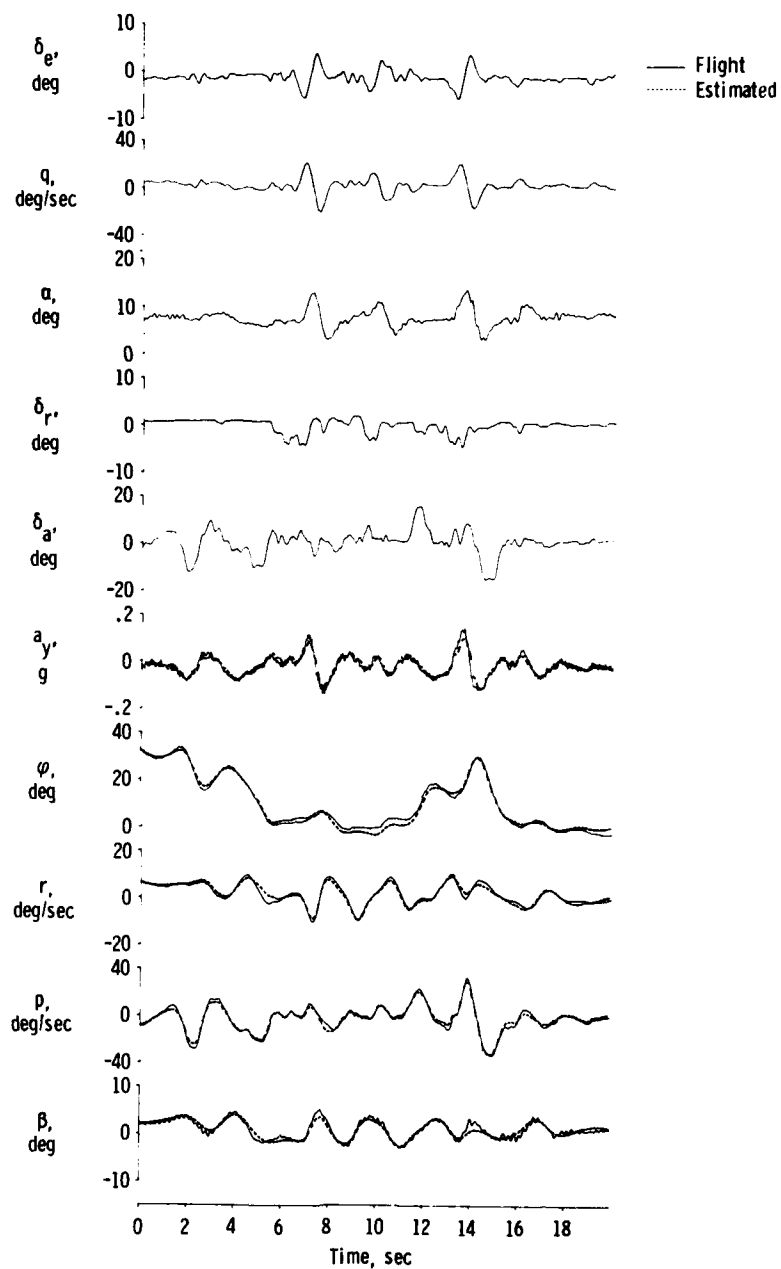


Figure 41. Comparison of measured and computed lateral-directional motions of oblique wing aircraft with 45° of wing skew where cross-coupling terms are included.

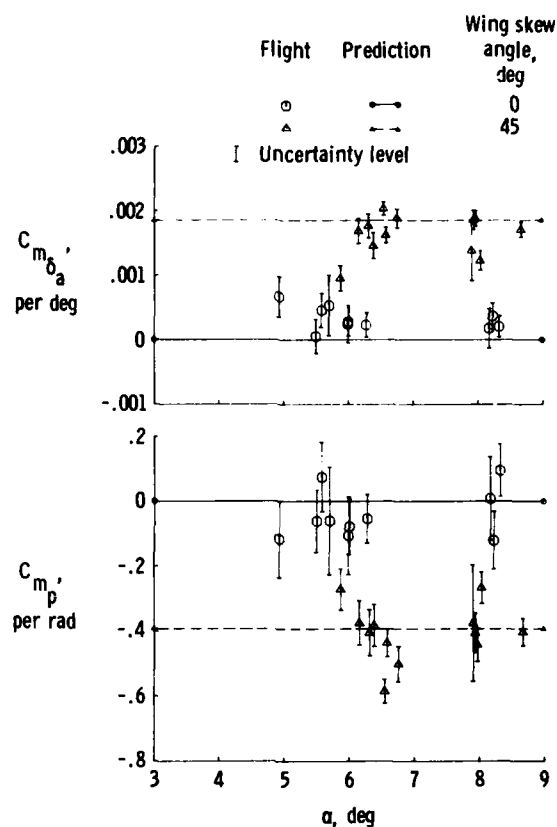


Figure 42. Maximum likelihood estimates of aerodynamic cross-coupling derivatives obtained for the oblique wing aircraft at two wing skew angles.

and reasonable estimates of  $C_{m_q}$  and  $C_{m_{\dot{\alpha}}}$ , as well as all the other longitudinal stability and control derivatives, were obtained. In figure 44, the estimate of  $C_{m_q}$  and  $C_{m_{\dot{\alpha}}}$  from 13 maneuvers are compared with simplified analytical predictions. Because the airplane undergoes a complete 360° roll in each of these maneuvers, the cross-coupling effects of the lateral-directional motion on the longitudinal analysis are extremely important. In fact, the removal of the linear dependence of  $C_{m_q}$  and  $C_{m_{\dot{\alpha}}}$  is primarily due to the cross-coupling effects. For the maneuver shown in

figure 43, dynamic pressure varies from 3.5 to 7.5 kN/m<sup>2</sup>, so a time-varying analysis is necessary. The altitude changes are sufficiently large and rapid that pressure lags in the static pressure measurements are significant. The 0.4-second lag of the static pressure system results in errors of up to 10 percent in the uncorrected dynamic pressure. The successful analysis of this maneuver is a good indication of the state of the art in the estimation of stability and control derivatives from dynamic flight test data without state noise at the Dryden Flight Research Center.

#### CONCLUDING REMARKS

During the past 13 years at the NASA Dryden Flight Research Center, the maximum likelihood estimator has been used to analyze over 3500 maneuvers from 32 different aircraft. Most of the analysis has involved the extraction of stability and control derivatives from dynamic flight maneuvers. In this lecture, procedures were discussed for obtaining high-quality estimates from dynamic maneuvers. The importance of well documented and accurate instrumentation as well as the analysis and interpretation of the estimates were discussed, and many examples of instrumentation problems and analysis difficulties were given. The lecture indicated the state of the art at the Dryden Flight Research Center in obtaining maximum likelihood estimates from dynamic flight data.

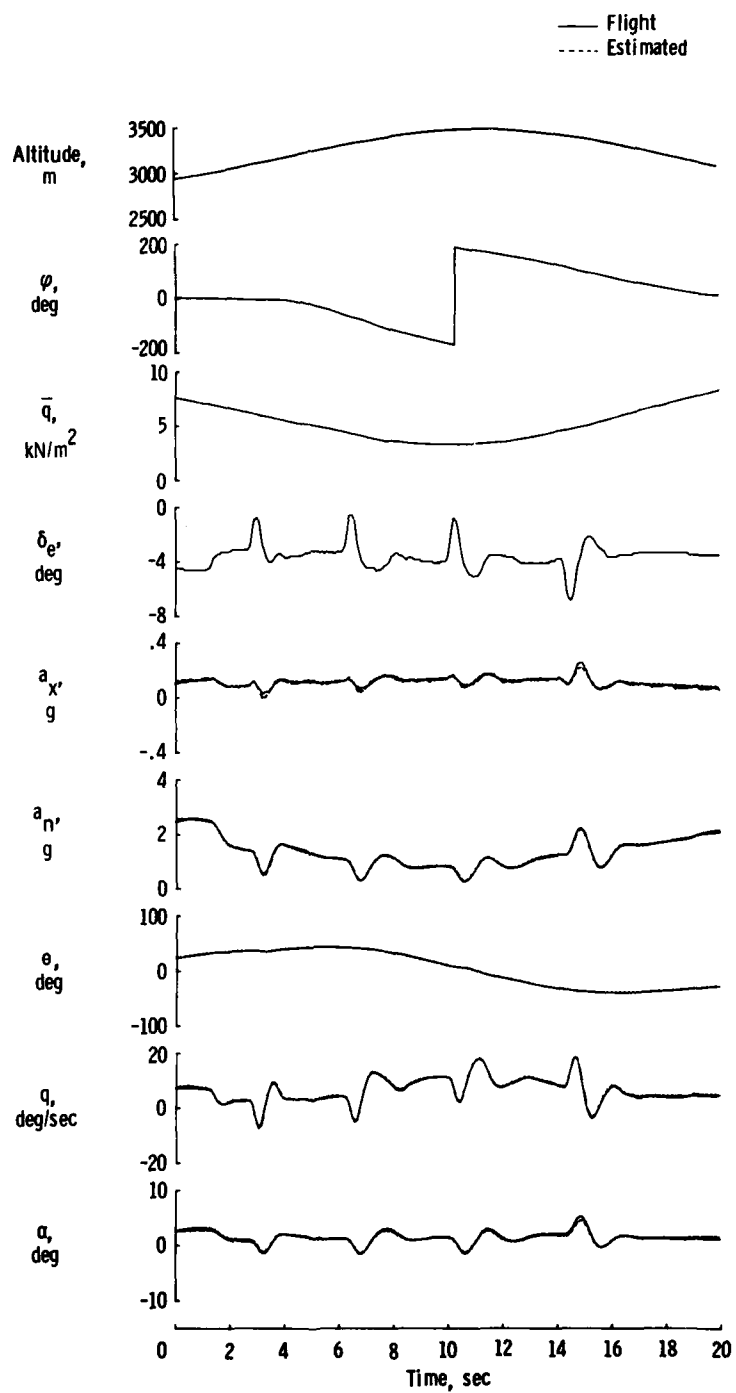


Figure 43. Fit of smooth roll.  $C_{m_q}$  and  $C_{m_{\dot{\alpha}}}$  estimated independently.

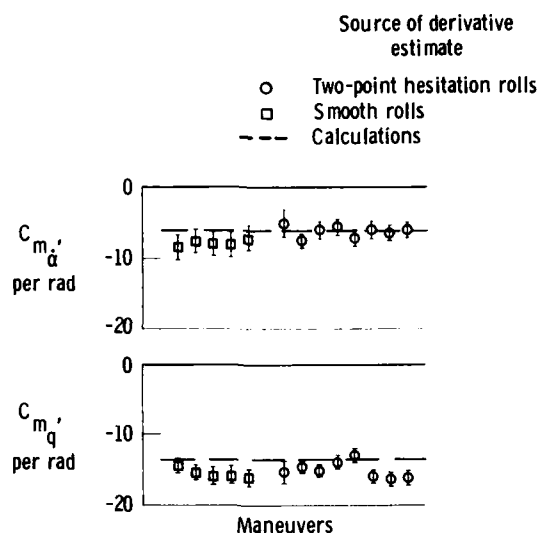


Figure 44. Comparison of independent flight estimates of  $C_{m_\alpha}$  and  $C_{m_q}$  with calculated values.

#### APPENDIX—FIVE-DEGREE-OF-FREEDOM MATHEMATICAL MODEL

The linear aerodynamic mathematical model considered in the following discussion is defined by the requirement that the first-order partial derivatives be used to describe the aerodynamic behavior of the aircraft. The differential equations of motion, which allow for nonzero  $I_{XZ}$  and  $I_{XY}$ , are written as follows:

$$\dot{\alpha} = -\frac{\bar{q}s}{mV} C_L + q + \frac{g}{V} [\cos(\theta) \cos(\varphi) \cos(\alpha) + \sin(\theta) \sin(\alpha)] - \tan(\beta) [p \cos(\alpha) + r \sin(\alpha)] \quad (15)$$

$$\dot{\beta} = \frac{\bar{q}s}{mV} C_Y + \frac{g}{V} \cos(\theta) \sin(\varphi) + p \sin(\alpha) - r \cos(\alpha) \quad (16)$$

$$\dot{p} I_X - \dot{r} I_{XZ} - \dot{q} I_{XY} = \bar{q} s b C_\ell + q r (I_Y - I_Z) + p q I_{XZ} - r p I_{XY} \quad (17)$$

$$\dot{q} I_Y - \dot{p} I_{XY} = \bar{q} s b C_m + r p (I_Z - I_X) + (r^2 - p^2) I_{XZ} + q r I_{XY} + r \omega_p I_{Xp} \quad (18)$$

$$\dot{r} I_Z - \dot{p} I_{XZ} = \bar{q} s b C_n + p q (I_X - I_Y) - q r I_{XZ} + (p^2 - q^2) I_{XY} - q \omega_p I_{Xp} \quad (19)$$

$$\dot{\theta} = q \cos(\varphi) - r \sin(\varphi) \quad (20)$$

$$\dot{\varphi} = p + r \cos(\varphi) \tan(\theta) + q \sin(\varphi) \tan(\theta) \quad (21)$$

If the aircraft is inertially symmetric in the horizontal plane, the  $I_{XY}$  term is zero and the terms including  $I_{XY}$  disappear.

For the purposes of this paper, the linear expansions of the nondimensional moments and forces are written as follows:

$$C_L = C_{L_\alpha} \alpha + C_{L_{\delta_e}} \delta_e + C_{L_0} + C_{L_\beta} \beta \quad (22)$$

$$C_Y = C_{Y_\beta} \beta + C_{Y_{\delta_a}} \delta_a + C_{Y_{\delta_r}} \delta_r + C_{Y_0} + C_{Y_\alpha} \alpha \quad (23)$$

$$C_\ell = C_{\ell_\beta} \beta + C_{\ell_p} \frac{pb}{2V} + C_{\ell_r} \frac{rb}{2V} + C_{\ell_{\delta_a}} \delta_a + C_{\ell_{\delta_r}} \delta_r + C_{\ell_0} + C_{\ell_q} \frac{qc}{2V} + C_{\ell_\alpha} \alpha \quad (24)$$

$$C_m = C_{m_\alpha} \alpha + C_{m_q} \frac{qc}{2V} + C_{m_{\delta_e}} \delta_e + C_{m_0} + C_{m_{\delta_a}} \delta_a + C_{m_p} \frac{pb}{2V} + C_{m_r} \frac{rb}{2V} + C_{m_\beta} \beta \quad (25)$$

$$C_n = C_{n_\beta} \beta + C_{n_p} \frac{pb}{2V} + C_{n_r} \frac{rb}{2V} + C_{n_{\delta_a}} \delta_a + C_{n_{\delta_r}} \delta_r + C_{n_0} + C_{n_q} \frac{qc}{2V} + C_{n_\alpha} \alpha \quad (26)$$

The underlined terms are normally not included in the linear analysis when the data are gathered during stabilized flight at low angles of attack. The underlined terms (referred to as the aerodynamic cross-coupling terms) are only needed when the aircraft is expected to have aerodynamic cross-coupling between the longitudinal and lateral-directional aerodynamic modes. For instance, these terms would be significant for an aircraft that is flying at high angles of attack or one that is aerodynamically asymmetric.

In the absence of either kinematic or aerodynamic cross-coupling terms, the equations can be divided into two sets: the two-degree-of-freedom longitudinal equations and the three-degree-of-freedom lateral-directional equations. The longitudinal equations are defined by equations (15), (18), and (20), with  $\delta_a$ ,  $\delta_r$ ,  $\phi$ ,  $\beta$ ,  $p$ , and  $r$  assumed known. The lateral-directional equations are defined by equations (16), (17), (19), and (21), with  $\delta_e$ ,  $\theta$ ,  $\alpha$ , and  $q$  assumed known.

#### REFERENCES

1. Iliff, Kenneth W.; and Taylor, Lawrence W., Jr.: Determination of Stability Derivatives From Flight Data Using a Newton-Raphson Minimization Technique. NASA TN D-6579, 1972.
2. Maine, Richard E.; and Iliff, Kenneth W.: A FORTRAN Program for Determining Aircraft Stability and Control Derivatives From Flight Data. NASA TN D-7831, 1975.
3. Iliff, Kenneth W.; Maine, Richard E.; and Montgomery, T. D.: Important Factors in the Maximum Likelihood Analysis of Flight Test Maneuvers. NASA TP-1459, 1979.
4. Suit, William T.: Aerodynamic Parameters of the Navion Airplane Extracted From Flight Data. NASA TN D-6643, 1972.
5. Ross, A. Jean: Determination of Aerodynamic Derivatives From Transient Responses in Manoeuvring Flight. Technical Memorandum Aero 1598, Royal Aircraft Establishment, [1974].
6. Gould, D. G.; and Hindson, W. S.: Estimates of the Stability Derivatives of a Helicopter and a V/STOL Aircraft From Flight Data. Methods for Aircraft State and Parameter Identification, AGARD-CP-172, May 1975, pp. 23-1 to 23-9.
7. Klein, V.: Longitudinal Aerodynamic Derivatives of a Slender Delta-Wing Research Aircraft Extracted From Flight Data. CIT-FI-74-023, Cranfield Inst. of Technology, July 1974.
8. Schuetz, A. J.: Low Angle-of-Attack Longitudinal Aerodynamic Parameters of Navy T-2 Trainer Aircraft Extracted From Flight Data: A Comparison of Identification Techniques. Volume I--Data Acquisition and Modified Newton-Raphson Analysis. NADC-74181-30, Naval Air Development Center, Warminster, Pa., June 23, 1975.
9. Marchand, M.; and Koehler, R.: Determination of Aircraft Derivatives by Automatic Parameter Adjustment and Frequency Response Methods. Methods for Aircraft State and Parameter Identification, AGARD-CP-172, May 1975, pp. 17-1 to 17-18.
10. Yazawa, Kenji: Identification of Aircraft Stability and Control Derivatives in the Presence of Turbulence. AIAA Paper 77-1134, Aug. 1977.
11. Rynaski, Edmund G.; Andrisani, Dominick, II; and Weingarten, Norman C.: Identification of the Stability Parameters of an Aeroelastic Airplane. AIAA Paper 78-1328, Aug. 1978.
12. Park, Gary D.: Determination of Tail-Off Aircraft Parameters Using Systems Identification. Proceedings of AIAA 3rd Atmospheric Flight Mechanics Conference, c. 1976, pp. 128-136.
13. Jeglum, Paul M.: Air Force Flight Test Center Experience in the Identification of Stability and Control Parameters from Dynamic Flight Test Maneuvers. Dynamic Stability Parameters, AGARD-CP-235, Nov. 1978, pp. 14-1 to 14-5.
14. Smith, Harriet J.: Flight-Determined Stability and Control Derivatives for an Executive Jet Transport. NASA TM X-56034, 1975.
15. Sim, Alex G.: A Correlation Between Flight-Determined Derivatives and Wind-Tunnel Data for the X-24B Research Aircraft. NASA SX-3371, 1976.
16. Shafer, Mary F.: Stability and Control Derivatives of the T-37B Airplane. NASA TM X-56036, 1975.
17. Maine, Richard E.: Aerodynamic Derivatives for an Oblique Wing Aircraft Estimated From Flight Data by Using a Maximum Likelihood Technique. NASA TP-1336, 1978.
18. Parameter Estimation Techniques and Applications in Aircraft Flight Testing. NASA TN D-7647, 1974.
19. Methods for Aircraft State and Parameter Identification. AGARD-CP-172, May 1975.
20. Hamel, P. G.: Status of Methods for Aircraft State and Parameter Identification. Flight/Ground Testing Facilities Correlation, AGARD-CP-187, Apr. 1976, pp. 8-1 to 8-16.

21. Balakrishnan, A. V.: *Communication Theory*. McGraw-Hill Book Co., c. 1968.
22. Balakrishnan, A. V.: *Stochastic Differential Systems I. Filtering and Control—A Function Space Approach. Lecture Notes in Economics and Mathematical Systems*, 84, M. Beckmann, G. Goos, and H. P. Künzi, eds., Springer-Verlag (Berlin), 1973.
23. Powell, J. David; and Tyler, James S., Jr.: Application of the Kalman Filter and Smoothing to VTOL Parameter and State Identification. 1970 Joint Automatic Control Conference of the American Automatic Control Council, Paper 18-G, American Soc. Mech. Eng., June 1970, pp. 449-450.
24. Iliff, Kenneth W.; and Maine, Richard E.: Practical Aspects of Using a Maximum Likelihood Estimation Method To Extract Stability and Control Derivatives From Flight Data. NASA TN D-8209, 1976.
25. Iliff, Kenneth W.; and Maine, Richard E.: Further Observations on Maximum Likelihood Estimates of Stability and Control Characteristics Obtained From Flight Data. AIAA Paper 77-1133, Aug. 1977.
26. Wolowicz, Chester H.; and Yancey, Roxanah B.: Experimental Determination of Airplane Mass and Inertial Characteristics. NASA TR R-433, 1974.
27. Gilyard, Glenn B.; and Belte, Daumants: Flight-Determined Lag of Angle-of-Attack and Angle-of-Sideslip Sensors in the YF-12A Airplane From Analysis of Dynamic Maneuvers. NASA TN D-7819, 1974.
28. Brenner, Martin J.; Iliff, Kenneth W.; and Whitman, Robert K.: Effect of Sampling Rate and Record Length on the Determination of Stability and Control Derivatives. NASA TM-72858, 1978.
29. Steers, Sandra Thornberry; and Iliff, Kenneth W.: Effects of Time-Shifted Data on Flight-Determined Stability and Control Derivatives. NASA TN D-7830, 1975.
30. Holleman, Euclid C.: Summary of Flight Tests To Determine the Spin and Controllability Characteristics of a Remotely Piloted, Large-Scale (3/8) Fighter Airplane Model. NASA TN D-8052, 1976.
31. Wilson, Donald B.; and Winters, Charles P.: F-15A Approach-to-Stall/Stall/Post-Stall Evaluation. AFFTC-TR-75-32, Air Force Flight Test Center, Edwards Air Force Base, Jan. 1976.
32. Edwards, John W.; and Deets, Dwain A.: Development of a Remote Digital Augmentation System and Application to a Remotely Piloted Research Vehicle. NASA TN D-7941, 1975.
33. Iliff, Kenneth W.; Maine, Richard E.; and Steers, Sandra Thornberry: Flight-Determined Stability and Control Coefficients of the F-111A Airplane. NASA TM-72851, 1978.
34. Powers, Bruce G.: Phugoid Characteristics of a YF-12 Airplane With Variable Geometry Inlets Obtained in Flight Tests Near a Mach Number of 2.9. NASA TP-1107, 1977.
35. Clark, Daniel C.; and Kroll, John: General Purpose Airborne Simulator-Conceptual Design Report. NASA CR-544, 1966.
36. Iliff, K. W.: Identification and Stochastic Control With Application to Flight Control in Turbulence. UCLA-ENG-7340, School of Engineering and Applied Science, Univ. Calif., Los Angeles, Calif., May 1973.
37. Iliff, Kenneth W.: Maximum Likelihood Estimation of Lift and Drag from Dynamic Aircraft Maneuvers. J. Aircraft, vol. 14, no. 12, Dec. 1977, pp. 1175-1181.
38. Orlik-Rückemann, K. J.: Aerodynamic Coupling between Lateral and Longitudinal Degrees of Freedom. AIAA J., vol. 15, no. 12, Dec. 1977, pp. 1792-1799.
39. Maine, Richard E.; and Iliff, Kenneth W.: Maximum Likelihood Estimation of Translational Acceleration Derivatives From Flight Data. AIAA Paper 78-1342, Aug. 1978.

# ROTORCRAFT IDENTIFICATION EXPERIENCE

by

J. Kaletka

Institut für Flugmechanik

Deutsche Forschungs- und Versuchsanstalt  
für Luft- und Raumfahrt e.V. (DFVLR)  
Braunschweig-Flughafen

## SUMMARY

The lecture presents an overview of the identification of stability and control derivatives of rotorcraft with respect to practical aspects and applications. First an introduction to the basic dynamics and control of helicopters is given. Then helicopter characteristics causing difficulties in the identification are discussed in detail: many coupled degrees of freedom lead to a large number of unknown parameters, instabilities limit the run length, vibrations deteriorate the flight test data quality. Measurement and sensor problems are discussed.

Approaches to overcome these difficulties are presented. Emphasis is placed on the following two key elements of the identification procedure:

1. The selection of adequate mathematical models and identifiable derivatives of the helicopter to isolate significant model effects.
2. Possibilities of increasing the information content of flight test data by appropriate system excitation and by multiple-run evaluations.

Identification results obtained from simulated and flight test data of helicopters by applying different identification methods are presented.

## 1. INTRODUCTION

The overall identification procedure includes four main phases: preparation, flight tests, evaluation, and conclusions (Figure 1). The preceding contributions to this lecture series have demonstrated that powerful tools have been developed to find solutions to specific problems of these phases. They include the design of appropriate input signals [1], aircraft instrumentation and data collecting [2], flight test data analysis [3], and finally, various identification methods of different complexity [4]. For fixed wing aircraft, it was shown that parameter identification yields reliable and accurate results which can be used for further investigations and conclusions, such as derivative verification, stability and control analysis, handling qualities assessment, etc. [5]. Fixed wing aircraft identifications have been conducted frequently for normal operational flight conditions. Approaches to evaluate extreme flight regimes and closed loop configurations are reported in two of the subsequent contributions [6, 7].

In contrast to the development of fixed wing aircraft identification the application of these methods to rotary wing aircraft is still not common. This is primarily due to adverse helicopter characteristics, such as coupled behaviour, high vibration level, and inherent instabilities which complicate the identification. But it is certainly also due to computational limitations: rotorcraft models usually include at least six degrees of freedom and, consequently, a large number of unknown parameters have to be identified, which requires both high computer storage capability and computation time. Furthermore it has to be considered that in the past only relatively few researchers have concentrated on rotorcraft identification. It was not until the early 1970's that the first extensive approach to obtain derivatives from helicopter flight test data was made by Molusis [8 to 11]. He placed the main emphasis on three aspects: 1. the definition of suitable rotorcraft models to be used in the identification, 2. the development of appropriate identification techniques, and 3. the application of these techniques to data from computer simulations and flight tests. At about the same time Gould and Hindson [12 to 14] identified a Bell 205 helicopter assuming longitudinal and lateral-directional motions to be uncoupled. The first attempt to evaluate the influence of different input signals on rotorcraft identification results was presented by Tomaine [15]. However, no specifically optimized signals were used. He continued his work with the identification of a Sikorsky CH-54B large 'crane' helicopter and a Boeing Vertol CH-47 [16, 17]. A research program for the extraction of parameters from both computer simulated and flight test data of a MBB BO 105 helicopter was presented by Rix, Huber, and Kaletka [18]. It was the first approach to identify a hingeless helicopter using optimized input signals. The influence of these signals on identification results together with a combined evaluation of different data runs was additionally demonstrated by Kaletka and Rix [19]. Within this research program emphasis was first placed on the medium speed regime; however, flight tests including hover and high speed flight conditions were then conducted in summer 1979. Recently, Hall, Gypta, and Hansen developed an integrated rotorcraft identification procedure consisting of data filtering, model structure estimation, identification technique, and input signal design [20].

Although the application of system identification techniques to rotorcraft has not been extensive, there is an urgent need for the determination of accurate mathematical models and the verification of existing analytical derivative calculations. Having in mind the improvement in today's helicopters and the development of future aircraft there is a keen interest in the stability and control analysis and handling qualities evaluation. Another motivating factor is the necessity to meet the increasing requirements of military helicopters, which are becoming more and more important in defense strategy.

At almost the same time as the identification of full-scale helicopters was being worked on, attempts were being made to apply system identification techniques to rotor models. The extraction of linear perturbation models from blade flapping measurements of a 4-bladed model rotor was investigated using both computer simulated and experimental data [21 to 24]. Rotor dynamic inflow models of varying complexity were used. Another approach to the identification of model rotors from simulated and dynamic wind tunnel tests is presented in [25].

This lecture concentrates on rotorcraft identification using flight test data of full-scale helicopters. It is divided into four major parts. The first part, based mainly on [26] and [27], is intended to give a physical understanding of helicopter dynamics and controls that influence system identification considerations. The necessity for the introduction of hinged or flexible rotor blade attachments as well as blade flapping and lagging motions is discussed. Helicopter controls are briefly described and rotor design trends are discussed. The second part summarizes the unique problems of rotorcraft identification. The complexity of helicopters, their coupled behaviour, and their inherent instabilities are described. Data measurement difficulties arising from rotorcraft characteristics are discussed in detail. In the third part of the lecture emphasis is placed on rotorcraft modeling. The structures of various mathematical linear models with different degrees of complexity are presented. Assumptions and mathematical reduction procedures to simplify these models as well as techniques to isolate significant model coefficients are given. Identification results are shown in the fourth part. These results were obtained from flight test data using different identification approaches. Both time history comparisons and identified parameters are presented.

## 2. BASIC DYNAMICS OF HELICOPTERS

The concept of using lift-producing rotating wings to achieve landing and takeoff in restricted areas, hovering and vertical flight is very old. The first flight trials of helicopters took place at about the same time as the first flights of fixed wing aircraft, but they were without success. Therefore much effort was concentrated on the development and improvement of fixed wing aircraft and only relatively few engineers continued the struggle against the adverse characteristics of the helicopter. The consequences of this fact are still felt in the standard of these two different types of aircraft today.

Figure 2 shows a helicopter in forward flight. For this flight condition the aerodynamic flow at the blades of the rotor consists of the rotational velocity and the speed of the helicopter itself. It is apparent that the blades advancing in the direction of flight on the upstream side of the rotor encounter higher velocities and consequently higher lift than the retreating blades on the opposite or downstream side of the rotor. For a rigid propeller - as designed for the first helicopters - the inequality in lift produced on the advancing and retreating blades causes a sizable moment. Although it is possible to utilize two rotors rotating in opposite directions to cancel the moments, high alternating blade loads and resulting material stresses cannot be avoided. Therefore, in the early helicopter development, when steel spar, fabric covered or wooden blades were normally used, material strength constituted a severe problem.

### 2.1 BLADE FLAPPING AND LAGGING MOTION

In 1926 it was Juan de la Cierva who created the prerequisites for the realization of technically satisfactory helicopter projects. His "Autogiro" incorporated freely hinged blades as a means of equalizing the lift of both sides of the rotor in translational flight. This so called "articulated blade attachment" or "articulated rotor" was found on all helicopters of the following period and still is used for most of today's rotorcraft.

The blade attachment to the rotor shaft through horizontal (flapping) hinges has three important effects:

1. The blades are free to rise and fall
2. Bending moments at the root of the blades are eliminated
3. No, or only small, moments can be transmitted to the hub.

As shown in Figure 3 the forces acting on the blade in flapping direction during flight are:



1. Air forces (lift) depending on airflow and blade geometry
2. Centrifugal forces depending on rotor rpm and blade mass distribution
3. Blade inertia
4. Blade weight

In general blade weight is relatively small and usually can be neglected.

These forces produce moments about the flapping hinge and, according to the equilibrium condition, the sum of these moments must be zero. With lift and centrifugal forces acting on it, a blade will take up a position which is roughly the resultant of these forces. Therefore the rotor looks like an inverted shallow cone, with the tip path plane for a base and  $\beta_0$  as coning angle.

For a rotor in forward flight the lift force varies with the azimuth angle  $\psi$  of the blade. The resulting blade motion is considered with the aid of Figure 4. In the downstream position ( $\psi=0^\circ$ ) the blade encounters no added velocity due to forward speed. As the blade moves forward, however, the velocity and thus the lift are increased: the blade flaps upwards. The flapping velocity must be of such a magnitude as to decrease the blade angle of attack so that the lift remains constant. Following the blade around, then, the maximum upward flapping velocity occurs at  $\psi=90^\circ$ , it is zero at  $\psi=180^\circ$ , maximum downward at  $\psi=270^\circ$  and zero again at  $\psi=0^\circ$ . Consequently, the advancing blade rises and reaches its highest position at  $\psi=180^\circ$ , the retreating blade falls to its lowest position at  $\psi=0^\circ$ : the rotor tilts backward by the amount of the longitudinal flapping  $\beta_{1c}$ .

Another effect of helicopter forward speed on the rotor arises from coning. Looking at the rotor from the side - as also depicted in Figure 4 - it can be seen that there is a difference in angle of attack of the blades at the front and the rear of the rotor. Again, this asymmetry in lift leads to blade flapping where the flapping velocity is maximum upward at  $\psi=180^\circ$ , maximum downward at  $\psi=0^\circ$ , and zero at  $\psi=90^\circ$  and  $270^\circ$ . It follows that the rotor tilts sideward to the right by the amount of the lateral flapping  $\beta_{1s}$  which can be in the same order of magnitude as the  $\beta_{1c}$  flapping.

For the understanding of the dynamic behavior of the rotor it is important to visualize that two periodic forces are acting on the blades of forward moving helicopters:

1. Changes in lift due to different flow at the advancing and retreating blades
2. Changes in lift due to different angle of attack at the blades of a coned rotor.

Because of these forces rotor pitch and roll motions are coupled, which results in an inherent coupling of the longitudinal and lateral-directional motion of the helicopter.

Analytically the flapping motion of the rotor can be expressed as a function of the azimuth angle  $\psi$  by the Fourier series:

$$\beta = \beta_0 - \beta_{1c} \cos \psi - \beta_{1s} \sin \psi \dots - \beta_{nc} \cos n\psi - \beta_{ns} \sin n\psi$$

The flapping angle  $\beta$  is defined as the angle between a blade and a plane perpendicular to the shaft. It is positive for upward flapping. As already explained,  $\beta_0$  is the coning angle,  $\beta_{1c}$  the backward tilt and  $\beta_{1s}$  the sideward tilt. The higher harmonics  $\beta_{nc}$  and  $\beta_{ns}$  may be viewed as a weaving of the blade in and out of the surface of the cone formed by the coning angle and the first harmonic motions of the blades. The sources of higher harmonic flapping lie in the forces produced by the periodically changing velocities at the blades, in higher harmonic components of nonuniform downwash, and in effects of reverse flow on the retreating side of the rotor. The higher harmonic blade motions are small and of little importance in problems of rotor control and rotor performance. However, as they cause a high level of helicopter vibration they are extremely important in material fatigue and passenger comfort considerations.

An observer who is viewing the tilted rotor from the powered shaft and who is rotating with the blades can see the blades flapping up and down. He can also notice that the distance between a blade element and the shaft axis changes with the flapping angle (Figure 5). This means that in addition to its tangential velocity the blade element moves radially. Whenever a mass moves radially in a rotating plane it experiences a tangential force, the Coriolis force. The direction of this force is opposite to the direction of rotation when the mass is moving outward and it is in the direction of rotation when the mass is moving inward. It follows that a flapping blade also experiences forces that tend to accelerate or decelerate the rotation of the blade and therefore produce high bending moments at the blade root. Consequently the use of flapping hinges necessitates the introduction of hinges in the inplane direction. Then the blades are free to lead and lag and the observer rotating with the shaft would see the blades move back and forth.

This lagging motion is mostly due to Coriolis forces. In forward flight it is also influenced by the asymmetric drag at the advancing and retreating blade. Similar to the flapping motion, the inplane motion can be described in terms of a Fourier series where higher harmonics also contribute to vibrational problems.

## 2.2 ROTORCRAFT CONTROL

The control of a helicopter is achieved by inclination and magnitude adjustment of the rotor lift vector. As this vector is almost normal to the tip path plane the question is how the desired tilt of the tip path plane can be achieved. The system commonly used

is based on varying the pitch of the rotating blades by means of a swashplate. As shown in Figure 6 the blades are hinged to the hub so that they are free to flap and lag. In pitch, however, the blades are constrained by a linkage connecting them to the upper rotating plate of the swashplate assembly. From the lower non-rotating plate, control rods lead off through the control transmission to the pilot's stick and collective lever. The swashplate can be tilted and moved vertically and hence produces a blade pitch change in reference to the shaft.

When the swashplate is tilted to the right side the pitch of the advancing blade alters from  $\theta_0$  at  $\psi=0^\circ$  to minimum at  $\psi=90^\circ$  and then increases again to  $\theta_0$  at  $\psi=180^\circ$  and - when the blade is retreating - to maximum at  $\psi=270^\circ$ . During this feathering motion the angle of attack at the blade also varies with the cyclic pitch. Consequently, the advancing blade falls and reaches its lowest position at the front of the rotor ( $\psi=180^\circ$ ) while the retreating blade rises to its highest position at the rear ( $\psi=0^\circ$ ): the rotor tilts forward, a component of the lift acts in the direction of the tilt so that the helicopter pitches nosedown and accelerates in the forward direction. Hence, a sideward tilt of the swashplate leads to helicopter motion along the longitudinal axis. Similarly, the lateral motion of the helicopter is controlled by a forward or backward tilt of the swashplate. For vertical control the swashplate is moved up and down to change the pitch of all blades simultaneously by the same amount (collective pitch). Thus the magnitude of the lift is controlled (in general rotor rpm is held constant automatically).

The feathering system provides a very convenient means to control the helicopter. It should be noted that three out of four pilot controls (engine control excepted) of a single rotor helicopter make use of collective or cyclic pitch change of the blades. These are:

1. Longitudinal cyclic: pilot's stick fore and aft, swashplate tilts sideward
2. Lateral cyclic: pilot's stick sideward, swashplate tilts forward or backward
3. Collective pitch: pilot's collective lever up and down, swashplate moves vertically.

The fourth control the pilot needs, the directional control, is usually provided by the use of the tail rotor. Primarily the tail rotor is necessary to balance the main rotor torque. However, by using the pedals, the pilot can alter the collective pitch of the tail rotor blades and - due to the resulting lift change - control the yaw motion of the helicopter.

### 2.3 ROTOR DESIGN TRENDS

It was the articulated rotor concept that made it possible to develop successfully flying helicopters. Although the use of flapping, lagging and feathering hinges caused a high degree of complexity they have been used and are still in use on many of today's helicopters. However, during the last few decades designers returned to projects with rigid blade attachments as in the beginning of rotorcraft history. Since then the knowledge of blade stresses has increased considerably. New materials, like titanium and fiber reinforced plastics (F.R.P.) have become available, their technology has been investigated and production techniques have been improved. On the basis of these developments it was possible to replace hinges by elastic components and to design and develop two new rotor concepts: the hingeless and the bearingless rotor.

Figure 7 compares a fully articulated rotor with a hingeless one [28]. It can be seen that flapping and lagging hinges are replaced by elastic elements whereas conventional feathering bearings are still used for blade control. The mechanical simplicity and its impact on reliability, maintainability and drag reduction is self-evident.

The bearingless rotor concept includes the elimination of all three hinges. In comparison with the hingeless rotor the feathering hinge is also replaced by flexible elements, for example a torque tube. While hingeless rotor helicopters - like the MBB BO 105 - have been flying successfully for years the bearingless rotor still has to prove its feasibility.

Both the hingeless and the bearingless rotor systems are sometimes erroneously called "rigid rotors". This is misleading because there is such a high degree of flexibility involved in the blades and the blade attachment that the dynamic behavior of the blades is almost comparable to that of articulated blades. Hence, the fundamentals of articulated blade motion and control are also valid for hingeless and bearingless rotors, although there may be significant differences in flying capabilities and handling qualities of these helicopters.

### 3. UNIQUE PROBLEMS OF ROTORCRAFT IDENTIFICATION

In comparison with fixed wing aircraft, parameter identification of rotorcraft is a more complicated task. This is mainly due to three problem areas: the complexity of the system, inherent instabilities, and data measurement difficulties.

### 3.1 SYSTEM COMPLEXITY

In the previous section the necessity of an articulated blade attachment was shown. It was also pointed out that hinges may be replaced by corresponding elastic blade deformations or specific elastic components. In any case, each blade has two degrees of freedom (DOF): it is free to flap and to lag. Hence, for the description of the motion of a four-bladed helicopter, as shown in Figure 8, as many as eight DOF are required to describe the blade motions. Additionally, 6 DOF are necessary to represent the rigid body motion. If the influences of stability augmentation and control systems and their dynamic behaviour, tail rotor dynamics, and blade and fuselage flexibilities are also considered, the result is a still larger number of degrees of freedom.

It has already been shown that blade DOF are highly coupled because flapping immediately causes a lead-lag motion. In addition blade flexibility causes elastic coupling effects that may have a significant influence on blade motion. Besides the motion coupling of individual blades there is also a pronounced coupling effect between the pitch and roll motion of the rotor itself. The rotor, however, is used to generate the main control forces and moments of the helicopter during all flight conditions. Hence, the dynamic behaviour of the rotor determines the rigid body motion to a high degree and it is evident that rotor and fuselage states are also coupled.

Because of the large number of coupled degrees of freedom, a mathematical description of helicopter dynamics requires a high order model (set of differential equations) with many parameters. However, successful application of system identification techniques is always limited by the size of the model, the number of unknowns that have to be identified, and the information content of the data. Therefore the selection of an appropriate model to be used in the identification is one of the key problems in rotorcraft identification.

### 3.2 ROTORCRAFT INSTABILITIES

Helicopters normally show an unstable flight behaviour without pilot actions. This stick-fixed instability is produced by the rotor which represents a rather unstable disc with respect to attitude and velocity changes. Consequently, the degree of instability depends to a large extent on rotor characteristics and helicopter speed. This is demonstrated in Figure 9 taken from [29]. It shows how long it takes for the time response of a stick-fixed helicopter to reach its double amplitude - when the system is unstable - or its half amplitude - when the system is stable -. Hence, decreasing time to double amplitude is related to more instability. Four rotors of different flapping frequency ratios  $\Omega_\beta$  are considered. ( $\Omega_\beta$  is the blade flapping frequency  $\omega_\beta$  divided by the rotor angular velocity  $\Omega$ ). It can be seen that only helicopters with  $\Omega_\beta$  close to 1, like articulated rotors with no or only small hinge offsets, become stable at higher speeds. However, increasing flapping frequencies, typical of stiffer rotors, produce a destabilizing effect. For a rotor with  $\Omega_\beta$  equal to 1.15, for example, the time to double amplitude approaches only 1 second for high speed conditions. Today's hingeless helicopters have flapping frequency ratios in the range of 1.1 to 1.2 (MBB BO 105:  $\Omega_\beta = 1.12$ ). Nevertheless, pilots do fly these helicopters without any particular difficulties by making use of the high control power of hingeless rotorcraft.

These inherent instabilities, however, complicate the system identification for two main reasons. First, there is a high sensitivity to gust disturbances and inaccurate trim - state variables diverge even with no control input. Second, the time for a data run is limited because increasing amplitudes quickly invalidate the small perturbation assumptions of the linear model. Therefore it is essential to obtain as much information as possible about the system under test within a short time span to allow a successful identification.

### 3.3 DATA MEASUREMENT DIFFICULTIES

System identification techniques are based on the evaluation of measured input and output data of the system under test. Therefore reliable identification results can only be obtained when the control and state variables are measured with high accuracy. Aircraft flight test data recording should include linear and angular accelerations, translational velocities, attitudes, rates, control inputs, and, for rotorcraft, rotor blade motions. Typical on-board sensors that are needed to fulfill these requirements consist of accelerometers, pressure transducers, vanes, attitude and rate gyros, potentiometers and strain gages. Many of these sensors have been designed and built for application in aircraft instrumentation. They are available as production units and meet high quality standards. It has already been demonstrated in part 4 of this lecture series that for a fixed wing aircraft the selection of adequate sensors together with proper adjustment and calibration of the transducers yields accurate data of the aircraft motion [2]. However, measurement of some rotorcraft states is still problematic. This is mainly due to the high vibration level of helicopters, the adverse signal to noise ratio of translational accelerations, and the inefficiency of conventional airspeed measuring devices for both the hover and the low speed flight condition.

### 3.4 HELICOPTER VIBRATION

The main sources of helicopter vibration are higher harmonic blade motions due to considerably varying aerodynamical loads on the rotating blades. First of all there are higher harmonic components of the flapping and lagging motion. But in addition natural blade bending modes may be excited by harmonic blade motions and by continuously changing lift distributions over the blade span. Although rotor blades are designed to have no resonance points it is extremely difficult or even impossible to avoid resonance effects for all operating flight conditions [28]. Vibratory blade responses, however, give rise to root shear forces and moments which are then transmitted to the rotor hub where they are combined and sent through the rotor shaft into the airframe. As forces go from the rotating system to the fixed fuselage system the rotor system in steady state flight acts like a filter and only transmits rotor harmonics that are integral multiples of the number of blades [30]. This is demonstrated by Figure 10, which shows the X-axis vibration frequency spectrum of a MBB BO 105 helicopter for two different flight conditions, a steady state flight and a flare maneuver. The measurement was made using an accelerometer rigidly attached to the suspension flange close to the lower part of the swashplate. Comparing the frequency spectra it is obvious that the maneuver data are much more vibratory than the steady state data. In both cases the high vibration content at 4, 8, and 12  $\Omega$  is clearly to be seen. But for the non-steady state data a variety of other frequencies can be distinguished, in particular those frequencies that are integral multiples of the rotor angular velocity  $\Omega$ . A more detailed discussion of the BO 105 vibrations is presented in [31]. As non-steady state flight test data are usually used for system identification these data contain high amplitude vibrations at various frequencies. This is especially true for rigid body acceleration and rate measurements, as shown in Figure 11. Although the data have already been filtered using a third order analogue filter with a cut-off frequency of 16 Hz, they are still very noisy. This causes severe identification problems, especially with equation error methods. Therefore procedures like high quality digital filtering techniques must be applied to smooth the data.

A comparison of the measured rates and linear accelerations clearly shows that two groups of different signal to noise ratios can be distinguished:

1. The signal to noise ratio is relatively high. The rigid body response to a control input is larger than the vibratory noise superimposed on the data. This is the case for the vertical acceleration and rate measurements.
2. The signal to noise ratio is relatively low. It is very difficult or almost impossible to recognize the rigid body motion from the measured longitudinal and lateral accelerations. This is also true for maneuvers where longitudinal or lateral cyclic control inputs were applied to produce significant horizontal accelerations. Nevertheless the rotorcraft response is still very small in comparison to the noise on the data.

Another problem arising from helicopter vibrations is the availability of appropriate sensors with high measuring accuracy in a strong vibratory environment. The sensors have to fulfill two main requirements:

1. Reliable functioning during all flight conditions of interest.
2. High linearity and sensitivity. As the measuring range is specified by the total signal (desired signal + noise), some sacrifice of data accuracy cannot be avoided. Since the desired signal only needs a small part of the full scale range, linearity errors may result in high distortion of the data.

In addition, it has to be carefully considered whether sensors with built-in filtering devices, like specific feedback-system, elastomeric bearings, etc., can be used. The benefit is that the measuring range can be chosen with respect to the desired signal. Higher frequency noise is filtered and thus cannot produce saturation. The drawback, however, is that filtering yields data phase shifts which may be intolerable for identification purposes and therefore have to be corrected during the data processing phase.

### 3.5 ACCELERATION MEASUREMENTS

A unique characteristic of single rotor helicopters is the deficiency of measured accelerations in the longitudinal (X-axis) and lateral (Y-axis) direction of a body fixed axis system. Even when large control inputs are applied, the acceleration remains relatively small. This phenomenon can be explained with the help of Figure 12. To measure longitudinal accelerations an accelerometer is rigidly attached to the helicopter fuselage. In Figure 12 it is represented by a spring-mass system with one degree of freedom. The acceleration is measured by the force acting on the spring or, in other words, by the movement of the mass with respect to its neutral position. Because of inertia forces a forward acceleration of the fuselage would cause the mass to move backward and vice versa. For a helicopter in horizontal steady state flight there are no X-forces acting on the accelerometer mass. When a longitudinal cyclic control input is applied the first response of the aircraft is a forward tilt of the rotor tip path plane generating a pitch moment around the helicopter's center of gravity. During this phase only minor accelerations are present. The fuselage then pitches nosedown to obtain momentum equilibrium again and the helicopter starts to increase its longitudinal speed. As a result of the inertia force the accelerometer mass would move backward. Because of

the fuselage tilt, however, a gravity force component is also acting on the mass and tries to move it forward. Using BO 105 flight test data Figure 13 demonstrates that these two forces, the inertia force  $m \cdot \ddot{x}$  and the gravity force component  $m \cdot g \cdot \sin \theta$ , are of the same order of magnitude. As they are acting in opposite directions there is a high compensation effect and the actually measured longitudinal acceleration  $a_x$  is very small.

It is easy to visualize that for the same reasons the measured lateral accelerations are also relatively small whereas the vertical acceleration measurement is almost unaffected by any compensation of gravity and inertia forces.

### 3.6 AIRSPEED MEASUREMENT

A prerequisite for successful rotorcraft identification is the accurate measurement of air data parameters, i.e. altitude, airspeed, angle of attack, and angle of sideslip. The conventional sources of air data are vanes and pitot static systems consisting of total and static pressure probes. Such devices have been developed for fixed wing aircraft but they are also still used on today's helicopters. In general the sensors are attached to the fuselage where the airflow is essentially unidirectional and clean for most flight conditions. Rotorcraft, however, pose special problems in accurate sensing of air data, which render conventional techniques ineffective at low airspeed. When the speed approaches zero the fuselage becomes deeply involved in rotor downwash that influences air data measurements and makes them unusable. For flight tests the mismatch between sensor measuring and vehicle motion is reduced by mounting the sensor on a noseboom to be out of downwash. But pitot static systems quit working at speeds below about 25 kts and vanes also require some aerodynamic flow and cannot be used at hover and very low speeds. In addition noseboom natural frequencies may be excited by helicopter vibratory frequencies, which results in oscillations, especially on the measurement obtained from vanes.

Alternative solutions to measure longitudinal, lateral, and vertical velocities of helicopters are rare. The integration of measured accelerations may yield poor accuracy, because of the measurement problems of accelerations themselves. Tracking systems, based on radar or laser techniques, have already been used for system identification purposes [17]. But such systems are usually not available.

Although the deficiencies of conventional air data systems in helicopters are obvious, there has been no major improvement in rotorcraft airspeed sensing for a long time. During the last decade, however, various different and innovating approaches have been made to solve the low airspeed and flow direction measurement problem [32 to 37]. Two of these systems which are available as production units are shown in Figure 14 and 15: the LORAS (Pacer Systems) and the LASSIE (Marconi Avionics).

The Low Range Airspeed System (LORAS) uses a motor driven rotating bar with a venturi tube at each end. The venturis are connected to either side of a differential pressure transducer where the measurements are converted to electrical signals. An on-board computer resolves these signals azimuthally and outputs forward and lateral airspeed, density altitude or air density. The best sensor position is above the rotor so that the LORAS installation usually requires a nonrotating standpipe through the main rotor shaft.

The Low Air Speed Sensing and Indicating Equipment (LASSIE) consists of a swivelling pitot static probe. It is installed on the fuselage and sited underneath the rotor. The sensor is free to rotate in pitch direction (angle of attack measurement) and it can rotate up to  $\pm 45$  degrees in yaw direction (sideslip angle measurement). Probe angles, static and dynamic pressure are fed to an on-board air data computer that outputs forward and lateral airspeed, height and height rate, and, except for low speeds, vertical velocity.

Both, LORAS and LASSIE, are based on pressure measurements. Therefore Figure 16 compares these systems with the conventional pitot static system. The main disadvantage of the pitot static system is the small difference between the static and dynamic pressure for low aircraft speed. This drawback can be removed by superimposing a defined dynamic pressure: due to its rotation the LORAS rotor generates a high constant dynamic pressure level for both sensors. When the helicopter moves, the pressure differences between the advancing and the retreating sensor can be measured with high accuracy. Evaluating these differences at defined sensor azimuth positions yields a linear pressure to airspeed relationship. In hover and at low speeds the LASSIE sensor works within the rotor downwash using the flow to adjust the swivelling probe and to raise the dynamic pressure level. When it is free from downwash the sensor works like a conventional swivelling pitot static system. Helicopter speed is calculated from measurements of both dynamic pressure and probe angles of attack and sideslip. It turns out that the calculation is based mainly on the probe angles when the sensor is in downwash, whereas it is primarily based on pressure measurement when the probe is free from the rotorwash. The transition phase, however, is highly nonlinear and requires accurate system characterization and calibration.

Various flight tests have been conducted to investigate the feasibility of low airspeed measuring systems. However, only steady state flight conditions have been evaluated and no in-flight dynamic behaviour of these systems has been considered. This is mainly due to the problem that true and measured airspeeds have to be compared. But what can be done when the "true" values can only be measured by equipment that may be even less

precise than the system under test itself? Parameter identification, however, is based on the evaluation of non-steady state flight maneuvers. Although the LASSIE has been used successfully for the identification of a MBB BO 105 helicopter at 70 knots forward speed, there is no unique solution to the airspeed measuring problem for system identification flight tests [18]. In addition, no measuring system is able to sense the vertical velocity in the low speed regime directly. In general, vertical velocity is calculated from acceleration or static pressure measurements.

#### 4. ROTORCRAFT MODELING

The selection of adequate mathematical helicopter models to be used in the identification is one of the most important steps of the identification procedure. This task is usually referred to as rotorcraft modeling or, more precisely, as model structure determination. The objective is to define the structure, that is the size and the order, of the required model. The quantification of the coefficients, then, is part of the parameter identification.

There are two principle aspects of rotorcraft modeling:

1. The determination of the degrees of freedom and, consequently, of the equations that are necessary to describe rotorcraft dynamic behaviour
2. The isolation of significant parameters to reduce the number of unknowns.

Within this section both aspects are discussed in detail.

##### 4.1 MODELING OF ROTORCRAFT DYNAMICS

It has already been pointed out that helicopters have a large number of coupled degrees of freedom (DOF) that occur in both rotating and nonrotating axes. The complete mathematical model of rotorcraft necessarily must be very complex, inasmuch as nonlinear and time variant aerodynamic effects also have to be considered. It has to be stated at the outset that the presently known and available system identification techniques are not able to determine such "global" systems. But these models are usually only needed for some detailed simulations or specific analyses and they may be very inefficient for handling more general problems, like control system design, stability and control analysis and direct correlation with flight test data for validation purposes. Therefore model simplifications are required and there is a need for simple and still accurate mathematical rotorcraft models. This is the problem area that provides both a challenge and strong motivation for applying system identification methods.

Considerations to simplify analytical models are mostly based on mode decoupling assumptions to split the model differential equations into independent subsystems. Usually, this can be done without significant loss of accuracy when 1. the coupling intensity is rather low or 2. the frequencies are well separated from each other and there is only interest in a specific frequency range or 3. an equation has only minor influence and can be neglected. For rotorcraft identification the reduction of the model to a reasonable size is required by the inherently limited data information content, by constraints of computational resources, and by the restricted applicability of identification algorithms. But this reduction has to be carried out very carefully as the assumptions it is based on are actually only approximations. Errors, like ignoring modes or modal couplings which are, in fact, significant, will lead to severe identification problems and to false results.

Taking the MBB BO 105 helicopter as an example, Figure 17 summarizes typical frequency ranges of the rigid body and rotor motions. A comparison of the frequency relationships clearly shows that rigid body long period and short period modes can be within the same frequency range. In addition, short period modes may also interfere with blade flapping and lagging motions, in particular with flap regressing and lag regressing. Higher harmonics are virtually uncoupled from rigid body modes but they can be within the same frequency range as blade flap and lag advancing modes. This consideration leads directly to one of the basic questions of rotorcraft identification, whether rotor DOF have to be included in the model and to what extent. Therefore, various models with different degrees of complexity are presented in the following section.

##### 4.2 ANALYTICAL ROTORCRAFT MODELS

Rotor blade motions are usually described and measured in a rotating coordinate system whereas rigid body motions are defined in non-rotating axes. The nonlinear equations of helicopter motions therefore contain fuselage states  $x_F$  and control variables  $u$  in the non-rotating axis system and also rotor states  $x_R$  in the rotating axis system, denoted by the subscript  $r$ . In addition, some equation terms are periodic with rotor blade azimuth or with time.

$$\dot{x}_F = f_F(x_F, x_R^r, u, t)$$

$$\dot{x}_R^r = f_R(x_F, x_R^r, u, t)$$

Linearization then yields linear equations with periodic coefficients:

$$\dot{x}_F = F_{FF}(t)x_F + F_{FR}(t)x_R^r + G_F(t)u$$

$$\dot{x}_R^r = F_{RF}(t)x_F + F_{RR}(t)x_R^r + G_R(t)u$$

where the block matrices  $F_{FF}$  and  $F_{RR}$  define the coefficients of the uncoupled fuselage and rotor motion and  $F_{FR}$  and  $F_{RF}$  describe the fuselage-rotor and the rotor-fuselage coupling.

The transformation from rotating to non-rotating axes physically means describing the attitude and shape of the tip path plane with respect to the shaft instead of describing the individual blade motions. However, tip path plane variables usually cannot be measured directly and therefore specific evaluation techniques are needed to calculate these variables from blade motion measurements. Such tip path plane resolving methods are Fourier analysis and Kalman estimation technique. When blade flapping angles  $\beta_i$  and blade azimuth angles  $\psi_i$  are measured the Fourier transform for the flapping motion yields for an N-bladed rotor [11]:

$$\beta_o = 1/N \sum_{i=1}^N \beta_i$$

$$\beta_{ns} = 2/N \sum_{i=1}^N \beta_i \sin n\psi_i$$

$$\beta_{nc} = 2/N \sum_{i=1}^N \beta_i \cos n\psi_i$$

$$\beta_d = 1/N \sum_{i=1}^N \beta_i (-1)^i \quad N \text{ even only}$$

The variables in the non-rotating coordinate system are then

$\beta_o$       the coning angle  
 $\beta_{1c}$      the tip path plane tilt in pitch  
 $\beta_{1s}$      the tip path plane tilt in roll  
 $\beta_d$       the differential coning  
 $\beta_{nc}/\beta_{ns}$  the tip path plane wrap ( $n>1$ )

The Kalman estimator technique for tip path plane resolving from flapping measurements is discussed in [38]. It was found to be superior to the Fourier method when data are noise-contaminated.

The lagging motion is transformed in a similar way as the flapping motion. The transformation of all variables of the rotating reference axes to the non-rotating axis system and the averaging of all periodic coefficients results in the linear constant coefficient model

$$\dot{x}_F = A_{FF}x_F + A_{FR}x_R + B_F u$$

$$\dot{x}_R = A_{RF}x_F + A_{RR}x_R + B_R u$$

This set of first order differential equations is suitable for use in system identification. The variables are defined in a non-rotating reference system. The matrices  $A_{FF}$  and  $A_{RR}$  define the uncoupled fuselage and rotor modes, the matrices  $A_{FR}$  and  $A_{RF}$  represent the corresponding coupling terms. The actual size of the matrices  $A_{FR}$  and  $A_{RF}$  vectors depends on the number of degrees of freedom considered and on the degree of approximation.

Taking a 4-bladed helicopter as an example Figure 18 demonstrates that a variety of candidate models of different complexity can be derived for use in flight dynamic studies. When all rigid body degrees of freedom (DOF) and blade flapping and lagging motions are considered the helicopter has 14 DOF. The nonlinear equations are first transformed to linear differential equations with periodic coefficients and then to constant coefficient equations. The resulting model still represents 14 DOF, however, two approximations already have been applied: small perturbation assumption and periodic coefficient averaging. There are about 325 state matrix coefficients, more than 300 of them have to be identified unless any derivatives are known or can be neglected. It depends on the studies the model is used for whether the model size can be reduced and to what extent. In general, however, higher harmonic terms (tip path plane wrap), differential coning and differential collective lag ( $\beta_d$  and  $\beta_{nc}$ ) can be ignored for most flight dynamic studies. This leads to

a 12 DOF model with a 6 DOF rotor representation (3 DOF for the tip path plane, 3 DOF for the inplane motion). It allows for coupling between the flapping and lagging motion. Further simplifications of this model result in 12 or 10 DOF models that use a first order representation of both flapping and lagging. The 10 DOF model is the most simple model that still includes the rotor DOF separately. The derivation of the first order model is shown for the flapping motion in a subsequent section.

So far, models have been presented which included both flapping and lagging DOF. The next level of approximation is based on the assumption that inplane DOF can be ignored because their influence on the overall rotorcraft response is very small. (Nevertheless, they may be required for high gain feedback studies and, in particular, for the investigation of resonance phenomena.) The flap-lag models can then be reduced to four models that include only the rotor flapping DOF and the rigid body DOF: a 10 DOF model that still accounts for higher harmonic components, a 9 DOF model representing coning and first harmonics, and two models with 9 and 8 DOF, which use a first order rotor representation.

One of the most often used assumptions to simplify rotorcraft models is the decoupling of high frequency rotor modes and low frequency fuselage modes. This yields a 6 DOF rigid body model. When deriving this model from higher order analytical models the rotor equations cannot simply be omitted, but a mathematical model reduction method, based on the assumption of quasi-static rotor behaviour, has to be used (this reduction technique is discussed in the subsequent section). The model obtained is often referred to as quasi-static model. It is identical in structure and size to the 6 DOF rigid body representation of fixed-wing aircraft. However, the separation into longitudinal and lateral-directional motions is, in general, not appropriate for helicopters because of strong coupling effects. But this separation may be possible for high speed flight conditions. For the hovering flight condition vertical forces and yaw moments may be virtually decoupled from longitudinal and lateral forces and from pitch and roll moments. Hence, a separation into 4 DOF and 2 DOF models may be possible.

#### 4.3 REDUCTION TO FIRST ORDER AND QUASI-STATIC MODELS

Usually, model simplifications are achieved by omitting defined equations and states. Some of the previously presented models, however, are obtained by the application of specific reduction techniques. This section first describes the derivation of the first order rotor representation for the flapping motion and then discusses the reduction to the quasi-static model [11].

The tip path plane motion (without inplane DOF) is described by

$$\dot{\mathbf{x}}_R = \mathbf{A}_{RR} \mathbf{x}_R$$

and in detail

$$\begin{bmatrix} \ddot{\beta}_0 \\ \ddot{\beta}_{1c} \\ \ddot{\beta}_{1s} \\ \dot{\beta}_0 \\ \dot{\beta}_{1c} \\ \dot{\beta}_{1s} \end{bmatrix} = \begin{bmatrix} a_{11} & \textcircled{a_{12}} & \textcircled{a_{13}} & a_{14} & \textcircled{a_{15}} & \textcircled{a_{16}} \\ \textcircled{a_{21}} & a_{22} & a_{23} & \textcircled{a_{24}} & a_{25} & a_{26} \\ \textcircled{a_{31}} & a_{32} & a_{33} & \textcircled{a_{34}} & a_{35} & a_{36} \\ 1 & 0 & 0 & 0 & 0 & 0 \\ 0 & 1 & 0 & 0 & 0 & 0 \\ 0 & 0 & 1 & 0 & 0 & 0 \end{bmatrix} \begin{bmatrix} \dot{\beta}_0 \\ \dot{\beta}_{1c} \\ \dot{\beta}_{1s} \\ \beta_0 \\ \beta_{1c} \\ \beta_{1s} \end{bmatrix}$$

Usually the circled equation terms have only minor influence on the overall rotor response characteristic and can be neglected. Then

$$\begin{bmatrix} \ddot{\beta}_0 \\ \dot{\beta}_0 \end{bmatrix} = \begin{bmatrix} a_{11} & a_{14} \\ 1 & 0 \end{bmatrix} \begin{bmatrix} \dot{\beta}_0 \\ \beta_0 \end{bmatrix}$$

$$\begin{bmatrix} \dot{\beta}_{1c} \\ \dot{\beta}_{1s} \end{bmatrix} = - \begin{bmatrix} a_{22} & a_{23} \\ a_{32} & a_{33} \end{bmatrix}^{-1} \begin{bmatrix} a_{25} & a_{26} \\ a_{35} & a_{36} \end{bmatrix} \begin{bmatrix} \beta_{1c} \\ \beta_{1s} \end{bmatrix}$$



Longitudinal and lateral flapping are described by two first order differential equations that model the flap regressive mode. The second order equation for the coning mode is considered to be decoupled and, since the coning mode frequency is usually much higher than the flap regressive frequency, this equation may be ignored. The advantage of this rotor representation is a relatively simple tip path plane characterization that still retains a good approximation of the flap regressive mode[39]. The inplane motion equations can be reduced in a similar way as the flapping equations are reduced.

The 6 DOF rigid body quasi-static model is derived from

$$\dot{x}_F = A_{FF}x_F + A_{FR}x_R + B_F u$$

$$\dot{x}_R = A_{RF}x_F + A_{RR}x_R + B_R u$$

Setting  $\dot{x}_R$  equal to zero yields for the second equation

$$x_R = -A_{RR}^{-1} \cdot A_{RF}x_F - A_{RR}^{-1} \cdot B_R u$$

Substituting this equation into the first equation results in

$$\begin{aligned} \dot{x}_F &= (A_{FF} - A_{FR} \cdot A_{RR}^{-1} \cdot A_{RF}) x_F + (B_F - A_{FR} \cdot A_{RR}^{-1} \cdot B_R) u \\ &= A_{FF}^* x_F + B_F^* u \end{aligned}$$

The obtained model considers only fuselage states, the matrices  $A_{FF}^*$  and  $B_F^*$  contain the quasi-static derivatives. It is clearly to be seen that the initial rigid body coefficients are modified by rotor and coupling terms. Thus the rotor contribution to the rotorcraft motion is lumped into the fuselage coefficients.

The quasi-static model was derived assuming the rotor dynamics to be neglected ( $\dot{x}_R=0$ ). Physically this means that the rotor tip path plane can be tilted instantaneously and immediately reaches its new trim position when an input is applied. This assumption is justified when rotor frequencies are essentially higher than rigid body frequencies. The rotor response is then virtually instantaneous in comparison with the fuselage response.

#### 4.4 ROTORCRAFT IDENTIFICATION MODELS

The linear constant coefficient models previously described are prime candidates for use in system identification. On the basis of experience, a priori knowledge and simulation results the minimum order model has to be selected that satisfies both the requirements of the studies the model will be used for and the requirements of the data evaluation methods. It is important to visualize that an adequate model has to be defined at an early stage of the preparation phase because of its great influence on rotorcraft instrumentation, input signal design, and data processing:

1. The variables to be measured are defined by the model used in the identification. Therefore, increasing the size of the mathematical model also increases the amount of effort and expense connected with sensor equipment and its installation, signal conversion, data recording, calibration, and analysis.
2. Input signals are designed to not only excite all modes of interest but also to avoid the excitation of those modes not considered by the model. It follows that an appropriate input signal can only be developed when the frequency ranges of interest have been defined.
3. Data processing has been discussed extensively in part 5 and 6 of this lecture series [3]. There are two main rotorcraft data characteristics that influence the processing phase: 1. large identification models require a multitude of variables to be processed, 2. high frequency modes necessitate high sampling rates. Both characteristics cause a large amount of data to be stored and evaluated, which requires much computing time.

Until now, only rigid body DOF models have been used for rotorcraft identification from flight test data. Major attempts to include rotor DOF as well have been made only for the evaluation of computer simulated data [11] but not for the extraction of parameters from flight test data. Obvious reasons for this development are certainly that rotor state measurements are often not available and that there is still the need for evaluation techniques that are able to process a large amount of data and to estimate a large number of unknown parameters within tolerable limits of computing time and costs. Other more subtle reasons may arise from the difficulties in increasing the data information content.

Analytical and identified rigid body models are identical in their structure. But there is a difference in the definition of the coefficients. The analytical models assume a quasi-static rotor behaviour. In reality, however, the rotor does not follow a control input instantaneously, but it reaches its new steady state only after some revolutions.

It is easy to imagine that there can be significant differences between the quasi-static and the actual rotor response when control inputs are applied and the helicopter is flying in non-steady state flight conditions. System identification is based on flight test data where specific control inputs are used to produce dynamic helicopter responses. Therefore, identified derivatives represent the rigid body derivatives plus an average rotor contribution. They cannot be identical to the quasi-static values. The differences between these averaged coefficients and the quasi-static derivatives may be relatively small, but they have to be considered when identified and analytical values are compared.

Figure 19 presents BO 105 time history responses obtained from a non-linear computer simulation that includes 5 rigid body DOF (without yaw motion) and 4 DOF per blade: flap, lag, torsion, and control flexibility [40]. The part of the roll acceleration response where the input signal changes its amplitude has been enlarged in Figure 20. The 4/rev vibration mode of the 4-bladed helicopter is clearly to be seen. In addition a 4.8 Hz oscillation due to blade inplane motion is indicated, which damps out after a couple of rotor revolutions. Although the input signal is filtered to avoid the excitation of rotor modes the influence of the rotor transient on the rigid body motion is so dominant that the 6 DOF model response is rather incorrect for this time period. It follows that a rigid body model may be used when higher frequency motions and rotor transient effects can be ignored but such a model is not appropriate for a more precise description of rotorcraft behaviour. Nevertheless fuselage-only models have been used and are still used extensively for both stability and control analysis and control system design and, consequently, they are used for system identification too. The need to also include rotor DOF into the model was first established and re-emphasised by Molusis [8, 10, 11], who strongly recommended the use of a 9 DOF model (rigid body, rotor coning, tip path plane tilt). A further extension is proposed by [20] requiring a minimum model of 12 DOF that also includes 3 rotor inplane DOF.

To demonstrate the significance of explicit rotor modeling Sikorsky CH-53 flight test data are compared with the pitch acceleration response of three different linear models:

1. A 6 DOF model with only fuselage states
2. A 9 DOF model with 6 rigid body DOF and 3 rotor flapping DOF, where the rotor is modeled as a first order system
3. A 9 DOF model where the flapping rotor is described by second order equations.

The results are shown in Figure 21, taken from [20]. They were obtained from a model estimation program based on regression analysis. When the 6 DOF model is used, only a relatively poor curve fit can be achieved because of the rotor transient effects. Hence, the additional modeling of rotor DOF results in a significant increase in model accuracy. When a second order representation is used instead of a first order rotor model no significant further improvement can be seen.

#### 4.5 ISOLATION OF SIGNIFICANT PARAMETERS

Once the decision is made which DOF are considered by the identification model the significant model parameters have to be determined. The basic idea is that parameters found to be significant, i.e. parameters which contribute distinctively to aircraft motion, can also be identified accurately. However, parameters with only minor influence on vehicle motion cannot be identified with reasonable confidence and, consequently, can be ignored. This step of rotorcraft modeling is of fundamental importance as it represents a powerful tool to reduce the number of unknown parameters to be identified.

One approach to determine which parameters are significant is based on Bode plots evaluation. This technique has been discussed in more detail in part 3 of this lecture series [1]. For each model equation a set of transfer functions multiplied by the corresponding equation coefficient is calculated and plotted as shown in Figure 22 for the roll moment equation of a linear model of the Sikorsky S-61 in hover. Considering the frequency range of the input signal used for the data run of interest the amplitudes of all equation terms are compared: high amplitudes indicate dominant terms that can be identified whereas low amplitude terms may be ignored. The main advantages of this evaluation method are that it is easy to implement and that it gives a considerable insight into the relationship of system excitation and parameter identifiability. The technique has been used successfully for fixed wing aircraft [41], for helicopters, however, it can lose part of its simplicity when plots of many parameters have to be evaluated. Figure 22 is based on a 6 DOF model where 4 DOF represent the rigid body and 2 DOF describe the tip path plane pitch and roll [42]. It demonstrates that the parameter curves often interfere with each other and sometimes can hardly be distinguished. In addition, there are also high amplitude changes within a small frequency range. The application of the Bode plot method then requires an accurate frequency analysis of the input signal.

Another method to isolate significant model equation terms uses the time domain. As it is also based on the separate evaluation of each equation the S-61 roll moment equation is again used as an example

$$\dot{p} = L_u u + L_v v + L_p p + L_q q + L_{\theta R} \theta_R + L_{\phi R} \phi_R + L_{pR} \dot{p}_R + L_{qR} \dot{q}_R + L_{\theta c} \dot{\theta}_c$$

For all variables the absolute values of the time histories are integrated over the time span used in the identification (Integral criterion). The equation terms are then

$$\int \dot{p} |dt, L_u \int |u| dt, L_v \int |v| dt \quad \text{etc.}$$

As the inertia term usually also is the reference term in the identification it is meaningful to normalize all terms by  $\int \dot{p} |dt$ . Figure 23 shows the magnitude of the resulting terms when a run is evaluated where an optimized input signal was applied to the lateral cyclic. It also presents results obtained from two modifications of this technique: the integral criterion is replaced by first, a route mean squares criterion and second, a maximum absolute value criterion. Comparing the amplitudes shown in Figure 23 it is obvious that for example,  $L_{\phi R}$  and  $L_v$  are dominant whereas  $L_{pR}$  and especially  $L_{qR}$  have only minor influence. Although three basically different criteria are used, almost identical tendencies in parameter significance can be seen. The magnitude of the inertia term is of special importance. If it is small in comparison to other equation terms there is no significant reference term in the equation. Hence, only parameter relationships can be determined.

The parameter isolation criteria were applied to the Sikorsky S-61 model. As much as 22 % of the stability and control derivatives (12 out of 54) were neglected and set equal to zero. Figure 24 compares the time responses of both the complete and the reduced model. This parameter isolation technique uses measured or simulated system response data directly. Therefore no special attention has to be given to any frequency analysis of the input signal.

Both the Bode plot technique and the time history method are powerful tools to isolate significant equation terms and identifiable parameters. The Bode plot method is certainly most valuable for the input signal design phase, whereas the time history technique may be more suited for the identification phase. As it is computationally very easy to implement it can be used within an iterative identification procedure to confirm or update the momentary model structure.

## 5. ROTORCRAFT IDENTIFICATION FROM FLIGHT TEST DATA

Helicopter identifications have been conducted using various identification techniques which include relatively simple equation error methods but also more sophisticated techniques like maximum likelihood, extended Kalman filter, and Bayesian approach. In general, however, only input signals like step, pulse and doublets were applied although both many unknown parameters and limited data length require the use of more efficient input signals to raise the data information content. This section therefore presents identification results from flight test data where optimized input signals were applied to a MBB BO 105 helicopter, equipped with a fly-by-wire system. A description of this helicopter is given in [43]. Flight tests were conducted at a trim speed of 70 knots TAS where the aircraft is slightly unstable. The identification results were obtained from least squares, instrumental variable, and maximum likelihood techniques.

### 5.1 EVALUATION OF SINGLE RUNS

To excite the rigid body helicopter modes pseudostochastic input signals were used that consist of a sequence of step functions. They have already been discussed in detail in part 3 of this lecture series [1]. The signals were generated electronically and fed to the helicopter's fly-by-wire control system. They were started by the pilot as soon as the aircraft had reached its defined steady state trim flight condition. Three different input signal combinations were used (Figure 25): first, the input signal was applied only once to one control, second the signal was applied twice to the same control. The moment to restart the signal was chosen by the pilot in such a way to keep the aircraft within small perturbation limits from trim position. The third combination was similar to the second one, but now the restarted signal was applied to another control.

Identification results for each of these combinations are now presented. The identification model considers 6 rigid body DOF, about 25 stability derivatives have to be determined. Using the least squares equation error method a 15 second duration run with a collective control input was evaluated. The time histories of the measured data and the identified model are shown in Figure 26. It is clearly to be seen that only a poor fit is obtained. Attempts to improve this result using the iterative techniques, instrumental variable and maximum likelihood, failed because of convergence problems. Figure 27 presents time histories obtained from the identification of a 30 second duration run with two sequential collective control input signals. In comparison with the previous run this run should have a significantly higher information content because an additional input signal was applied and a longer time span is evaluated. But no noticeable improvement in the least squares result was obtained. However, the instrumental variable converged and the improvement is obvious. Nevertheless the curve fit is still not satisfactory.

During the evaluation of various flight tests it became clear that it is very difficult or sometimes even impossible to accurately identify the helicopter when only one control is used to excite all rigid body modes. This may be caused by the fact that, for example, a collective control input primarily excites the longitudinal motion (Z-force) whereas the lateral-directional motion is only influenced because of coupling effects. Although there is a high coupling intensity - this is clearly indicated by almost the same magnitude of the pitch rate and roll rate response - no sufficient information about

the system can be obtained from inputs to a single control. Consequently, an additional excitation of another control may help to improve this situation. Therefore a run was evaluated where a control input was first applied to the collective and then to the lateral cyclic. Now both longitudinal and lateral-directional motions are excited directly. Figure 28 presents flight test data and the time histories of the identified models obtained from the least squares and the instrumental variable technique. These time histories are almost identical and show a good agreement with the measured data. This run was also identified using the maximum likelihood method. As can be seen from Figure 29 a satisfactory result was obtained which confirms that a successful identification can be accomplished when both longitudinal and lateral-directional motions are excited directly by appropriate controls and optimized input signals.

However, the use of different controls within one run is always problematic for a helicopter. As shown in the last two examples, a time duration of about 25 to 30 seconds is required when the so-called "3-2-1-1" pseudostochastic signal is used sequentially. More unstable helicopter flight conditions will not allow this data length without any stability augmentation systems or pilot actions, which leads directly to the closed loop identification problem. The time duration can be reduced by simultaneous excitations of two controls. This can easily be accomplished when an automatic input device is available. But even for very skilled pilots it is certainly extremely difficult to give two signals - well defined in both amplitude and timing and also statistically independent from each other - simultaneously to different controls.

## 5.2 EVALUATION OF MULTIPLE RUNS

When all possibilities during the preparation and flight test phase have been utilized to fulfill system identification requirements and it is still not possible to accurately identify the helicopter from one data run, more powerful identification procedures have to be used. One approach to this problem is the application of identification techniques that allow use of information from multiple data runs. As shown in Figure 30, the single run evaluation considers each run independently of the others, which also results in one identified model for each run. It has been demonstrated that poor results are often obtained because of insufficient data information content. In the multiple run evaluation, however, a combination of various independent runs is identified. The result, then, is one model that is valid for each of the identified runs.

Identification results obtained from a combination of three different runs are now presented. In the first run a collective control input was used primarily to excite the longitudinal aircraft motion, in the second run the lateral-directional motion was excited by a lateral cyclic control input and the third run was included to provide additional information about the yaw characteristic. Figure 31 shows the flight test data and the time histories of the identified models obtained from both the least squares and the instrumental variable technique, whereas Figure 32 presents the maximum likelihood results. It can be seen that each of these methods yields a satisfactory curve fit which is especially true for the maximum likelihood result. Discrepancies in the lift equation (vertical acceleration  $a_z$ ) probably arise from inaccurate vertical velocity measurements.

The first of the three runs (collective input) has already been presented in Figure 26. It was used for a single run evaluation, however, only unsatisfactory results could be obtained. Only the combination with additional data from other runs makes it possible to accurately identify the helicopter. This example clearly shows the main advantages of the multiple run evaluation with respect to rotorcraft identification:

1. A physically meaningful combination of different runs provides a large amount of information about the system under test although the individual runs may contain only a certain part of this information.
2. It is sufficient if an individual run contributes only a specific part or the total information content to the overall evaluation. This requirement simplifies the input signals and, consequently, improves the signal flyability, as only a part of all modes of interest has to be excited within one run.
3. Insufficient data length, for example due to system instabilities, can be compensated to a certain extent by the use of additional data from other runs. The example presented includes three runs of 15 seconds duration each. However, to conduct one run of 45 seconds duration is usually not possible without any stabilization efforts.

Furthermore, Gould and Hindson [14] have demonstrated that the combined evaluation of various similar runs makes it possible to reduce the influences of external inputs, like atmospheric disturbances, on identification results.

The main parameter identification objective is the determination of flight mechanical derivatives that can be related to analytical calculations or to wind tunnel measurements. Therefore Figure 33 presents the identified values of some of the main stability derivatives together with their quasi-static a priori values for each of the previously discussed evaluations. In addition, results are given that were obtained from the combined identification of two different runs, where a collective control input (first run) and a lateral cyclic control input (second run) were applied. For some of these cases various runs or various combinations of different runs were identified:

Evaluation of	1 input signal applied to	No of runs or combinations	ID method	Notation in Fig. 33
single run	collective	4	least squares	A
multiple runs				
2 runs	collective (1st run) lat cyclic (2nd run)	13	instrumental variable	D
3 runs	collective (1st run) lat cyclic (2nd run) tail rotor (3rd run)	7	instrumental variable	E

The mean value and the standard deviation of the resulting derivatives are presented. Derivatives shown without standard deviation were obtained only from one run or one combination. This is the case for those runs where two signals were applied sequentially (B, C) and for the maximum likelihood results. Comparing the identified derivatives it should be noted that they are obtained from different runs, various combinations of different runs and also from different identification methods. Therefore identical values cannot be expected. However, it can be stated that there is a good agreement between the results, except for the first two cases shown (A and B) where only one control was used to excite all rigid body modes. Once more, this result confirms the need for excitations using different controls.

When the results obtained from the instrumental variable and the maximum likelihood method are compared it can be seen that the maximum likelihood technique yields a better curve fit. This is almost self-evident as the maximum likelihood criterion is defined to minimize the output error whereas the instrumental variable method minimizes the equation error. The identified derivatives, however, are of the same order. It also has to be considered that the computation times of the least squares, of the instrumental variable, and of the maximum likelihood techniques differ roughly by a factor of ten. The maximum likelihood identification of three runs, for example, required about 3 1/2 hours CPU-time on a Siemens 7.755 computer. The instrumental variable result was obtained within about 20 minutes CPU-time. Of course, these numbers cannot be representative as the CPU-time depends to a large extent on program convergence and the number of iterations. But it turned out that the computing time relationships are similar even when other data were evaluated. Therefore the decision, which method is used for the identification of a helicopter may often be dictated by computing time availability and cost considerations, especially when even larger systems (inclusion of rotor DOF) have to be identified.

#### 6. CONCLUDING REMARKS

In this lecture an overview of rotorcraft identification with respect to practical applications was given. Problems associated with the identification were discussed. Reliable identification results can only be obtained when flight test data have been measured with high accuracy. Therefore, measuring difficulties due to helicopter characteristics were discussed in detail. Emphasis was also placed on rotorcraft modeling. Various candidate models of different complexity to be used in the identification as well as techniques to isolate significant parameters and to reduce the number of unknowns were presented.

Identification results obtained from MBB BO 105 flight test data were given. Identification techniques that allow use of information from different data runs were applied. This multiple run evaluation is ideally suited for rotorcraft identification for two main reasons: 1. only a part of all modes of interest has to be excited within a single run, which simplifies both input signal and flight test conduction. 2. insufficient data length, due to helicopter instabilities, can be compensated to a certain extent by the use of additional data from other runs. It was demonstrated that a physically meaningful combination of different runs provides a sufficient amount of information about the system under test to successfully identify rotorcraft derivatives.

The multiple run evaluation together with the application of optimized input signals and a high quality flight test instrumentation are powerful tools for the identification of helicopters. Future flight test data evaluations still have to prove that these techniques can also be used to satisfy two main rotorcraft identification objectives: 1. the identification of models including rotor degrees of freedom and 2. the identification of highly unstable flight conditions. In addition, attempts have to be made to consider also non-linear effects of rotorcraft behaviour.

## 7. REFERENCES

1. Plaetschke, E., Schulz, G., "Practical Input Signal Design", AGARD Lecture Series No. 104, 29 October - 2 November 1979.
2. Breeman, J.H., Mulder, J.A., van Woerkom, K., "Aspects of Flight Test Instrumentation" AGARD Lecture Series No. 104, 29 October - 2 November 1979.
3. Mulder, J.A., Jonkers, H.L., Horsten, J.J., Breeman, J.H., Simons, J.L., "Analysis of Aircraft Performance, Stability and Control Measurements", AGARD Lecture Series No. 104, 29 October - 2 November 1979.
4. Klein, V., "Identification Evaluation Methods", AGARD Lecture Series No. 104, 29 October - 2 November 1979.
5. Iliff, K.W., "Aircraft Identification Experience", AGARD Lecture Series No. 104, 29 October - 2 November 1979.
6. Ross, A.J., "Identification Experience in Extreme Flight Regimes", AGARD Lecture Series No. 104, 29 October - 2 November 1979.
7. Koehler, R., Wilhelm, K., "Closed Loop Aspects of Aircraft Identification", AGARD Lecture Series No. 104, 29 October - 2 November 1979.
6. Molnisi, J.A., "Helicopter Stability Derivative Extraction and Data Processing Using Kalman Filtering Techniques", 28th Annual National Forum of the American Helicopter Society, Washington, D.C., Preprint No. 641, May 1972.
9. Molnisi, J.A., "Helicopter Stability Derivative Extraction from Flight Data Using the Bayesian Approach to Estimation", Jour. American Helicopter Society, Juli 1973.
10. Molnisi, J.A., "Analytical Study to Define a Helicopter Stability Derivative Extraction Method", NASA CR-132371, May 1973.
11. Molnisi, J.A., "Rotorcraft Derivative Identification from Analytical Models and Flight Test Data", Session V: Rotorcraft Parameter Identification, AGARD Conference Proceedings No. 172, November 1974.
12. Gould, D.G., Hindson, W.S., "Estimates of the Lateral-Directional Stability Derivatives of a Helicopter from Flight Measurements", National Research Council Canada, Aeronautical Report LR-572, December 1973.
13. Gould, D.G., Hindson, W.S., "Estimates of the Stability Derivatives of a Helicopter from Flight Measurements", 9th Congress of the International Council of the Aeronautical Sciences, Haifa, Israel, August 1974.
14. Gould, D.G., Hindson, W.S., "Estimates of the Stability Derivatives of a Helicopter and a V/STOL Aircraft from Flight Data", Session V: Rotorcraft Parameter Identification, AGARD Conference Proceedings No. 172, November 1974.
15. Tomaine, R.L., "The Effect of Pilot Control Input Shape on the Identification of Six Degree-of-Freedom Stability and Control Derivatives of a Transport Helicopter", Master's thesis, George Washington University, Washington, D.C., December 1976.
16. Tomaine, R.L., "Flight Data Identification of Six Degree-of-Freedom Stability and Control Derivatives of a Large "Crane" Type Helicopter", NASA TM X-73958, 1976.
17. Tomaine, R.L., Bryant, W.H., Hodge, W.F., "VALT Parameter Identification Flight Tests", 4th European Rotorcraft and Powered Lift Aircraft Forum, Stresa, Italy, September 1978.
18. Rix, O., Huber, H., Kaletka, J., "Parameter Identification of a Hingeless Rotor Helicopter", Preprint No. 77.33-42, 33rd Annual National Forum of the American Helicopter Society, Washington, D.C., Mai 1977.
19. Kaletka, J., Rix, O., "Aspects of System Identification of Helicopters", 3rd European Rotorcraft and Powered Lift Aircraft Forum, Aix-en-Provence, France, September 1977.
20. Hall, W.E., Gupta, N.K., Hansen, R.S., "Rotorcraft System Identification Techniques for Handling Qualities and Stability and Control Evaluation", Preprint No. 78-30, 34th Annual Forum of the American Helicopter Society, Washington, D.C., May 1978.
21. Hohenemser, K.H., "Rotor Dynamic State and Parameter Identification from Simulated Forward Flight Transients", Part 1: NASA CR-137963, 1976 (co-authors: Banerjee, D., Yin, S.K.), Part 2: NASA CR-137964, 1976 (co-author: Crews, S.T.).
22. Hohenemser, K.H., Crews, S.T., "Unsteady Hovering Wake Parameters Identified from Dynamic Model Tests", NASA CR-132022, 1977.
23. Hohenemser, K.H., Banerjee, D., "Application of System Identification to Analytical Rotor Modeling from Simulated and Wind Tunnel Dynamic Test Data", NASA CR-152023, 1977.

24. Banerjee, D., Hohenemser, K.H., "Optimum Data Utilization for Parameter Identification with Application to Lifting Rotors", *Journal of Aircraft*, Vol. 13, pp. 1014-1016, December 1976.
25. Kanning, G., Biggers, J.C., "Application of a Parameter Identification Technique to a Hingeless Helicopter Rotor", NASA TN D-7834, 1974.
26. Gessow, A., Myers, G.C., "Aerodynamics of the Helicopter", Frederick Ungar Publishing Co., New York, 1967.
27. Reichert, G., "Basic Dynamics of Rotors, Control and Stability of Rotary Wing Aircraft, Aerodynamics and Dynamics of Advanced Rotary-Wing Configurations ", AGARD Lecture Series No. 63, April 1973.
28. Berrington, D.K., "The Development of the WG.13 (Lynx)", 3rd European Rotorcraft and Powered Lift Aircraft Forum, Aix-en-Provence, France, September 1977.
29. Huber, H., "Parametric Trends and Optimization-Preliminary Selection of Configuration-Prototype Design and Manufacture", AGARD Lecture Series No. 63, April 1973.
30. Bramwell, A.R.S., "Helicopter Dynamics", Edward Arnold Publishers, London, 1976.
31. Langer, H.J., Stricker, R., "Results of Dynamic Measurements with a Model Hingeless Rotor", 5th European Rotorcraft and Powered Lift Aircraft Forum, Amsterdam, Netherlands, September 1979.
32. Carter, J., "The Measurement of Helicopter Air Data Using a Swivelling Pitot-Static Pressure Probe", Air Data Symposium Proceedings, Session V: Helicopter/VSTOL Sensors, Naval Postgraduate School, Monterey, Cal., USA, June 1976.
33. De Leo, R.V., Jensen, D.P., "Low Range Orthogonal Airspeed System", Air Data Symposium Proceedings, Session V: Helicopter/VSTOL Sensors, Naval Postgraduate School, Monterey, Cal., USA, June 1976.
34. Rotier, D.J., Ferrin, F.J., "Ultrasonic Wind Vector Sensor", Air Data Symposium Proceedings, Session V: Helicopter/VSTOL Sensors, Naval Postgraduate School, Monterey, Cal., USA, June 1976.
35. DuBro, G.A., Kim, D.G., Rudd, M.J., "An Electro-Optic Airspeed Sensor", Air Data Symposium Proceedings, Session IV: Helicopter/VSTOL Sensors, Naval Postgraduate School, Monterey, Cal., USA, June 1976.
36. Joy, D., "Airspeed and Direction Measurement by Vortex Detection", Air Data Symposium Proceedings, Session IV: Helicopter/VSTOL Sensors, Naval Postgraduate School, Monterey, Cal., USA, June 1976.
37. Abbot, W.Y., Boirun, B.H., Hill, G.E., Tavares, E.J., "Flight Evaluation Pacer Systems Low-Range Airspeed System LORAS 1000", Final Report, US AAEFA Project No. 75-17-1, Edwards Air Force Base, Cal., May 1977.
38. Briczinski, S.J., Cooper, D.E., "Flight Investigation of Rotor/Vehicle State Feedback", NASA CR-132546, January 1975.
39. Hohenemser, K.H., Yin, S.K., "On the Use of First Order Rotor Dynamics in Multiblade Coordinates", Preprint No. 831, 30th Annual National Forum of the American Helicopter Society, Washington, D.C., May 1974.
40. Huber, H., "Effect of Torsion-Flap-Lag Coupling on Hingeless Rotor Stability", 29th Annual National Forum of the American Helicopter Society, Washington, D.C., May 1973.
41. Marchand, M., Koehler, R., "Determination of Aircraft Derivatives by Automatic Parameter Adjustment and Frequency Response Methods", Session IV: Analysis of Flight Test Data, AGARD Conference Proceedings No. 172, November 1974.
42. Hall, W.E., Bryson, A.E., "Inclusion of Rotor Dynamics in Control Design for Helicopters, *Journal of Aircraft*", Vol. 10, pp. 200-206, 1973.
43. Attifellner, S., Rode, M., "BO 105 In-Flight Simulator for Flight Control and Guidance Systems", 1st European Rotorcraft and Powered Lift Aircraft Forum, Southampton, Great Britain, September 1975.

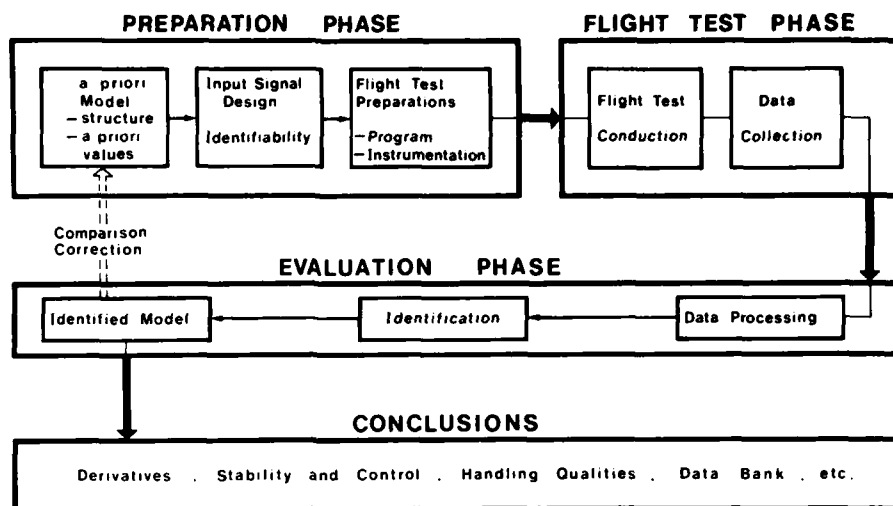


Fig. 1 System Identification Procedure

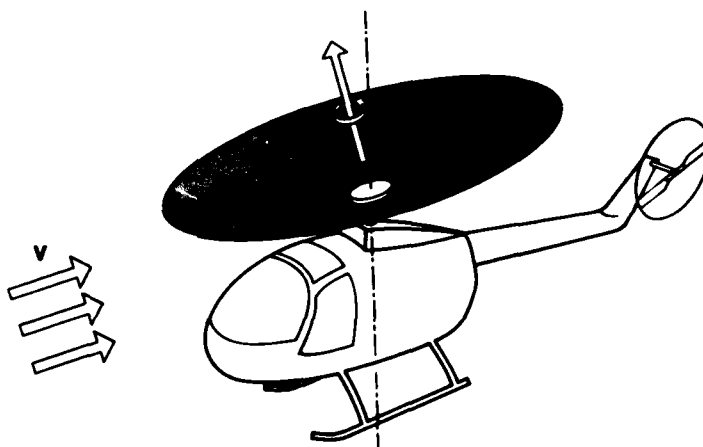


Fig. 2 Helicopter in Forward Flight

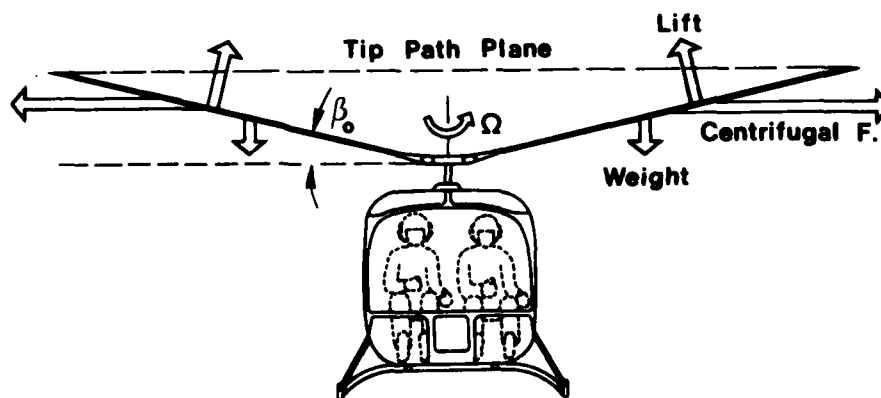


Fig. 3 Forces Acting on Rotating Blades



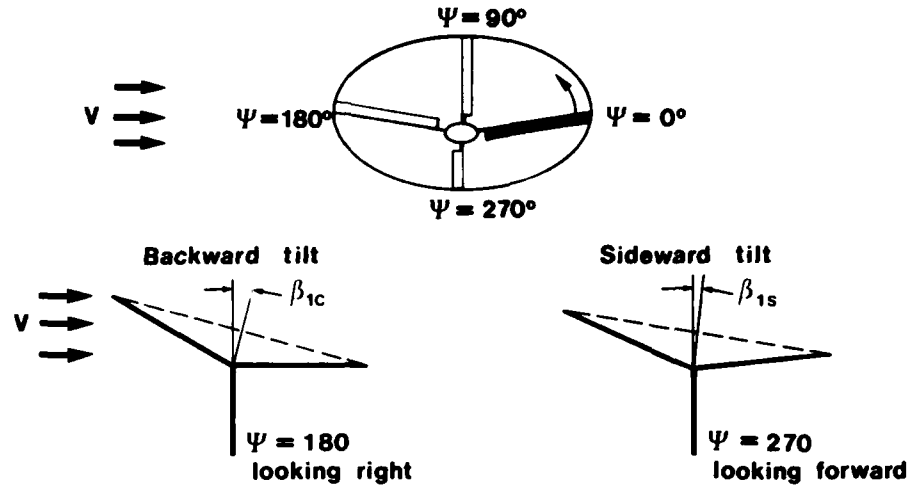
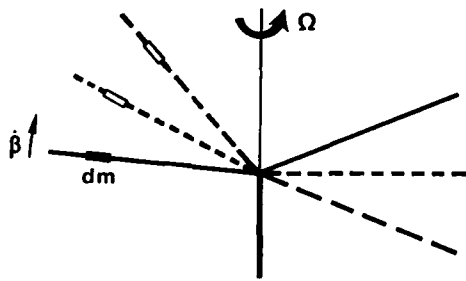


Fig. 4 Rotor Tilt Due to Blade Flapping

ROTOR SEEN FROM THE SIDE



ROTOR SEEN FROM ABOVE

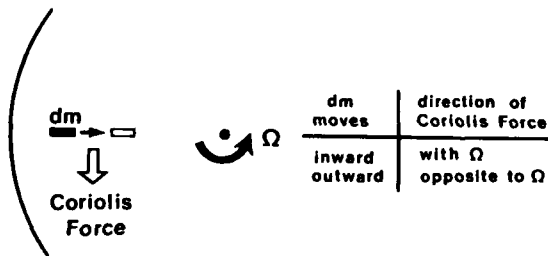


Fig. 5 Inplane Coriolis Forces Due to Blade Flapping

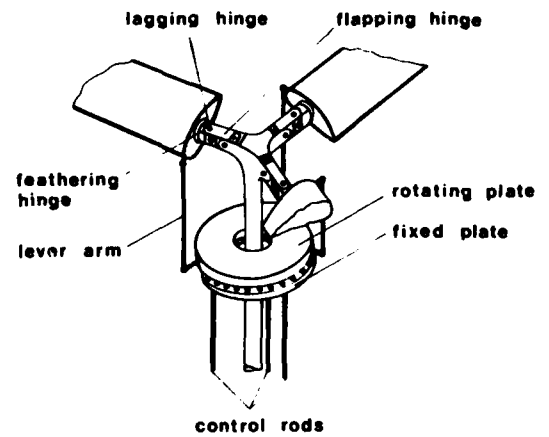
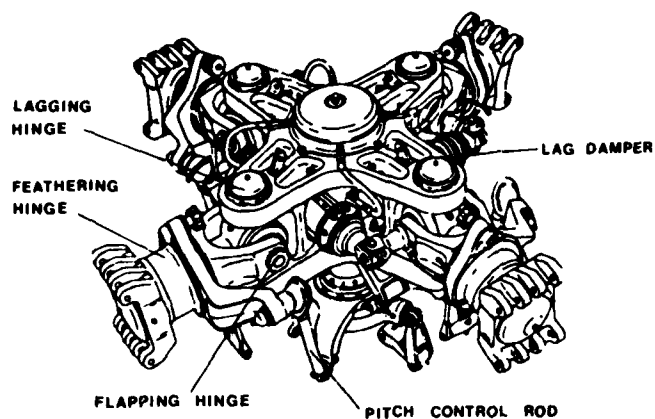
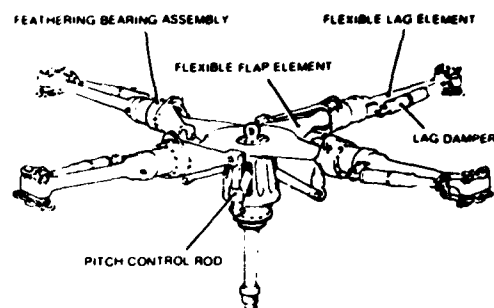


Fig. 6 Swashplate Assembly



ARTICULATED ROTOR (WESSEX/S 58)



HINGELESS ROTOR (LYNX)

Fig. 7 Rotorhead Comparison

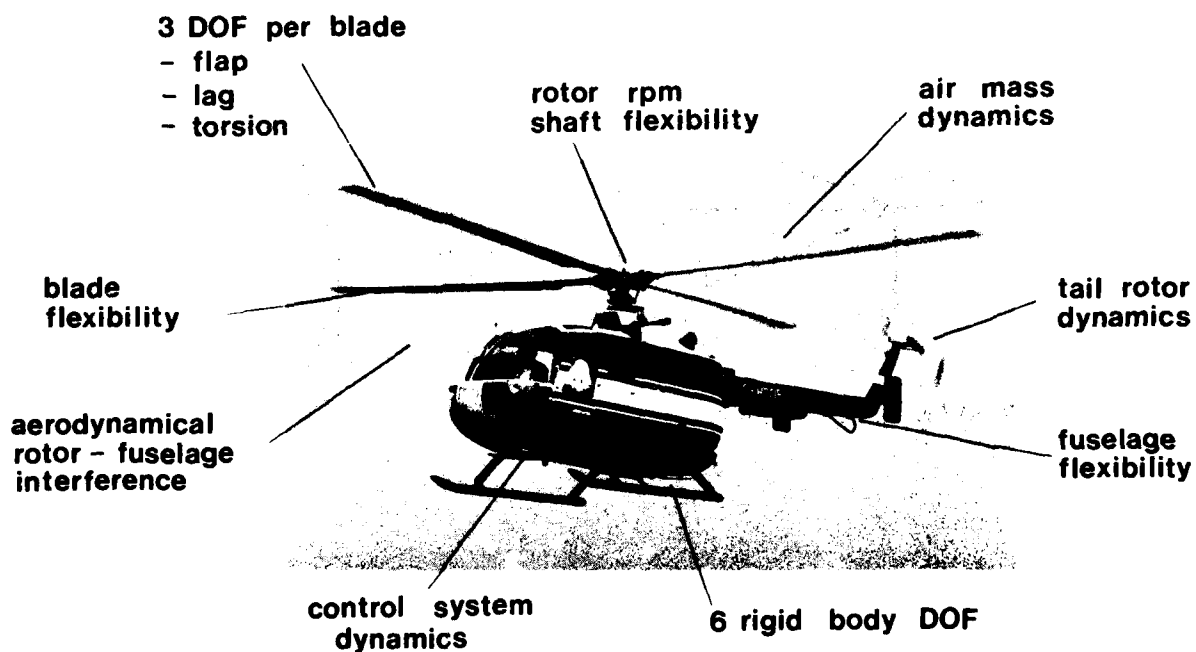


Fig. 8 Rotorcraft Degrees of Freedom and Influences on Vehicle Motion

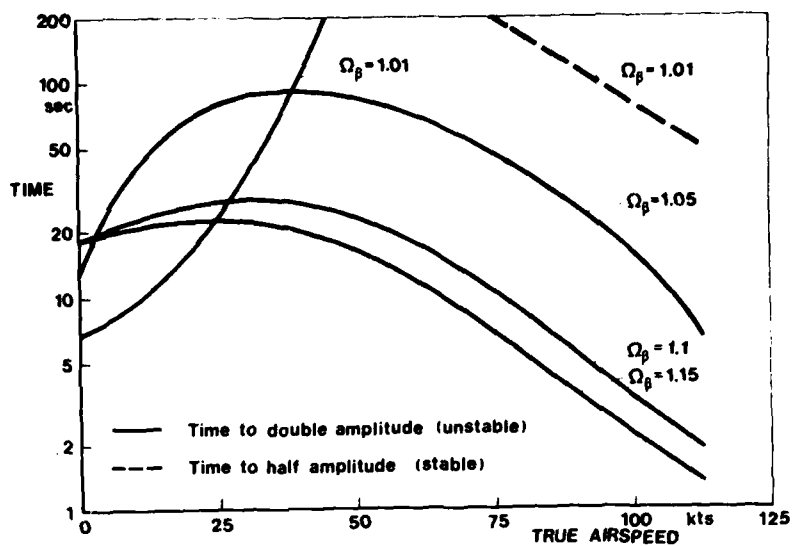


Fig. 9 Helicopter Dynamic Stability

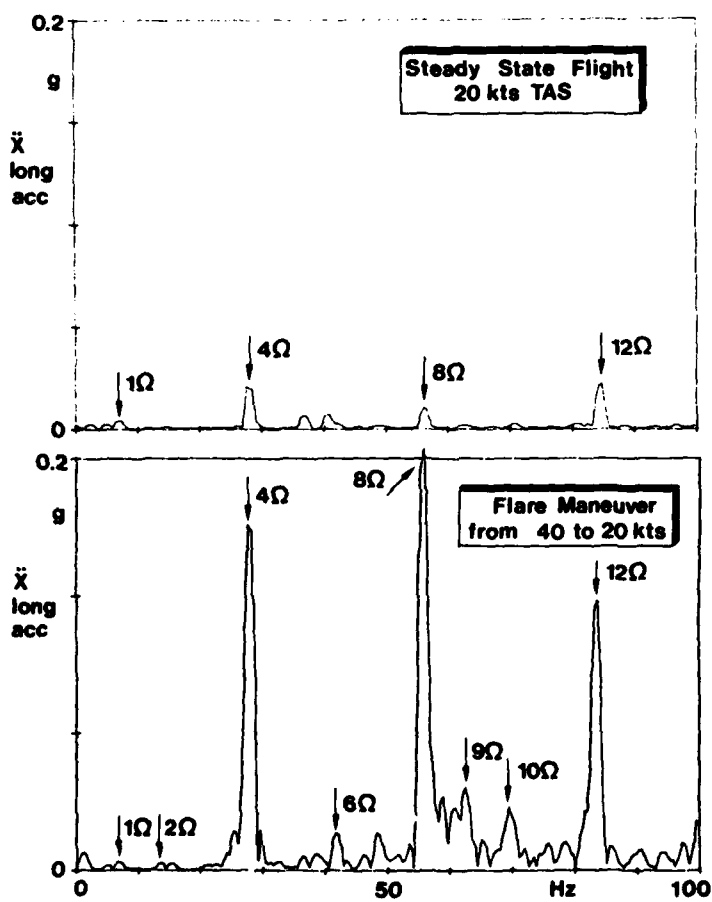


Fig. 10 Helicopter Vibration Frequency Spectra

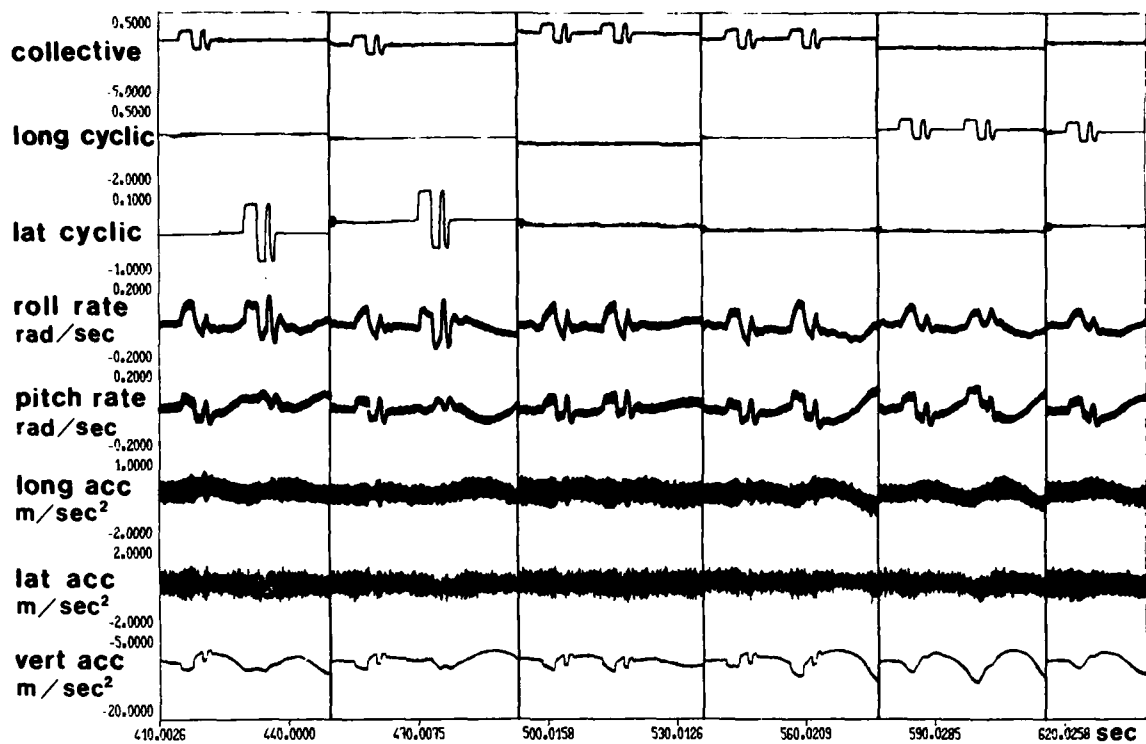


Fig. 11 Helicopter Vibratory Flight Test Data (BO 105, 70 kts)

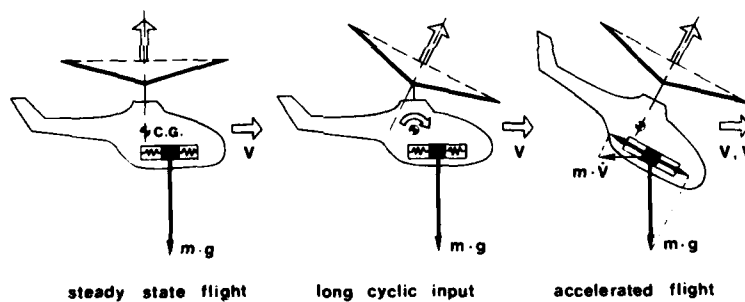


Fig. 12 Longitudinal Acceleration Measurement

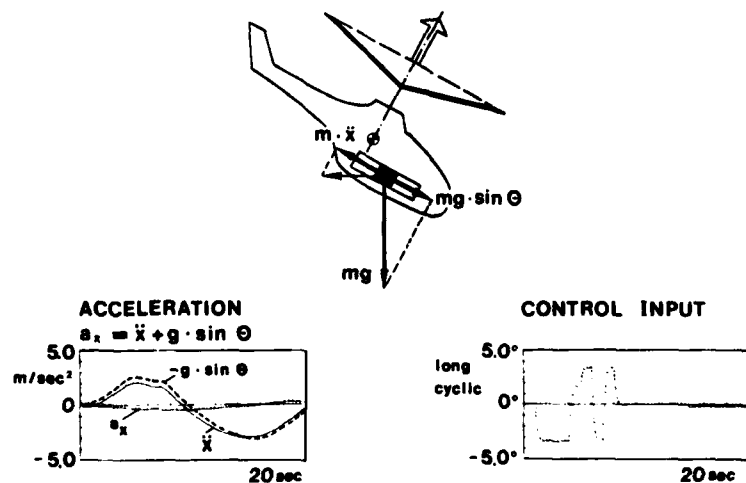


Fig. 13 Compensation of Helicopter Acceleration and Gravity Force

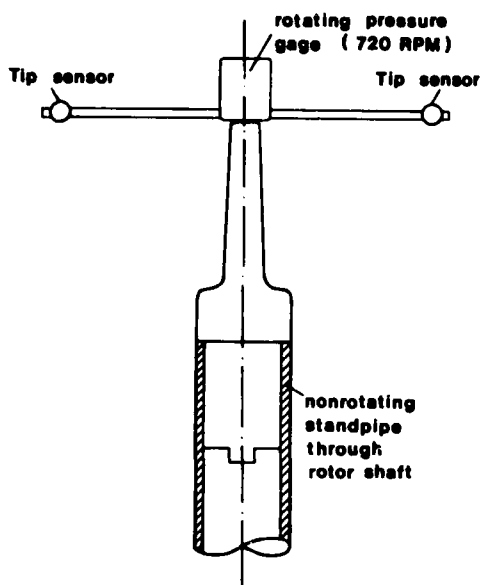


Fig. 14 LORAS Sensor

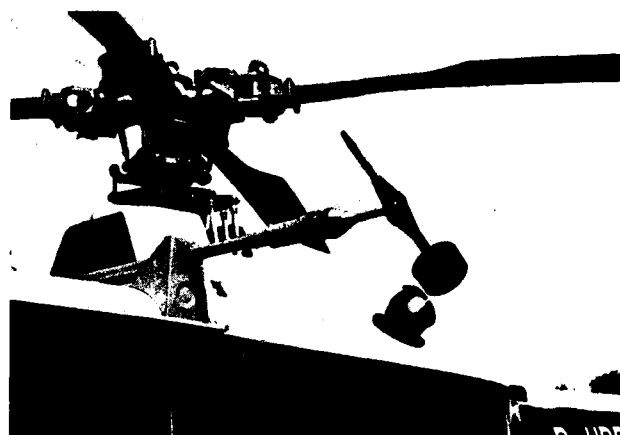


Fig. 15 LASSIE Sensor

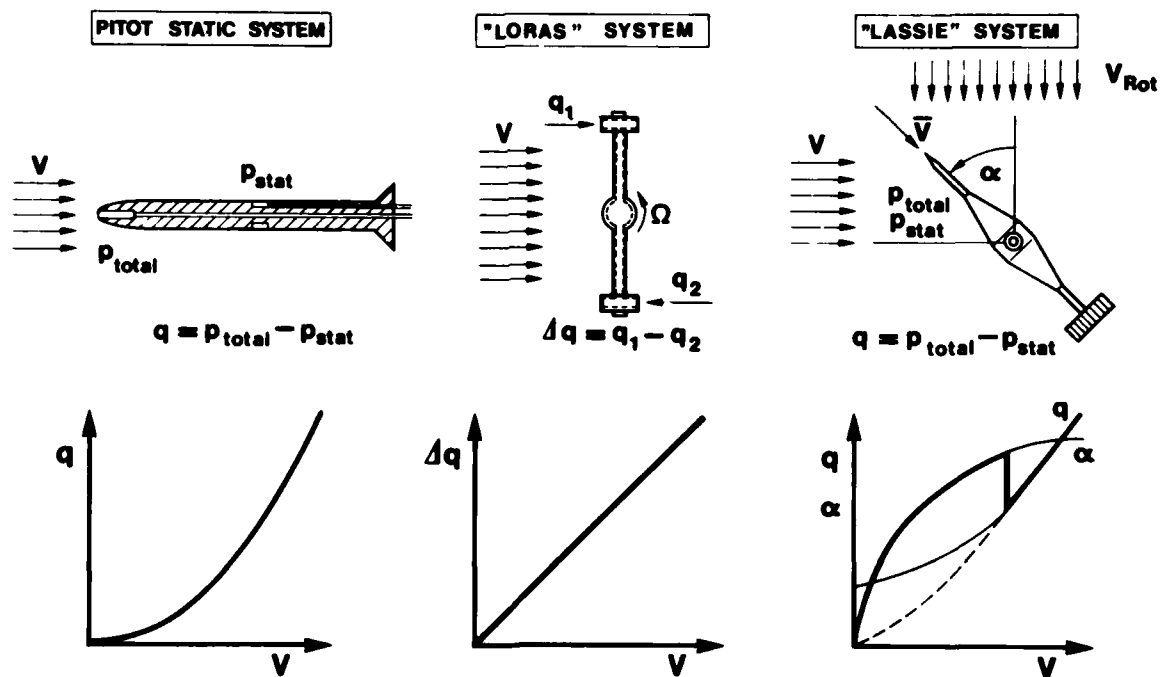


Fig. 16 Airspeed Measuring Systems Comparison

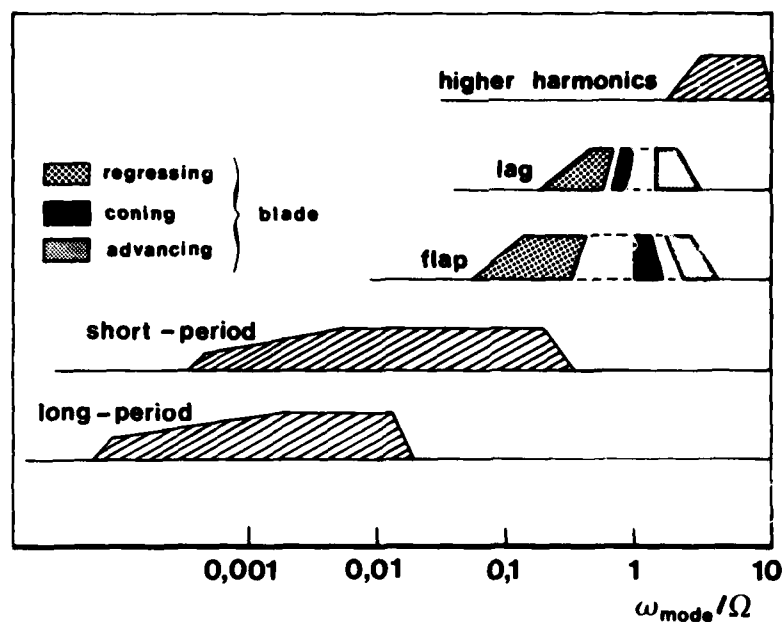


Fig. 17 Typical Frequency Ranges of Rotorcraft Motions (BO 105)

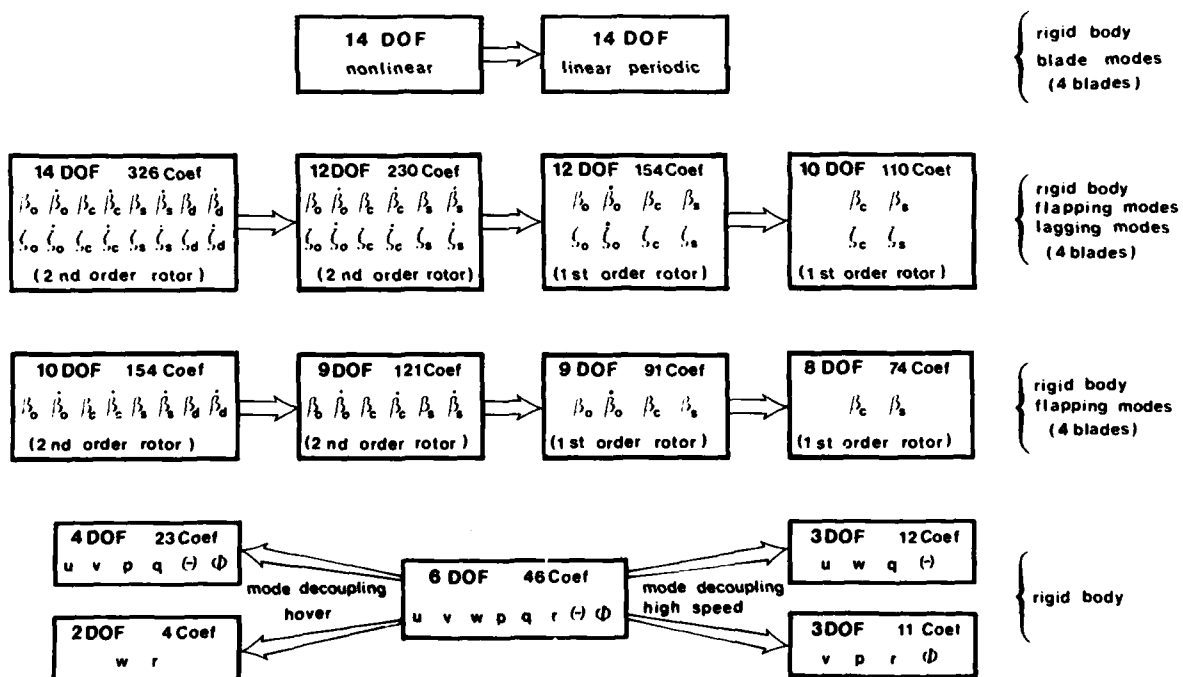


Fig. 18 Rotorcraft Models for a 4-bladed Helicopter

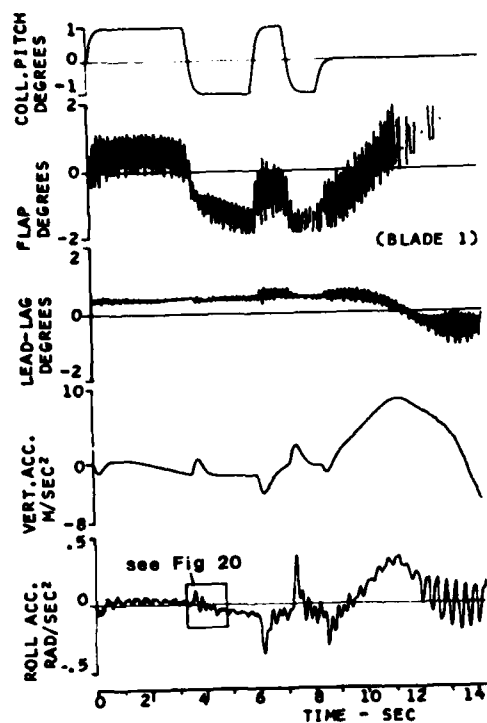


Fig. 19 Time Histories of Non-linear Computer Simulation (BO 105, 65 kts)

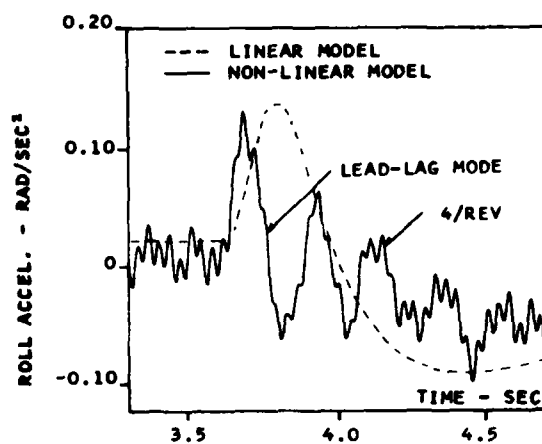
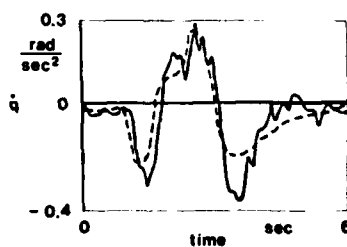
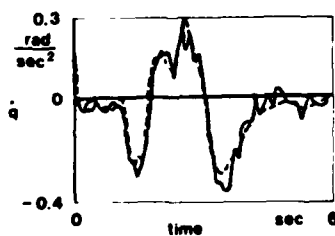


Fig. 20 Influence of Rotor Transient Effects on Roll Acceleration (enlarged from Fig. 19)

Rigid body model (6 DOF)

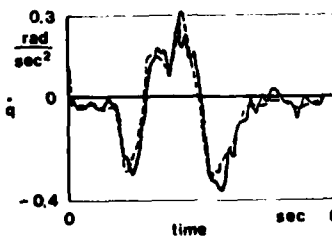


Inclusion of Rotor DOF



9 DOF (1st order rotor)

— CH-53A flight test data



9 DOF (2nd order rotor)

--- regression fit

Fig. 21 Model Structure Influence

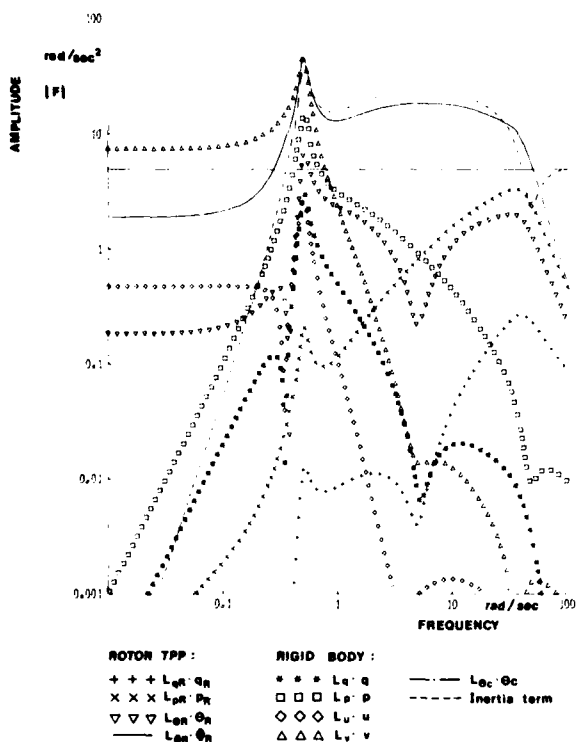


Fig. 22 Bode Plot of Roll Moment Equation Terms (Sikorsky S-61 in Hover)

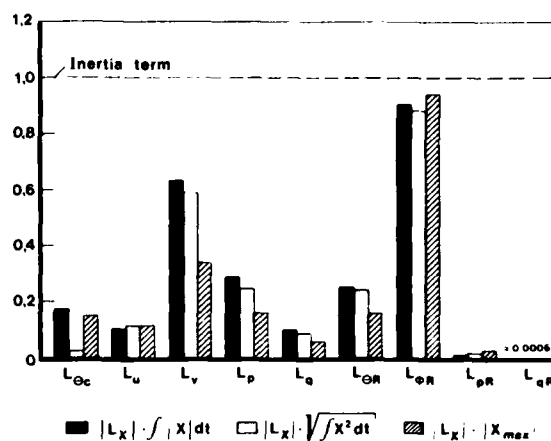


Fig. 23 Significance of Roll Moment Equation Terms (Sikorsky S-61 in Hover)

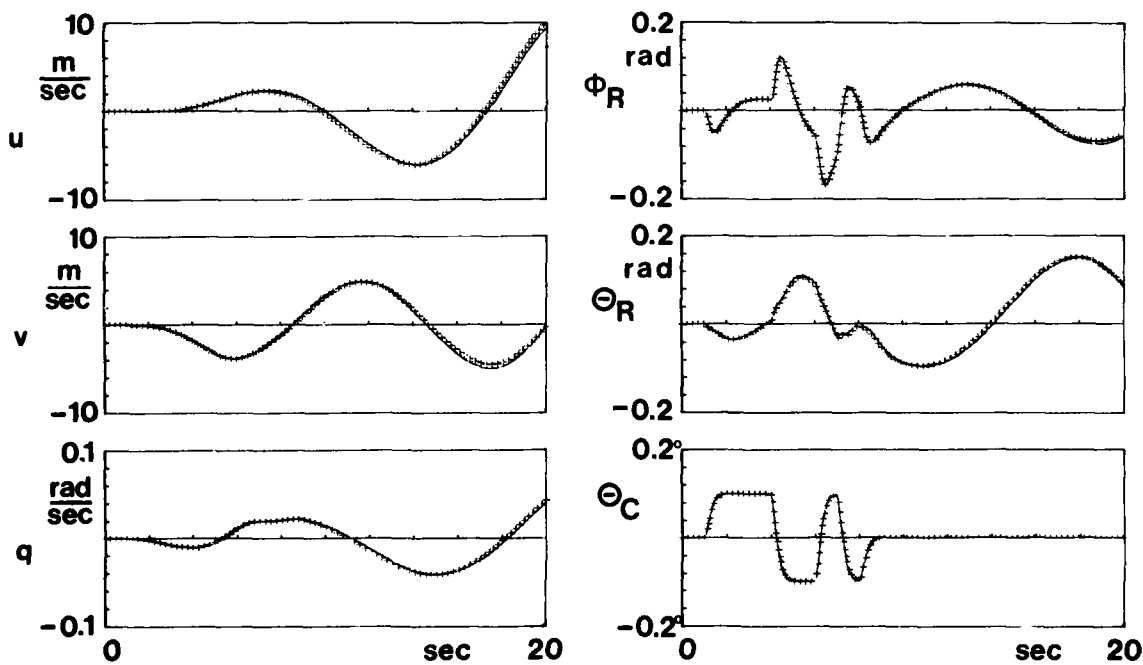


Fig. 24 Time Histories from S-61 Simulation Model ( + + + ) and the Reduced Model ( — )



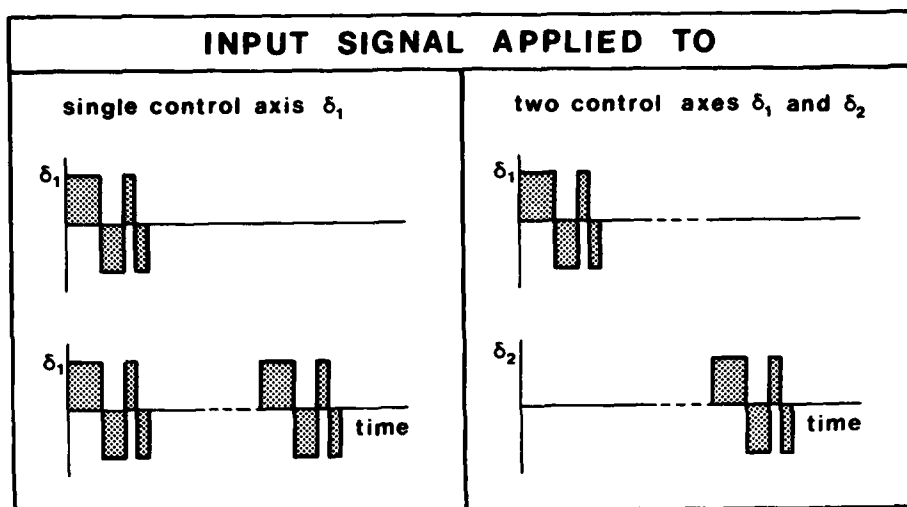


Fig. 25 Application of DFVLR 3211 Inputs Signals

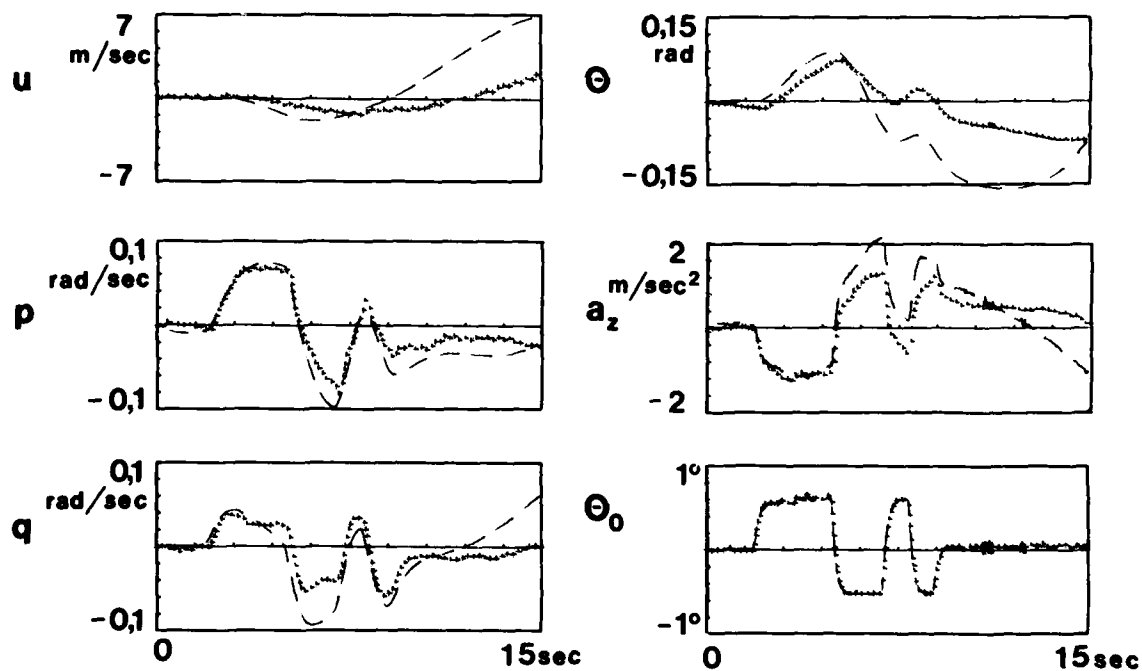


Fig. 26 Time Histories of Flight Test Data ( + + + ) and Identified Least Squares Model ( - - - ), one run evaluated (BO 105, 70 kts).

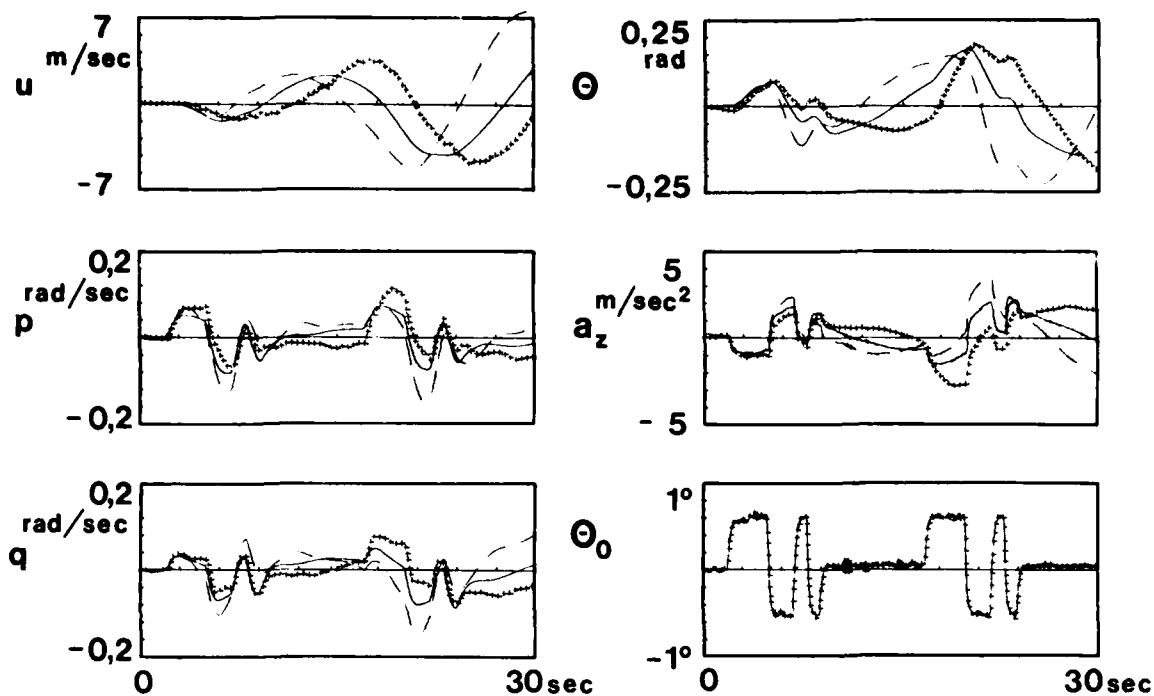


Fig. 27 Time Histories of Flight Test Data ( + + + ), Identified Least Squares ( - - - ), and Instrumental Variable ( — ) Models, one run evaluated (BO 105, 70 kts)

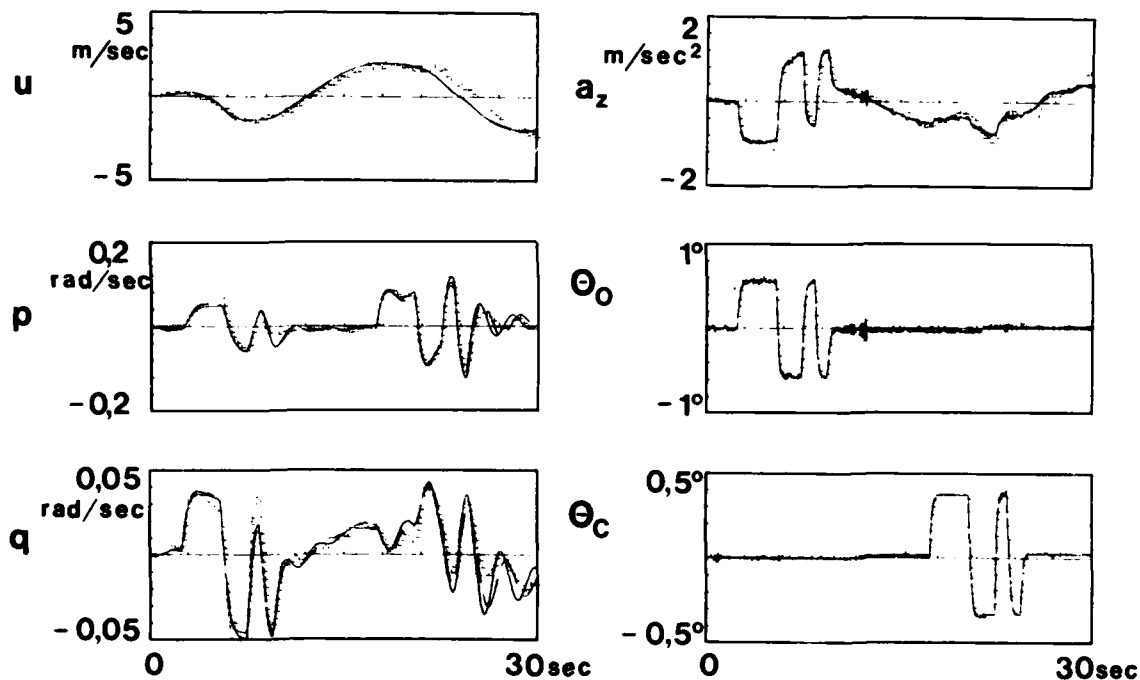


Fig. 28 Time Histories of Flight Test Data ( + + + ), Identified Least Squares ( - - - ), and Instrumental Variable ( — ) Models, one run evaluated (BO 105, 70 kts)

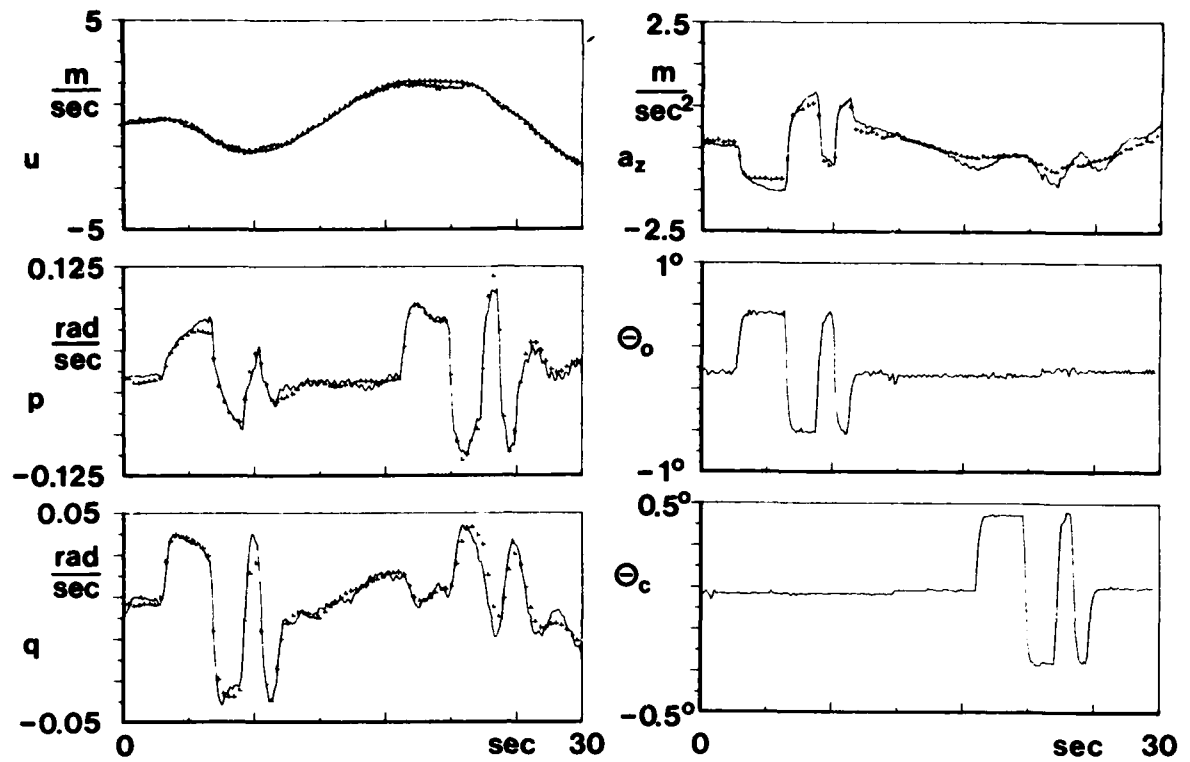


Fig. 29 Time Histories of Flight Test Data (—) and Identified Maximum Likelihood Model ( + + + ), one run evaluated (BO 105, 70 kts)

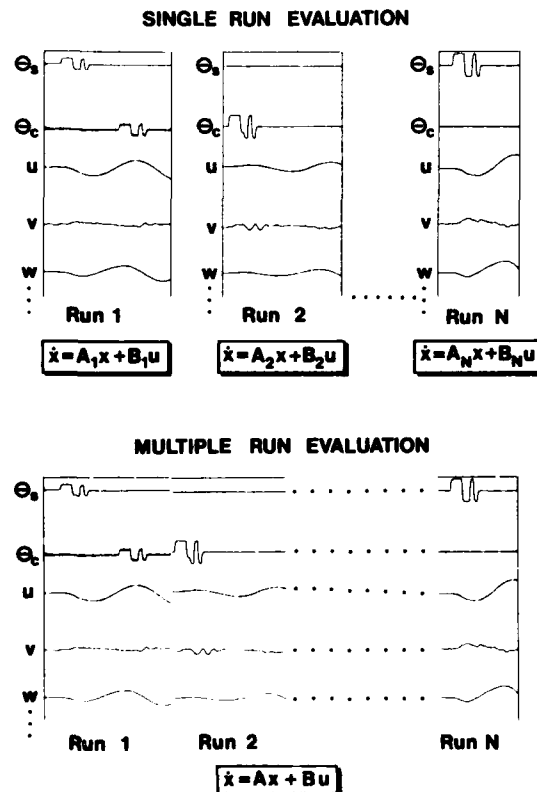


Fig. 30 Single and Multiple Run Evaluation

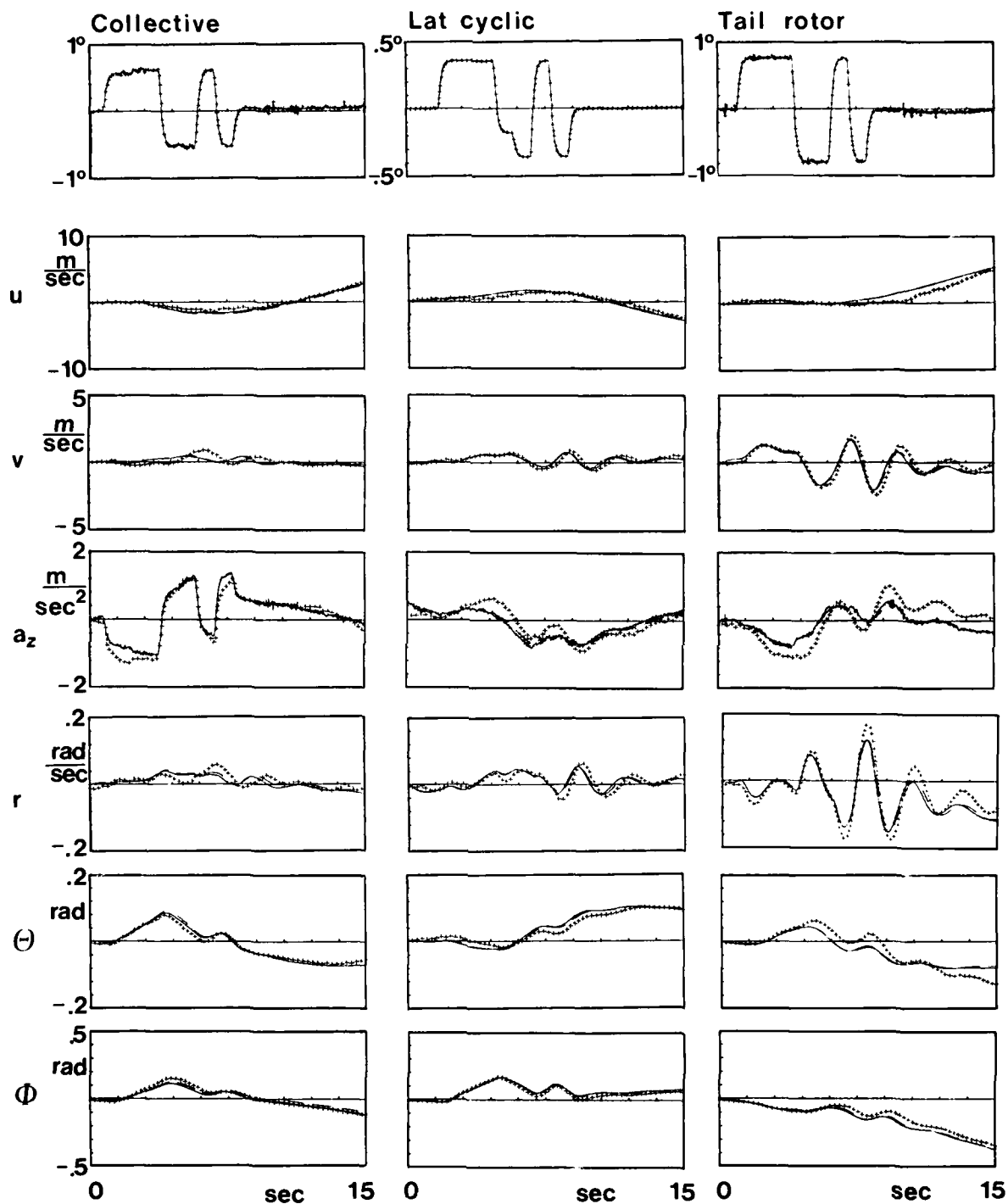


Fig. 31 Time Histories of Flight Test Data ( + + + ), Identified Least Squares ( - - - ), and Instrumental Variable ( — ) Models, three runs evaluated (BO 105, 70 kts)

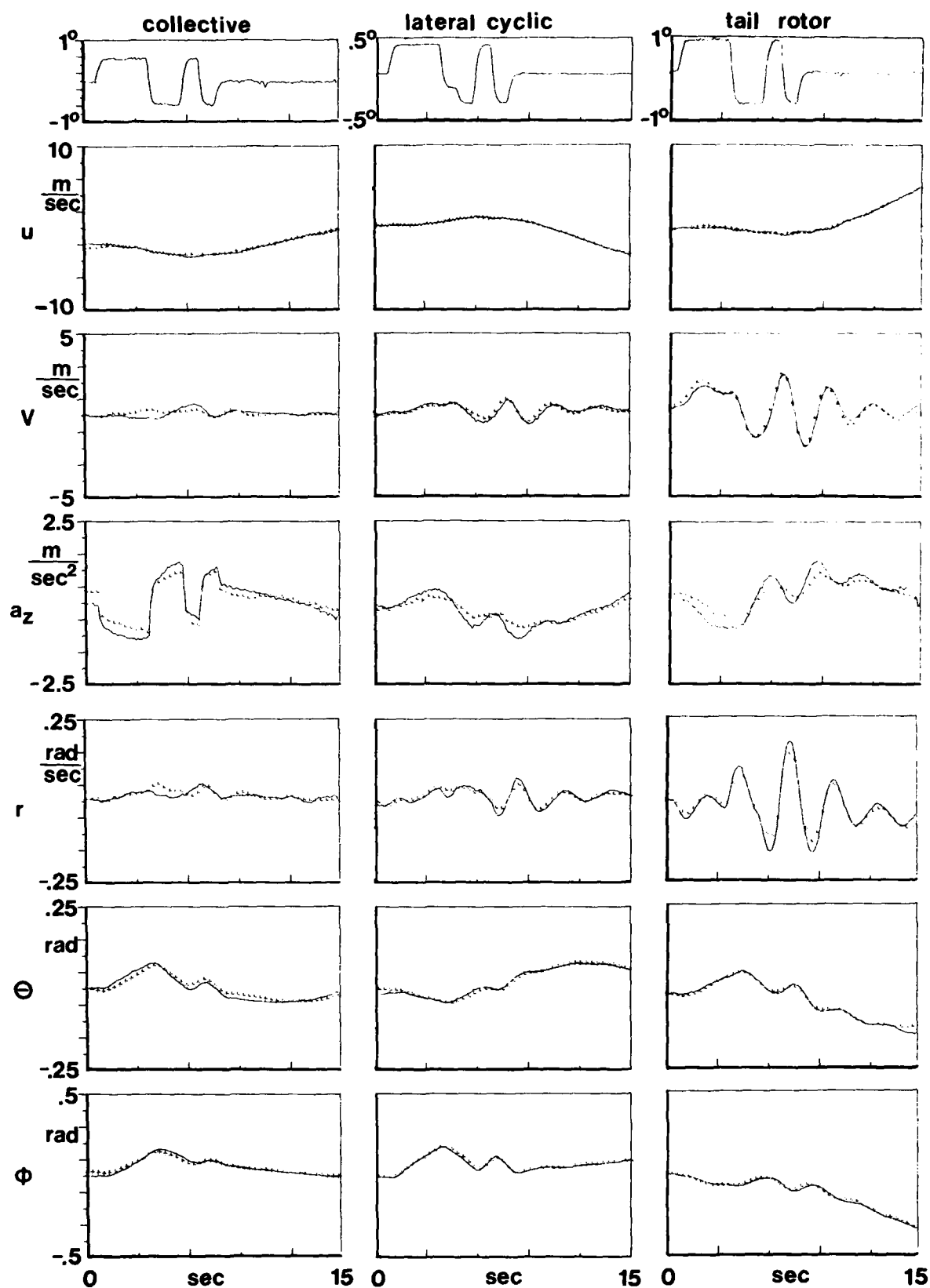


Fig. 32 Time Histories of Flight Test Data (—) and Maximum Likelihood Identified Model (+ + +), three runs evaluated (BO 105, 70 kts)

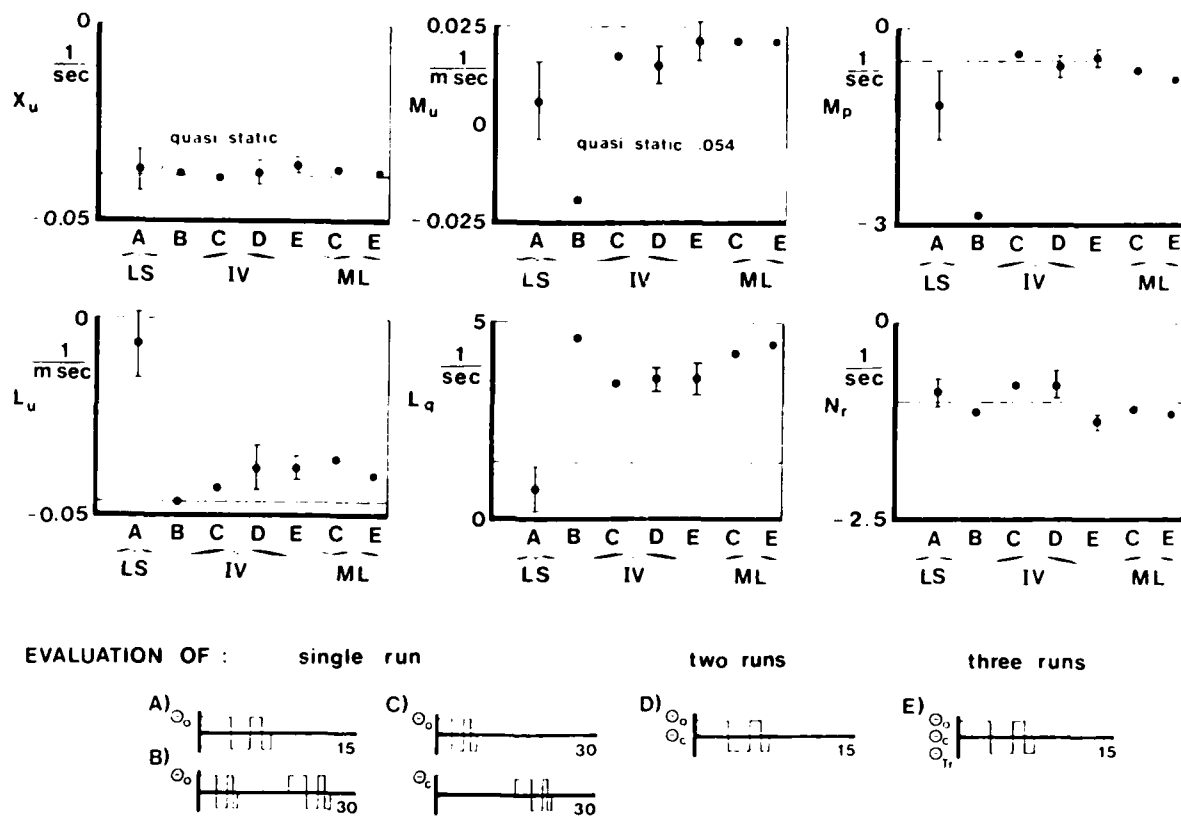


Fig. 33 Identification Results from the Least Squares (LS), the Instrumental Variable (IV), and the Maximum Likelihood (ML) Methods Compared with Quasi-Static Derivatives (BO 105, 70 kts)

## IDENTIFICATION EXPERIENCE IN EXTREME FLIGHT REGIMES

by

A. Jean Ross

Flight Systems Department  
 Royal Aircraft Establishment  
 Farnborough, Hampshire  
 England

## 1 INTRODUCTION

Those of you involved with combat aircraft will know that much effort goes into obtaining acceptable flying qualities during manoeuvring, that is at high angles of attack. The design and implementation of the control laws, which are almost invariably necessary for today's high performance aircraft, depend on the values of the stability and control derivatives, and so a number of research programmes have been directed towards identifying them from full-scale flight tests, or from free-flight model tests. The derivatives are often varying significantly with angle of attack, perhaps with Mach number, and nonlinearities can be expected. As a result, the responses to control pulses may not be the typical longitudinal short-period or lateral Dutch roll oscillations, so that the classic equations of motion based on linear derivatives cannot always be used. This fact is the crux of the problem, as we have to choose the form of the mathematical model\* of the aerodynamics (and kinematics) which will reproduce the response adequately. There are two different approaches to the problem, either to start with a very complicated mathematical model (with power series expansions of the aerodynamic forces and moments) and choose the most significant terms on a statistical basis for each response, or to use a simpler model with only those nonlinear terms suggested by physical considerations. The latter approach is advocated here, even though it usually calls for additional work and thought by the analyst, and I hope that you will appreciate the reasons for this choice by the end of the lecture.

The principles of the statistical approach are described briefly in section 2.1, and some results are used to illustrate the reservations that some flight dynamicists have in 'leaving out the physics'. Once the form of the mathematical model has been chosen, then any of the output error methods developed for parameter identification can be used to abstract the aerodynamic coefficients. The treatment of the nonlinear terms is described in section 2.2, and the tests which should be applied to assess the validity of the results are discussed in section 2.3.

A particular problem that we have approached at RAE, using as simple a model as possible to represent wing rock response, is described in some detail in section 3, to show how other information is incorporated in the identification process. Unfortunately, I have not found an example to compare the two approaches to the choice of the form of the mathematical model for the same set of responses. Selected results from investigations of other manoeuvres at high angles of attack are given in section 4, to show the types of problems which have been solved, and to illustrate some effects of nonlinearities.

## 2 MATHEMATICAL TECHNIQUES

## 2.1 Form of the mathematical model

The equations of motion of an aircraft are usually expressed, via Newton's laws of motion, in terms of the forces and moments acting on the moving body, together with equations giving the kinematic relationships. These latter equations can be expressed in their exact form, or can be approximated according to the responses being analysed. For example, the kinematic equation for the rate of change of bank angle is given exactly by

$$\dot{\phi} = p + r \cos \phi \tan \Theta + q \sin \phi \tan \Theta \quad (1)$$

For lateral disturbances from straight and level flight, when  $\Theta = 0$ , equation (1) can be replaced by the linear equation

$$\dot{\phi} = p \quad (2)$$

However, it is not necessary to linearise the kinematic equations used in the identification process, and the exact equations may be retained if necessary. It is the representation of the aerodynamic forces and moments in the equations of motion which causes the difficulty. At low angles of attack, experience has shown that the aerodynamic

---

\* It should be noted that 'mathematical model' can be used in two ways, either to denote the form of the equations, or to denote the numerical values of the coefficients in the equations. In this Lecture, the term is used for the form of the equations.

forces and moments are adequately represented by retaining only the linear terms in the Taylor series expansions, i.e. the stability and control derivatives. Thus pitching moment is expressed as

$$M = M_0 + \frac{\partial M}{\partial \alpha} \alpha' + \frac{\partial M}{\partial q} q' + \frac{\partial M}{\partial \dot{\alpha}} \dot{\alpha}' + \frac{\partial M}{\partial \dot{\eta}} \dot{\eta}' \quad (3)$$

where the dimensional form is used for clarity, and the prime ' denotes perturbation from a steady state. It is not usually necessary to introduce pitching moments due to the lateral response variables, as these are negligible for most configurations. (This is not true, of course, for such asymmetric layouts as the oblique wing<sup>1</sup>.)

For flight at higher angles of attack, it is possible that this linear representation is not adequate, and so additional terms in the Taylor series expansions have to be retained. The problem comes in choosing which terms. The 'physical' approach is to use data from other sources, mainly wind-tunnel results, to guide in the choice of terms, and only those needed to give the indicated degree of nonlinearity are retained. The 'statistical' approach is to include all possible terms up to a given order in a particular expansion, and to choose the terms having statistical significance in a given response. The polynomial representation of the aerodynamic forces and moments may not be appropriate for some phenomena, and it may be necessary to introduce discontinuities or hysteresis if the responses are due in part to forces arising from flow separation and reattachment effects near stalling conditions. Gust penetration and ground effect are other examples which require other forms of modelling. However, we shall concentrate on polynomial representation in this Lecture.

In order to fix ideas, we now consider the pitching moment at high angle of attack for the F-4 (Phantom) aircraft. Two longitudinal responses, in which angle of attack varied between  $20^\circ$  and  $40^\circ$ , have been analysed and reported<sup>2,3</sup>, using different mathematical models and different techniques to determine them. The wind-tunnel results for  $C_m(\alpha)$  at zero sideslip are shown in Fig 1a, together with the results from the identification of two different responses designated Run 20 in Ref 2, and Run 14 in Ref 3. If we use the physical approach to choose the maximum order of the polynomial to represent  $C_m(\alpha)$ , it is obvious that a fairly high order would be required to fit the  $C_m$ - $\alpha$  curve over the complete range of wind-tunnel tests, ( $0 < \alpha < 52^\circ$  shown in Fig 1a). However, there can be no information in the flight responses to determine  $C_m(\alpha)$  for  $\alpha < 20^\circ$  or  $\alpha > 40^\circ$ , and so it is logical to restrict the representation to the range  $20^\circ < \alpha < 40^\circ$ . We may then use a second-order polynomial to model the variation of  $C_m(\alpha)$  with reasonable accuracy. A datum value of angle of attack has to be introduced, and the incremental change in angle of attack is then used as the state variable in the equations of motion. It appears that such a model was chosen in Ref 2, although discussion of the results in that paper is confined to another response at lower angles of attack; no results for variation of pitching moment with sideslip are quoted.

In contrast, the statistical approach is used in Ref 3 where each of the static coefficients, control effectiveness derivatives and dynamic derivatives are expanded in the form

$$c = c_0(\bar{\alpha}, \bar{\beta}) + \sum_i c_{\alpha i} \alpha^i + \sum_j c_{\beta j} \beta^j + \sum_i \sum_j c_{\alpha i \beta j} \alpha^i \beta^j \quad (4)$$

The static forces and moments, such as  $C_m(\alpha, \beta)$ , are expanded so that all terms in  $\alpha^i \beta^j$  obtained from linear combinations of  $(k_1 \alpha + k_2 \beta)^n$ ,  $n = 1, 2, 3$  are included. For pitching moment, the polynomial in angle of attack had order 9 (i.e.  $i_{\max} = 9$ ). It is stated that  $\bar{\alpha}, \bar{\beta}$  are the reference angles of attack and sideslip respectively, which implies that  $\alpha, \beta$  in equation (4) are again incremental changes from the reference condition. The pitching moment equation then takes the form

$$\begin{aligned} \dot{q} = & m_0 + m_{\alpha} \alpha' + m_{\alpha 2} \alpha'^2 + m_{\alpha 3} \alpha'^3 + \dots + m_{\beta} \beta' + m_{\beta 2} \beta'^2 + \dots \\ & + m_{\alpha \beta} \alpha' \beta' + \dots + m_q q' + m_{\alpha q} \alpha' q' + \dots + m_{\eta} \eta' + m_{\alpha \eta} \alpha' \eta' + \dots \end{aligned} \quad (5)$$

If time histories of  $\dot{q}, \alpha, \beta, q, \eta$  are available, then it is possible to determine the correlation of  $\dot{q}$  and the subsets of the complete variable set  $(\alpha, \alpha^2, \alpha^3, \dots, \beta, \beta^2, \dots, \alpha \beta, \dots, q, \alpha q, \dots, \eta, \alpha \eta)$  as each of the parameters  $m_{\alpha}, m_{\alpha 2}, \dots, m_{\alpha \eta}$  are added one at a time, using regression analysis. However, angular accelerations such as  $\ddot{q}$  are not often measured, and so the pitch rate response has to be differentiated with respect to time. The process is not described in Ref 3, but is achieved in Ref 2 by first performing a compatibility check between the recorded  $(p, q, r, a_x, a_y, a_z)$  and the measured  $(V, \gamma, \eta, \delta, \psi, \text{altitude, and Euler angles } \phi, \theta, \psi)$ . An iterated Kalman filter/fixed-point smoother<sup>4</sup> is used to generate an optimal estimate of the aircraft trajectory,  $(V, \alpha, \beta, \phi, \theta)$ , and the angular accelerations are obtained by differentiating the filtered  $(p, q, r)$ . The analysis of equation (5), and the other equations of motion, is



basically the equation error method of parameter identification, but the error obtained as each parameter is added to the expansion is tested for significance. (See Appendix A of Ref 3 for details.) The regression analysis thus yields some initial values for the significant parameters, which may be used to start the identification using output error methods. In contrast to the quadratic form used in Ref 2, the static pitching moment was found to have a significant dependence on  $\alpha'^3$  for the response 'Run 14'. This response also contains a variation of sideslip between  $-6^\circ$  and  $12^\circ$ , and the  $m_{\beta 8}$  term was significant. It should be noted that the parameters  $m_{\beta 8}$  and  $m_{\alpha 2}$ , which could be unexpected from the point of view of symmetry, arise due to the non-zero reference angles of sideslip and attack. The approximate numerical values of the parameters, as obtained from Fig 8 of Ref 2 and Fig 17 of Ref 3, are given by

$$\text{Run 20 (quadratic specified)} \quad C_m = -0.07 - 0.38\alpha' - 0.28\alpha'^2 \quad (6)$$

$$\text{Run 14 (cubic derived)} \quad C_m = -0.126 - 0.48\alpha' - 0.18\alpha'^2 + 4.2\alpha'^3 \quad (7)$$

where  $\alpha'$  is the incremental angle of attack, in radians, from the reference angle of attack of  $30^\circ$ . Variation in angle of sideslip is assumed to be zero.

It is not possible to compare the actual flight records, but simulated responses have been calculated, assuming that speed remains constant and that lateral responses are zero, in order to assess the effect of the different models. A trim angle of attack of  $\bar{\alpha} = 30^\circ$  has been taken, and the responses shown in Fig 1b are due to a steady pull on the elevator from an initial out-of-trim condition, so that the angle of attack response covers the range  $20^\circ < \alpha < 40^\circ$ . The difference in level of  $C_m$  at  $\bar{\alpha} = 30^\circ$  implies different trim speeds, but the indicated air speed only differs by 3%, so the motion about the trim state should not be significantly affected. Although the responses do not match precisely, the residual error in pitch rate and angle of attack are in fact similar to those obtained in the actual fit to the flight data for Run 14, (for which the control input is not given in Ref 3). The computed and flight responses are shown in Fig 2, plotted to the same scale as Fig 1b for comparison. Thus it seems that the introduction of the cubic in the expansion for  $C_m$  as a function of angle of attack is not absolutely necessary for an adequate fit to be obtained. Unfortunately the response analysed using the quadratic form (Run 20) is not given in Ref 2 for comparison.

An alternative treatment is possible if a sufficient number of flight records of reasonable length can be obtained, each of which is a small perturbation from different mean states, so that a linear mathematical model can be retained. The experiments<sup>5,6</sup> with a remotely-controlled 3/8-scale model of the F-15 were designed to give such responses. The local value of the linear derivative  $C_{m\alpha}$  has been identified from responses with small variations in angle of attack about the mean flight condition. About 50 flight records were analysed, covering the range  $-20^\circ < \alpha < 50^\circ$  with typical increments in  $\alpha'$  of  $\pm 3^\circ$ . The variation of  $C_{m\alpha}$  with angle of attack obtained from flight tests is highly nonlinear, indicating that  $C_m(\alpha)$  itself is also nonlinear, but agreement with the results for  $C_{m\alpha}$  obtained from static wind-tunnel results is good (Fig 3), (although there are some changes in level at the extremes of the angle of attack range, near  $\alpha \approx -20^\circ$  and for  $\alpha = 40^\circ$  to  $50^\circ$ ). Since this localised linear representation of  $C_m(\alpha)$  yields satisfactory results, it is interesting to take the comparisons made in Fig 1 one stage further, i.e. to linearise the results for  $C_m$  of the F-4 over the range  $20^\circ < \alpha < 40^\circ$ , and to calculate the response. The wind-tunnel results were used for this comparison and the second-order polynomial giving the best fit to the value of  $C_m$  at  $\alpha = 20^\circ(5^\circ)40^\circ$ , about the trim state of  $\bar{\alpha} = 30^\circ$ , was found to be

$$C_m = -0.122 - 0.5\alpha' - 0.33\alpha'^2 \quad (8)$$

The corresponding linear fit is

$$C_m = -0.127 - 0.5\alpha' \quad (9)$$

The various representations of  $C_m(\alpha)$  are shown in Fig 4a, and the resulting responses are compared in Fig 4b. An idealised elevator doublet was used to generate the response instead of the pull-up assumed in Fig 1b. As may be seen in Fig 4b, the increase in angle of attack from  $30^\circ$  to  $40^\circ$  is followed by an overswing to  $\alpha = 14^\circ$ , i.e. just outside the range chosen to fit the tunnel data, and it is mainly due to the discrepancy in the linear and quadratic representations of  $C_m(\alpha)$  for  $14^\circ < \alpha < 20^\circ$  which causes the slight differences in the responses.

The same elevator input has also been used with the quadratic equation for  $C_m(\alpha)$  obtained by fitting Run 20, i.e. flight results for the coefficients in  $C_m(\alpha)$ , equation (6), and the resulting angle of attack is also shown in Fig 4b. A genuine difference is apparent, in both frequency and amplitude, which can be associated with the change in level of the mean values of  $\partial C_m / \partial \alpha$ . The values corresponding to the expansions given in equations (6) to (8) are shown in Fig 5, and it may be seen that  $\partial C_m / \partial \alpha$  from the fitted quadratic to the wind-tunnel results is about 20% greater in magnitude than the

results from Run 20. Since the frequency is approximately proportional to  $(\partial C_m / \partial \alpha)^{1/2}$ , for nonlinear systems with small nonlinearities, we could expect a change of 10% in the responses, as is observed in Fig 4b. It is noticeable (Fig 3) that the values of  $\partial C_m / \partial \alpha$  obtained from the tunnel tests on an F-15 configuration are also greater in magnitude than the values identified from the flight records, over the similar angle of attack range  $10^\circ < \alpha < 35^\circ$ , so the trends shown in the analysis of the F-4 records are consistent.

This somewhat lengthy discussion on possible ways of representing  $C_m(\alpha)$  has been included to demonstrate the importance of establishing which nonlinear terms are likely to make a significant contribution to particular types of responses, before embarking on a complicated identification process.

The statistical approach to selecting the form of the mathematical model is being developed, eg Refs 7 to 10, but the various methods suggested are not discussed further here.

## 2.2 Identification process

As stated in the introduction, the methods based on output error techniques described in previous lectures can be used to identify the unknown parameters. However, two different ways of treating the nonlinear terms are currently in use. If the computer algorithm requires that the equations of motion are linear in the state variables, then it is necessary to consider the additional nonlinear terms as pseudo-control inputs, ie terms such as  $m_{\alpha^2} \cdot \alpha^2$  are replaced by  $m_{\alpha^2} \cdot \alpha_{obs}^2$ , where  $\alpha_{obs}$  is obtained from the observed value of angle of attack. This has often to be derived from the recorded responses, to correct for instrument position. Thus if the linear equations of motion are represented by the matrix equation

$$\dot{x} = Ax + Bu + \delta \quad (10)$$

and the instrument equations by

$$y = Cx + Du + \epsilon, \quad (11)$$

then, in order to retain linearity, the matrix product  $Bu$  is replaced by the partitioned product  $[B : F]\{u : s_{obs}\}$ . The matrix  $F$  contains the additional parameters, such as  $m_{\alpha^2}$  and  $m_{q\alpha}$  and the vector  $s$  contains the nonlinear combinations of variables, such as  $\alpha^2$  and  $q\alpha$ , but these are treated as known inputs.

The alternative treatment retains the nonlinear equations of motion, and usually necessitates changes to the algorithms, due to extra terms arising in the sensitivity matrix. Instead of changing the input matrix, the product  $Ax$  is replaced by  $[A : F]\{x : s\}$ , where  $F$  and  $s$  contain the same terms as previously, but the nonlinear terms in  $s$  are obtained from the calculated state variables. In order to illustrate the different techniques, we consider again the term such as  $m_{\alpha^2} \cdot \alpha^2$ , contributing to the pitching moment. The sensitivity of  $q$ , the rate of pitch, to the unknown parameters is obtained by partially differentiating the pitching moment equation with respect to each parameter, so that, for example,  $\frac{d}{dt} \left( \frac{\partial q}{\partial m_q} \right)$  contains the term  $\frac{\partial}{\partial m_q} \left( m_{\alpha^2} \cdot \alpha^2 \right)$ . For the first method,  $\alpha_{obs}$  is independent of  $m_q$ , and so the term is zero, but for second method, the partial differentiation gives the term  $m_{\alpha^2} \cdot 2\alpha \frac{\partial \alpha}{\partial m_q}$ . When the iterative process of solution has converged, and if the calculated values of the variables are close to the observed values, then the different treatments of the equations of motion should not affect the values of the identified parameters significantly.

It is usually necessary to take particular notice of the degree of correlation between parameters, especially between the coefficients associated with expansions of given derivatives as functions of angle of attack or sideslip. For example, if the damping-in-pitch derivative is expanded as  $(m_q + m_{q\alpha} + m_{q\alpha^2})$ , then it is likely that the parameters  $m_q, m_{q\alpha}, m_{q\alpha^2}$  are strongly correlated, since the main contribution to the response will be associated with the 'total' damping. The final values of strongly correlated parameters are likely to be dependent on the initial values chosen to start the iteration, and so it is probably best to identify the dominant parameters first (eg  $m_q$ ) keeping the higher-order nonlinear parameters fixed. The development of the correlation can then be traced as the iteration process converges, for each additional nonlinearity introduced. Experience needs to be gained on both the effects of various nonlinearities on the response, and on the design of suitable control inputs, to generate responses which are identifiable in terms of the important parameters.

A different approach to the algorithms needed for identification is taken in Ref 11 where functionals are used to determine the dependence of the state variables on the parameters, ie the sensitivity. The description of the method is lengthy, and so reference should be made to the original Report for details. The process yields a time history of the variation of each parameter value throughout the response, and this may be used as an additional check on the form of the mathematical model (see section 2.3).

## 2.3 Assessment of results

The numerical values of the identified parameters can be assessed in two ways, which often complement each other, viz their plausibility (judged on a physical basis) and on the statistical measures produced by the identification process. If the values are totally unexpected, in terms of magnitude and/or sign, then it is probable that the response is not sensitive to that parameter, and so the calculated likely error is probably large, and the associated elements in the sensitivity matrix are relatively small. In addition, there may be correlation with other parameters, which could then have associated unexpected values. Such tests have already been described in earlier lectures, and so no further details are given here. However, there are further tests which should be used when there is uncertainty about the form of the mathematical model.

An obvious test is to check that the time history of the residual error in each response variable is not correlated with any state variable. Significant correlation is due to terms being omitted from the mathematical model, and the information can be used to define the form of the additional terms needed. An example<sup>12</sup> of such correlation is given in Fig 6, where the residual from the linear model is seen to correlate with  $n_z$ . The response is due to an elevator pulse applied to a slender-wing research aircraft (HP 115) and so nonlinear aerodynamic terms can be expected to be significant. The expansions for normal force and pitching moment included terms in  $a^2$ ,  $q\dot{a}$  and  $\dot{n}_a$  (and also an additional linear term in  $\dot{h}$ ), and when these were added to the identified parameters the residual has near white noise characteristics (Fig 6b). However, the sensitivities to the nonlinear terms in the normal force expansion were found to be small, and so the identification was repeated, successively dropping the  $Z_{a^2}$ ,  $Z_{q\dot{a}}$  and  $Z_{\dot{n}_a}$  terms. An adequate model could be defined without using these normal force derivatives, for which the sensitivities of the remaining parameters increased, the likely errors in some parameter estimates were reduced, and the fit errors to the responses were only slightly larger, i.e. the statistical measures described earlier were used in the choice of significant terms. Again, such a process of reducing the number of identified parameters is similar to that used for assessing significant derivatives in any linear model.

Some identification methods, (especially those based on extended Kalman filters, in which parameters are treated as state variables) also give a time history of the value of each parameter as it is updated throughout the response. An example using this technique is given in Ref 11. It was found that linear representation of the lateral derivatives for the C-8A (Buffalo) did not lead to stabilised values of rolling moment due to roll rate and rolling moment due to aileron, even though the fit to the response was acceptable. The C-8A is an STOL aircraft, with a jet-augmented flap on the wing, and so the form of the mathematical model needed at this low-speed extreme of the flight envelope is not well defined. It was known from previous simulator studies that rolling moment due to roll rate depended on flap deflection and jet coefficient, and these second-order derivatives were added to the mathematical model. The parameter corrections are shown in Fig 7, for three pairs of representations of  $\dot{x}_p$  and  $\dot{x}_\xi$ . Although adding the nonlinear derivatives dependent on  $C_J$  and  $\delta_F$  to the terms in  $C_J(p)$  stabilised that derivative, (Fig 7b), the aileron power is not converging to an acceptable level. It was necessary to add the dependence of  $C_J(\xi)$  on  $C_J$ , to give good convergence for  $\dot{x}_{\xi_0}$ , and acceptable convergence for  $\dot{x}_{p_0}$ . It should be noticed that the magnitude of the dispersion envelopes ( $\pm 1\sigma$  covariance level) are also converging, indicating that the parameter is at its best estimate.

If more than one set of responses are available from flight tests at the same Mach number, and over the same ranges of variables, then it is possible to use the values of the parameters identified from one set to predict the response to the different control inputs. Analysis of the residuals between the predicted and flight responses gives an indication of the adequacy of the mathematical model and of the accuracy of the numerical values. It is particularly important to have a reasonable number of flight records suitable for analysis, so that the results can be checked for consistency over the ranges of flight conditions covered, e.g. angle of attack, and/or Mach number, and/or angle of sideslip. Although the fit obtained for a particular response could be excellent, the values of some of the identified parameters may be quite different to values obtained from other responses, and so it would be necessary to recheck that the sensitivities and correlations are at acceptable levels. Such anomalies are more likely to occur if the form of the mathematical model is determined for each response, when different terms may or may not be deemed significant. The different models which could be used for  $C_m(\alpha)$  have already been discussed in section 2.1, and illustrate the difficulty which can arise if the terms are chosen from a purely statistical basis.

Some guidelines have been suggested by Dr Iliff in Ref 6, which are worthy of being repeated here, as they summarise and emphasise the process of evaluation of results:

- "(i) The higher order statistics of the estimated coefficients of the power series (such as  $f$  tests) must indicate that the estimates are valid.
- (ii) The quality of the fit must be good, and even small discrepancies must be explained since these discrepancies can result in serious misinterpretations of nonlinear systems.
- (iii) The simplest model that adequately fits the data should be chosen; a more complex model cannot be justified.

- (iv) A consistent trend must result for each estimated coefficient as each independent variable is changed.
- (v) A plausible physical explanation for each resulting model should be found.
- (vi) The resulting model must be evaluated on a completely independent set of data."

### 3 IDENTIFICATION OF WING ROCK RESPONSES

#### 3.1 Description of problem

A number of combat aircraft experience lateral handling problems at high angles of attack and high subsonic speeds, and one adverse phenomenon has been termed 'wing rock' by pilots. It is defined as an "uncommanded lateral/directional oscillation viewed by the pilot as oscillations primarily in roll" and its cause was not obvious. At the RAE, we used a Gnat aircraft to investigate the phenomenon<sup>13,14</sup>, as it encounters a controllable wing rock, and we applied parameter identification techniques to relate the dynamic responses to the aerodynamic forces and moments causing the oscillation. We used a relatively simple computer program, based on the least-squares technique, and chose a mathematical model which produced an adequate fit to the flight data, and which was supported by evidence from other experimental or theoretical sources. When we began the investigation, we knew that the frequency of the wing rock oscillation was similar to that of the Dutch roll oscillation, and so we planned the flight tests to obtain records of Dutch rolls throughout the angle of attack range up to the onset of wing rock. The pilots also told us that wing rock was delayed to higher angles of attack if external fuel tanks were carried on the wings. This gave us added opportunity to identify the crucial aerodynamic forces and moments for the different flight characteristics.

Examples of typical flight responses for the clean aircraft are shown in Fig 8. The pilot applied rudder and aileron inputs to excite the Dutch roll mode, and possibly the roll subsidence mode, while maintaining a constant angle of attack of about  $7^\circ$  in a  $3.2\text{ g}$  turn. When the angle of attack is increased to about  $10^\circ$ , then the wing rock oscillation starts (after an initial wing drop) without any input to rudder or aileron. At this Mach number of 0.78, the oscillation is still diverging, but at lower Mach numbers, the amplitude of the oscillation tended to become near-constant, indicating the presence of nonlinear effects. For the aircraft with tanks on, the pilot was able to excite a damped Dutch roll oscillation at comparable flight conditions ( $M = 0.77$  and  $\alpha = 9.75^\circ$ ), and did not encounter wing rock until  $\alpha = 14^\circ$  at such Mach numbers.

#### 3.2 Supporting work

##### 3.2.1 Theoretical studies

The preliminary theoretical studies<sup>15</sup> were directed towards predicting the variation of Dutch roll characteristics with angle of attack and Mach number, for which estimates of the stability derivatives were required. Some results from static tunnel tests were available up to  $\alpha \leq 10^\circ$ , and so these were used to provide a basis for extrapolation of the linear values for the derivatives due to rates of roll and yaw to the moderate angles of attack, where flow separation effects are significant ( $\alpha > 6^\circ$  to  $8^\circ$ ). A parallel study was made on Phantom, for which measurements were available for all the derivatives, in order to check the empirical factors used in the extrapolations. The results showed that the damping of the Dutch roll mode increased initially as angle of attack increased, but tended to zero at higher angles of attack, beyond flow separation. At the lower Mach numbers, the effect of the presence of fuel tanks was to maintain the damping to higher angles of attack. The predicted frequency of the Dutch roll mode remained near-constant over the angle of attack range, due to the fact that the tunnel measurements of yawing moment due to sideslip showed no loss at the highest angles of attack tested.

These results suggested that the usual linear model of aerodynamics could be used in the identification of both the pilot-induced Dutch roll oscillations, and the initial growth of the wing rock oscillations. However, nonlinear terms have to be added in order to account for the near-constant amplitude responses encountered in flight. Previous work on the HP 115 experimental aircraft<sup>16</sup> had shown that nonlinear moments due to sideslip could produce limit cycles, i.e. the initially diverging oscillation tends to a finite amplitude oscillation, but the tunnel tests did not show any large nonlinearities in sideslip for the Gnat. It can also be expected that moments due to roll rate are nonlinear when flow separation effects are considered, and so the approximate analysis was extended to explore the influence of nonlinear  $C_q(p)$ . It was found that such characteristics did cause limit cycles<sup>14</sup>, and so nonlinear terms in both sideslip and roll rate were included in the mathematical model for the identification analysis. Other types of nonlinearity, particularly hysteresis, were investigated, but were not used to model the Gnat aircraft, since the results from the wind-tunnel tests did not show any discontinuities.

##### 3.2.2 Experimental studies

A small model of the Gnat had been tested in wind tunnels previous to the flight tests, but two 1/6-scale models were built as part of the research programme. One was used to measure static and control (and buffet) characteristics<sup>18</sup>, and the other was tested on an oscillatory rig<sup>17</sup> to give the derivatives due rates of roll and yaw. High Reynolds numbers could be achieved, but the angle of attack range was limited, mainly by

load considerations. However, the tests on the oscillatory rig were further limited by the large amplitude rolling oscillations which occurred at angles of attack just below those for onset of wing rock. The maximum angles of attack achieved at  $M = 0.7$  and  $0.8$  were  $10.5^\circ$  and  $7^\circ$  respectively, and the results show that significant flow separation has occurred at such conditions. Comparisons have been made between the values of the linear derivatives obtained from the tunnel tests, and those identified from the flight responses, in order to substantiate the mathematical model used in the identification.

Recently we have measured the moments of inertia in roll and pitch, using a ground-based rig<sup>19</sup>. The theoretical estimates of the inertias were originally made 20 years ago, before the advent of computerised weight analysis, and so were unreliable. In addition, all the rolling moment derivatives identified using the estimated inertias were smaller in magnitude than the values measured in the tunnel tests, indicating a consistent error. It was found that the estimated inertia in roll was about 30% too small, and the corresponding revised values of the derivatives are now in reasonable agreement with the tunnel values.

### 3.3 Discussion of results

#### 3.3.1 Linear aerodynamic model

Some selected results are shown here to illustrate the problems we encountered, (some of which could have occurred in the analysis of responses about straight and level flight conditions), and to show how the choice of mathematical model was validated. It is important to realise that the mean flight path was a steady turn, often diving to maintain Mach number, and so we had to include the nonlinear kinematic and inertia terms in our mathematical model. The recorded angle of attack and pitch rate were used as pseudo-control inputs, and were not included in the matching process. We were thus able to retain only the three lateral equations of motion, and we used linear stability and control derivatives for the analysis of the Dutch roll oscillations and the initial growth of the wing rock oscillations.

The results (Fig 9) for moments due to sideslip, at the mean Mach number of  $0.7$ , show greater scatter than is usually expected, although it is possible to choose a mean curve through the likely error band to include most of the points. We think that this is due to the fact that most of the flights at the lower Mach numbers were done in our first series of tests, with just a few check flights after the aircraft had been re-instrumented. In particular, a better angle of attack vane was installed, but we did not realise until later that the original vane had given consistently low readings. This became apparent when we plotted our original values for normal force coefficient, rolling moment due to sideslip, and yawing due to roll rate, as functions of angle of attack, and found that the results fell on two distinct curves in each case, one for the first series of tests, and one for the second. We have applied empirical corrections to the angle of attack as recorded in the earlier flights, but cannot be precise, so some scatter remains in the revised values (Fig 9). Even so, the values from the flight tests agree with the values obtained from the tunnel tests, although the static tunnel tests show greater effects of flow separation on rolling moment, for  $\alpha > 8^\circ$ . The four values at the highest angles of attack ( $\alpha > 11^\circ$ ), were obtained from flight responses of the initial growth of wing rock, and follow the trend and level obtained from the Dutch roll responses, an indication that the linear form of the mathematical model is adequate.

There is less scatter in the results obtained from the later series of flight tests, for which  $M \approx 0.8$ . The sideslip characteristics are similar to those at  $M \approx 0.7$ , and so the values are not presented here. The variation of rolling moment due to roll rate with angle of attack was confirmed to be the crucial factor in the occurrence of wing rock, as the results in Fig 10 show. For the clean aircraft, we were able to analyse the initial growth of one wing rock oscillation at this Mach number, from which a positive value of  $C_{lp}$  was identified, and the results given by analysis of the Dutch roll oscillations at the moderate angles of attack also showed this trend. (At  $M \approx 0.7$ , two of the values of  $C_{lp}$  obtained from the wing rock oscillations were positive, and two were near-zero.) In contrast,  $C_{lp}$  remains near-constant up to similar angles of attack for the aircraft with fuel tanks on. It seems that the presence of the tanks, carried close to the under-wing surface at midspan, delays the spread of flow separation from the tips to the inner portions of the wing, so that damping-in-roll is maintained. Identified values of aileron power also showed less variation with angle of attack for the aircraft with tanks on, which supports this hypothesis.

It was not found possible to determine both  $C_{np}$  and  $C_{nr}$  from most of the responses, even though the control inputs for the later flights should have excited the roll subsidence mode as well as the Dutch roll oscillation. The iterative process usually converged, but  $C_{np}$  and  $C_{nr}$  were obviously correlated, so final values probably depended on the initial guesses used to start the iteration. As the damping-in-yaw derivative is well determined from the oscillatory rig tests, and does not affect the damping of the Dutch roll so strongly as  $C_{np}$  at higher angles of attack, it was decided to keep  $C_{nr}$  fixed at the tunnel value. The presence of the aileron input in some responses did not appear to uncouple the effects of  $C_{np}$  and  $C_{nr}$  sufficiently for them both to be determined consistently, and this was probably due to the high level of damping of the roll subsidence mode. The variation of  $C_{np}$  with angle of attack is

well-defined (see Fig 11), and the trends agree with the values obtained from the tests on the oscillatory rig in the wind-tunnel.

The mean variation of each of the identified derivatives with angle of attack was used to determine the characteristics of the Dutch roll mode, and it was found that zero damping occurred near angles of attack corresponding to the onset of wing rock, at both  $M = 0.7$  and  $0.8$ . This substantiates the assumption that the initial growth of the wing rock oscillation of the Gnat aircraft is a divergent Dutch roll, and that a linear mathematical model is adequate to explain the onset of the phenomenon.

### 3.3.2 Nonlinear model

As mentioned earlier, the wing rock oscillation tends to become a constant-amplitude oscillation, particularly at the lower Mach numbers, and, of course, nonlinear terms have to be introduced to model such responses. Attempts to match the flight responses using nonlinear moments due to sideslip led to divergence, and so the alternative plausible nonlinearity in roll rate was used instead. The initial growth of the wing rock was analysed first, using the linear aerodynamic model to give good starting values for the analysis of the complete record. A linear term plus cubic term were used to represent  $C_l(p)$ . The supporting theoretical work had shown that both parts of the response had to be included for matching, because the same constant amplitude can be obtained if the coefficients of the linear and cubic terms are linearly related<sup>14</sup>, i.e. any attempt to match only the constant-amplitude response would lead to strong correlation in these two parameters. The rate of initial growth is needed to determine the linear derivative. We have only had opportunity to examine a few records, and a typical matched response is shown in Fig 12. It is obvious that more work needs to be done before good agreement is achieved, but the main characteristics of the flight response are reproduced by the mathematical model. The linear derivatives agree well with those obtained at similar flight conditions, e.g.  $C_{l\beta} = -0.104$ ,  $C_{n\beta} = 0.061$ ,  $C_{np} = -0.1$  at  $\alpha = 13^\circ$ ,  $M = 0.65$ . The nonlinear rolling moment due to roll rate obtained from this response is shown in Fig 13, and it may be seen that the corresponding linear value identified from the smaller amplitude initial growth is a good mean value.

## 4 IDENTIFICATION OF OTHER RESPONSES AT HIGH ANGLES OF ATTACK

### 4.1 Longitudinal response near stalling conditions.

The analysis and results described in Ref 20 illustrate some of the points made earlier, and give a comparison of identification using either nonlinear models or locally linearised models for the same response. The aircraft is a variable-sweep fighter, with twin vertical tails, and the longitudinal response analysed was for the fully-swept configuration. An elevator input was applied at an initial Mach number of 0.5, increasing from a trim elevator setting of  $5^\circ$  to  $32^\circ$  in one second. The aircraft stalled at about  $45^\circ$  angle of attack, and the elevator was then held at about  $30^\circ$  deflection, for several seconds. A rudder input did not excite any significant lateral response. Altitude remained essentially unchanged during this manoeuvre, but Mach number dropped to about 0.2 at the end of the run.

Linear derivatives were retained for forces and moments due to rate of pitch and elevator, but lift and pitching moment were expressed as second-order polynomials in incremental angle of attack, e.g.

$$C_m = C_{m_0} + C_{m_\alpha}(\alpha - \alpha_0) + C_{m_{\alpha^2}}(\alpha - \alpha_0)^2 + C_{m_q}\left(\frac{q\bar{c}}{2V}\right) + C_{m_{\dot{\eta}}}\dot{\eta}.$$

The calculated response in angle of attack is shown in Fig 14, which also shows the fit obtained for the normal acceleration (as an example), using the nonlinear representation of  $C_z$  and  $C_m$ . The reference angle of attack was taken to be the initial angle, ( $8.2^\circ$ ) for the nonlinear analysis. A study was also made using the linearised model (i.e.  $C_{z_{\alpha^2}} = 0$ ,  $C_{m_{\alpha^2}} = 0$ ), about three nominal angles of attack,  $\alpha_0 = 20.9^\circ$ ,  $29.9^\circ$  and  $41.6^\circ$ , although it is not clear which portions of the flight record were used for each.

The results for  $C_z$  and  $C_m$  as functions of angle of attack may be displayed in two ways, either as total  $C_z(\alpha)$ ,  $C_m(\alpha)$ , i.e. as  $C_{z_0}$  and  $C_{m_0}$  for various  $\alpha_0$ , or as local slope,  $\frac{\partial C_z}{\partial \alpha}$ ,  $\frac{\partial C_m}{\partial \alpha}$  evaluated as functions of angle of attack. Comparisons are made between results from wind-tunnel tests and the two sets of results from the flight test in Fig 15. The results obtained with the nonlinear model are shown as a continuous line, and those from the linear analysis and wind-tunnel tests as discrete points. The values of  $C_z(\alpha)$  and  $C_m(\alpha)$  given by the linear model agree well with the nonlinear results, and are close to the tunnel values, except for  $C_m(\alpha)$  at  $\alpha > 20^\circ$ . This discrepancy is also apparent in the results for  $\frac{\partial C_m}{\partial \alpha}$ , where the local slopes derived from the original wind-tunnel results are appreciably smaller than the flight results for  $20^\circ < \alpha < 30^\circ$ . The presentation of the results as slopes highlights the departure of the flight results from tunnel results for  $\alpha > 40^\circ$ , i.e. near the stall, when  $\frac{\partial C_z}{\partial \alpha} \approx 0$ . This may be due in part to Reynolds number effects on the onset of flow separation, which can be expected to be delayed to higher angles of attack in flight.

The values of damping-in pitch derivative identified at the various nominal angles of attack do not agree well with results from oscillatory tests in the wind-tunnel, being about half the tunnel values for  $\alpha < 30^\circ$ , and of opposite sign at  $\alpha = 40^\circ$ . Identifications were also made with  $C_{m_{q\alpha}}$ ,  $C_{m_{q\alpha^2}}$ , and  $C_{Z_{q\alpha}}$  terms in the mathematical model,

but the values of  $C_{m_q}(\alpha)$  did not change significantly. It was observed that some of the nonlinear parameters were highly correlated with the corresponding linear parameter, and this appears to be a common occurrence. Although this analysis of only one flight record has yielded encouraging results, more flight records should be studied in order to give added confidence in the values obtained, particularly for the damping derivatives.

#### 4.2 Small perturbation responses

A radio-controlled model of the F-15 aircraft mentioned in section 2.1 has been extensively tested at NASA, Dryden, and 136 manoeuvres have been successfully analysed<sup>5</sup>. The longitudinal and lateral responses were excited at angles of attack between  $-20^\circ$  and  $50^\circ$ . Since the manoeuvres were designed to have small amplitudes about a steady flight condition, it was possible to use a linear representation of the aerodynamic forces and moments. The variation of the derivatives with angle of attack was well-defined by the identified values, even through the stall region. However, there was some evidence of nonlinear effects, and the two examples quoted in the original paper are repeated here, to show how results from linear models could be used to build nonlinear models.

The effectiveness of the elevator (all-moving tail) is one parameter showing nonlinear behaviour. The values for  $C_{m_\eta}$  are shown in Fig 16, and it may be seen that for negative and low angles of attack ( $\alpha < 10^\circ$ ), the scatter in the results is minimal, but between  $15^\circ < \alpha < 30^\circ$  there is a factor of about 2 between the greatest and least values, although the likely error is much smaller. It was noticed that the more negative (larger magnitude) values of  $C_{m_\eta}$  were obtained from manoeuvres with small elevator deflections, and so there seems to be an appreciable loss of effectiveness at large angles of deflection. A pitching moment proportional to  $\eta^2$  would be needed to represent this effect, and a first estimate of its magnitude could be derived from the linearised identified values, and the elevator angles used.

The second example is shown in Fig 17, where the results for yawing moment due to sideslip indicate two distinct levels near  $\alpha = 38^\circ$ , about  $-0.086$  or  $-0.23$  with large likely errors. The three full symbols refer to values of  $C_{n_\beta}$  obtained from manoeuvres performed a few seconds before an unexplained rapid roll-off or upset, of which four were observed during the flight programme. The open symbol at  $\alpha = 38^\circ$  indicates a value obtained from a manoeuvre not followed by an upset, but it is conjectured that the large negative values of  $C_{n_\beta}$  may have been caused by the same phenomenon, the upset being prevented by other occurrences. Such changes in  $C_{n_\beta}$  can be expected if the vortex flow generated by the nose and forebody of the aircraft is not symmetric with respect to the aircraft's plane of symmetry. With twin fins, it is possible for the vortices to be concentrated on the same side of the fins, so that an asymmetric yawing moment would be induced, causing departure from controlled flight. A change in sideforce could also be expected, and may be indicated by the results, as the likely errors for  $C_{Y_\beta}$  are larger in this angle of attack range ( $\alpha \approx 38^\circ$ ) than elsewhere. The effect on the rolling moment due to sideslip seems to be smaller, as the results for this derivative are well-behaved. Wind-tunnel tests on forebodies have revealed the presence of large yawing moments and sideforces at high angles of attack, and zero angles of sideslip, and these would have to be modelled as inputs, rather than higher-order derivatives. The alternative phenomenon is nonlinear yawing moment due to sideslip, which may also be significant.

#### 4.3 Rapid roll manoeuvres

One of the manoeuvres used in flight clearance tests of combat aircraft is to perform rapid rolls at various g-levels at high speeds. The control inputs required are, first, elevator to give the desired g-level in the turn, then step input to the roll motivator, with rudder and elevator held nominally constant. The resulting motion has to be represented by coupled longitudinal and lateral equations, and the responses had originally to be analysed using analogue matching techniques. The dominant parameter is usually yawing moment due to sideslip, and its variation with angle of attack and Mach number has to be monitored during the flight test programme, in order to avoid flight conditions where  $C_{n_\beta}$  tends to zero, i.e. where inertia cross-coupling effects could be catastrophic. The other derivatives due to sideslip, roll rate and angle of attack are also significant, and it may be necessary to include their variation with angle of attack (via second-order derivatives) in the mathematical model. Additional terms may be needed for adequate representation of this coupled motion; for example, if spoilers are used as a roll motivator, then the associated lift and pitching moment should be included.

An example of a rapid roll response<sup>21</sup> is shown in Fig 18, with the computed response obtained using an output error method of analysis, and the fit is seen to be quite good. The values of the derivatives agreed well with the values obtained by identifying other manoeuvres, such as Dutch roll and wing rock oscillations. However, the main interest in using digital computer techniques to analyse rapid roll records is due to the fact that



values of the important derivatives can be obtained much more quickly than other analysis methods can achieve, so that the flight test programme is not delayed.

#### 4.4 Spin

The remotely-controlled model technique mentioned in section 4.2 above is also being used to obtain spinning characteristics of combat aircraft, and work is in progress to extract aerodynamic data from the flight responses. No results have been published yet, but the approach to the problem being taken at NASA, Dryden is described in Ref 6. There has been a long history of spin investigations, and so previous experience can be drawn upon, to guide in the choice of mathematical model for the necessarily coupled equations of motion. The simplest possible form of mathematical model is to be used initially, and the simplest response, the steady-state spin, is to be studied first. In this steady state, the aerodynamic forces and moments must balance the known kinematic effects, and so approximate values of the principal derivatives can be estimated directly. The next step is to study the responses due to small control inputs applied during the steady state spin, and it is hoped to use a near-linear perturbation model in the maximum likelihood estimator, to identify important parameters more precisely. A parallel wind-tunnel experiment is also planned, using a rotary balance to simulate the spinning modes, so that comparisons between flight and tunnel data will be possible.

Analysis of the responses during spin entry is likely to prove more difficult, as they are not usually repeatable, indicating the presence of discrete inputs due to flow separation and vortex interference at the large angles of attack. These inputs are very sensitive to the values of other response variables, and so appear to be random. Spin recovery is more predictable, and the transient motion is largely dependent on the control powers, so should be more amenable to analysis.

Experience needs to be gained to establish which aerodynamic parameters are important for any particular configuration, and some work is being done at RAE<sup>22</sup> to study the effects of some cross-coupling derivatives. The work is in support of free-flight experiments to investigate high angle of attack and spinning characteristics of a combat aircraft, using a 1/4-scale model controlled by pre-set series of control inputs. A striking example of the difference in predicted response, due to a derivative which is usually neglected (variation of yawing moment due to sideslip and elevator deflection) is shown in Fig 19. A trim angle of attack of about  $21^\circ$  is first achieved, before full rudder is applied for 8.5 seconds, and then the rudder is centralised again, with reduced elevator deflection to effect recovery. In flight, the model executed post-stall gyrations after the rudder input, but did not enter a spin, and the control inputs for recovery led to steady flight conditions. The 'basic prediction' of the response shown in Fig 19 was close to that actually achieved, although the amplitude of the oscillation in the post-stall gyrations was not so large as predicted. The theoretical mathematical model included the term  $C_{n\dot{\beta}}$ , and the magnitude of this second-order derivative was obtained from wind-tunnel tests. It is found to have an appreciable effect on the predicted response, and if neglected, the calculations indicate a departure into a fast, flat spin in the opposite sense to the yaw rate experienced earlier in the post-stall gyration. The predicted effects of other second-order derivatives have been discussed in Ref 22, and it is concluded that specially designed wind-tunnel tests are needed to provide insight into the form and magnitude of the aerodynamic forces and moments at high angles of attack and sideslip. It is planned to analyse the responses of the free-flight models using parameter identification techniques, as one of the next steps in the research programme.

#### 5 CONCLUDING REMARKS

The major problem in extracting aerodynamic forces and moments from responses near the extremes of the flight envelope is the definition of the form of the mathematical model, on which the optimisation process has to be based. The usual linear stability and control derivatives may not be adequate to represent the aerodynamics, and extensions to the classic longitudinal and lateral equations of motion may be needed. The usual practice is to retain higher-order terms in the Taylor's series expansions of the forces and moments as polynomials in the state variables, so that the problem becomes that of choosing which of these 'derivatives' to include. Although some computer programs have been written using statistical criteria to determine the terms which are significant in each response, only a brief description of these methods has been included in this lecture. Many flight dynamicists prefer to specify the form of the mathematical model, basing the choice of terms on supporting experimental and theoretical evidence, ie only introducing terms which have physical significance. This latter approach is advocated here, and some examples have been given to demonstrate the effect (or lack of it) of nonlinear terms, and to show how linear forms can sometimes be used. The maxim for any work in this area is "Keep the model as simple as possible", but at the same time "Remember that the numerical values obtained will not apply to ranges of variables outside those covered by the analysed responses". Flight in extreme regimes is, by definition, near some point of departure, structural limit or engine limit, and so extrapolation to untested regions is not justified.



## REFERENCES

- 1 R.E. Maine, Maximum likelihood estimation of aerodynamic derivatives for an oblique wing from flight data. AIAA Paper 77-1135 (1977) (Also NASA TP 1336)
- 2 E.J. Eulrich, E.G. Rynaski, Identification of nonlinear aerodynamic stability and control parameters at high angle of attack. Paper 2 of AGARD CP 172 (1974)
- 3 W. Earl Hall, N.K. Gupta, J.S. Tyler, Model structure determination and parameter identification for nonlinear aerodynamic flight regimes. Paper 21 of AGARD CP 172 (1974)
- 4 V. Klein, J.R. Scheiss, Compatibility check of measured aircraft responses using kinematic equations and extended Kalman filter. NASA TN D-8574 (1977)
- 5 K.W. Iliff, R.E. Maine, Subsonic stability and control derivatives for an unpowered, remotely piloted 3/8-scale F-15 airplane model obtained from flight test. NASA TN D-8136 (1976)
- 6 K.W. Iliff, Estimation of aerodynamic characteristics from dynamic flight test data. Paper 15 of AGARD CP 235 (1978)
- 7 L.W. Taylor, Application of a new criterion for modelling systems. Paper 4 of AGARD CP 172 (1974)
- 8 S. Ramachandran, *et al.*, Identification of aircraft aerodynamic characteristics at high angles of attack and sideslip using the estimation before modelling (EBM) technique. AIAA Paper 77-1169 (1977)
- 9 N.K. Gupta, W. Earl Hall, T.L. Trankle, Advanced methods of model structure determination from test data. AIAA Paper 77-1170 (1977)
- 10 P.H. Fiske, C.F. Price, A new approach to model structure identification. AIAA Paper 77-1171 (1977)
- 11 T.J. Galbraith, T.J. Petersen, Nonlinear parameter identification and its application to transport aircraft. Paper 18 of AGARD CP 235 (1978)
- 12 V. Klein, Longitudinal aerodynamic derivatives of a slender delta-wing research aircraft extracted from flight data. Cranfield Report Aero 27 (1975)(or Ref 21 below)
- 13 A. Jean Ross, G.W. Foster, T. Turvey, An investigation of Dutch roll and wing rock oscillations of a Gnat Trainer aircraft: Flight tests and linear analysis. RAE Technical Report 78032 (1978)
- 14 A. Jean Ross, Lateral stability at high angles of attack, particularly wing rock. Paper 10 of AGARD CP (being published) (1978)
- 15 H.H.B.M. Thomas, A. Jean Ross, The role of theoretical studies of flight dynamics in relation to flight testing. Paper 22 of AGARD CP 119 (1972)
- 16 A. Jean Ross, L.J. Beecham, An approximate analysis of the nonlinear lateral motion of a slender aircraft (HP 115) at low speeds. ARC R & M 3674 (1971)
- 17 C. O'Leary, Wind-tunnel measurements of lateral aerodynamic derivatives using a new oscillatory rig and comparisons for a Gnat aircraft. RAE Technical Report 77159 (1977)
- 18 P.J. Haynes, S. Lineham, RAE Technical Report (to be published)
- 19 R.W. Poulter, Measurements of inertia characteristics of a Gnat aircraft using a ground rig. RAE Technical Memorandum FS (to be published)
- 20 S. Ramachandran, W.R. Well, Estimation of nonlinear aerodynamic derivatives of a variable geometry fighter aircraft from flight data. AIAA 74-790 (1974)
- 21 A. Jean Ross, Determination of aerodynamic derivatives from transient response in manoeuvring flight. Paper 14 of AGARD CP 172 (1974)
- 22 H.H.B.M. Thomas, Geraldine Edwards, Mathematical models of aircraft dynamics for extreme flight conditions (Theory and experiment). Paper 27 of AGARD CP 235 (1978)

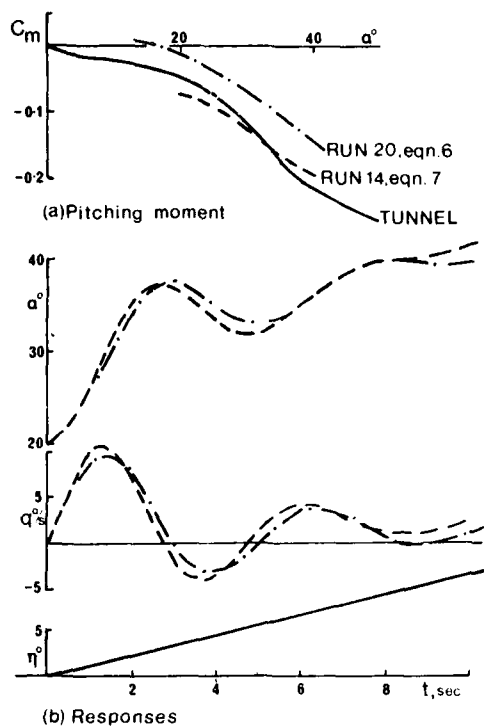


Fig 1 Pitching moment and responses, F-4 (Phantom)

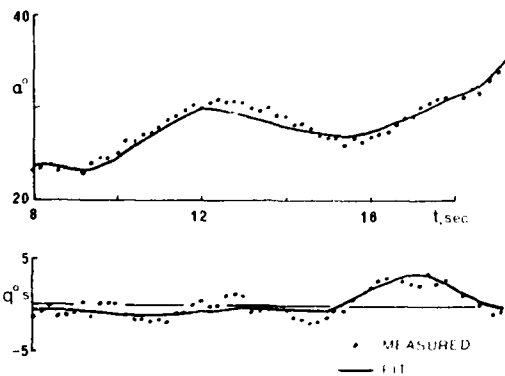


Fig 2 Matched response, Run 14, F-4 (Phantom)

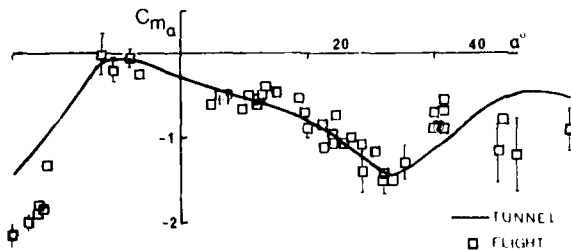


Fig 3 Pitching moment due to angle of attack derivative, F-15 model

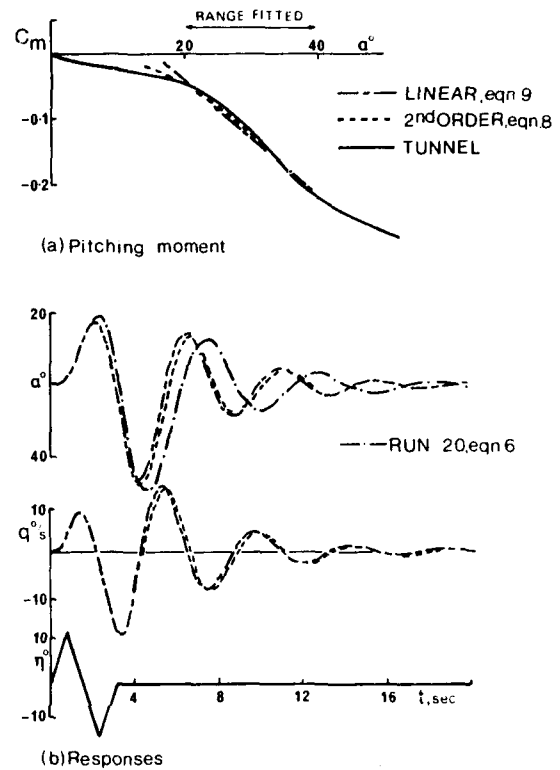


Fig 4 Linear and quadratic pitching moment and responses, F-4 (Phantom)

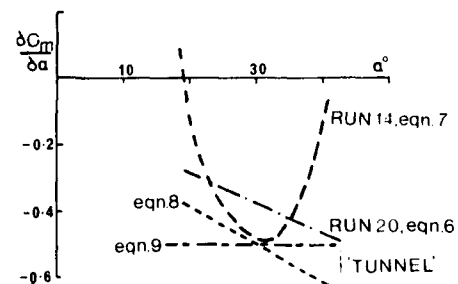


Fig 5 Slope of pitching moment due to angle of attack, F-4 (Phantom)

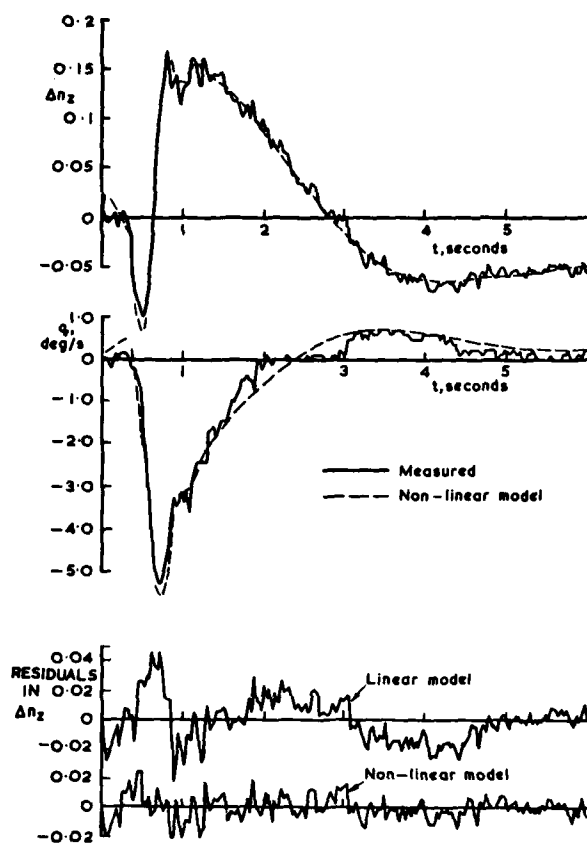


Fig 6 Longitudinal response, nonlinear model, HP 115

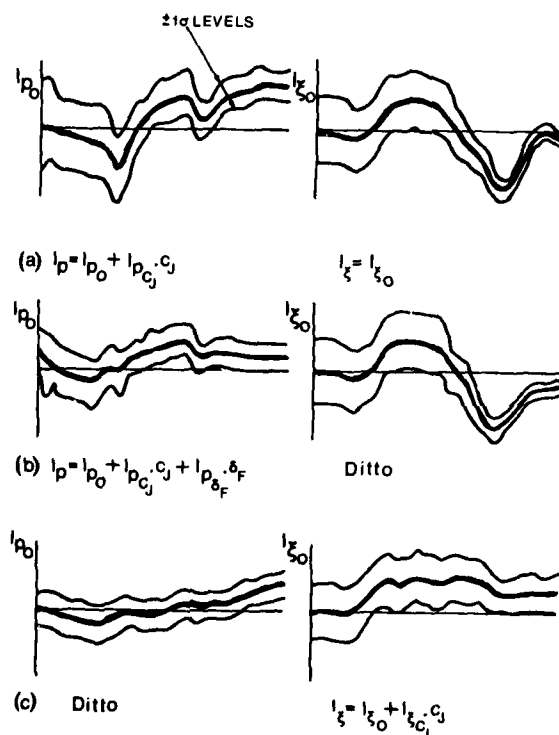


Fig 7 Development of nonlinear rolling moments, C-8A (Buffalo)

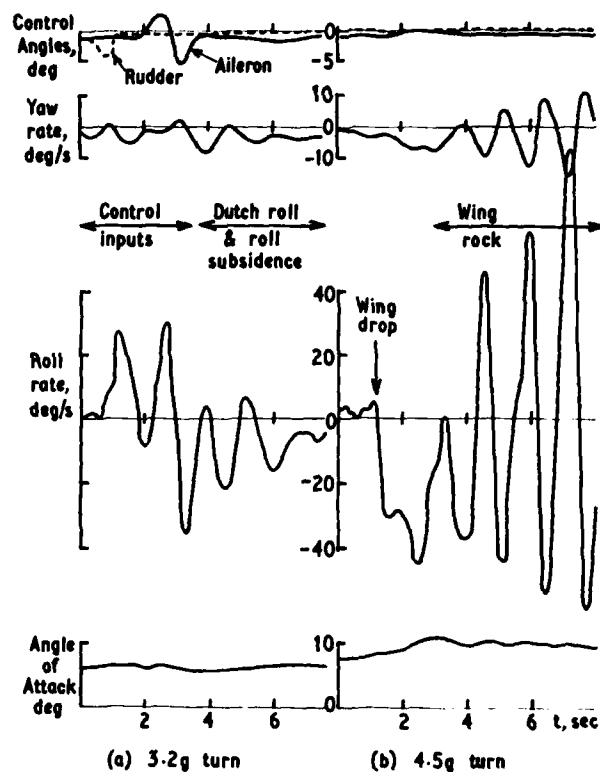


Fig 8 Responses in turns, clean aircraft, Gnat

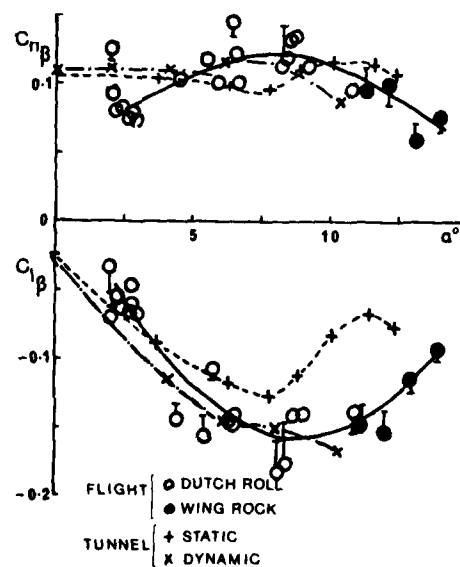


Fig 9 Moment derivatives due to sideslip,  $M = 0.7$ , Gnat

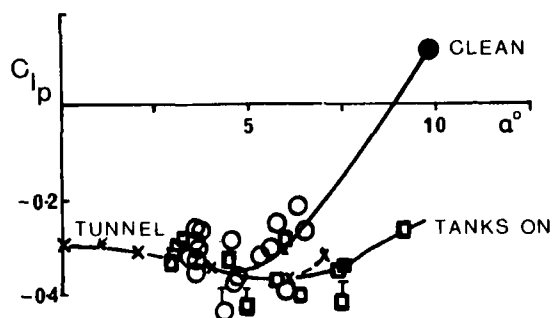


Fig 10 Rolling moment due to roll rate derivative,  $M = 0.8$ , Gnat

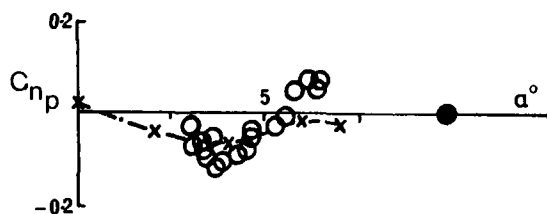


Fig 11 Yawing moment due to roll rate derivative,  $M = 0.8$ , Gnat

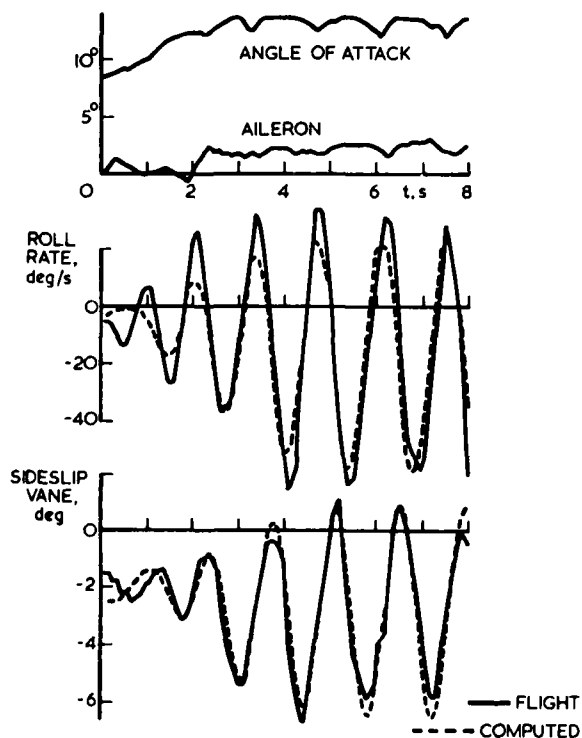


Fig 12 Match obtained for wing rock, with cubic  $C_l(p)$ , Gnat

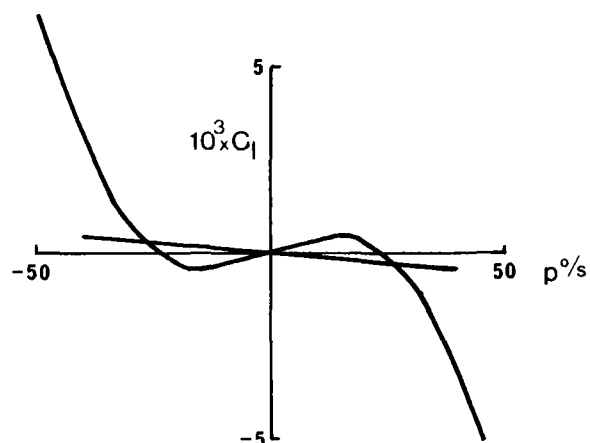


Fig 13 Linear and cubic models for rolling moment due to roll rate

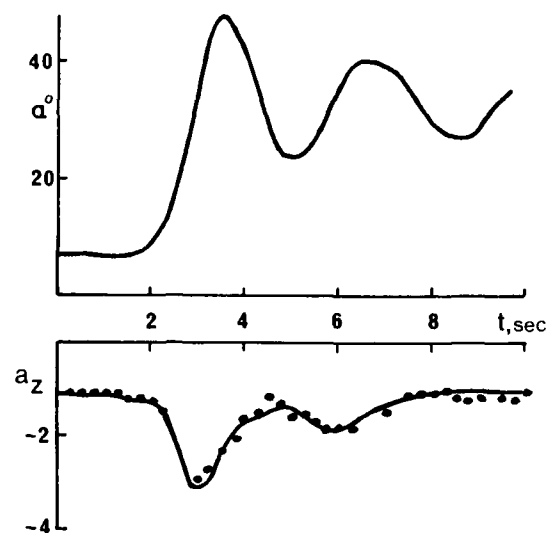


Fig 14 Angle of attack and matched response, variable sweep fighter

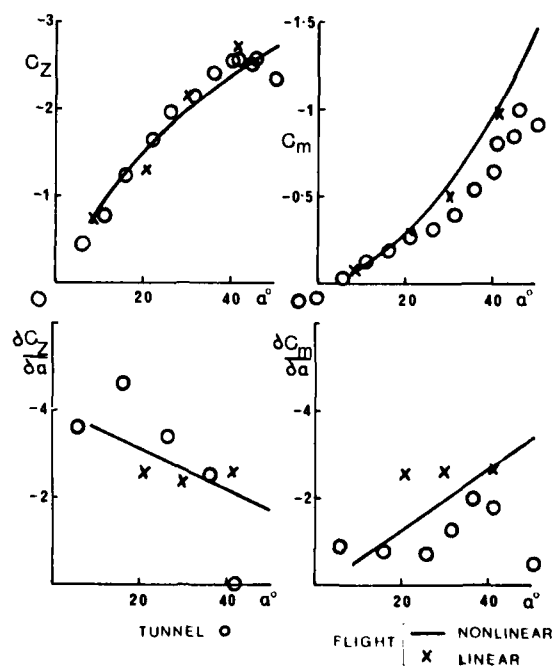


Fig 15 Normal force and pitching moment at angle of attack, variable sweep fighter

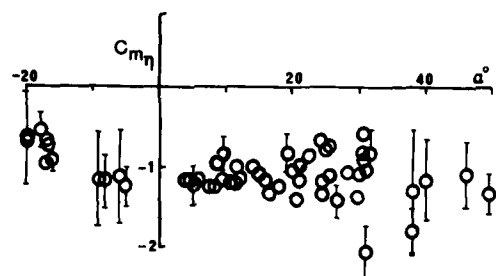


Fig 16 Pitching moment due to elevator derivative, F-15 model

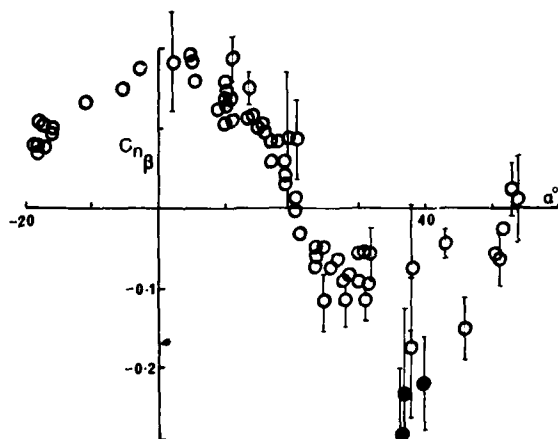


Fig 17 Yawing moment due to sideslip derivative, F-15 model

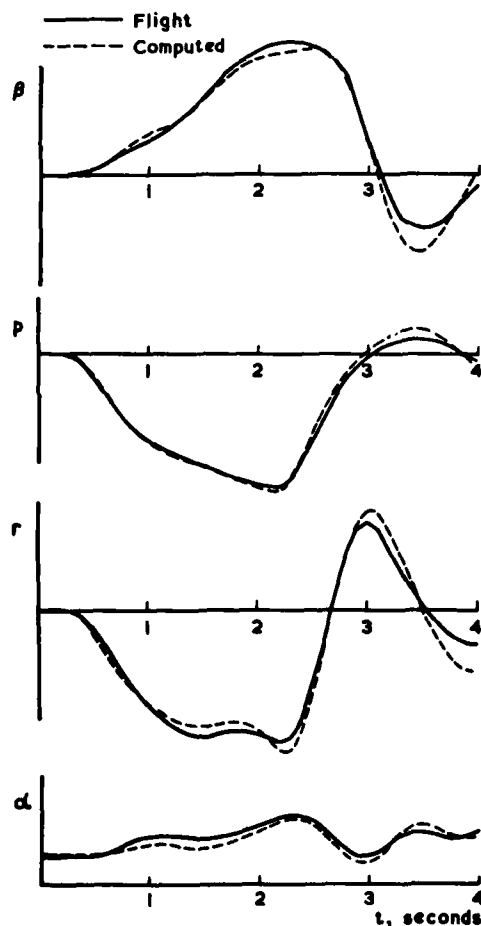


Fig 18 Matched rapid roll of combat aircraft

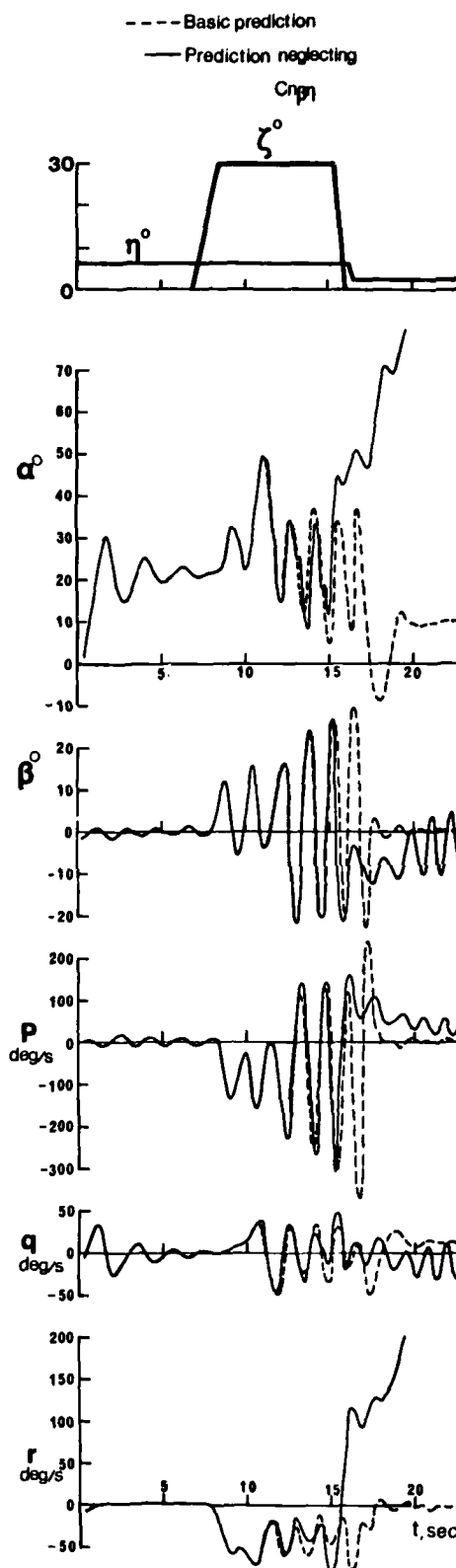


Fig 19 Effect of neglecting yawing moment due to sideslip and elevator on predicted response of free-flight model

## WIND TUNNEL AND FREE FLIGHT MODEL IDENTIFICATION EXPERIENCE

R.A.Verbrugge and W.Charon

Institut de Mécanique des Fluides  
I.M.F.L. (France) 5 bd Painlevé, Lille

M.Marchand

Institut für Flugmechanik  
Deutsche Forschungs- und Versuchsanstalt für Luft- und Raumfahrt e.V. (DFVLR)  
Braunschweig-Flughafen**ABSTRACT**

The first part of this lecture gives an overview of different experimental techniques used for parameter identification based on dynamic model tests in wind tunnel or in free flight. The specific domain of application is defined for each test technique : ability for identification, range of Mach and Reynolds number, angle of attack, nature of inputs, environment conditions, gust applications, kind of motion, etc ..

The second part considers particular aspects of semi-free and free model tests techniques in wind tunnel or laboratory mainly based on DFVLR (Germany) and IMFL (France) experiences : input signals, mathematical modelisation, simulations and test design.

Third part concerns data processing from the collection until the application of identification procedure : nature and quality of the informations, data acquisition software, state vector elaboration, some specific filter aspects and evaluation methods. A set of results will illustrate each particular point.

As conclusion a review of the present state of these techniques is given and future field of application is discussed.

**INTRODUCTION**

Prediction of flight qualities or performance characteristics of modern aircraft needs more than in the past years the development of ground tests and their adaptation to the new aircraft flight domain.

In fact the investigation field to be considered is extensively enlarged more especially in high angle of attack domain including large amplitude motion often with high rotation rate inducing generally large flow asymmetries inducing to strong coupling effects between longitudinal and lateral characteristics. Complex flow fields are generated introducing highly non linear stability characteristics for the aircraft. Such a possible extension of flight domain, mainly due to the integration of generalized automatic controls on the aircraft, needs at design stage particularly for simulation studies a good prediction of the aerodynamic derivatives in an increasing range of angle of attack and sideslip.

Further the environment effects such as gusts requires a particular attention introducing unstationary inputs which interfere in the optimisation of automatic flight control system of the aircraft and therefore in the flight qualities definition.

We can also observe that for low angle of attack flights, dynamic stability parameters have not a determinative influence on flight qualities due to their low value and quasi-independence of the fundamental aerodynamic terms : angle of attack or sideslip. It is not at all the same for higher angle of attack domain in which stability parameters can vary in a wide range and are strongly connected to flow characteristics as well as to local geometric definition of the aircraft. In this case knowledge of dynamic stability parameters is absolutely necessary to define the final specifications of flight qualities and performance.

Usually two different approaches are considered in the prediction of dynamic stability characteristics. The analytical methods and the experimental techniques on scale model in ground based facilities.

The usual analytical methods based on linear potential theories developed for low angle of attack flight regime are now irrelevant to high  $\alpha$  because highly non linear phenomena appear and viscous effects and separated flow must be considered in such flight configuration.

Considering the preliminary remarks mentioned above the experimental techniques have considerably progressed during the past years in various laboratories in order to permit direct determination of stability parameters and also to provide an experimental support and a data-bank necessary for the validation of analytical methods. A progress in this field is no doubt indispensable to reach a comprehensive approach of the complex phenomena observed.

A lot of experimental methods have been developed in order to measure or identify dynamic stability parameters on the base of a "representative" mathematical model grounded on restrictive assumptions (linear model, small perturbations, etc). New apparatus or test techniques were also created to provide global aerodynamic data relative to large amplitude, high rate motion or continuous rotation (i.e rotary balances).

Analysis of such data and application of parameter identification techniques requires new developments of representative models, including new derivatives definition and the opportunity to consider simultaneously all degrees of freedom.

In front of such a new complexity of the problems encountered in dynamic stability parameter prediction it is clear that none model test method is able to cover the whole needs to be considered in an extensive domain, of angle of attack, Mach and Reynolds Number, etc ... It is the reason why many attempts are devoted to develop in many laboratories various and complementary experimental techniques.

The objective of this lecture is to present a short review of some facilities and associated experimental methods with a particular development on semi free of free model test techniques. The aim is to bring out the specific aspects of system identification applied to such experiences and their original contribution to actually solve the difficult problems of predicting modern aircraft flight qualities. These experimental methods are currently in progress. The informations provided as example of recent applications are relative to a limited area inside the field of possible applications. They mainly concern longitudinal motion and gust effects.

# **1 - SHORT REVIEW OF DIFFERENT EXPERIMENTAL TECHNIQUES USED FOR STABILITY PARAMETER IDENTIFICATION.-**

## **1.1 - General frame.**

This review is not exhaustive. Numerous and various test methods exist and a considerable work should be necessary for a complete presentation. (More informations in Ref. 1). Only the main general methods will be shortly presented and illustrated by a few specific examples in order to compare semi free model or laboratory free model experiences with more conventional techniques.

The area we consider here will be mainly restricted to incompressible aerodynamic in which free or ~~free~~ model tests techniques are mostly developed to day. The present field of application is shown on fig.1.

The first generally formulated comment on these methods concerns the test Reynolds number. It is sure as mentioned by Mr Orlik Ruckeman in Ref. 1, that captive model tests in wind tunnel offer the advantage of a wide range of Reynolds number which can sometimes reach, in new facilities, the flight Reynolds Number. Nevertheless many attempts to perform free tests at higher Reynolds numbers have been made. Reynolds numbers are now situated in the range of  $10^6$ .

Also we can observe that for a lot of aerodynamic phenomena, which are currently considered as strongly dependant on Reynolds number, it is not systematically demonstrated what could be the necessary specifications, in the matter of limit Reynolds number, which warrant a direct prediction of aircraft characteristics. Further and as mentioned by Mr Orlik Ruckeman (Ref. 1) it is of great interest to establish between full scale and model results the necessary correlations in order to define the relative importance of various derivatives to be identify and to appreciate more completely the validity or the justification of different methods. In fact it is clear that conjunction of various requirements, relative to flow characteristics, structural representation, working field of new flight control system ... to be considered in aircraft characteristics prediction, tend to invalidate all direct experiences on scale models. The procedure most often considered will consist in performing more and more numerous tests, that are partly representative and complementary. They are realized in order to validate a modelisation of the phenomena investigated considering the basic assumptions and specific characteristics of the test. Transposition to full scale aircraft is afterwards considered (see fig. 2).

## **1.2 - Presentation of main experimental techniques.**

Figure 3 suggests a summary classification of various experimental techniques applied to the determination of dynamic stability parameters. Main outstanding characteristics of each technique will be examined and more details will be given on semi-free or free model tests.

### **1.2.1 - Dynamic Balance Test Techniques.**

#### **1.2.1.1 - Introduction.**

These wide spread techniques are the most classical ones and in constant development. The main characteristics are presented on figure 4. The possibilities to realize high Reynolds or Mach Number and to conduct parametric studies (effect of  $R$ ,  $M$ ,  $\alpha$  or reduced frequency ...) are doubtless the most important advantages of the method. Also many improvements have been made in the mechanical area : balance system, model, pivots and suspension system design as well as in instrumentation, data acquisition and reduction procedures. We may point out for memory's sake the multi degree of freedom techniques based on motion analysis during forced oscillations of an elastically suspended model, different from forced oscillations with constant torque (electromagnetic drive) or constant amplitude (mechanical or hydraulic drive) and the derivatives obtained from reactions measurements. Sometimes usual measurements : frequency, amplitude, forces and moments are completed with accelerometric measurements extended to the whole model. This method not only allows a convenient motion analysis but also the more direct determination of the dynamic components taking into account structural modes of the support. It also forwards the application of parameter identification methods. (See Ref. 2).

A few examples are now given to illustrate such captive model tests.

#### **1.2.1.2 - Low speed derivatives balances of DFVLR (Germany).**

Figure 5 shows different types of dynamic mountings in use in West Germany (DFVLR).

The mobile oscillatory derivative balance (MOD) can work in several 3 m low speed wind tunnels in W.Germany. Excitation can separately be imposed on pitch, roll, yaw and heave by means of a drive system using a rigid mechanically forced excitation, frequency is adjustable up to 3 Hz.

Measurements consist in : instantaneous position of the model, Forces and Moments obtained by a 5 components strain-gauge balance, frequency of oscillations.

MOD balance can also operate up to 50 degrees angle of attack with a special extension device.

A Fourier analysis method is applied for reduction of MOD data. Static, direct and coupled damping derivatives can be obtained with this method. A new program based on a regression analysis method is in run to identify the derivatives. The application of this method requires accelerations and velocities informations which can be obtained with suitable precision by fitting the model with accelerometers (see Ref. 2).

The multi degree of freedom derivative balance MFD presented is a forced oscillation apparatus design to work in low-speed wind tunnel with angle of attack up to 25°. Model is supported by an elastic sting which consists of two spring elements with different stiffness. The forced oscillation at constant amplitude is applied to the model by an electro mechanical drive. Varying excitation frequency separated or combined motion can be performed (see Ref. 3).

Informations are obtained on excitation and damping of model motion, excitation frequency, amplitudes and phases of the motion.

Analysis of the data for derivative evaluation is based on integral energy equations relative to the motions of an aeroelastic system. (Ritz Galerkin Energy Equation - see Ref. 4).

An example of results obtained on MOD and MFD balances compared to flight test results is shown on fig.6. The results are relative to the damping in roll  $C_{lp}$  and coupling derivative  $C_{Np}$ . For  $C_{lp}$  the results of the two balances are in good agreement and are essentially confirmed by the flight tests. For  $C_{Np}$  accordance is reasonably good and difference appears particularly at low  $\alpha$ . It can be suggested that for one part the engine not simulated can interfere.

#### 1.2.1.3 - Rotary balance of IMFL France.

Usual oscillatory balances such as those presented are designed to work with small amplitudes oscillations in the  $\alpha$ ,  $\beta$  domain and the mean value of  $p$ ,  $q$  or  $r$  is zero. The derivatives obtained are in relation to the classic assumptions made in modelling the equations of motion based on small perturbations.

Nevertheless some kinds of motion of the aircraft flying at high angle of attack, departure, spin motion and recovery include very large amplitude motion, even continuous rotation and generally high rates of rotation are encountered.

In this case the data produced by oscillatory test rigs are not valid also a more general formulation of equations of motion is necessary, adding terms relative to continuous rotary motion and non linear coupling effects. (Reference 5).

To provide specific data in this domain a quite new rotary balance apparatus was design and built at IMFL France in 1978 (Ref. 6).

The test apparatus is designed to work in two specific domains :

- . High angle of attack evolution up to 65° on large scale model.
- . Spin domain ( $\alpha$  up to 120°,  $\beta \pm 90^\circ$ ). All the characteristic parameters of the spin can be represented.

The movable apparatus can take place in the four metres test section of the vertical wind tunnel of IMFL also used to perform free spin model studies. This particular arrangement presents the advantages to reduce pulsatory gravity forces on the balance and allows also to recreate stationary spin conditions getting zero signals on the balance and performing stability or control efficiency tests around the equilibrium point.

A general sketch of the apparatus showing the various degrees of freedom is presented in fig.8.

Fixed value in  $\theta$  or continuous rotation can be realized in order to study autorolls at high angle of attack.  $\theta$  angle is adjustable continuously from 0 to 45° and 45° to 90° by means of the curved arm. Motions in  $\theta$  and  $\theta$  don't move the C.G. in the test section. At the junction with the  $\Omega$  rotation axis two independant adjustings can introduce spin radius and relative heading.  $\vec{V}$  and  $\vec{a}$  vectors can be dissociated introducing  $\lambda$  angle. Periodic fluctuations of  $\alpha$  and  $\beta$  and dynamic terms  $\dot{\alpha}$  and  $\dot{\beta}$  are obtained during the rotation. Such terms are particularly important for high  $\alpha$  departure studies (Reference 5).

$\Omega$  rotation in both directions is obtained by a servo-torque-motor. Main characteristics of the rotary balance are presented on fig. 9.

All the data are on line digitized and the present reduction procedure provides all the motion informations combined to the aerodynamic components.



Data analysis is presently introduced regarding to a new math formulation particularly in the spin domain. Further details will be available on this subject in a next future. Also as an extension of the possibilities of the apparatus forced oscillations could be superimposed to the continuous rotation in the spin domain. This scheme is under consideration.

#### 1.2.1.4 - Dynamic balance for large amplitude motions (IMFL France)

In addition to the rotary balance apparatus and to investigate in large amplitude motion with high rate of rotation a new balance was created at IMFL working in the horizontal wind-tunnel. The general arrangement is presented on figure 10. The system is initially designed to provide pitch and yaw motion with large amplitudes (up to 45°), and high rotation speed of 200°/s in  $\alpha$ ,  $\beta$  domain up to 45°.

An hydraulic drive is used to generate forced motion, various laws of motion can be performed.

Measurements, data acquisition and data reduction are analog to those realised for the rotary balance apparatus.

Roll oscillation will later be introduced.

#### 1.2.2 - Semi free model test techniques.

##### 1.2.2.1 - Introduction.

These techniques have two main advantages. They combine wind tunnel performances : Mach, Reynolds number, test duration, ground based measurement systems ... and the possible representation of a semi-free motion considering the most demonstrative degree of freedom. On this point of view it's a more global representative test technique. Generally the model has 4 to 5 degrees of freedom : (excluding X and often Y motions are not represented).

The basic characteristics of these techniques are proposed in fig.11 and will be illustrated by two typical examples giving more details on the dynamic simulation tests in wind tunnel performed by the DFVLR. Specific aspects regarding to parameter identification techniques will be given in the next chapter.

##### 1.2.2.2 - Dynamic simulation in wind tunnel (DFVLR).

DFVLR has developed a new wind tunnel test technique, using semi-free flying and remotely controlled models. The model flies in a special suspension frame which allows freedom of motion in pitch, yaw, roll and heave (fig.12), it has scale inertial properties which give it a dynamic response similar to the original aircraft. The experimental installation includes a gust generator, a weight reduction system, and a measurement container with model control devices, measurement data processor, and various monitoring devices. The advantage of this type of simulation is the good observability of all state variables and all inputs acting on the model. All standard tests for parameter identification and dynamic response evaluation, such as harmonic, impulse and stochastic excitations, can be programmed in the computer and performed. The gust generator flaps and/or the onboard control surfaces can be used to excite the model. The response can be evaluated immediately after the test to show time histories, frequency responses or power spectra. Data are recorded on magnetic tape to perform off-line evaluations such like parameter identification.

As example for an application, a model of small transport aircraft DO 28 TNT used for gust alleviation system development and parameter identification is shown in figs 13 (and 14). This model is representative of a rigid aircraft. All control surfaces are driven by electric torque motors. The model is equipped with rate gyros, accelerometers, pressure transducers and angle of attack probes. The model motion and the deflections of the control surfaces can be measured using built-in potentiometers. Power supply, control signals and measured data, flow to and from the model via an umbilical cable.

Two gust generator flaps driven by an electro hydraulic actuator allow a deflection of the airstream within the test-section up to 10 degrees. It is possible to generate various types of gust profiles, such as impulses, harmonic oscillations or stochastic gust in a frequency range up to 15 Hz. The properties of the gust generator allow the simulation of a scaled down stochastic gust field with a Dryden- or v.Karman characteristic.

Fig. 15 summarizes the special features of this test technique when being used in the low speed wind tunnel of DFVLR at Braunschweig.

##### 1.2.2.3 - Semi free flight. Simulation in wind tunnel. (Cable mount system) (NASA Langley)

Another interesting example of application of system identification techniques to data obtained from semi-free wind tunnel tests is shortly presented here (All details in Ref. 7).

Suspension system is issued from those currently applied to flutter or gust response tests in the NASA Langley transonic tunnel (fig. 16).

Two cable loops upstream and downstream are connected to the model with pin joints. In the rear loop stiffness is adjustable depending on the geometric arrangement of the cables. Limited freedom in all direction is permitted except in fore and aft.

In order to perform test on model having static unstable characteristics and also to provide excitation forces for response measurements, cables are active controlled by two servo-motors in the loops.

Models are dynamically and often elastically scaled and fully instrumented mainly with three axes gyro and accelerometers. Cables strains, displacement and velocity are measured.

Generally the model is excited with an harmonic signal varying frequency until a resonance appears by visual observation of the model and the transducers signals. When modes of the system are found, the applied excitation contains the modal frequencies and the responses are measured and collected for data processing.

Parameter identification is based on a maximum likelihood program only modified to include some specific aspects of the experimental method (influence of cable system).

Some results are presented in fig.17 (reproduced from Réf. 7).

Very reasonable results were obtained both for lateral and longitudinal motions. Further experiences will be performed and application will be extended to flexible aircraft.

#### 1.2.3 - Wind tunnel free model test technique.

Main characteristics of this technique are presented in fig.19.

One of the most demonstrative example of this method was performed a few years ago by NASA in the Langley full scale wind tunnel. The well known pictorial view showing the general arrangement is reproduced on fig.19 (see Réf.8).

The powered free model (except safety cable, pneumatic, electric and control signals connections) flies in the open test section of the wind tunnel (30 x 60 ft) under control of three operators : for pitch control, power control and roll and yaw control.

Flight qualities or pilot control studies up to high angle of attack were performed with this technique.

Qualitative results issued from motion visualisation can mainly be obtained with this method which is a rather complex technique not used for parameter identification.

#### 1.2.4 - Atmospheric free flight model tests.

Dynamically scale models are dropped from helicopters or aircraft and are radio-controlled. This technique was used for several fighter aircraft by NASA and AFFDL (Edwards) specifically to provide informations on post-stall and spin entry and also to evaluate control efficiency during such fights.

Test procedure is similar to those used in full scale test but a lot of limitations appears : complexity of the technique, cost of the model and of the test program, duration of the tests, influence of atmospheric environment ...

#### 1.2.5 - Laboratory free flight model test technique.

This experimental method has been developed by IMF Lille since 1965 and is now applied to many domains : parameter identification (stability and control parameters, ground and gust effects), flight qualities studies (high  $\alpha$ , active control, gust alleviation) or impact studies (fig.1).

Information will be given here on this technique to introduce the specific aspects of parameter identification experiences (more details can be found in Ref. 9).

Specific aspects of the method are presented on fig.20.

Basically the test method is very simple.

Unpropelled models, dynamically scale, are launched in free flight by means of a catapult system. The flight is performed over 50 metres in a laboratory and the model is recovered.

The general arrangement of the facility is presented on fig.21.

All initial conditions of the flight can be adjusted. The flights can be performed in still air. Lateral as well as longitudinal gusts can be created and flights with ground effect realized. A schematic illustration of these possibilities is shown on fig. 22-23.

Main specifications of the tests are presented on fig.24.

This technique is in constant progress due to the integration, in large model of high performance transducers and actuators associated to digital telemetry and telecontrol systems. All that contributes to the development of quantitative tests.

Identification of stationary coefficients was initially realized by performing permanent trimmed fights. Comparative studies with low speed wind-tunnel results are presently systematically conducted.

For dynamic stability parameters identification numerous original and various sensitizing inputs can be realized (see chap.2) : various combined inputs as initial conditions of the flight, control inputs in flight and external inputs such as gusts. Typical motions may be performed (for example flights at  $\alpha$  or  $\theta$  constant).

To realize such tests various specific software was developed : data acquisition and real time control loops, general flight simulation, state variable elaboration from trajectographic and dynamic data, parameter identification programs.

## 2 - SPECIFIC ASPECTS OF SEMI FREE AND FREE FLIGHT MODEL TEST TECHNIQUES.-

### 2.1 - Mathematical modelisation used for simulation.

#### 2.1.1 - Introduction.

We generally consider two modelisation concepts : the physical and the representative modelisation.

In flight mechanics, a physical modelisation would be a mathematical description of the aerodynamic phenomena around the aircraft. But even for the general flight of the aircraft, such a model would be very complicated. Therefore in flight mechanics, a mathematical structure of the forces and moments is used to describe the aerodynamic phenomena. Nevertheless, it stands to reason that the more the phenomena are complicated the more the modelisation is near to be a physical one.

It is the reason why, at the basis of every representative modelisation, a set of assumptions strongly restricts the application field of this modelisation. As an example, let us take the "small perturbations" assumption. The global aerodynamic coefficients are developed in series and the terms of second order are disregarded in relation to the terms of the first order. Which are the magnitudes of the disregarded terms in relation with the others ? Haven't any out of those other terms the same magnitudes as the disregarded ones ? All these problems should be carefully solved for some use requirements.

A simulator may have multiple uses :

- flight forecasting determination of safe trajectories from the estimated coefficients
- comparison between simulations and actual flights
- determination of the parameters sensitized with a particular input
- inversely, determination of the flights to be performed in order to be able to identify such and such parameter
- base of the identification process.

It is obvious that the two last uses should require the solution of the problems involved by the "minor perturbations" to be sure that the results are significant.

#### 2.1.2 - Examples of modelisation.

##### 2.1.2.1 - IMPL free flight modelisation.

Up to now IMPL has developed digital simulations with the following characteristics :

- the modelling is on a representative form with the "minor perturbations" assumption in relation with an almost permanent "reference flight" described in the catapult frame. The outputs of the system are therefore deviations in relation with this "reference flight"
- the variables introduced in the model are non dimensional variables. It enables a comparison between mock-ups of different sizes and shapes
- those simulations are adapted to the particular inputs which may be produced during our experiments. Thus we can simulate the response to initial condition steps (incidence, attitude, longitudinal velocity, mass, C.G. location, control surface), the motions due to any in flight control deflection particular motion due to long vertical gusts
- they enable piloting and control laws to be elaborated such as maintaining constant attitude or incidence or giving them a linear function of time.

All those characteristics are summarized in fig. 25.

For the mathematical model refer to fig. 26.

##### 2.1.2.2 - Mathematical modelling for free flight evaluation.

Fig.28 shows a set of mathematical models used for ATA free flight model test evaluation. From first runs, with the equation error regression model (A), no satisfactory results for derivatives and time histories could be achieved. For this reason, model B was defined introducing the following modifications : (1) the output errors of  $u$ ,  $y$ ,  $h$ ,  $q$ , and  $\theta$  were included in the performance criteria ; (2) to avoid the high correlation between  $\dot{\alpha}$  and  $q$ -derivatives,  $\dot{\alpha}$ -derivatives were fixed at the a-priori values ; (3) bias terms in the differential and observation equations were added. For better efficiency of the identification the data from several different flights were used in the same computation run. In the case of seven flight tests to be evaluated, seven sets of bias terms have to be estimated, this giving a total number of 99 unknown parameters. This would lead to numerical difficulties. To reduce this number, the model was divided into three parts as shown in fig.29. Now for the X-, Z- and M-degree of freedom separate identification runs can be performed with a maximum number of 38 unknown parameters. Based on model B, two additional model versions have been defined for investigation of special non-linear aerodynamic effects (model types C and D from fig.28). Some typical results from these evaluations are shown later.

### 2.1.2.3 - Mathematical modelling for semi free test technique.

Fig.30 shows specific features of mathematical modelling for semi-free test technique. Geodetic axis system is used. The reasons for this choice are : (1) translatory motion is only possible in the geodetic  $z$ -direction ; (2) gust field and the suspension frame influence are described as function of time and geodetic coordinates, and (3) some signals such as weight reduction force, vertical speed and position are measured directly in the geodetic  $z$ -direction.

The various types of inputs are shown in fig.31. The model structure shown in this figure is complex. To perform a good identification of the derivatives a detailed and very carefully performed modelling and identification of the flow field and mechanical system characteristics is required. These additional identifications should be done using special tests before identification of aircraft parameters to avoid an enlarging of the mathematical model structure and an increasing of the number of unknown parameters in the identification model.

### 2.1.2.4 - Wing-tail interference modelling.

A problem, to be considered in aircraft identifications when using high frequency inputs is the modellisation of the downwash effect at the tailplane. Three different approaches are shown in fig.32. If the local angle of attack can be measured at the tailplane position, separate signals of  $\alpha_{wing}$  and  $\alpha_{tail}$  can be used for identifying separate derivatives for the wing- and tail contributions (see n° 1 of fig.32). But these two signals,  $\alpha_{wing}$  and  $\alpha_{tail}$ , are very high correlated in the low frequency regime, so separate identification of wing- and tail derivatives may not be possible with low frequency inputs.

The same problem exists when  $\alpha_{tail}$  is replaced by a time shifted signal  $\alpha_{wing}(t - t_L)$  (see n° 2 of fig.32). In both cases,  $\alpha_{tail}$  cannot be used as a state variable of a linear mathematical model, so only identification methods of regression type can be used.

A linear model can be obtained by a Taylor-series expansion of  $\alpha_{wing}(t - t_L)$  (see n° 3 of fig.32). When doing so, two uncorrelated signals  $\alpha(t)$  and  $\dot{\alpha}(t)$  are obtained. But it is important to know, that this type of mathematical model is valid only in the low frequency regime. Especially in the case of quick flow deflection at the wing (flaps, gusts symmetric aileron, spoiler) the time lag of the downwash effect cannot be described by a Taylor-series of first order. It can be shown, that the relative error of the Taylor-series exceeds 10 %, when  $\omega > .45/t_L$ . As example, for a low speed model test with  $V = 30$  m/sec and a model with a 1 m distance from wing to tailplane,  $t_L$  is .033 sec and  $f_{limit} = 2.2$  Hz.

It is evident, that this type of mathematical model is not applicable in the case of tests with high frequency or step inputs. So, for the identification of the high frequency behaviour above the short period frequency (dynamic and transient effects, elastic modes, ...) the use of time shifted signals (n° 2 of fig. 32) gives more exact results than the Taylor-series expansion (n° 3). Fig. 33 shows a comparison of the outputs of two simulated models corresponding to these different formulations. From the curves it can be seen, that for higher input frequencies the model based on Taylor-series expansion gives no realistic time history of pitch acceleration and pitch rate.

## 2.2 - Input signals - Simulation and sensitivity tests.

### 2.2.1 - Nature of inputs - Classification - Frequency domain.

#### 2.2.1.1 - Scheme.

Fig.34 proposes a classification of different inputs (external-, internal-, combined inputs) that may be used for 2 or 3 dimensional-, stationary or non stationary-, free flight or semi free flight tests. These inputs may be discrete, harmonic or stochastic.

#### 2.2.1.2 - Nature of inputs.

It has been shown in lecture 3 (Ref.10) of this series, that the choice of input signals is of great importance for the identifiability of the aircraft parameters. Therefore, practical test design should include always the choice of input type and signal shape as well as a carefully performed definition of amplitude- and time scaling characteristics.

Fig.35 shows some examples of input types applicable in free and semi-free model testing. For parameter estimation, signals with large bandwidth should be applied, e.g. the multistep signal shown in this figure. (The properties of this signal type are discussed in detail within lecture 3). Harmonic and stochastic signals are only restrictively applicable in free flight tests due to their short duration. Used in semi-free flight tests, they lead to very long test and evaluation times.

As another type of input, initial conditions can be chosen so that the aircraft's natural modes are excited. They can be combined to control inputs in flight. In the case of free flight, initial values of angle of attack, speed, flight path angle ... or deviations of the mass, c.g.location ... can be applied.

Initial condition values and control input characteristics can be optimized by numerical methods. For practical work sensitivity tests can be performed to get an insight into the relationships between input signal characteristics, system behaviour and parameter identifiability. Two examples of sensitivity tests are given later on — the first performed in the time domain and the second one in frequency domain.

### 2.2.2 - Sensitivity tests.

#### 2.2.2.1 - Sensitivity tests in time domain.

Sensitivity tests are performed with simulations in the time domain. The purpose is to contribute to define an efficient set of tests for identification.

The sensitivity study was carried out on the quasi-stationary model described previously.

For a successive variation of each coefficient  $P_i$  ( $C_{z\dot{x}}$ ,  $C_{z\dot{y}}$ ,  $C_{zq}$ ,  $C_{m\dot{x}}$  ... of 20 % we examine the relative deviation  $\Delta j/j$  for  $j = V, \alpha, q, \theta$ . For each type of input we compare the  $\Delta j/j$  obtained with each parameter. To make the comparison easier, we define a criterion

$$\Delta_i = \frac{\sum_{j=V, \alpha, q, \theta} \frac{\Delta j}{j}}{\sum_{i=1}^n \left( \sum_{j=V, \alpha, q, \theta} \frac{\Delta j}{j} \right) P_i}$$

The results are given in fig.36 for some of the possible input combinations.

Derivatives such as  $C_{x\dot{v}}$ ,  $C_{z\dot{v}}$ ,  $C_{x\dot{\alpha}}$ ,  $C_{x\dot{\delta}_m}$  and  $C_{z\dot{\delta}_m}$  which are not shown in the table are negligible, whatever input is being considered. From these results we can draw out a test protocol for the identification of the derivatives of longitudinal dynamic stability based on 5 kinds of flights ( $\Delta \ddot{z}$ ,  $\Delta \ddot{z} + \Delta \ddot{\theta}$ ,  $\Delta \ddot{z} + \Delta \alpha$ ,  $\Delta \ddot{z} + \Delta \delta_m$ , reference flight).

A much more effective sensitivity test is going to be adjusted. It is a general simulation of the identification process (see fig.37). In this case, the test protocol that is to be defined, depends on the cost function and on the algorithm used for its minimization. For example, it has been developed a conjugated gradient method to minimize the output error for many tests kept all together in the same process.

With the best known aerodynamic coefficients, we simulate a lot of various tests (28) which are now considered as experiments. We know the maximum of error we may have made in the estimation of the aerodynamic coefficients and we employ those values to start the identification process because we need an initial vector of unknowns.

Obviously, the more the tests are numerous, the more the identification is accurate. But the aim is to reduce the number of flights to be performed as far as possible. We are helped in this purpose by some outputs of the program that give us for any iteration, for any flight and any unknown parameter, the contribution to the gradient and each flight contribution to the cost function. The final result of the process is the definition of the number and characteristics of the flights we have to perform.

#### 2.2.2.2 - Sensitivity tests in frequency domain.

Such tests contribute also to define the kinds of tests to be performed. A method used by DFVLR is already described in paper 3 Ref.10 of this lecture series. This method gives for each derivative an illustration of its contribution to the measured forces or moments over the frequency of the input signal. From this, it can be decided 1.) whether a parameter has to be identified or to be neglected in the mathematical model and 2.) which is the best input frequency or frequency range. Fig.38 shows, as example, the Bode plots of the pitch equation terms of ATA free flight model. It can be seen, that the best frequency for identifying  $C_{m\dot{x}}$ ,  $C_{mq}$  and  $C_{m\dot{\delta}_e}$  is the S.P.O. frequency. Because a narrow band input is not sufficient for identifying more than two derivatives of the pitch equation, a signal with a large bandwidth should be applied. In semi-free tests, for a given input signal shape (step, doublet, multistep,...) the time scaling can be defined in such a way that the maximum of the input power spectrum is lying near the S.P.O. frequency. In free flight tests, the lowest applicable input frequency is given by  $1/T$  ( $T$  = duration of free flight phase) and is closed to the S.P.O. frequency. In this case, the best way to excite the short period oscillation is to use an initial condition input  $\Delta \alpha(0) \neq 0$ . Fig.39 shows the possibility of combining initial condition inputs with in flight control inputs. These input combinations give information as well for identification of stationary and dynamic derivatives as for investigation of high frequency behaviour of the aircraft (unstationary and transient effects, elastic modes, ...)

### 2.3 - Examples of test design for longitudinal identification of DO 28 TNT

#### 2.3.1 - DO 28 TNT semi free flight test procedure (DFVLR)

Fig.40 shows the procedure for semi-free model tests for parameter identification using onboard control and gust inputs. Before aircraft model identification, preliminary tests are performed (determination

of the characteristics of wind tunnel flow field, frame influence, gust wave propagation,  $\alpha$  - transducers etc). With the model fixed at c.g. and spring mounted at the tail, free oscillation tests without wind for determination of actual moment of inertia can be done. With the model fixed at c.g. and/or tail, aerodynamic forces due to gust or onboard control inputs can be measured directly by strain gages. As the last tests, semi-free flight manoeuvres with different input types on the gust generator and the onboard controls are performed.

As an example of test design fig.41 shows results for different input signal types applied on elevator. For evaluation, the three tests are combined to obtain one set of derivatives representative for a wide range of input types and frequencies. It can be seen, that the output information contents are quite different. The third signal (3.2.1.1 multistep signal) produces more information in the pitch response (high amplitude and long duration) than the other two conventional inputs.

### 2.3.2 - DO 28 TNT free flight test program at IMFL

#### 2.3.2.1 - Determination of the reference flight.

We have the choice for the initial angle of attack and the whole configuration. Then from the  $C_z$ ,  $C_m$ ,  $C_x$  curves obtained in wind-tunnel we find  $\delta m_0$  ( $C_m = 0$ ) and at last  $C_{x0}$  and  $C_{z0}$  that induce the glide path :

$$\gamma_0 = -\arctan \frac{C_{x0}}{C_{z0}} \quad \text{and the velocity} \quad V_0 = \sqrt{\frac{2m \cdot g \cos \gamma_0}{\rho_0 S C_{z0}}}$$

All this values allow us to determine the characteristics of the facilities (catapult length and height, air pressure in the jack ...). The steady permanent flight is obtained by a flight adjustment procedure.

#### 2.3.2.2 - Design of the flights with steps.

From the sensitivity tests we choose four flights :

- 1 -  $\Delta M + \Delta \delta_z$  (weight increasing at I.C. and lift increasing during the flight)
- 2 -  $\Delta M + \Delta CG + \Delta \delta_m$  (weight increasing and C.G. displacement at I.C. and step of the elevator in flight)
- 3 -  $\Delta M + \Delta \theta + \Delta \delta_m$
- 4 -  $\Delta M + \Delta CG + \Delta \theta + \Delta \delta_z$

As the simulation system is linear we simulate 5 different steps :  $\Delta M$ ,  $\Delta CG$ ,  $\Delta \theta$ ,  $\Delta \delta_m$ ,  $\Delta \delta_z$  and afterwards we determine the maximum step amplitudes that keep the model safe and out of the ground effect.

The simulations of the designed tests are shown fig.42.

#### 2.3.2.3. - Free flight procedure.

As example we shortly describe the DO 28 TNT free flight procedure (details in Ref.9). The model is unmoved under the catapult. Its instrumentation is supplied with external current. There are three accelerometers, three gyrometers, three pressure transducers, six electric actuators and their potentiometers for position information, a photocell, the P.C.M. codeur, the transmitter and of course batteries.

The on-ground computer is ready to collect the data. All the on-ground system is preprogrammed. When starting the test, a flash operates and commutes through a photocell the whole on-board system. All data from on board transducers are collected. The lens of the ground based cameras are opened and the model light spots are turned on. After half a second, the mock-up is moving under the catapult and just after the release the optic barriers measure the initial velocity. Passing the cameras, the model light spots produce trails on the negatives. Furthermore the space-time synchronisation system (flasches and photocell tops) will determine the times of the events.

## 3 - DATA PROCESSING AND EVALUATION METHODS.-

### 3.1 - Data acquisition.

On board data digitalisation is performed with a 150 kb frequency. In each P.C.M. cycle two key words are checked by the computer for synchronisation. Indeed it sometimes happens that a cycle isn't well transmitted or is even lost. This cycle isn't taken in account and the computer has to decide when the transmission is good again. We exactly know the time of each cycle transmission owing to an on-board cycles counter whose value is transmitted inside each cycle.

At a 150 kb frequency with two subcycles we collect 781 values/sec/parameter. The bandwidth (about 260 hz) is thus sufficient to describe the transient and non-stationary phenomena.

### 3.2 - State vector evaluation and filtering aspects.

#### 3.2.1 - State vector evaluation.

Two main programmes are implemented to process the data relating to the flight (see fig.43).

. The trajectography programme processes the spatial traces of the model references obtained by the optical recordings made on bases. It uses 48 measuring points per base to work out a set of characteristic values for a given position of the model. Linearisation by least squares on each spatial trace is performed and a coherence test for the data is drawn up using the criteria of the geometrical positioning of the optical references in the model centerlines. For each base we therefore obtain the Euler angles and the coordinates of the center of gravity ( $\psi$ ,  $\theta$ ,  $\phi$ ,  $X_G$ ,  $Y_G$ ,  $Z_G$ ) in addition to the coordinates for the spatial glide path.

. The processing programme for the dynamic recordings processes on about 40,000 values. It operates on the values obtained by the difference between the free flight and the reference values recorded immediately before the launching. The first set of initial conditions is determined either by direct measurements (instant values supplied by the transducers at the time of release) or by independent measurements such as glide path, attitude, initial velocity, etc ...

For each PCM sub-cycle (1.28 ms) the following magnitudes are restituted or visualized  $\psi$ ,  $\theta$ ,  $\phi$ ,  $X_G$ ,  $Y_G$ ,  $Z_G$  (t) and their derivatives,  $V$ ,  $\alpha$ ,  $\beta$ , control surface positions, data relating to the tail plane.

. The results obtained from both independent data sources are then used in a validation test and for final adjustment of the initial flight conditions. In actual fact, the trajectographic data remain the most accurate, enabling correlation to be made with the integrated dynamic data. The flights are validated when, for each of the variables, the value occurs inside "precision tubes" defined by the geometric accuracy of the data. A least square is implemented to deal with the various optical bases. The adjustments are made on the initial flight conditions ( $\psi_0$ ,  $\theta_0$ ,  $\phi_0$ ,  $X_{G0}$ ,  $Y_{G0}$ ,  $Z_{G0}$ , first and second derivatives) taking into account the confidence in each measured parameter.

This flight validation procedure therefore specifies the initial conditions and enables full use to be made of the flights there after : working out of the state vector and its derivatives in particular. Checks on the passing times through the velocity measuring barriers check the release abscissa and the space-time synchronisation.

The means taken as a whole allow us to validate flights in a laboratory over distances of about 50 m inside "precision tubes" with geometric magnitudes  $X$ ,  $Y$ ,  $Z$  of 0.01 m and 0.1° on attitudes.

The quality of the information for accelerations and angular and linear velocities is therefore particularly precious for the aerodynamic exploitation of the flights.

During the same computer restitution program, these various elaborated data are projected into flight-path axis system.

#### 3.2.2 - Filtering aspects.

Three examples of filters are shown on fig. 44 :

- First order filter : to remove from the dynamic data the residual structural noise (above 20 Hz) associated with release, a reverse-direct digital first order filter is implemented. It allows us to precisely determine the initial dynamic conditions ; this filter is not use when transient or non stationary effects are concerned.

- Polynomial filter is an interactive software mostly used to process the flights with high frequency inputs. In this method, a succession of polynomials approximates the experimental curve. Then the first order filter is implemented to treat the difference between the experimental curve and the polynomial curve.

- F.F.T. filter : in this method, the signal is decomposed into Fourier Series by a fast Fourier transform method. The coefficients related to the perturbing frequencies are set equal to zero. Then the signal is recomposed. Let us notice (fig.45) that the method is very efficient for cyclic applications but it induces non physical perturbations for the other applications (fig.44).

### 3.3 - Evaluation methods.

#### 3.3.1 - Preliminary identification at IMFL

##### 3.3.1.1 - Stationary coefficients.

The determination of stationary characteristics from free flights are obtained through a flight adjustment procedure. The preliminary aerodynamic data, wherever they come from, are not sufficiently rigorous to determine a permanent flight over 200 chords at set trim. An adjustment phase for stabilized symmetrical flights is undertaken according to the procedure outlined in fig.46.

The initial conditions ( $\Delta V_0, \Delta \alpha_0, \Delta \delta_{mo} \dots$ ) required to obtain a permanent flight are adjusted by the digital simulator on the basis of the information obtained during the previous flight. When the permanent flight is established (each variable remaining stable inside the defined "precision tubes") balanced aerodynamic characteristics of the model are obtained with great accuracy.

### 3.3.1.2 - Identification of the longitudinal derivatives.

For the identification, the system  $\dot{CX} = AX + BU$  shown on fig.47 is written in the form  $0 = AX - CX + BU$

By replacing the simulated values  $X$  and  $\dot{X}$  with the experimental values, the first member will no longer be void and we can then write

$$E = MY$$

where  $M$  is the matrix composed of the combined matrixes  $[A \quad -C \quad B]$  and  $Y^T$  the vector composed of the combined vectors  $[X^T \quad \dot{X}^T \quad U^T]$

the vector  $E$  is an error vector with 4 parts and we can reduce to the minimum  $\sum_{k=1}^n (E_k^2)$  line by line using the least squares method.

A principle used in this IMFL identification system is the simultaneous use of the greatest possible number of tests and the use of the elaborated state vector and derivatives in the criterion. It was demonstrate as very efficient.

Fig.48 shows the overall identification results achieved with this method.

For 6 different flights we obtain a good general agreement with the identified set of coefficient.

It must be pointed out that for these tests we produced low amplitude motion. While remaining coherent with the model hypotheses, more marked steps will allow us to perfect the definition of the parameters looked for.

### 3.3.2 - Definition of the evaluation method used at DFVLR.

A schematic of the main evaluation method is given in fig.49. Based on this method, a computing program was developed by DFVLR, which has a high adaptability to different field of applications and different model structure definitions. Some special features of this computing program are listed in fig.50. The program can be used for equation error regression, output error regression (weighted least squares) or maximum-likelihood estimation. Because model definition can be changed during calculation, the evaluation can be started in the output error regression mode without any knowledge of a-priori-information and finished in the maximum-likelihood-mode. Using a subroutine for the calculation of non-linear functions of measured input- and output signals, also non-linear terms in the mathematical model can be taken into account. In this way, the different model types A, B, C and D from fig.28 could be identified using the same computing program.

In identification from ATA free flight experiments, seven selected flight tests were combined in one identification run.

Fig.51 shows the final identification result for the pitch-degree-of-freedom part of model C from fig.28 such good curve fittings were obtained also for the others degree of freedom (fig. 52-53).

Fig. 54 gives a comparison with the results obtained from the preliminary evaluation and for varied a-priori-values of  $C_{Z\dot{\alpha}}$  and  $C_{m\dot{\alpha}}$ . A comparison of results from different static and dynamic techniques and evaluation methods applied to DO 28 TNT-model is given in fig.55.

## 4 - CONCLUSION.-

A large variety of methods and techniques are now available for the determination of aircraft dynamic stability parameters. The question is to satisfy the requirements dictated by the new flight domain considered.

The most usual methods based on captive model tests in wind tunnels, mainly progress in the field of : type and number of the informations collected during the experiments, data acquisition, elaboration of the dynamic components, filtering aspects, extension to the other methods ...

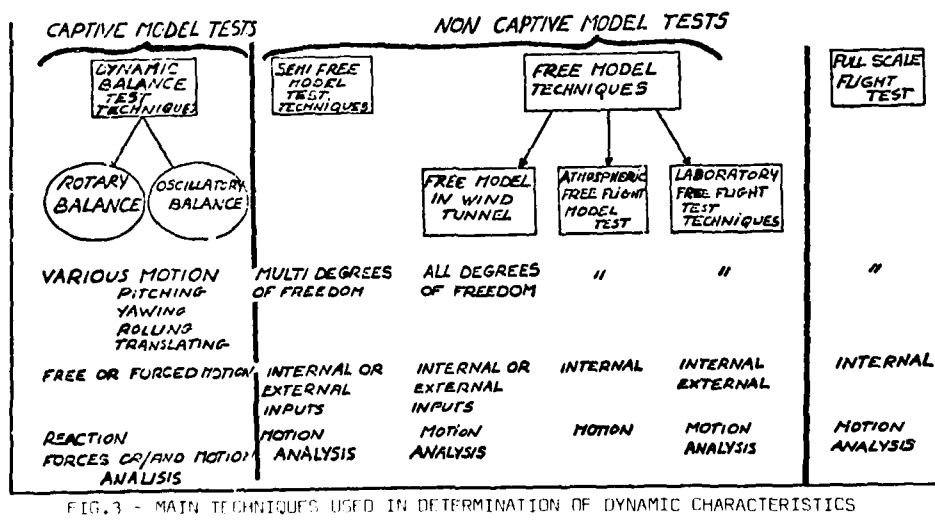
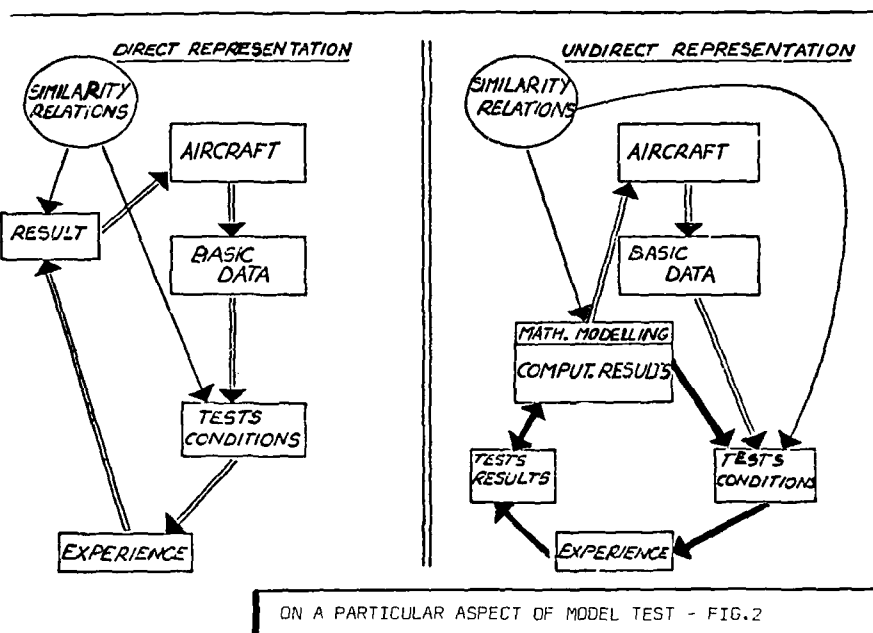
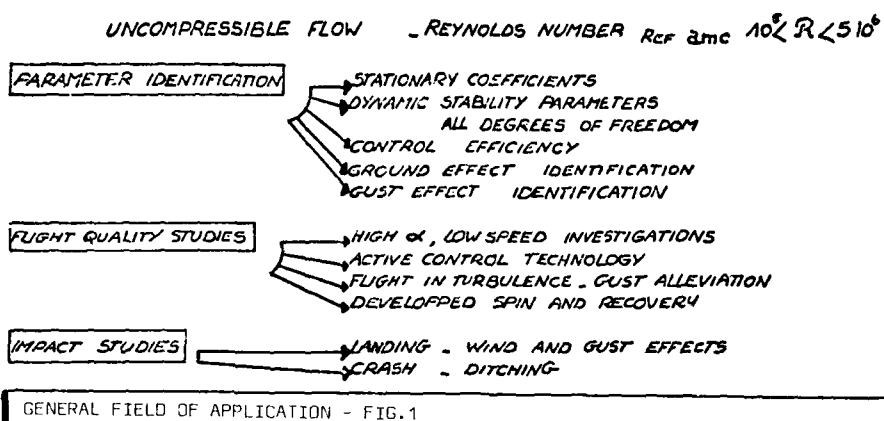
Other methods based on semi-free models in wind tunnel or free models in laboratory are also available in this field. Accurate quantitative results can be obtained by the application of parameter identification methods, which have recently been introduced. These methods are presently extended to the determination of lift and lift control and are flexible enough to

be applied to what would be the mathematical model of the whole aircraft for the whole



## REFERENCES

- (1) Techniques for dynamic stability testing in wind tunnels  
K.J. ORLIK RUCKEMANN - NAE - NRC Canada  
AGARD C.P. 235, 1978
- (2) Nouvelle methode de mesure de forces aerodynamiques  
F. GAIGNEBET  
A.A.A.F. Novembre 1977
- (3) Wind tunnel testing of dynamic derivatives in W.Germany  
X. HAFFER  
AGARD C.P. 235, 1978
- (4) On the test procedures of the derivative balances used in W.Germany  
J. von der DECKEN - F. SCHMIDT - B. SCHULZE  
AGARD C.P. 235, 1978
- (5) Aerodynamic characteristics of fighter configurations during spin entries and developed spins  
E. ANGLIN - NASA Langley  
J.Aircraft vol 15 n° 11, November 1978
- (6) Rotary balance of IMFL and associated experimental techniques  
R.A. VERBRUGGE  
A.A.A.F. 1979 (In preparation Available Dec. 79)
- (7) A wind tunnel technique for determining stability derivatives from cable mounted aeroelastic models  
Robert M. BENNET - Moses G. FARMER - NASA Langley  
A.I.A.A. Flight Mechanics Conference, August 8-10, 1977
- (8) Wind tunnel free flight investigation of a model of a spin resistant fighter aircraft  
S.B. GRAFTON - J.R. CHAMBERS - P.L. COE - NASA TN
- (9) Nouvelle technique d'essais sur maquettes libres pour la détermination de caracteristiques aérodynamiques  
W. CHARON - R.A. VERBRUGGE  
AGARD C.P. 235, 1978
- (10) Practical input signal design  
Dr E. PLAETSCHKE - DFVLR Braunschweig - LS 104
- (11) Filtre polynomial  
Manuels theoriques de programmation et d'utilisation  
W. CHARON - I.M.F.L. Février 1978
- (12) Méthode du gradient conjugué en identification en Mécanique du Vol  
W. CHARON - T. COTILLON - IMFL (rapport interne), Septembre 1978
- (13) Filtrage par transformée de Fourier rapide  
P. COTTON - IMFL, Février 1979
- (14) Programme de restitution tridimensionnelle du vol libre des maquettes  
W. CHARON - R. ARCZYNSKI - M. VANMANSART - IMFL (mis à jour, Août 1979)
- (15) Dépouillement de la trajectographie optique des vols libres  
W. CHARON - IMFL, Juin 1977
- (16) Ermittlung von dynamischen derivativen der längs- und seitenbewegung mit der mobilen oszillierenden derivativwaage und systematische untersuchungen zum einfluss einiger parameter auf die ergebnisse  
O. DETERMANN  
FGLR 78-115, 1978 - Jahrestagung der DGLR, Darmstadt, 19-23 September 1979
- (17) Die AVA-Derivativwaage  
E. SCHMIDT  
DLR-Mitt. 74-32, 1974
- (18) Test installations to investigate the dynamic behaviour of aircraft with scaled models in wind tunnels  
H. SUBKE  
Symposium "Dynamic Analysis of Vehicle Ride and Manoeuvring Characteristics,  
London 28-30 nov.78, preprint p.137-148
- (19) The wind tunnel behaviour of a scaled model with a gust alleviation system in a deterministic gust field  
B. KRAG - Symposium "Dynamic analysis of vehicle ride and manoeuvring characteristics,  
London 28-30 nov.78, preprint p.149-166
- (20) Dynamic wind tunnel simulation of active control systems  
P.G. HAMEL - B. KRAG  
AGARD Conference Proc. N° 260 Stability and Control, p. 16 A.1 - 16 A.10
- (21) Dynamic simulation in wind tunnels part.1  
H. HÖLTINGER - O. ENSBURG  
AGARD Conference Proc. N° 187 on Flight/Ground testing facilities correlation p. 5.1 - 5.27
- (22) Active Control Technology for Gust Alleviation  
B. KRAG  
v.Kaman Lecture Series "Active Control Technology" Brüssel, 4-8 December 1978



- EXTENSIVE DOMAIN OF  $Re$  OR  $M$  NUMBER
- EXTENSIVE DOMAIN OF ANGLE OF ATTACK AND SIDESLIP } NOT COMBINED  
(90°)
- SEPARATE MOTION OR COMBINED (3 D.O.F) POSSIBLE
- POSSIBILITY OF VARYING IN A LARGE RANGE REDUCED FREQUENCY AND AMPLITUDE INDEPENDENTLY { FORCED OSCILLATION  
WITH RIGID  
EXCITATION ONLY
- TEST WITH AERODYNAMIC INSTABILITIES
- CONTROLS INPUTS POSSIBLE
- EXTENSIVE INSTRUMENTATION { 5 OR 6 COMPONENTS BALANCE  
ACCELEROMETERS IN THE MODEL  
FREQUENCY - AMPLITUDE MEASUREMENTS  
- VISUALISATIONS  
PRESSURE DISTRIBUTION - etc ...
- GOOD ADAPTATION TO PARAMETRIC STUDIES
- WIND TUNNEL AND SUPPORT INTERFERENCE : AERODYNAMIC OR MECHANIC SENSITIVITY PROBLEMS
- NO SIMULATION OF FREE MOTION

FIG.4 - DYNAMIC BALANCE TEST TECHNIQUES MAIN CHARACTERISTICS

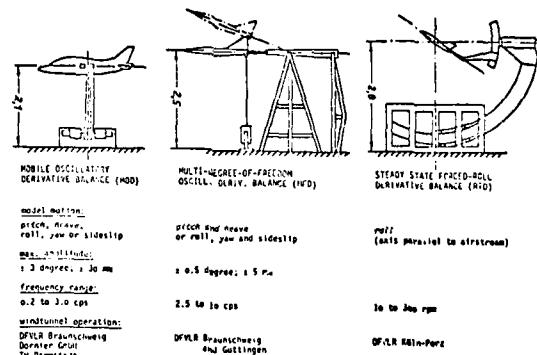


FIG.5 - EXAMPLES OF LOW-SPEED DERIVATIVE BALANCES

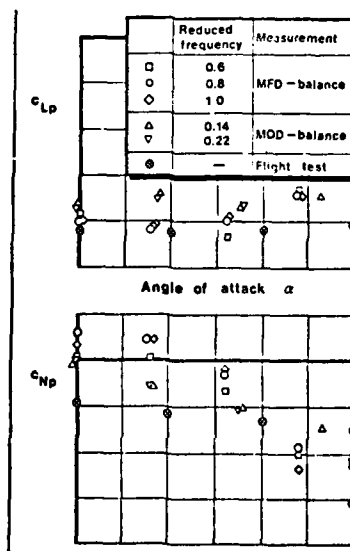
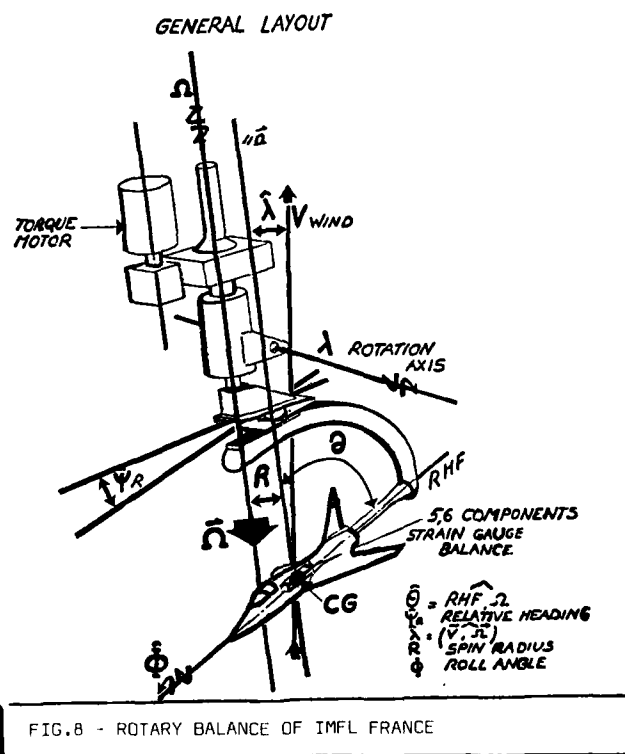
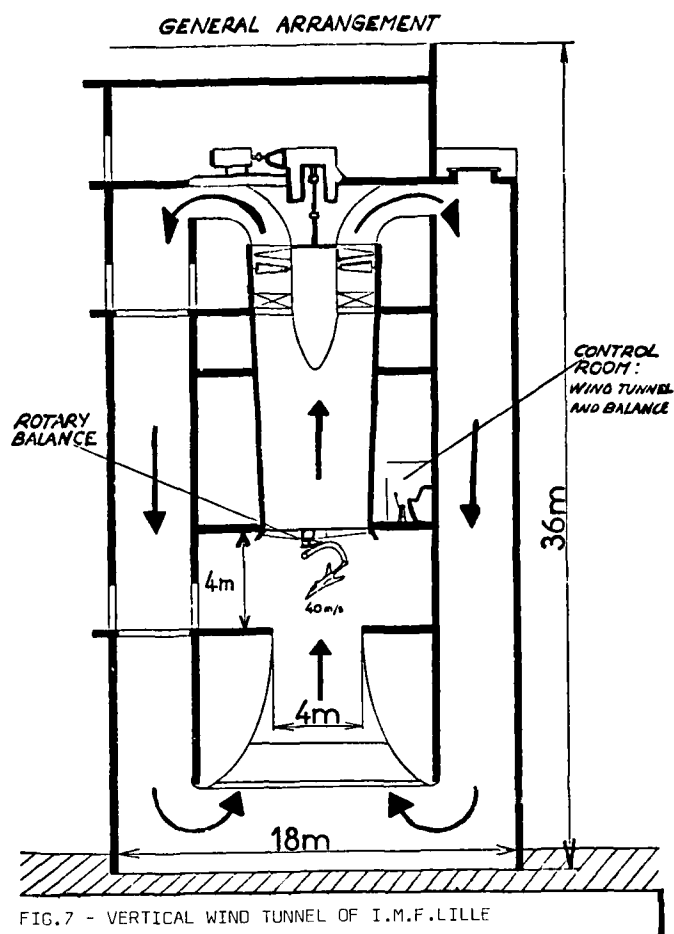


FIG.6 - CORRELATION OF RESULTS



## MAIN CHARACTERISTICS

PARAMETERS	DOMAIN	ADJUSTMENT		
		AUTO	WINDOW	RESOLUTION
V	40 m/s	x	x	CONTINUOUS
$\Omega$	$\pm 11$ rad/s	x	x	$.1^\circ/s$
$\lambda$	$\leq 30^\circ$	x	x	CONTINUOUS
$\theta$	0-45° 45-90°	x		$.1^\circ$
$\phi$	$\pm 180^\circ$	x	x	$.1^\circ$
R	.20 m	x		CONTINUOUS $10^{-3}$ m
$\gamma_R$	$\pm 180^\circ$			CONTINUOUS $.1^\circ$
MODEL MASS	< 50 kg			
MEAN SIZE	1.5 m			
CONTROL POSITION	-	x	x	

FIG. 9 - ROTARY BALANCE  
OF IMFL FRANCE

## COLLECTED INFORMATIONS

- ALL TEST PARAMETERS : DIRECT DIGITAL MEASUREMENT
- 5,6 COMPONENTS BALANCE
- 9 CHANNELS FOR ACCELEROMETERS
- PRESSURE MEASUREMENTS - LOCAL FORCES i.e. (FIN or ELEVATOR CONTROLS)
- FLOW VISUALISATION
- ALL DATA ON LINE DIGITALISED

30 CHANNELS  
WORDS 12 BITS  
200 HZ PER CHANNEL

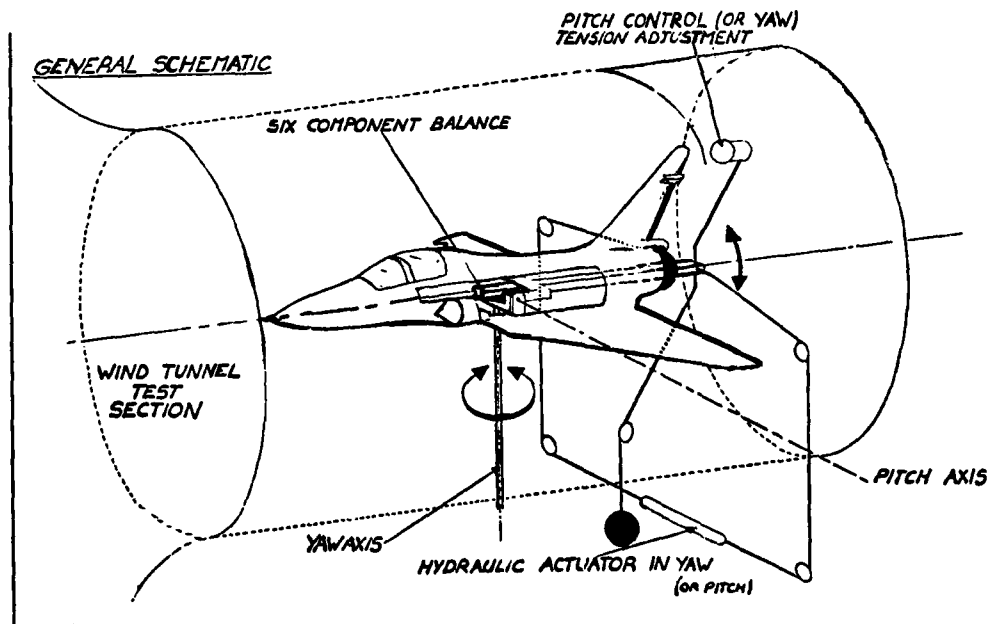


FIG.10 - LARGE AMPLITUDE MOTION DYNAMIC BALANCE

- WIDE RANGE POSSIBLE IN
  - { MACH AND REYNOLDS NUMBER
- USUAL FLIGHT ENVELOPPE ( $\alpha, \beta$ ) CAN BE INVESTIGATED
- NUMEROUS DEGREE OF FREEDOM REPRESENTED (4 to 5). GENERALLY LOW AMPLITUDE
- VARIOUS INPUTS POSSIBLE : EXTERNAL EXCITATION
  - CONTROL INPUTS
  - SIMULATION OF GUST OR GROUND EFFECT POSSIBLE
- IN BOARD OR GROUND BASED INSTRUMENTATION
- FLIGHT QUALITIES TEST PERFORMED
- APPLICATION OF PARAMETER IDENTIFICATION TECHNIQUES
- WIND TUNNEL AND SUPPORT INTERFERENCE (Aerodynamic-Mechanic)  
-Structural

FIG.11 - SEMI FREE MODEL TEST TECHNIQUES

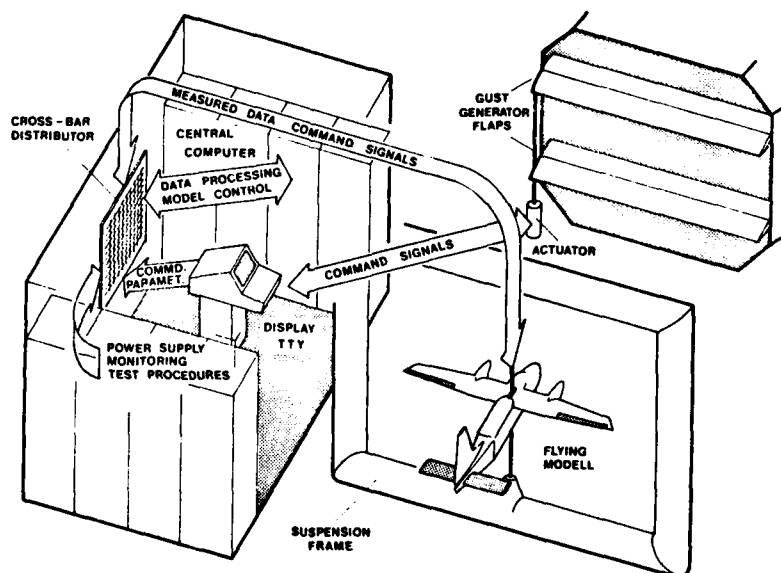


FIG.12 - GENERAL VIEW OF THE INSTALLATION FOR DYNAMIC SIMULATION IN WIND TUNNELS

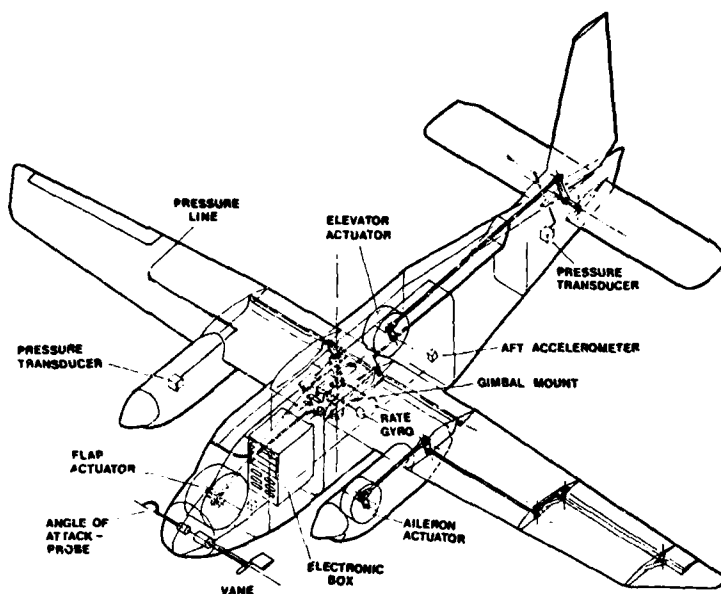


FIG.13 - DO 28 TNT WIND TUNNEL MODEL

DEGREES OF FREEDOM : PITCH, HEAVE, YAW, ROLL

V, Re : V UP TO 70 M/SEC, Re = .5 ...  $1 \times 10^6$

$\alpha$ -RANGE :  $\pm 2^\circ$  (GUST FLAPS)  
:  $\pm 10^\circ$  (PITCH MOTION)

Z-RANGE :  $\pm .5$  M

INPUTS ON : CONTROL SURFACES OF MODEL  
: GUST GENERATOR SYSTEM  
: WEIGHT REDUCTION SYSTEM

TYPE OF INPUTS : STEPS, STOCHASTIC, HARMONIC, ...

FREQUENCY RANGE : 0 - 12 Hz

(VALUES ARE GIVEN FOR 3-M WIND TUNNEL OF DFVLR)

FIG. 15 - CHARACTERISTICS OF DFVLR SEMI-FREE TEST TECHNIQUE

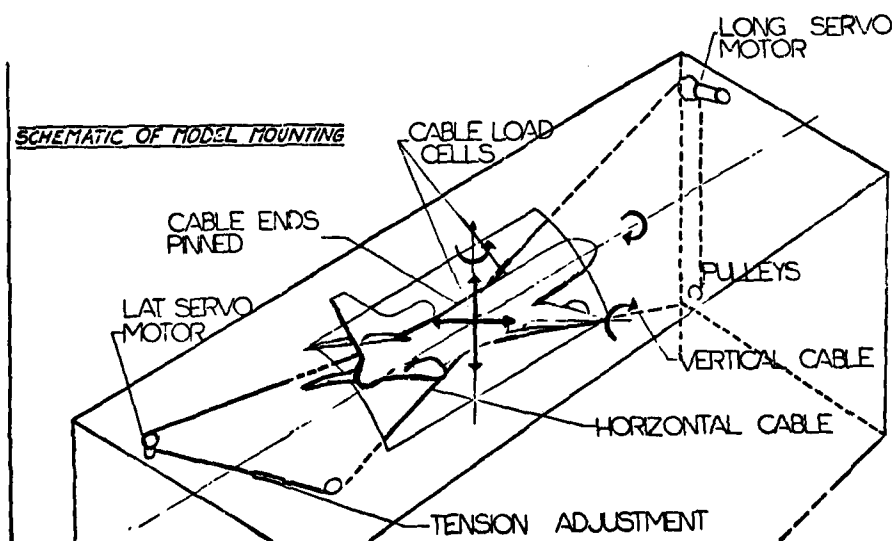


FIG.16 - SEMI-FREE FLIGHT SIMULATION IN TRANSONIC WIND TUNNEL (NASA LANGLEY from REF. 7)

EXAMPLE OF RESULTS (FROM REF 7) F14  
PARAMETER VALUE (STANDARD DEVIATION)

PARAMETER	INITIAL ESTIMATES	IDENTIFICATION RESULT FROM LOW AND HIGH FREQUENCY EXCITATION
$C_{Z\alpha}$	-5.88	-5.51(.013)
$C_{m\alpha}$	-2.87	-2.92(.0062)
$C_{mq} + C_{m\dot{\alpha}}$	-24.5	-14.8(.20)
$C_{Y\beta}$	-1.06	-.827(.020)
$C_{l\beta}$	-.077	-.028(.0006)
$C_{l\dot{\beta}}$	-.186	-.174(.0027)
$C_{n\beta}$	.15	.088(.0027)
$C_{n\dot{\beta}}$	-.123	-.473(.072)

FIG. 17 - SEMI FREE FLIGHT SIMULATION NASA LANGLEY

- ALL DEGREES OF FREEDOM COMBINED
  - SOME ADVANTAGES OF THE WIND-TUNNEL CAN BE KEPT UP
  - REDUCED OR NON EXISTING MECHANICAL INTERFERENCE DURING THE FLIGHT
  - FLIGHT ENVELOPE INCLUDING HIGH  $\alpha$ . DOMAIN
  - FLIGHT QUALITIES OR PILOT TEST CAN BE PERFORMED
  - COMPLEXITY OF THE TECHNIQUE : INSTRUMENTATION  
CONTROL OF THE MODEL (TIME SCALE)  
MOTION ANALYSIS ...
- ↑  
QUALITATIVE RESULTS  
EXPECTED

- WIND TUNNEL INTERFERENCE -

FIG. 18 - WIND TUNNEL FREE MODEL TEST TECHNIQUE

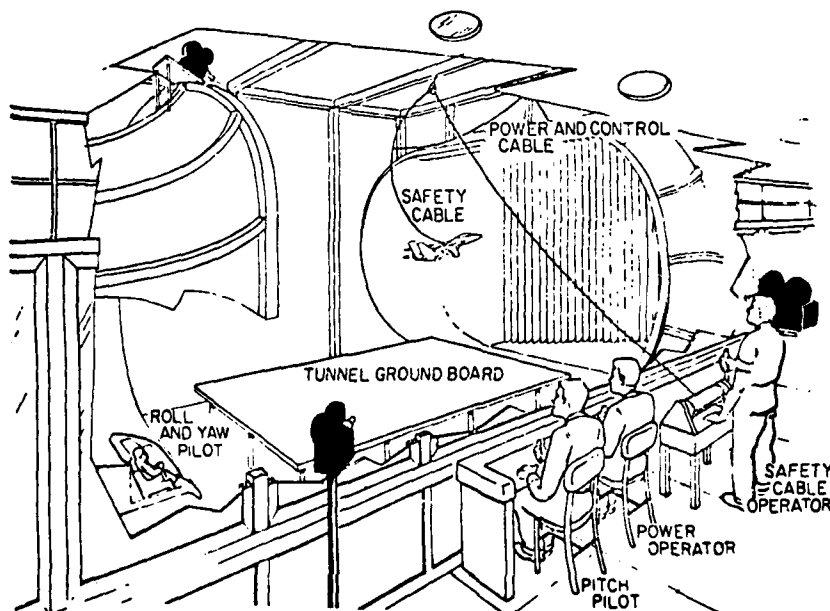


FIG. 19 - REMOTELY CONTROLLED FREE FLIGHT NASA LANGLEY



## SPECIFIC ASPECTS

- LOW SPEED TEST - REYNOLDS NUMBER IN THE RANGE OF  $10^6$  (on a.m.c)
- ALL DEGREES OF FREEDOM REPRESENTED
- WELL KNOWN ENVIRONMENT (LABORATORY CONDITIONS)
- HIGH ACCURACY IN MASS INERTIA AND STRUCTURAL CHARACTERISTICS OF THE MODEL
- FLIGHT ENVELOPE INCLUDING HIGH  $\alpha$  - POSTSTALL.
- LARGE DIVERSITY OF ACCURATELY CONTROL INPUTS
 

DEFINED INPUTS :	INITIAL CONDITION INPUTS	LONGITUDINAL OR
	EXTERNAL INPUTS	LATERAL GUST
		GROUND EFFECT
- EXTENSIVE INSTRUMENTATION
  - IN BOARD : GYROS, ACCELEROS, PRESSURE TRANSDUCERS:  $V, \alpha, \beta, \dots$
  - GROUND BASED : OPTICAL TRAJECTOGRAPHY SYSTEM,
  - IN BOARD OR GROUND BASED AUTOMATIC CONTROL LOOP
  - IN APPLICATION OF PARAMETER IDENTIFICATION TECHNIQUES
- SHORT DURATION OF THE TEST (5 TO 15 sec Full scale)
- WIDELY COMPLEMENTARY WITH LOW SPEED WIND-TUNNELS

FIG.20 - LABORATORY FREE FLIGHT MODEL TEST TECHNIQUE (I.M.F.LILLE)

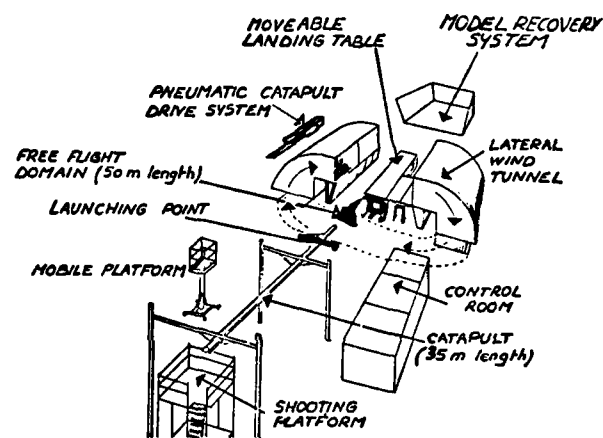


FIG.21 - GENERAL ARRANGEMENT OF FREE FLIGHT FACILITY (I.M.F.LILLE)

### GROUND EFFECT - LATERAL WIND or GUSTS TEST CONFIGURATION

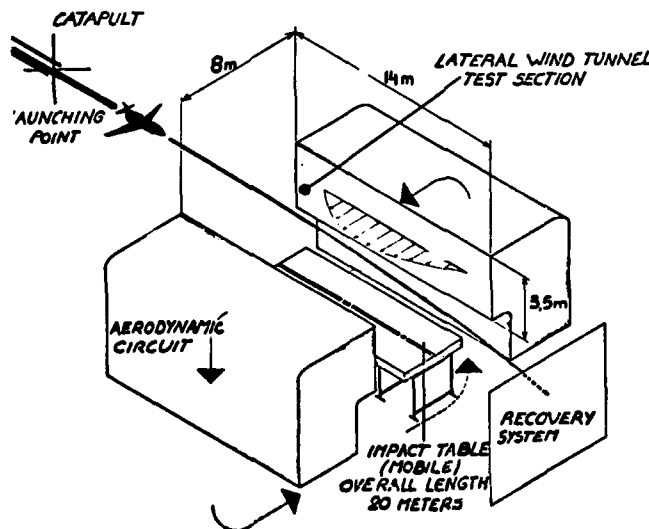


FIG.22 - FREE FLIGHT FACILITY (I.M.F.LILLE)

## VERTICAL GUSTS TESTS CONFIGURATION

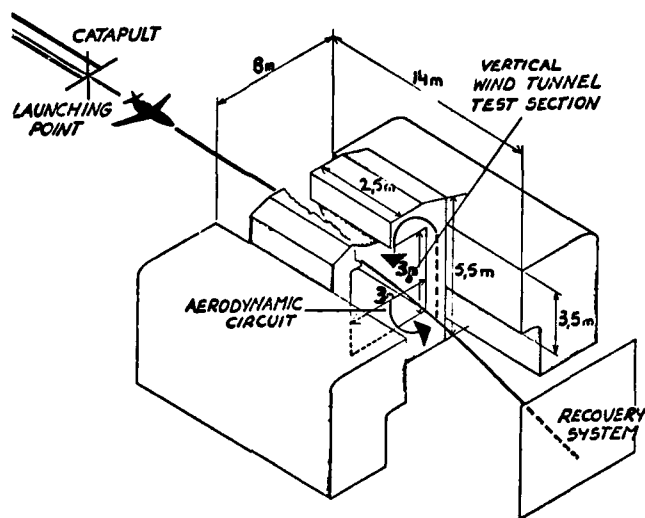


FIG.23 - FREE FLIGHT FACILITY (I.M.F.LILLE)

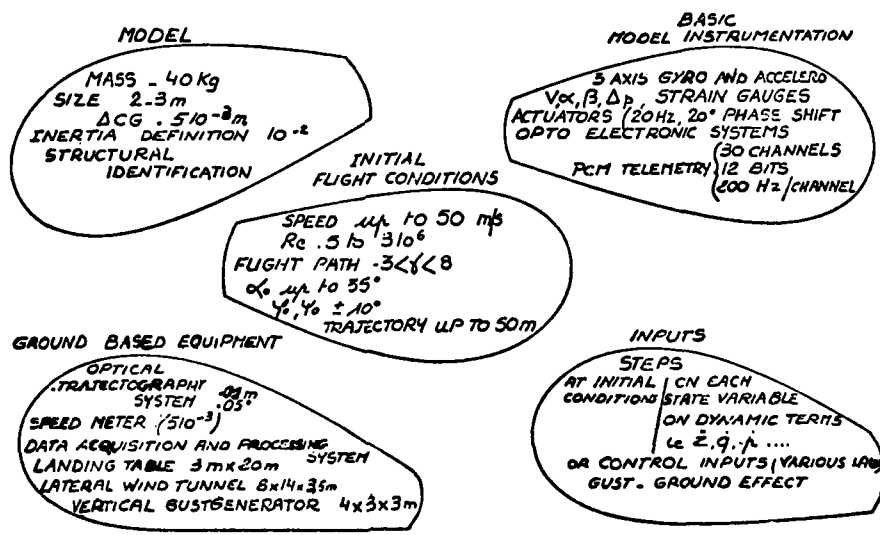


FIG.24 - I.M.F.L. FREE FLIGHT TEST TECHNIQUE MAIN SPECIFICATIONS

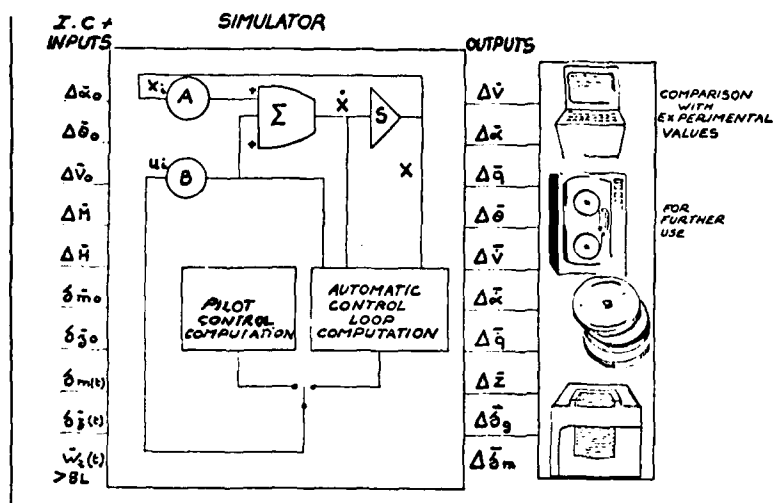


FIG. 25 - SIMULATOR DIAGRAM

## ACCEPTED FORM OF THE SYSTEM

$$\begin{aligned} \dot{X} &= \bar{A}X + \bar{B}u \\ X^T &= (\dot{V}, \dot{\alpha}, \dot{q}, \dot{\delta}) \\ u^T &= (\Delta \delta_m, \Delta \delta_z, \Delta \mu, \Delta \tilde{x}) \end{aligned}$$

$$\bar{A} = \begin{bmatrix} \frac{-2C_{x0}}{2\mu} & \frac{C_{z0} - C_{x0}\alpha}{2\mu} & 0 & -\frac{C_{z0}}{2\mu} \\ \frac{-2C_{z0}}{2\mu + C_{z0}\alpha} & \frac{-C_{z0}\alpha + C_{x0}}{2\mu + C_{z0}\alpha} & \frac{C_{z0}\tilde{q}}{2\mu + C_{z0}\alpha} & \frac{C_{x0}}{2\mu + C_{z0}\alpha} \\ \frac{-C_{m0}\alpha}{(2\mu + C_{z0}\alpha)\beta} & \frac{C_{m0}\alpha - C_{m0}\alpha + C_{x0}}{\beta(2\mu + C_{z0}\alpha)} & \frac{C_{m0}\tilde{q} + C_{m0}\tilde{q}}{\beta} & \frac{C_{m0}\tilde{q}}{\beta(2\mu + C_{z0}\alpha)} \\ 0 & 0 & 1 & 0 \end{bmatrix}$$

$$\bar{B} = \begin{bmatrix} -\frac{C_{x0}\delta_m}{2\mu} & -\frac{C_{x0}\delta_z}{2\mu} & \frac{g\ell \sin \delta_0}{2\mu V_0^2} & 0 \\ -\frac{C_{z0}\delta_m}{2\mu + C_{z0}\alpha} & -\frac{C_{z0}\delta_z}{2\mu + C_{z0}\alpha} & \frac{g\ell \cos \delta_0}{V_0^2(2\mu + C_{z0}\alpha)} & 0 \\ \frac{C_{m0}\delta_m - C_{m0}\alpha}{\beta(2\mu + C_{z0}\alpha)} & \frac{C_{m0}\delta_z - C_{m0}\alpha}{\beta(2\mu + C_{z0}\alpha)} & \frac{C_{m0}g\ell \cos \delta_0}{\beta V_0^2(2\mu + C_{z0}\alpha)} & \frac{C_{w0} \cos \theta_0}{\beta} \\ 0 & 0 & 0 & 0 \end{bmatrix}$$

FIG. 26 - SIMULATOR MODEL

Model	Curve fitting of signals	Identified parameters
A Equation - error regression	$\dot{u}, \dot{y}, \dot{q}$	10 derivatives: $C_{x\alpha}, C_{x\delta}, C_{z\alpha}, C_{z\delta}, C_{zq}, C_{z\dot{\alpha}}, C_{m\alpha}, C_{m\delta}, C_{mq}, C_{m\dot{\alpha}}$
B Output - error regression	$\dot{u}, u, \dot{y}, y, h, \dot{q}, q, \theta$	8 derivatives (without $C_{z\dot{\alpha}}$ and $C_{m\dot{\alpha}}$ ) + bias terms
C = model B plus dynamic flap derivatives	as model B	as model B plus $C_{z\delta}, C_{m\delta}$
D = model C plus nonlinear flap terms	as model B	as model C plus $C_{z\alpha\delta}, C_{m\alpha\delta}$

FIG. 28 - MATHEMATICAL MODELS FOR IDENTIFICATION

Part	Degree of freedom	Equations of motion	Measurement equations	Number of parameters to be identified		
				Derivatives	Constants $k_{ij}$	Total number
I	X	$\Delta \dot{u}_i = \{ \dots \} + k_{1i}$	$\Delta \dot{u} = \Delta \dot{u}_i + k_{2i}$ $\Delta u = \Delta u_i + k_{3i}$	$C_{x\alpha}, C_{x\delta}$ $\Rightarrow 2$	3 for each flight i $\Rightarrow 21$	23
II	Z	$\Delta \dot{y}_i = \{ \dots \} + k_{4i}$ $\Delta \dot{h}_i = \Delta y_i + k_{5i}$	$\Delta \dot{y} = \Delta \dot{y}_i + k_{6i}$ $\Delta y = \Delta y_i + k_{7i}$ $\Delta h = \Delta h_i + k_{8i}$	$C_{z\alpha}, C_{z\delta}, C_{zq}$ $\Rightarrow 3$	5 for each flight i $\Rightarrow 35$	38
III	M	$\Delta \dot{q}_i = \{ \dots \} + k_{9i}$ $\Delta \dot{\theta}_i = \Delta q_i + k_{10i}$	$\Delta \dot{q} = \Delta \dot{q}_i + k_{11i}$ $\Delta q = \Delta q_i + k_{12i}$ $\Delta \theta = \Delta \theta_i + k_{13i}$	$C_{m\alpha}, C_{m\delta}, C_{mq}$ $\Rightarrow 3$	5 for each flight i $\Rightarrow 35$	38
Total model B		5 differential equations	8 measurement equations	8	91	99

FIG.29 - EQUATIONS AND PARAMETERS OF MODEL B

- GEODETIC AXIS SYSTEM
- REDUCED NUMBER OF DEGREES OF FREEDOM (E.G. HEAVE AND PITCH ONLY)
- ADDITIONAL Z-FORCE FROM WEIGHT REDUCTION SYSTEM
- ADDITIONAL FORCES AND MOMENTS DUE TO CABLE CONNECTIONS
- INFLUENCE OF SUSPENSION FRAME ON  $\alpha$  ( $\partial \alpha / \partial x, \partial \alpha / \partial z, \dots$ )
- INPUT FROM GUST GENERATOR FLAPS AND WINDTUNNEL TURBULENCE
- TIME LAG AND AMPLITUDE RESPONSE OF  $\alpha_{\text{vane}}, \alpha_{\text{wing}}, \alpha_{\text{tail}}$  DUE TO  $\alpha_G$
- SPECIAL EQUATIONS, WHEN MODEL IS FIXED AT C.G. OR TAIL FOR DIRECT MEASUREMENT OF FORCES AND MOMENTS

FIG.30 - SPECIFIC CHARACTERISTICS OF MATHEMATICAL MODEL FOR SEMI-FREE TEST TECHNIQUE

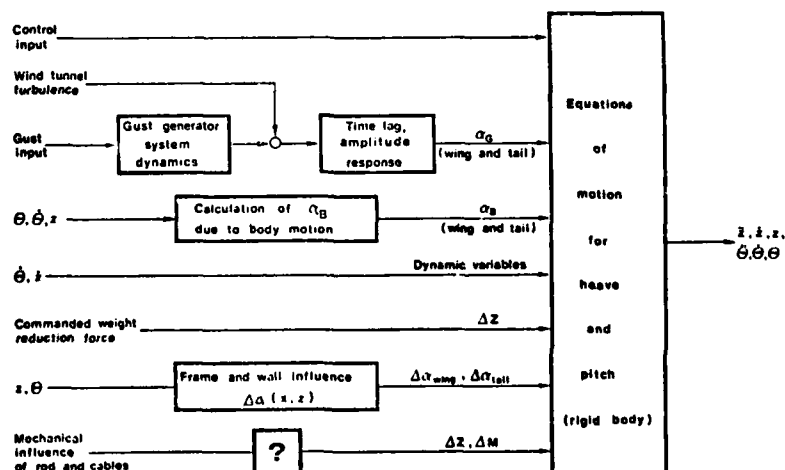


FIG.31 - EXAMPLE OF MATHEMATICAL MODEL FOR SEMI FREE FLIGHT

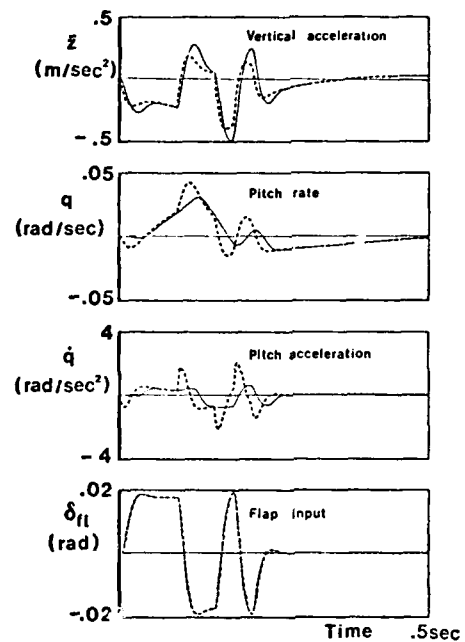
## 1) SEPARATE DERIVATIVES FOR WING AND TAIL

E.G.  $C_{Z\text{wing}} \cdot C_{Z\text{tail}}$ PROBLEMS: • MEASUREMENT OF  $\alpha_{\text{tail}}$ •  $\alpha_{\text{wing}}, \alpha_{\text{tail}}$  CORRELATED FOR  $\omega \rightarrow 0$ 2) CALCULATION OF  $\alpha_{\text{tail}}$  BY TIME SHIFTING OF  $\alpha_{\text{wing}}$ 

$$\alpha_{\text{tail}}(t) = \alpha_{\text{wing}}(t - t_L) + \frac{\partial \alpha_{\text{tail}}}{\partial C_{Z\text{wing}}} \Delta C_{Z\text{wing}}(t - t_L) + d\alpha_{\text{tail}}(q)$$

PROBLEMS: • NONLINEAR MODEL WITH TIME LAG  $t_L$ •  $\frac{\partial \alpha_{\text{tail}}}{\partial C_{Z\text{wing}}}$  AS UNKNOWN PARAMETER•  $\alpha(t), \alpha(t - t_L)$  CORRELATED FOR  $\omega \rightarrow 0$ 3) CALCULATION OF  $\alpha(t - t_L)$  BY FOURIER SERIES EXPANSION

$$\alpha(t - t_L) \approx \alpha(t) - t_L \dot{\alpha}(t)$$

PROBLEMS: • MODEL LINEAR, BUT NOT VALID FOR  $\omega t_L > 0.45$ • MODEL NOT APPLICABLE FOR STEP INPUTS ON WING  
CONTROLS WITH LARGE  $\Delta C_L$  (FLAPS, SYN. ALLERON, ...)FIG.32 - PROBLEMS OF MODELISATION  
OF WING AND TAIL CONTRIBUTIONS

--- Model with simulated time lag for downwash effects  
 — Model with  $\dot{\alpha}, \dot{\delta}$  - derivatives  
 (Fourier series expansion of time lag effect)

FIG.33 - SIMULATION RESULT FROM  
2 MODELS

	DIM 2, 3	INPUTS			
		STATIONARY Y N	TYPE (*) SI H ST		
EXTERNAL INPUTS	GUSTS	SIDE VERTICAL	I	I	I
			I	I	I
			I	I	I
INTERNAL INPUTS	DEFLECTION CONTROL IN FLIGHT	INITIAL CONDITIONS FOR STATE VECTOR	I	I	I
			I	I	I
			I	I	I
			I	I	I
			I	I	I
COMBINED INPUTS			I	I	I
			I	I	I

(\*) SI: SINGLE - H: HARMONIC - ST: STOCHASTIC

I: IMFL FREE FLIGHT

D: DFVLR SEMI FREE FLIGHT

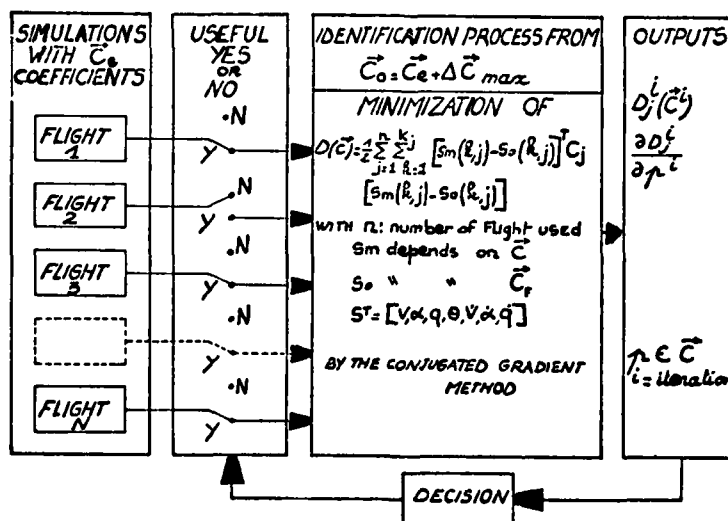
FIG.34 - INPUT MATRIX FOR IMPL

Type	Signal form	Remarks	Application in free(F)/semi-free(S) model flight
Discrete	or	Less information in 1 test	F, (S)
		Small bandwidth	F, (S)
		Large bandwidth, useful signal for identification	F, S
	1-cos cut	Small bandwidth, MIL-gust-input	F, S
Harmonic		Very small bandwidth, signal for frequency response test, very long test time	S
Stochastic		Signal for statistical evaluation (e.g. of response on v, Karman gust spectrum), long test time	S

FIG.35 - TYPE OF INPUTS

$$\frac{(\sum_{j=1}^n \frac{\Delta j}{J}) \rho_L}{(\sum_{i=1}^n (\sum_{j=1}^n \frac{\Delta j}{J}) \rho_L)} \quad \text{CRITERION}$$

COEFFICIENTS INPUTS	$C_{Z\alpha}$	$C_{Z\alpha}$	$C_{Zq}$	$C_{m\alpha}$	$C_{m\alpha}$	$C_{mq}$	$C_{x\alpha}$
$\Delta CG (2\%)$	35	0,1	1,3	44	2	13	5
CONTROL SURFACE (1')	35	0,0	1,2	44	2	12	6
$\Delta\alpha (1')$	28	0,5	1,8	38	11	19	3
MASS (7%)	23	0,1	(24)	36	3	(34)	3
$\Delta CG + \Delta\alpha$	37	0,1	0,8	46	3	9	6
$\Delta CG$ CONTROL SURFACE	36	0,1	1,1	44	2	11	5
$\Delta CG + MASS$	(42)	0,1	0,4	44	2	4	9
CONTROL SURFACE + $\Delta\alpha$	33	0,2	1,4	42	4	14	5
CONTROL SURFACE + MASS	32	0,1	0,9	(50)	2	8	8
$\Delta\alpha + MASS$	24	(05)	1,7	39	(13)	22	1

FIG.36 - SENSITIVITY TESTS  
IN TIME DOMAINFIG.37 - IDENTIFICATION  
SIMULATION PROCESS

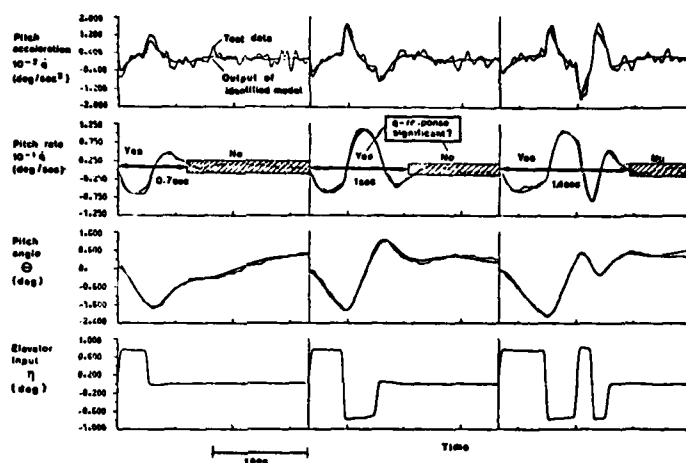


FIG.41 - DIFFERENT INPUT SIGNALS IN SEMI-FREE MODEL IDENTIFICATION

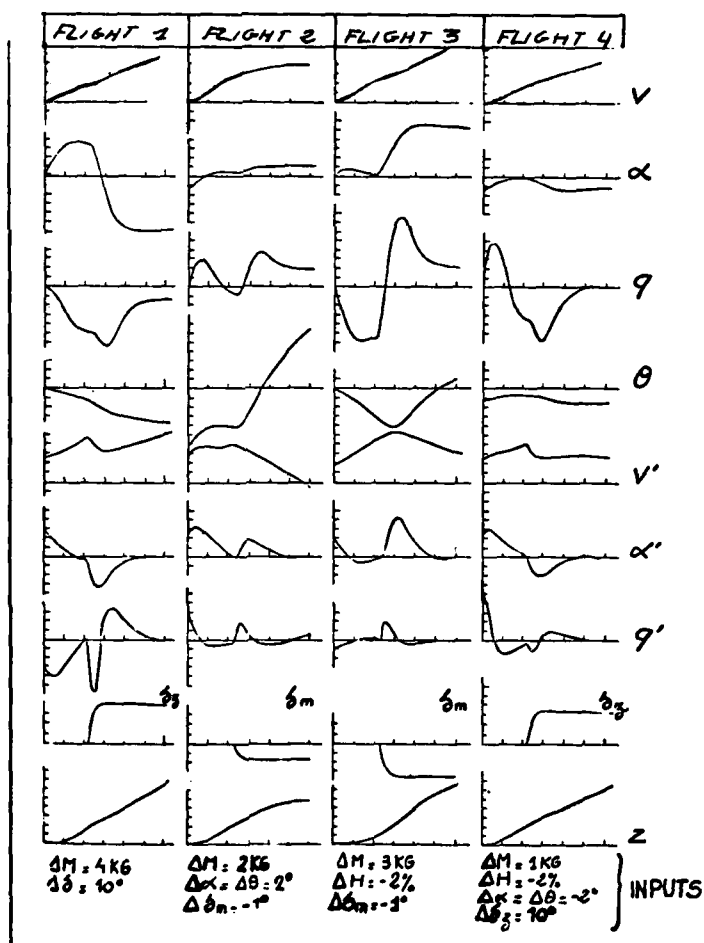
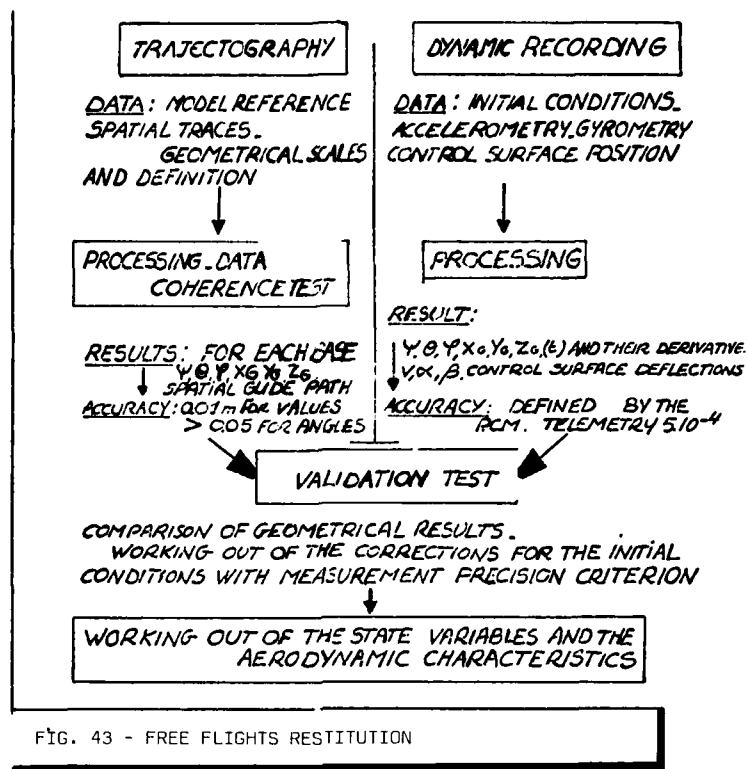


FIG.42 - DD 2A TNT FIRST TEST PROTOCOL



## EXAMPLE : VERTICAL ACCELEROMETER DATA

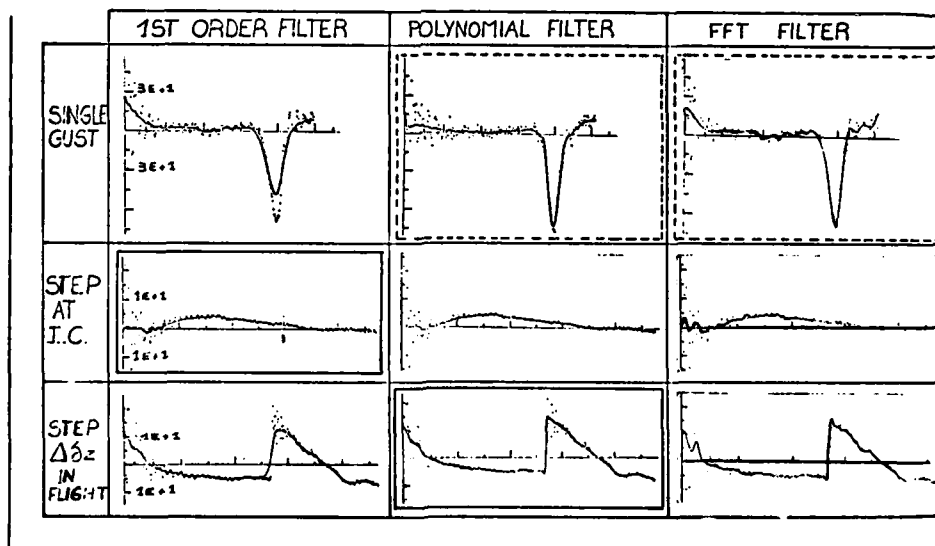


FIG. 44 - FILTERING ASPECTS



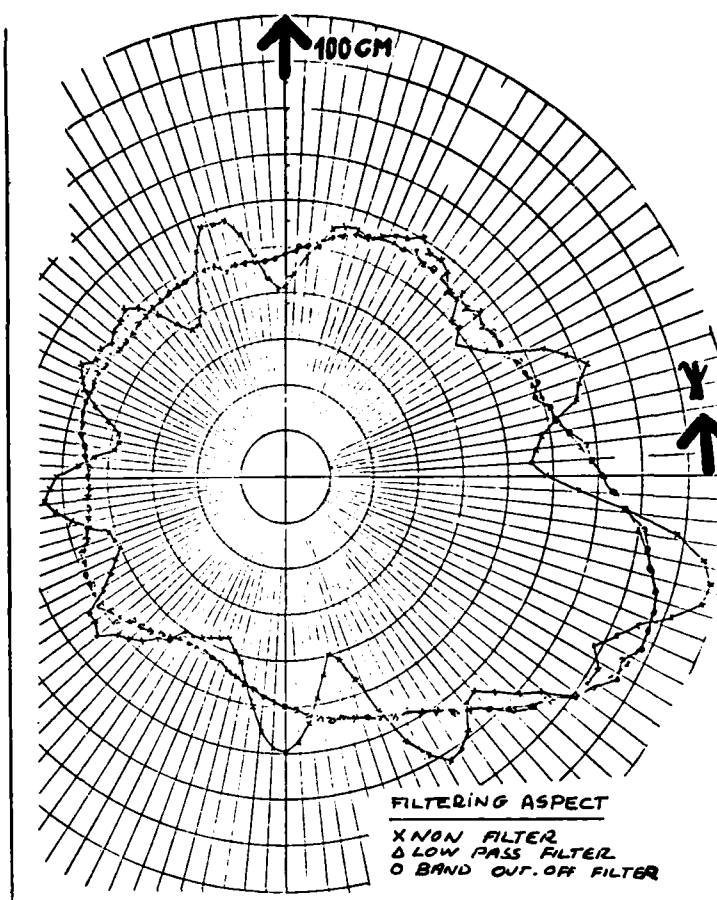


FIG. 45 - ROTARY BALANCE DATA F.F.T. FILTER

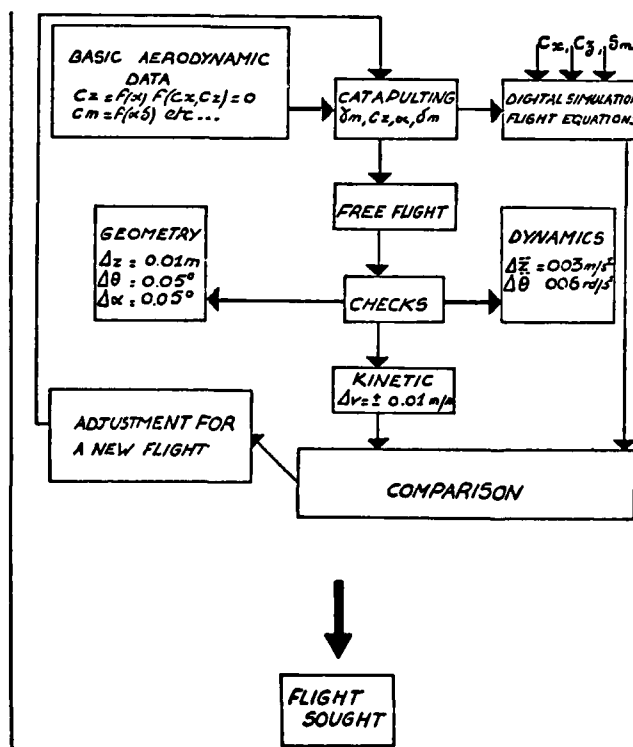


FIG. 46 - DEFINITION OF STATIONARY VALUES

## FORM FOR THE IDENTIFICATION

$$C\dot{x} = Ax + Bu + D\delta$$

with:  $x^T = (\dot{V}, \dot{\alpha}, \dot{q}, \theta)$   
 $u^T = (\Delta \delta_m, \Delta \delta_z, \Delta \delta_r, \Delta \delta_x)$

$$B = \begin{bmatrix} 0 & -C_{x\dot{\alpha}} & g \frac{C_{x\dot{\alpha}}}{V_0} & 0 \\ 0 & -C_{z\dot{\alpha}} & g \frac{C_{z\dot{\alpha}}}{V_0} & 0 \\ C_{m\dot{\delta}_m} & C_{m\dot{\delta}_z} & 0 & 0 \\ 0 & 0 & 0 & 0 \end{bmatrix}$$

$$A = \begin{bmatrix} -2C_{x0} & C_{x0} - C_{x\dot{\alpha}} & 0 & C_{z0} \\ -2C_{z0} & -C_{x0} - C_{z\dot{\alpha}} & 2\mu - C_{z\dot{q}} & C_{x0} \\ 0 & C_{m\dot{\alpha}} & C_{m\dot{q}} & 0 \\ 0 & 0 & 1 & 0 \end{bmatrix} \quad \begin{bmatrix} 2\mu & 0 & 0 & 0 \\ 0 & 2\mu + C_{m\dot{\alpha}} & 0 & 0 \\ 0 & -C_{m\dot{\alpha}} & B & 0 \\ 0 & 0 & 0 & 1 \end{bmatrix}$$

$$D = \begin{bmatrix} -2C_{x0} & -C_{x\dot{\alpha}} & 0 \\ 0 & C_{m\dot{\alpha}} & C_{m\dot{q}} \\ 0 & 0 & 0 \end{bmatrix} \quad \Delta y_a = \begin{bmatrix} W_L \\ W_L \\ \frac{\partial W_L}{\partial T} \end{bmatrix} \left. \vphantom{\begin{bmatrix} W_L \\ W_L \\ \frac{\partial W_L}{\partial T} \end{bmatrix}} \right\} \text{SPECIFIC FOR GUST}$$

FIG. 47 - BASIC MATRIXES FOR IDENTIFICATION

PRINCIPLES: SEPARATE EXPLOITATION OF THE INITIAL CONDITIONS.  
 - COMBINED CRITERIA ON SHAPE AND DISTANCE.  
 - SIMULTANEOUS USE OF ALL FLIGHTS

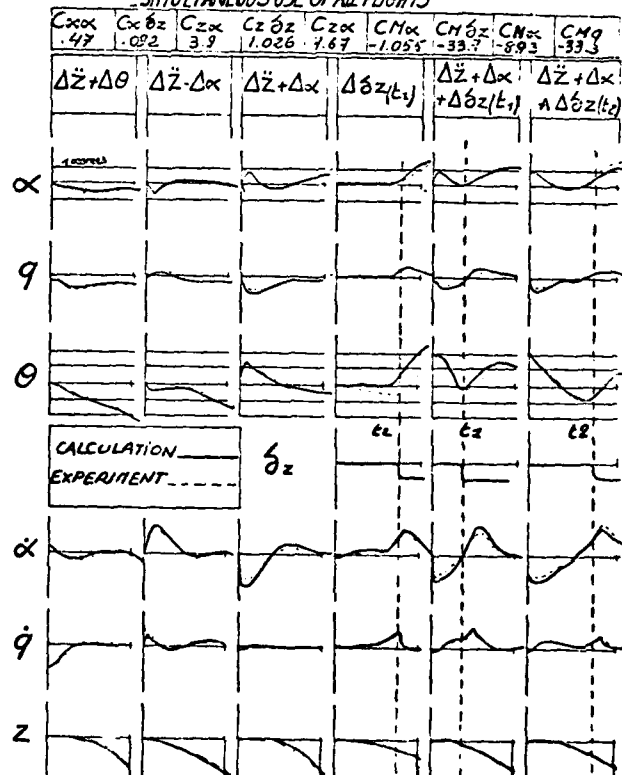


FIG. 48 - IDENTIFICATION RESULTS

- HIGH ADAPTABILITY TO DIFFERENT MODEL DEFINITIONS  
(FREE FLIGHT, SEMI-FREE FLIGHT, CONTROLLED AIRCRAFT, TRANSIENT EFFECTS, ...)
- NO A-PRIORI-VALUES NEEDED DUE TO SPECIAL MODEL DEFINITION  
FOR THE FIRST ITERATION STEPS:

FIRST ITERATIONS	FINAL ITERATIONS
$\dot{x} = A x_{\text{MEASURED}} + B u$	$\dot{x} = A x + B u$
$y = C x_{\text{MEASURED}} + D u$	$y = C x + D u$

- MULTI-MANOEUVRE EVALUATION  
→ 1 SET OF DERIVATIVES FROM SEVERAL MANOEUVRES OR FLIGHTS  
WITH DIFFERENT KINDS OF INFORMATION CONTENT
- CALCULATION OF NONLINEAR FUNCTIONS OF MEASURED DATA  
AS NEW OR ADDITIONAL INPUT/OUTPUT SIGNALS

FIG.50 - SPECIAL FEATURES OF DFVLR IDENTIFICATION PROGRAM

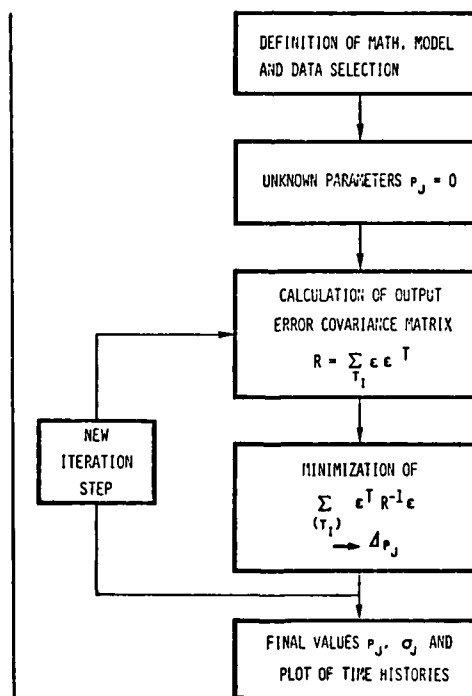


FIG.49 - DFVLR IDENTIFICATION METHOD

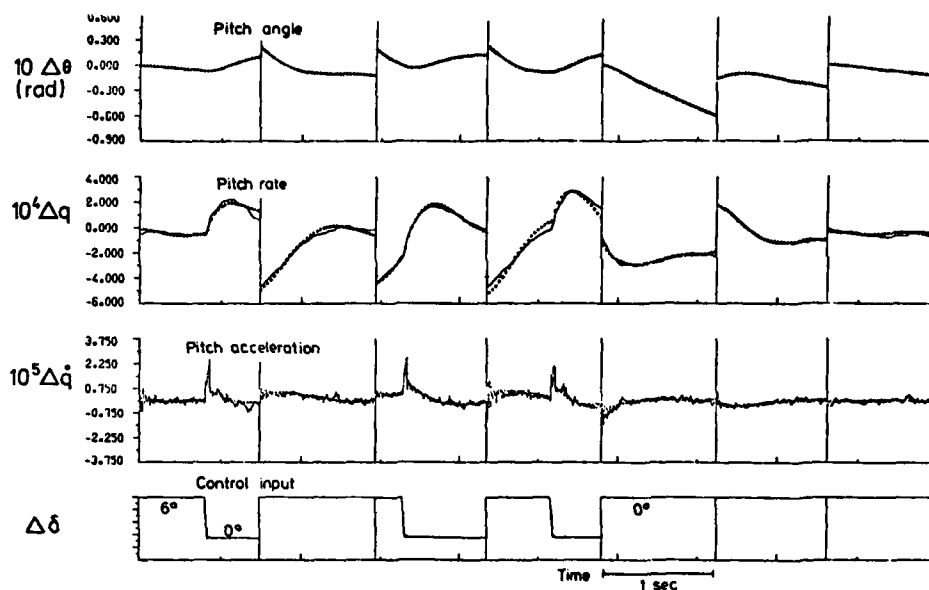


FIG. 51 - CURVE FITTINGS FROM FINAL IDENTIFICATION (M-EQUATIONS)

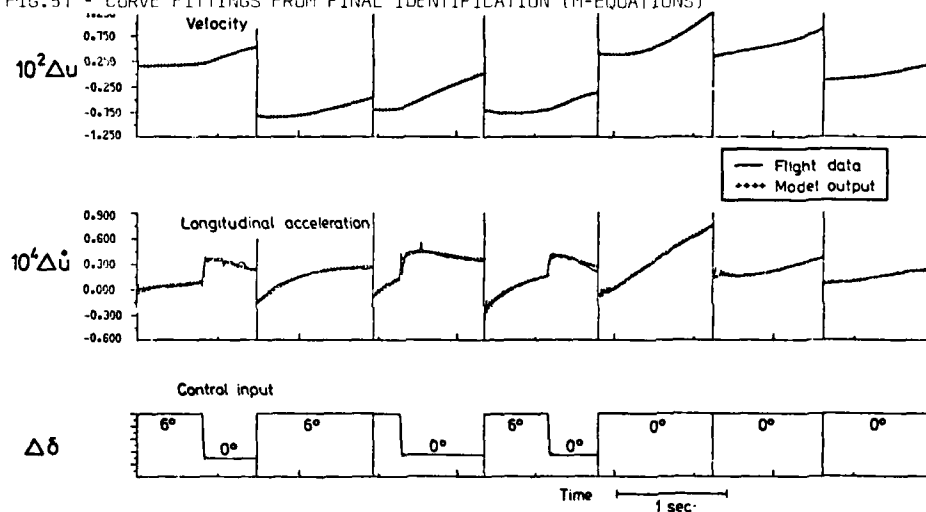


FIG. 52 - CURVE FITTINGS FROM FINAL IDENTIFICATION (X-EQUATIONS)

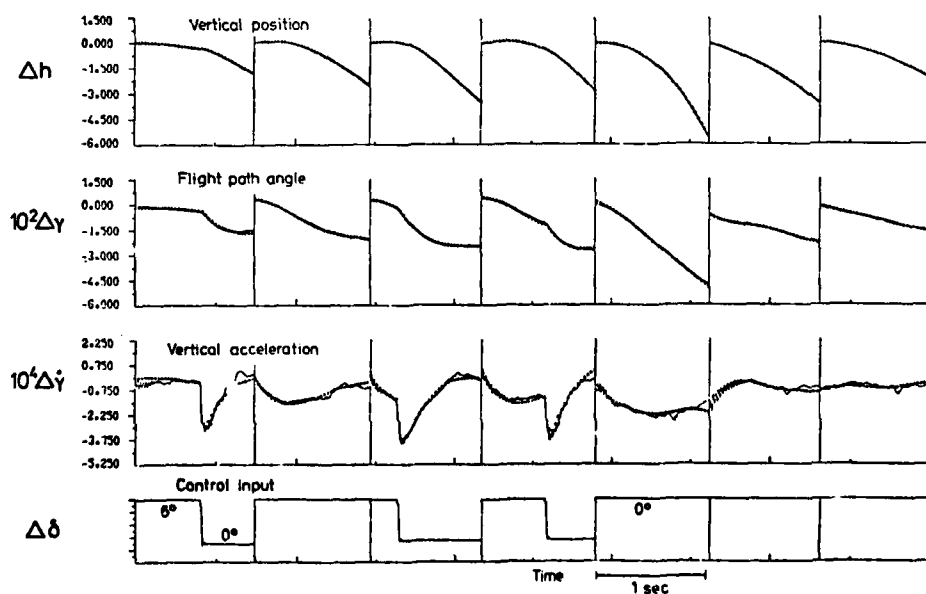


FIG. 53 - CURVE FITTINGS FROM FINAL IDENTIFICATION (Z-EQUATIONS)

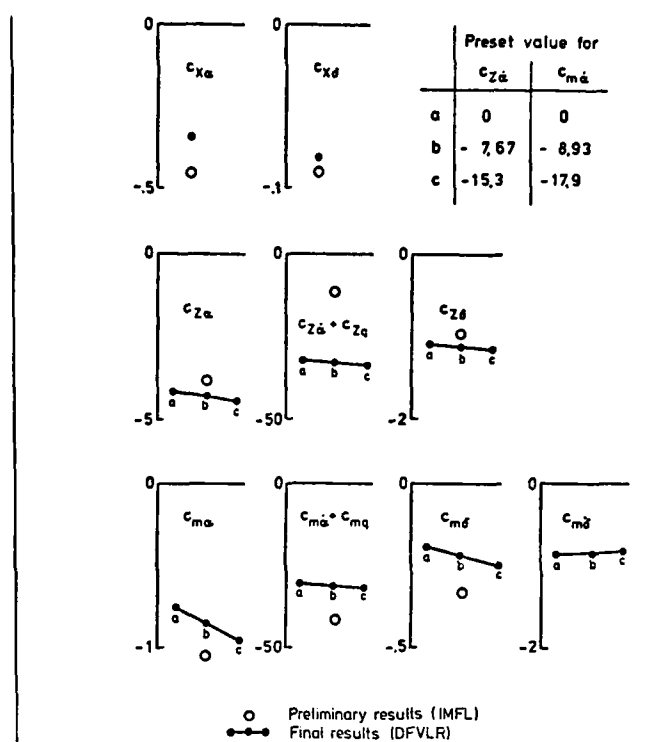


FIG. 54 - IDENTIFICATION RESULTS

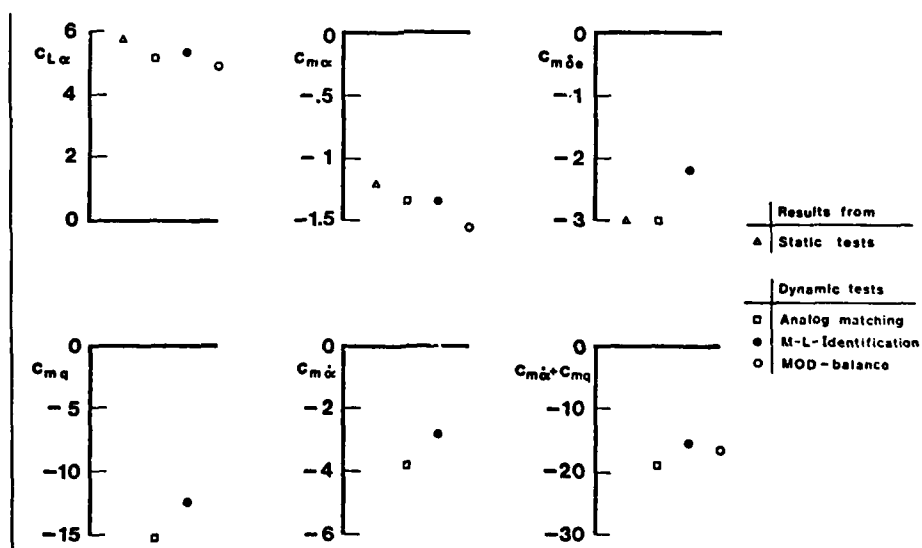


FIG. 55 - RESULTS OF DO 28 TNT WIND TUNNEL MODEL TESTS

## CLOSED LOOP ASPECTS OF AIRCRAFT IDENTIFICATION

by

R. Koehler  
K. Wilhelm

Institut für Flugmechanik

Deutsche Forschungs- und Versuchsanstalt  
für Luft- und Raumfahrt e.V. (DFVLR)  
Braunschweig-Flughafen

## SUMMARY

The lecture deals with specific problems of system identification applied to highly augmented aircraft with respect to flying qualities assessment. An introduction to the influence of augmentation system on dynamic response and flying qualities is given. The application of parameter estimation techniques to control loop systems and problems of control loop identification and equivalent system modellization are discussed.

## 1. INTRODUCTION

The purpose of system identification is the determination of a mathematical model which corresponds to the structure of the system under test and yields model responses that are equal to system responses for any arbitrary inputs. Aircraft parameter estimation techniques usually determine the aerodynamic derivatives from flight tests carried out with the augmentation system disengaged.

The current design trends are towards even more highly augmented aircraft with advanced control concepts. In these cases security reasons often do not permit the stability augmentation system to be removed during an identification experiment. Consequently identification experiments frequently have to be performed on aircraft operating in closed loop. The important influence of the augmentation system and the dependency of its behaviour on flight conditions requires system identification of the augmentation system.

In this paper some practical aspects are discussed, which are important in closed loop identification. The application of system identification results to flying qualities assessment is stressed. The theoretical background is only mentioned when problems are discussed which occurred during flight test data evaluations.

In the literature there are only a few papers which deal with practical evaluations of closed loop identification e.g. [1] and [2], whereas theoretical aspects of closed loop system identification are treated rather extensively [3 - 34]. The most comprehensive survey of recent results is given in the paper by Gustavsson et al. [3].

## 2. INFLUENCE OF AUGMENTATION SYSTEM ON MODELLIZATION

To assess flying qualities of aircraft various evaluation methods are applied. One method is the evaluation of characteristic motion to determine the dynamic characteristics - eigenvalues and eigenvectors - of the system (Figure 1). The results are compared with flying quality specifications, for example in the case of military aircraft with MIL-F-8785 B (ASG). The specifications are valid when the aircraft is unaugmented or when the dynamic behaviour is similar to an unaugmented aircraft.

The augmentation system dynamics can influence the dynamic response of the aircraft significantly. Figure 2 shows the block diagram of an aircraft operating with and without Stability Augmentation System (SAS). When the aircraft is unaugmented the pilot commands are fed directly to the control surfaces. The control surface deflections lead to aerodynamic forces which result in aircraft responses. When the aircraft is augmented aircraft motion and pilot command is measured and fed into the stability augmentation system. The control system moves the control surfaces. Aircraft responses due to the control surface deflections are aircraft motions, which are again measured and fed back to the control system. This way the control loop is closed.

Aircraft responses can be described by linearized equations of motion. As an example the equation of longitudinal motions are given:

$$\begin{aligned} \dot{u} - X_u u - X_w w - X_q q + g \theta &= X_\delta \delta_e \\ \dot{w} - Z_u u - Z_w w - (V + Z_q) q &= Z_\delta \delta_e \\ \dot{q} - M_u u - M_w w - M_q q &= M_\delta \delta_e \\ \dot{\theta} &= q = 0 \end{aligned} \quad (1)$$

These equations can be written using matrices and vectors in the following form

$$\begin{bmatrix} \dot{u} \\ \dot{w} \\ \dot{q} \\ \dot{\theta} \end{bmatrix} + \begin{bmatrix} -X_u & -X_w & -X_q & g \\ -Z_u & -Z_w & -(V+Z_q) & 0 \\ -M_u & -M_w & -M_q & 0 \\ 0 & 0 & 0 & 0 \end{bmatrix} \begin{bmatrix} u \\ w \\ q \\ \theta \end{bmatrix} = \begin{bmatrix} X_\delta \\ Z_\delta \\ M_\delta \\ 0 \end{bmatrix} \delta_e \quad (2)$$

or

$$\dot{x} + Ax = Bu \quad (3)$$

with the open loop system matrices A and B, the state vector x and the control vector u. Some types of feedback configurations will now be discussed to show their influence on the model structure (Figure 3).

*Control system with constant feedback.* A stability augmentation system with constant feedback of pitch rate can be described by

$$\delta_e = a q + b \delta_{es} \quad (4)$$

$\delta_e$  and  $\delta_{es}$  are elevator surface and stick deflections, a and b are constants and q is the pitch rate. Inserting the feedback law (4) in (1) gives

$$\begin{aligned} \dot{u} - X_u u - X_w w - (X_q + a X_\delta) q + g \theta &= b X_\delta \delta_{es} \\ \dot{w} - Z_u u - Z_w w - (V + Z_q + a Z_\delta) q &= b Z_\delta \delta_{es} \\ \dot{q} - M_u u - M_w w - (M_q + a M_\delta) q &= b M_\delta \delta_{es} \\ \dot{\theta} &= -q \end{aligned} \quad (5)$$

The structure of these equations is not changed compared to the structure of Eq. (1). Only the coefficients in the column of the feedback signal are varied. These equations, therefore, could be valid for another aircraft without augmentation system, but another set of aerodynamic derivatives which are called equivalent derivatives.

In a more general discussion a feedback law of

$$u = Cx + Du_s \quad (6)$$

is used with the feedback matrix C, the feedforward matrix D, and the vector of pilot command signals  $u_s$ . Inserting the feedback law (6) in (3) gives

$$\dot{x} + (A - BC)x = BDu_s \quad (7)$$

The structure of this equation is also not changed compared to the structure of Eq. (3). Only the coefficients in the columns of the feedback signals are varied.

*Control system with differential feedback.* A stability augmentation system with differential feedback can be described by the control law

$$u = Cx + E\dot{x} + Du_s \quad (8)$$

When the feedback law (8) is inserted in Eq. (3), then

$$(I - BE)\dot{x} + (A - BC)x = BDu_s$$

or

$$\dot{x} + (I - BE)^{-1} (A - BC)x = (I - BE)^{-1} BDu_s \quad (9)$$

with the unit matrix I. The Eq. (9) has the same structure as Eq. (3), but all coefficients in the matrices are varied, even if only one signal is fed back by the stability augmentation system.

*Control system with integrating feedback.* In the case of a stability augmentation system with dynamic behaviour the control law is given by

$$\dot{u} + Fu = Cx + Du_s \quad (10)$$

This equation together with Eq. (3) can be written in the form

$$\begin{bmatrix} \dot{x} \\ \dot{u} \end{bmatrix} + \begin{bmatrix} A & -B \\ -C & F \end{bmatrix} \begin{bmatrix} x \\ u \end{bmatrix} = \begin{bmatrix} 0 \\ D \end{bmatrix} u_s \quad (11)$$

This differential equation system has a different structure compared to Eq. (3). The number of poles increases with the number of equations and for highly augmented aircraft no equivalent unaugmented aircraft model with similar dynamic behaviour can be found.

Some MIL-specifications, therefore, cannot be applied to aircraft with stability augmentation systems having a significant dynamic behaviour. In these cases other evaluation methods have to be used.

One possibility is to apply system identification methods. This paper deals specially with the aspects of the application of system identification to the assessment of flying qualities of augmented or automatically controlled aircraft. System identification has the great advantage of yielding a mathematical model of the augmented aircraft, which may be used immediately to calculate the dynamic response for arbitrary inputs. In addition, it also allows the assessment to be carried out with reference to general aspects of system theory, e.g. stability limits in precision flight. Figure 4 shows the two evaluation methods. As system identification requires much greater effort the flight test engineer generally will prefer the simpler method of evaluation of characteristic motion. This, however, may cause problems, especially in the flying qualities assessment of highly augmented aircraft.

### 3. AIRCRAFT WITH LONGITUDINAL AUGMENTATION SYSTEM

To assess flying qualities with respect to the longitudinal short period MIL-F-8785 specification involves criteria which are based on a second order model. The same approach may result in good fits for the short period time histories even in the case of an aircraft with a stability augmentation system that has a significant dynamic behaviour. An example is given in Figure 5. Satisfactory fits of flight test data and model response data were obtained in all evaluations of characteristic longitudinal motions using a simple second order model. Thus, the augmentation system dynamics could not be detected during characteristic motion evaluations, and the flight test engineer may apply the handling criteria without being warned. But the quantitative assessment based on the MIL-Specification would give conflicting results when compared to pilot rating evaluations.

To overcome the deficiencies of handling qualities investigations based on characteristic motion evaluations, system identification methods were applied. A modified maximum likelihood identification method which can be started without knowledge of a priori values for the unknown parameters was used. The flight test data were obtained using various pilot applied control inputs (mainly steps and doublets). However, special input signals designed for system identification were not employed. During these manoeuvres the SAS was engaged. Signals were measured at points A, B and C shown in the sketch of Figure 6.

The flight test data measured at the points A and B were used to identify the SAS. The outputs from the identification were the SAS parameters. Elevator surface deflection and aircraft response, points B and C, were used to determine the aerodynamic derivatives of the basic aircraft. The results of the two identifications can be used to calculate the behaviour of the closed loop model. In addition, a system identification of the augmented aircraft from point A to C was carried out using an unaugmented aircraft model structure. This identification yields so called equivalent derivatives.

The results of some representative flight test data time histories and corresponding system identification curve fits are shown in Figure 7. The curve fittings based on the identification of the aerodynamic derivatives on the left of Figure 7 are satisfactory. On the right hand side, equivalent derivative curve fittings are shown. The pitch rate fit is unsatisfactory, while the vertical acceleration fit is acceptable but not good. The deficiencies are caused by the inadequate model structure which did not include the augmentation system dynamics.

As a check, two models were used for identification of the control system. On the left of Figure 8 results using the complete dynamic model are shown. On the right are results using a simplified model which neglected augmentation system dynamics. The poorer fit on the right again shows the influence of the augmentation system dynamics.

Another time sequence is shown in Figure 9. Again as shown on the left, identification of aerodynamic derivatives yielded satisfactory fits. The model structure is equal to the system structure. As shown on the right, identification of equivalent derivatives also yielded satisfactory fits. Although the model structure is not equal to the system structure, the fits are still good. The flight test engineer may assume that the influence of the stability augmentation system dynamics is small and can be neglected for handling qualities assessment.

In Figure 10 the corresponding identification results for the stability augmentation system are shown. On the left, the identified model included the SAS dynamics. On the right, the identified model did not include SAS dynamics. It is clear that the SAS dynamics should not be neglected.

For the cases where a good fit of aircraft response was possible using equivalent derivatives, the augmentation system dynamics were approximated by modifying the derivatives. It was found that the modification of the derivatives was dependent on the particular input signal used. Therefore, the identified equivalent derivatives could not be used to predict aircraft responses for other arbitrary input signals.



In Figure 11 poles of the short-period motion for both the open and closed loop cases are shown. Three different regions can be distinguished. The poles of the basic aircraft are at relatively low frequencies. The poles of the augmented aircraft, which were calculated from both the identified SAS and basic aircraft models, are at relatively high frequencies. In between are the poles of the aircraft modeled with equivalent derivatives. These poles should be in the same region as the poles for the augmented aircraft. Thus, aircraft models using equivalent derivatives can lead to erroneous conclusions during handling qualities investigations. All aircraft configurations investigated showed similar results.

#### 4. AIRCRAFT WITH LATERAL DIRECTIONAL AUGMENTATION SYSTEM

In contrast to the evaluations of the longitudinal motion the influence of the lateral-directional augmentation system dynamics could at least be partially identified by evaluations of characteristic motions.

In the following some examples of such evaluation results will be given. Figure 12 shows time histories of the lateral directional characteristic motion. Flight test data are plotted using solid lines. The crosses represent the best fit possible using a second and fourth order model. For this dutch roll example, yaw rate and sideslip angle are matched fairly well, whereas the fit for roll rate is unsatisfactory using a second order model. A satisfactory fit was obtained using a fourth order model consisting of two conjugate complex pole pairs. One of these pole pairs represents the dutch roll motion, the other pair represents the control system dynamics. Another data run is shown in Figure 13. As can be seen, the unsatisfactory roll rate fit using a second order model is again improved when a fourth order model is used. In this case also better fits for yaw rate and angle of sideslips are obtained with the fourth order model.

In the two examples shown in Figure 12 and 13, the SAS dynamics could be detected during the evaluation of characteristic motions. The flight test engineer is warned that the stability augmentation system has significant dynamic behaviour. The response of the augmented aircraft does not conform to the basic assumptions of the MIL Spec 8785 and these criteria cannot be readily applied.

In other cases of lateral-directional characteristic motions the augmentation system dynamics could not be detected. Figure 14 shows an example of a good fit for a second order model. In cases like this the flight test engineer may apply the handling criteria without being warned. But the quantitative assessment based on the MIL-specifications would give conflicting results when compared to pilot rating evaluations.

In order to gain a deeper insight into the influence of augmentation system dynamics on the lateral-directional motions, system identifications analogous to those for the longitudinal motion were effected. Some representative flight test data time histories and the corresponding system identification curves are shown on Figure 15. The curve fits based on the identification of the aerodynamic derivatives are satisfactory.

In Figure 16 curve fits based on identified equivalent derivatives are shown. Although the model structure is not equal to the real system structure, the fits are still satisfactory. The flight test engineer may assume that the influence of the stability augmentation system dynamics is small and that the augmented aircraft may be represented by a model of an unaugmented aircraft. This conclusion is only permissible if for normal pilot control inputs the augmentation system dynamics are not excited.

To check this it is necessary to apply system identification to a model with and without augmentation system dynamics. This approach is analogous to that for longitudinal motions (Figure 6). The lateral-directional augmentation system has two parts: the roll and the yaw augmentation system (see Figure 17).

In Figure 18 the identification results for the roll augmentation system with two model structures are compared. In addition, the response of the model given by the contractor is shown. Inputs to the roll augmentation system are roll rate and stick deflection. The identification was made applying the same two models to four time periods. Application of proportional feedback model (see first diagram, Figure 18) resulted in good fits in the first and fourth time period. But in the two middle time periods the augmentation system behaviour represented by this model is wrong. The dynamic behaviour of the augmentation system in this case cannot be neglected. This example shows also that an identification model of the augmentation system may yield good fits for some pilot inputs without being representative for other arbitrary inputs.

In the second diagram flight test data and the response of the contractor's model are shown. The fit is satisfactory but there are some discrepancies in the first and last time period. The third diagram shows the curve fit using a model obtained by system identification including augmentation system dynamics. Here the fit is good for all time periods.

In an analogous manner the yaw augmentation system was analysed (Figure 19). Also in this case there are partly good fits using a proportional feedback model but in the second time period the fit is less satisfactory. The contractor's model shows curves which are too high at peaks of the output signal (see second diagram). Here again the best fit is given by the model obtained by system identification including augmentation system dynamics even though there remain small deviations.

## 5. CLOSED LOOP IDENTIFICATION PROBLEMS

In the identifications presented so far no difficulties occurred in the determination of the mathematical model of the closed loop system consisting of the basic aircraft and the augmentation system. However, problems may arise if some laws of identifiability are violated.

In the following it is assumed that some system noise must be taken into account in the equations of flight dynamics. The equations are

$$\dot{x} + Ax = Bu + r \quad (12)$$

with  $x$  = aircraft response,  
 $u$  = control surface inputs,  
 $r$  = system noise.

The augmentation system may consist of proportional feedback channels or the augmentation system dynamics may only be so weakly excited during the measurement period that the augmentation system may be approximately represented by the equation

$$u = Cx + Du_s \quad (13)$$

with  $u_s$  = pilot control input. The task of closed loop system identification is to determine elements of the open loop system matrices  $A$  and  $B$ , the feedback matrix  $C$ , and the feedforward matrix  $D$ .

Multiplication of Eq. (13) by an arbitrary matrix  $\Lambda$  and adding the product to Eq. (12) yields

$$\dot{x} + (A + \Lambda C)x = (B + \Lambda)u + r - \Lambda Du_s \quad (14)$$

When applied to basic aircraft parameter estimation, the identification method treats the sum  $r - \Lambda Du_s$  as noise and determines the coefficients so as to minimize the values of this noise. If the control inputs  $u_s$  during the measuring time are large, the elements of  $\Lambda$  become very small and may, therefore, be neglected in all terms of Eq. (14). This equation then is approximately the same as Eq. (12) and the feedback, consequently has only little influence on the precision of the identification results. If, however, the control inputs  $u_s$  during the measuring time are small or restricted to very short periods, the term  $\Lambda Du_s$  will be small compared to the system noise  $r$  even for rather large values of  $\Lambda$ . Eq. (14) then also has the same structure as Eq. (12) but the matrix  $\Lambda$  is involved in the coefficient matrices of  $x$  and  $u$ . Variation of  $\Lambda$  does not influence the model response and the cost function of the system identification method. The result of identification will then be the matrices  $A + \Lambda C$  and  $B + \Lambda$  instead of  $A$  and  $B$ , with an arbitrary matrix  $\Lambda$ .

The difficulties in this case are caused by the fact that the control surface deflections become linear combinations of the aircraft response variables, as may be seen from Eq. (13) in neglecting the control inputs  $u_s$ . Similar difficulties may arise when aircraft response signals are correlated or become linear combinations due to augmentation system influence. This yields

$$x = Gx, \quad G \neq I \quad (15)$$

with  $I$  = unit matrix. Inserting Eq. (15) in Eq. (12) gives

$$\dot{x} + [A + \Lambda(I - G)]x = Bu + r \quad (16)$$

Here again an arbitrary matrix  $\Lambda$  is involved in the coefficient matrix of  $x$ . It does not affect model responses and the value of the cost function and the elements of matrix  $A$  cannot be determined.

In evaluation of flight test data from closed loop measurements both cases may occur together. This means that control surface deflections and aircraft response variables may be highly correlated or that an aircraft response variable is highly correlated to another one. In the following, two examples will be given.

A dutch roll excitation using a rudder pedal doublet caused the signals of Figure 20.  $\xi$ ,  $p$  and  $q$  are highly correlated to one another. In the figure it is demonstrated that the extreme values occur at the same time. Results of system identification were not satisfactory. When this time period was supplemented by another one with aileron stick deflection satisfactory results were obtained.

Time histories of curve fits of lateral-directional motion using harmonic oscillation, with SAS fully engaged, are shown in Figure 21. As can be seen, the signals are highly correlated. The peaks of the signals are often at the same time. Again the results of system identification were disappointing.

In flight tests harmonic oscillation inputs are scarcely ever applied. Short time excitation, for instance doublets, are used more frequently. It is necessary, therefore, to evaluate also the characteristic motion by the system identification procedure. In these cases the correlation of the signals are characterized by the phase angle of the eigenvectors. Thus a significant influence of eigenvector phase angle on the correlation and

identifiability of derivatives can be expected. Figure 22 shows an example of a highly augmented aircraft. The eigenvector phase angle of  $p$  and  $\delta$  is in many cases near to  $180^\circ$  due to stability augmentation system. The correlation coefficient of  $N_\delta$  and  $N_p$  is sometimes nearly 1 at the maximum of the envelope at  $180^\circ$ . In this region the standard deviation of the derivatives increases. As an example, standard deviations of  $N_\delta$  are shown in Figure 23.

To overcome the difficulties in the identification it is necessary to apply well designed input signals. Evaluation of several time periods with different modes of excitation is also advantageous. Another possibility, which will be discussed in the following, is shown by Gilyard [1].

The lateral directional flying qualities of a mach 3 cruise aircraft is significantly influenced by engine inlet forces. The engine inlet was controlled by an inlet computer (see Figure 24). A simplified block diagram of the control loop is shown in Figure 25. The linearized equation of motion can be written in the form

$$\dot{x} + Ax = B_1 u_1 + B_2 u_2 + r \quad (17)$$

with two control inputs  $u$ .  $u_1$  means rudder deflection and  $u_2$  inlet position variations. The control law can be approximated by the equation

$$u_2 = Cx \quad (18)$$

Inserting the feedback law (18) in Eq. (17) gives

$$\dot{x} + (A + \Lambda C)x = B_1 u_1 + (B_2 + \Lambda) u_2 + r \quad (19)$$

Flight tests with inlet computer engaged yields correlated signals, as shown by Eq. (18). Using only these flight test data it is not possible to identify the unknown coefficients due to the arbitrary matrix  $\Lambda$ . A second flight test with inlet computer disengaged yielded flight test data which meet the equation

$$\dot{x} + Ax = B_1 u_1 + r \quad (20)$$

From identification of both flight tests with the same model good results can be obtained. Using the test with the inlet computer disengaged the elements in the matrices  $A$  and  $B_1$  are identified corresponding to Eq. (20) and the matrix  $\Lambda$  in Eq. (19) is set to zero. Using the test with inlet computer engaged the elements of matrix  $B_2$  are estimated (see Eq. (19)). The results of curve fits are shown in Figure 26. This method can also be applied using two flight tests with different gains in the augmentation system to meet the identifiability requirements in a closed loop system.

## 6. CONCLUSIONS

To conclude, when identifying an aircraft with a dynamic stability augmentation system, the following points are important

- Evaluation of flight test data may yield satisfactory curve fits but give unsatisfactory results for closed loop handling qualities investigations. In particular the flight test engineer must be aware of the shortcomings of characteristic motion evaluations, equivalent derivative estimations, and investigations based on equivalent derivatives. Using these methods, augmentation system dynamics and its influence cannot be detected in all cases.
- Satisfactory fits and also satisfactory results can be obtained using expanded models and methods. System identification of the basic aircraft and the dynamic stability augmentation system yields a correct mathematical model. Separate identification of basic aircraft and SAS instead of using equivalent derivatives proved to be absolutely necessary.
- Problems of identifiability in system identification of closed loop systems can be overcome by applying well designed input signals. To improve system identification it is recommended to use several selected flight tests with different modes of excitation for one parameter estimation. An additional possibility is to use different feedback control gains in flight tests.

## 7. REFERENCES

1. Gilyard, G.B., "Determination of Propulsion-System-Induced Forces and Moments of a Mach 3 Cruise Aircraft", NASA Symposium on Parameter Estimation Techniques and Applications in Aircraft Flight Testing, Edwards, 24-25 April 1973.
2. Koehler, R., Marchand, M., "Open/Closed Loop Identification of Stability and Control Characteristics of Combat Aircraft", AGARD FMP Symposium on Stability and Control, Ottawa, 25-28 Sept. 1978, Conference Proceedings 260 (1979).
3. Gustavsson, I., Ljung, L., Söderström, T., "Identification of Processes in Closed Loop - Identifiability and Accuracy Aspects", Automatica, Vol. 13, pp. 59-75, 1977.
4. Prasad, R.M., Sinha, A.K., Mahalanabis, A.K., "Two-Stage Identification of Closed-Loop Systems", IEEE Transactions on Automatic Control, Vol. AC-22, No. 6, 1977.
5. Balakrishnan, A.V., Peterka, V., "Identification in Automatic Control Systems", Automatica, Vol. 5, pp. 817-829, 1969.
6. Caines, P.E., Chan, C.W., "Feedback between Stationary Stochastic Processes", IEEE Transactions on Automatic Control, Vol. AC-20, pp. 498-508, 1975.
7. Caines, P.E., Chan, C.W., "Estimation, Identification and Feedback", in Advances in System Identification, R.K. Mehra, D.G. Lainiotis, Eds., Academic Press, New York, 1976.
8. Gustavsson, I., Ljung, L., Söderström, T., "Identification of Linear, Multivariable Process Dynamics Using Closed Loop Experiments", Dept. of Automatic Control, Lund Institute of Technology, Lund, Jan. 1974, Report 7401.
9. Ljung, L., Gustavsson, I., Söderström, T., "Identification of Linear, Multivariable Systems Operating under Linear Feedback Control", IEEE Transactions on Automatic Control, Vol. AC-19, pp. 836-840, 1974.
10. Söderström, T., Gustavsson, I., Ljung, L., "Identifiability Conditions for Linear Systems Operating in Closed Loop", Int. J. Control, Vol. 21, pp. 243-255, 1975.
11. Box, G.E.P., MacGregor, J.F., "The Analysis of Closed-Loop Dynamic-Stochastic Systems", Technometrics, Vol. 16, pp. 391-398, 1974.
12. Akaike, H., "On the Use of a Linear Model for the Identification of Feedback Systems", Ann. Inst. Stat. Math., Vol. 20, pp. 425-439, 1968.
13. Box, G.E.P., MacGregor, J.F., "The Analysis of Closed-Loop Dynamic-Stochastic Systems", Dept. of Statistics, University of Wisconsin (the 4th chapter in a series Topics in Control), 1972, Technical Report No. 309.
14. Priestley, M.B., "Estimation of Transfer Functions in Closed Loop Stochastic Systems", Automatica, Vol. 5, pp. 623-632, 1969.
15. Rödder, P., "Systemidentifikation mit stochastischen Signalen im geschlossenen Regelkreis - Verfahren und Fehlerabschätzung", Dissertation, TH Aachen, 1973.
16. Rödder, P., "Statistischer Fehler bei der Systemidentifizierung im geschlossenen Regelkreis", Regelungstechnik und Prozeß-Datenverarbeitung, Vol. 22, pp. 282-283, 1974.
17. Thöm, H., Krebs, V., "Identifizierung im geschlossenen Regelkreis - Korrelationsanalyse oder Parameterschätzung?", Regelungstechnik und Prozeß-Datenverarbeitung, Vol. 23, pp. 17-19, 1975.
18. Söderström, T., Ljung, L., Gustavsson, I., "Identifiability Conditions for Linear Multivariable Systems Operating under Feedback", IEEE Transactions on Automatic Control, Vol. AC-21, 1976.
19. Vorchik, V.G., "Plant Identification in a Stochastic Closed-Loop System", Automation Rem. Control, Vol. 36, pp. 550-565, 1975.
20. Box, G.E.P., MacGregor, J.F., "Parameter Estimation with Closed-Loop Operating Data", Proc. 6th IFAC Congress, Boston, 1975, Paper 38-5.
21. Schulze, H., "Anwendung von Schätzverfahren für die Kenngrößen von Regelstrecken aufgrund von Messungen im geschlossenen Regelkreis", Regelungstechnik und Prozeß-Datenverarbeitung, Vol. 19, pp. 113-119, 1971.
22. Goodwin, G.C., Payne, R.L., Murdoch, J.C., "Optimal Test Signal Design for Linear Single Input-Single Output Closed Loop Identification", Conference on Computer Aided Control System Design, IEE Publication No. 96, Cambridge, 1973.
23. Lindberger, N.A., "Stochastic Modelling of Computer-Regulated Linear Plants in Noisy Environments", Int. J. Control, Vol. 16, pp. 1009-1019, 1972.

24. Lindberger, N.A., "Stochastic Identification of Computer-Regulated Plants in Noisy Environments", Int. J. Control, Vol. 17, pp. 65-80, 1973.
25. Panich, Yu. V., Trachevskii, M.L., "Identification of a Class of Closed-Loop Control Systems", Automation rem. Control, Vol. 34, pp. 1457-1466, 1973.
26. Vorchik, B.G., Fetisov, V.N., Steinberg, Sh. E., "Identification of a Closed-Loop Stochastic System", Automation rem. Control, Vol. 34, pp. 1069-1081, 1973.
27. Kurz, H., Isermann, R., "Methods for On-Line Process Identification in Closed Loop", Preprints 6th IFAC World Congress, Boston, 1975.
28. Caines, P.E., Sinha, S., "An Application of the Statistical Theory of Feedback to Power System Identification", Preprints 1975 IEEE Conference on Decision and Control, Houston, Dec. 1975.
29. Graupe, D., "On Identifying Stochastic Closed-Loop Systems", IEEE Transactions on Automatic Control, Vol. AC-20, pp. 553-555, 1975.
30. Wellstead, P.E., Edmunds, J.M., "Least-Squares Identification of Closed-Loop Systems", Int. J. Control, Vol. 21, pp. 689-699, 1975.
31. Lobbia, R.N., Saridis, G.N., "On-Line Identification of Multivariable Stochastic Feedback Systems", Preprints JACC, Stanford, 1972.
32. Defalque, B., Gevers, M., Installé, M., "Combined Identification of the Input-Output and Noise Dynamics of a Closed-Loop Controlled Linear System", Int. J. Control, Vol. 24, pp. 345-360, 1976.
33. Froisy, J.B., Smith, C.L., Corripio, A.B., Murrill, P.W., "Closed-Loop Identification of System Dynamics in the Presence of Noise and Unmeasured Disturbances", Proc. JACC 1974, Austin.
34. Schwalm, D., "Bestimmung des Frequenzganges eines linearen rückgekoppelten Systemes mit zwei unabhängigen stochastischen Eingangssignalen", Regelungstechnik und Prozeß-Datenverarbeitung, Vol. 18, pp. 453-455, 1970.

#### 8. ACKNOWLEDGEMENTS

The authors wish to thank the following for their contributions to this paper:

- Dr. E. Plaetschke for the development of a system identification program based on maximum likelihood function, identification of longitudinal motion and longitudinal augmentation system,
- M. Marchand for the development and application of a computer program to evaluate characteristic motions, identification of lateral-directional motion and lateral-directional augmentation system, and interpreting problems of system identification in closed loop,
- Mrs. M. Nagel and Mrs. A. Froben for drawing the figures and typing the manuscript.

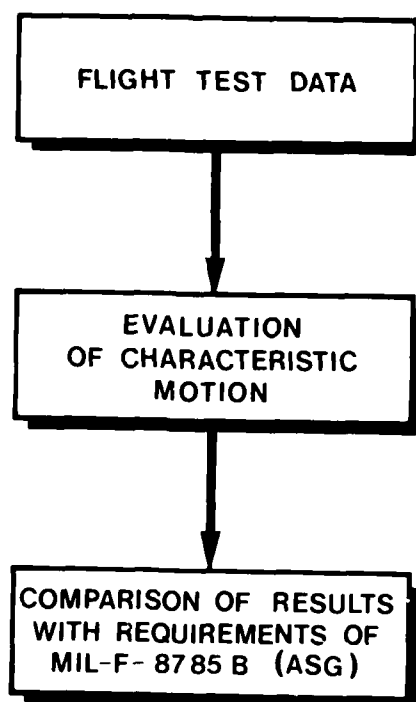
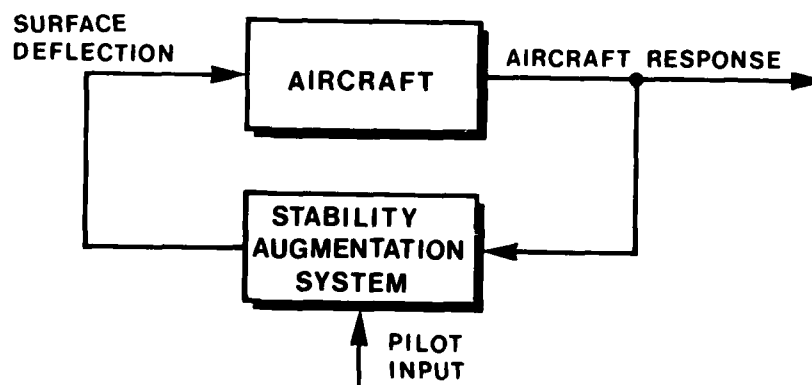


Fig. 1 Evaluation for Flying Qualities Assessment



UNAUGMENTED AIRCRAFT



AUGMENTED AIRCRAFT

Fig. 2 Aircraft with and without Stability Augmentation System

FEEDBACK TYPE	CHANGES IN THE MODEL OF AUGMENTED AIRCRAFT
PROPORTIONAL	DERIVATIVES OF FEEDBACK VARIABLES
DIFFERENTIAL	ALL DERIVATIVES
INTEGRATING	MODEL STRUCTURE ( ADDITIONAL POLES )

Fig. 3 Influence of SAS on Modellization

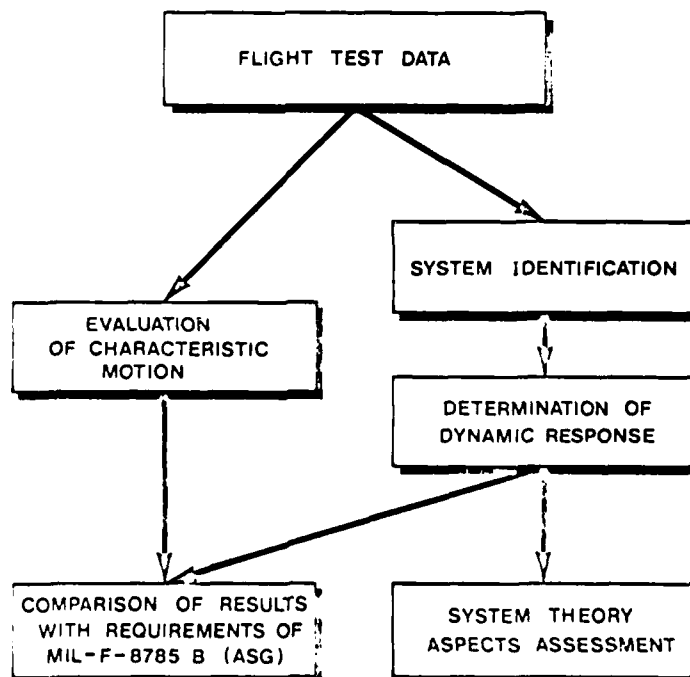


Fig. 4 Evaluation Methods

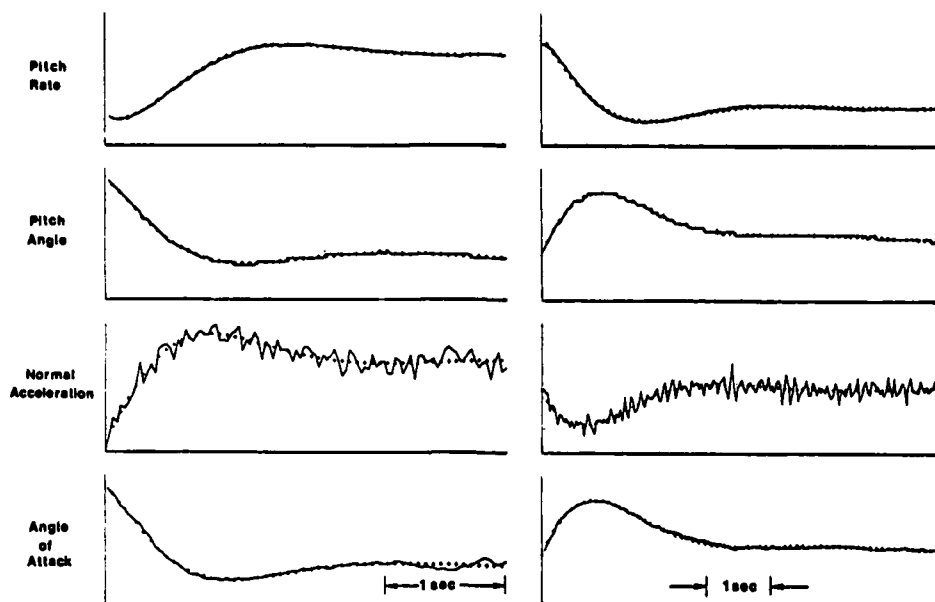
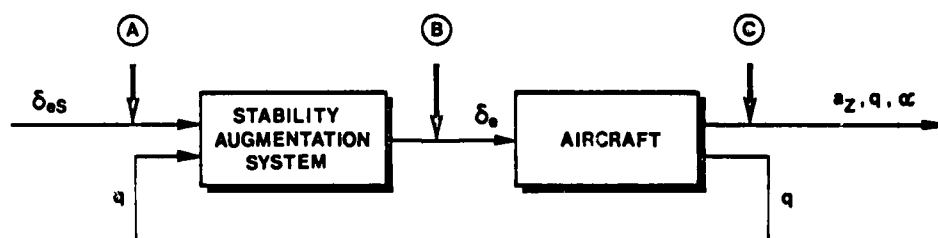


Fig. 5 Examples of Satisfactory Fit Using Second Order Model

— Flight Test Data  
 + + + Model Output



POINTS	SYSTEM	IDENTIFICATION RESULTS
(A) - (B)	STABILITY AUGMENTATION SYSTEM	SAS PARAMETERS
(B) - (C)	BASIC AIRCRAFT	AERODYNAMIC DERIVATIVES
(A) - (C)	AUGMENTED AIRCRAFT	EQUIVALENT DERIVATIVES

Fig. 6 Closed Loop System Identification



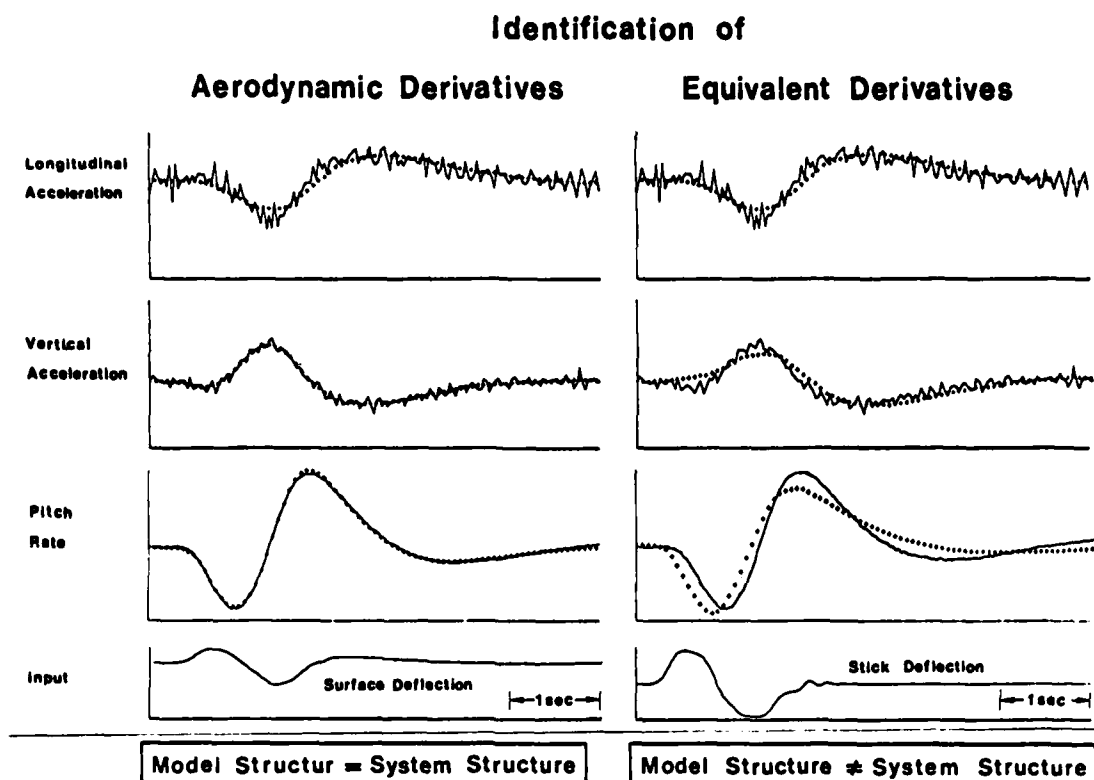


Fig. 7 Example of Degraded Fits in Identification of Equivalent Derivatives

— Flight Test Data  
 + + + Model Output

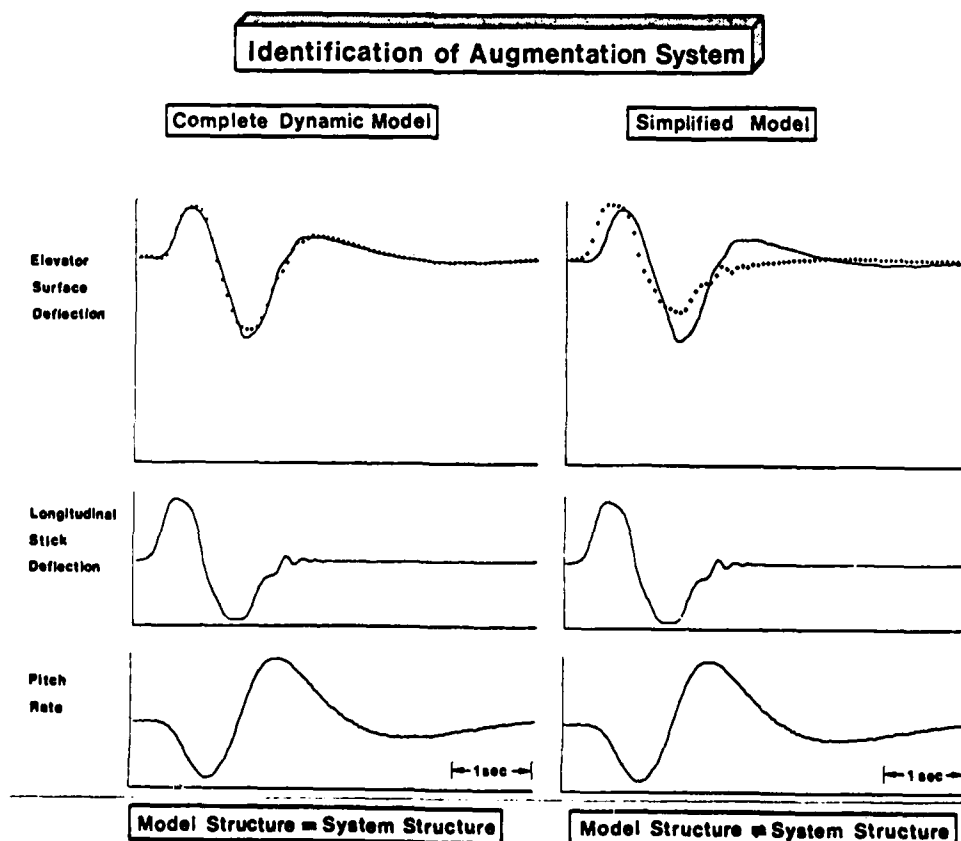


Fig. 8 Comparison of Fits in Identification of the Augmentation System

— Flight Test Data  
 + + + Model Output

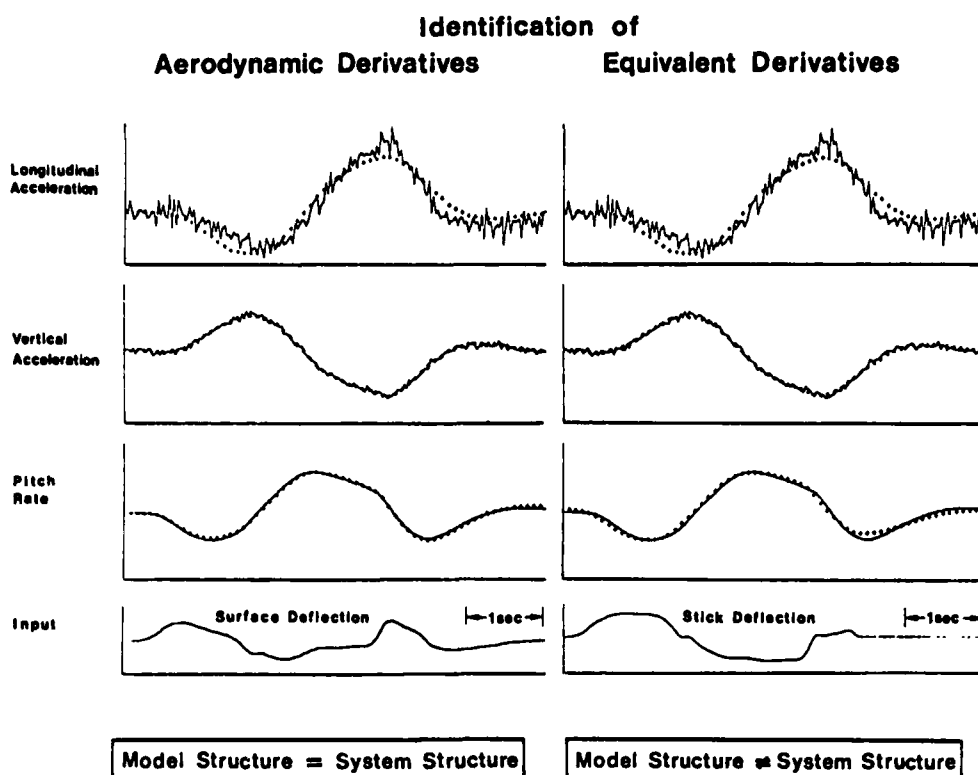


Fig. 9 Example of Good Fits in Identification of Aerodynamic and Equivalent Derivatives

— Flight Test Data  
+ + + Model Output

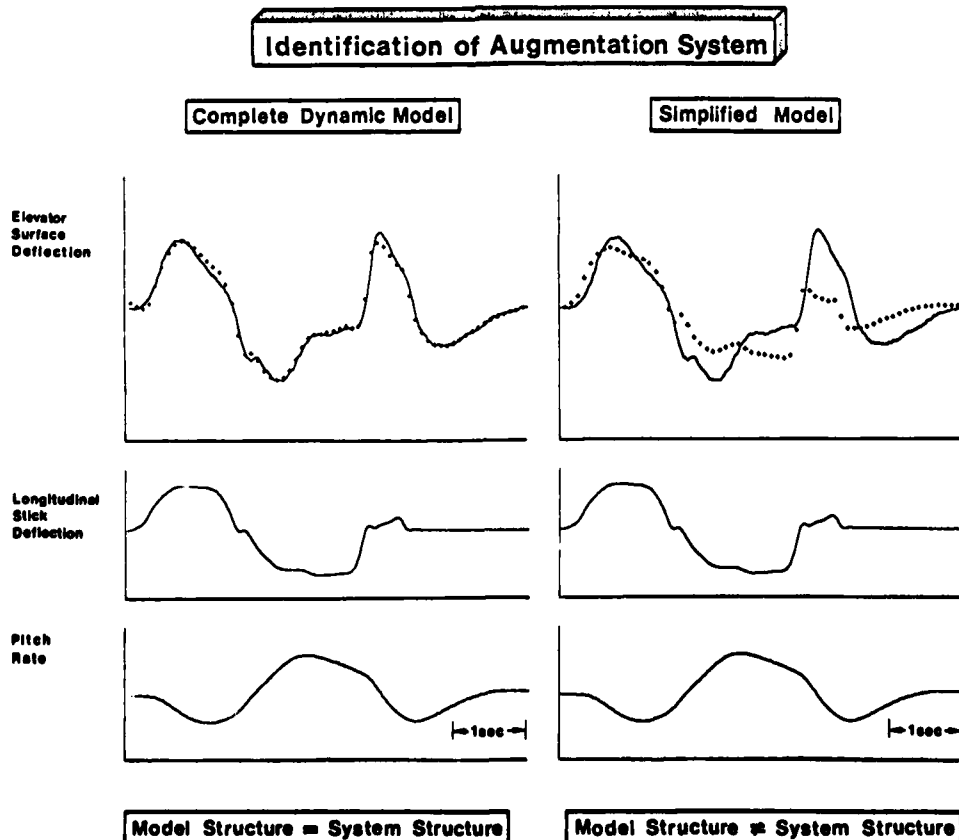


Fig. 10 Influence of Augmentation System Dynamics on Time Histories

— Flight Test Data  
+ + + Model Output

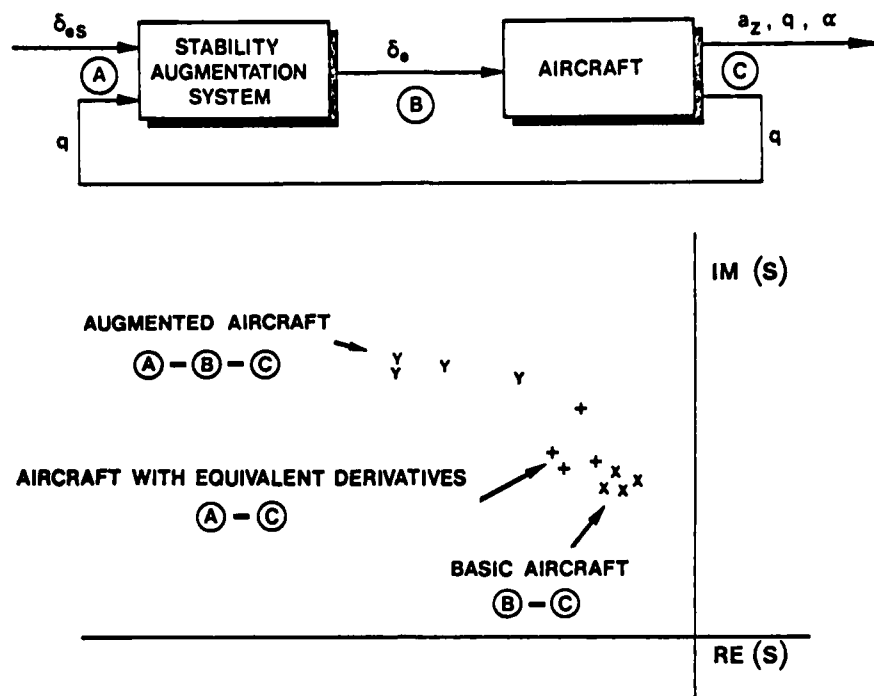


Fig. 11 Poles of Short Period Motion in Open and Closed Loop System

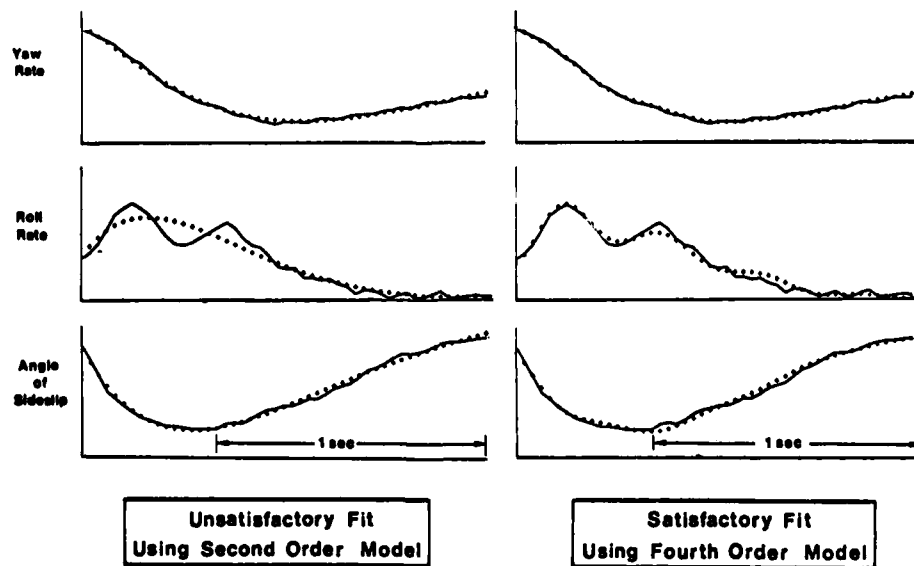


Fig. 12 Comparison of Fits Using Second and Fourth Order Models

— Flight Test Data  
 + + + Model Output

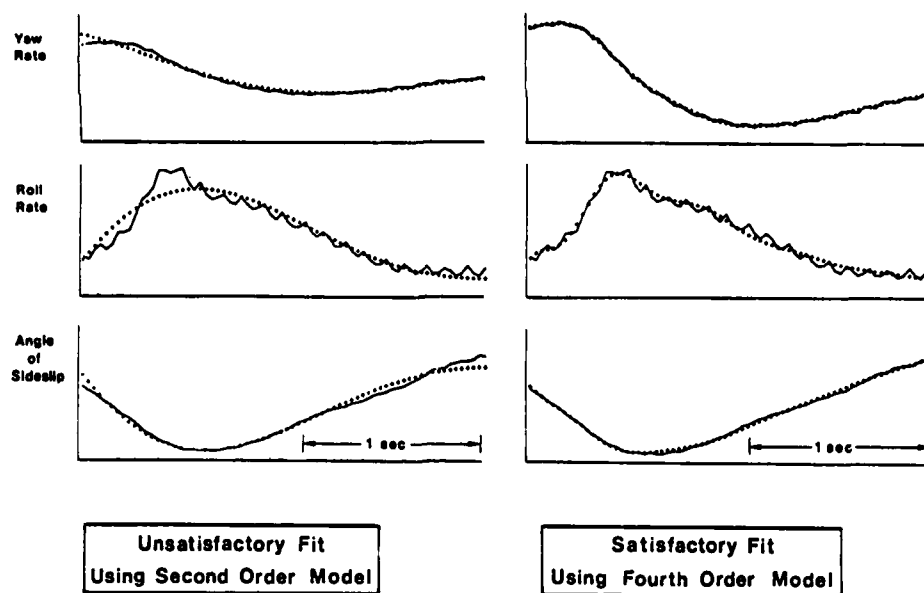


Fig. 13 Improvement of Fits in Three Output Signals Using a Fourth Order Model

— Flight Test Data  
 + + + Model Output

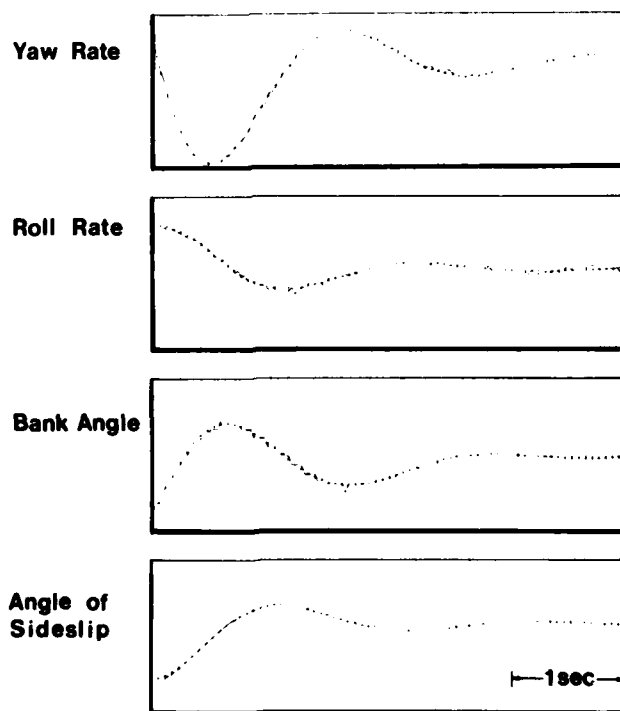


Fig. 14 Examples of Satisfactory Fit Using Second Order Model

— Flight Test Data  
 + + + Model Output

# IDENTIFICATION OF AERODYNAMIC DERIVATIVES

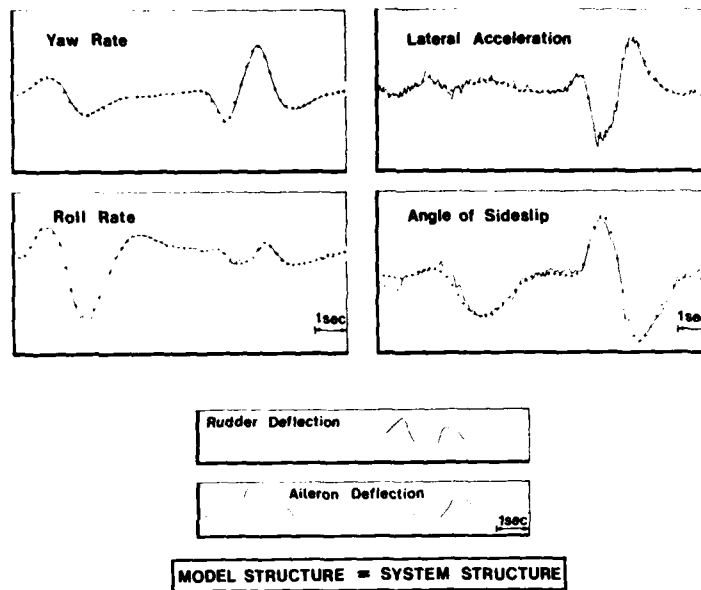


Fig. 15 Example of Good Fits in Identification of Aerodynamic Derivatives  
 — Flight Test Data  
 + + + Model Output

# IDENTIFICATION OF EQUIVALENT DERIVATIVES

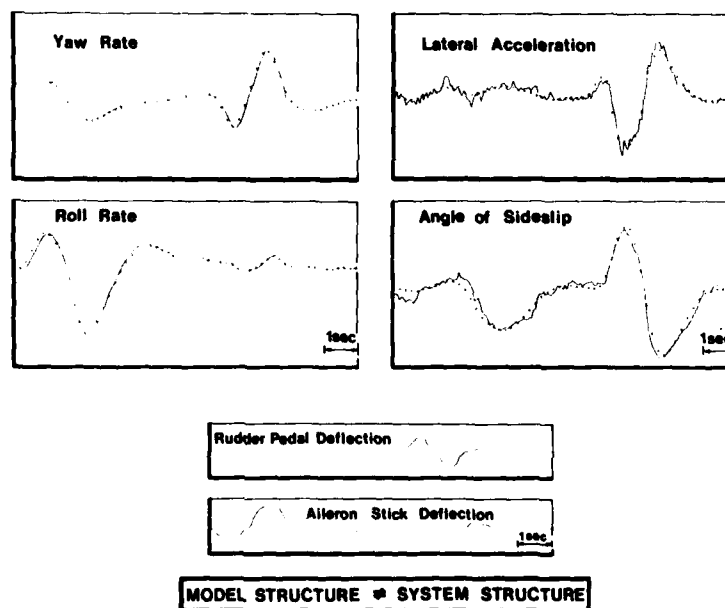


Fig. 16 Example of Good Fits in Identification of Equivalent Derivatives  
 — Flight Test Data  
 + + + Model Output

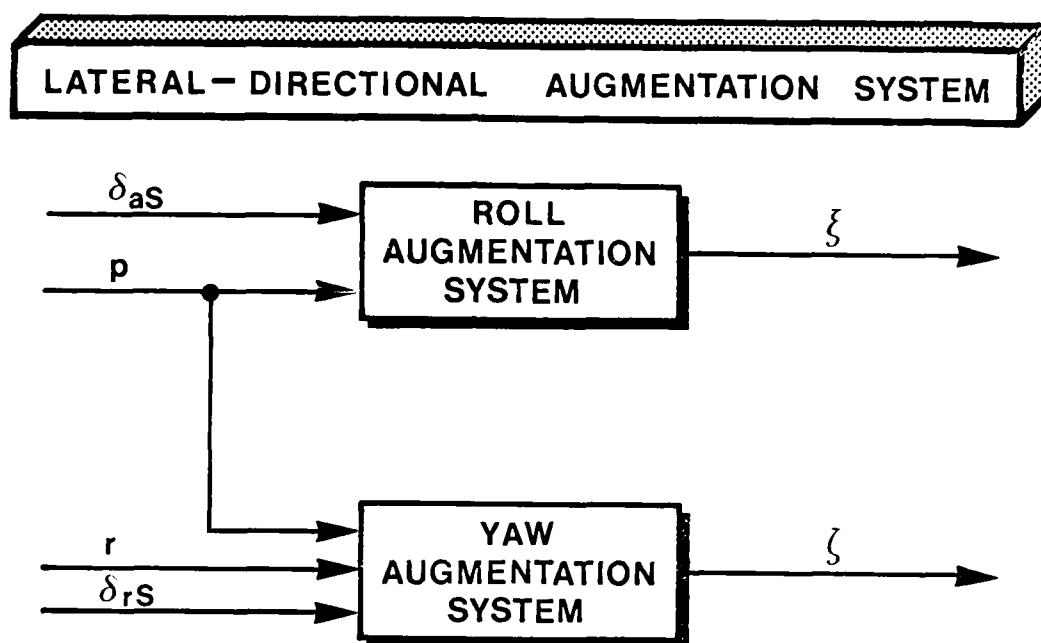


Fig. 17 Block Diagram of Stability Augmentation System

# IDENTIFICATION OF ROLL AUGMENTATION SYSTEM

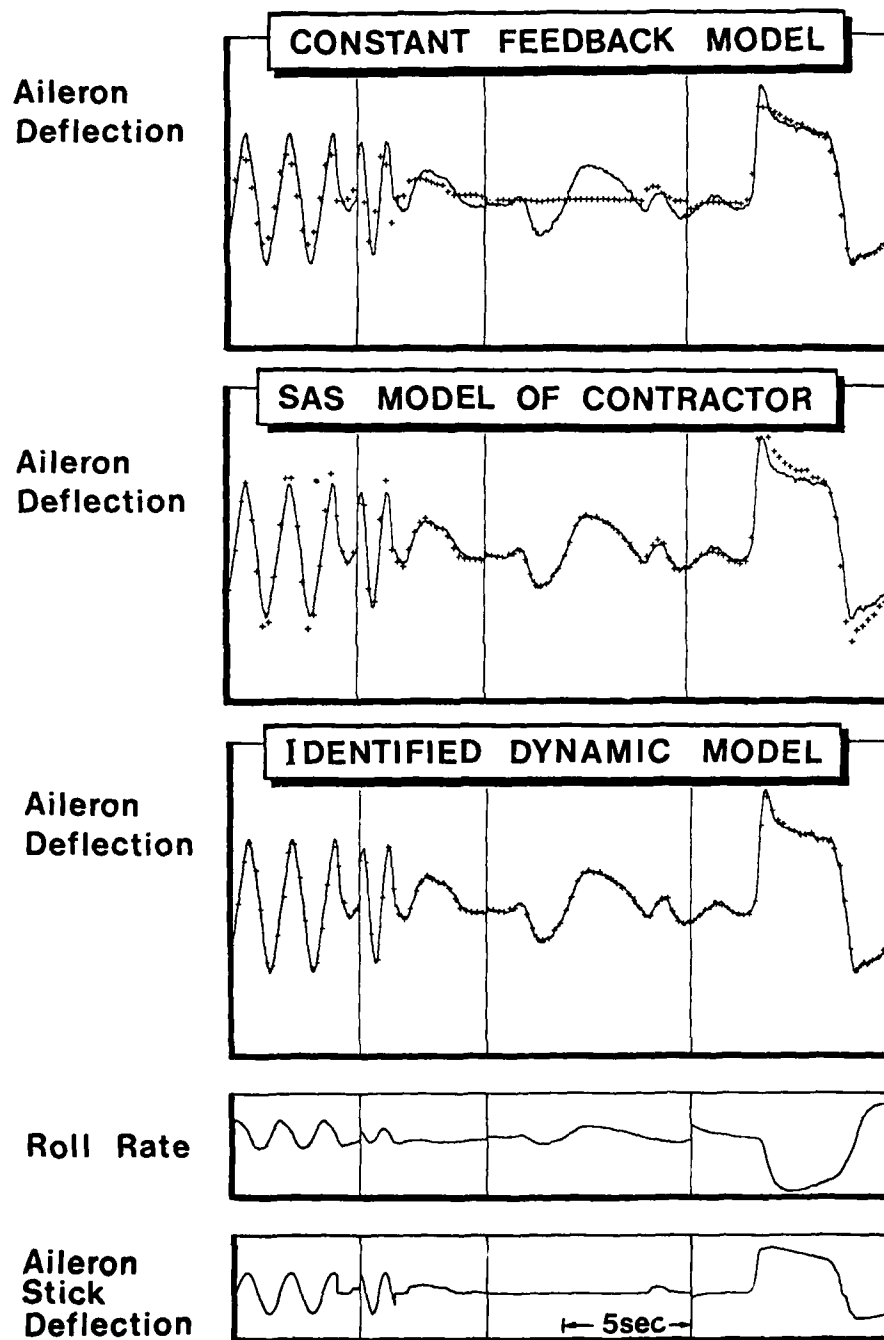


Fig. 18 Comparison of Fits in Identification of the Roll Augmentation System

— Flight Test Data  
 + + + Model Output

# IDENTIFICATION OF YAW AUGMENTATION SYSTEM

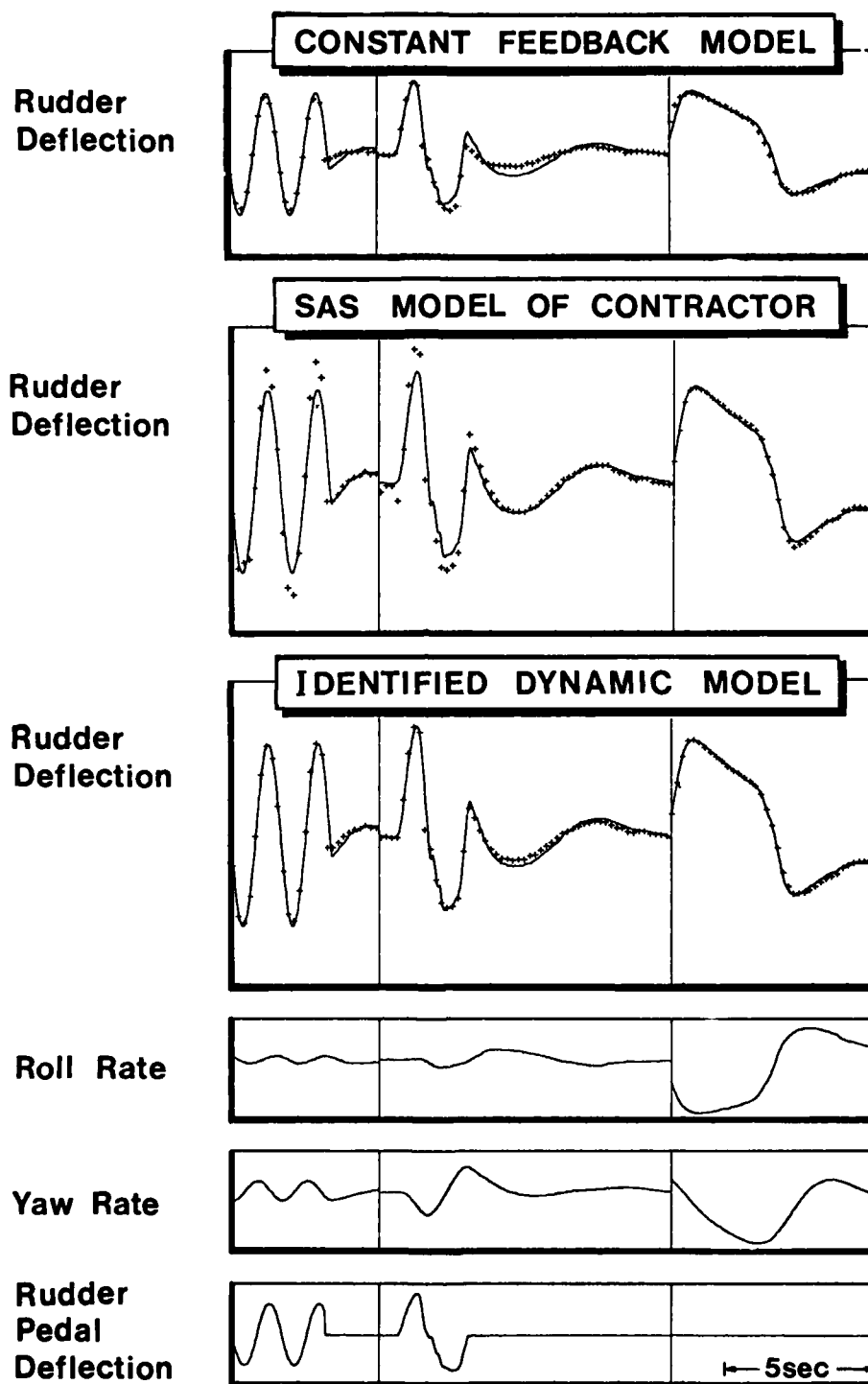


Fig. 19 Comparison of Fits in Identification of the Yaw Augmentation System

— Flight Test Data  
 + + + Model Output



# PROBLEMS IN IDENTIFICATION DUE TO SIGNAL CORRELATION

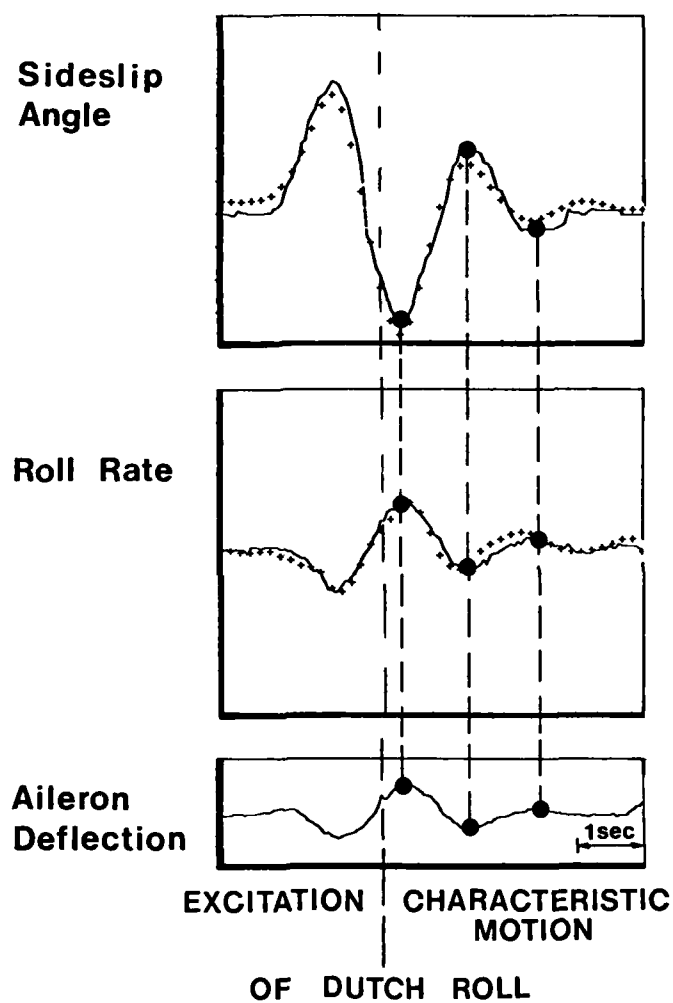


Fig. 20 Example of Signal Correlation in Characteristic Motion  
 — Flight Test Data  
 + + + Model Output

# PROBLEMS IN IDENTIFICATION DUE TO SIGNAL CORRELATION

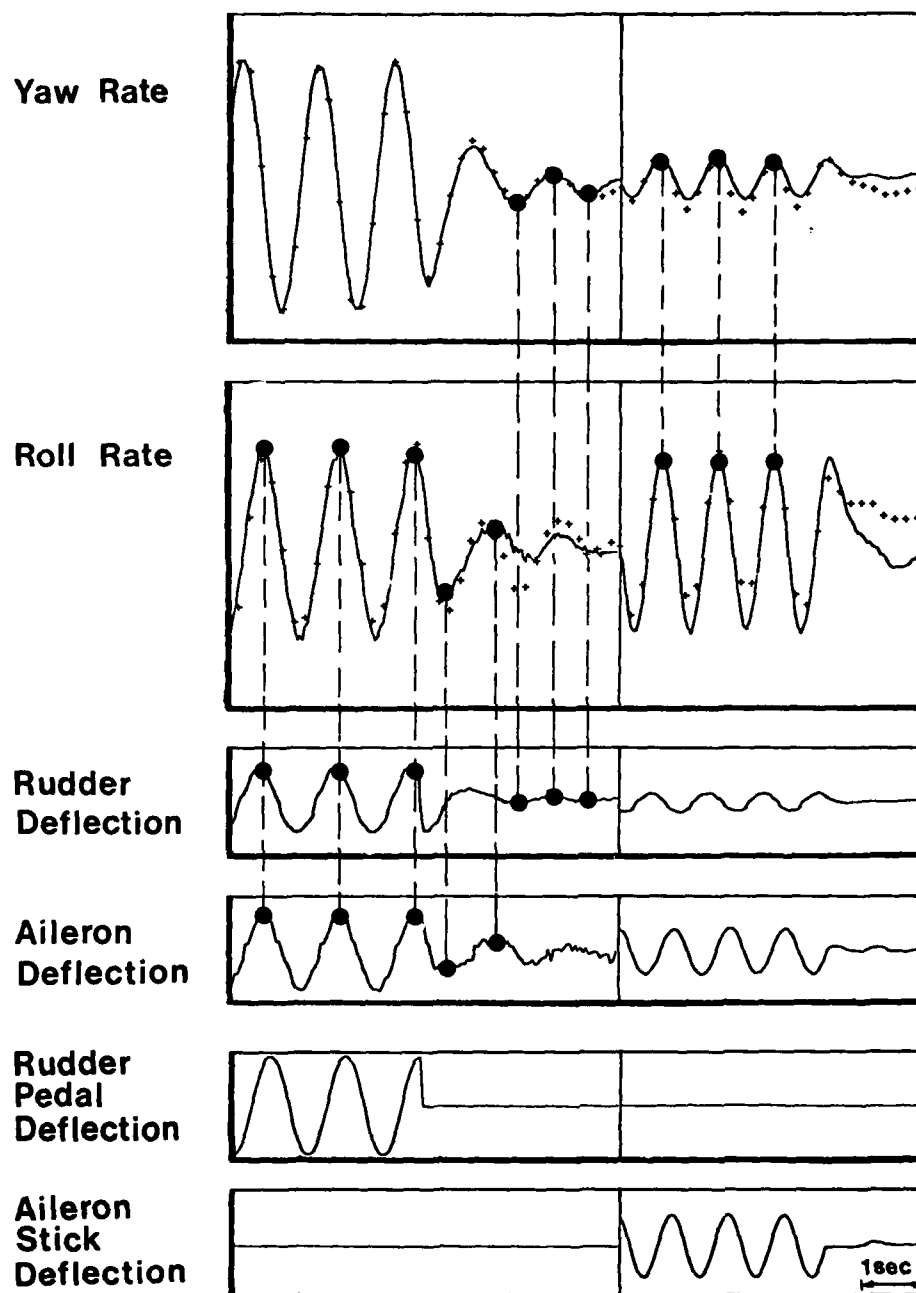


Fig. 21 Example of Signal Correlation in Harmonic Oscillation  
 — Flight Test Data  
 + + + Model Output

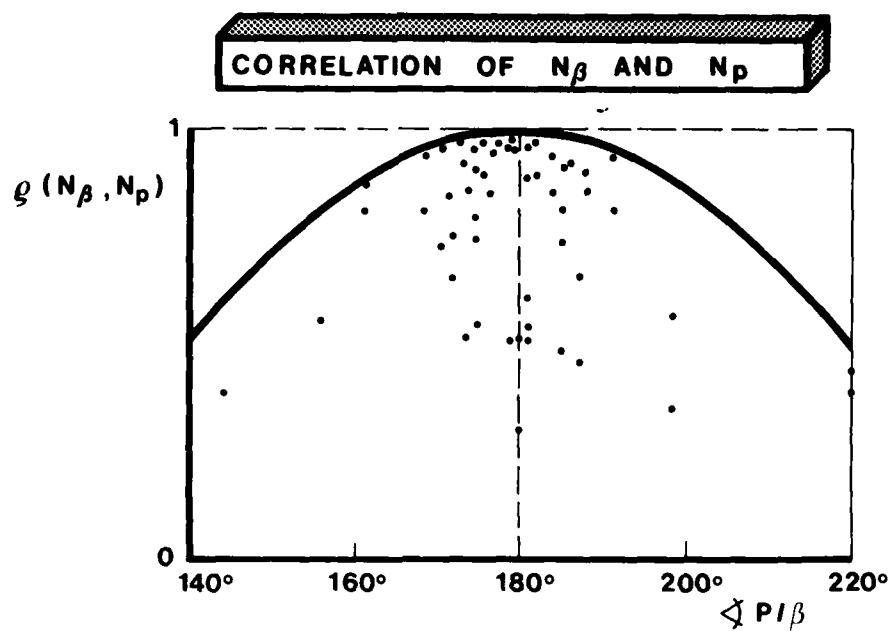


Fig. 22 Influence of Eigenvector Phase Angle  
on Correlation Coefficient of  $N_\beta$  and  $N_p$

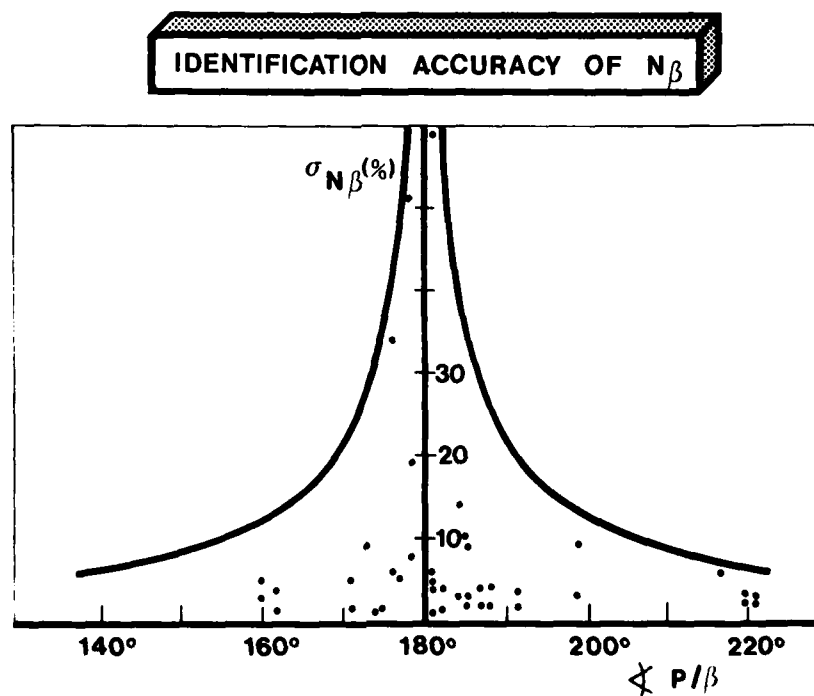


Fig. 23 Influence of Eigenvector Phase Angle  
on Identifiability of  $N_\beta$

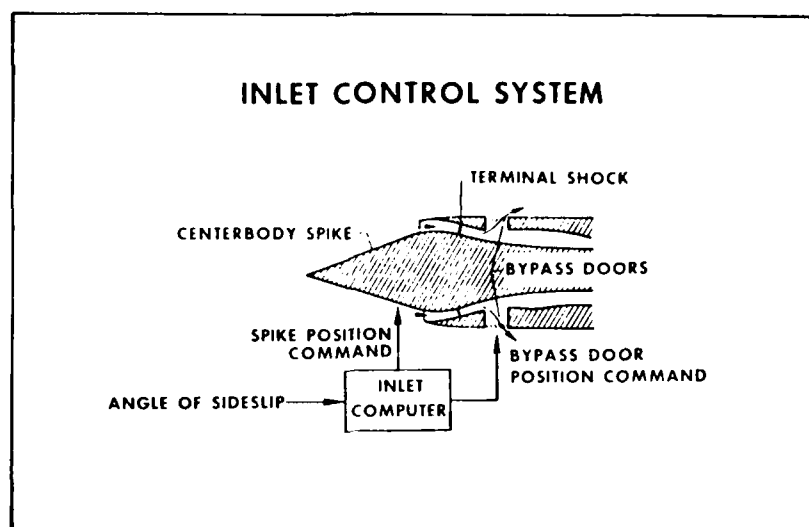
**EXAMPLE OF GLENN B. GILYARD**

Fig. 24 Inlet Control System of a Mach 3 Cruise Aircraft

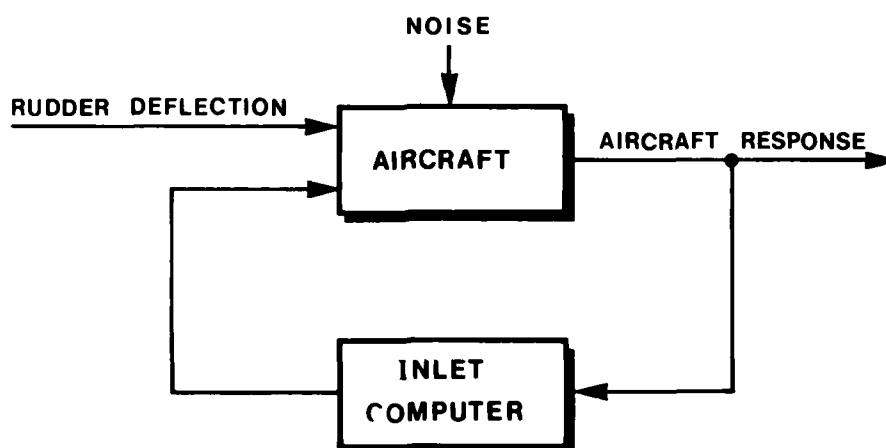


Fig. 25 Block Diagram of Inlet Control System

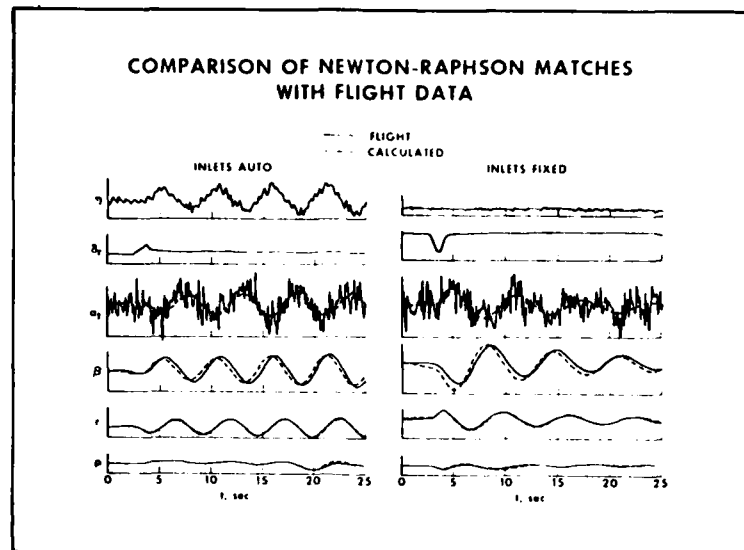
**EXAMPLE OF GLENN B. GILYARD**

Fig. 26 Identification Using Two Different SAS Modes

## BIBLIOGRAPHY

This Bibliography with Abstracts has been prepared to support AGARD Lecture Series No.104 by the Scientific and Technical Information Branch of the US National Aeronautics and Space Administration, Washington, D.C., in consultation with Dr P.Hamel of Braunschweig, Federal Republic of Germany.

Section 1	Input Design	B-1
Section 2	Aircraft Identification	B-5
Section 3	Extreme Flight Regime Identification	B-13
Section 4	Closed Loop Identification	B-19
Section 5	Rotorcraft Identification	B-25
Section 6	Identification of Aeroelastic Systems	B-33
Section 7	Miscellaneous	B-39

SECTION 1

INPUT DESIGN

**UTTL:** Application of optimal input synthesis to aircraft parameter identification

**AUTH:** A/GUPTA, N. K.; B/HALL, W. E., JR.; C/MEHRA, R. K.; PAA: B/(Systems Control, Inc., Palo Alto, Calif.); C/(Harvard University, Cambridge, Mass.) CORP: Harvard Univ., Cambridge, Mass.; Systems Control, Inc., Palo Alto, Calif. (American Society of Mechanical Engineers, 1976.) ASME, Transactions, Series G - Journal of Dynamic Systems, Measurement, and Control, vol. 98, June 1976, p. 139-145.

**ABS:** The Frequency Domain Input Synthesis procedure is used in identifying the stability and control derivatives of an aircraft. By using a frequency-domain approach, one can handle criteria that are not easily handled by the time-domain approaches. Numerical results are presented for optimal elevator deflections to estimate the longitudinal stability and control derivatives subject to root-mean square constraints on the input. The applicability of the steady state optimal inputs to finite duration flight testing is investigated. The steady state approximation of frequency-domain synthesis is good for data lengths greater than two time cycles for the short period mode of the aircraft longitudinal motions. Phase relationships between different frequency components become important for shorter data lengths. The frequency domain inputs are shown to be much better than the conventional doublet inputs.

**RPT#:** ASME PAPER 76-AUT-U 76/06/00 76A36158

**UTTL:** Effects of control inputs on the estimation of stability and control parameters of a light airplane

**AUTH:** A/CANNADAY, R. L.; B/SUIT, W. T. CORP: National Aeronautics and Space Administration, Langley Research Center, Hampton, Va.

**ABS:** The maximum likelihood parameter estimation technique was used to determine the values of stability and control derivatives from flight test data for a low-wing, single-engine, light airplane. Several input forms were used during the tests to investigate the consistency of parameter estimates as it relates to inputs. These consistencies were compared by using the ensemble variance and estimated Cramer-Rao lower bound. In addition, the relationship between inputs and parameter correlations was investigated. Results from the stabilator inputs are inconclusive but the sequence of rudder input followed by aileron input or aileron followed by rudder gave more consistent estimates than did rudder or ailerons individually. Also, square-wave inputs appeared to provide slightly improved consistency in the parameter estimates when compared to sine-wave inputs.

**RPT#:** NASA-TP-1043 L-11355 77/12/00 78N13071

**UTTL:** Computation of optimal inputs for parameter identification with Walsh and other orthogonal basis functions

**AUTH:** A/REID, J. G. PAA: A/(USAF, Avionics Laboratory, Wright-Patterson AFB, Ohio) In: Productivity: Proceedings of the Joint Automatic Control Conference, West Lafayette, Ind., July 27-30, 1976. (A77-28626 12-63) New York, American Society of Mechanical Engineers, 1976, p. 495-500.

**ABS:** A recently obtained matrix-operator representation of the parameter sensitivities in linear time-invariant systems is used to provide a straightforward and computationally efficient algorithm for computing the optimal input for parameter identification. The computational algorithm is based upon the use of the Rayleigh-Ritz-Galerkin direct method of solution and theoretical results of Mehra. If Walsh functions are selected as the basis functions in the direct method, then computation requirements of the algorithm are reduced still further. The specific reduction technique should also be of general interest to control design and system simulation with Walsh function in linear time-invariant systems. 76/00/00 77A26544

**UTTL:** Flight test design for efficient extraction of aircraft parameters

**AUTH:** A/WELLS, W. R.; B/RAMACHANDRAN, S. PAA: B/(Cincinnati, University, Cincinnati, Ohio) CORP: Cincinnati Univ., Ohio. In: Atmospheric Flight Mechanics Conference, 3rd, Arlington, Tex., June 7-9, 1976. Proceedings. (A76-36901 17-08) New York, American Institute of Aeronautics and Astronautics, Inc., 1976, p. 101-107.

**ABS:** This paper considers the design of flight control inputs which result in a minimization of the nonuniqueness problem of parameter identification due to statistical correlation. The performance index for the control design is taken as a linear weighted sum of the squares of the correlation coefficients of the aerodynamic stability and control derivatives as computed from the Cramer-Rao lower bound matrix. An optimal input design is demonstrated for an F-8 aircraft with supercritical wing. Reduced correlations are noted and corresponding estimates and confidence levels presented. 76/00/00 76A36912



differential and integral constraints. The criteria used are either expressed in terms of the Cramer-Rao lower bound on the covariance matrix of the parameter estimates or in terms of the maximum prediction error variance. Both time-domain longitudinal and lateral dynamics of C-8 and Jet Star aircrafts and comparison with doublet type inputs are made. 75/05/00  
75N30009

UTTL: Optimal input design for parameter identification of dynamic systems  
AUTH: A/RAMACHANDRAN, S. CORP: Cincinnati Univ., Ohio.  
ABS: Nonlinear multi-input multi-output multi-parameter systems are considered. The design criterion is that the optimal input should minimize statistical correlations between parameters. The performance index for the control design is taken as a linear weighted sum of the squares of the correlation coefficients of the aerodynamic stability and control derivatives as computed from the Cramer-Rao lower bound matrix. The optimal control is bang-bang when the system is linear in control and amplitude constraint is imposed on the input. Optimal aileron and rudder inputs are designed for an F-8 aircraft with super-critical wing. Reducing the correlation results in improved estimates and confidence levels. Flight tests for parameter identification are designed for a light aircraft using optimal inputs. Simulations are carried out using the optimal inputs and lateral derivatives are extracted from flight data. 76/00/00 77N15048

UTTL: Input design for aircraft parameter identification. Using time-optimal control formulation

AUTH: A/CHEN, R. T. N. CORP: Calspan Corp., Buffalo, N. Y.  
CSS: (Flight Research Dept.) In AGARD Methods for Aircraft State and Parameter Identification 15 p (SEE N75-29997 21-01)

ABS: A new formulation and a practical and useful solution to the input design for identification of aircraft stability and control parameters is presented. Necessary conditions and the structure of the optimal control input are discussed. By using Walsh functions and calculating the Cramer-Rao lower bounds recursively, a practical and useful design procedure is then presented. Application of the new approach are then made to the design of flight test inputs for identification of stability and control parameters of several types of aircraft. 75/05/00 75N30010

UTTL: Status of input design for aircraft parameter identification

AUTH: A/MEHRA, R. K.; B/EUPTA, N. K. PAA: B/ISystems Control, Inc.) CORP: Harvard Univ., Cambridge, Mass. In AGARD Methods for Aircraft State and Parameter Identification 21 p (SEE N75-29997 21-01)

ABS: Results are presented on the design of aircraft inputs (i.e. elevator, rudder and aileron deflection time histories) to identify aircraft stability and control derivatives from flight test data. The problem is first reduced to an optimization problem with

SECTION 2

AIRCRAFT IDENTIFICATION

aircraft performance model. AIDES may run under interactive graphics or as a batch program. While under interactive operation, AIDES may be controlled as an 'analog matching' process, wherein the operator may vary the system parameters and observe the effects on the match. A maximum likelihood algorithm can be used to compute improved estimates of the parameters. At each iteration, the operator has complete control over what parameters are to be identified, and may assign them any values. The program modular construction, identification algorithm, and an overview of parameter identification methods are presented. 76/00/00 77A38014

UTTL: Parameter identification and study of properties within the scope of flight testing a high-performance aircraft

AUTH: A/SCHAEUFELÉ, H.; B/EIBL, H. PAA: B/Messerschmitt-Boelkow-Blohm GmbH, Ottobrunn, West Germany) Deutsche Gesellschaft fuer Luft- und Raumfahrt, Jahrestagung, 9th, Munich, West Germany, Sept. 14-16, 1976, 53 p. In German

ABS: The paper describes the method of subsystems for calculating stability and control derivatives from parameter identification tests of aircraft. Differential equations for computing a number of derivatives of longitudinal and transverse motions are set up. Measurement matrices that minimize the effects of angle of attack and sideslip angle measurement errors are introduced. Calculations of poles and zeros of transfer functions are shown

RPT#: DGLR PAPER 76-220 MBB-UFE-1268 76/09/00 77A16528

UTTL: Recursive identification and tracking of parameters for linear and non-linear multivariable systems

AUTH: A/SIDAR, M. PAA: A/NASA, Ames Research Center, Moffett Field, Calif.) CORP. National Aeronautics and Space Administration, Ames Research Center, Moffett Field, Calif. International Journal of Control, vol. 24, Sept. 1976, p. 351-378.

ABS: The problem of identifying constant and variable parameters in multi-input, multi-output, linear and nonlinear systems is considered, using the maximum likelihood approach. An iterative algorithm, leading to recursive identification and tracking of the unknown parameters and the noise covariance matrix, is developed. Agile tracking and accurate and unbiased identified parameters are obtained. Necessary conditions for a globally asymptotically stable identification process are provided; the conditions proved to be useful and efficient. Among different

UTTL: Aircraft aerodynamic coefficient estimation

AUTH: A/GUPTA, N. K.; B/HALL, W. E.; C/KUHR, R. L. PAA: C/Systems Control, Inc., Palo Alto, Calif.) In: Conference on Decision and Control, and Symposium on Adaptive Processes, 16th, and Special Symposium on Fuzzy Set Theory and Applications, New Orleans, La., December 7-9, 1977, Proceedings, Volume 1, (A79-14957 04-63) Piscataway, N.J., Institute of Electrical and Electronics Engineers, Inc., 1977, p. 296-302. Navy-supported research.

ABS: The paper reviews advanced statistical and computational techniques used during the last decade to estimate aircraft aerodynamic coefficients from flight test data. Topics considered include system identification for aircraft aerodynamic coefficient estimation, preflight test design, post-flight data processing, and model verification. Data reconstruction, model structure estimation, and parameter identification are discussed. Examples involving input design, instrument analysis, and post-flight data processing are presented. 77/00/00 79A14974

UTTL: Estimation of the aerodynamic stability and control parameters for the F-106A aircraft from flight data - Maneuver design and flight data analysis

AUTH: A/EULRICH, B. J.; B/GOVINDARAJ, K. S.; C/HARRINGTON, W. W. PAA: B/Calspan Corp., Buffalo, N.Y.); C/(USAF, Flight Dynamics Laboratory, Wright-Patterson AFB, Ohio) In: Atmospheric Flight Mechanics Conference, Palo Alto, Calif., August 7-9, 1978. Technical Papers. (A78-46526 20-08) New York, American Institute of Aeronautics and Astronautics, Inc., 1978, p. 1-19.

RPT#: AIAA 78-1326 78/00/00 78A46527

UTTL: AIDES - A parameter identification program

AUTH: A/CLIFF, E. M.; B/HECTOR, R. G. PAA: A/(Virginia Polytechnic Institute and State University, Blacksburg, Va.); B/(USAF, Flight Test Center, Edwards AFB, Calif.) In: The many disciplines of flight test; Proceedings of the Seventh Annual Symposium, Eastsound Orcas Island, Wash., August 4-6, 1976. (A77-38003 17-05) Lancaster, Calif., Society of Flight Test Engineers, 1976, p. 13-1 to 13-20.

ABS: AIDES (Aircraft Identification and Derivative Extraction System), a computer program for identifying parameters in mathematical models of a dynamical system from measured data, is described. Models currently under investigation are a new linearized aircraft stability and control model and a linearized

cases studied, the stability derivatives of an aircraft were identified and some of the results are shown as examples. 76/09/00 76A44369

UTTL: Flight test evaluation of predicted lift aircraft drag, performance, and stability

AUTH: A/SMETANA, F. O.; B/FOX, S. R. CORP: North Carolina State Univ., Raleigh. CSS: (Dept. of Mechanical and Aerospace Engineering.)

ABS: A technique was developed which permits simultaneous extraction of complete lift, drag, and thrust power curves from time histories of a single aircraft maneuver such as a pullup (from V sub max to V sub stall) and pushover (to sub V max for level flight.) The technique is an extension to nonlinear equations of motion of the parameter identification methods of Haff and Taylor and includes provisions for internal data compatibility improvement as well. The technique was shown to be capable of correcting random errors in the most sensitive data channel and yielding highly accurate results. This technique was applied to flight data taken on the ATLIT aircraft. The drag and power values obtained from the initial least squares estimate are about 15% less than the 'true' values. If one takes into account the rather dirty wing and fuselage existing at the time of the tests, however, the predictions are reasonably accurate. The steady state lift measurements agree well with the extracted values only for small values of alpha. The predicted value of the lift at alpha = 0 is about 33% below that found in steady state tests while the predicted lift slope is 13% below the steady state value.

RPT#: NASA-CR-158076 79/00/00 79N15943

UTTL: Nonlinear parameter identification and its application to transport aircraft

AUTH: A/GALBRAITH, T. J.; B/PETERSEN, T. J. CORP: Boeing Commercial Airplane Co., Renton, Wash. In AGARD Dyn. Stability Parameters 20 p (SEE N79-15061 OG-08)

ABS: A nonlinear parameter identification computer program and results obtained from analyzing jet transport flight data characterized by nonlinear motion and parameters is described. The program is called NLAK for nonlinear aerodynamics and kinematics and is part of a system of computer programs for analyzing airplane dynamic response data. NLAK's formulation is based on the full six degrees-of-freedom equations of motion and up to third order polynomials for aerodynamic coefficients and thrust parameters. NLAK employs a maximum likelihood estimation algorithm which is capable of both recursive and batch processing. The flight data analyzed was low speed.

below 150 knots. The analysis system is outlined and all interfaces with the NLAK program are described. The basic concepts and some of NLAK's formulation details are also described in relation to obtaining consistent estimation results, especially for the nonlinear problem. 78/11/00 79N15078

UTTL: Air Force Flight Test Center experience in the identification of stability and control parameters from dynamic flight test maneuvers

AUTH: A/JEGLUM, P. M. CORP: Air Force Flight Test Center, Edwards AFB, Calif. In AGARD Dyn. Stability Parameters 5 p (SEE N79-15061 OG-08)

ABS: Air Force Flight Test Center experience in the flight test determination of stability derivatives is generalized in terms of the attainment of known benefits, and the practical and philosophical necessity for the use of the technique are discussed. Data from recent flight test programs is used to illustrate that Stability Derivative Extraction (STABDEX) techniques result in savings of flight time, a significantly better and safer flight test program and high quality data which would otherwise be unobtainable. Concluding remarks discuss the importance of the technique for the flight testing of advanced designs. 78/11/00 79N15074

UTTL: More effective aircraft stability and control flight testing through use of system identification technology

AUTH: A/BURTON, R. A.; B/BISCHOFF, D. E. CORP: Naval Air Test Center, Patuxent River, Md.

ABS: The development of system identification technology was undertaken to provide for more effective aircraft flight testing by reducing the time required to conduct specific tests and/or to provide for a more comprehensive data analysis. F-14A and TA-4J flight test results presented demonstrate that the flight time required to obtain stability and control data can be significantly reduced without loss in accuracy of conventional flight test derived parameters.

Presentation of S-3A and EA-6B system identification results demonstrate that this technology can be successfully used to update the aerodynamic data bases of modern jet aircraft from flight test data. These system identification results are compared with wind tunnel data and flight test derived parameters to demonstrate the accuracy of this new technology. Applications of this technology to integrate several areas of aircraft flight testing are discussed.

RPT#: AD-A032293 NATC-TM-76-2-SA 76/11/04 77N21086

**UTTL:** Adaptive estimation and parameter identification using multiple model estimation algorithm  
**AUTH:** A/ATHANS, M.; B/CHANG, C. B. CORP: Lincoln Lab., Mass. Inst. of Tech., Lexington.

**ABS:** The purpose of this report is to introduce an adaptive estimation and parameter identification scheme which the authors call Multiple Model Estimation Algorithm (MMEA). The MMEA consists of a bank of Kalman filters with each matched to a possible parameter vector. The state estimates generated by these Kalman filters are then combined using a weighted sum with the a posteriori hypothesis probabilities as weighting factors. If one of the selected parameter vectors coincides with the true parameter vector, this algorithm gives the minimum variance state and parameter estimates. Algorithms for filtering, smoothing, and prediction are derived for linear and nonlinear systems. They are described in a tutorial fashion with results stated explicitly so that they can be readily used for computer implementation. Approaches for the extension of MMEA to a more general class of adaptive estimation problems are outlined. Several further research topics are also suggested.  
**RPT#:** AD-A028510 TN-1976-28 ESD-TR-76-184 76/06/23 77N16803

**UTTL:** Simultaneous identification of short period and phugoid stability parameters using an advanced likelihood method

**AUTH:** A/BRYAN, F. T. CORP: Naval Postgraduate School, Monterey, Calif.

**ABS:** An investigation was conducted to determine the feasibility of obtaining the short period and phugoid stability derivatives from one maneuver, simultaneously. It was concluded that the maximum likelihood identification program SCIDNT-1 showed great promise in obtaining the short period and phugoid stability derivatives from one maneuver. Extraction of the short period stability parameters in the presence of the phugoid was easy, straight forward, and yielded results similar to those obtained from pure short period data. Estimation of the phugoid stability parameters was possible when they were estimated in conjunction with  $Z_0$ ,  $X_0$ ,  $M_0$ , and  $\Theta_0$ . It was recommended that a new set of data be obtained at a flight condition where the phugoid is at least moderately damped and that this data be analyzed to resolve the present anomalies.

**RPT#:** AD-A021760 75/12/00 76N26167

**UTTL:** Status of methods for aircraft state and parameter identification  
**AUTH:** A/HAMEL, P. G. CORP: Deutsche Forschungs- und Versuchsanstalt fuer Luft- und Raumfahrt, Brunswick (West Germany). In AGARD Flight/Ground Testing Fac. Correlation 16 p (SEE N76-25266 16-09)

**ABS:** The report of a meeting on aircraft system identification for flight test engineers and pilots, handling qualities and simulation experts, and aircraft and control system designers, was presented. It was shown that in recent years several identification procedures have evolved for obtaining aircraft parameters from inflight measurements. These approaches have been shown to have good success for conventional (winged) aircraft and have become practical to apply. The parameter identification problem becomes a much more complicated task for large and slender body aircraft where the elastic deformations at high dynamic pressure can no longer be neglected. For helicopters, simplifying assumptions are also, in general, considerably more difficult due to the strong coupling of the rigid body degrees-of-freedom, because of the different flexible motions introduced by the rotor blades, and because of the shortness of the test period which can be recorded due to the inherent instability of these vehicles.  
 76/04/00 76N25282

**UTTL:** Low angle-of-attack longitudinal aerodynamic parameters of Navy T-2 trainer aircraft extracted from flight data: A comparison of identification techniques. Volume 1: Data acquisition and modified Newton-Raphson analysis

**AUTH:** A/SCHUETZ, A. J. CORP: Naval Air Development Center, Warminster, Pa. CSS: (Air Vehicle Technology Dept.)

**ABS:** A Navy T-2 jet trainer aircraft was instrumented to measure and record all motion variables. Motion time histories were recorded for a variety of carefully selected pilot inputs. A unique problem with the data was the high noise level in the measurement of the control input. Longitudinal motion data were analyzed with three digital computer parameter identification techniques: modified Newton-Raphson, Kalman filtering/smoothing, and maximum likelihood. Reported in Volume I are data gathering and modified Newton-Raphson analysis.

**RPT#:** AD-A013181 NADC-74181-30-VOL-1 75/06/23 76N13084

**UTTL:** Model structure determination and identifiability problems in system identification

**AUTH:** A/TSE, E.; B/GUPTA, N. K. CORP: Systems Control, Inc., Palo Alto, Calif.

**ABS:** System identification has become one of the most active areas in system theory and its applications. In many engineering applications where the system to be identified or estimated is governed by differential or difference equations with known structure, the problem is mainly that of parameter estimation. As the authors extend the concept of system identification to those classes of problems where prior knowledge on structure is limited, some basic problems other than parameter estimation become important. System identification consists of three basic sub-problems: (1) pre-estimation, where one is concerned with structure specification, types of data to be collected, and experimental design. (2) estimation, where the main emphasis is on estimation algorithm development, and (3) post-estimation, where one has to test the validity of using the model for a specific objective. The program of studies reported here is on the basic problem in system identification, with more emphasis on pre-estimation and post-estimation problems.

**RPT#:** AD-A009404 75/04/00 75N31800

**UTTL:** Advancement in parameter identification and aircraft flight testing

**AUTH:** A/BURTON, R. A. CORP: Naval Air Test Center, Patuxent River, Md. CSS: (Flight Test Div.) In AGARD Methods for Aircraft State and Parameter Identification 16 p (SEE N75-29997 21-01)

**ABS:** Results are presented from a program to develop parameter identification technology with specific emphasis placed on studies conducted in parameter identifiability and (optimal) control inputs for parameter estimation. Navy applications for parameter identification technology are discussed with specific areas in aircraft stability and control testing outlined. Specific criteria required for defining optimal control inputs and establishing parameter identifiability are discussed. Parameter identification results from the analysis of flight test data are presented which establish the need for considering input design in planning tests for extracting aerodynamic coefficients from flight test data. Parameter identifiability results for specific control inputs used are presented. In cases where identifiability problems are shown to exist the use of a rank deficient solution to improve parameter identifiability is demonstrated. 75/05/00 75N30012

**UTTL:** Methods for aircraft state and parameter identification

**CORP:** Advisory Group for Aerospace Research and Development, Paris (France). Meeting held at Hampton, Va., 5-8 Nov. 1974

**RPT#:** AGARD-CP-172 75/05/00 75N29997

**UTTL:** Recursive identification and tracking of parameters for linear and nonlinear multivariable systems

**AUTH:** A/SIDAR, M. CORP: National Aeronautics and Space Administration, Ames Research Center, Moffett Field, Calif.

**ABS:** The problem of identifying constant and variable parameters in multi-input, multi-output, linear and nonlinear systems is considered, using the maximum likelihood approach. An iterative algorithm, leading to recursive identification and tracking of the unknown parameters and the noise covariance matrix, is developed. Agile tracking, and accurate and unbiased identified parameters are obtained. Necessary conditions for a globally, asymptotically stable identification process are provided; the conditions proved to be useful and efficient. Among different cases studied, the stability derivatives of an aircraft were identified and some of the results are shown as examples.

**RPT#:** NASA-TM-X-62446 A-6115 75/05/00 75N25960

**UTTL:** User's manual for a parameter identification technique

**AUTH:** A/KANNING, G. CORP: National Aeronautics and Space Administration, Ames Research Center, Moffett Field, Calif.

**ABS:** A digital computer program written in FORTRAN is presented that implements the system identification theory for deterministic systems using input-output measurements. The user supplies programs simulating the mathematical model of the physical plant whose parameters are to be identified. The user may choose any one of three options. The first option allows for a complete model simulation for fixed input forcing functions. The second option identifies up to 36 parameters of the model from wind tunnel or flight measurements. The third option performs a sensitivity analysis for up to 36 parameters. The use of each option is illustrated with an example using input-output measurements for a helicopter rotor tested in a wind tunnel.

**RPT#:** NASA-TM-X-62366 A-5752 75/03/00 75N25623

UTTL: Extraction of flight mechanic derivatives from flight data by a manual analog matching technique  
 AUTH: A/PIETRASS, A. CORP: European Space Agency, Paris (France). Transl. into ENGLISH of Ermittlung von Flugmechanischen Derivativen aus Flugmessungen durch manuelle Variation der Modellparameter am Analogrechner. DLR-FB-73-111, DFVLR, 8 Sep. 1973  
 Original German report available from DFVLR, Porz, West Ger. 27. 90 DM

ABS: Starting from linearized equations of motion of conventional jet aircraft, relations are established between single derivatives or groups of derivatives and characteristics of the transient motion in measured responses. An iterative procedure is given for parameter identification by manual analog model matching. Some parameters extracted from flight measurements of a business jet aircraft differ considerably from predicted values. Beyond the widely used linear equations with constant aerodynamic derivatives, parameters were identified of nonlinear increase of drag with incremental angle of attack, and nonstationary flap effectiveness.

RPT#: ESRO-TT-118 DLR-FB-73-111 74/12/00 75N20347

UTTL: Parameter identification applied to aircraft  
 AUTH: A/KLEIN, V. CORP: Cranfield Inst. of Technology Bedfordshire (England). CSS: (Coll. of Aeronautics.)  
 ABS: All three steps in the identification, namely characterization, parameter estimation and verification are considered and applied to the determination of aircraft parameters from flight data. The estimation procedure includes the equation error method and the output error method with the weighted least squares, maximum likelihood and Bayesian estimation technique. The problems concerning accuracy and identifiability are also discussed. A general computing algorithm is developed covering all estimation techniques described. It is applicable to linear as well as nonlinear systems and is flexible enough for the solution of various identifiability problems. Using this algorithm the computing program has been compiled in general terms to enable the user to achieve the objectives mentioned. As examples, the results of the identification of aircraft parameters and aerodynamic derivatives for four different aircraft are presented. They include the analysis of flight data from the Basset variable stability aircraft and the simulated data for a nonlinear model of the F-100 aircraft, and the flight data from the longitudinal motion of the Hp-115 slender delta-wing research aircraft.

RPT#: CRANFIELD-AERO-26 74/00/00 75N19177

SECTION 3

EXTREME FLIGHT REGIME IDENTIFICATION



**UTTL:** System identification technology for estimating re-entry vehicle aerodynamic coefficients

**AUTH:** A/GUPTA, N. K.; B/HALL, W. E., JR. PAA: B/(Systems Control, Inc., Palo Alto, Calif.) Journal of Guidance and Control, vol. 2, Mar.-Apr. 1979, p. 139-146.

**ABS:** The paper describes how a general system identification approach was specialized for the estimation of aerodynamic coefficients from maneuvering reentry vehicle (MARV) flight data. The overall system identification approach consists of two main phases, the preflight system evaluation phase and the postflight data processing phase. The basic features of the algorithms for the preflight phase, including instrument analysis, telemetry bandwidth evaluation, and trajectory perturbation determination, are described. Steps developed for postflight analysis are data reconstruction, model structure development, maximum likelihood parameter identification, and verification, and the techniques adopted for these aspects of the analysis are briefly considered. The identification methodology has been applied to some simulated responses to test the accuracy of the algorithms, and some of these results are discussed.

79/04/00 79A26321

**UTTL:** Identification of aircraft aerodynamic characteristics at high angles of attack and sideslip using the estimation before modeling (EBM) technique

**AUTH:** A/RAMACHANDRAN, S.; B/SCHNEIDER, H.; C/MASON, J. D.; D/STALFORD, H. L. PAA: D/(Dynamics Research Corp., Wilmington, Mass.) In: Atmospheric Flight Mechanics Conference, Hollywood, Fla., August 8-10, 1977. Technical Papers. (A77-43151 20-08) New York, American Institute of Aeronautics and Astronautics, Inc., 1977, p. 374-385. Navy-supported research.

**ABS:** This paper presents the EBM technique for aircraft parameter identification in stall/poststall flight regime. This method uses a unique two-step approach. The first step is the model independent estimation of states and aerodynamic forces and moments using a nonlinear spline estimation method. In the second step, the angles of attack and sideslip and control input space is divided into several small subspaces. Data from all flights that fall within the chosen subspace is used in modeling the force and moment coefficients. The state and control dependent model is obtained using Stepwise Multiple Linear Regression (SMLR). The technique is demonstrated for a light jet trainer aircraft.

**RPT#:** AIAA 77-1169 77/00/00 77A43192

**UTTL:** A nonlinear method for parameter identification applied to a trajectory estimation problem

**AUTH:** A/HULL, D. G.; B/WILLIAMSON, W. E. PAA: A/(Texas, University, Austin, Tex.); B/(Sandia Laboratories, Albuquerque, N. Mex.) In: Atmospheric Flight Mechanics Conference, Hollywood, Fla., August 8-10, 1977. Technical Papers. (A77-43151 20-08) New York, American Institute of Aeronautics and Astronautics, Inc., 1977, p. 148-150. ERDA-supported research.

**ABS:** The trajectory estimation problem is formulated as a parameter identification problem. The performance index is that of weighted least squares, and the unknown parameters are the initial conditions of the trajectory and the parameters which are used to represent the aerodynamic constants or functions. The optimization problem is solved using a square-root variable-metric algorithm. Also, to avoid having to linearize the equations defining the model, the derivatives needed by the optimization algorithm are computed numerically. Finally, the nonlinear estimation method is used to compute the initial state and drag coefficient history of a reentry vehicle using simulated radar data.

**RPT#:** AIAA 77-1137 SAND-77-0065C 77/00/00 77A43168

**UTTL:** Practical applications of parameter identification

**AUTH:** A/FREL, D. R. PAA: A/(Grumman Aerospace Corp., Bethpage, N.Y.) In: Atmospheric Flight Mechanics Conference, Hollywood, Fla., August 8-10, 1977. Technical Papers. (A77-43151 20-08) New York, American Institute of Aeronautics and Astronautics, Inc., 1977, p. 134-147.

**ABS:** A modified maximum-likelihood parameter-estimation technique was developed at Grumman and applied to the F-14 and the Shuttle Training Aircraft (STA). The algorithm operated in an interactive mode, providing for control of the number of active parameters and state equations, while the program was running. Initial F-14 work was for trimmed level flight. STA flight data were analyzed in both forward and reverse-thrust modes, providing reliable derivatives during flight development tests. Lateral-directional derivatives were extracted from F-14 high-angle-of-attack maneuvers, from 7.5 to 36 degrees. Work done to date with this program employed a linear model, no data smoothing techniques, and normal stability and control flight test maneuvers. The program provided a rapid and reliable method of determining aircraft stability and control derivatives in a flight test environment.

**RPT#:** AIAA 77-1136 77/00/00 77A43167

UTTL: Aerodynamic parameter identification for the A-7 airplane at high angles of attack

AUTH: A/MCDRINN, D. E.; B/BRASSELL, B. B. PAA: B/(V)ught Corp., Dallas, Tex.) In: Atmospheric Flight Mechanics Conference, 3rd, Arlington, Tex., June 7-9, 1976. Proceedings. (A76-36901 17-08) New York, American Institute of Aeronautics and Astronautics, Inc., 1976, p. 108-117.

ABS: Methods are developed for the practical determination of aircraft stability coefficients from flight test data at nonlinear flight regimes. The emphasis throughout is on development of practical techniques for everyday use. Modeling is performed by step up/step down regression analysis. Kalman filter techniques are used for data preprocessing. Parameter identification is by quasi-linearization techniques, extended to embrace multiple maneuvers and nonlinear plants. The techniques developed are applied to actual flight test data for the A-7 aircraft. This produces a model which is then tested by using it to predict the dynamics of a maneuver which was not used in the analyses. The results validate the usefulness of the techniques. 76/00/00 76A36913

UTTL: Model structure determination and test input selection for identification of nonlinear regimes

AUTH: A/GUPTA, N. K.; B/HALL, W. E.; JR. CORP: Systems Control, Inc., Palo Alto, Calif. CSS: (Aeronautical and Marine Systems Div.)

ABS: This report describes techniques for model structure estimation and test input design for system identification in nonlinear vehicle regimes. Optimal methods for parameterizing estimation problems are discussed. For those regions where aerodynamic or hydrodynamic force and moment models are not known, the use of splines in approximating unknown nonlinear effects is discussed. Finally, methods for selecting inputs which enhance system identifiability are described.

RPT#: AD-8037831 SCAMS-TR-107 ONR-CR215-213-5 76/08/00 77N26131

UTTL: Model structure determination and parameter identification for nonlinear aerodynamic flight regimes

AUTH: A/HALL, W. E.; JR.; B/GUPTA, N. K.; C/TYLER, J. S.; JR. CORP: Systems Control, Inc., Palo Alto, Calif. In AGARD Methods for Aircraft State and Parameter Identification 21 p (SEE N75-29997 21-01)

ABS: The identification of nonlinear stall/spin regime aerodynamic forces and moments is discussed, along with applications to simulated and flight test response

data. For this development, a two-step method is presented. The first step is the application of an algorithm which determines the order and coefficients of polynomial expansions which determines the order and coefficients of polynomial expansions which determines the order and coefficients of polynomial expansions of the nonlinear aerodynamic forces and moments which characterize the stall/post-stall flight regime. The second step is the use of a nonlinear six degree-of-freedom maximum likelihood algorithm which accurately estimates the values of the polynomial coefficients. This method was applied to simulated and flight test data for a twin engine swept wing fighter aircraft. Suggested approaches to general nonlinear flight regime identification are given. 75/05/00 75N30018

UTTL: Identification of nonlinear aerodynamic stability and control parameters at high angle of attack

AUTH: A/EULRICH, B. J.; B/RYNASKI, E. G. CORP: Calspan Corp., Buffalo, N. Y. In AGARD Methods for Aircraft State and Parameter Identification 15 p (SEE N75-29997 21-01)

ABS: A procedure is described for the estimation of the nonlinear aerodynamic stability and control coefficients at high aircraft angles of attack. It is based on a nonlinear, iterated Kalman filter/fixed-point smoother identification algorithm and a least squares equation error method. Key ingredients for successful identification are the mathematical model, instrumentation system, control inputs, and the identification algorithm. The major emphasis is placed on the use of the identification procedure in analyzing high angle of attack flight data. Specifically, model form and initial estimates are established from wind tunnel data using series expansions to represent the nondimensional force and moment coefficients for selected ranges of angle of attack. This high dimensional representation is reduced by: (1) preprocessing the flight data using the instrumentation system model and the six-degree-of-freedom aircraft kinematic equations to perform optimal state estimation and hence decrease the effects of instrumentation errors, and (2) separating the six equations of motion into two separate four-degree-of-freedom systems: one for extracting the longitudinal coefficients and the other for the lateral-directional coefficients. Specific problems associated with the identification procedure at high angles of attack and parameter identifiability problems caused by poorly conditioned flight data are reviewed. Selection of the coordinate system for the

aircraft model, the determination of the initial covariance estimates, and the measurement and process noise statistics required to use the iterated Kalman technique are discussed. 75/05/00 75N29999

UTTL: Modelling of systems with a high level of internal fluctuations

AUTH: A/JONES, J. G. CORP: Royal Aircraft Establishment, Bedford (England). In AGARD Methods for Aircraft State and Parameter Identification 18 p (SEE N75-29997 21-01)

ABS: The problem of modelling the structure of systems with a high level of internally generated fluctuations is discussed and problems in parameter identification are reviewed. The systems considered typically have two types of behavior, determined by the magnitude of a controlling parameter which influences stability. For a finite range of parameter values the system is stable and its structure may be described by a deterministic set of differential equations. If not subjected to external disturbances the system will achieve a state of equilibrium. At some 'critical' value of the parameter, however, the system becomes unstable and beyond this boundary the system no longer achieves a state of equilibrium but may exist (as a result of nonlinearities) in a steady state typified by continuous fluctuations. This state may either be described as a regular limit-cycle type of oscillation or may be essentially random in nature. Practical examples include aircraft buffeting and wing-rocking. Forms of fluctuating motion which occur respectively in structural and rigid-body modes. In these examples aircraft incidence may be regarded as the controlling parameter and the fluctuating motion is associated with the existence of extensive areas of separated flow at high incidence. A structure which falls into the type considered, is the standard human-pilot model in which the internal fluctuations are represented by a 'remnant'. An example is discussed which illustrates problems that can arise in the identification of this type of system when operating as part of a closed loop. 75/05/00 75N29998

SECTION 4

CLOSED LOOP IDENTIFICATION

before using the parameters in an on-line design process. The on-line design process is an algebraic mapping of the parameters of the model into primary control system feedback and feedforward gains. The mapping was selected to satisfy specific flying quality characteristics over the range of parameter variations expected. Results are presented from simulation studies on the identification algorithm made during the development of the system. 77/10/00 78A12361

UTTL: An implementable digital adaptive flight controller designed using stabilized single-stage algorithms

AUTH: A/ALAG, G.; B/KAUFMAN, H. PAA: B/(Rensselaer Polytechnic Institute, Troy, N.Y.) CORP: Rensselaer Polytechnic Inst., Troy, N.Y. IEEE Transactions on Automatic Control, vol. AC-22, Oct. 1977, p. 780-788.

ABS: An explicit adaptive controller, which makes direct use of on-line parameter identification, has been developed and applied to both the linearized and nonlinear equations of motion for the F-8 aircraft. This controller is composed of an on-line weighted least squares parameter identifier, a Kalman state filter, and a real model following control law designed using single-stage performance indices. The corresponding control gains are readily adjustable in accordance with parameter changes to ensure asymptotic stability if the conditions of perfect model following are satisfied, and stability in the sense of boundedness otherwise. Simulation experiments with realistic measurement noise indicate that the controller was effective in compensating for parameter variations and capable of rapid recovery from a set of erroneous initial parameter estimates which defined a set of destabilizing gains. 77/10/00 78A12360

UTTL: A moving-window parameter adaptive control system for the F8-DFBW aircraft

AUTH: A/MONTGOMERY, R. C.; B/DUNN, H. J. PAA: B/(NASA, Langley Research Center, Flight Dynamics and Control Div., Hampton, Va.) CORP: National Aeronautics and Space Administration, Langley Research Center, Hampton, Va. In: Conference on Decision and Control and Symposium on Adaptive Processes, 15th, Clearwater, Fla., December 1-3, 1976, Proceedings. (A77-28801 12-63) New York, Institute of Electrical and Electronics Engineers, Inc., 1976, p. 15-22.

ABS: This paper describes the moving-window parameter adaptive control system developed for the NASA F8-DFBW aircraft. The control system employs a parameter identification process that, iteratively, adjusts

UTTL: On-line parameter estimation using a high sensitivity estimator

AUTH: A/MISHNE, D.; B/BRYSON, A. E.; JR. PAA: B/(Stanford University, Stanford, Calif.) CORP: Stanford Univ., Calif. In: Guidance and Control Conference, Palo Alto, Calif., August 7-9, 1978, Technical Papers. (A78-50159 22-01) New York, American Institute of Aeronautics and Astronautics, Inc., 1978, p. 413-423.

ABS: An on-line parameter identification method is presented. The method is based on a recursive formulation of the maximum likelihood method, with a significant modification on the gains of the state estimator. In the conventional maximum likelihood method, the Kalman gains are used in the state estimator. This produces unbiased, minimum variance parameter estimates in the presence of process noise and measurement noise, but it also slows the convergence rate when the identification is done on-line. Here we suggest choosing the gains to maximize a measure of the sensitivities of the state estimates to parameter variations. One such criterion is to minimize the trace of the inverse information matrix. This increases the convergence rate significantly. After one or two time constants, the gains are switched to the Kalman values to assure unbiased, minimum-variance estimates. The state estimate will initially be nonoptimal, and may not be adequate for control purposes. In this case, a parallel Kalman filter which uses the identifier's parameter estimates can be used. This method is applied here for the identification of a simple first-order system, and for the identification of short-period stability derivatives of an F-8 aircraft from simulated data.

RPT#: AIAA 78-1303 78/00/00 78A50205

UTTL: A moving window parameter adaptive control system for the F8-DFBW aircraft

AUTH: A/DUNN, H. J.; B/MONTGOMERY, R. C. PAA: B/(NASA, Langley Research Center, Hampton, Va.) CORP: National Aeronautics and Space Administration, Langley Research Center, Hampton, Va. IEEE Transactions on Automatic Control, vol. AC-22, Oct. 1977, p. 788-795.

ABS: This paper describes the moving window parameter adaptive control system developed for the NASA F8-DFBW aircraft. The control system employs a parameter identification process that, iteratively, adjusts parameters of a model of the aircraft motions in a batch-processing manner so that responses generated from the model fit the outputs of sensors stored in a finite record referred to as the moving window. Tests are made on the validity of the parameter estimates

parameters of a model of the aircraft motions in a batch processing manner so that responses generated from the model fit the outputs of sensors stored in a finite record referred to as the moving window. Tests are made on the validity of the parameter estimates before using the parameters in an on-line design process. The on-line design process is an algebraic mapping of the parameters of the model into primary control system feedback and feedforward gains. The mapping was selected to satisfy specific flying quality characteristics over the range of parameter variations expected. Results are presented from simulation studies on the identification algorithm, tests for parameter validity, and the on-line design process. 76/00/00 77A28805

UTTL: An adaptive flight controller for the F-8 without explicit parameter identification

AUTH: A/MABLIUS, L.; B/KAUFMAN, H. PAA: A/(Analytical Sciences Corp., Reading, Mass.); B/(Rensselaer Polytechnic Institute, Troy, N.Y.) In: Conference on Decision and Control and Symposium on Adaptive Processes, 15th, Clearwater, Fla., December 1-3, 1976. Proceedings. (A77-28801 12-63) New York, Institute of Electrical and Electronics Engineers, Inc., 1976 p. 9-14.

ABS: A stabilizing adaptive control algorithm which does not require the presence of an identification algorithm has been developed and applied to the F-8 aircraft. Results using linear dynamics with no disturbances showed the procedure to be capable of stabilizing motion even in the presence of rapidly varying parameters. Using the linearized lateral F-8 equations, the algorithm is shown to be capable of adjusting to sudden flight condition changes within 1-2 seconds. 76/00/00 77A28804

UTTL: Estimation of the parameters of the dynamic model of an aircraft with the purpose of designing adaptive numerical control

AUTH: A/BELONGOV, V. D.; B/NIKOLAIEV, I. U. A.; C/TERIAEV, E. D.; D/SHARLIKOV, B. M. In: Identification and estimation of system parameters; Symposium, 4th, Tiflis, Georgian SSR, September 21-27, 1976. Preprints. Part 2. (A77-25276 10-99) Tiflis, Izdatel'stvo Metsniereba, 1976, p. 211-222. In Russian.

ABS: Necessary and sufficient conditions are formulated for the identifiability of control plants in a closed adaptive numerical control system of an aircraft, and a parameter-identification algorithm based on a recursive least squares method is developed. Methods

for raising the accuracy and reducing the time of the identification of optimal control characteristics, in the presence and absence of random disturbances, are described. 76/00/00 77A25281

UTTL: A recursive on-line estimation method with application to aircraft dynamics parameter identification

AUTH: A/SIDAR, M. PAA: A/(Ministry of Defense, Armament Development Authority, Haifa, Israel) (Israel Annual Conference on Aviation and Astronautics, 18th, Tel Aviv and Haifa, Israel, May 19, 20, 1976.) Israel Journal of Technology, vol. 14, no. 1-2, 1976, p. 56-65.

ABS: The problem of identifying constant system parameters and identifying and tracking variable parameters in multi-input, multi-output, linear and nonlinear systems is considered in this paper. An identification algorithm is developed on the basis of the one step prediction error concept using the minimum variance and the maximum likelihood approach. The identification is performed by applying the 'output error' approach. The novel iterative algorithm, leading to recursive identification and tracking of the unknown parameters and the noise covariance matrix, is developed and presented here. Agile tracking, accurate, consistent and unbiased parameter estimates are obtained. Necessary conditions for a stable identification process are provided. Among different cases studied, special emphasis was focused on the aircraft dynamics identification problem, the stability and control derivatives of aircraft being identified. Some results are shown as examples in this paper. 76/00/00 77A15033

UTTL: Adaptive optimal input synthesis for linear system identification

AUTH: A/UPADHYAYA, B. R.; B/SORENSEN, H. W. CORP: California Univ., San Diego. CSS: (Dept. of Applied Mechanics and Engineering.)

ABS: Optimal open-loop feedback formulation of the input synthesis problem for parameter estimation in linear dynamic systems is presented. The combination of recursive estimation and synthesis technique features a marked improvement in the behavior of estimates over the open-loop formulation. These methods are also applied in designing probing signals when the discrete a priori distribution of the parameters is known.

RPT#: AD-A013809 AFOSR-75-1093TR 75/00/00 76N14862

UTTL: Parameter identification of minimal realizations

AUTH: A/PASSERI, D.; B/HERGET, C. J. CORP: Iowa State Univ. of Science and Technology, Ames. CSS: (Engineering Research Inst.)

ABS: The report is concerned with the problem of identifying the unknown parameters of a multiple-input/multiple-output, linear, constant, discrete time system from measurements made on the inputs and the outputs. The class of systems to be considered must satisfy the requirements of a specified canonical form. Necessary and sufficient conditions for systems to satisfy this canonical form are given, and as demonstrated by the examples in the report, a large class of useful systems falls into the category for which this identification algorithm is applicable.

RPT# : AD-747693 ERI-72189 72/07/00 73N12653

UTTL: Adaptive parameter identification

AUTH: A/KAUFMAN, H.; B/BEAULIER, D. CORP: Rensselaer Polytechnic Inst., Troy, N. Y. CSS: (Systems Engineering Div.)

ABS: An extended Kalman filter with a fictitious noise input is developed for tracking time varying parameters. An adaptation algorithm is used for adjusting the covariance of the fictitious noise according to the magnitude of the measured residuals. Application of the filter to the tracking of time varying VTOL parameters is shown to give an off line model that reproduces the process behavior much better than a model with fixed parameters.

RPT# : AD-739694 71/00/00 72N28024

SECTION 5

ROTORCRAFT IDENTIFICATION



simulated and actual flight data processing are given to illustrate each phase of processing. The procedure is shown to provide means of calibrating sensor errors in flight data, quantifying high order state variable models from the flight data, and consequently computing related stability and control design models.

RPT#: AHS 78-30 78/00/00 79A18156

UTTL: VALT Parameter Identification flight test  
A/TOMASINE, R. L.; B/BRYANT, W. H.; C/HODGE, W. F.  
PAA: A/U.S. Army, Structures Laboratory, Hampton, Va.; C/(NASA, Langley Research Center, Hampton, Va.)  
CORP: National Aeronautics and Space Administration, Langley Research Center, Hampton, Va.; Army Structures Lab., Hampton, Va.; Associazione Italiana di Aeronautica ed Astronautica and Associazione Aerospaziale, European Rotorcraft and Powered Lift Aircraft Forum, 4th, Stresa, Italy, Sept. 13-15, 1978. Paper, 14 p.

ABS: The paper describes a method of establishing the accuracy of previously developed analytical models of research vehicles for a program for developing avionics technology for VTOL aircraft. The research vehicle is a Boeing-Vertol CH 47 tandem rotor transport helicopter equipped with a fly-by-wire control system. The specialized flight test was designed to take into account the presence of winds at flight conditions from hover through transition to cruise. The test provided data to obtain estimates of derivatives by parameter identification. 78/09/00 78A45439

UTTL: Parameter Identification of a hingeless rotor helicopter

AUTH: A/RIX, O.; B/KALETKA, J.; C/HUBER, H. PAA: B/(Deutsche Forschungs- und Versuchsanstalt fuer Luft- und Raumfahrt, Braunschweig, West Germany); C/(Messerschmitt-Boelkow-Blohm GmbH, Munich, West Germany) In: American Helicopter Society, Annual National Forum, 33rd, Washington, D.C., May 9-11, 1977, Proceedings. (A77-40048 1B-01) Washington, D.C., American Helicopter Society, Inc., 1977, 17 p.

ABS: The three-step research program discussed was carried out with the aim of identifying the parameters of the BO 105 hingeless-rotor helicopter. The derivation of mathematical models describing rotorcraft behavior, with allowance for helicopter dynamics and flight mechanics is discussed, along with the application of digital simulation to in-flight data identification and interpretation of the results. Identification results are presented, showing that helicopters, in general, can be described by linear models, and that

UTTL: Parameter identification applied to analytic hingeless rotor modeling  
A/BANERJEE, D.; B/CREWS, S. T.; C/HOHENEMER, K. H. PAA: A/(Hughes Helicopters, Culver City, Calif.); B/U.S. Army, Systems Development and Qualification Div., St. Louis, Mo.; C/(Washington University, St. Louis, Mo.) CORP: Hughes Helicopters, Culver City, Calif.; Army Aviation Research and Development Command, St. Louis, Mo.; Washington Univ., St. Louis, Mo. American Helicopter Society, Journal, vol. 24, Jan. 1979, p. 26-32. Army-sponsored research;

ABS: It is known that dynamic rotor inflow has a substantial effect on rotor dynamic loads. Despite the complexity of the unsteady flow problem, simple analytical models can be made useful by identifying their parameters from transient response tests without performing flow measurements. Two analytical inflow models are studied; the first is based on an equivalent blade lock number, the second is based on a time delayed unsteady momentum inflow. In preparation for the experimental data analysis, identifications from simulated test data and an eigenvalue analysis are performed. The experimental results show that the first analytical inflow model is accurate for rotor advance ratios of 0.4 and above. For lower advance ratios, the second inflow model provides better accuracy. Prediction studies with experimental data not used for the identification are performed to determine the accuracy of the mathematical models. 79/01/00 79A22475

UTTL: Rotorcraft system identification techniques for handling qualities and stability and control evaluation

AUTH: A/HALL, W. E., JR.; B/GUPTA, N. K.; C/HANSEN, R. S. PAA: C/(Systems Control, Inc., Palo Alto, Calif.) CORP: Systems Control, Inc., Palo Alto, Calif. In: American Helicopter Society, Annual National Forum, 34th, Washington, D.C., May 15-17, 1978, Proceedings. (A79-18126 05-01) Washington, D.C., American Helicopter Society, 1978, 23 p.

ABS: An integrated approach to rotorcraft system identification is described. This approach consists of sequential application of (1) data filtering to estimate states of the system and sensor errors, (2) model structure estimation to isolate significant model effects, and (3) parameter identification to quantify the coefficient of the model. An input design algorithm is described which can be used to design control inputs which maximize parameter estimation accuracy. Details of each aspect of the rotorcraft identification approach are given. Examples of both

the 80 105 helicopter's behavior at moderately high air speeds is adequately described by a model which includes a single aerodynamic derivative in each of the force equations.

RPT#: AHS 77-33-42 77/00/00 77A40073

UTTL: Optimum data utilization for parameter identification with application to lifting rotors  
AUTH: A/BANERJEE, D.; B/HOHENEMSER, K. PAA: A/Washington University, St. Louis, Mo.) CORP: Washington Univ., St. Louis, Mo. Journal of Aircraft, vol. 13, Dec. 1976, p. 1014-1016.

ABS: The work is concerned with determining the minimum quantity of data needed for achieving best possible accuracy of identified parameters in transient testing of a lifting rotor blade. Specifically, the problem is that of determining from blade flapping transients caused by blade pitch inputs the equivalent Lock number and the equivalent collective pitch setting. For a given time-dependent blade pitch input function, the running time for the test less than which insufficient parameter accuracy is obtained and more than which little accuracy improvement is achieved was calculated with the aid of the Cramer-Rao lower bound for the parameter covariance matrix. 76/12/00 77A14554

UTTL: Identification of helicopter parameters  
AUTH: A/GMELIN, B.; B/KALETKA, J.; C/RIX, O. PAA: C/(Deutsche Forschungs- und Versuchsanstalt fuer Luft- und Raumfahrt, Institut fuer Flugmechanik, Braunschweig, West Germany) Zeitschrift fuer Flugwissenschaften, vol. 22, Nov. 1974, p. 367-372. In German.

ABS: Parameter identification employing a hybrid computer is performed using a simulation of the Sikorsky S-61 helicopter as baseline data. The solution technique was successfully used in the Institute for Flight Mechanics of DFVLR for the evaluation of flight test data obtained from fixed wing aircraft. The relationship between the given inputs to the simulation and the resulting derived parameters is discussed in particular. The results are presented graphically showing pole distribution and some frequency and time responses.

RPT#: DFVLR-SONDDR-428 74/11/00 75A15038

UTTL: Application of system identification to analytic rotor modeling from simulated and wind tunnel dynamic test data

AUTH: A/BANERJEE, D. CORP: Washington Univ., Seattle.  
ABS: Aircraft state and parameter identification methods are introduced. A simplified form of the Maximum Likelihood method is selected to extract analytical aeroelastic rotor models from simulated and dynamic wind tunnel tests results for accelerated cyclic pitch stirring excitation. The goal is to determine the dynamic inflow characteristics for forward flight conditions from the blade flapping responses without direct inflow measurements. Reverse flow effects are considered for high rotor advance ratios. Two inflow models are studied; the first is based on an equivalent blade Lock number, the second is based on time delayed momentum inflow. Basic rotor parameters are identified together with measurement bias values. The effect of the theoretical dynamic inflow on the rotor eigenvalues is studied. A relation between the accuracy of the identified parameters and the length of input data is established in simulation studies. 77/00/00 78N18040

UTTL: Unsteady hovering wake parameters identified from dynamic model tests

AUTH: A/CREWS, S. T. CORP: Washington Univ., Seattle.  
ABS: The development of a four bladed model rotor that can be excited with a simple eccentric mechanism in progressing and regressing modes with either harmonic or transient inputs was reported. Parameter identification methods were applied to the problem of extracting parameters for linear perturbation models, including rotor dynamic inflow effects, from the measured blade flapping responses to transient pitch-stirring excitations. These perturbation models were then used to predict blade flapping response to other pitch-stirring transient inputs, and rotor wake and blade flapping responses to harmonic inputs. The viability and utility of using parameter identification methods for extracting the perturbation models from transients are demonstrated through these combined analytical and experimental studies. 77/00/00 78N16992

UTTL: Application of system identification to analytic rotor modeling from simulated and wind tunnel dynamic test data, part 2

AUTH: A/HOHENEMSER, K. H.; B/BANERJEE, D. CORP: Washington Univ., St. Louis, Mo. CSS: (Dept. of Mechanical Engineering.)  
ABS: An introduction to aircraft state and parameter

Identification methods is presented. A simplified form of the maximum likelihood method is selected to extract analytical aeroelastic rotor models from simulated and dynamic wind tunnel test results from accelerated cyclic pitch stirring excitation. The dynamic inflow characteristics for forward flight conditions from the blade flapping responses without direct inflow measurements were examined. The rotor blades are essentially rigid for inplane bending and for torsion within the frequency range of study, but flexible in out-of-plane bending. Reverse flow effects are considered for high rotor advance ratios. Two inflow models are studied; the first is based on an equivalent blade lock number, the second is based on a time delayed momentum inflow. In addition to the inflow parameters, basic rotor parameters like the blade natural frequency and the actual blade lock number are identified together with measurement bias values. The effect of the theoretical dynamic inflow on the rotor eigenvalues is evaluated.

RPT#: NASA-CR-152023 77/06/00 77N26078

UTTL: Unsteady hovering wake parameters identified from dynamic model tests, part 1

AUTH: A/HOHENEWSEER, K. H.; B/CREWS, S. T. CORP: Washington Univ., St. Louis, Mo. CSS: (Dept. of Mechanical Engineering.)

ABS: The development of a 4-bladed model rotor is reported that can be excited with a simple eccentric mechanism in progressing and regressing modes with either harmonic or transient inputs. Parameter identification methods were applied to the problem of extracting parameters for linear perturbation models, including rotor dynamic inflow effects, from the measured blade flapping responses to transient pitch stirring excitations. These perturbation models were then used to predict blade flapping response to other pitch stirring transient inputs, and rotor wake and blade flapping responses to harmonic inputs. The viability and utility of using parameter identification methods for extracting the perturbation models from transients are demonstrated through these combined analytical and experimental studies.

RPT#: NASA-CR-152022 77/06/00 77N26077

UTTL: Methods studies on system identification from transient rotor tests

AUTH: A/HOHENEWSEER, K. H.; B/BANERJEE, D.; C/YIN, S. K. CORP: Washington Univ., St. Louis, Mo. CSS: (Dept. of Mechanical Engineering.)

ABS: Some of the more important methods are discussed that have been used or proposed for aircraft parameter

identification. The methods are classified into two groups: Equation error or regression estimates and Bayesian estimates and their derivatives that are based on probabilistic concepts. In both of these two groups the cost function can be optimized either globally over the entire time span of the transient, or sequentially, leading to the formulation of optimum filters. Identifiability problems and the validation of the estimates are briefly outlined, and applications to lifting rotors are discussed.

RPT#: NASA-CR-137965 AR-2-PT-1 75/06/00 77N10005

UTTL: Rotor dynamic state and parameter identification from simulated forward flight transients, part 2

AUTH: A/HOHENEWSEER, K. H.; B/CREWS, S. T. CORP: Washington Univ., St. Louis, Mo. CSS: (Dept. of Mechanical Engineering.)

ABS: State and parameter identifications based on a form of the maximum likelihood method are applied to the problem of extracting linear perturbation models, including rotor dynamic inflow effects, from transient blade flapping measurements. The estimation method is first studied in computer simulations and then applied to cyclic pitch stirring transients generated with a four-bladed rotor model operating in hovering trim conditions. The analytical perturbation models extracted from the transient test results are compared with transient and frequency response tests not used in the state and parameter identification. The identified analytical perturbation model is also compared with a simple theory. The method that is applicable both to small scale and full scale dynamic rotor testing is being extended to perturbations from forward flight trim conditions.

RPT#: NASA-CR-137964 REPT-3 76/06/00 77N10004

UTTL: Rotor dynamic state and parameter identification from simulated forward flight transients, part 1

AUTH: A/HOHENEWSEER, K. H.; B/BANERJEE, D.; C/YIN, S. K. CORP: Washington Univ., St. Louis, Mo. CSS: (Dept. of Mechanical Engineering.)

ABS: State and parameter identifications from simulated forward flight blade flapping measurements are presented. The transients were excited by progressing cyclic pitch stirring or by hub stirring with constant stirring acceleration. Rotor dynamic inflow models of varying degree of sophistication were used from a one parameter inflow model (equivalent Lock number) to an eight parameter inflow model. The maximum likelihood method with assumed fixed measurement error covariance matrix was applied. The rotor system equations for both fixed hub and tilting hub are given. The

identified models were verified by comparing true responses with predicted responses. An optimum utilization of the simulated measurement data can be defined. From the numerical results it can be anticipated that brief periods of either accelerated cyclic pitch stirring or of hub stirring are sufficient to extract with adequate accuracy up to 8 rotor dynamic inflow parameters plus the blade lock number from the transients.

RPT#: NASA-CR-137963 REPT-3 76/06/00 77N10003

UTTL: Flight data identification of six degree-of-freedom stability and control derivatives of a large crane type helicopter

AUTH: A/TOWAINE, R. L. PAA: A/(USAMRDL, Hampton, Va.)  
CORP: National Aeronautics and Space Administration, Langley Research Center, Hampton, Va.

ABS: Flight test data from a large 'crane' type helicopter were collected and processed for the purpose of identifying vehicle rigid body stability and control derivatives. The process consisted of using digital and Kalman filtering techniques for state estimation and Extended Kalman filtering for parameter identification, utilizing a least squares algorithm for initial derivative and variance estimates. Data were processed for indicated airspeeds from 0 m/sec to 152 m/sec. Pulse, doublet and step control inputs were investigated. Digital filter frequency did not have a major effect on the identification process, while the initial derivative estimates and the estimated variances had an appreciable effect on many derivative estimates. The major derivatives identified agreed fairly well with analytical predictions and engineering experience. Doublet control inputs provided better results than pulse or step inputs.

RPT#: NASA-TM-X-73958 76/09/00 76N33212

UTTL: Analytical evaluation of tilting prop rotor wind tunnel test requirements

AUTH: A/HALL, W. E., JR.: B/BUENZ, D. CORP: Systems Control, Inc., Palo Alto, Calif.

ABS: Specific test requirements related to the wind tunnel testing of the XV-15 advanced tilt rotor research aircraft were determined. The following analytical tools were developed: (1) digital simulation of the XV-15, incorporating a simplified tunnel support model, control system loop, measurement lags, gust disturbances, and sensor noise. (2) Specialization of existing data analysis programs to the high order XV-15 dynamical model (transfer function program, a time series analysis program, an advanced maximum likelihood parameter identification program). (3)

several auxiliary programs to provide estimates of damping from transfer functions as well as calculations of model decomposition of system response. The following results were discussed: (1) modelling of the aircraft, instrumentation, and controls. (2) results of the rotor/cantilever wing model and coupled wing. (3) examples of data prediction with system identification techniques, and (4) detailed conclusions and recommendations.

RPT#: NASA-CR-137826 76/01/00 76N19146

UTTL: Instrumentation requirements for aircraft parameter identification with application to the helicopter

AUTH: A/SORENSEN, J. A.: B/MOHR, R. L.: C/CLINE, T. B. CORP: Systems Control, Inc., Palo Alto, Calif.

ABS: The extent to which instrumentation errors cause degradation in the knowledge of stability and control derivatives identified for flight tests was studied along with the resultant degradation of the flight system performance based on these derivatives. The error in measurement and data processing systems used for parameter identification, error analysis techniques, and the effects of instrumentation, errors on the accuracy of parameter estimates are discussed. The analysis programs were used to study instrumentation error effects on the accuracy of the identified stability and control derivatives of the CH-46 helicopter.

RPT#: NASA-CR-132675 75/06/00 75N32112

UTTL: Rotor systems research aircraft (RSRA) requirements for, and contributions to, rotorcraft state estimation and parameter identification

AUTH: A/CONDON, G. W. CORP: National Aeronautics and Space Administration, Langley Research Center, Hampton, Va.: Army Air Mobility Research and Development Lab., Hampton, Va. In AGARD Methods for Aircraft State and Parameter Identification 18 p (SEE N75-29997 21-01)

ABS: Rotor System Research Aircraft (RSRA) is designed to provide the capabilities necessary for the effective and efficient in-flight test and verification of promising rotor concepts and supporting technology developments. The RSRA requirements for, and possible contributions to, rotorcraft state estimation and parameter identification technology are discussed.

75/05/00 75N30022

UTTL: Application of a parameter identification technique to a hingeless helicopter rotor

AUTH: A/KANNING, G.; B/BIGGERS, J. C. CORP: National Aeronautics and Space Administration, Ames Research Center, Moffett Field, Calif.

ABS: A mathematical model of a gyro-controlled, three-bladed hingeless helicopter rotor was developed and parameters of the model were estimated using a parameter identification technique. The flapping and feathering degrees of freedom of the blades were modeled. The equations of the model contain time-varying, periodic coefficients due to the forward speed of the rotor. A digital simulation of the analytical model was compared with wind-tunnel measurements to establish the validity of the model. Comparisons of steady-state and transient solutions of the analytical model with the tunnel measurements gave reasonably good matching of gyro angle but less satisfactory matching of hub moment measurements. Further improvements were obtained by use of a parameter identification technique to adjust as many as 10 parameters of the analytical model. The sensitivity of the blade response to small changes in the parameters was also calculated.

RPT#: NASA-TN-D-7834 A-5289 74/12/00 75N12906

SECTION 6

IDENTIFICATION OF AEROELASTIC SYSTEMS

mathematical model to one obtained from the flight tests of the actual aircraft.  
 RPT#: AIAA 78-1328 78/00/00 78A46520

UTTL: Instrumental variables algorithm for modal parameter identification in flutter testing  
 AUTH: A/JOHNSON, W.; B/GUPTA, N. K. PAA: A/(NASA, Ames Research Center, Aeromechanics Laboratory, Moffett Field, Calif.); B/(Systems Control, Inc., Palo Alto, Calif.) CORP: National Aeronautics and Space Administration, Ames Research Center, Moffett Field, Calif.; Systems Control, Inc., Palo Alto, Calif.  
 AIAA Journal, vol. 16, Aug. 1978, p. 800-806.

ABS: The paper is concerned with the task of estimating modal parameters from system response measurement in aircraft flutter testing. A frequency-domain derivation of an instrumental-variables algorithm is presented for a linear time-invariant dynamic system of order  $n$ . Basically, this algorithm fits a set of poles and zeros to the measured transfer function. An illustrative example is provided regarding the application of the algorithm to aeroelasticity testing. It is shown that the algorithm can be implemented for on-line data reduction with a microcomputer-based analysis system. By using instrumental variables the sensitivity of the modal parameter estimates to noise in the system-response measurements is reduced greatly. The algorithm is expected to be a powerful and valuable tool for on-line estimation of modal parameters in flutter testing and should be useful in control system and structural dynamics tests. 78/08/00 78A44904

UTTL: Identification of structural system parameters from dynamic response data  
 AUTH: A/LINK, M.; B/VOLLAN, A. PAA: B/(Dornier System GmbH, Friedrichshafen, West Germany) Zeitschrift fuer Flugwissenschaften und Weltraumforschung, vol. 2, May-June 1978, p. 165-174. Bundesministerium fuer Forschung und Technologie

ABS: A description is presented of a method which can be used to extract from the vibration test additional information on the structure's dynamic parameters, including natural frequencies, natural modes, generalized mass, stiffness, and damping. The method, which is designated ISSPA (Identification of Structural System Parameters), represents an alternative to the modal survey test which is also directed towards the determination of these parameters. The discrete equation of motion of a structure represented by a finite element model and subjected to base excitation and force excitation is

UTTL: Maximum likelihood identification of aircraft parameters with unsteady aerodynamic modelling  
 AUTH: A/RESKAR, D. A.; B/WELLS, W. R. PAA: A/(Cincinnati University, Cincinnati, Ohio); B/(Wright State University, Dayton, Ohio) CORP: Cincinnati Univ., Ohio.; Wright State Univ., Dayton, Ohio. American Institute of Aeronautics and Astronautics, Aerospace Sciences Meeting, 17th, New Orleans, La., Jan. 15-17, 1979, 10 p.

ABS: A simplified aerodynamic force model based on the physical principle of Prandtl's lifting line theory and trailing vortex concept has been developed to account for unsteady aerodynamic effects in aircraft dynamics. Longitudinal equations of motion have been modified to include these effects. The presence of convolution integrals in the modified equations of motion led to a frequency domain analysis utilizing Fourier transforms. This reduces the integro-differential equations to relatively simple algebraic equations, thereby reducing computation time significantly. A parameter extraction program based on the maximum likelihood estimation technique is developed in the frequency domain. The extracting algorithm contains a new scheme for obtaining sensitivity functions by using numerical differentiation. The paper concludes with examples using computer generated and real flight data  
 RPT#: AIAA PAPER 79-0400 79/01/00 79A19710

UTTL: Identification of the stability parameters of an aeroelastic airplane  
 AUTH: A/RYNASKI, E. G.; B/ANDRISANI, D.; II; C/WEINGARTEN, N. C. PAA: C/(Calspan Corp., Buffalo, N.Y.) CORP: Calspan Corp., Buffalo, N. Y. In: Atmospheric Flight Mechanics Conference, Palo Alto, Calif., August 7-9, 1978, Technical Papers, (A78-46526 20-08) New York, American Institute of Aeronautics and Astronautics, Inc., 1978, p. 20-27. NASA-supported research.

ABS: Phase variable transformations are used to construct the mathematical model of an aeroelastic aircraft in a form that is amenable to partial or piecemeal acceptance of parameters estimated from flight data. The problem is one of parameter identification of large scale dynamic systems involving a system matrix characterized by about 200 elements. A mathematical model of the USAF Total In-Flight Simulator was computed using the FLEXSTAB program. As data became available during the progress of the flight test program, it was processed and substituted in the mathematical model for parameters obtained from the FLEXSTAB program. Results tend to show a progressive and orderly transition from an analytically defined

considered. The extraction of eigenmodes and generalized masses is discussed along with the determination of the modal damping matrix. Investigations of the effects of various factors on the accuracy of the identification method are reported, giving attention to closely spaced eigenfrequencies, a nondiagonal generalized damping matrix, the number of measuring points compared to the number of excitation frequencies, and the number of effective degrees of freedom. 78/06/00 78A41395

UTTL: Simplified unsteady aerodynamic concepts, with application to parameter estimation  
AUTH: A/WELLS, W. R.; B/QUEIRO, M. J. PAA: A/(Wright State University, Dayton, Ohio); B/(NASA, Langley Research Center, Hampton, Va.) CORP: Wright State Univ., Dayton, Ohio.; National Aeronautics and Space Administration, Langley Research Center, Hampton, Va. In: Atmospheric Flight Mechanics Conference, Hollywood, Fla., August 8-10, 1977, Technical Papers, (A77-43151 20-08) New York, American Institute of Aeronautics and Astronautics, Inc., 1977, p. 39-45.

ABS: A simplified aerodynamic force model based on the physical principle of Prandtl's lifting line theory and trailing vortex concept has been developed to account for unsteadiness in the aircraft dynamics. The wake is assumed to be compressed to a single shed vortex element of appropriate strength moving downstream at a speed sufficient to approximate the Wagner function. Results are presented illustrating the ability of the simplified theory to duplicate exact solutions in unsteady aerodynamics. Further, consideration is given to the utility of the model in a parameter identification application.  
RPT#: AIAA 77-1124 77/00/00 77A43157

UTTL: Nonlinear parameter identification from a

vibration test  
AUTH: A/KOHLER, H. PAA: A/(Vereinigte Flugtechnische Werke-Fokker GmbH, Lemwerder, West Germany) Zeitschrift fuer Flugwissenschaften und Weltraumforschung, vol. 1, Jan.-Feb. 1977, p. 50-57. In German.

ABS: A theory for the determination of the nonlinear vibration behavior of a discrete, holonomic, elastomechanical system is described by means of a substitute system reduced, after a general survey, to two degrees of freedom. The method is applied to the nonlinearities in frequency/angle of rotation diagrams of the VFM 614 lateral control system measured during a static vibration test. A detailed discussion of the overall vibration behavior compared to the linear

theory follows. 77/02/00 77A36394

UTTL: Identification of the stability parameters of an aeroelastic airplane  
AUTH: A/RYNASKI, E. G.; B/ANDRISANI, D., II; C/WEINGARTEN, N. CORP: Calspan Corp., Buffalo, N. Y. CSS: (Flight Sciences Dept.) In AGARD Dyn. Stability Parameters 9 p (SEE N79-15061 06-08)

ABS: The problem of the parameter identification of large scale dynamic systems involving a system matrix characterized by approximately 200 elements is addressed. By using phase variable transformations, a mathematical model of an aeroelastic airplane is described in a form that is amenable to partial or piecemeal acceptance of parameters estimated from flight data. A mathematical model of the U.S. Air Force Total In-Flight Simulator was computed using the FLEXSTAB digital computer program. As data became available during the progress of the flight test program, this data was processed and substituted in the mathematical model for parameters analytically obtained from the FLEXSTAB program. The results tend to show a progressive and orderly transition from an analytically defined mathematical model to one obtained from the flight tests of the actual aircraft. 78/11/00 79N15077

UTTL: Identification of stability derivatives from wind tunnel tests of cable-mounted aeroelastic models  
AUTH: A/MOHR, R. L.; B/HALL, W. E., JR. CORP: Systems Control, Inc., Palo Alto, Calif.

ABS: The test models were mounted within the wind tunnel on a cable support system which allowed five degrees of freedom in the model's motion. A parameter identification algorithm was computer coded to calculate the maximum likelihood estimates of the stability and control derivatives based on an assumed structure of the equations of motion. Models of the F-14 aircraft and the space shuttle orbiter were tested in the transonic dynamics tunnel to demonstrate the feasibility of identifying aerodynamic coefficients from wind tunnel test data of cable-mounted models.  
RPT#: NASA-CR-145123 77/00/00 77N29166

UTTL: Dynamics and identification of flexible aircraft  
AUTH: A/WELLS, W. R. CORP: Cincinnati Univ., Ohio. CSS: (Dept. of Aerospace Engineering.) NASA  
ABS: The equations of motion and a maximum likelihood parameter identification formulation are developed for a flexible aircraft. The various levels of



approximation associated with the modal substitution representation of the elastic displacement field are discussed and illustrated when appropriate. The necessary extension of the parameter set of stability and control derivatives due to the aeroelastic effects is obtained.

RPT#: NASA-CR-2672 76/04/00 76N21158

SECTION 7

MISCELLANEOUS

is shown that the regression analysis is insensitive to noise, as expected, so that the improvement in the measuring data could not improve the results. Tests with simulated data also show that the filter is very well qualified to filter out systematic errors. In the flight test results this is also seen in the improvements of the multiple correlation coefficient. To summarize, studies with a Kalman-filter-algorithm show the technique to be a valuable tool in dynamic systems parameter identification.

RPT#: BMVG-FBWT-77-6 77/00/00 75N18057

UTTL: Flight instrumentation specification for parameter identification: Program user's guide  
AUTH: A/MOHR, R. L. CORP: Systems Control, Inc., Palo Alto, Calif.

ABS: A set of four digital computer programs is presented which can be used to investigate the effects of instrumentation errors on the accuracy of aircraft and helicopter stability-and-control derivatives identified from flight test data. The programs assume that the differential equations of motion are linear and consist of small perturbations about a quasi-steady flight condition. It is also assumed that a Newton-Raphson optimization technique is used for identifying the estimates of the parameters. Flow charts and printouts are included.

RPT#: NASA-CR-132676 75/06/00 75N32113

UTTL: A Monte Carlo analysis of the effects of instrumentation errors on aircraft parameter identification  
AUTH: A/BRYANT, W. H.; B/HODGE, W. F. CORP: National Aeronautics and Space Administration, Langley Research Center, Hampton, Va. In AGARD Methods for Aircraft State and Parameter Identification 19 p (SEE N75-2997 21-01)

ABS: An output error estimation algorithm was used to evaluate the effects of both static and dynamic instrumentation errors on the estimation of aircraft stability and control parameters. A Monte Carlo analysis, using simulated cruise flight data, was performed for a high performance military aircraft, a large commercial transport, and a small general-aviation aircraft. The effects of variations in the information content of the flight data, resulting from two different choices of control input maneuvers, were also determined. The results indicate that unmodeled instrumentation errors can cause inaccuracies in the estimated parameters which are comparable to their nominal values. Control input errors and angular accelerometer lags were found to be

UTTL: Aerodynamic coefficient estimation for dynamic wind tunnel models

AUTH: A/MOHR, R. L.; B/SMITH, R. G. PAA: B/(Systems Control, Inc., Palo Alto, Calif.) CORP: Systems Control, Inc., Palo Alto, Calif. In: Annual Aeronautics Conference on Circuits, Systems, and Computers, 10th, Pacific Grove, Calif., November 22-24, 1976.

ABS: Maximum likelihood parameter identification is used to estimate the aerodynamic coefficients of a 'flying' aircraft model which is mounted in a transonic wind tunnel by a system of cables and pulleys. The model's motion is governed by both cable and aerodynamic forces, where the parameters to be identified are functions of the aerodynamic forces but cable forces greatly predominate. The test data were successfully processed assuming a linear equation model in the identification procedure. In one instance, the procedure was able to detect a failing measurement instrument. The final parameter estimates are compared to estimates obtained in independent tests of a similar aircraft model. 77/00/00 78A18058

UTTL: Gust-vehicle parameter identification by dynamic simulation in wind-tunnels

AUTH: A/KRAG, B. CORP: Institut fuer Flugmechanik, Brunswick (West Germany). In AGARD Dyn. Stability Parameters 6 p (SEE N79-15061 06-08)

ABS: A description of the DiVLR (Deutsche Forschungs- und Versuchsanstalt fuer LUFT- und Raumfahrt) installation for dynamic simulation in wind tunnels is given. The application of this research installation in a research program and its capability and limitation are described. 78/11/00 79N15097

UTTL: Improvement of flight measuring data with a Kalman filter

AUTH: A/PLATZIEDER, L. CORP: Dornier-System G.m.b.H., Friedrichshafen (West Germany). DOKZENTBW

ABS: Improvement of Fiat G91-T3 flight test measuring data using a Kalman filter algorithm was studied. The system equations and the Kalman filter equations are given and the regression analysis is presented. Tests with the Kalman filter FORTRAN computer program, listed in the appendix, are reported and results are discussed. Both the filtering and the one channel smoothing of the measuring data produce an improvement in the regression analysis, but not nearly to the expected extent. Indeed the filtering produces a distinct reduction of the measuring data noise. But it

most significant of the instrumentation errors evaluated, and the perturbations they produce are much larger than those arising from the combined effects of static errors and white noise in the output response measurements. 75/05/00 75N30002

UTTL: SCIP2 flight instrumentation specification for parameter identification: User's guide

AUTH: A/TANIGUCHI, N. CORP: Systems Control, Inc., Palo Alto, Calif. NASA

ABS: SCIP2 which is a digital computer program that can be used to investigate the effects of instrumentation errors on the accuracy of aircraft stability and control derivatives identified from flight test data is presented. The program is based on the assumptions that the aircraft differential equations of motion are linear and consist of small perturbations about a quasi-steady flight condition. It is also assumed that a Newton-Raphson optimization technique is used for identifying the estimates of the parameters. A summary of the equations which are coded in the program are included.

RPT#: NASA-CR-112122 72/05/00 72N32041

REPORT DOCUMENTATION PAGE									
1. Recipient's Reference	2. Originator's Reference	3. Further Reference	4. Security Classification of Document						
	AGARD-LS-104	ISBN 92-835-1340-1	UNCLASSIFIED						
5. Originator	Advisory Group for Aerospace Research and Development North Atlantic Treaty Organization 7 rue Ancelle, 92200 Neuilly sur Seine, France								
6. Title	PARAMETER IDENTIFICATION								
7. Presented at	a Lecture Series under the sponsorship of the Flight Mechanics Panel and the Consultant and Exchange Programme of AGARD on 29-30 October 1979 at Delft in The Netherlands and 1-2 November 1979 in London, UK.								
8. Author(s)/Editor(s)	Various		9. Date November 1979						
10. Author's/Editor's Address	Various		11. Pages 372						
12. Distribution Statement	This document is distributed in accordance with AGARD policies and regulations, which are outlined on the Outside Back Covers of all AGARD publications.								
13. Keywords/Descriptors	<table border="0"> <tr> <td>Aircraft</td> <td>Reviews</td> </tr> <tr> <td>Flight tests</td> <td>Flight characteristics</td> </tr> <tr> <td>Data processing</td> <td>Design criteria</td> </tr> </table>			Aircraft	Reviews	Flight tests	Flight characteristics	Data processing	Design criteria
Aircraft	Reviews								
Flight tests	Flight characteristics								
Data processing	Design criteria								
14. Abstract	<p>The aim of this Lecture Series is to review the present state of the art of Aircraft Parameter Identification Techniques and to provide a critical appraisal of current methods developed and applied to the problems of Analysis of Flight Test Data in a number of NATO countries. Particular emphasis is placed on the practical aspects of Aircraft Parameter Estimation to generate information useful for the Flight Test Engineer.</p> <p>The material in this publication was assembled to support a Lecture Series under the sponsorship of the Flight Mechanics Panel and the Consultant and Exchange Programme of AGARD presented on 29-30 October 1979 at Delft in The Netherlands and 1-2 November 1979 in London, UK.</p>								

<p>AGARD Lecture Series No.104 Advisory Group for Aerospace Research and Development, NATO PARAMETER IDENTIFICATION Published November 1979 372 pages</p> <p>The aim of this Lecture Series is to review the present state of the art of Aircraft Parameter Identification Techniques and to provide a critical appraisal of current methods developed and applied to the problems of Analysis of Flight Test Data in a number of NATO countries. Particular emphasis is placed on the practical aspects of Aircraft Parameter Estimation to generate information useful for the Flight Test Engineer.</p> <p>P.T.O.</p>	<p>AGARD-LS-104</p> <p>Aircraft Flight tests Data processing Reviews Flight characteristics Design criteria</p>	<p>AGARD Lecture Series No.104 Advisory Group for Aerospace Research and Development, NATO PARAMETER IDENTIFICATION Published November 1979 372 pages</p> <p>The aim of this Lecture Series is to review the present state of the art of Aircraft Parameter Identification Techniques and to provide a critical appraisal of current methods developed and applied to the problems of Analysis of Flight Test Data in a number of NATO countries. Particular emphasis is placed on the practical aspects of Aircraft Parameter Estimation to generate information useful for the Flight Test Engineer.</p> <p>P.T.O.</p>	<p>AGARD-LS-104</p> <p>Aircraft Flight tests Data processing Reviews Flight characteristics Design criteria</p>
<p>AGARD Lecture Series No.104 Advisory Group for Aerospace Research and Development, NATO PARAMETER IDENTIFICATION Published November 1979 372 pages</p> <p>The aim of this Lecture Series is to review the present state of the art of Aircraft Parameter Identification Techniques and to provide a critical appraisal of current methods developed and applied to the problems of Analysis of Flight Test Data in a number of NATO countries. Particular emphasis is placed on the practical aspects of Aircraft Parameter Estimation to generate information useful for the Flight Test Engineer.</p> <p>P.T.O.</p>	<p>AGARD-LS-104</p> <p>Aircraft Flight tests Data processing Reviews Flight characteristics Design criteria</p>	<p>AGARD Lecture Series No.104 Advisory Group for Aerospace Research and Development, NATO PARAMETER IDENTIFICATION Published November 1979 372 pages</p> <p>The aim of this Lecture Series is to review the present state of the art of Aircraft Parameter Identification Techniques and to provide a critical appraisal of current methods developed and applied to the problems of Analysis of Flight Test Data in a number of NATO countries. Particular emphasis is placed on the practical aspects of Aircraft Parameter Estimation to generate information useful for the Flight Test Engineer.</p> <p>P.T.O.</p>	<p>AGARD-LS-104</p> <p>Aircraft Flight tests Data processing Reviews Flight characteristics Design criteria</p>

<p>The material in this publication was assembled to support a Lecture Series under the sponsorship of the Flight Mechanics Panel and the Consultant and Exchange Programme of AGARD presented on 29–30 October 1979 at Delft in The Netherlands and 1–2 November 1979 in London, UK.</p> <p>ISBN 92-835-1340-1</p>	<p>The material in this publication was assembled to support a Lecture Series under the sponsorship of the Flight Mechanics Panel and the Consultant and Exchange Programme of AGARD presented on 29–30 October 1979 at Delft in The Netherlands and 1–2 November 1979 in London, UK.</p> <p>ISBN 92-835-1340-1</p>
<p>The material in this publication was assembled to support a Lecture Series under the sponsorship of the Flight Mechanics Panel and the Consultant and Exchange Programme of AGARD presented on 29–30 October 1979 at Delft in The Netherlands and 1–2 November 1979 in London, UK.</p> <p>ISBN 92-835-1340-1</p>	<p>The material in this publication was assembled to support a Lecture Series under the sponsorship of the Flight Mechanics Panel and the Consultant and Exchange Programme of AGARD presented on 29–30 October 1979 at Delft in The Netherlands and 1–2 November 1979 in London, UK.</p> <p>ISBN 92-835-1340-1</p>